TOC

IUE-401-76-099

SYSTEM DESIGN REPORT
For The
INTERNATIONAL ULTRAVIOLET EXPLORER

VOLUME II
SPACECRAFT DESIGN

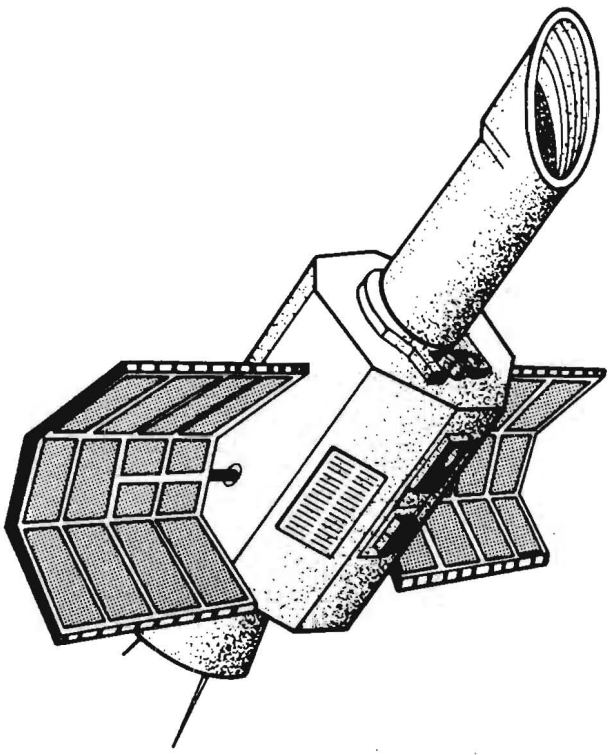

June 1976

GODDARD SPACE FLIGHT CENTER
GREENBELT, MARYLAND

PREFACE

This document was prepared by OAO Corporation under contract NAS5-23559 for Goddard Space Flight Center in Greenbelt, Maryland. The contract covers the revision of two volumes of the International Ultraviolet Explorer (IUE) System Design Report. This volume (Volume II) presents the IUE spacecraft design; whereas, Volume I, to be republished later this year, devotes its attention to the scientific instrument. The third volume titled Ground System Plan was published in December of 1974 and will not be revised under this contract. It is anticipated that both Volumes I and II will be updated periodically to reflect design and performance changes, as the IUE program evolves to completion. These revisions along with a document history sheet delineating the changes will be available from the IUE Project Office, GSFC, Code 401. Additional copies of Volumes I and II will also be available from the Project Office.

CONTENTS

CONTENTS (cont)

CONTENTS (cont)

CONTENTS (cont)

CONTENTS (cont)

CONTENTS (cont)

CONTENTS (cont)

CONTENTS (cont)

ILLUSTRATIONS (cont)

CONTENTS (cont)

ILLUSTRATIONS (cont)

ILLUSTRATIONS (cont)

CONTENTS (cont)

ILLUSTRATIONS

ILLUSTRATIONS (cont)

CONTENTS (cont)

ILLUSTRATIONS (cont)

ILLUSTRATIONS (cont)

CONTENTS (cont)

ILLUSTRATIONS (cont)

TABLES

CONTENTS (cont)

TABLES (cont)

SECTION 1. INTRODUCTION

1.1 BACKGROUND

The International Ultraviolet Explorer (IUE) was first considered in late 196[illegible] as a result of recommendations made by the NASA Astronomy Mission Board (AMB) their publication (Reference 1-1), a Long-Range Program in Space Astronomy, whi recommended an integrated space astronomy plan for the 1970s. Various programs were identified for UV astronomy such as the Orbiting Astronomical Observatory (OAO) and the Large Space Telescope (LST). By the end of 1969, however, it appeared unlikely that it would be possible for NASA to launch anothe OAO-type spacecraft after OAO-C. As a result, it was recommended that an Explorer-class satellite should be investigated to see if it could meet the needs of a UV astronomy program. A study, known as the UVAS study, was conducted earlier by the Culham group in the United Kingdom for the European Space Research Organization (ESRO) concerning a 45-cm telescope having an echelle spectrograph. As a result of this study and the recommendation by the AMB for an Explorer-class satellite, Goddard Space Flight Center conducted an "in-house" Phase A Study during the summer of 1970. The GSFC Phase A study focused on a system that had the following general characteristics:

a. Delta launch vehicle.

b. 45-cm UV telescope with an echelle spectrograph.

c. Lifetime of 3 to 5 years.

d. Geosynchronous orbit.

e. Three-axis control with 1 arc sec pointing accuracy.

f. International (guest observer) facility.

A Phase A report (Reference 1-2) was published in March 1971. The results of the study, conducted by a group of scientists and engineers at GSFC, documented the technical approach, with some options, and determined that a UV astronomy satellite having these characteristics was indeed feasible. In July 1971, the GSFC study group was given the go-ahead to conduct the system design phase (Phase B) of the program. This phase was to further define the subsystem parameters, settle on a specific subsystem design, develop specifications and drawings necessary for the execution phase, demor strate feasibility by breadboarding the critical or developmental hardware and produce an overall program plan including the involvement and interac

tions between GSFC, the United Kingdom, and ESRO in the context of an international, cooperative program. An interim design report was published as a three volume document in August 1972 (Reference 1-3). A second report (Reference 1-4) issued in June and September of 1973 was an update to the August 1972 publication and was used during the preliminary hardware specification and procurement period. This report is a correction and expansion of the 1973 report and represents the IUE hardware and mission configuration as of May 30, 1976.

1.2 REFERENCES

1-1. A Long Range Program in Space Astronomy, NASA Astronomy Mission Board.

1-2. Phase A Report for Small UV Astronomy Satellite, SAS-D. Technical Plan, NASA GSFC, March 1971.

1-3. Systems Design Report for International Ultraviolet Explorer (IUE), NASA GSFC, August 1972.

1-4. Systems Design Report for International Ultraviolet Explorer (IUE) - Volume I, Scientific Instrument, NASA GSFC, June 1973, Volume II, Spacecraft Design, NASA GSFC, September 1973.

SECTION 2. GENERAL DESCRIPTION

2.1 DESIGN REQUIREMENTS AND GOALS

The general system design requirements and goals have not changed since the publication of the Phase A report. The scientific objectives are covered in Volume I of this report as well as in earlier reports. However, for completeness and to allow this volume to be used independently, some of the basic requirements and goals that propelled the spacecraft design to its present configuration are given below.

2.1.1 SCIENTIFIC

It is desired to place a 45-cm diameter telescope of f/15 Cassegrain design, using an echelle spectrograph, for ultraviolet astronomy in the spectral region between 1150 and 3200A, into geosynchronous orbit. In this spectral region, it is required to perform high-resolution spectroscopy (0.1 Å) with stars having brightness down to 7th magnitude and to perform low resolution spectroscopy (6 Å) with faint stars, 12th magnitude or dimmer.

2.1.2 SPACECRAFT

The spacecraft must be able to point anywhere on the celestial sphere, except within 45^{o} of the sun, with an accuracy of ± 1 arc-second. The control system must be able to repoint the telescope to a new target star over a fairly wide angle (up to 60^{o}) with a rate of 4.5 degrees per minute per axis and guarantee that the desired new target star falls within the 16 arc-minute diameter field-of-view of the fine error sensor. To perform spectroscopy on the faint stars with the desired resolution, the control system must hold a 1 arc-second diameter star image within a 3 arc second-diameter spectrograph entrance aperture long enough to permit an integrated exposure of 1 hour duration by the spectrograph camera. Battery storage is required on the spacecraft to provide sufficient power to maintain attitude control and critical spacecraft subsystems during solar eclipses.

The IUE is being developed as an international guest observer facility. The design lifetime of the hardware is 3 years, with a goal, including the sizing of consumables and degradable hardware, of 5 years. Moreover, to be consistent with the Explorer-class satellites, the spacecraft must be sized to be launched with a Delta vehicle.

2.1.3 GROUND OPERATIONS

The satellite is to be placed into an elliptical geosynchronous orbit that will give 24 hours a day coverage from a ground station in the United States and at least 10 hours a day coverage from a ground station located in Europe. Once in orbit, continuous telemetry and command communications will be maintained from a control center located at GSFC. This requires a dedicated ground facility to ensure continuous uplink-command and downlink-telemetry capabilities. Telemetry and command communications will also be maintained from the European Control Center during its period of coverage.

2.2 CONTROL SYSTEM CONCEPT

The primary attitude sensor is the Inertial Reference Assembly (IRA) consisting of six precision single-axis, torque-rebalanced, rate-integrating gyros with gas bearings, implemented in a strapdown mode. The input axes of the six gyros are skewed for redundancy so that any 3 gyros can perform complete 3-axis attitude sensing. Coordinate transformation and attitude computation is done by an on-board computer. Control torques are provided by a momentum exchange system using conventional reaction wheels. Three are arranged in an orthogonal triad and a fourth wheel is skewed relative to all three axes for redundancy. Telescope pointing is controlled by astronomers from the ground.

Figure 2-1 is a block diagram of the essential components of the system. The system design makes extensive use of the continuous spacecraft-to-ground communications capability provided by a synchronous orbit. On a single day, the system can make observations anywhere in the celestial sphere to within 45 degrees of the sun or the earth, and the entire celestial sphere is observable within three months.

To envision the operation of the system, assume that the gyros in the IRA have been trimmed and that the telescope is pointed at an object whose celestial coordinates are known. To move the telescope to a new target requires that the celestial coordinates of the new target be inserted into the ground computer. The ground computer will calculate the magnitude and direction of the pitch, yaw, and roll slews required to move the telescope to a new target. Through a series of ground commands, the spacecraft is instructed to perform the slews, one axis at a time, using the IRA as a reference. The IRA can preserve its inertial reference to better than 2 minutes of arc even for large angle slew maneuvers. This gyro accuracy guarantees that the new target star will lie well within the 16 arc-minute field-of-view of the fine error sensor at the completion of any slew.

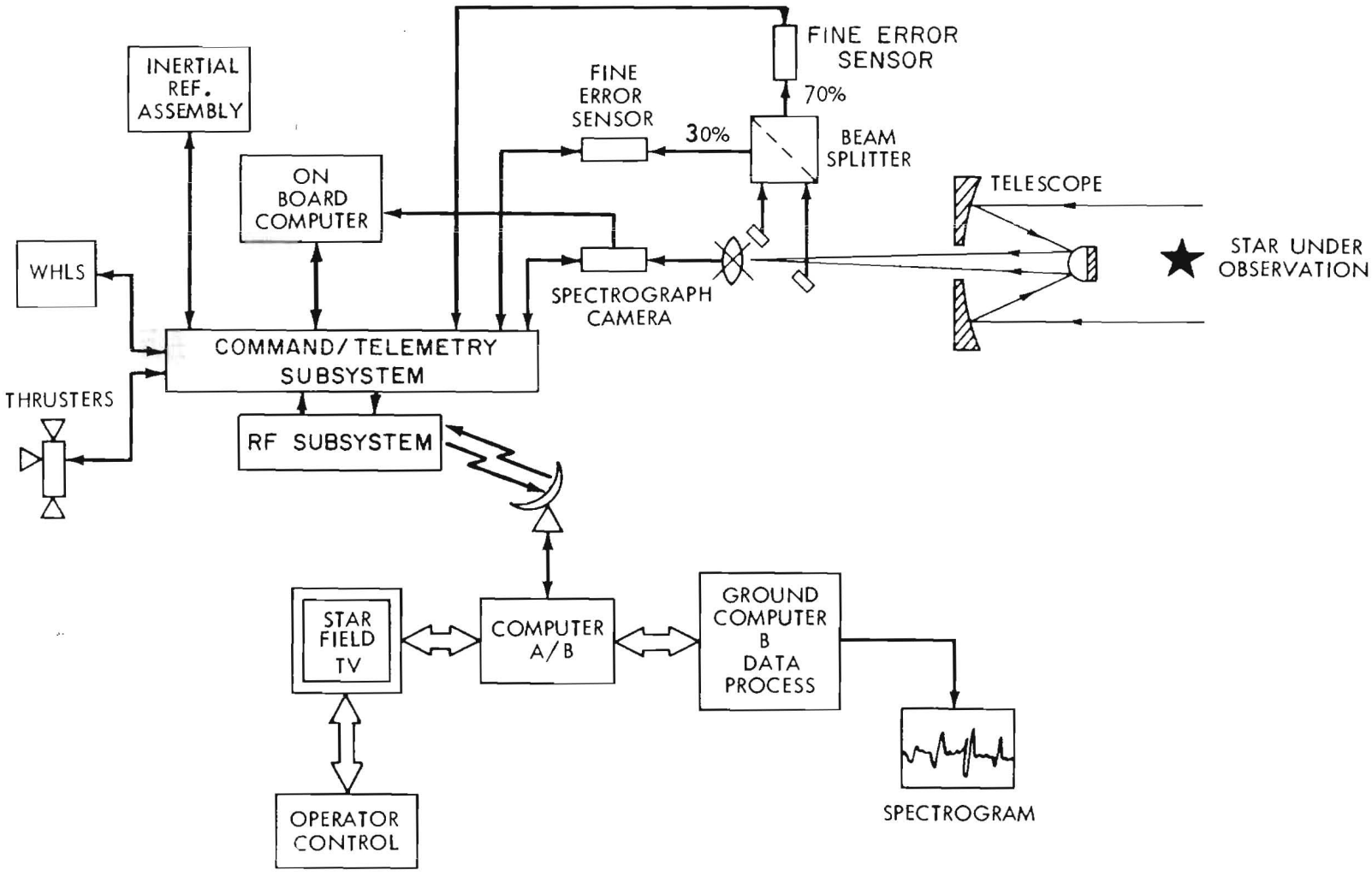

Figure 2-1. Block Diagram of IUE Essential System Elements

After completion of the slew, the fine error sensor is operated in its Field Camera Mode and the telescope image is relayed to the ground by the spacecraft telemetry system. The image is recorded in the ground computer and displayed on a television monitor. From the pattern, coordinate changes necessary to correct the pointing of the telescope to the desired star can be derived. The principal of operation resembles that of the finder telescope used with ground-based telescopes. The sensitivity of the fine error sensor will permit 14th magnitude objects to be recorded.

The guest observer, using a star atlas having about the same scale and limiting magnitude as the fine error sensor display, identifies the object he wishes to observe. Using an interactive device (x-y coordinate track ball), he then communicates this identification to the computer. The computer will calculate the magnitude of the pitch and yaw fine slews that are required to move the target star into the spectrograph aperture. The maximum permissible slew magnitude under these conditions is 5 arc-minutes, and the slew accuracy is 1 part in 1000. Such a slew will easily position the star into the aperture.

Members of the Astronomy Working Group and others have expressed a desire to observe objects fainter than 12th magnitude. Many factors influence the limiting magnitude of stellar objects that are observable with the instrument and ground test results cannot accurately predict the faintest object that will be visible to the system in orbit.

Once the desired target star has been placed into the 3 arc-second entrance aperture, fine pointing is maintained using information derived from another star within the 16 arc minute Field-of-View (FOV) of the Fine Error Sensor (FES). In this mode the FES is used as an offset star tracker, and its instantaneous FOV is commanded to offset point to a known star position within its FOV. Pitch and yaw position error information can be obtained from stars as faint as 14th magnitude. These signals may be used directly by the attitude control system, together with the IRA outputs, to maintain the target star within the spectrograph's entrance aperture. Alternatively, attitude control can be attained using the IRA outputs alone. In this mode of operation, the FES error signals may be used to provide IRA drift trim and position update information. Additional fine error sensor characteristics may be found in Volume I.

If objects to be observed cannot be recorded directly by the FES, the same procedure is followed, except that the celestial coordinates of the faint or invisible target object, relative to the observed guide star, are manually inserted into the ground computer. There is no fundamental limitation on the length of an exposure made in this manner, and the technique will permit observations to be made down to the sky background limit.

Planets and comets generally subtend an angle larger than 3 arc-second entrance aperture of the spectrograph. In such cases, the image recorded by the FES will be used to determine which area of the object is being processed. The fine-slew maneuver described for the initial-acquisition sequence will point the telescope initially at the area of interest. A small bias inserted into the pitch and yaw control loop can be used to provide the spacecraft motion necessary to generate a scan of the target or to follow a target's orbital motion.

2.3 SIGNIFICANT CHANGES FROM SYSTEM DESIGN REPORT (PHASE B)

There have been some conceptual changes in the spacecraft system design since the Phase B report and some additional changes as a result of these conceptual changes. The most important of these are included in the following discussions.

2.3.1 CONCEPTUAL CHANGES

2.3.1.1 On-board Computer. The primary user of the on-board computer as presented in the Phase B report was the stabilization and control subsystem. The purpose of the on-board computer has now been expanded to include service and diagnostic routines for other subsystems as well.

2.3.1.2 Digital Sun Sensors. The two Digital Sun Sensors (DSS) have been relocated on a mounting block providing identical view angles and allowing either sensor to cover the expected operational range of 15 to 135 degrees in Beta.

2.3.1.3 Antenna Location. Pattern tests performed on the VHF receiver system indicated that relocation of the VHF antennas to the bottom of the spacecraft would provide better coverage on the ground. The S-band transmitting antenna located on the telescope sunshade was relocated to the bottom of the spacecraft to provide redundancy for the prime-use antenna already there and to avoid the need and expense of a deployment mechanism that would have been required to resolve a shroud interference problem.

2.3.1.4 Radiation Shield Philosopy. Many IUE electronic subsystems were designed around microcircuits using CMOS technology. As a result of changes in the manufacturing process, the currently available CMOS circuits are more susceptible to high energy particle radiation damage. Therefore, it has become necessary to provide several millimeters of aluminum shielding around electronics units with a consequent increase in weight. This has been countered by changes to permit a greater in-orbit payload capability and by other changes to reduce spacecraft subsystem weight.

2.3.2 CHANGES INCREASING ORBITAL PAYLOAD WEIGHT

2.3.2.1 Orbital Parameters. A substantial increase in payload weight was obtainable by changing the parameters of the orbit from a circular, geosynchronous orbit to an elliptical orbit with the same period. The parameters of the revised orbit are as follows:

a. Semi-major axis: 42,164 km.
b. Radius of perigee: 30,686 km.
c. Radius of apogee: 53,642 km.
d. Apogee bias: 10,556 km.
e. Inclination: 26.50°.
f. Eccentricity: 0.27221.
g. Period: 23.934 hours.

2.3.2.2 Apogee Boost Motor. The Apogee Boost Motor (ABM) has been changed to a TE-M-604-4. This motor provides the required velocity increment to place the IUE in its geosynchronous, elliptical orbit. The standard "604" was lengthened 1½ inches for IUE.

2.3.3 CHANGES TO REDUCE SUBSYSTEM WEIGHT

A large number of weight reduction actions have been implemented. Major examples follow:

2.3.3.1 OBC Memories. The number of OBC memories has been reduced from four (two available to each Central Processor Unit [CPU]) to three. However, these three units have been made available to both CPU's, thereby enhancing redundancy at no loss in function.

2.3.3.2 Redundant Fine Error Sensor. The Fine Error Sensor (FES) has been augmented with a second unit and the two acquisition cameras have been deleted. This saves weight and provides critical redundancy in the ACS fine pointing loop.

2.3.3.3 Spacecraft Batteries. The two, 12 ampere-hour (AH) batteries have been replaced by two 6 AH units. As a result of this change, the provision for experimentation in the earth's shadow has been eliminated and the orbital parameters changed to minimize the number and duration of eclipse events.

2.3.3.4 Solar Array. The array has been reduced in size.

2.3.3.5 Heat Pipes. The number of heat pipes has been reduced from three to two with no adverse effects on the thermal design.

2.3.3.6 Command Subsystem. The S-band redundant command receivers and the hybrids and diplexers required to allow use of common antennae with the S-band transmitters have been removed. The VHF command system will be used for mission operations as well as the transfer orbit phase.

SECTION 3. SPACECRAFT SUMMARY

3.1 SPACECRAFT CONFIGURATION

The frontispiece shows the IUE spacecraft in mission-orbit configuration. The spacecraft's main body is octagonal in shape; its telescope extends from the upper end of the main body; and its fixed solar array extends outward from two opposite sides. After stabilization in mission orbit, the attitude control system will maintain spacecraft orientation such that the front of the solar array always faces toward the sun. This also means that the thermal louvers, seen on the spacecraft main body, will always face away from the sun. The louvers together with thermal blankets covering the spacecraft, heat pipes mounted to the underside of the main equipment platform, and heaters within the spacecraft provide thermal control, maintaining temperatures within acceptable ranges. The main equipment platform carrying most of the electronic equipment is located within the main body adjacent to the louvers. Temperatures are maintained between 0°C and 40°C.

Figure 3-1 provides another view of the spacecraft. An apogee boost motor located in the lower part of the spacecraft is used to insert the spacecraft from transfer orbit to synchronous orbit. Also located in the lower part of the spacecraft is a Hydrazine Auxiliary Propulsion System (HAPS) used for nutation control, precession, despin, sun acquisition, reaction wheel momentum unloading, station acquisition, and east-west stationkeeping. The HAPS consists of tanks, plumbing, thruster assemblies, and supporting structure, all forming an integrated unit. Figure 3-2 shows the spacecraft in launch configuration with solar array folded. The array remains folded throughout the park and transfer orbits and is deployed only after apogee motor burn and despin.

The Scientific Instrument (SI), consisting of the telescope and spectrograph, is mounted to the spacecraft structure by the strong ring. The strong ring rests on three columns which carry the load to the lower structure and are supported laterally by truss members of the main body structure. The Inertial Reference Assembly (IRA) is mounted directly to the SI at the strong ring to minimize relative movement between the two and to simplify alignment. This arrangement permits alignment of the IRA and SI as an integral assembly and assures maximum precision in controlling the pointing of the telescope. The IRA is the primary rate and position sensor and provides position data accurate to a fraction of an arc-second. Two Fine Error Sensors (FES) mounted within the spectrograph also determine and control telescope pointing to within one arc-second.

A summary of spacecraft characteristics appear in table 3-1.

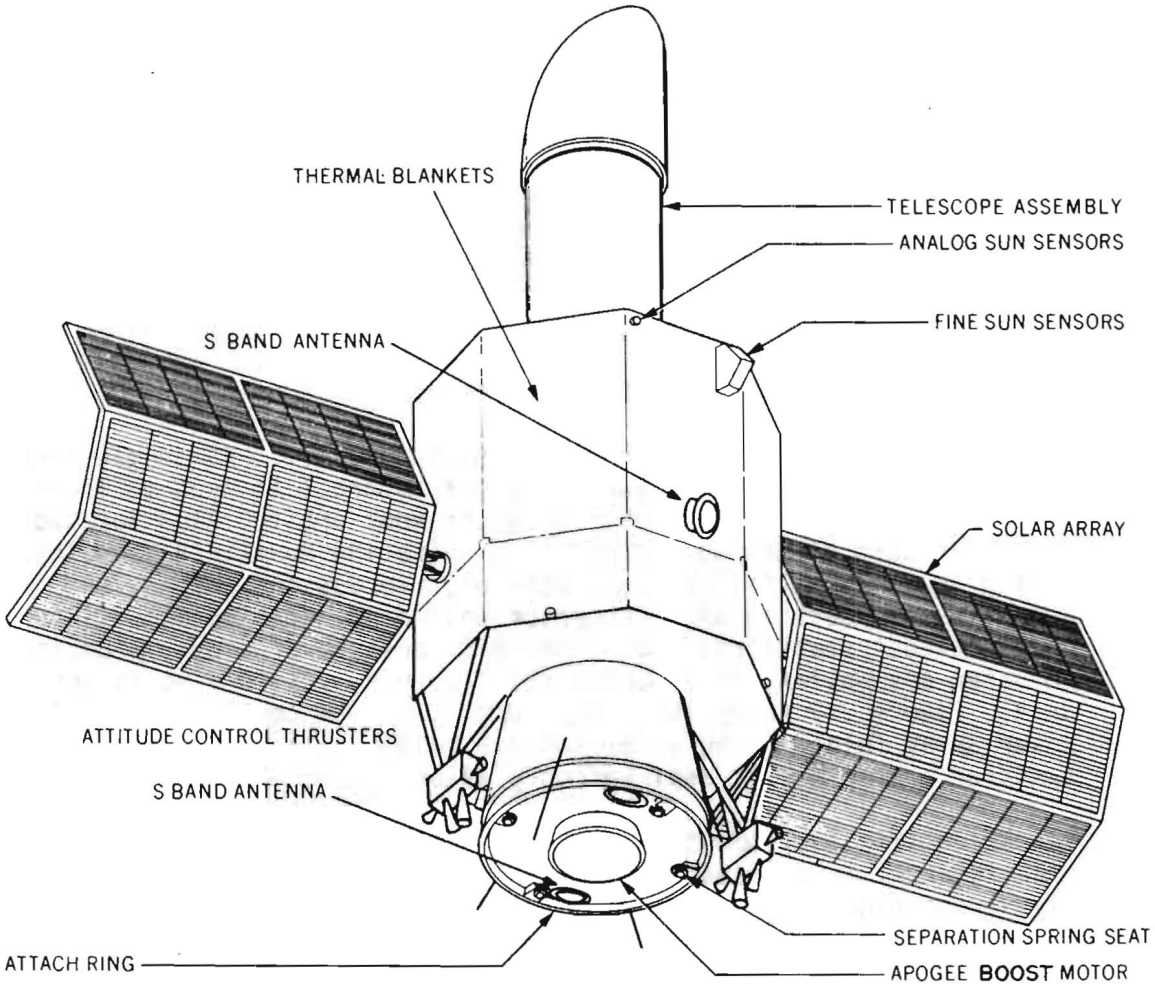

Figure 3-1. IUE Spacecraft

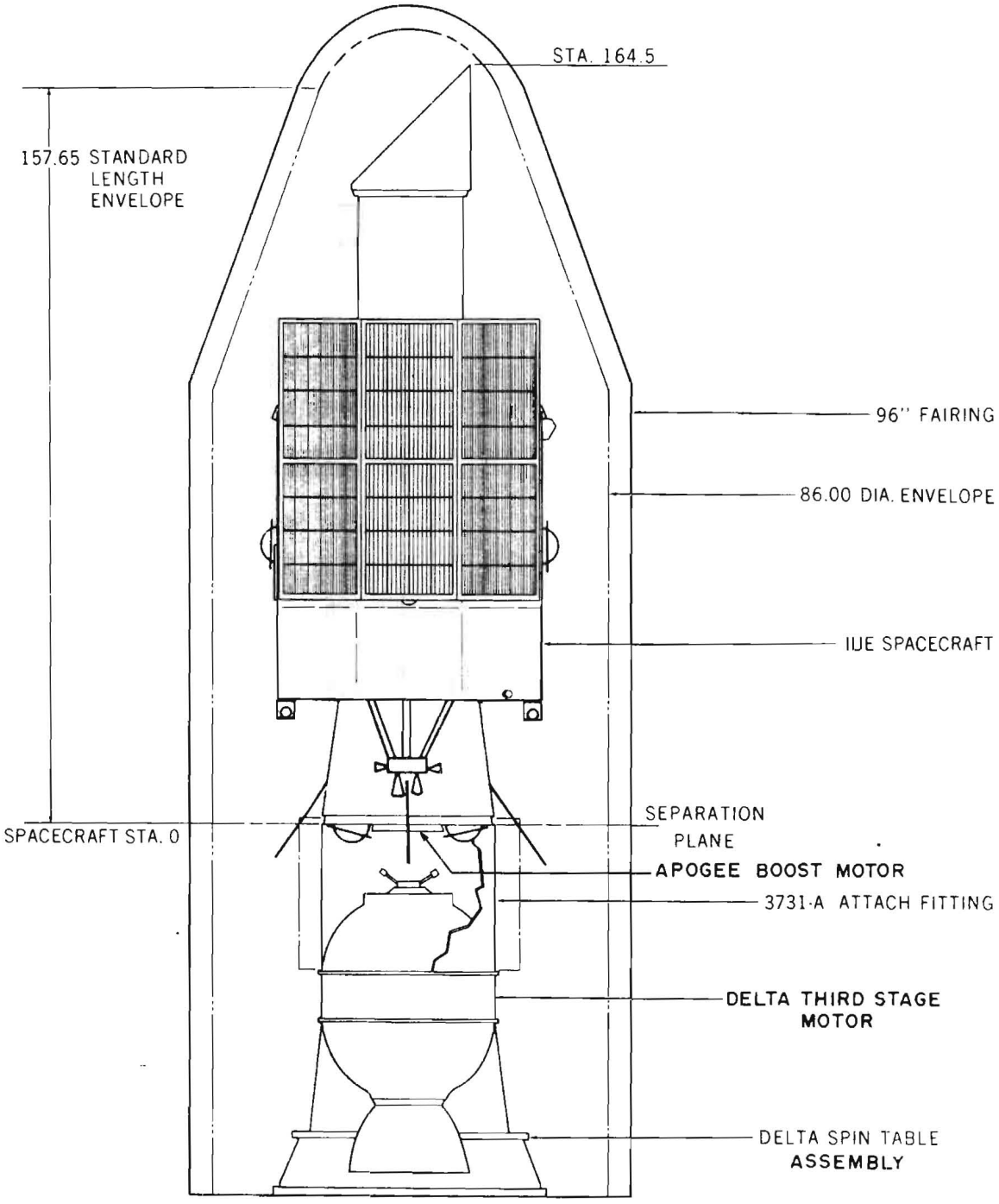

Figure 3-2. IUE Launch Configuration

Table 3-1. IUE Summary

Characteristics	Description
Spacecraft Weight	656.8 lbs
Experiment Weight	272.1 lbs
Apogee Motor	490.3 lbs
Total Spacecraft Weight	1419.2 lbs
Launch Vehicle	Delta 2914
Life	3 - 5 Years
Orbit (Mission)	Elliptical Geosynchronous (26.5° inclination)
Power Required (Spacecraft and Experimentation)	218 watts avg.
Array Capability (Beginning of Life)	424 watts at β = 67.5° 238 watts at β = 0° and 135°
Batteries (2)	6-AH NiCad Cells (17 each)
Telemetry Bit Rate	1.25 KB/s to 40 KB/s with fixed and reprogrammable formats
Command	PCM/FSK/AM, 1200 B/S
Stabilization and Control	Spinning during transfer orbit, 3-axis stabilized with 1 arc-second control for synchronous orbit.

3.2 MISSION SEQUENCE

A detailed mission sequence of events is given in Section 8.2. A brief overview of the maneuvers and operations required during the various phases of the mission is given here. Section 14 is a detailed discussion of the mission analysis.

While attached to the Delta vehicle, the spacecraft will have no control or operational requirements. Prior to the Delta third stage burn for injection into the transfer orbit, the spacecraft and third stage assembly is spun-up to 60 rpm by the Delta spin table. After injection from the parking orbit into the transfer orbit and separation from the Delta's third stage, an Automatic Nutation Control (ANC) system on the spacecraft is initiated. Spacecraft control is by the ANC or ground initiated commands. With the solar arrays folded about the spacecraft, the moment of inertia ratio with respect to the spin vector is unfavorable, thus the requirement for the active nutation control. A detailed analysis of this can be found in section 8.2 of this volume.

Since it is planned to fire the apogee boost motor at the second apogee of the transfer orbit, the spin mode duration in the transfer orbit will be about 21 hours. However, it is optional to wait for the fourth apogee and hydrazine fuel quantity for the nutation control takes this into account. Precession of the spin vector will have to be performed in order to align the apogee motor in the proper direction for boost into the synchronous orbit. Approximately 180^0 rotation is required. Figure 3-3 depicts the mission sequence required during the early phase of the transfer orbit if a January 1978 launch date is assumed. Range and range rate measurements will be required during the transfer orbit to accurately predict the orbit and time of apogee motor firing. Figure 3-4 shows the transfer orbit geometry with sun position depicting a January launch.

Mission sequences are grossly dependent on the time-of-year launch. The sequence and the launch profile shown in figure 3-3 assumes a January launch. Launches in May or September would require the 180^0 precession to occur in two steps in order to ensure a favorable sun angle for spacecraft power.

At apogee, the motor is commanded to ignite by ground command. A backup command sequence may be provided by the onboard computer to perform the burn sequence if something should happen to the ground command link. For the planned transfer orbit injection point, second apogee motor burn would occur over the Pacific Ocean at about W 150^0 longitude and the desired station point is W 47^0 longitude. The bias obtained by a nominal Delta third stage burn and a nominal apogee motor burn will be such that an eastward drift will result at about 6^0 per day. However, when the 3 sigma values are considered, the resultant drift could be anywhere from 6^0 per day, westward drift, to 18^0 per day, eastward drift. Therefore,

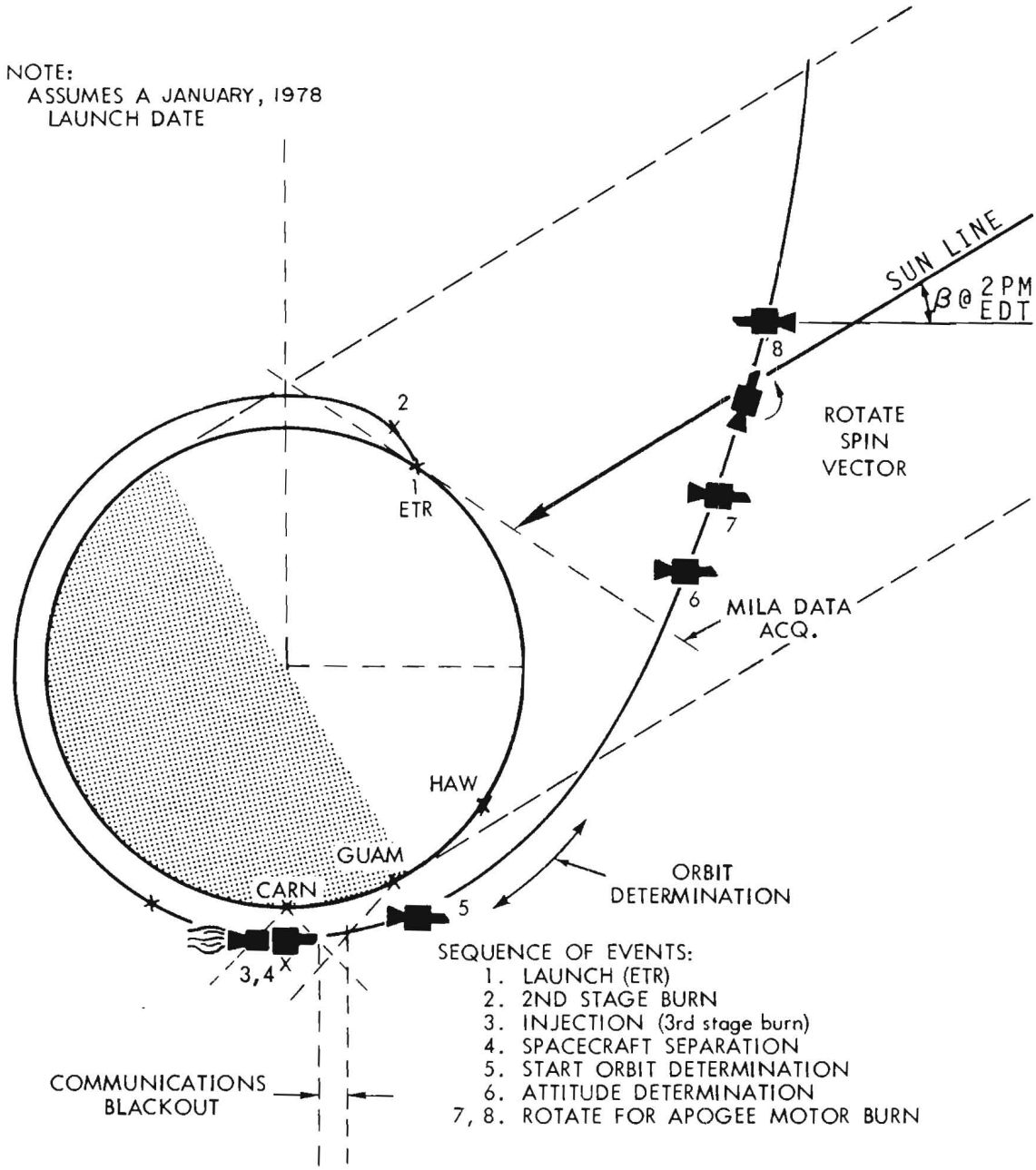

Figure 3-3. Transfer Orbit Profile

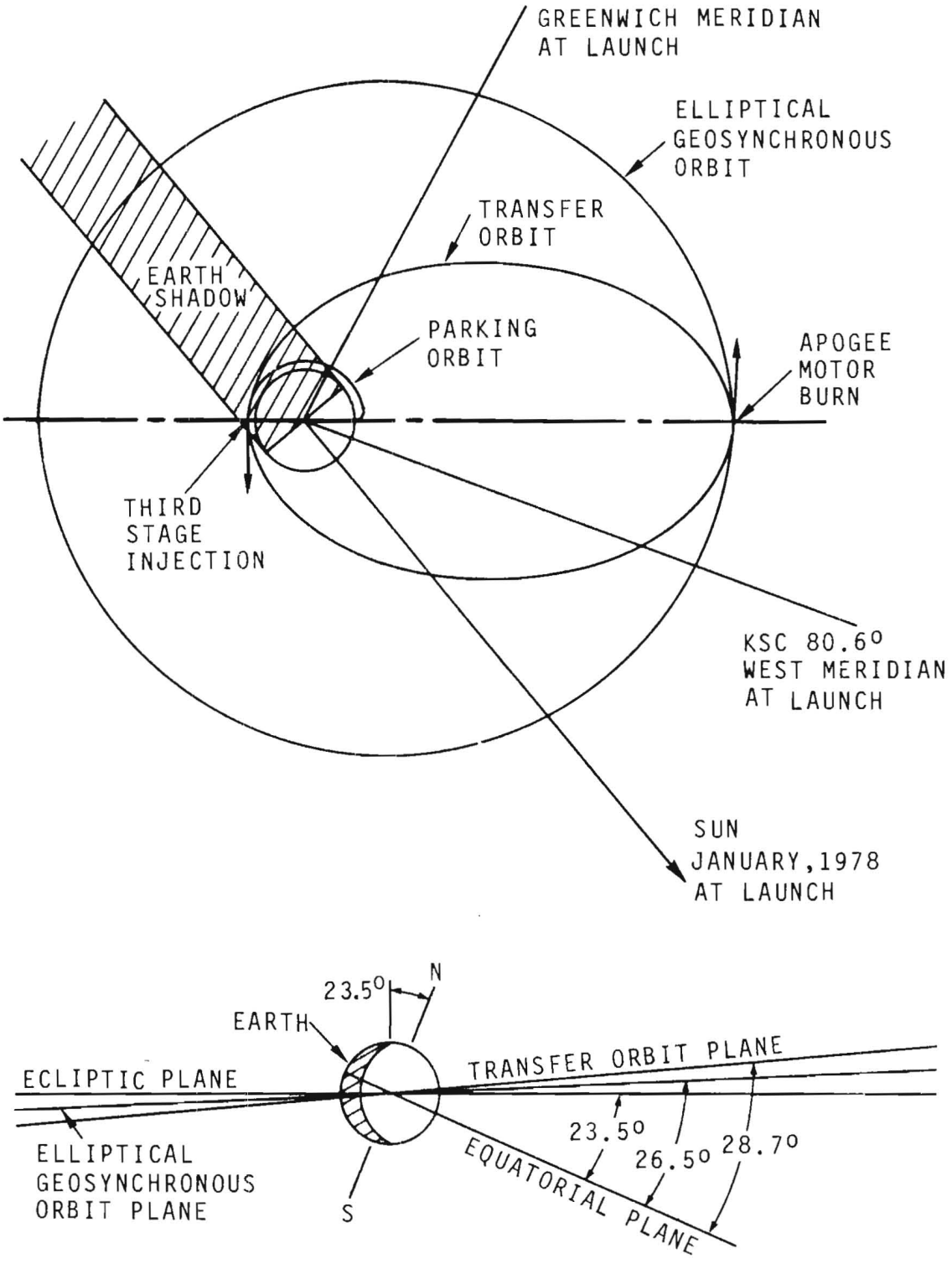

Figure 3-4. Transfer Orbit Geometry

following the apogee motor burn, the spacecraft will remain in a spun-up mode for approximately two hours for an orbit (drift) determination to be obtained. Energy would have to be removed from the orbit to get an eastward drift greater than 3^0 per day if deemed necessary. In this case, some hydrazine fuel would have to be expended to obtain the desired drift. The hydrazine weight carried in the weight budget allows for the 99% worst case velocity change required to get on station.

When the desired drift is obtained, the spacecraft will be despun in two phases to calibrate HAPS thrusters and gain 3 axis gyro rate control. The IUE will then be spun up to 2 to 5^0 per second and the solar arrays deployed. After deployment, the IUE will be rate damped to 0.25^0/sec. The solar acquisition phase is then initiated and the spacecraft will be aligned with the sunline normal to the primary plane of the solar arrays. As the drift progresses near the desired station point, two 5-pound thrusters will be fired along a pre-aligned axis to increase orbit energy to achieve a synchronous orbit period.

3.3 ELECTRICAL SYSTEM SUMMARY

Figure 3-5 is the overall block diagram of the IUE electrical system. The discussion in this section will give a brief description of the subsystem designs that are detailed in Sections 4 through 8 of this report.

Two solar paddles and two 6-amp-hour nickel-cadmium batteries will support a nominal spacecraft load of 217 watts for a period of 5 years. The spacecraft will experience solar eclipse periods for about 45 days twice a year. Table 3-2 shows the power profile as a function of operating mode. During the park and transfer orbits, the nonessential electronic packages will be turned off. The solar arrays will be folded until the apogee motor burn is complete and the spacecraft has been despun to 2 to 5°/second. During the spinning phase the spacecraft power required is in the order of 107 watts which is well within the solar array power available when the sunline is within 40 degrees of normal to the spin axis. The solar array power is clamped to +28 volts with a regulation of ±2% by a shunt regulator and fed directly to the system voltage bus. When the solar array cannot support the required power, the battery voltage is boosted to maintain the +28 volt bus with the same ±2% regulation.

The RF Communications System is comprised of a pair of redundant VHF transponder systems radiating and receiving through a turnstile VHF antenna system and a pair of redundant S-band transmitters driving four S-band power amplifiers and antennas.

Two redundant command decoders detect and route the frequency shift keying/amplitude modulation/pulse code modulation (FSK/AM PCM) command messages from the ground, or in a time-shared mode, route the digital command messages generated by an onboard computer. The command rate from the ground is 1200 bits per second, where the 1200 bit per second clock is amplitude modulated on "one" and "zero" tones. The tones are FSK signals at the clock rate and will have a discrete frequency assigned for each tone. The frequencies assigned will be within a 7 kHz to 12 kHz band.

The data handling system is comprised of analog and digital multiplexers, data source format control memories, and a split-phase generator. The analog and digital multiplexers are time shared with the onboard computer whereby the transmitted telemetry data and computer data may be programmed to sample different multiplexer input gates. Furthermore, the telemetry data sample rate and the computer data sample rate may be of different ratios depending on the bit rate being transmitted to the ground. The telemetry and computer controlled format memories are either generated by Read-Only-Memories (ROM's) or by variable reprogrammable memories.

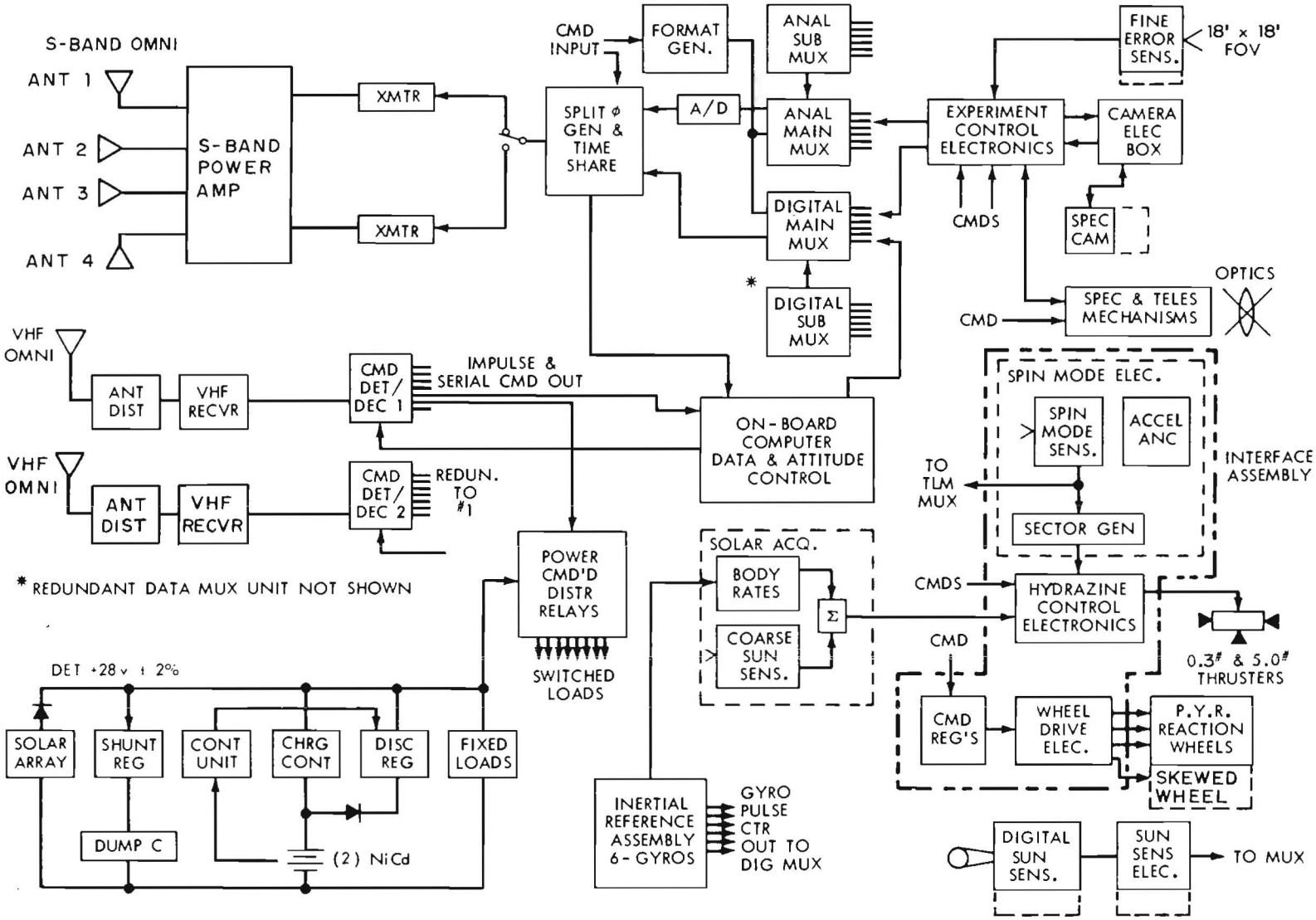

Figure 3-5. IUE Electrical System Block Diagram

Table 3-2. IUE Power Profile (Watts)

	Transfer Orbit	Mission Orbit
SCIENTIFIC INSTRUMENT		
Cameras	0.0	5.56
CEB and CSIU	0.0	13.82
Fine Error Sensor	0.0	4.30
EEA	0.0	11.47
Mechanisms and Lamps	4.0	1.95
Heaters	5.0	13.00
Subtotal	9.0	50.10
SPACECRAFT		
Communications		
S-Band	0.0	27.00
VHF	14.80	3.40
Command & Data Handling		
OBC	16.40	16.40
DMS	3.60	3.60
Command	1.30	1.30
Attitude Control		
CSS	0.0	0.0
FSS	1.35	1.35
SMSS	0.42	0.0
PAS	4.00	0.0
IRA	30.00	67.00
NSA	1.00	0.0
RWA	0.0	9.00
WDA	5.00	8.00
CEA	0.0	0.0
HAPS	15.00	25.00
Power Subsystem	5.50	5.50
Subtotal	98.37	167.55
Spacecraft Total	107.37	217.65

The on-board computer interfaces with the analog and digital multiplexers and the command decoder. The primary function of the computer is to synthesize the stabilization and control parameters and to generate signals through the command decoder to maintain the required attitude pointing and stability needed to perform UV astronomy with one arc-second pointing accuracy. It is envisioned that much more will be done with the computer, such as the sequencing and managing of the experiment's image tube detectors. Because the computer is interfaced only with the telemetry and command systems, the ground computer can act as functional redundancy to the onboard system. The throughput-rate ratio of the onboard system (which includes the addressing of the data source, computer processing time, and command execution time to the control device) can be as low as 30 milliseconds, as opposed to approximately 500 milliseconds if the ground computer is required.

A strapped-down Inertial Reference Assembly (IRA), consisting of six skewed gas-bearing gyros, senses motion about any axis to an accuracy of 0.005°/hr to maintain precise three-axis pointing. The six gyros have their input axes skewed in such a manner that some information is derived from any one gyro about all three control axes. Six gyros are required to achieve sufficient reliability for a 5-year mission, but any three can meet the mission control requirements. The skewed input axes of the gyros are transformed to the control axes of the spacecraft by appropriate algorithms within the onboard computer. Appropriate control signals are computed and sent to the three momentum reaction wheels via the command decoder. A fourth wheel, mounted in an offset configuration, is provided to increase reliability. A hydrazine propellant system unloads the stored momentum in the reaction wheels by actuation of a pair of the 0.1 pound hydrazine thrusters. The hydrazine system also supplies the thrust required for orbit-injection error correction, attitude orientation during the transfer orbit, and stationkeeping for the life of the satellite at synchronous altitude.

The Panoramic Attitude Sensor (PAS) provides spin-axis attitude information and sun position relative to a spacecraft spin period during the transfer orbit. These data and control signals are required to maintain appropriate sun-to-spin-axis alignment during the transfer orbit and to align the thrust axis of the apogee boost motor for its burn phase. Active nutation control is employed during the spin phase by sensing torque motion perpendicular to the spin axis with an accelerometer.

Analog sun sensors combined with IRA body rate information, provide the control signals to align the spacecraft during sun acquisition so that the solar arrays are favorably illuminated by the sun. The combination of the digital sun sensors obtaining a sun-to-IUE vector and the PAS obtaining an earth-to-IUE vector when combined with ephemeris data, allow IUE attitude determination and slew to point the Fine Error Sensor (FES) to the North Ecliptic Pole (NEP). At this attitude stellar acquisition (or reacquisition) is accomplished

and precise pointing attitude is obtained by comparison of the star field as viewed by the fine error sensor with sectional star maps. The digital sun sensor (or Fine Sun Sensor [FSS]) and the FES are used to readout gyro drift which is then eliminated via ground computed and commanded compensation.

SECTION 4. COMMUNICATIONS SUBSYSTEM

4.1 GENERAL DESCRIPTION

The Communications System consists of two redundant VHF transponder systems, two redundant S-band transmitters with four power amplifiers, and associated antenna systems. A block diagram of the IUE Communications, System is shown in figure 4-1. The Communication Subsystem interfaces with the power supply subsystems, telemetry encoder output, and command decoder input. Functionally, this subsystem provides the means for transmission of telemetry data, reception of ground generated commands, and a way of tracking the spacecraft using the Goddard Range and Range Rate system.

4.2 IUE S-BAND SYSTEM DESCRIPTION

The S-band System consists of two redundant transmitters and four power amplifiers with individual antennas. A block diagram of the S-band system is shown in figure 4-2 and figure 4-3 is the DC power flow diagram for the S-band system.

The S-band system is used for transmission of telemetry data. Both of the transmitters are connected to each of the power amplifier/antenna combinations. Only one transmitter and one power amplifier/antenna are activiated by command, at any one time. Selection of a particular power amplifier depends upon a favorable view of the earth by its associated antenna.

Characteristics of the S-band system include the following:

a. Transmitter Frequency . . . . 2249.80 MHz

b. Power Output . . . . . 6 Watts

c. Output Modulation . . . . . PM

d. Antenna Polarization. . . . . Circular

4.3 VHF TRANSPONDER SYSTEM DESCRIPTION

The VHF Transponder System consists of a turnstile antenna system, antenna distribution system and two VHF transponders. The VHF system block diagram is shown in figure 4-4. Figures 4-5 and 4-6 are the power flow diagram and the data flow diagram.

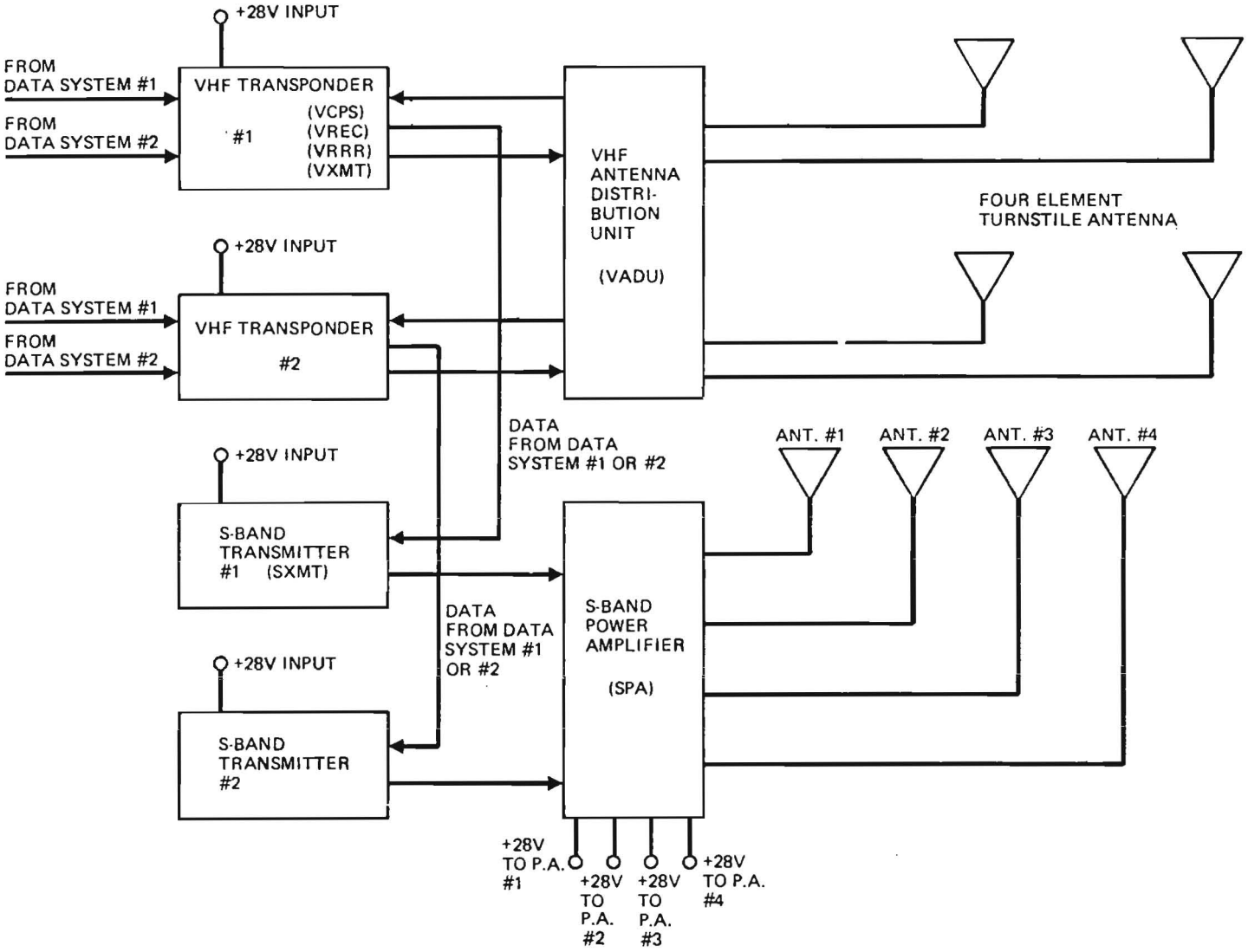

Figure 4-1. Block Diagram of IUE Communications System

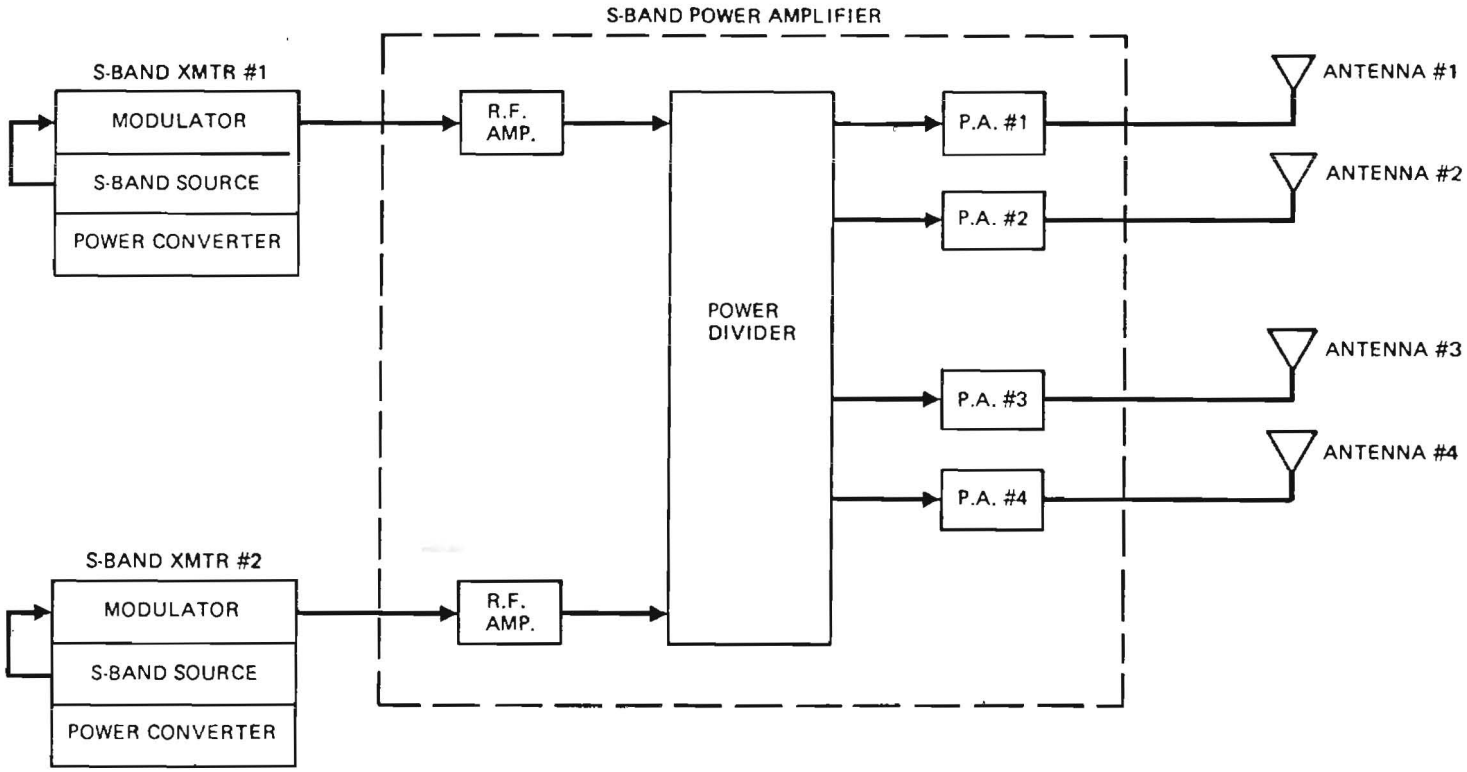

Figure 4-2. Block Diagram of S-Band System

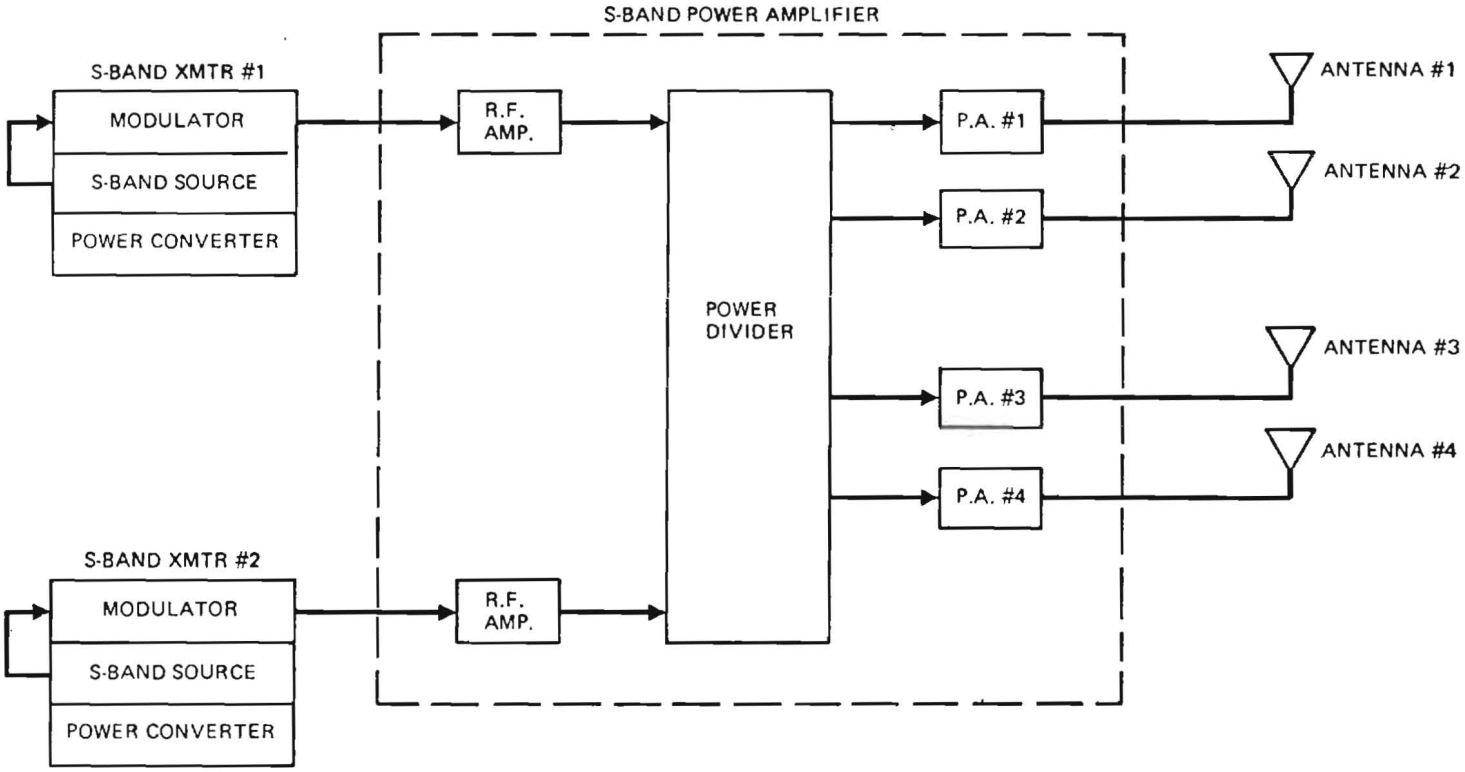

Figure 4-2. Block Diagram of S-Band System

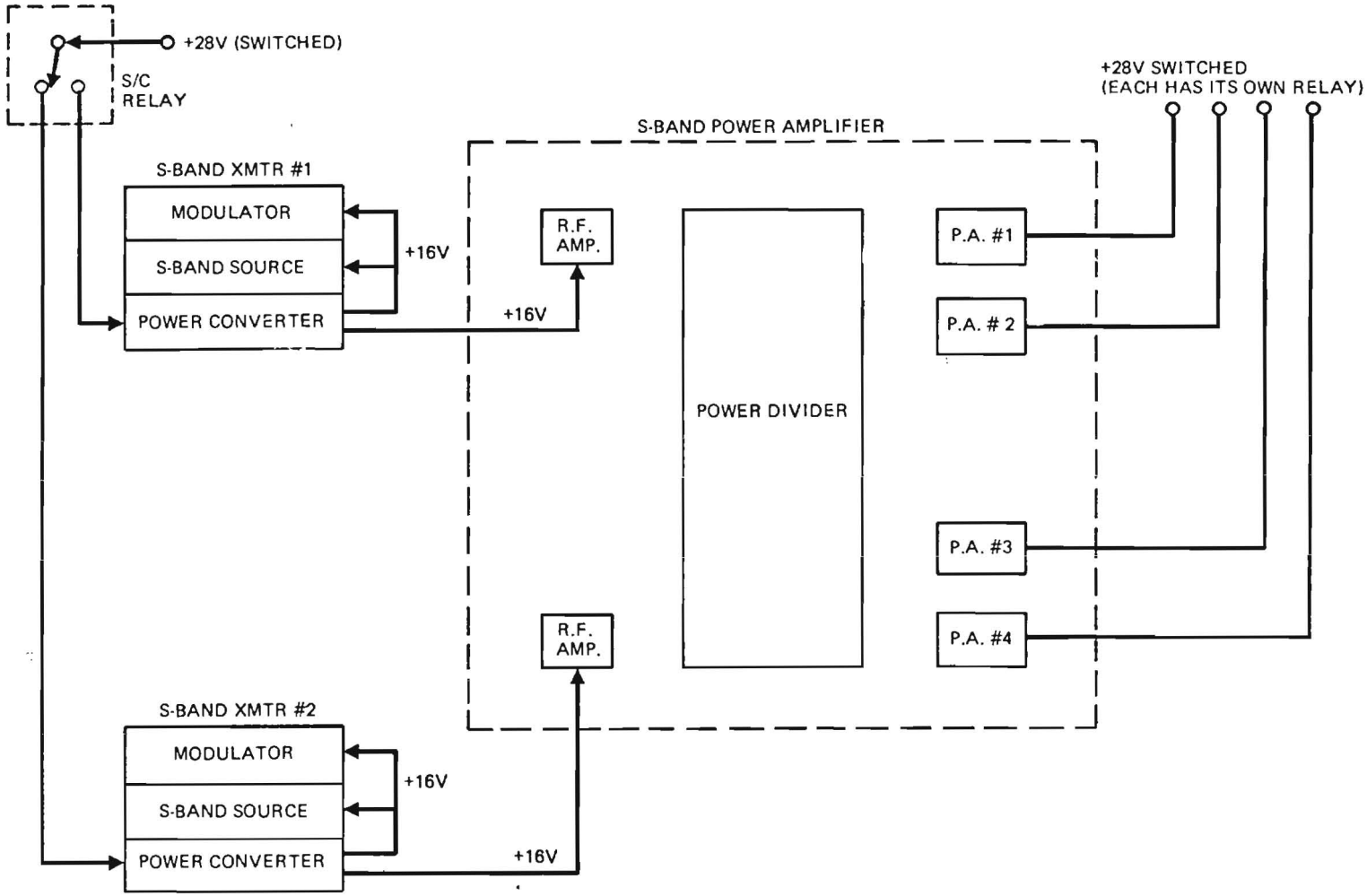

Figure 4-3. DC Power Flow Diagram of S-Band System

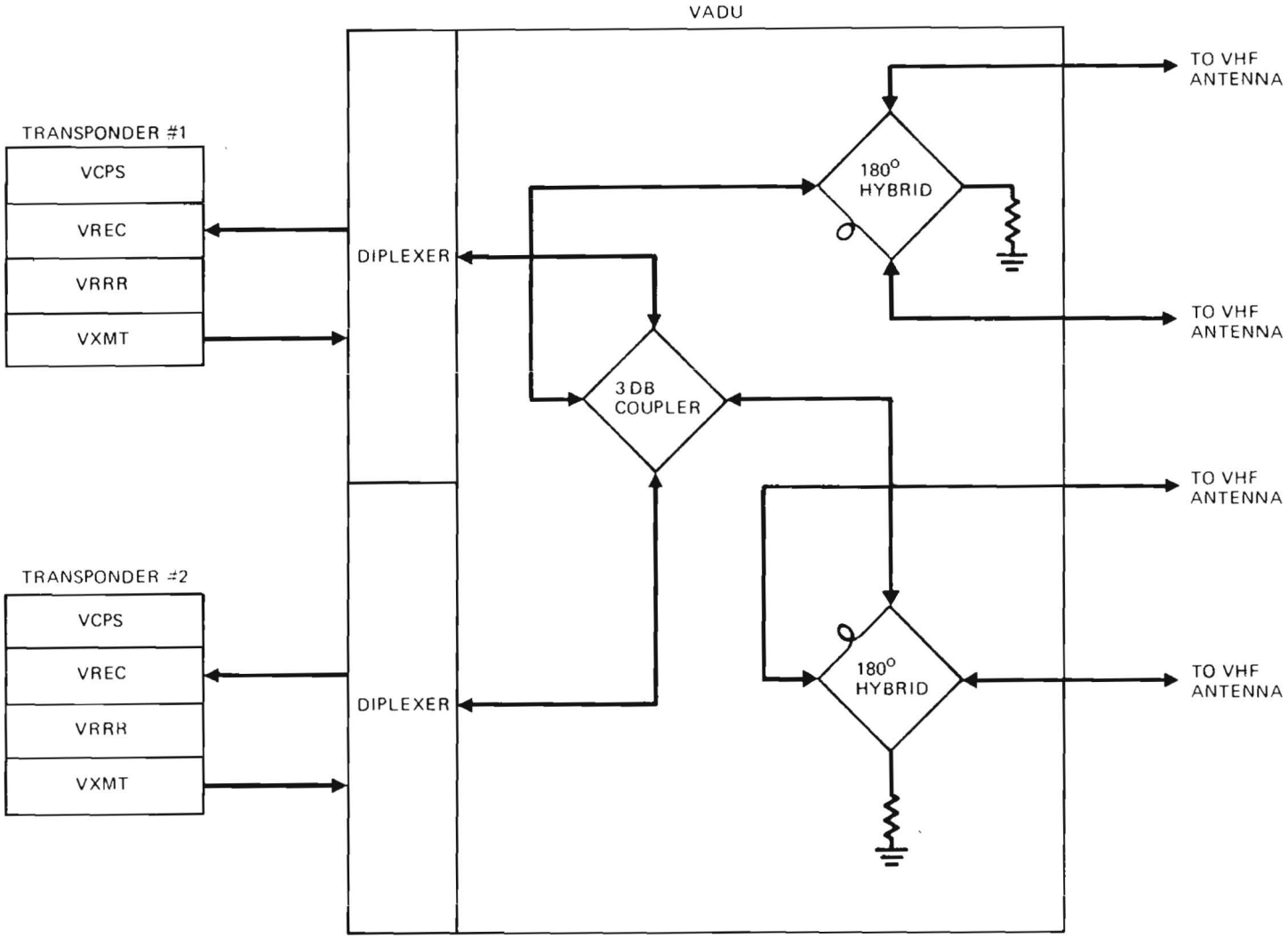

Figure 4-4. VHF System Block Diagram

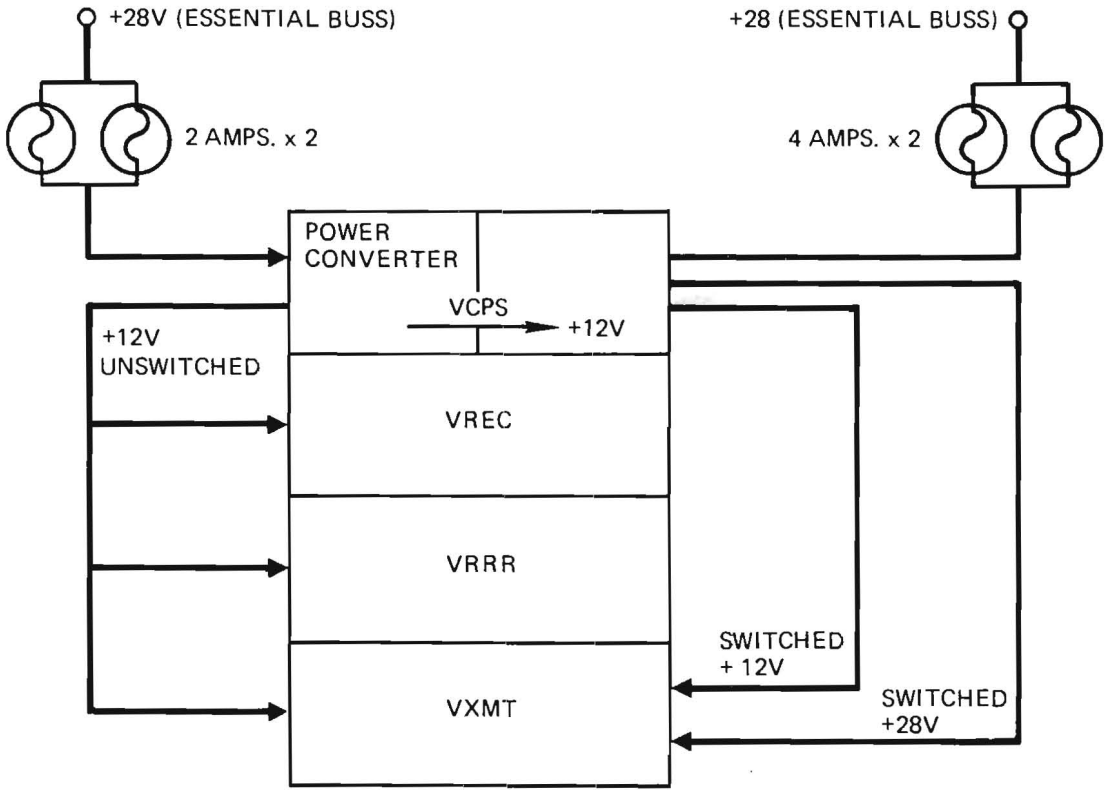

NOTE: EACH TRANSPONDER HAS ITS OWN FUSES, POWER CONVERTER AND WIRING.

Figure 4-5. VHF Power Flow Diagram

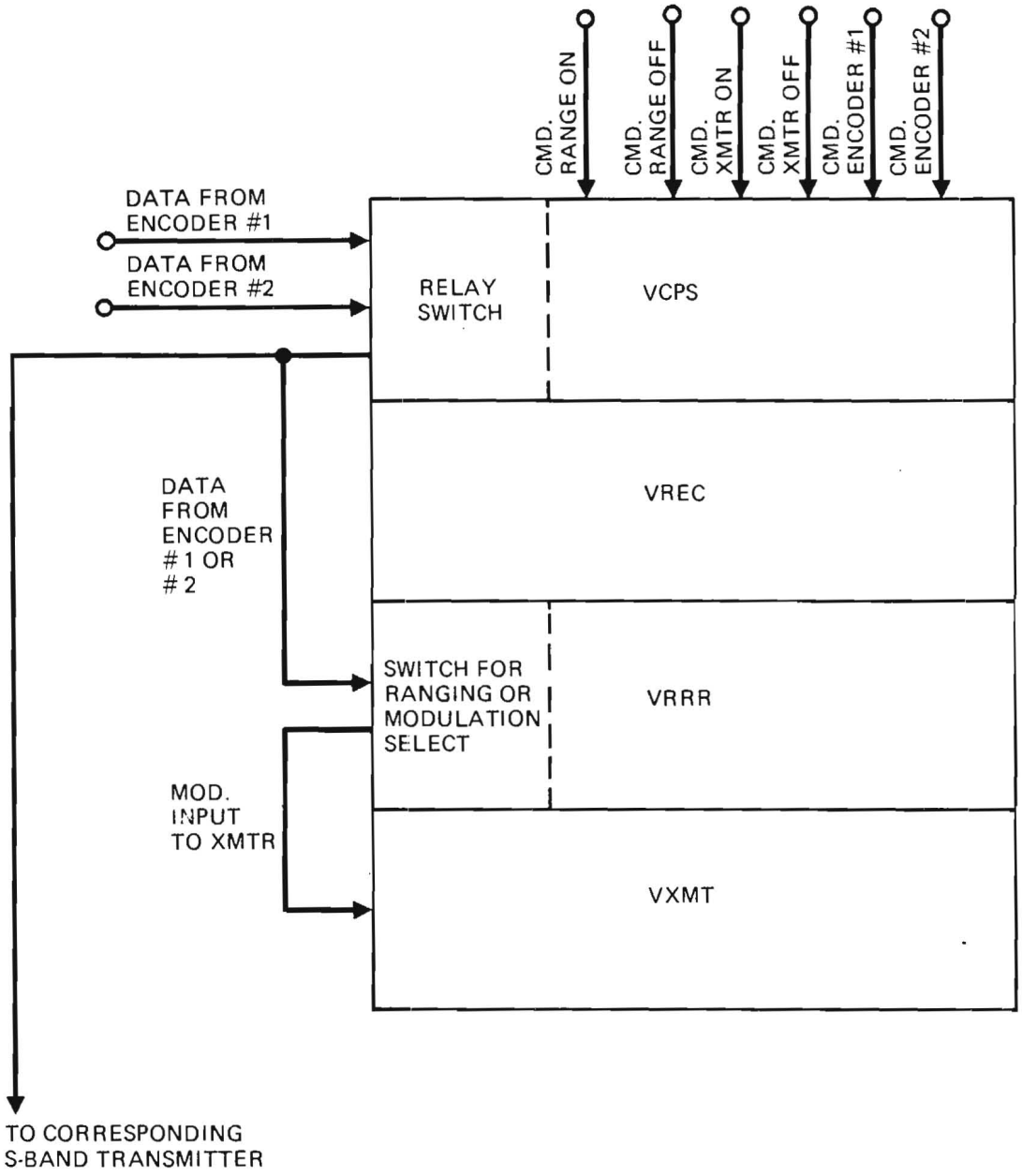

Figure 4-6. VHF Data Flow Diagram

The VHF System provides for the transmission of telemetry data, reception of ground generated commands, and the turnaround transmission of range and range rate signals for metric tracking of the spacecraft using the Goddard range and range rate system.

The VHF transponders are connected to an antenna system having four active elements.

Characteristics of the VHF transponder system include the following:

a. Receiver Frequency: 148.980 MHz

b. Transmitter Frequency: 136.860 MHz

c. Power Output: 6 Watts.

d. Output Modulation: PM.

e. Receiver Sensitivity: -106 dbm.

f. Antenna Polarization: Turnstile.

g. Antenna Pattern: Omnidirection.

The IUE RF system antenna locations are shown in figure 4-7.

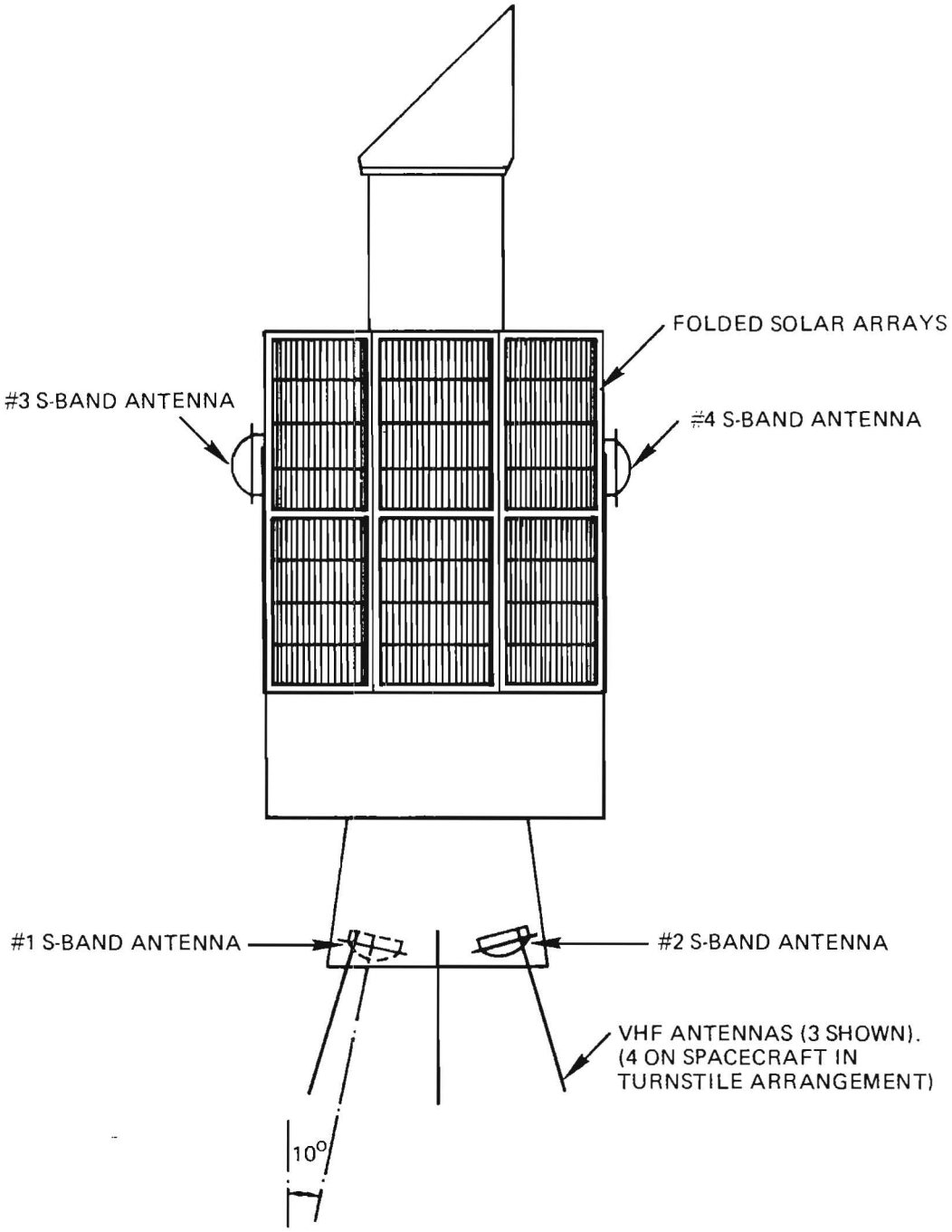

Figure 4-7. IUE RF System Antenna Locations

SECTION 5. COMMAND AND COMMAND DISTRIBUTION SUBSYSTEM

5.1 GENERAL SUBSYSTEM BLOCK DIAGRAM AND DESCRIPTION

The IUE command subsystem, shown in figure 5-1 consists of redundant command decoders and a command relay unit. The Command Relay Unit (CRU) contains circuit redundancy up to the individual relay and relay driver stage. Three distinct types of commands are available; discrete and serial commands are distributed by decoders A and B, and relay closures are provided by the CRU.

The discrete command is a positive ten volt pulse with a fifteen millisecond duration. There are 128 discrete commands available from each command decoder. Each serial command will provide 37 bits of programmable information. The serial command interface consists of 37 bits NRZ data, 37 bits clock, and a data envelope signal. There are 48 individually buffered serial commands available from each command decoder. All serial command outputs are ten volt logic signals and the clock transfer rate is 4.27 KHz. The relay closure commands are executed using a serial command to the CRU. Sixty latching relay closures are provided. Most of the CRU relays are used to switch primary +28 volt power to spacecraft subsystems.

A second function provided by the CRU is the Pyrotechnic circuitry. This circuitry controls by serial and discrete commands the apogee boost motor ignition, the solar array deployment, and the telescope cover release. The pyrotechnic circuitry is completely redundant.

Each command decoder can process command messages from two sources; a VHF receiver analog signal or digital information from the On-Board Computer (OBC). The decoders use time share command execution to avoid priority conflict. The OBC will generate commands based on software decision or execute delayed commands. The OBC will issue commands through one decoder only and commands from the VHF receivers will address the same decoder; this selection can be changed by command.

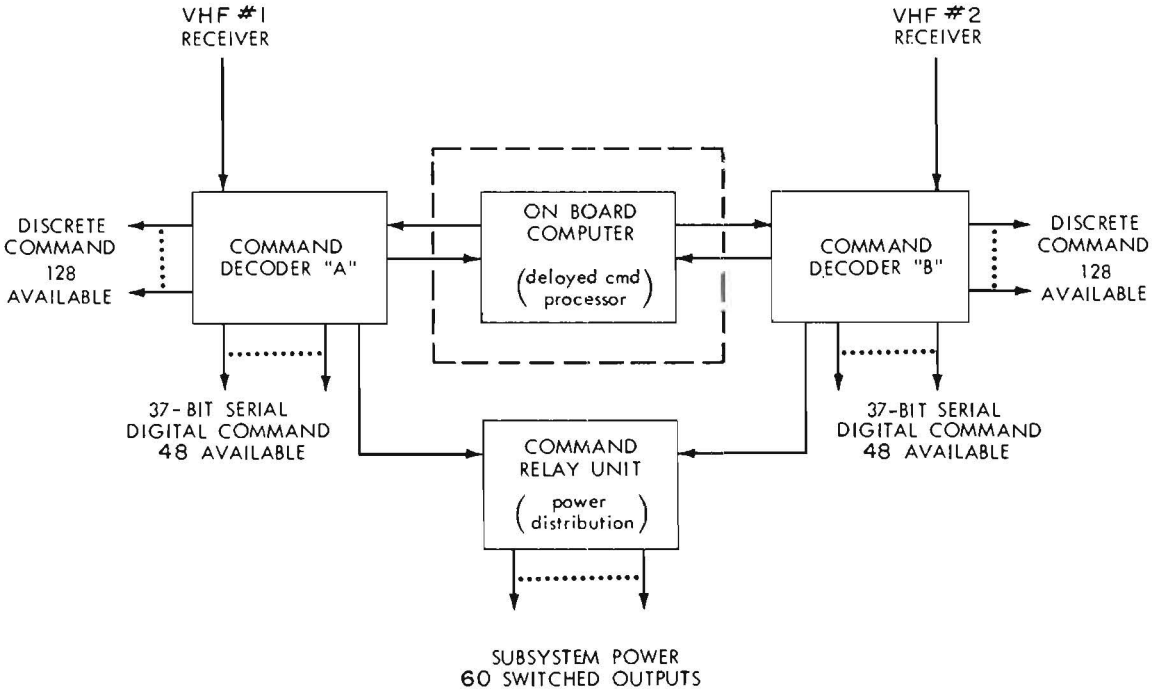

Figure 5-1. Block Diagram, IUE Command Subsystem

5.2 COMMAND DETECTOR AND DECODER DESIGN

5.2.1 GENERAL CHARACTERISTICS

a. Input Signal

(1) Modulation: PCM/FSK - AM.

(2) Subcarriers: 8 KHz/12 KHz.

(3) Bit rate: 800 Hz.

b. Command Rate

(1) Ground station originated: 13/second.

(2) Computer or stored command: 33/second.

(3) All commands time shared: no command priority required.

c. Command Capacity

(1) Discrete: 128 outputs/10 v, < 1 KΩ source impedance, 15 ms positive duration.

(2) Serial: 48 individually addressed and buffered/37 bits each with NRZ data, 4.27 KHz clock, 37 bit positive envelope, all 10 v logic, < 1 KΩ source impedance, rise/fall times < 5 μs.

5.2.2 POWER REQUIREMENTS

(1) +28 volts DC ±2% consumption < 0.60 watts.

(2) DC/DC converter operating at 19 KHz ±3% supplies all operating voltages.

(3) Internal undervoltage switch.

5.2.3 PHYSICAL CHARACTERISTICS

(1) Dimensions ≃ 6" w x 8" l x 3 5/8" h.

(2) Weight ≃ 3.5 pounds (unshielded).

(3) Electrical connectors: 8 flight and 1 test all AMP-type HD-22.

5.2.4 ELECTRICAL DESIGN

5.2.4.1 Circuit Description. The command decoder contains three distinct circuit groups. See block diagram, figure 5-2. The three groups are the analog circuits, DC/DC converter, and digital logic circuits. The analog circuits are fabricated on two circuit boards, the digital logic on nine circuit boards, and the DC/DC converter is separately housed in a shielded enclosure.

5.2.4.2 Analog Circuit. The analog circuits demodulate the composite FSK/AM signal and convert the information contained in the signal to three digital output signals. The three outputs are data, VCO clock, and a data present signal. The data and clock signals transfer the uplink command information to the digital logic circuits for processing. The data present signal provides the decoder with signal confidence information. Data present allows the digital logic to proceed with command processing only when adequate bit error rate probability exists. The analog circuits also contain an under-voltage threshold detector which disables the decoder should the positive ten volt level drop below approximately eight volts. This circuit provides abrupt voltage on/off characteristics should the input power bus exhibit a gradual rise or fall.

5.2.4.3 Digital Logic Circuits. The digital logic circuits process command information from two sources, the analog circuits and OBC command data. The uplink command data from the analog circuits is tested for correct address and parity prior to command execution. The OBC command data is assumed to be transferred by error free channel and is therefore executed as received. Should an address or parity error be detected in any uplink command, the decoder will terminate processing the command with an error and all subsequent continuous commands. An alarm flag is sent to the ground indicating the error and the subcarrier must be terminated to clear the alarm state of the decoder. An eight-bit command execution counter is advanced for each uplink command properly processed, this data is then sent to the ground and enables verification of commands executed by the decoder. Figure 5-3 contains the command formats used for both real-time (uplink) commands and OBC issued commands. Sixty bits of data are processed for each uplink command executed and forty-four bits are processed for OBC issued commands.

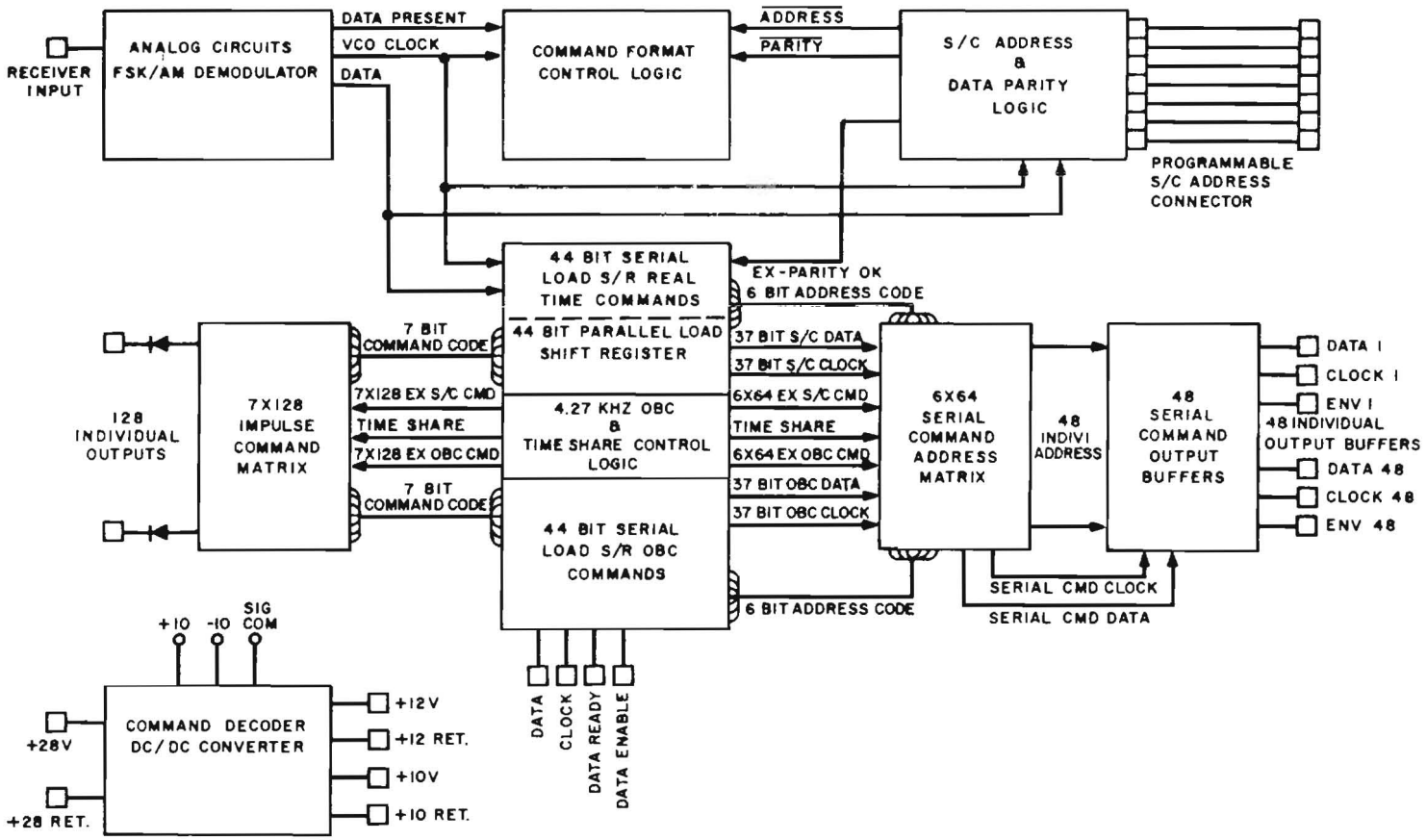

Figure 5-2. Command Decoder Block Diagram

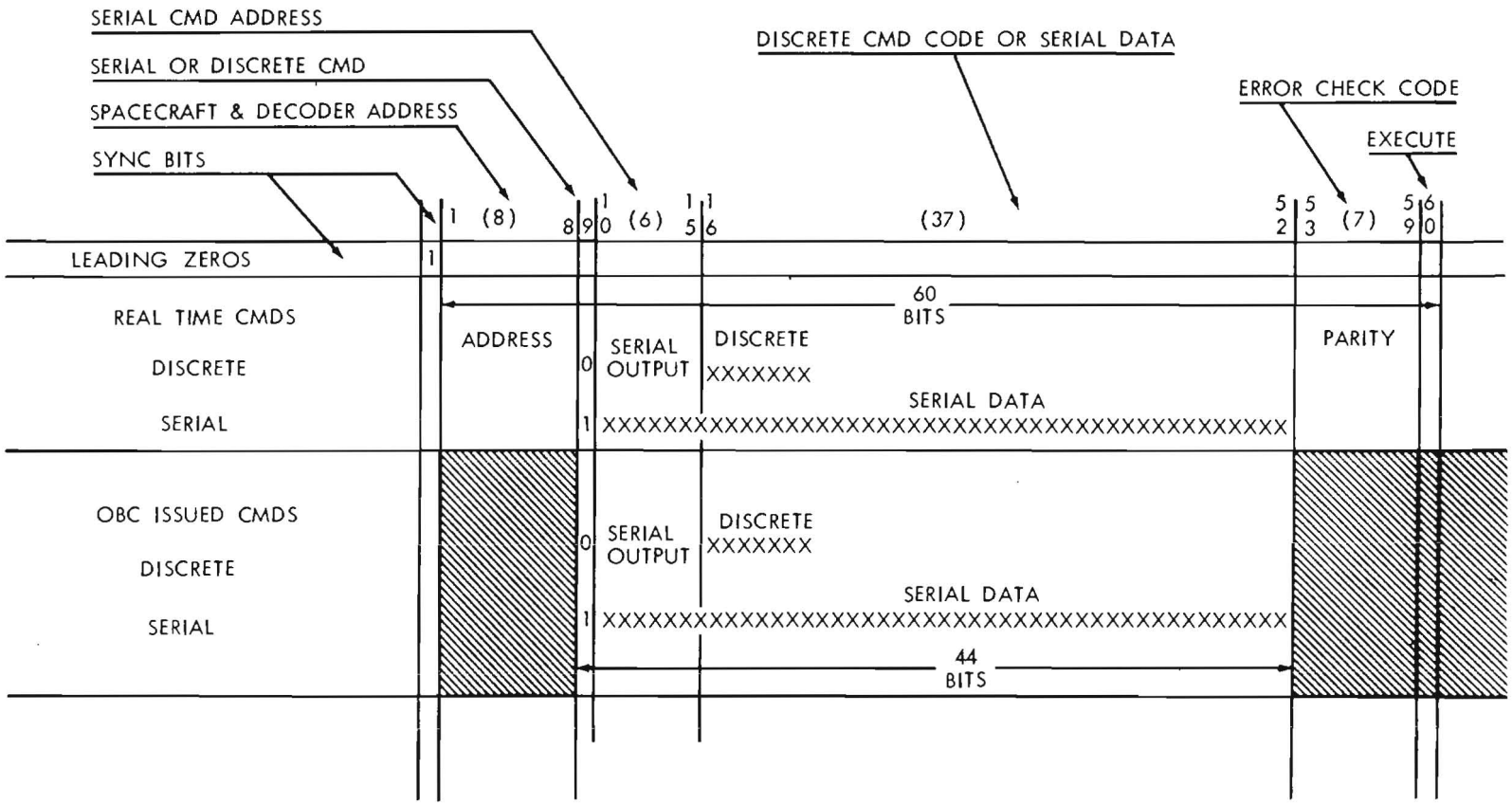

Figure 5-3. Command Format

5.2.4.4 Command Timing. Uplink and OBC command data are serially transferred, stored, and execution is performed based on timing generated by decoder time share logic. Figure 5-4 indicates the relationships which are imposed by the timing. Alternate fifteen millisecond intervals are provided for command execution. OBC command data is transferred to a decoder during the time interval when uplink (S/C) commands are being executed. The time share intervals of Command Decoder A and Command Decoder B are not synchronized; thus, it is important to ensure that uplink and OBC commands are addressed to only one decoder. If this condition is violated, the possibility exists that uplink and OBC commands to an individual user could overlap.

5.2.4.5 Command Interfaces. The command decoder issues two types of commands; discrete commands and serial commands.

a. Discrete Commands. Discrete commands are provided from circuits whose characteristics are shown in figure 5-5. All discrete commands use diode coupled outputs. The receiver circuit is responsible for noise immunity and the discharging of any cable capacitance. A fifteen millisecond, positive ten volt (minus diode drop) output pulse is developed on a true output. The one thousand ohm maximum output impedance is maintained for all loads in excess of ten thousand ohms. Ninety-six of the one hundred-twenty-eight outputs can be disabled by command and are always disabled when power is first applied to a decoder. These outputs can be enabled by a command from either decoder.

b. Serial Commands. Serial commands are provided from a three signal interface as shown in figure 5-6. The signals shown will only exist on the addressed serial command outputs. Signal levels will be zero to ten volts with rise and fall times less than five microseconds. A maximum output impedance of one thousand ohms will be maintained for load impedance of ten thousand ohms or greater. All forty-eight serial command output circuits can be enabled or disabled in the same manner as the discrete commands.

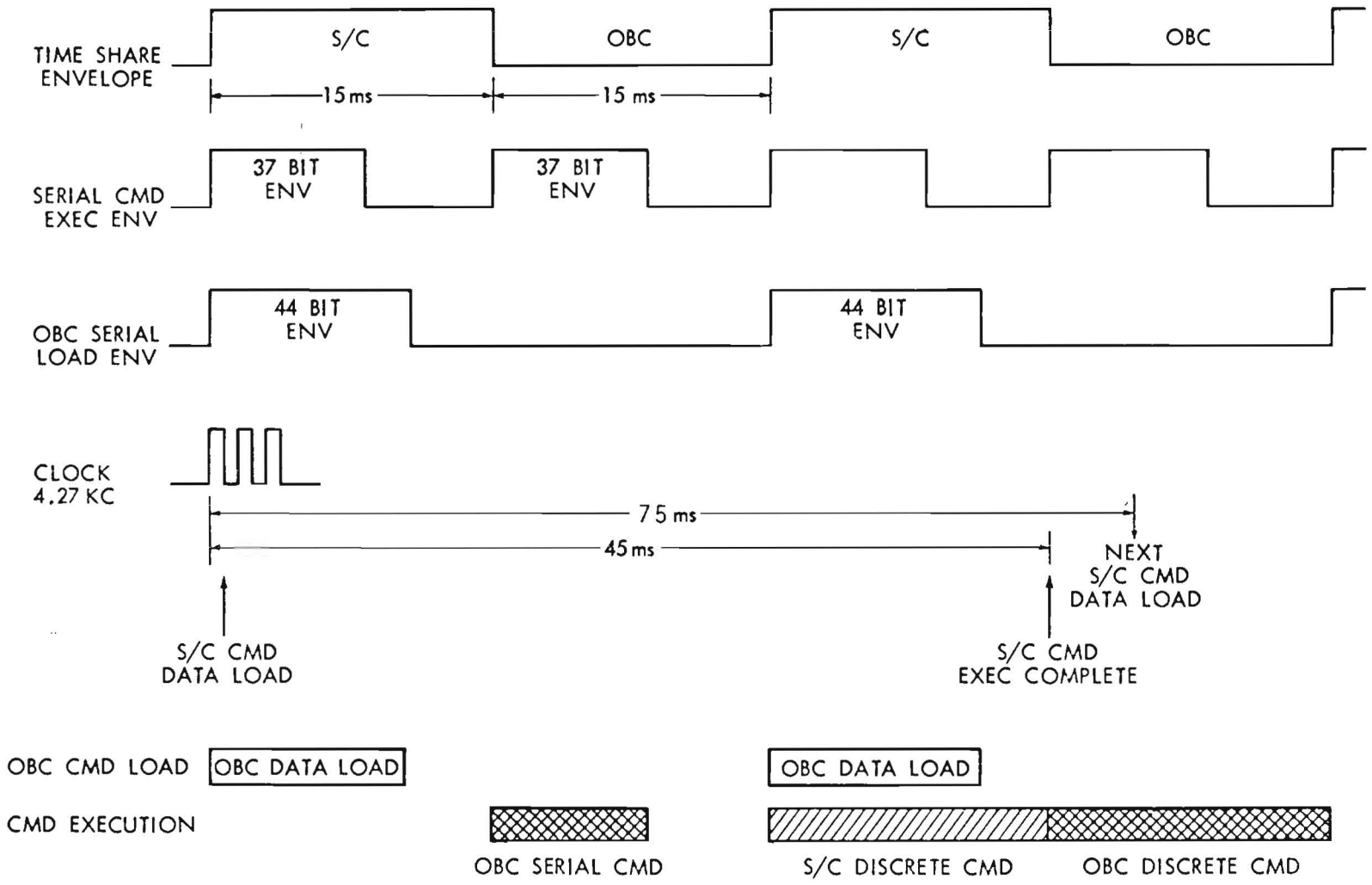

Figure 5-4. Timing Diagram, Time Share Logic

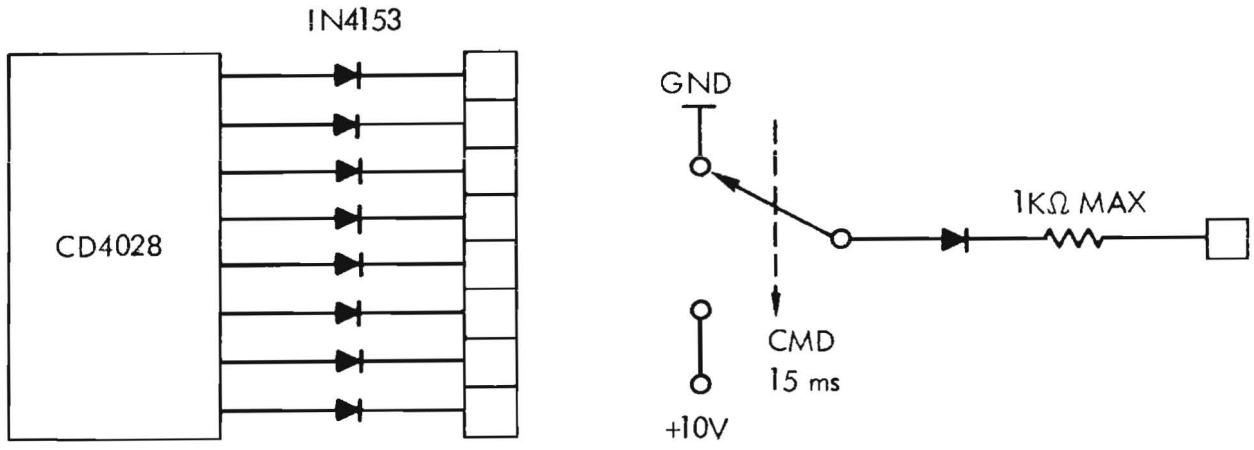

Figure 5-5. Discrete Commands

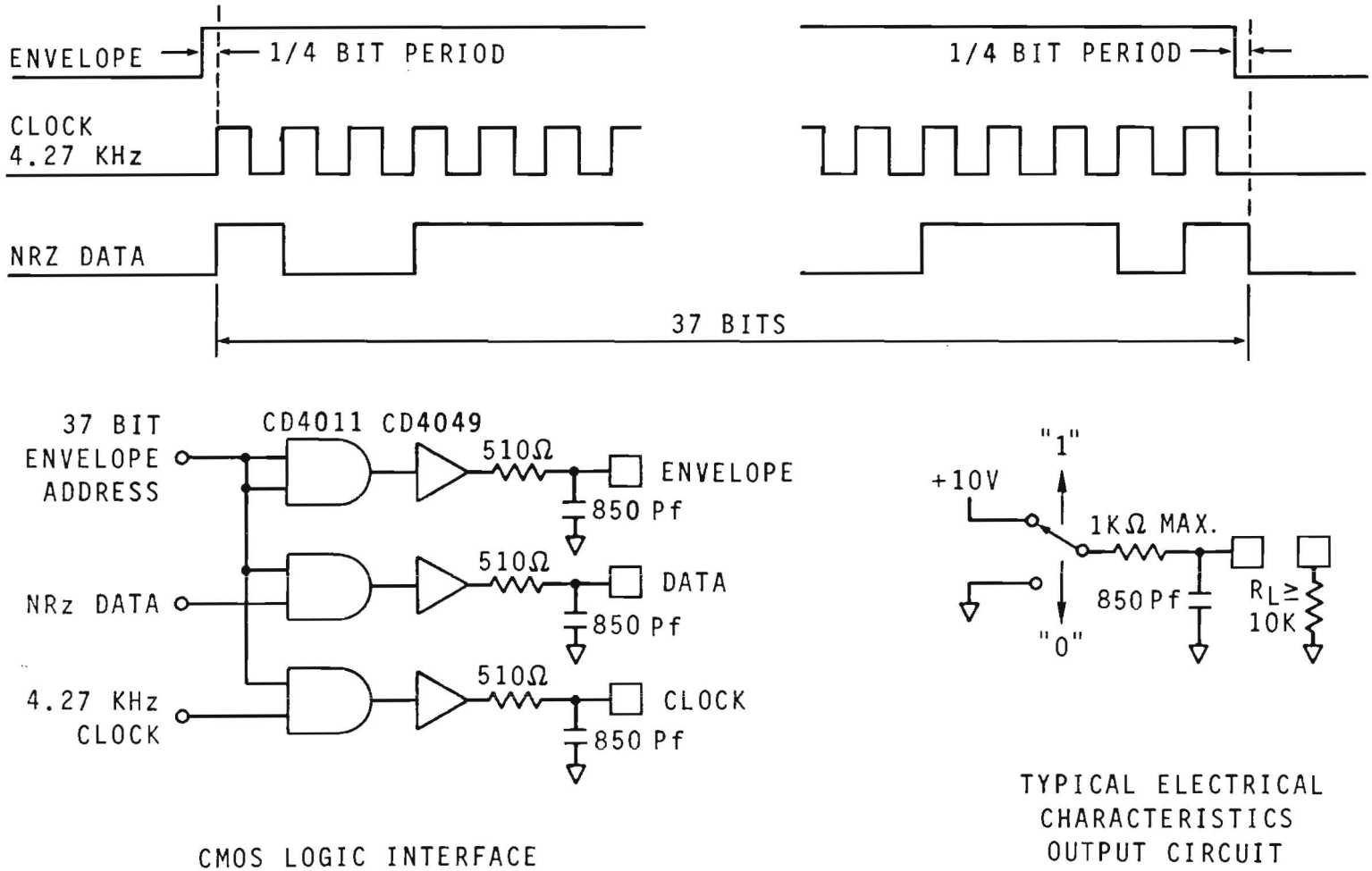

Figure 5-6. 37-Bit Serial Command Interface and Timing

5.3 COMMAND RELAY UNIT DESIGN

5.3.1 GENERAL CHARACTERISTICS

a. Input Signals

(1) Redundant serial commands control on/off states of 64 relays.

(2) Redundant discrete commands energize pyrotechnic outputs.

(3) Auxiliary off inputs energize 57 latching relay off states.

b. Relay Outputs

(1) 60 latching DPDT relays.

(2) 8 momentary > 40 ms closures.

c. Power Requirements

(1) Redundant +10 volt supplies, < 1 ma average current.

(2) +28 volt essential bus, < 1 ma average current.

(3) Redundant spacecraft batteries, current for pyrotechnic firing only.

d. Physical Characteristics

(1) Dimensions: ≈ 6" w x 8" 1 x 4½" h.

(2) Weight: ≈ 8.8 pounds (unshielded).

(3) Electrical connectors: 9 flight all AMP type HD-22.

5.3.2 ELECTRICAL DESIGN

5.3.2.1 CRU Spacecraft Functions. The CRU provides two spacecraft functions; primary power distribution using 60 commandable latching relays and electrical pyrotechnic circuitry using an additional 12 relays. Figure 5-7 is a block diagram which shows these functions. The block diagram also shows the redundant serial command registers and logic which control the on/off states of the 60 power distribution latching relays, and 4 pyrotechnic arming latching relays.

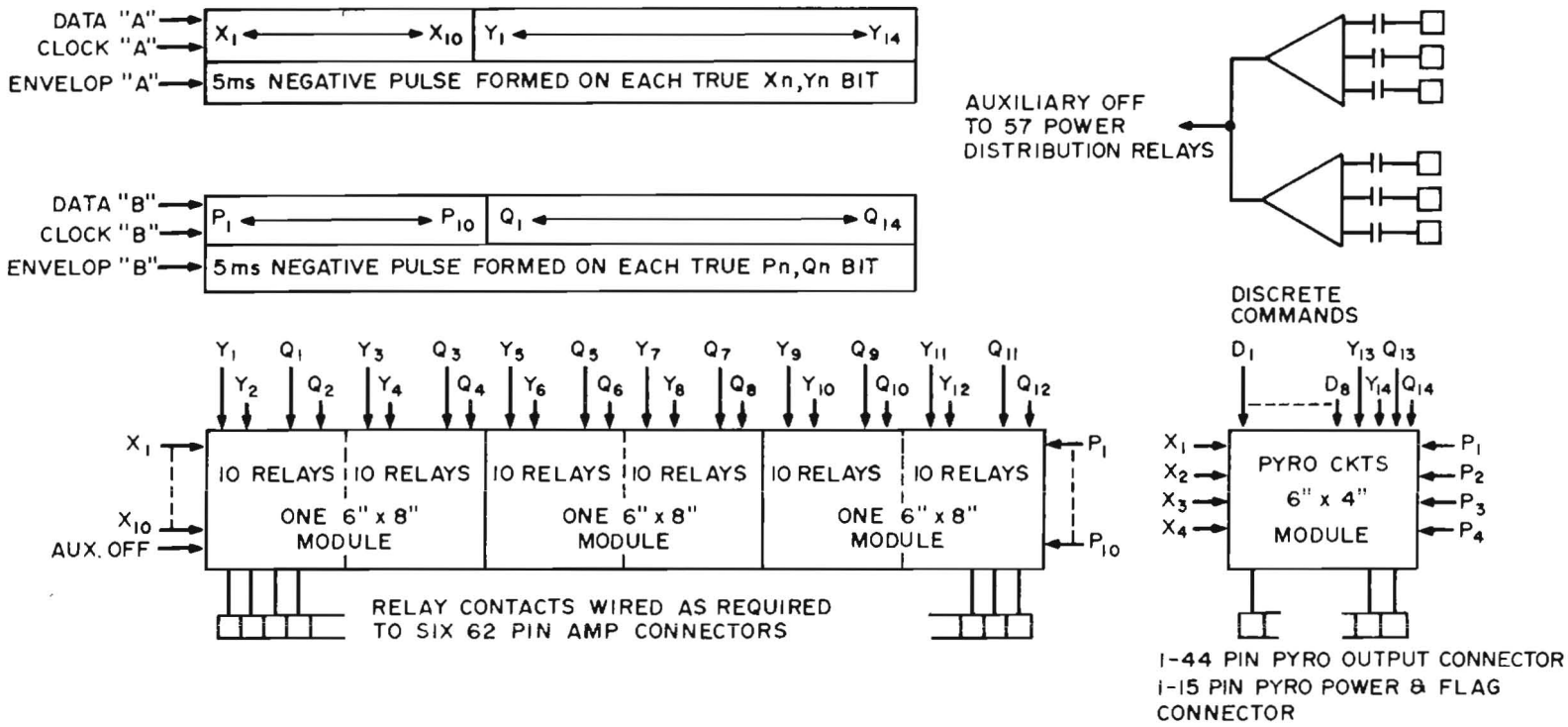

Figure 5-7. Block Diagram Command Relay Unit

5.3.2.2 Relay Logic. The redundant registers and logic are each operated separately from 10 volt supplies provided by the redundant command decoders. The redundant auxiliary off circuits are also on the separate 10 volt supplies. Figure 5-8 is a relay driver showing the two 10 volt supplies "or" connected for operating the relay driver logic element. The figure also shows a latching relay connected to the driver; however, the same driver, using additional charging capacitors, is used to drive momentary relays in the pyrotechnic circuitry. The auxiliary off circuit is a power buffer which receives a signal whenever a spacecraft undervoltage or overcurrent condition exists and 57 power distribution relays are turned off.

The pyrotechnic circuits are entirely redundant electrically, two spacecraft batteries supply energy, through the third stage separation switches, for ignition of the pyrotechnic devices. The circuit uses latching relays which are flagged and closed by serial command to arm two groups of momentary relays. Until third stage separation and arming has occurred, closure of the momentary relays will not ignite any device. The circuit is designed to supply approximately seven amperes of current for a minimum of 40 milliseconds when firing selected devices. The apogee boost motor is on a separate arming circuit from the solar array deploy and telescope cover release. The separate arming circuits provide additional safety to ensure against false ignition. The final ignition is by discrete command.

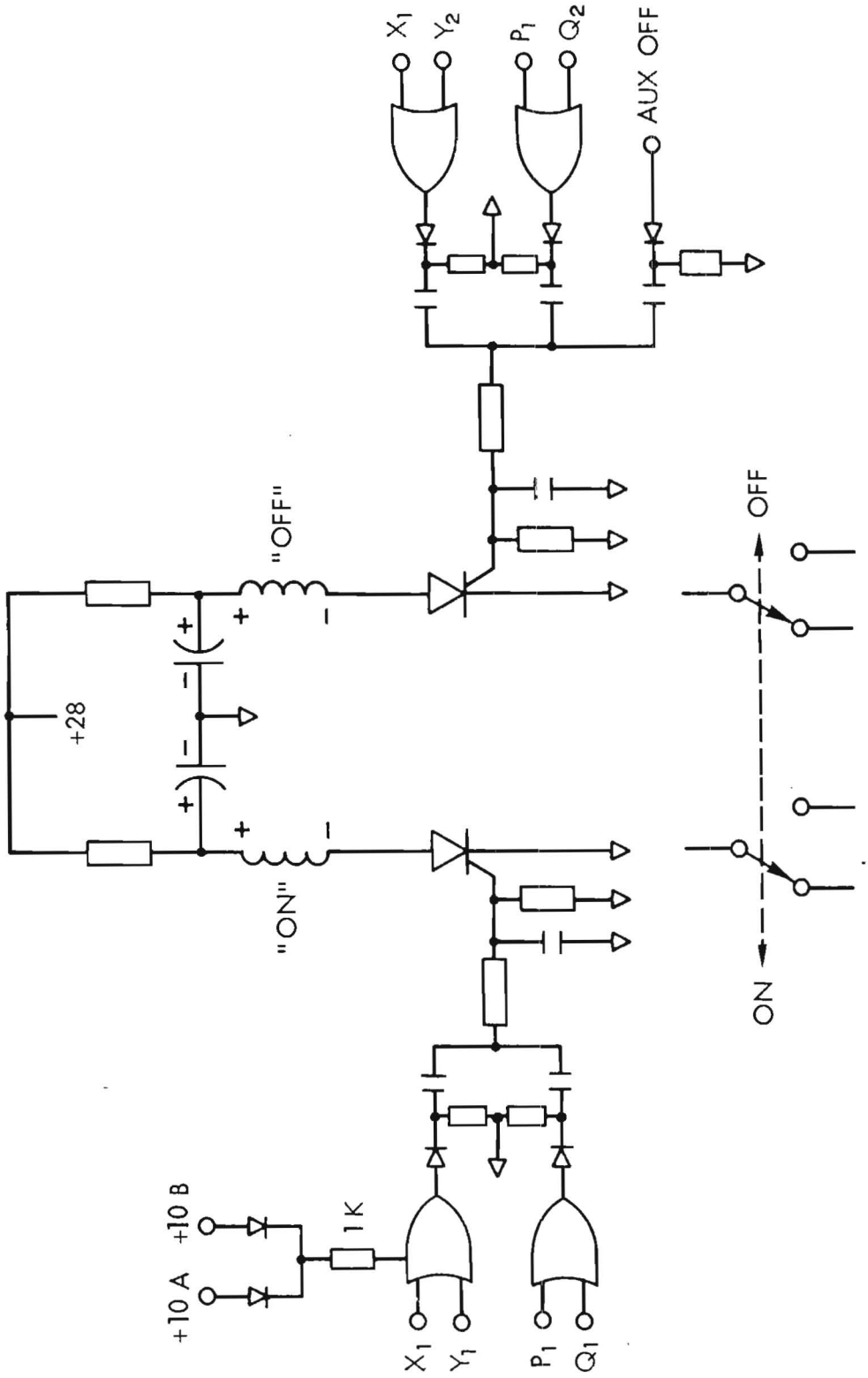

Figure 5-8. Relay Driver

SECTION 6. DATA HANDLING SUBSYSTEM

6.1 GENERAL DESCRIPTION

6.1.1 THE IUE DATA HANDLING SYSTEM

The IUE Data Handling System is composed of two major components, the Data Multiplexer Subsystem (DMS) and the Onboard Computer (OBC). The DMS serves as the spacecraft telemetry encoder and as the input data interface between the OBC and the rest of the spacecraft. The primary function of the OBC is to perform calculations and, based on the results, send attitude control commands to the stabilizations and control system (Section 8).

In performing its function as encoder, the DMS has access to engineering or scientific data from all onboard systems. By using a time-sharing technique, this data can be made available to the OBC. The computer also has the capability of sending all spacecraft commands through the command system, again on a time-shared basis. Thus, the combined data handling and command systems provide, in addition to their basic tasks, a flexible and powerful backup capability for most of the onboard systems. Figure 6-1 illustrates this concept.

6.1.2 THE DMS

The DMS was designed to satisfy the commonality of requirements among several different spacecraft. The resulting design uses solid state memories to generate the telemetry format. The contents of a memory, read out in consecutive order, controls the sequence followed by the multiplexer in the sampling of data. Thus, the DMS can be adapted to any of a variety of missions by using memories tailored to the mission requirements. The basic portion of the DMS, called the dataplexer, contains the main analog and digital multiplexers, the spacecraft clock, and timing and control signal logic all in one box. Provision is also made for convolutional encoding. One or more submultiplexer units, called Subplexers, each in its own box, can be added as required to expand the data handling capacity of the DMS.

6.1.3 THE ONBOARD COMPUTER

The onboard computer to be used on IUE is the GSFC developed Advanced Onboard Processor (AOP). This computer, or its predecessor the OBP, is being used on several Goddard missions. The AOP was developed specifically for the requirements common to the types of mission flown by Goddard. A Special Input Output (SIO) unit is designed for each spacecraft to adapt the AOP to the different mission requirements. Memory capacity can be expanded, in 4 K word modules, to a maximum capacity of 65 K.

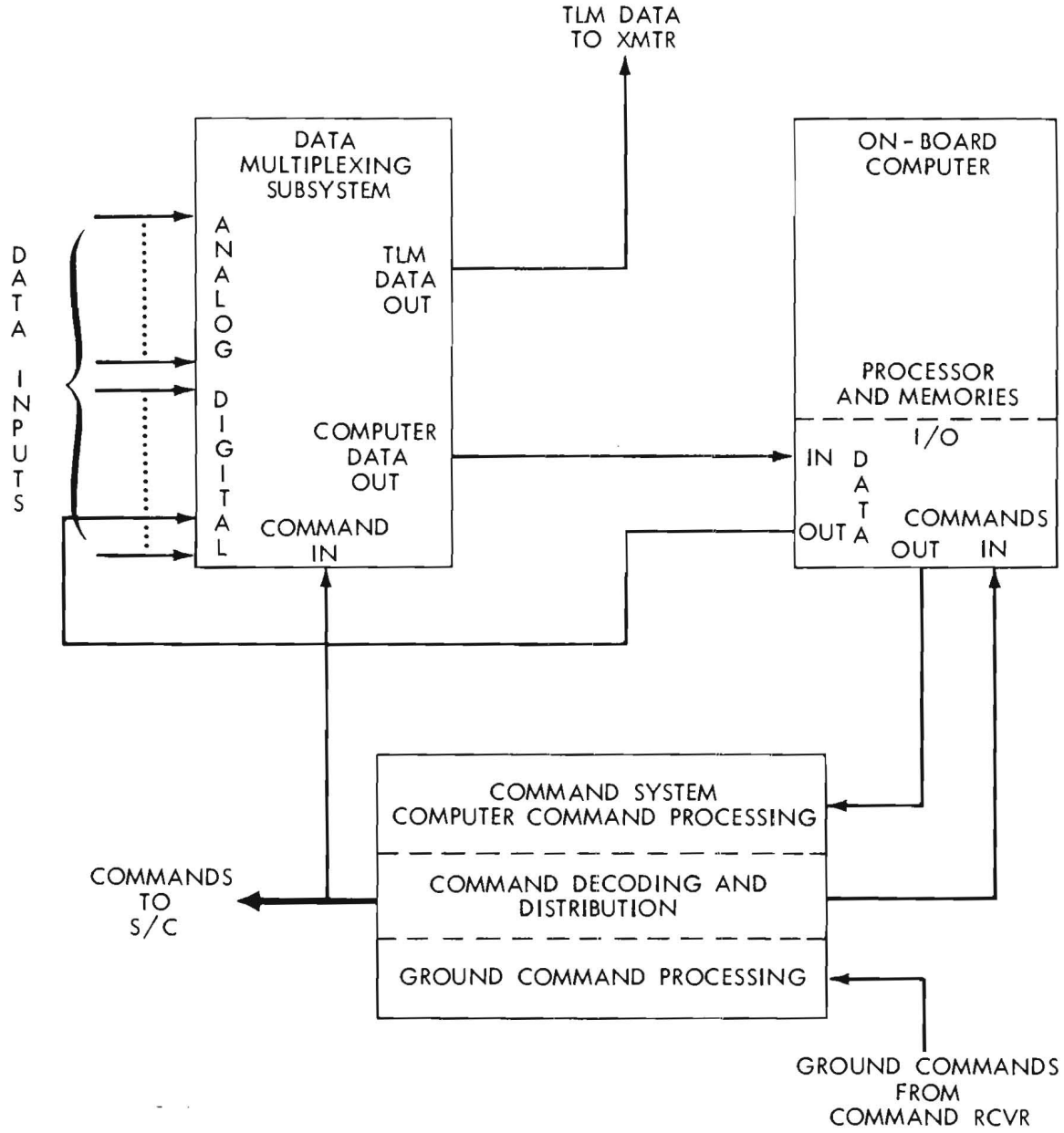

Figure 6-1. Data Multiplexer, Computer, Command System Configuration

6.2 DATA MULTIPLEXER SUBSYSTEM

6.2.1 DATAPLEXER SAMPLING

The Dataplexer selects digital or analog data samples in a time sequence controlled by a format memory. Each data sample is transformed into an 8-bit data word and transferred to a serial data bit stream. One complete sequence is called a minor frame and is 128 words in length. Each minor frame contains words dedicated to fixed parameters that always appear in the same locations independent of format memory. These parameters include frame sync words and information such as the contents of the frame counter, the spacecraft clock, variable format memory contents, and the spacecraft status bits. Figure 6-2 shows the typical telemetry minor frame format and table 6-1 lists the parameters associated with each dedicated word. A major frame is defined as 256 minor frames. All submultiplexer data samples are included in each major frame occurring each 64 minor frames. Table 6-2 lists the dataplexer input lines from the various subsystems.

6.2.2 SCIENTIFIC INSTRUMENT DATA

During the readout of the Scientific Instrument, most of a telemetry frame will be devoted to the spectrograph image data. It is desirable to synchronize an image tube scan line to a telemetry frame. If a spectrograph image was divided into 768 resolution elements by 768 lines, then the figure 6-3 would represent one telemetry frame out of 8 frames per line scan. At the 40 kilobit per second telemetry readout rate, the following computation would represent an image picture readout time:

$$8 \text{ frames} \times 25.6 \text{ msec/frame} = 0.2048 \text{ sec/line}$$

Thus:

$$0.2048 \text{ sec/line} \times 768 \text{ lines} = 2.62 \text{ minutes/picture}$$

6.2.3 THE DATAPLEXER

The dataplexer includes a 32-input analog multiplexer, a 16 analog sync pulse multiplexer, and a 32-input digital multiplexer. In addition it contains a 32-output word-gate multiplexer and a 32-output shift pulse multiplexer. These are control signals needed for serial digital data transfer from the data source connected to the selected input. Each digital input has corresponding word gate and shift pulse outputs, and all three are selected simultaneously. Figure 6-4 shows the timing of these signals.

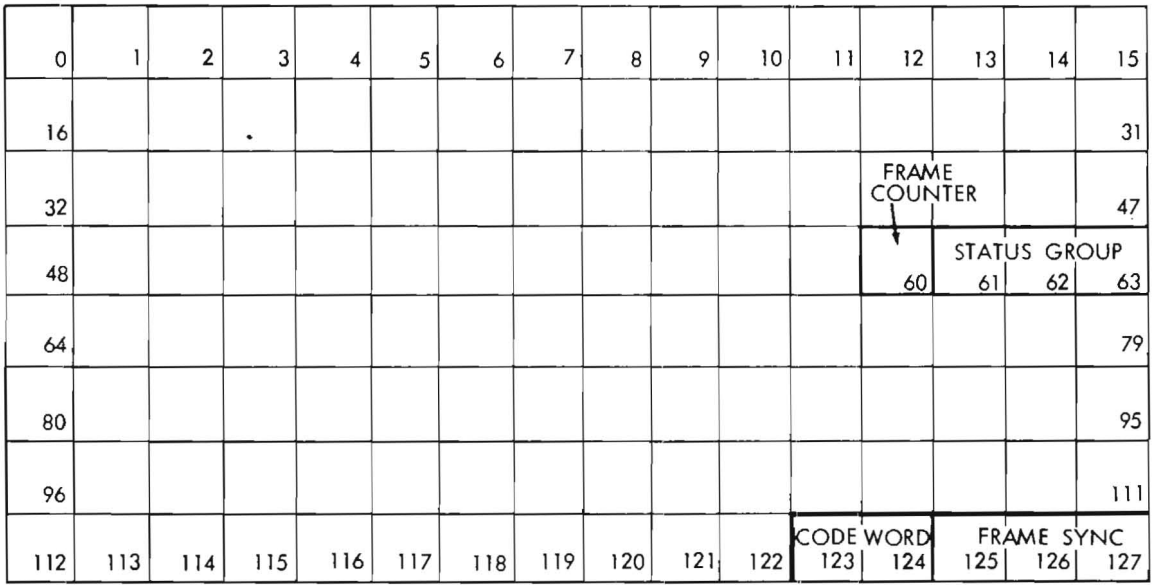

Figure 6-2. Data Multiplexer Telemetry Format

Table 6-1. Fixed Word Parameters

Word 60 (FRM CTR) 2 LSB	Word 61	Word 62	Word 63
0	Spacecraft Clock 8 MSB's	Spacecraft Clock Bits 9-16	Spacecraft Clock 8 LBS's
1	Variable Memory Readout	Indirect Address Register	Execute Address Register
2	Status Register Bits 1-8	Status Register Bits 9-16	Status Register Bits 17-24
3	Variable Memory Readout	Command Register Bits 1-8	Command Register Bits 9-16

Table 6-2. Input Lines from Subsystems to DMS

Subsystems	No. of Input Lines					
	Dataplexer			Subplexer		
	Analog	Digital	Status Bits	Temp	Analog	Digital
Power	3		2	6	14	2
Command		2	8	1	5	
Communications			4	5	6	
Computer		4		3	2	6
Data Systems	5		3	1	1	
Experiment	6	6	2	14	11	10
Attitude Control	14	11	2	16	44	11
Hydrazine				26	3	1
Ordnance				1		2
Spacecraft			2			

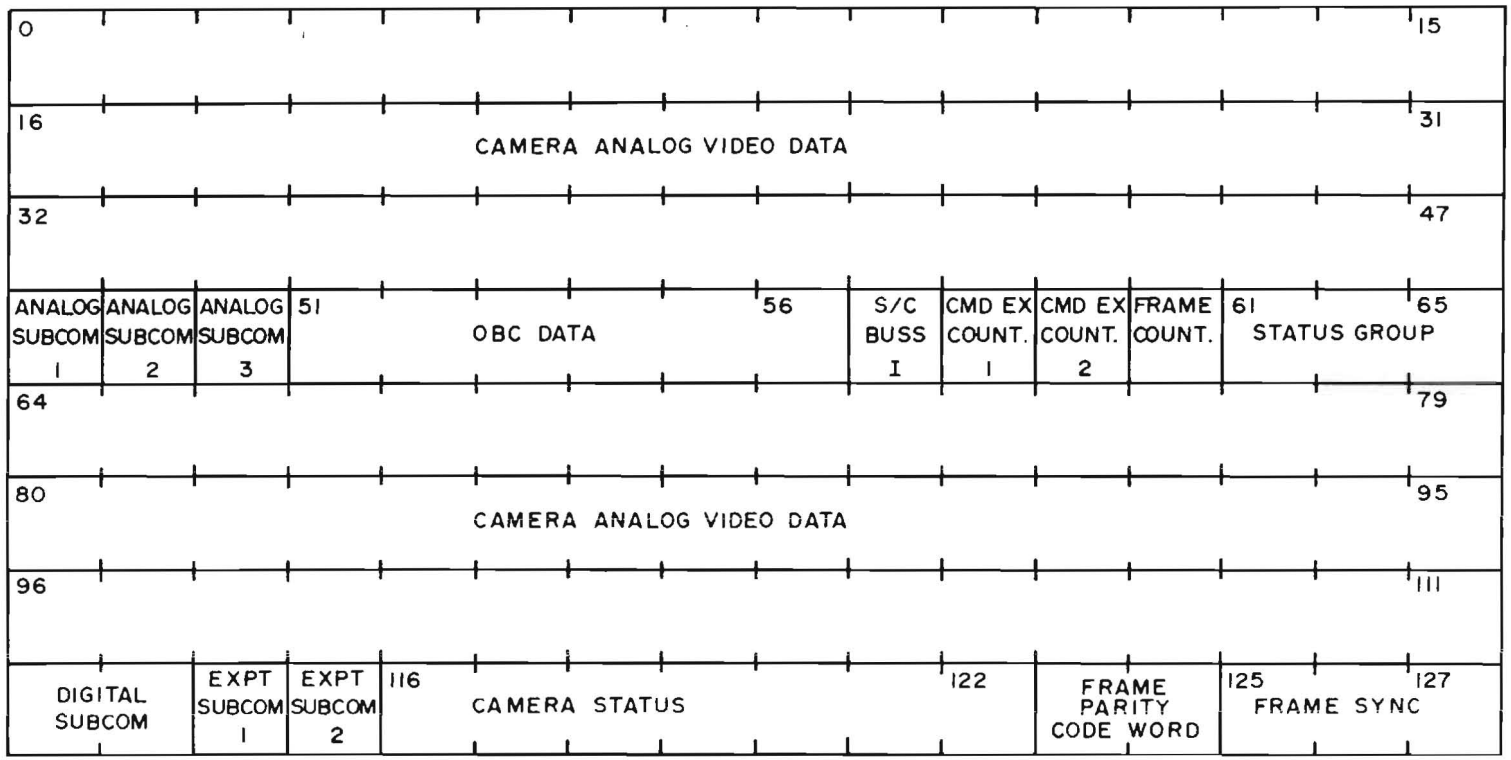

Figure 6-3. Minor Frame Format During Camera Readout

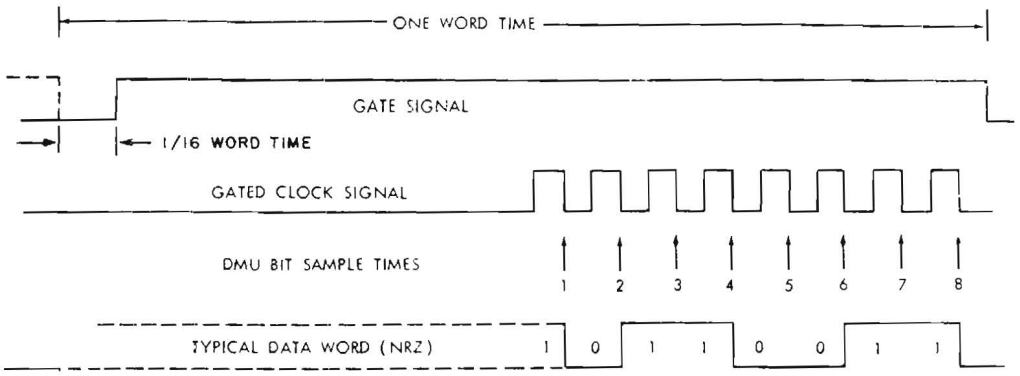

Figure 6-4. Digital Interface Signal

A particular input to the dataplexer is selected and the information present is transmitted through the multiplexer when the appropriate combination of enabling voltages is applied to the multiplexers' address lines. The address lines are driven by the contents readout of a location in the selected format memory. Format memories contain 128 locations of 8 bits each. Format generation is accomplished by stepping through successive memory locations and transferring data from the addressed dataplexer input at each location. Any desired sequence of dataplexer addresses may be loaded into the memory to compose a format. It should be noted that at the times dedicated to the fixed parameter words, mentioned earlier, the required information is inserted into the bit stream internally, and no input information is processed in the dataplexer. This eliminates the possibility of having an error in format composition jeopardize the data reduction process on the ground. As indicated earlier, 4 fixed-format and 1 variable format memories are supplied for telemetry formatting, two fixed, 1 variable and a computer controlled input for the computer portion of the time-sharing operation are available for computer formatting.

The ROM memories mentioned earlier are used for the fixed formats. The contents of these memories cannot be altered after fabrication, hence the term "fixed" formats. These memories are random-access, P-channel devices. They are each actually 256 word memories but a bit from the commandable memory selection decoder will permit only half to be selected at a time by putting a "1" or a "0" on the most significant memory address line. Thus, the four telemetry fixed format memories require two chips. In addition, two fixed format memories for the computer's use are supplied on a single chip. Memory location selection is controlled by a counter, incremented once per read out. Figure 6-5 shows a typical fixed format memory configuration.

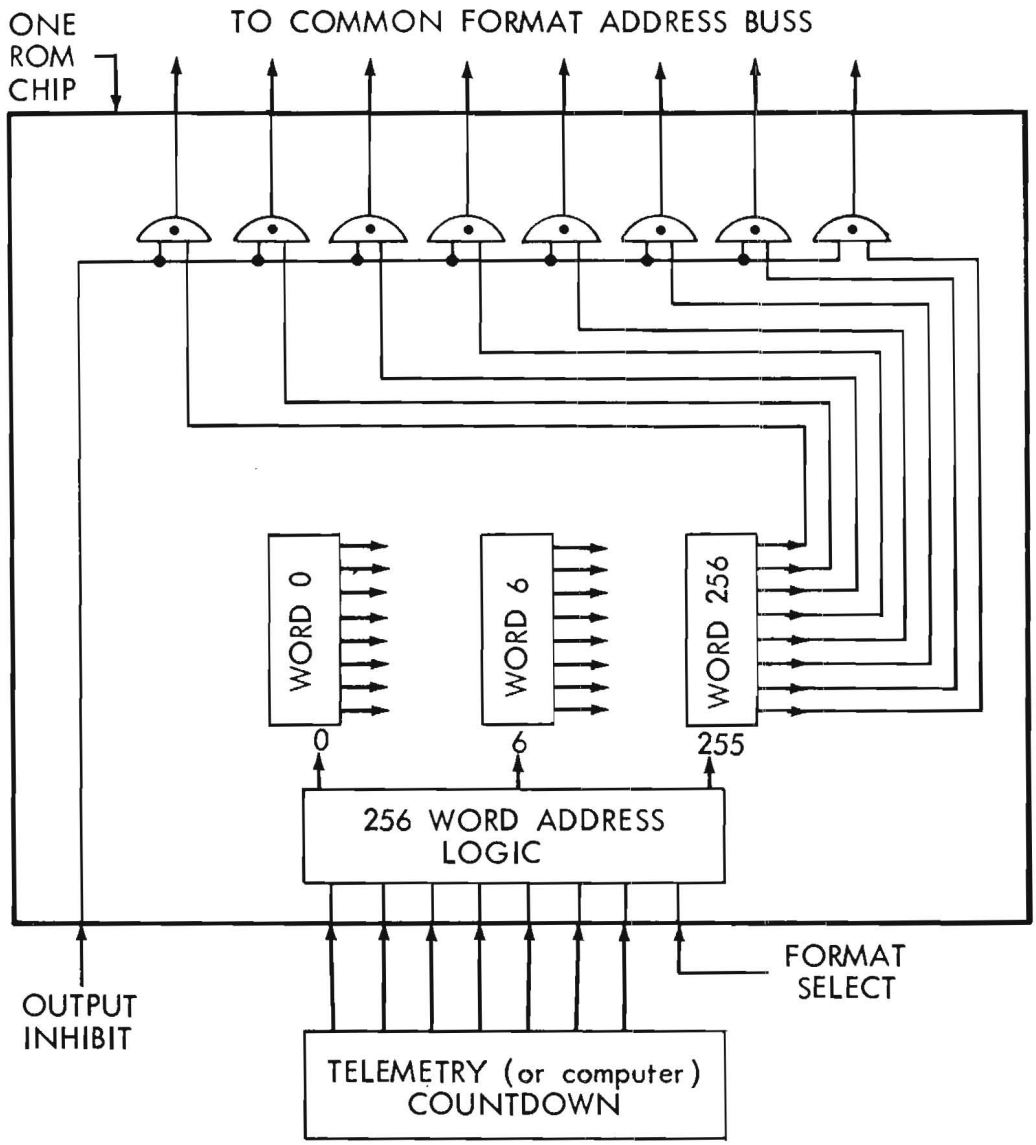

Figure 6-5. Fixed Format Memory Configuration

Each of the two variable format memories is formed by the parallel combination of 8 serial shift registers 128 bits long. Figure 6-6 illustrates this concept. Each 128 bit serial shift register is a single PMOS chip so that 8 chips are required per memory for a total of 16 chips for both. One variable format memory can be selected for either telemetry or the computer's use. An additional computer variable addressing technique will be discussed later. Memory location advance for these memories is achieved by supplying a single pulse on the shift inputs and circulating the contents. Note that this configuration is not a random-access memory, rather a "pipe-line" memory.

Figure 6-7 is a simplified block diagram showing the multiplexers and format memories. It combines the concepts described above. The total number of analog and digital inputs is 64, requiring 6 address bits. The 7th address bit shown is used to enable sync pulses when required. The 8th bit is used to generate an indirect address in the fixed formats. It is reserved for parity checking of the variable format memory output.

6.2.4 INPUT/OUTPUT CHARACTERISTICS

There are 32 digital data input lines available in the dataplexer. One-hundred-twenty-eight additional submultiplexed lines will be provided by the subplexer. Two control lines can be supplied to the user for each digital input, the word gate and shift pulse signals referred to in the previous subsection and shown in figure 6-3.

Digital output signal characteristics at 80 kHz sample rate are:

a. Word Gate Length: 87.5 microseconds.

b. Shift Pulses: 8 pulses per word at 160 kHz .

c. Logical "1" Voltage: $3\ V \leq v_1 \leq 7\ V$.

d. Logical "0" Voltage: $0\ V \leq v_0 \leq 1.0\ V$.

A partial schematic of a typical digital output circuit is given in figure 6-8. Rise and fall times are functions of circuit resistance at both ends and stray wiring capacitance.

Digital input signal characteristics to the multiplexer should be similar to those given for the outputs to guarantee successful data transfer. A partial schematic of the input circuit is shown in figures 6-9 and 6-10.

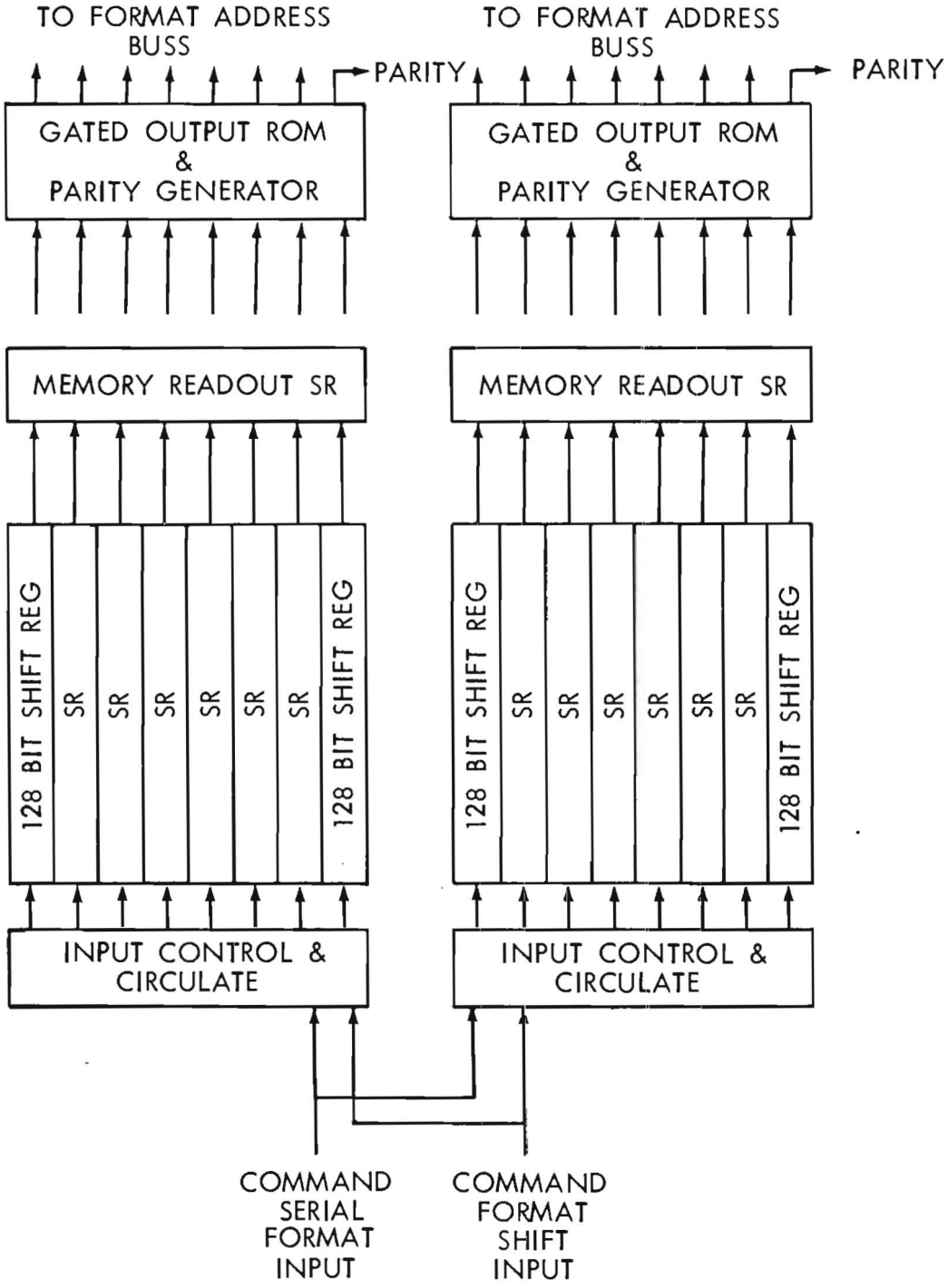

Figure 6-6. Variable Format Memories

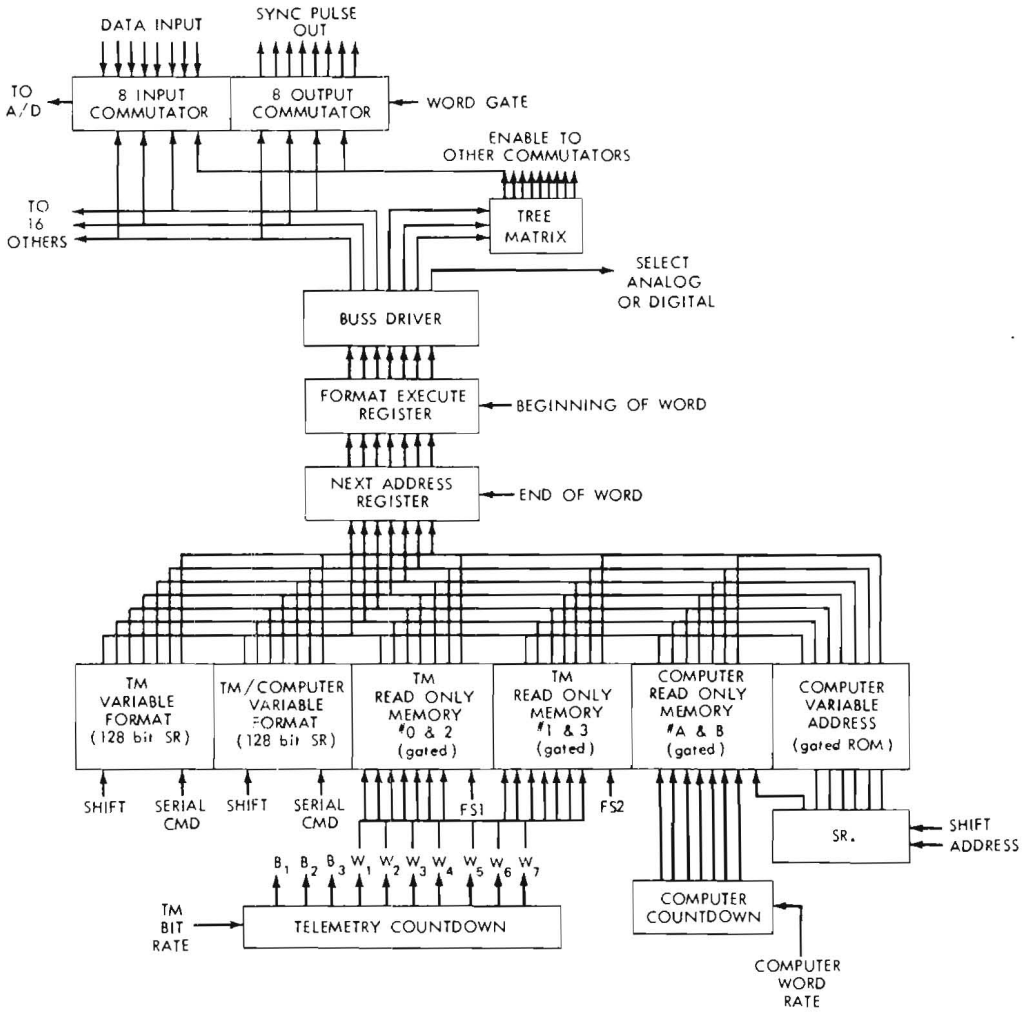

Figure 6-7. Simplified Block Diagram

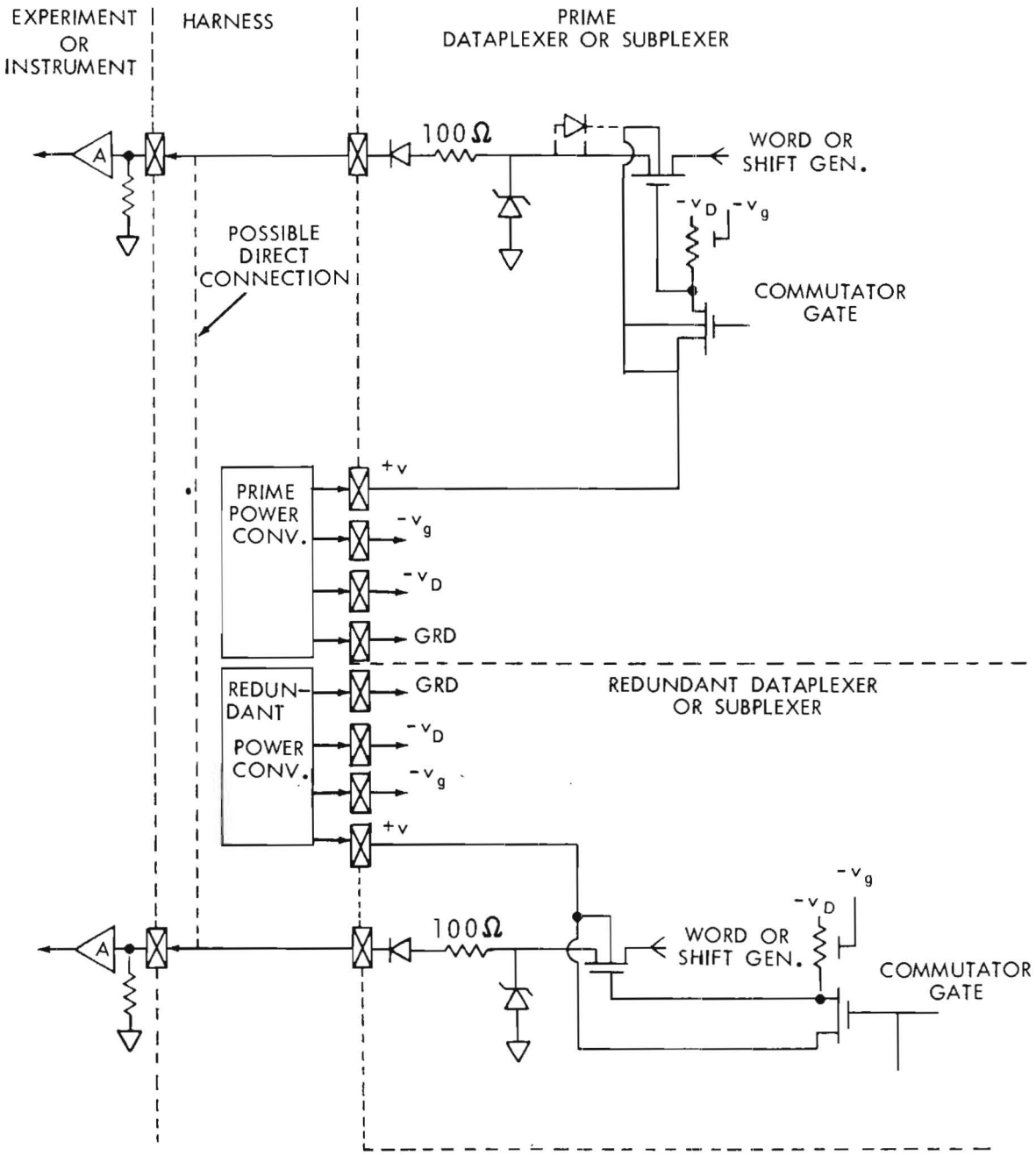

Figure 6-8. Digital Output Interfaces

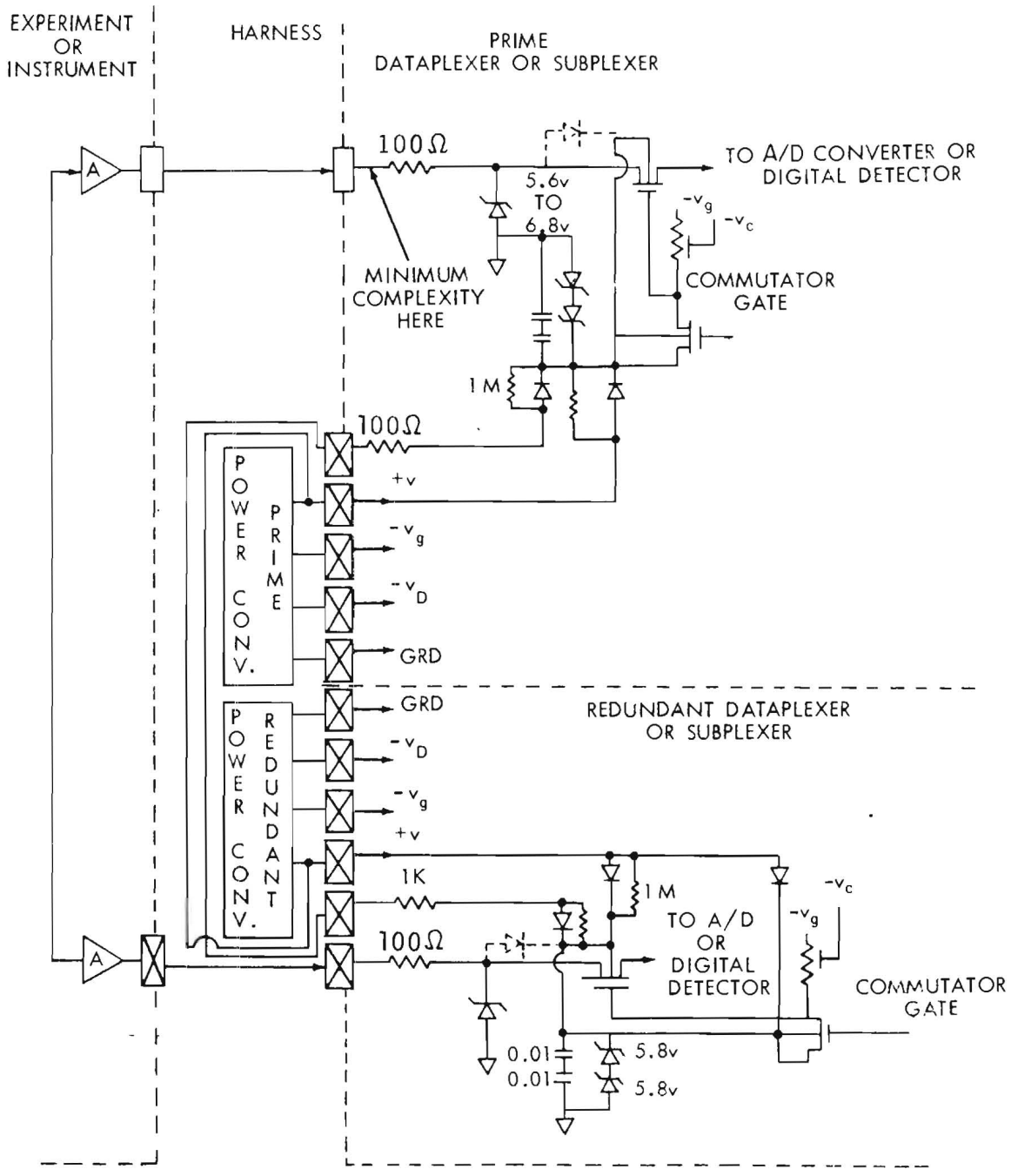

Figure 6-9. Digital Input Interfaces

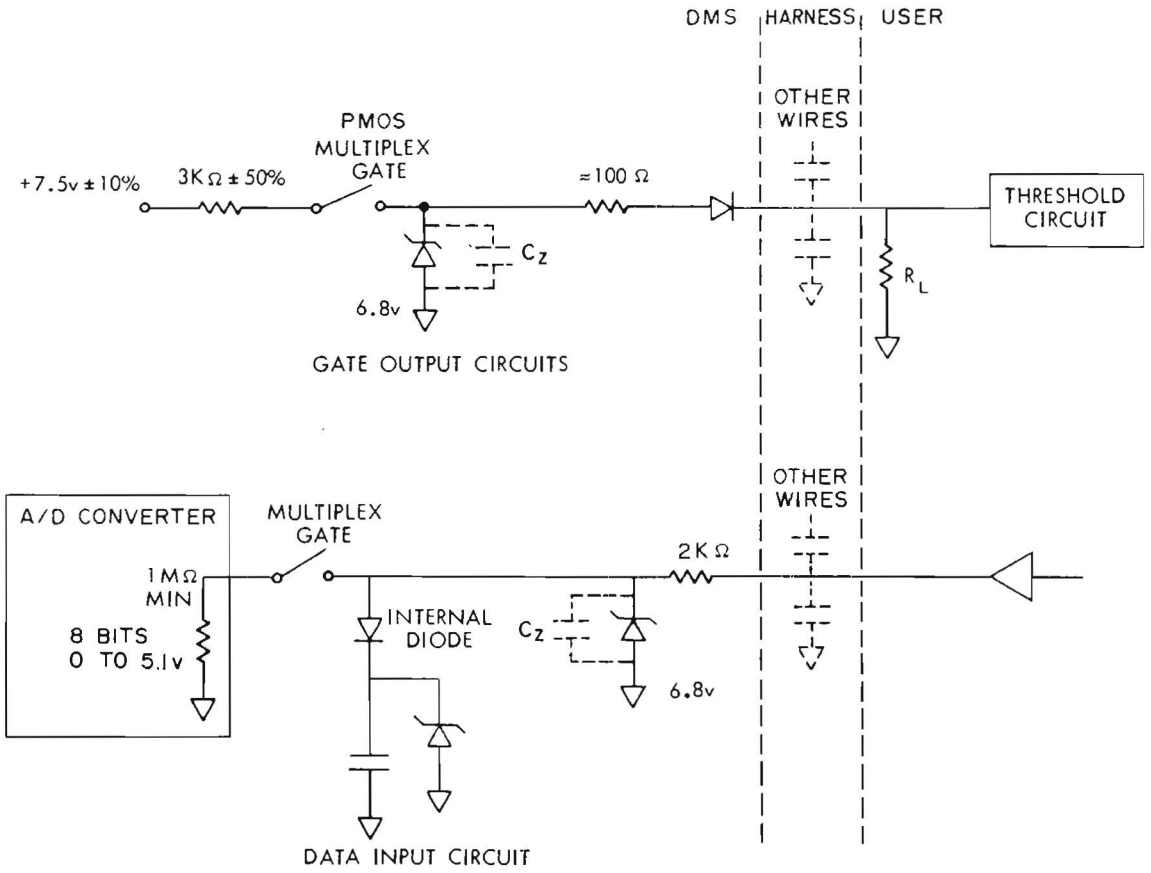

Figure 6-10. Analog Interface Equivalent Circuit

6.2.5 ANALOG TO DIGITAL CONVERTER

The analog data inputs are routed to an 8-bit Analog to Digital (A/D) converter. The A/D converter is a successive approximation type, running at the rate of 160,000 comparisons per second. The conversion time for a word is 50 microseconds. The maximum conversion word rate is 10,000 words per second, which is identical to the maximum word transmission rate through the dataplexer for telemetry and computer combined. The range of analog signal voltage input is from 0 volts to +5.1 volts. The analog input circuit is as shown in figure 6-10.

6.2.6 SUBMULTIPLEXING

Submultiplexing of up to 128 analog or digital inputs is handled by the subplexer, a box containing eight 16-input multiplexer units. The subplexer is designed so that combinations of these units can be interconnected internally as digital or analog submultiplexers. For example,

a 32-input analog submultiplexer and a 32-input digital submultiplexer with their associated 32 word gates and 32 shift pulses could be selected. The specific allocation of inputs between analog and digital signals is readily accomplished by the installation of jumper wires in otherwise identical boxes. If more inputs are needed, two subplexers could be used with one dataplexer. The dataplexer supplies all control signals needed by the subplexer, except OBC direct addressing.

6.2.7 TELEMETRY AND COMPUTER SAMPLE RATES

It was mentioned earlier that the DMS is used for both telemetry and computer data-collecting functions. The input data are transformed into 8-bit words and split into 2 serial data bit channels, one for each use.

The maximum data sample rate through the multiplexer is 80 kilobits with 40 kilobit maximum telemetry data rate. Thus, the computer and telemetry channels would receive alternate words from the multiplexer if the telemetry bit rate were maximum. In this case, the ratio of computer to telemetry words, called the multiplex ratio, is 1:1. At lower telemetry bit rates, the multiplex ratio can be greater than this and can be selected by ground command. Figure 6-11 illustrates the time-sharing technique and table 6-3 lists the various multiplex ratio options.

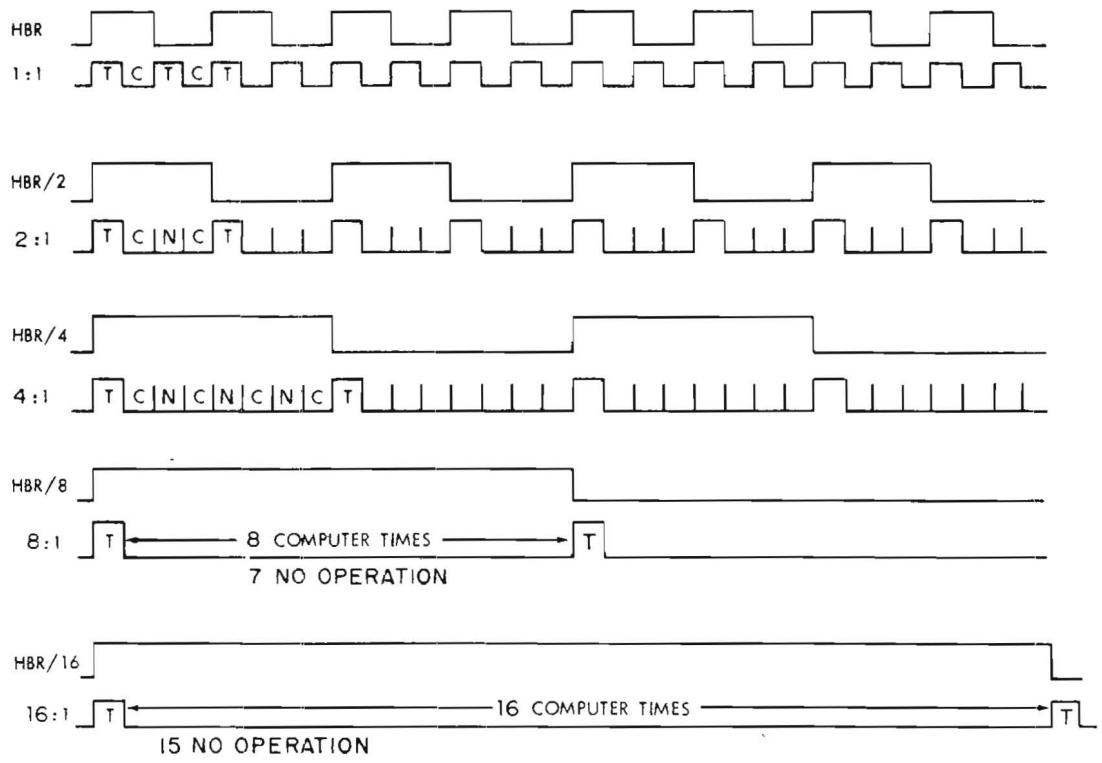

Figure 6-11. Time Share Arrangement

Table 6-3. Multiplex Ratio Options

TLM Bit Rate (bps)	Multiplex Ratio	Data Sample Rate (bps)	Computer Input Rate (bps)
40,000	1:1	80,000	40,000
20,000	2:1	80,000	40,000
20,000	1:1	40,000	20,000
10,000	4:1	80,000	40,000
10,000	2:1	40,000	20,000
10,000	1:1	20,000	10,000
5,000	8:1	80,000	40,000
5,000	4:1	40,000	20,000
5,000	2:1	20,000	10,000
5,000	1:1	10,000	5,000
2,500	16:1	80,000	40,000
2,500	8:1	40,000	20,000
2,500	4:1	20,000	10,000
2,500	2:1	10,000	5,000
2,500	1:1	5,000	2,500
1,250	32:1	80,000	40,000
1,250	16:1	40,000	20,000
1,250	8:1	20,000	10,000
1,250	4:1	10,000	5,000
1,250	2:1	5,000	2,500
1,250	1:1	2,500	1,250

Selection of multiplexer inputs for the computer channel is controlled by the computer format memories described earlier. Multiplexer addresses are switched between the selected telemetry and computer memories by the address multiplexer during the respective channel times.

In the computer variable format mode, the computer has additional capability of directly addressing the multiplexer and submultiplexer during the computer channel time. This affords complete flexibility for the computer to accumulate data from specific data sources in any desired sequence. In this way, the computer can become an important diagnostic aid for trouble-shooting problems during the missions.

6.2.8 THE COMMAND SYSTEM INTERFACE

The Command System Interface provides the means of controlling format, bit rate, multiplex ratio, and other DMS functions as shown in figure 6-12. A 24-bit command word is shifted serially into the command input register under control of shift pulses supplied from the command system. After the "execute" envelope has ended, the new command word is parallel transferred into the command control register at the end of the current minor frame. The new commands are then decoded and take effect at once. The command word bits and their related functions are listed in table 6-4.

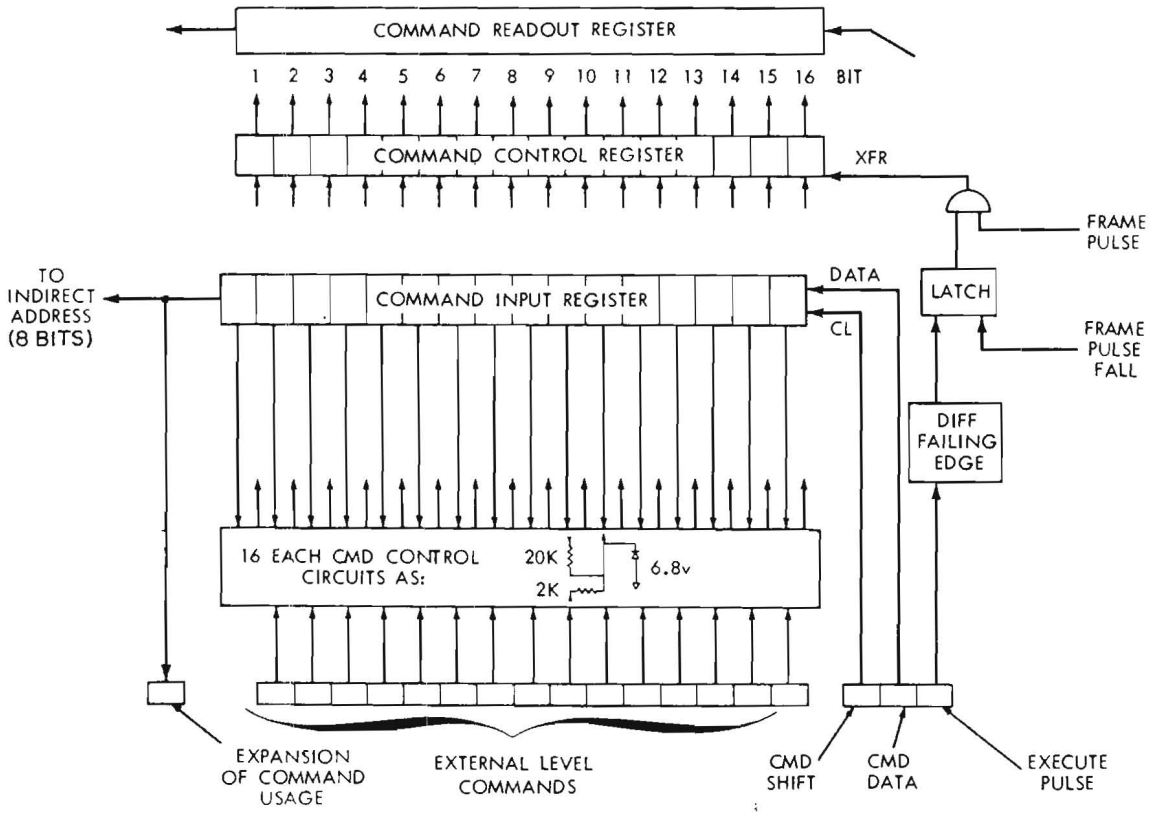

Figure 6-12. Command and Control Registers

Table 6-4. Command Word Bits

Command Register Bits	Mnemonic	Function Operation
1-8	1A	Indirect Address
9	--	0 Not Used 1 Not Used
10	XVAM	0 Circulate T/M VAM, Load OBC VAM (Bits 13 & 14 ≠ 0) 1 Circulate OBC VAM, Load T/M VAM (Bit 15 ≠ 0)
11	XCLOCK	0 Redundant Clock 1 Main Clock (Internal)
12	ALTROM	0 Address only one ROM (Bit 15 = 0) 1 Alternate ROMS (Bit 15 ≠ 0)
13, 14*	CPFMT	0 OBC VAM 1 ROM 2 Direct Address from OBC 3 NOP
15	TMFMT	0 T/M VAM 1 T/M ROM (Fixed)
16, 17*	TMROM	0 T/M ROM Format 1 1 T/M ROM Format 2 2 T/M ROM Format 3 3 T/M ROM Format 4
18	CODED	0 Block Code 1 Convolutional Code

*Least Significant Bit (LSB)

Note

A logic "1" is a positive voltage for serial inputs.
A logic "1" is a negative voltage for parallel inputs.
Bit 1 is first bit shifted serially into DMU.

Table 6-4. Command Word Bits (cont)

Command Register Bits	Mnemonic	Function Operation
19, 20, 21*	MXRATIO	0 All T/M 1 1:1 Multiplex Ratio 2 2:1 Multiplex Ratio 3 4:1 Multiplex Ratio 4 8:1 Multiplex Ratio 5 16:1 Multiplex Ratio 6 32:1 Multiplex Ratio
22, 23, 24*	SRATE	0 80 kb Transfer Rate 1 40 kb Transfer Rate 2 20 kb Transfer Rate 3 10 kb Transfer Rate 4 5 kb Transfer Rate

*LSB

Note

A logic "1" is a positive voltage for serial inputs.
A logic "1" is a negative voltage for parallel inputs.
Bit 1 is first bit shifted serially into DMU.

6.2.9 THE OSCILLATOR AND COUNTDOWN CHAIN

All spacecraft time is derived from a crystal oscillator and countdown chain included as an integral part of the dataplexer. These circuits comprise the spacecraft clock. Twenty-four bits of the spacecraft clock are telemetered to the ground in every fourth minor frame as shown in figure 6-13.

The oscillator and countdown chain are shown in figure 6-13. A single crystal oscillator is employed with binary dividers to obtain the desired drive frequency for the clock. The crystal oscillator frequency is 640 kHz. Oscillator stability, to ensure that the ground data reduction bit synchronizer can maintain reliable synchronization even when noise in the telemetry link masks the synchronization information, is $\pm$0.02%. A Pierce oscillator was chosen because:

a. The circuit does not require weldable inductors, difficult to procure with high reliability.

b. The circuit is self-starting and reliable over a wide range of crystal frequencies and circuit parameters.

c. Since oscillator requires the inductance of the crystal, spurious modes of oscillation are minimized.

The telemetry rate countdown binaries are synchronized to the constant-rate satellite clock countdown chain. Commands from the command system define input sample rates and multiplex ratio for computer time-sharing. The result of these two factors determine the telemetry rate.

The first three binaries (B1, B2, B3) in the telemetry countdown chain define the 8-bit times required for each telemetry word. The next 7 binaries (W1 to W7) define the 128 words of each minor frame. The last 8 binaries (F1 to F8) define the 256 minor frames which make up the maximum major frame. These binaries are set in the proper phase to ensure agreement with the satellite clock binaries running at the same rates.

6.2.10 POWER ESTIMATE FOR THE DMS

Power estimate for the DMS, including converter inefficiency, is 4.3 watts maximum. Weight is estimated at 6 pounds per system, or a total of 12 pounds for redundant systems.

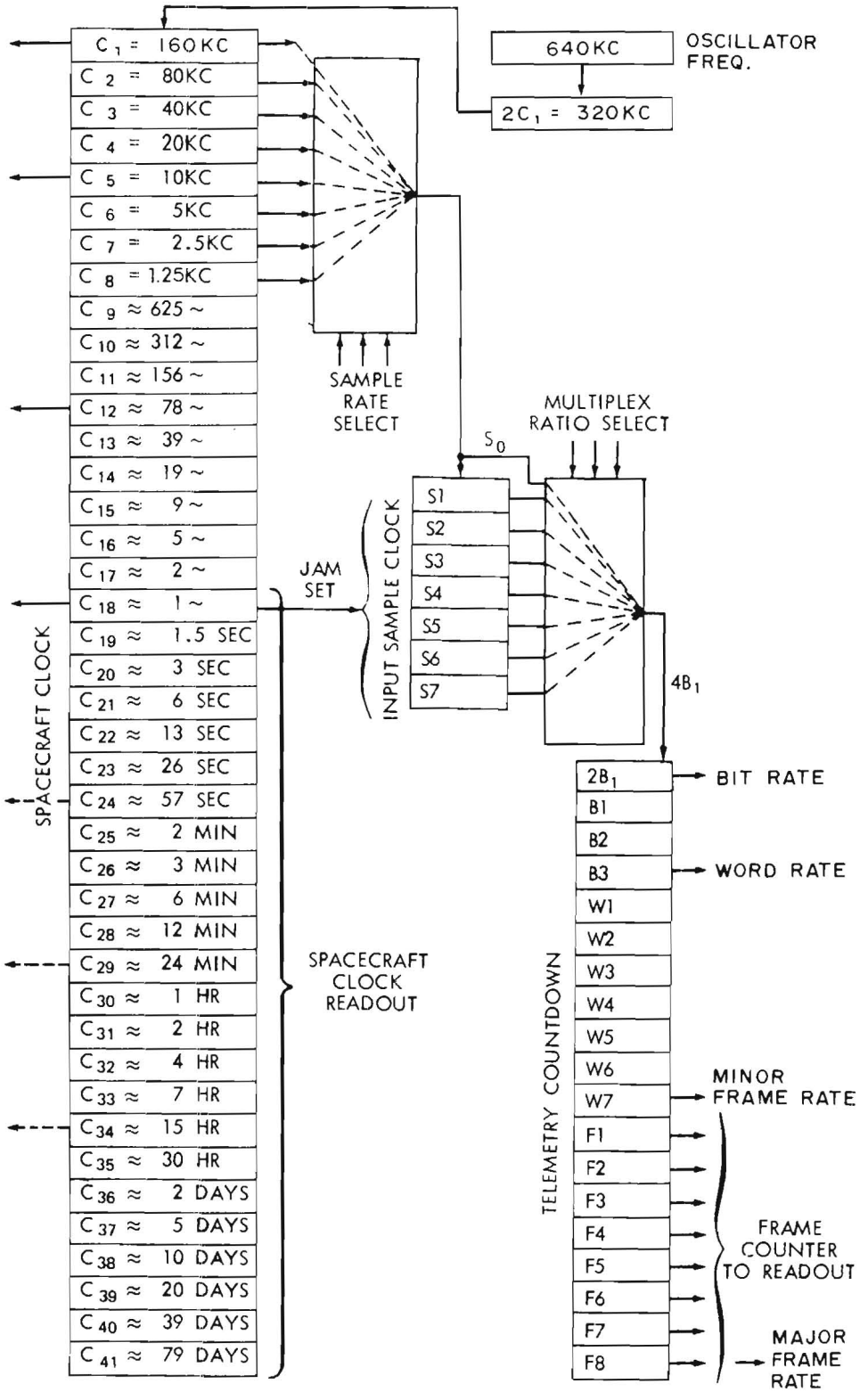

Figure 6-13. Spacecraft Clock and Countdown Block Diagram

6.3 SPECIAL SIGNAL CONDITIONING REQUIREMENTS

Up to 16 analog multiplexer and submultiplexer input lines can be modified to service thermistor circuits. The modifications consist of adding jumper wires in such a way that the remotely located thermistors receive the necessary operating voltage from the DMS. The output voltage of one of these circuits is proportional to the temperature of the environment where the associated thermistor is mounted. This voltage is in the 0 to +5.1 volts range and is switched to the A/D converter. Figure 6-14 shows the type of circuits used for this purpose.

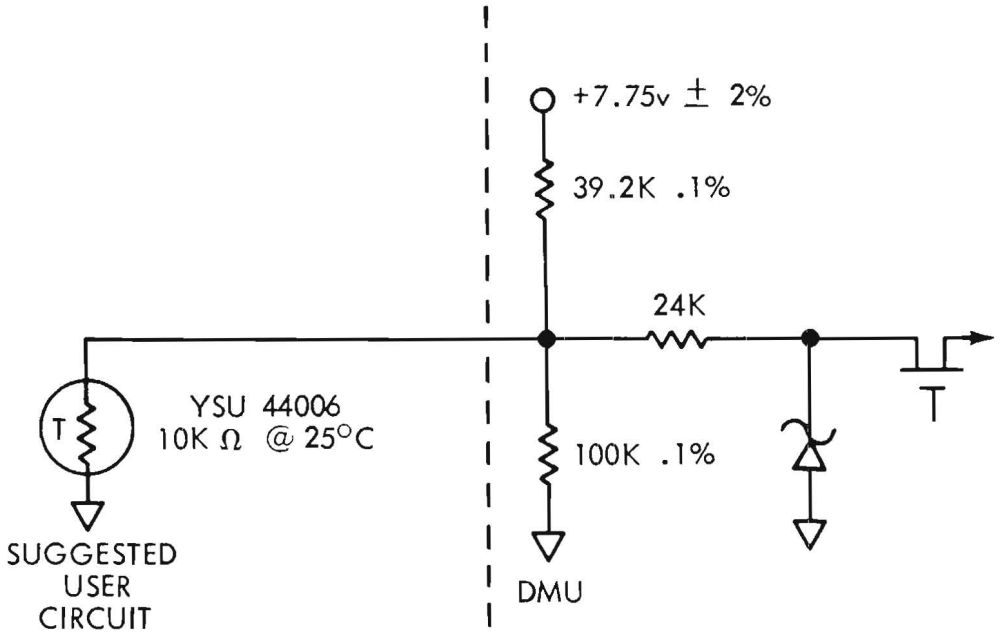

Figure 6-14. Thermister Interface Circuit

6.4 ON-BOARD COMPUTER

6.4.1 AOP DESCRIPTION

The architecture of the Advanced On-board Processor (AOP) is based on a modular approach to provide for standby spare redundancy. The system is composed of two module types: a processor module which performs the instruction execution and input/output functions and a basic memory module which is 4096 words in size. These modules are interconnected by means of dual redundant "data" buses which provide the parallel data paths and control lines necessary for data transfers between storage and processor unit. Figure 6-15 shows this architecture.

The processor module contains the Central Processing Unit (CPU) and special interface circuitry used for Input/Output (I/O). Although the special interface circuitry is unique to the mission it is packaged in the processor box so that each processor is really a stand-alone functional unit requiring only memory. The processor employs a fully parallel adder, and parallel data transfers between registers and at the processor/memory interface. Data words and instructions are 18 bits in length with negative numbers being represented in two's complement form. The instruction repertoire contains 55 instructions, 31 utilizing operand fetch. These instructions include a 5 microsecond add, a 37 microsecond multiply, and a 75 microsecond divide.

The basic memory module for the AOP is a random access 4096 by 18-bit word, plated wire unit. A minimum of 3 of these modules are being utilized for the IUE application. The memories feature cycle by cycle power switching, have a 500 nanosecond access time, and a 1 microsecond cycle time. They are nonvolatile and readout is nondestructive.

The AOP employs 16 individually armed priority interrupts, which allow asynchronous spacecraft events to gain access to computer operation at event dependent intervals. The interrupt handling logic is designed so that when an interrupt is honored, three critical registers are automatically saved and initialized to new values from fixed memory locations. These are the instruction counter, the interrupt lockout register, and the storage limit register. The hardware handling to these registers is important in providing security of program execution in a long term unattended environment.

In addition to the asynchronous events which require program interruption, there are a great many data acquired and generated onboard at various rates that should be transferred to and from computer memory without disturbing program execution. Program independent data transfers are accomplished by the AOP through the use of buffered I/O channels, operated in a cycle steal mode similar to the priority interrupt technique. These channels time-share a single set of Direct Memory Access (DMA) hardware.

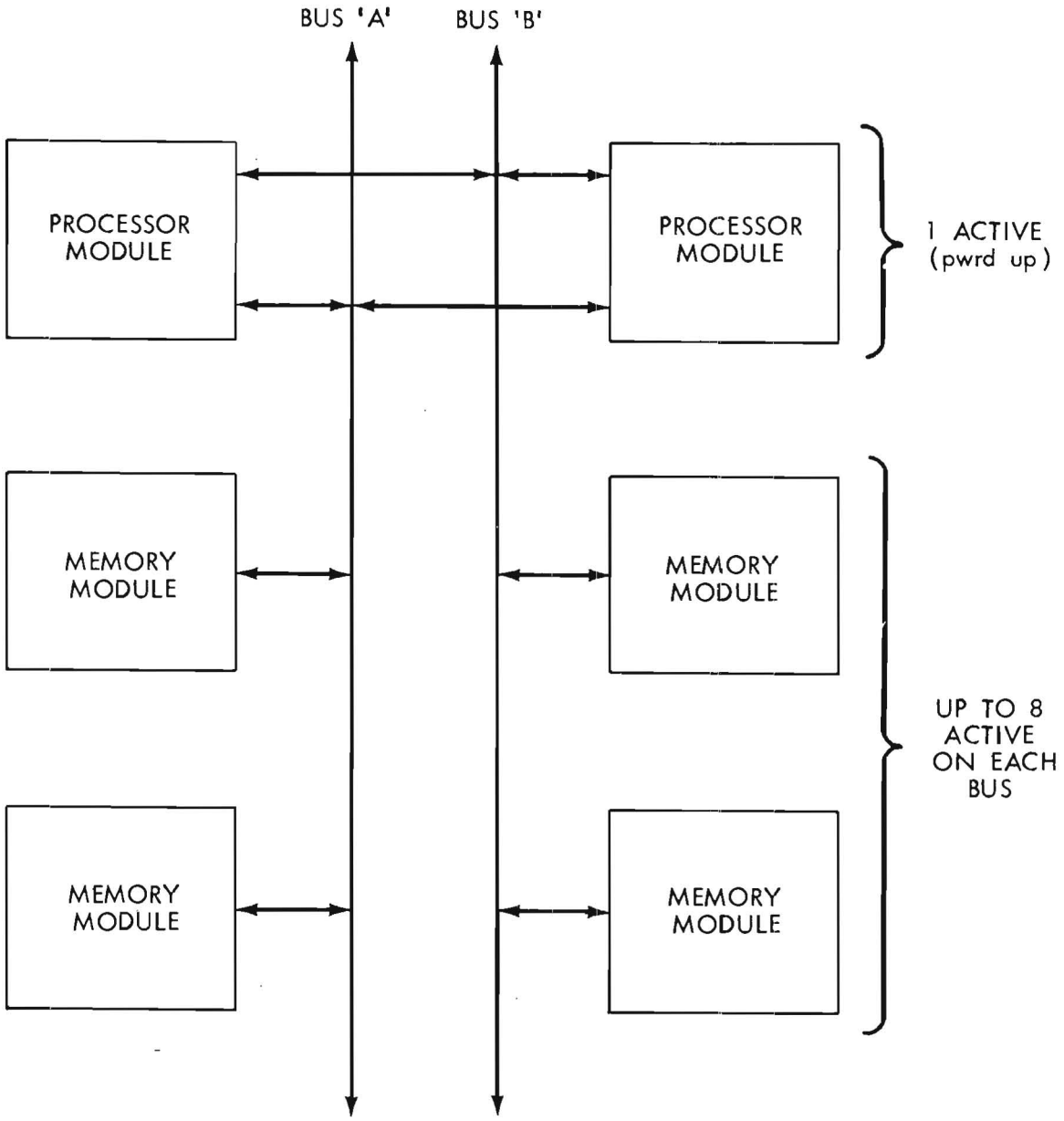

Figure 6-15. AOP System Block Diagram

6.4.2 COMMAND AND CONTROL CAPABILITIES

The command system accepts commands from both the computer and the command receiver on a time-shared basis. Therefore, the computer can control any commandable system if it is programmed to do so. This includes the capability of issuing stored commands on a time delayed or event dependent basis. Commands related to the computer's basic task of attitude control are computed, formatted, and sent to the reaction wheels or jets via the command system.

6.4.3 SPECIAL INPUT/OUTPUT

All communication between the computer and the outside world is channeled through the Special Input/Output unit (SIO). In most cases, information is transmitted to or from memory locations in a "background," or cycle-steal, mode of operation. Direct program-controlled transfer is also possible but must be used with care to avoid timing conflicts arising from the inherently asynchronous nature of the operations. The AOP has 8 input channels and 8 output channels available for use. These channels must be armed via software. In addition, 1 direct access channel is provided, and is used primarily for initial program loading.

The SIO also contains control logic to process cycle steal requests, ground commands, and interrupts. External timing signals from the DMS and the command systems are gated with enabling signals from the CPU to synchronize the data transfers and the arming of external interrupts and I/O cycle steal requests. Figure 6-16 is a functional block diagram of the SIO.

6.4.4 DMS INTERFACE REQUIREMENTS

As indicated earlier, the computer receives its data via the DMS. In addition, the computer must insert data into the telemetry stream via the multiplexer, just as any other data source must do. For the latter, the computer receives the standard digital word gate and shift pulse lines to control this output of information.

However, additional timing signals are required to control the incoming data from DMS and to enable the computer to keep in sync with the telemetry and computer formats. Table 6-5 lists the necessary interface signal lines between the SIO and the DMS, along with the function of each.

Each input signal to the SIO is fed to an input stage as shown in figure 6-17. This circuit also serves as a level shifter to convert the DMS signal levels to Transistor-Transistor Logic (TTL) levels. The two lines from the redundant DMS units are then combined in a logic circuit as indicated in the figure. A short to ground in either input line does not prevent the other from being used. A failure where an input

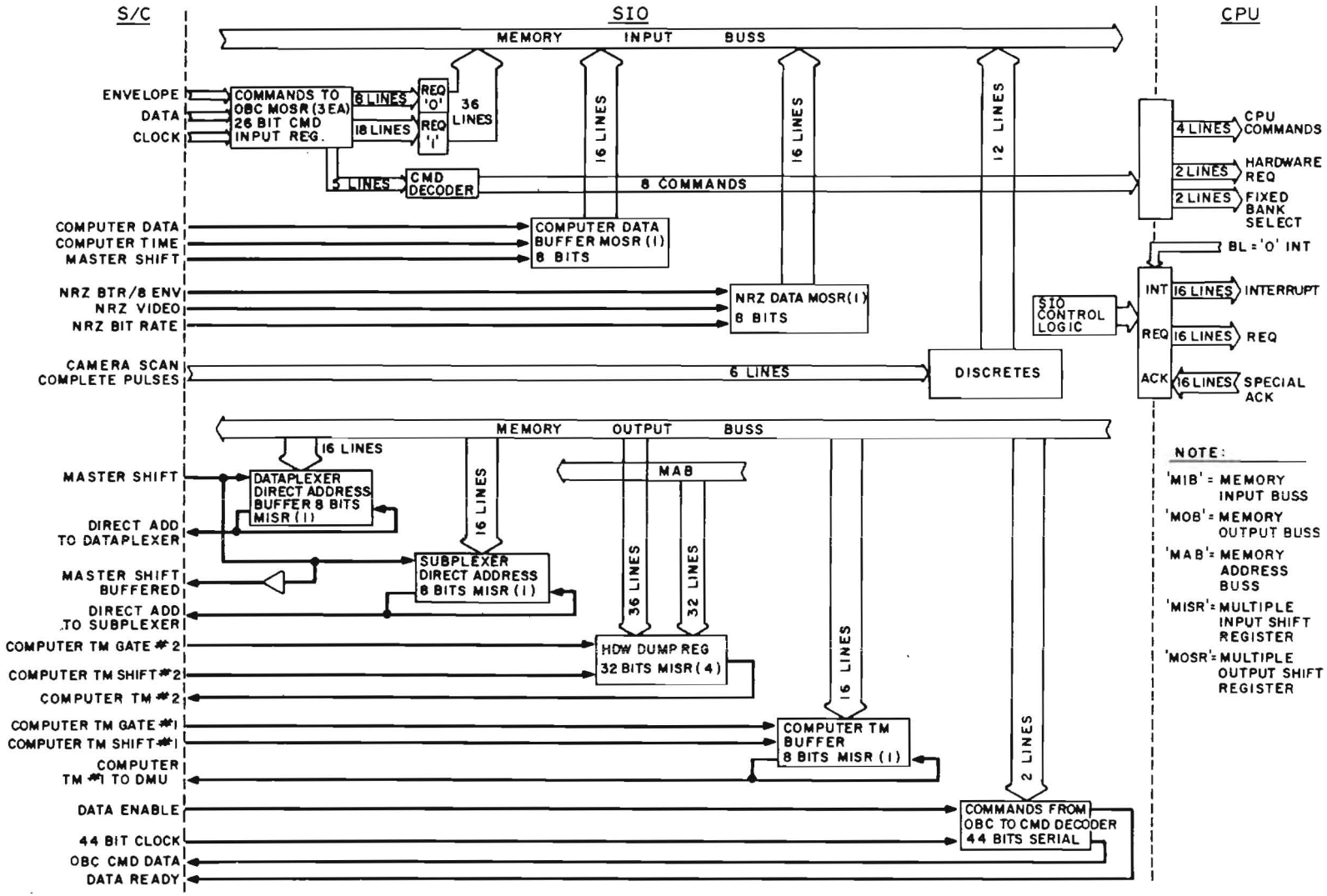

Figure 6-16. SIO Block Diagram

Table 6-5. SIO/DMS Signal Interface

Interface Signal Lines	Function
(1)	DATA INPUT
(2)	MASTER WORD GATE
(3)	MASTER SHIFT PULSE
(4)	COMPUTER TIME
(5)	MINOR FRAME SPIKE
(6)	FIXED WORD SYNC PULSE
(7)	DATA OUTPUT
(8)	DATA WORD GATE
(9)	DATA SHIFT PULSES
(10)	MUX ADDRESS OUTPUT
(11)	SUBMUX ADDRESS OUTPUT

Note
Two of each line is required.

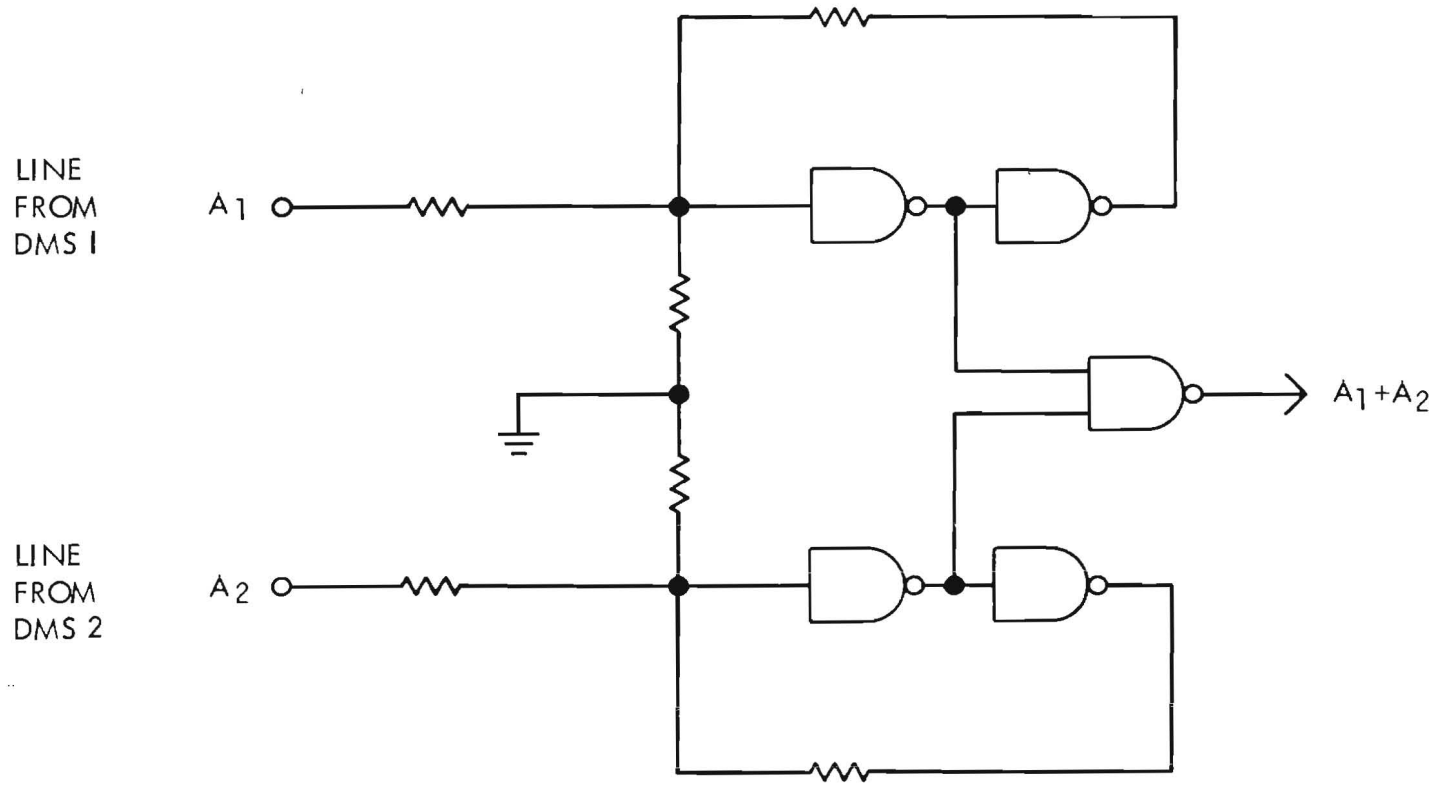

Figure 6-17. SIO/DMS Buffering

line was held positive would require turning off the offending DMS unit and switching to the redundant unit. Floating or open input lines look like zero volts and have no adverse effect. Protection against internal damage due to an external failure is provided for by the series resistor.

Output lines from each SIO to the two DMS units are buffered and driven separately. These should be buffered separately and then combined at the DMS.

6.4.5 COMMAND SYSTEM INTERFACE REQUIREMENTS

The AOP interfaces with the command system through the SIO. All timing signals are supplied by the command system, one set of signals for incoming commands and the other for computer generated commands to be routed via the command system. The computer requires both serial digital and discrete command inputs. Table 6-6 lists the required interface signal lines between the SIO and the command system.

Since the computer has the potential of sending commands to all onboard systems, ground control of computer operations is essential. Therefore the integrity of real time operation of ground control command capability is of primary importance to the mission.

The transfer of commands from the computer to the command decoder is controlled by the decoder-supplied "data enable" signal and shift pulses. Two sets of these signals come to the SIO, one from each of the redundant command decoders. The command decoders will both be powered, and will be operating at the same time, asynchronously. Therefore, the computer must be commanded to ignore one set of output command control signals.

Similarly, an active "data ready" line must be supplied to the command decoders from the SIO in use. The decoder will use this to gate commands from the "on" computer to avoid the possibility of executing spurious commands due to noise on the line from the unused SIO. Serial digital commands to the computer are 37 bits long. The format is shown in figure 6-18.

Output commands from the computer are 44 bits long. The command formats are shown in figure 6-19. The bit numbers given refer to position in the computer command memory buffer.

6.4.6 POWER AND WEIGHT BREAKDOWN

The weight breakdown for the OBC is based on seven boxes: two 2.5 lb boxes, each containing a CPU and its associated SIO, three 5.5 lb boxes, each containing a 4 K plated-wire memory unit and two 3.75 lb boxes, each containing a power converter and controls for selecting the

Table 6-6. SIO/Command System Signal Interface

Interface Signal Lines	Command System
	Serial Command Input to SIO
(1)	Real Time Data from Command Decoder A
(2)	Real Time Data from Command Decoder B
(3)	Shift Pulses from Command Decoder A
(4)	Shift Pulses from Command Decoder B
(5)	Execute Envelope from Command Decoder A
(6)	Execute Envelope from Command Decoder B
	Command Output from SIO to Command Decoder
(1)	Computer Command Data to Command Decoder A
(2)	Computer Command Data to Command Decoder B
(3)	Computer Command Shift Pulses from Command Decoder A
(4)	Computer Command Shift Pulses from Command Decoder B
(5)	Data Enable from Command Decoder A
(6)	Data Enable from Command Decoder B
(7)	Data Ready to Command Decoder A
(8)	Data Ready to Command Decoder B
	Control Commands to SIO*
(1)	Master Clear Serial Digital
(2)	Interrupt Level "0"
	Line from SIO to Command Decoder A - (GND when ON; Floating when OFF)
	Line from SIO to Command Decoder B - (GND when ON; Floating when OFF)
	* There will be several other serial digital commands to the SIO to control CPU/Memory configurations.

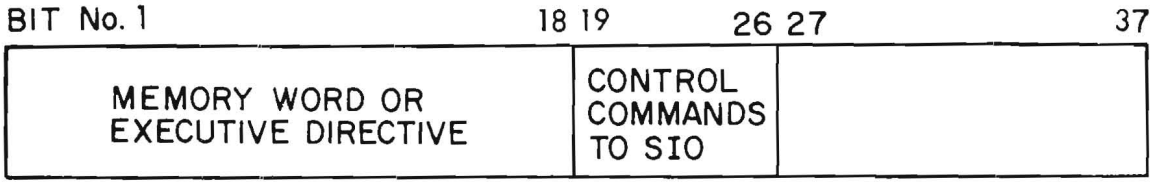

Figure 6-18. Serial Digital Command Format

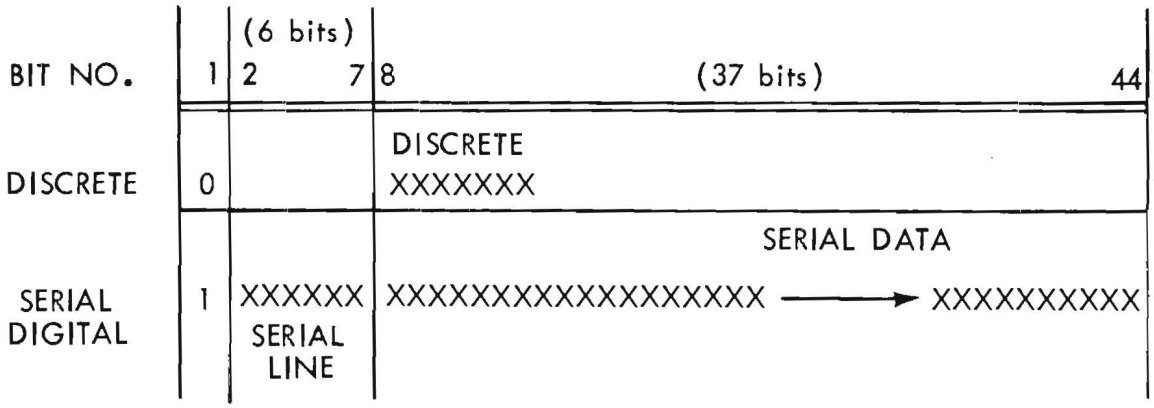

Figure 6-19. Command Formats

redundant CPU/SIO in use and memory bank combinations. The total weight for the OBC system is therefore 31.0 lbs.

The power estimate is broken down in the same manner. The CPU/SIO boxes require 7 watts per box but only one will be powered at a time. The memory units require 4 watts when running at maximum speed and 150 mW when on standby for each unit. Only one memory unit will be running at any given time and the other two will be drawing standby power. This totals 4.3 watts, (worst case for the memory units). The total power for memory units and CPU/SIO boxes is therefore 11.3 watts. The power converters have an efficiency of approximately 70%. This means that the power to the power converter must be 16 watts in order to deliver 11.3 watts to the rest of the OBC system. That is, the OBC requires 16 watts, total 4.7 watts of which are lost in power converter inefficiencies.

6.5 REDUNDANCY AND RELIABILITY

6.5.1 IUE MISSION LIFE

The IUE mission life of 3 to 5 years required particular attention to reliability of spacecraft systems. On the component level, careful selection of part types, vendors, and screening procedures were instituted. Where nonstandard parts are used, well known processes and thorough screening was applied. Fabrication techniques and box test procedures were controlled through the entire process.

6.5.2 DATA MULTIPLEXER SUBSYSTEM

The Data Multiplexer Subsystem is fully redundant. That is, two complete systems will be flown. One will be powered and the other turned off at any given time, in parallel, and no switching is employed in any of the input or output lines except the input power bus. Therefore, two wires are required for each signal interconnection between the DMS and another system. Figure 6-20 illustrates this. The DMS interface circuits provide protection against the possibility of an external failure causing a malfunction in the DMS. However, it does not protect against loss of signal. The user must take proper precautions against a single failure causing the loss of both lines to the two DMS units. This is especially important in the case of critical information that cannot be derived from another source. Figure 6-8 shows methods of protecting against this. The simplest interconnection, directly tying the two lines together, is the riskiest. In addition, the user should exercise care in cross-strapping between his own redundant units and the DMS units.

6.5.3 ADVANCED ON-BOARD PROCESSOR

The first concern in building a reliable AOP system is to design it in the simplest possible manner utilizing the fewest possible components. Minimization of interconnections is also important, but with the advent of LSI wherein most of the interconnection is done "on-the-chip," this factor is not nearly as significant as it once was. The reliability of the basic components, the building blocks of the system modules, is of paramount importance. The use of new LSI components in the AOP has introduced an unknown into the reliability equation. However, the impact of this is minimized by the fact that this component is built using well proven processes. Both the active devices (which have seen wide usage on a smaller scale) and two-layer metallization technology (which has undergone extensive evaluation) have demonstrated a very high reliability.

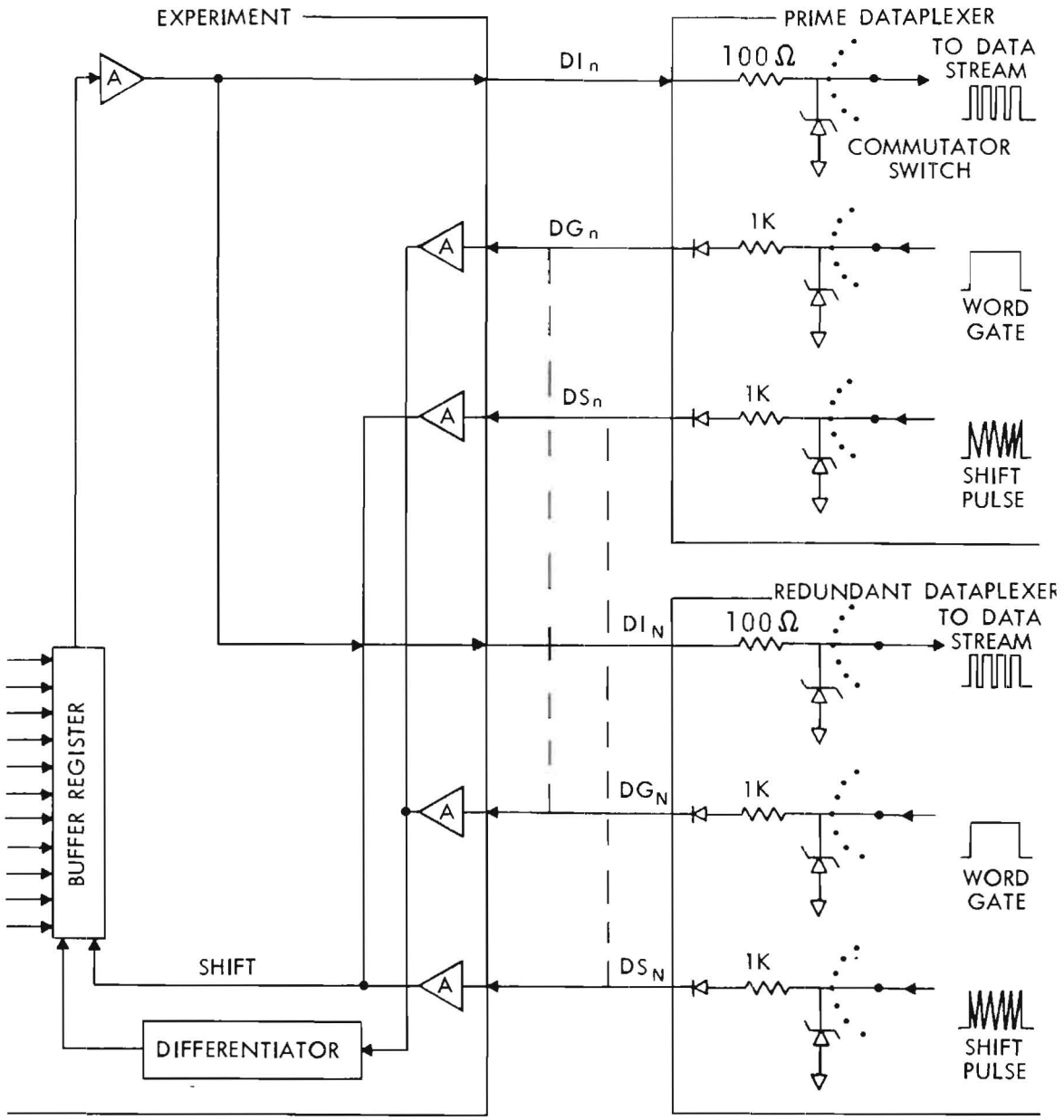

Figure 6-20. DMS Redundant Interconnection

6.6 SYSTEM LEVEL RELIABILITY

At the system level the probability of mission success can be improved either by connecting two or more simplex systems in parallel (this is the configuration allowed by computer designs available today), or by adding redundant modules in parallel with the simplex systems modules to form a duplex system (this is the configuration allowed by the AOP architecture). The reliability models of each of these configurations are depicted in figure 6-21. Assuming an application required 8K words of memory and an equal Mean Time Between Failure (MTBF) for individual modules, relative success probabilities as a function of time have been calculated and are plotted in figure 6-22. From these curves it can be seen that, with the same amount of hardware, the duplex (AOP) configuration is nearly twice as reliable as the dual simplex design. In addition, since the AOP memories have power-switching features, all four units of the duplex system including spares are available for use early in the mission. This effectively increases the memory size for non-critical tasks without cost to the system.

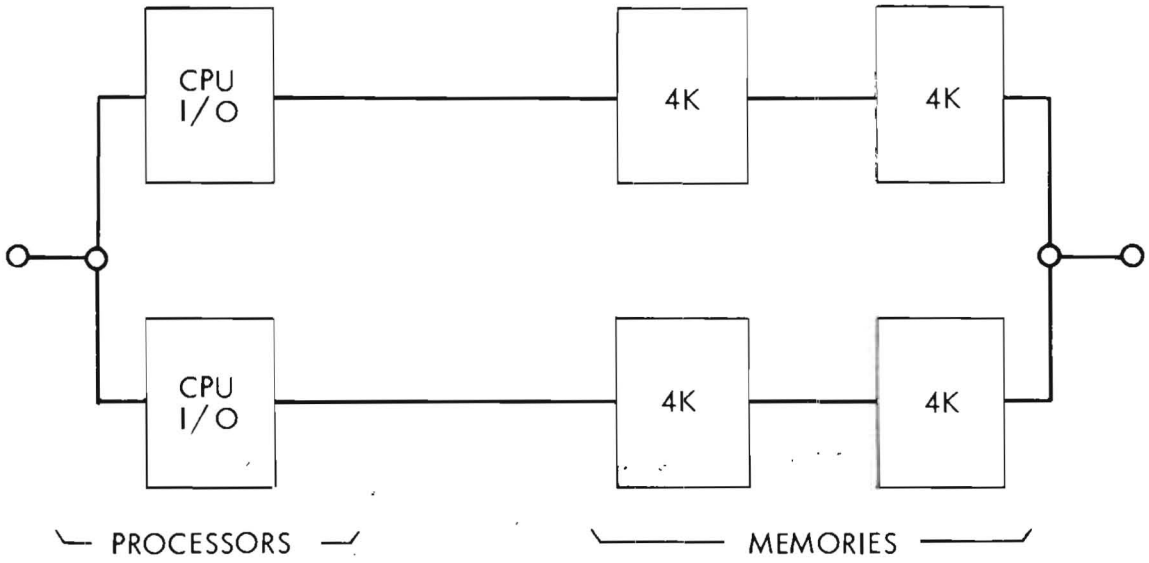

(a) DUAL SIMPLEX DESIGN

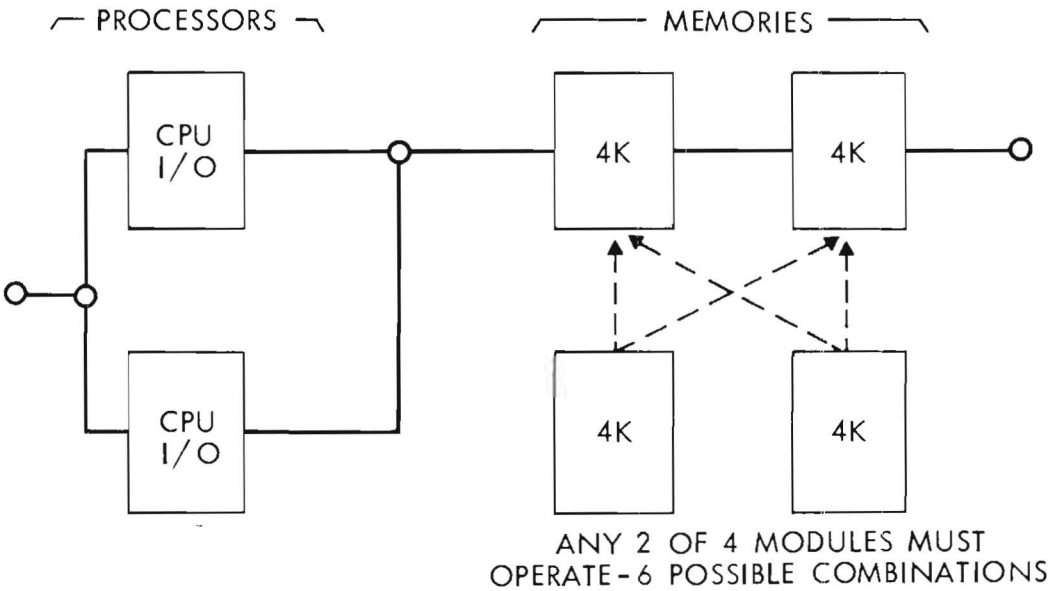

(b) SINGLE DUPLEX DESIGN (AOP)

Figure 6-21. Realiability Models

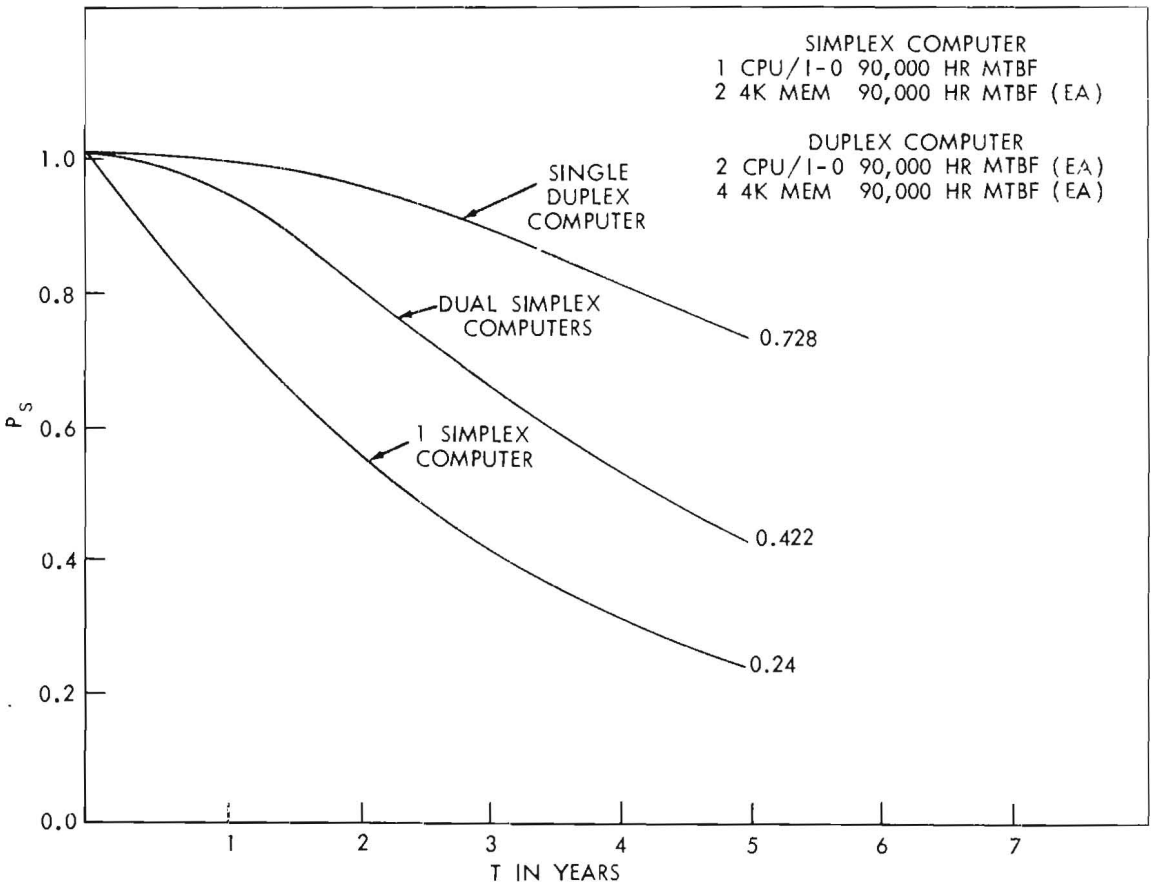

Figure 6-22. Reliability Curves

SECTION 7. POWER SUBSYSTEM

7.1 CONFIGURATION AND FUNCTIONAL OPERATION

The power subsystem on the IUE spacecraft is a Direct Energy Transfer (DET) system. The primary source of power is the spacecraft solar array which consists of two deployable paddles mounted to the spacecraft structure. Power from the solar paddles is transferred directly to the spacecraft bus which is regulated at +28.0 volts ±2 percent. The lack of any series elements between the solar array and the spacecraft loads provides for a transfer of array power to the loads at nearly 100 percent efficiency. Power during solar eclipses and other periods when demand exceeds solar array output is provided by two 6 ampere-hour nickel-cadmium batteries through a boost regulator. These basic elements of the IUE power subsystem are depicted in figure 7-1.

The Power Supply Electronics (PSE) is of modular design and consists of two power modules operating in unison through a mission adapter module. The PSE conditions the outputs from the solar array and the batteries at 28.0 volts ±2%. As shown in figure 7-2, three modes of operation exist, depending on the available solar array power and the spacecraft load requirements. If the array power is greater than the spacecraft load, the PSE will first provide battery charge current and then dump the excess array power. If the spacecraft load exceeds the solar array output, the difference in power will be supplemented by discharging the batteries through the boost regulator. If the spacecraft load is equal to the solar array power, the PSE will be in a dead-band or non-operational mode.

A simplified diagram of the IUE Power Supply Electronics is given in figure 7-3. The Power Subsystem block diagram is shown in figure 7-4. The Power Subsystem weight for each major component is summarized in table 7-1.

Table 7-1. IUE Power Subsystem Weight Summary

Subsystem	Weight (lbs)	
Solar Array	51.7	(23.5 kg)
Batteries (2, 6 ampere-hour)	27.2	(12.4 kg)
Power Supply Electronics	29.5	(13.4 kg)
Diode Filter Boxes	1.2	(0.5 kg)
Total	109.6	49.8 kg

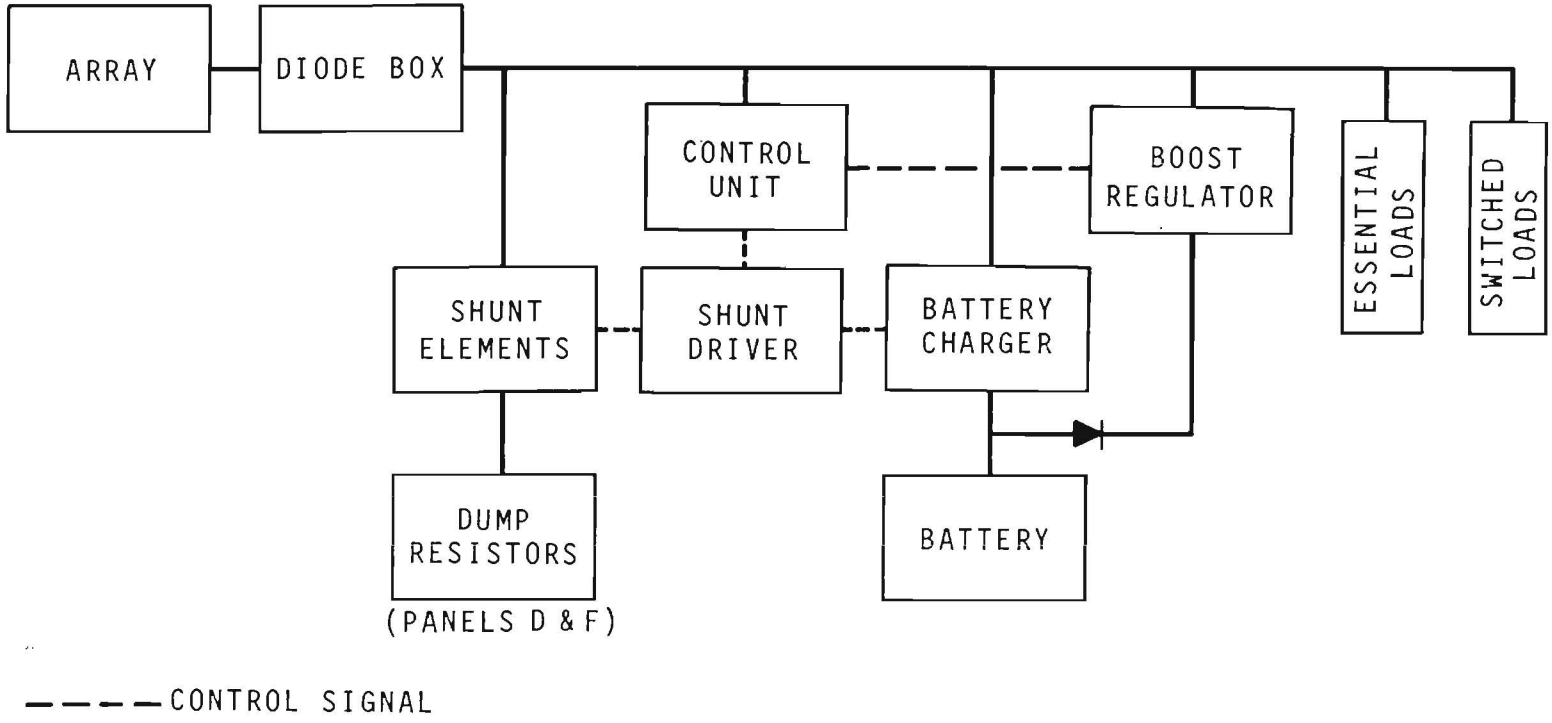

Figure 7-1. Functional Block Diagram - IUE Power Module

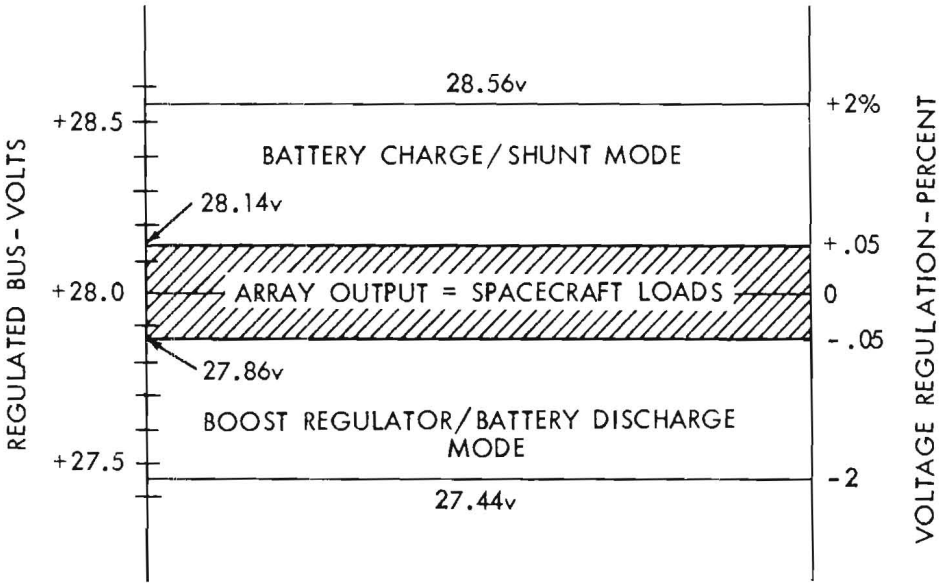

Figure 7-2. Spacecraft 28.0-Volt Bus Regulation Modes

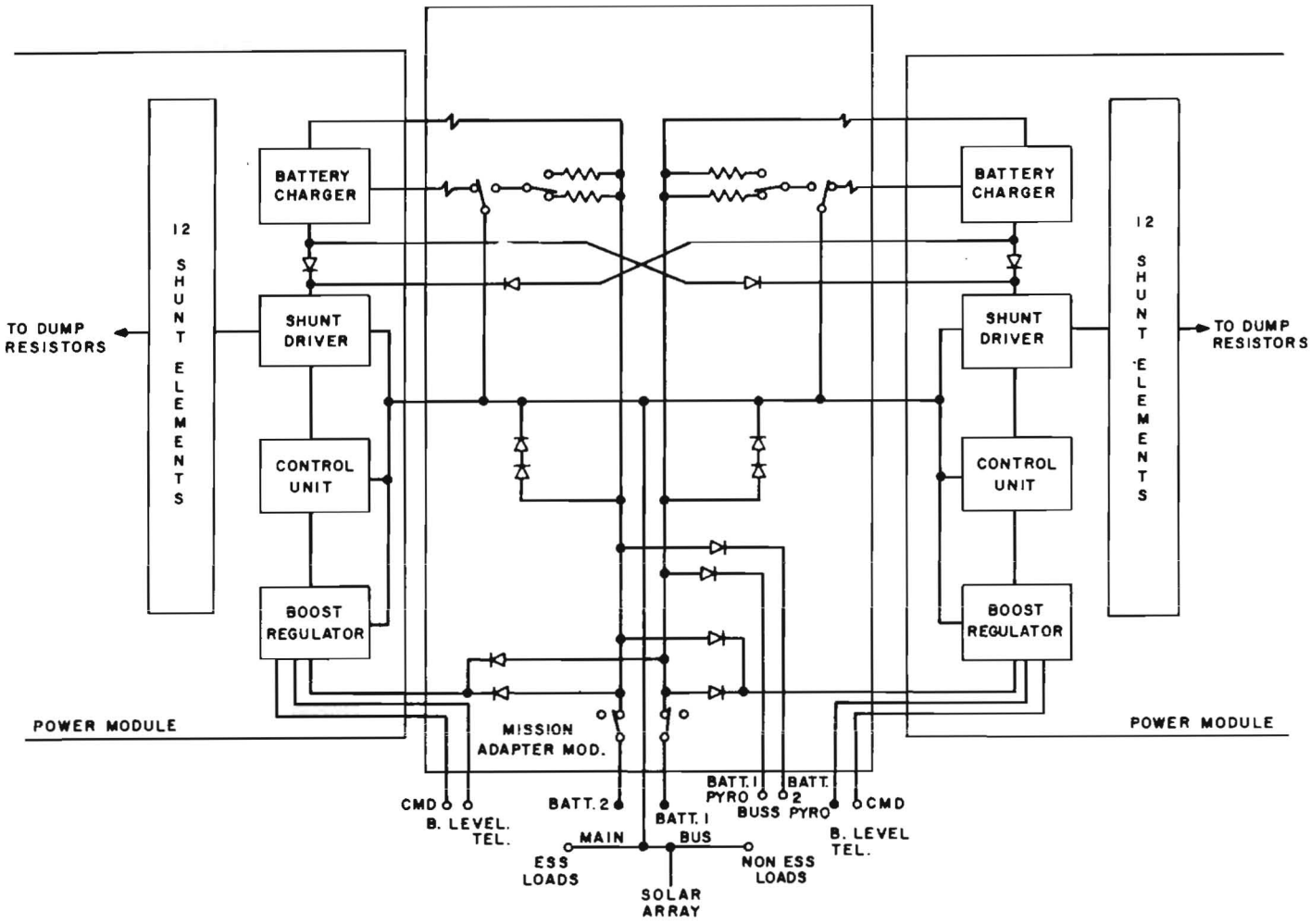

Figure 7-3. IUE Power Supply Electronics

7.2 POWER SUBSYSTEM CAPABILITY AND REQUIREMENTS

The design of the IUE power subsystem was influenced by the following basic requirements:

a. Three-year mission design life with a 5-year design goal.

b. Use of conventional solar conversion/energy storage system with proven design techniques.

c. Redundant units where necessary to assure maximum confidence in achieving design goal.

d. Automatic switchover to redundant units is prohibited.

e. Standardization of basic subsystem functions for maximum commonality with other spacecraft designs.

f. Loads: hold and experiment, 186 watts; transfer orbit, 90 watts.

Specific IUE power requirements involve two phases of the mission: the launch, park and transfer orbit and the mission orbit. During the launch, park and transfer orbit period, the solar paddles are stowed along the sides of the spacecraft. Thus, their output is considerably diminished. However, the spacecraft is in a relatively quiescent mode during this phase, i.e., many components are off and, therefore, the power demand is relatively low. The present estimate of average spacecraft load during the transfer orbit is 107.3 watts. During the mission orbit, the average spacecraft load is estimated to be 217.6 watts. The power subsystem design is based on the requirements imposed by the hold and experiment mode (mission orbit) as an analysis of this mode shows an excess of power demand over the other phases of operation. In addition, the power subsystem must have sufficient battery capacity to support a minimum spacecraft load for a period of 72 minutes. This requirement is due to the fact that the spacecraft will experience solar eclipse periods near this magnitude during the vernal and autumnal equinox periods.

The solar array capability in the stowed configuration is shown in figure 7-7. Power output in the deployed configuration is shown in figure 7-8. It will be noticed that maximum array power (deployed) occurs at a sun angle of $\beta = 67.5^0$. Maximum power expected at Beginning-Of-Life (BOL) and winter solstice is 432 watts. Worst case BOL is 365 watts. For BOL-best case, the array can support the mission orbit requirements from $\beta = 0^0$ through 135^0. BOL-worst case, the system is power positive from $B = 1^0$ through 134^0. After three years in orbit, the worst case prediction shows the system to be power positive from $\beta = 27^0$ through 108^0.

The Power Supply Electronics contains two Power Modules (PM) interfaced by a Mission Adapter Module (MAM), see figure 7-3. The design objective for both power modules was for a nominal 200 watts output capability with 300 watts peak sustainable for an indefinite period. Beyond 300 watts, the supply goes into current limiting. When array output power exceeds spacecraft load requirements, the balance is dissipated through shunt elements and dump resistors. Each power module contains 12 shunts and can dissipate a maximum of 474 watts (948 watts total for both units). A worst case analysis of the solar array (BOL array maximum, nonessential loads off and sun angle $\beta = 67°$) shows that conditions could exist that require dumping approximately 400 watts. The two power modules are identical and operate in parallel through the MAM to control the main bus at 28.0 volts ±2%.

7.3 SOLAR ARRAY

The solar array for the IUE spacecraft is supplied by the European Space Agency (ESA) with the design and development under the cognizance of the European Space and Technology Center (ESTEC), Noordwijk, Holland. Aspects of the solar array mechanical design (including deployment) and predicted thermal performance are covered in Sections 9 and 10, respectively. The information presented in the following technical discussion as well as in the sections referenced above has been abstracted from material supplied by ESA and their contractors, Aerospatiale and AEG Telefunken.

7.3.1 FUNCTIONAL DESCRIPTION

The solar array consists of two rigid solar cell paddles. In the launch configuration, they will be stowed along the satellite body. They will be deployed along the pitch (Y) axis, rotated, and locked at a 22.5^0 angle with respect to the spacecraft roll (X) axis (see figure 7-5).

The orbital power requirements amount to 218 watts to be delivered over 3 years of orbital lifetime. The array illumination is determined by two constraints:

a. The attitude of the spacecraft will be controlled in such a way as to keep the sun vector in the (X, +Z) half plane.

b. The solar array should support the full mission for values of beta between 22.5° and 112.5° for 3 years.

In addition to the supply of power in orbit, the solar array has to provide power in the stowed mode.

7.3.2 POWER OUTPUT

The power output from the array in the stowed configuration is shown in figures 7-6 and 7-7, both of which represent worst case conditions. The loss factors for these figures are presented in table 7-2.

The power output from the array in the deployed configuration is shown in figure 7-8. Again, this is the worst case condition. The loss factors for this case are shown in table 7-3.

The maximum power expected from the array at the beginning of life at winter solstice is 432 watts.

Figure 7-5. Solar Array (Deployed)

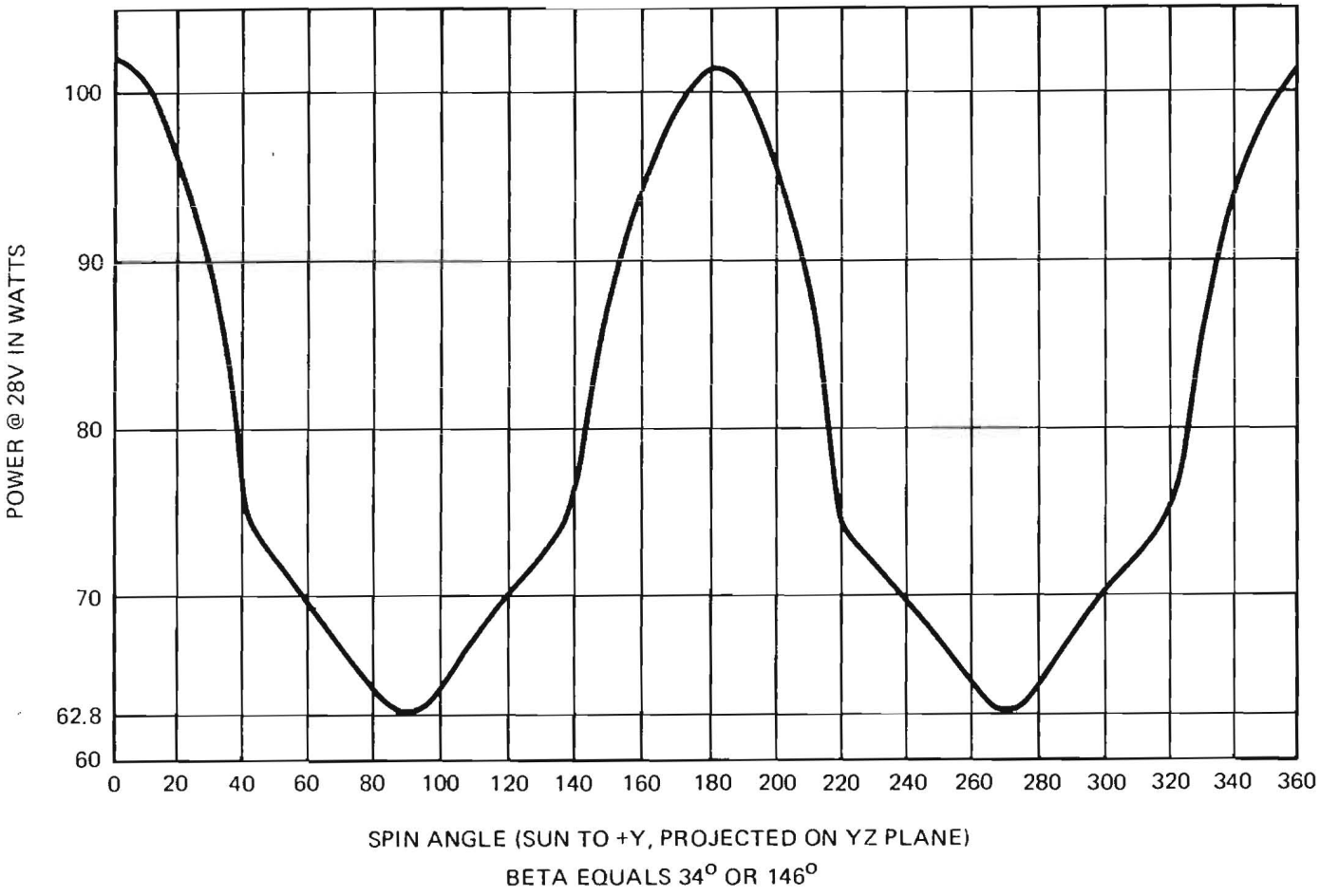

Figure 7-6. IUE Solar Array Power Output in Stowed Configuation

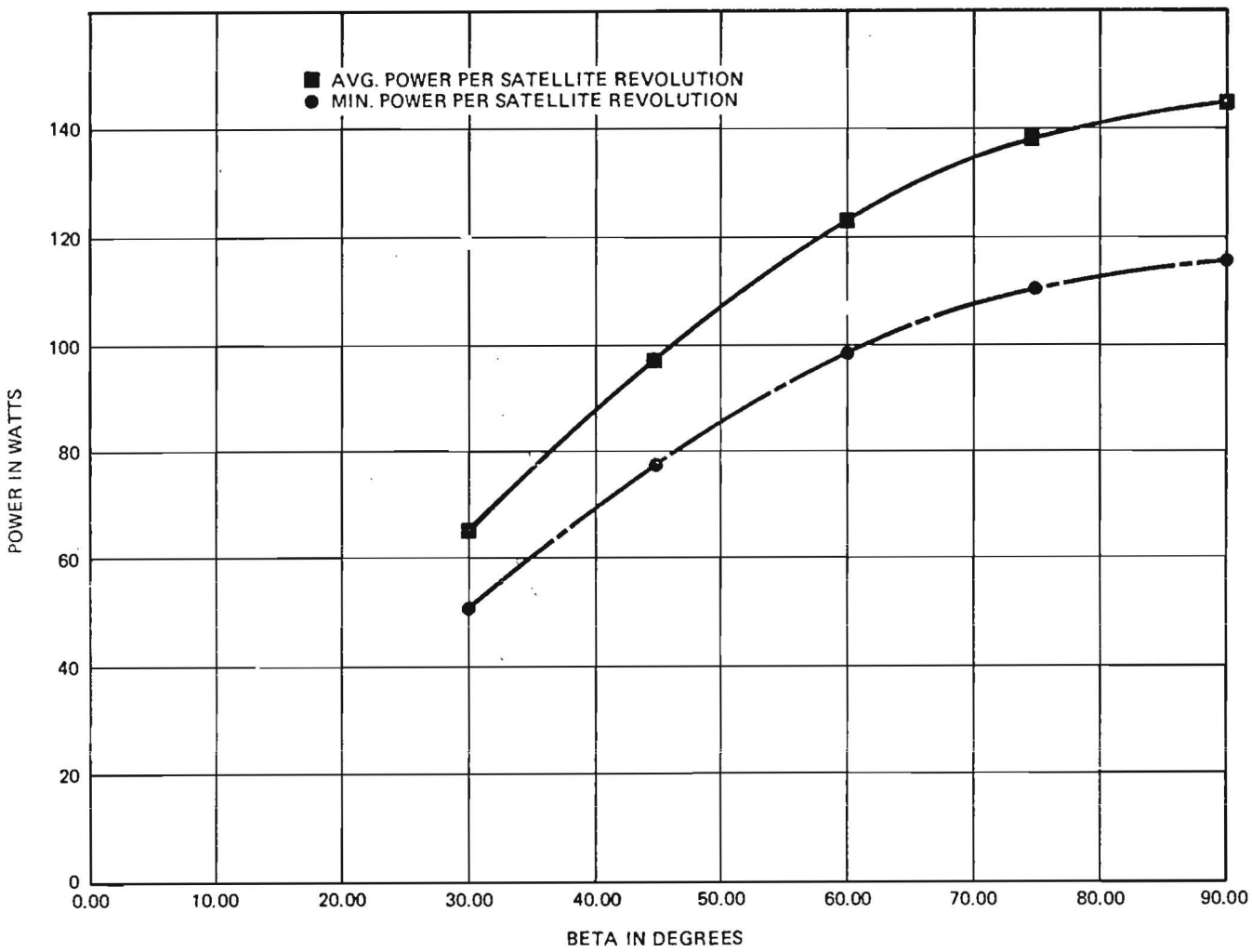

Figure 7-7. Power vs Beta for IUE Solar Array in Stowed Configuration

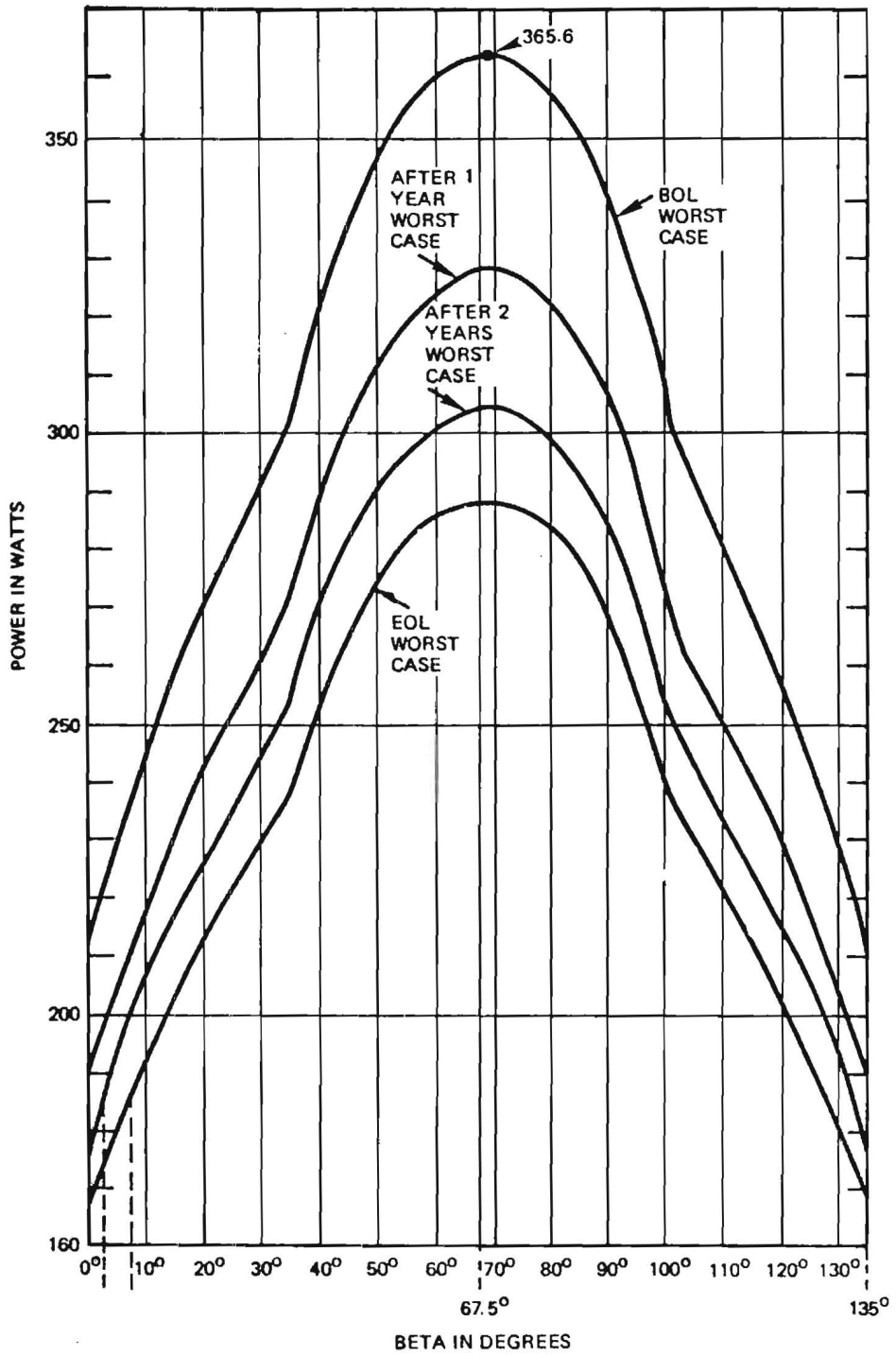

Figure 7-8. Solar Array Available Power

Table 7-2. Array Loss Factors in the Stowed Mode (after 3 transfer orbits)

Sun Intensity	.97
Orientation Error	.999
UV & Micrometeoroids	1.00
Radiation Damage	.986
Mismatching	.99
Reliability Margin	1.00
Design Margin	1.00

Table 7-3. Array Loss Factors in the Deployed Mode (after 3 years)

Sun Intensity	.97
Orientation Error	.999
UV & Micrometeoroids	.99
Radiation Damage	.82
Mismatching	.99
Reliability	.98
Design Margin	.99

7.3.3 SOLAR CELL MODULES

7.3.3.1 Radiation Damage. In the elliptical geosynchronous orbit, the IUE solar array will encounter a total dosage of 4×10^{14} equivalent 1 MeV electrons. This figure includes an allowance for up to five transfer orbits. The radiation damage loss factor of 0.82 in table 7-3 is a result of this dosage.

7.3.3.2 Solar Cells. The cells used on the IUE are nominal 2 cm x 2 cm x .02 cm, and have a resistivity of 1 Ω - cm. The cells are exceptionally efficient, producing 65 mW at 25° C at the beginning of life. The cell anti-reflection coating is TiO_2.

7.3.3.3 Cell Covers. The coverglasses are .01 cm thick cerium doped microsheet. The unusually thin glasses were selected in order to save weight. Even at the end of life, this choice results in a higher power to weight ratio than would be obtained with thicker glasses. The coverglasses extend over the full area of the solar cell including the bar contact. This gives optimum protection against low energy protons.

7.3.3.4 Adhesives. The coverslides will be mounted using DC-93-500 and the cell using RTV 566. This choice of adhesives is dictated primarily by the outgassing requirements of a maximum 1% weight loss and a 0.1% evaporation of condensable materials.

7.3.3.5 Interconnectors. The deep thermal cycles predicted for IUE have made it necessary to employ very carefully designed silver coated molybdenum interconnects. These interconnects will be welded to the cells as opposed to soldering. Welding is preferred over soldering in deep thermal cycles as it is more reliable.

7.3.3.6 Magnetic Cleanliness. The solar array contains only non-magnetic parts and materials. The maximum induced magnetic stray field from the array is 24.3 γ at 1 m from the array in the stowed configuration and 6.0 γ in the deployed configuration.

7.3.3.7 Wiring. To improve wiring reliability and reduce the risk of short circuit on the 28 volt main bus, it has been found preferable to mount the blocking diodes in the spacecraft. Multiple wires link the diode board to all subpanels, thereby ensuring current equalization in the pins of the connectors. One single connector is used per paddle. It is located next to the hinge and thus is accessible on a buttoned up spacecraft. For a 28 volt bus, the voltage drop across the diodes and wiring requires a cell string output of 29.2 volts. Each paddle is also equipped with three temperature sensors.

7.3.3.8 Module Layout. The complete solar array consists of 8 identical lateral subpanels and 4 identical central subpanels which are equally divided between the two paddles. The "upper" subpanels of one paddle are rotated by 180° relative to the "lower" subpanels. This design was chosen to optimize the wiring system on the subpanel rear sides and the harness with respect to mass and structure interface.

Each of the lateral (central) subpanels is equipped with 4 (2) solar cell strings consisting of 75 (69) cells in series and 3 (5) cells in parallel. For design, configuration and manufacturing reasons, each string is divided into solar cell modules using module types of 3 x 15 cells on the lateral subpanels and 5 x 11 or 5 x 12 cells on the central subpanels.

7.3.3.9 Repairs. The 3 x 15, 5 x 11, and 5 x 12 modules are the smallest repair units which will be removed and replaced in case the specially developed repair technique for single cells cannot be used. In either case, the electrical interconnection of the repaired module unit or cell will be done by welding. Both repair types are being subjected to thermal cycling and other design verification tests.

The repairs made on single cells will be done using specially designed equipment. With this equipment, the welding process can be performed outside the manufacturing area.

7.4 BATTERIES

7.4.1 BATTERY DESIGN

The IUE power subsystem utilizes two nickel cadmium batteries interfaced through the mission adapter module in a parallel discharge/independent charge configuration. The batteries are of 6 ampere-hour capacity and are to be used to power the essential loads during shadow periods (which occur during transfer orbit and during the equinox solar eclipse periods). The selection of nickel cadmium batteries was predicated on the three-year design life requirement (five-year design goal) and the demonstrated cycle capability under repetitive deep discharges. Each battery contains 17 series connected cells and weighs 13.6 pounds. Each cell has both the positive and negative terminal insulated from the cell case to assure maximum reliability. In addition, each battery contains one cell which incorporates a third-electrode for overcharge control.

7.4.2 THERMAL CONSIDERATIONS AND CHARGE CONTROL

The IUE battery size is predicated on an average battery life temperature of 10^0 C with variations during the three-year life of $\pm 10^0$ C. The 10^0 C is considered an optimum design temperature for overall life considerations. While battery temperature may vary as much as $\pm 10^0$ C during normal orbital use, it has been demonstrated that batteries operated at 0^0 C will yield twice the life as those operated at 20^0 C and above. Consequently, good thermal control is a necessity for the IUE battery design if the stringent requirements imposed by the mission are to be met.

Battery dissipation usually falls into two categories: dissipation from battery discharging and dissipation from battery overcharging.. During periods when the battery is supporting the spacecraft load, the battery dissipates approximately 16 percent of the electrical energy being supplied to the load as heat. For an average spacecraft load of 186 watts and a boost regulator efficiency of 90%, the dissipation will be approximately 18 watts per battery during discharge and about 3 watts per battery during overcharge.

Since charging is an endothermic process of relatively small magnitude, only the dissipation resulting from overcharge is considered. The selection of the charge control scheme was based primarily on thermal and battery life considerations. Each battery is charged from the 28 volt bus through a series type charger which is a pulse width modulated buck regulator. Charging is accomplished using a maximum current/maximum voltage limit concept. Inasmuch as the available charge time each day is on the order of 23 hours during the eclipse seasons, the selection of a maximum charge rate is based primarily on a tradeoff of available

power (Beta angle), battery recharge time desired, and dependency of battery charge efficiency on charge rate. With a charge rate of 0.6 amperes (c/10), the battery recharge time following a 72 minute eclipse would be approximately 11 hours. Since battery charge efficiency is not appreciably enhanced with higher charge rates and the charge control parameters become more critical with higher charge rates, the c/10 rate is considered to be optimum for the IUE mission.

Battery charging at the c/10 rate is maintained until the third-electrode signals the battery charger to begin reducing the rate of charge. Thereafter, charge rate is a function of third-electrode voltage. When the charge rate is c/50, the battery terminal voltage should be 24 to 25 volts. The primary advantage gained with third-electrode overcharge control for the IUE mission is the reduction of battery thermal dissipation during the long periods when the spacecraft is power positive. In addition, an upper voltage limit of 25.0 volts (1.47 v/cell) is designed into the charger to provide a battery voltage limit at the low temperature (0^0 to 10^0 C) range. No temperature compensation is contemplated for the voltage limit, i.e., the charger will not require a temperature feedback from the battery. Thermal dissipation at the c/50 charge rate is approximately 2.5 watts.

Redundant battery chargers are not provided, however, each charger can fail without loss of the battery associated with the charger. This feature is accomplished by charging the battery from the 28 v bus, through one of two resistors which can be selected by a commandable relay. This maintains the c/10 and c/50 capability with only a few watts sacrifice in power in the event of charger failure. Operating the batteries in this mode requires that the battery charge disable command be sent prior to eclipse to prevent power loss. This requirement is not considered to be a serious consequence since the resistor charge mode is provided for failure contingency only.

The maximum battery discharge rate for eclipse periods is c/1.5 or 4 amperes per battery. At this rate, the batteries will each provide 4.8 ampere-hours over a 72 minute period, resulting in a battery depth of discharge of 80%. For a new battery, the expected terminal voltage is 21.25 v. For a one year old battery at 80% DOD, the expected terminal voltage is 17.85 v. Battery discharge rates greater than c/1.5 can be tolerated for short time intervals, e.g., 12 amperes for 2 minutes.

7.4.3 BATTERY LIFE AND UNDER-VOLTAGE PROTECTION

The original IUE mission profile required a daily solar eclipse period ranging from 55 to 77 minutes per day. A survey of battery life tests which could be related to the IUE mission requirements revealed very little data applicable to predicting IUE battery life performance. As a result, a cell test program relevant to the IUE mission profile was initiated at NAD - Crane in March, 1971. During the interim, the IUE mission profile was changed to preclude the daily eclipse requirement. This action was the result of a spacecraft weight problem which was

solved, in part, by reducing the batteries to one-half their previous size (i.e., from 12 amp-hrs to 6 amp-hrs per battery). Consequently, the batteries will only be used to support necessary loads during the launch, park, and transfer orbit stages, to support necessary loads during solar eclipses (approximately 90 per year). The data from the cell test program is repeated here because even though it does not reflect precisely the ability of the cells to perform the current mission profile the data, nevertheless, gives some insight into the cell's performance capabilities as well as explaining how the under-voltage threshold value was chosen.

The cell test program consisted of subjecting four five-cell test packs to a 24-hour (60-minute daily eclipse) cycle. The daily depth of discharge was 60 percent of rated capacity and each pack was maintained at a different temperature. The test packs 109B (20°C), 75E (10°C), and 123B (0°C) are of particular interest to the IUE design because these packs are at temperatures representative of the design environment for the IUE batteries. Figure 7-9 illustrates the performance for a discharge after 356 cycles at 20° C and compares the discharge with that obtained from the pre-cycling discharge. While the degradation in ampere-hour capacity discharged to 1.25 volts and to 1.10 volts per cell is quite significant, the total loss in capacity to 1.0 volt per cell is only about 16 percent. The exact nature of the battery degradation is more clearly depicted in figure 7-10. It becomes obvious for the IUE mission that the design of the equipment operating from the battery bus voltage should be capable of operating with a minimum input of 17 volts (1.0 volts per cell).

Under-voltage protection is provided by two voltage detectors on each battery. One detector is connected to 8 cells, the other is connected to 9 cells. The threshold level on each detector is set to correspond to 1.0 volts per cell and the two outputs on each battery are OR'ed together. Detection of an under-voltage condition on either battery will result in the removal of all nonessential loads.

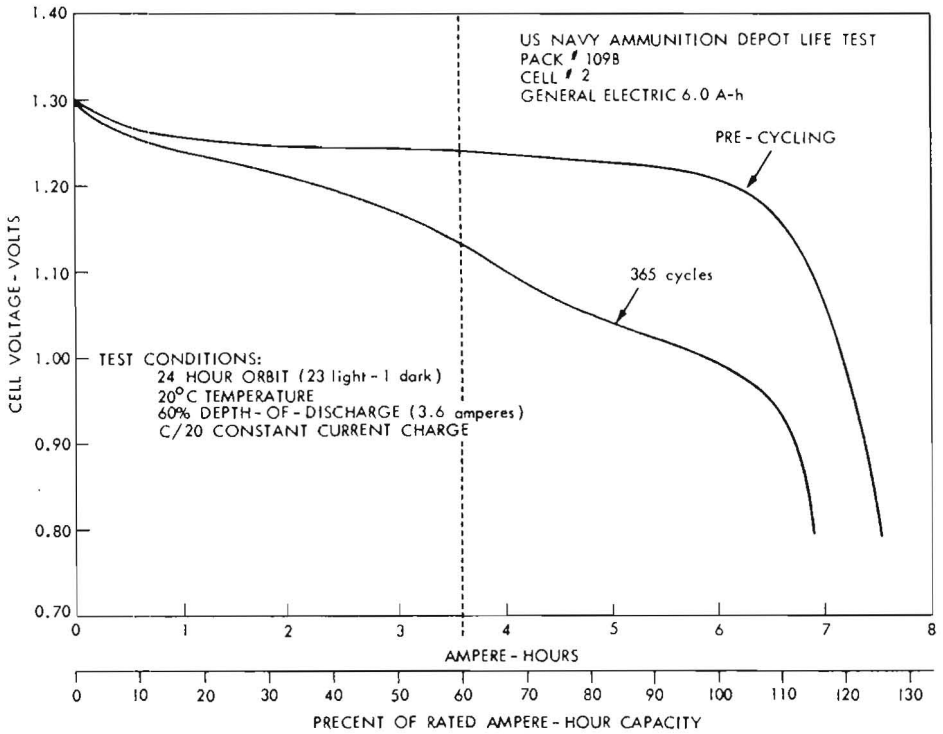

Figure 7-9. Ampere-Hour Characteristics of Ni-Cad Cells on 24 hr. Orbit Test

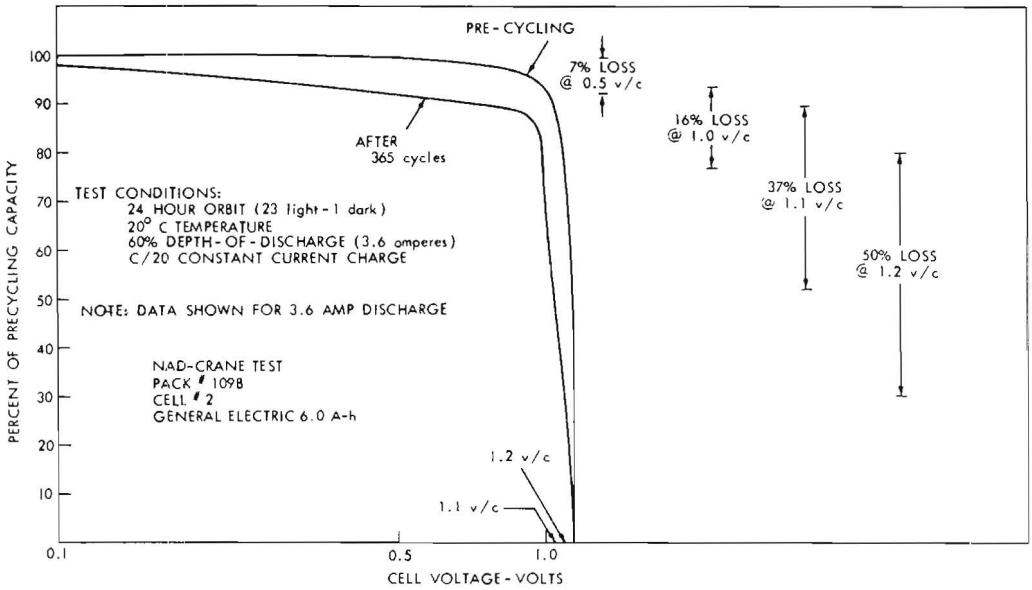

Figure 7-10. Voltage and Ampere-Hour Degradation of Ni-Cad Cells After 365 Cycles

7.5 POWER SUPPLY ELECTRONICS

7.5.1 OVERALL DESIGN CONSIDERATIONS

Design consideration for commonality with other spacecraft has significantly influenced the Power Supply Electronics (PSE) design for IUE. During the study phase for the power system, an additional task was undertaken to develop a modular design for the PSE that would lend itself to a wide range of applications. The concept of a standard power conditioning unit for a DET system was explored in detail and resulted in establishing a modular approach for the power conditioning electronics. Since the DET system had already been chosen for the IUE power system, all work was oriented toward the modularization of the electronics for the DET system.

A basic power unit of 200 watts (nominal) was chosen for the study. This selection was based primarily on the IUE requirement. A review of other spacecraft designs revealed that the basic power unit of 200 watts could be adapted to several missions by adding modules as required to meet power demands up to 1 kw. It also became apparent that for very low power systems (<50 watts) a smaller unit of power should be considered especially where weight and volume are critical.

To standardize on a basic power module requires that each module of power conditioning be capable of operating as a single unit, in parallel with other units and/or as a redundant unit to other units. A second consideration is that functions within a basic power module be capable of continued operation even though other functions within the same module fail, i.e., the failure of a boost regulator within a module should not render the battery charger, control unit or shunt driver inoperative.

The basic power module consists of a battery charger, battery charger/shunt drive, boost regulator, control unit, twelve dump transistors and twelve dump resistors. The dump transistors are packaged in the module. All dump resistors are located external to the PSE. To meet the IUE mission requirement, two of the basic power modules are required, both on line at all times. Each power module contains the functions required for power conditioning in a DET system and either can handle the required power. All interface circuits are located external to the power module.

The successful implementation of this concept is within the Mission Adapter Module (MAM). Figure 7-3 shows the adapter module configured for the IUE mission. The design of this module is mission dependent and provides the flexibility for interfacing the basic power modules to meet the requirements of a variety of missions. One compromise with standardization is an increase in complexity of circuits required to interface modules. This inevitably results in an increase in weight and volume when compared with designs tailored to each specific mission.

7.5.2 MODES OF OPERATION

The Power Supply Electronics (PSE) conditions the solar array energy source and the battery storage element to provide a spacecraft regulated bus as 28 v ±2%. Three modes of operation exist, depending on the available solar array power and the spacecraft load requirements. If the array power is greater than the spacecraft load, the PSE will first provide battery charge current and then dump the excess array power. If the spacecraft load exceeds the solar array output, the difference in power will be supplemented by discharging the batteries through the boost regulator. If the spacecraft load is equal to the solar array power, the PSE will be in a dead-band, or non-operational mode. To ensure these three modes of operation, the 28 volt bus tolerance consists of three bands: the boost-band, from 27.44 to 27.86 v (-2% to -½%); the dead-band, from 27.86 v to 28.14 v (-½% to +½%); and the charge/shunt band, from 28.14 to 28.56 volts (+½% to 2%).

The block diagram shown in figure 7-3 illustrates the functions required in the DET system as applicable to IUE. The control unit controls either the battery/shunt driver or the boost regulator by sampling the bus voltage to determine which operational mode is required. The battery/shunt driver drives the two battery chargers and then the shunt elements in sequence. Redundancy of the PSE is accomplished by the following:

a. Control Unit Two separate reference and error amplifiers.

b. Battery Shunt Driver Two separate complete circuits.

c. Shunt Elements Twelve separate shunt elements for each battery/shunt driver, each element controlling the shunt current through its respective dump resistor located external to the PSE.

d. Battery Charger Battery chargers are two separate complete circuits, each one dedicated to a particular battery and disabled by ground command. Back-up charging is done through resistors controlled by ground command.

e. Boost Regulator Two separate complete circuits.

7.5.3 ELECTRICAL CHARACTERISTICS

a. Control Unit The control unit consists of a single reference element, a voltage divider network, and a differential amplifier. The differential amplier provides two control signals necessary for controlling the operational modes. The control signals consist of: 0 volts for a bus voltage of 0 to 28.14 v, and 0 to 5 volts for a bus voltage of 28.14 v to 28.56 v, and 5 volts for a bus voltage greater than 28.56 v; 0 volts for a bus voltage greater than 27.86, 0 to 5 volts for a bus voltage from 27.86 to 27.44 volts, and 5 volts for a bus voltage less than 27.44 v.

b. Battery Charge Shunt Driver The battery charge shunt/driver is a buffer stage composed of an emitter follower type circuit.

c. Battery Charger Battery charger circuit is a pulse width modulated buck type. The rate of charge is controlled linearly by the battery charge/shunt driver up to the charger preset current limit (approximately 0.6 amperes). A battery voltage sensing circuit maintains the battery voltage at a preset level. In addition a 3rd electrode sensing circuit reduces the battery charge to c/50 rate as the 3rd electrode voltage approaches a preselected limit.

d. Shunt Elements There are 12 linear shunt elements which are driven sequentially to dump any excess solar array power. Only one element can be in the active region at any one time. Each element consists of an operational amplifier driving a Darlington pair. Each Darlington pair is connected to a power dissipating resistor located externally to the PSE to dissipate the excess power at a remote location. The dump resistors are located on the power dump panels on faces D and F of the spacecraft structure. Operating characteristics of the shunt elements are shown in figure 7-11.

e. Boost Regulator The boost regulator consists of a step-up autotransformer and low pass filter. Pulse width modulation is used to maintain the bus voltage within the specified tolerance, in accordance with the output of the control signal, 0 to 5 volts. Input characteristics to the regulator depend on the battery and its state of charge, plus the load required. The regulator is designed for a minimum input of 16 volts and a maximum steady state power of 250 watts. Current limit exists only in the form of limiting maximum transistor current to correspond to an output power of 300 watts. As a result, the output current capability of the regulator depends on the current capacity of the output and input rectifiers and the battery. The boost regulator also has a self-inhibit function which prevents the regulator from driving the 28 v main bus out of limits in the event of a boost regulator or controller failure. Minimum efficiency at maximum load (250 watts) and minimum input voltage (16 v) is 90%.

7.5.4 TELEMETRY AND COMMAND REQUIREMENTS

Telemetry functions and number of channels required for the power system are listed in table 7-4. Note that due to the large dynamic range of battery currents, two sensors per battery are required to provide adequate resolution. Also, due to the large dynamic temperature range predicted for the solar arrays (60 to -165 C) and the variation in

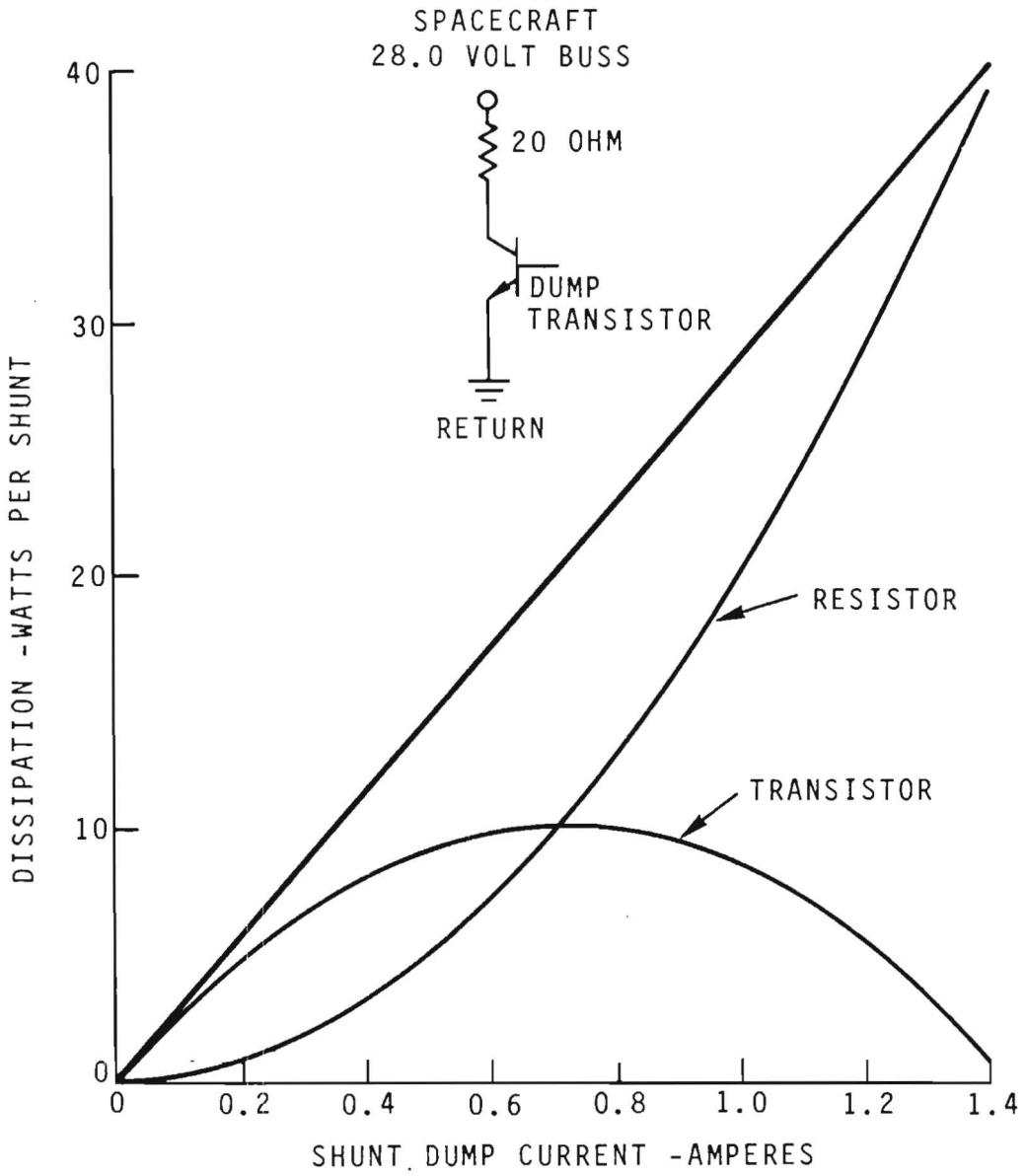

Figure 7-11. Operation of IUE Power Subsystem Shunt Element

Table 7-4. Power System Analog Telemetry Requirements

Function	Number	Comment
Telemetry - Analog		
Solar Array Current (Left Paddle)	1	
Solar Array Current (Right Paddle)	1	
Shunt Dump Current (Total)	2	Parallel operation of shunts requires 2 sensors
Battery 1 Chg/Dischg Current (High/Low Range)	2	Range of currents requires two sensors
Battery 2 Chg/Dischg Current (High/Low Range)	2	Range of currents requires two sensors
Spacecraft Load Current	1	
Essential Load Current	1	
Solar Array Temperature (Left)	3	Three per paddle
Solar Array Temperature (Right)	3	Three per paddle
Battery 1 Temperature	1	
Battery 2 Temperature	1	
Power Supply Electronics Temperature	3	One per module
Battery 1 Voltage	1	One provides high resolution
Battery 2 Voltage	1	
28.0 Bus Voltage	2	
Third Electrode Voltage #1	1	
Third Electrode Voltage #2	1	

temperature of each paddle section with Beta, three platinum wire temperature sensors are required on each paddle. Table 7-5 lists those functions related to the power subsystem that require command capability. All functions are of the latching type.

7.5.5 MECHANICAL AND THERMAL DESIGN

The packaging concept for the PSE is shown in figure 7-12. Each power module is packaged in a magnesium frame approximately 6.13" (15.57 cm) x 8.06" (20.47 cm) x 5.00" (12.70 cm). The bottom of each power module has the heat sink for mounting the large heat dissipating components in the PM. The Mission Adapter Module (MAM) is mounted on top of the two power modules and contains the necessary connectors for interfacing the PSE to the other power system components (array and batteries) and spacecraft harness. The MAM is approximately 4.34" (11.02 cm) high.

Since the MAM contains the battery-to-boost regulator diodes and the signal conditioning circuits, provision is made in the design for conduction of some heat through the PSE to the equipment platform. The overall dimensions of the PSE are 12.29" (31/19 cm) x 8.06" (20.47 cm) x 9.35" (23.75 cm) high. Total weight is 29.5 pounds. Circuits which generate Electromagnetic Interference (EMI) are independently shielded to prevent interactions with sensitive circuits as well as to provide double shielding to external portions of the PSE.

The high power dissipating units of the PSE are as follows:

a. Power Module

   (1) Boost regulator (2 units).

   (2) Shunt elements (1 to 12 units).

   (3) Battery charger (2 units).

b. Mission Adapter Module

   (1) Battery-to-boost regulator diodes.

   (2) Signal conditioning circuits.

Power dissipation in the battery chargers is a nominal 2.5 watts each during charge. Power dissipation in the shunt elements will depend on the difference between the solar array power available and spacecraft power demand (see figure 7-11 for shunt element power dissipation). When in the boost mode, power dissipation in the boost regulator is approximately 11 percent of the spacecraft load. In addition, when the boost regulator is on, the battery-to-boost regulator diodes dissipate

Table 7-5. Power System Command Requirements

Function	Number	Telemetry Bi-Level	Comments
Boost Regulator #1 (ON/OFF)	2	1	All functions are latching type (no toggle)
Boost Regulator #2 (ON/OFF)	2	1	
Battery 1 (Disable/Enable)	2	1	
Battery 2 (Disable/Enable)	2	1	
Battery 1 Charger (Enable/Disable)	2	1	
Battery 2 Charger (Enable/Disable)	2	1	
Load Remove Comm'd (Inhibit)	2	1	
Battery Undervoltage Detector (Enable/Disable)	4	2	
Main 28.0 Bus Over Current Detector (Enable/Disable)	2	1	
Main 28.0 Volt Bus Detector (Enable/Disable)	2	1	
Third Electrode 1 (Enable/Disable)	1	1	Battery 1 & 2 enable cmds enable 3rd electrode
Third Electrode 2 (Enable/Disable)	1	1	
Battery 1 Charge (High/Low)	2	1	Low rate is trickel charge command.
Battery 2 Charge (High/Low)	2	1	Performs function of Third Electrode in active control mode.

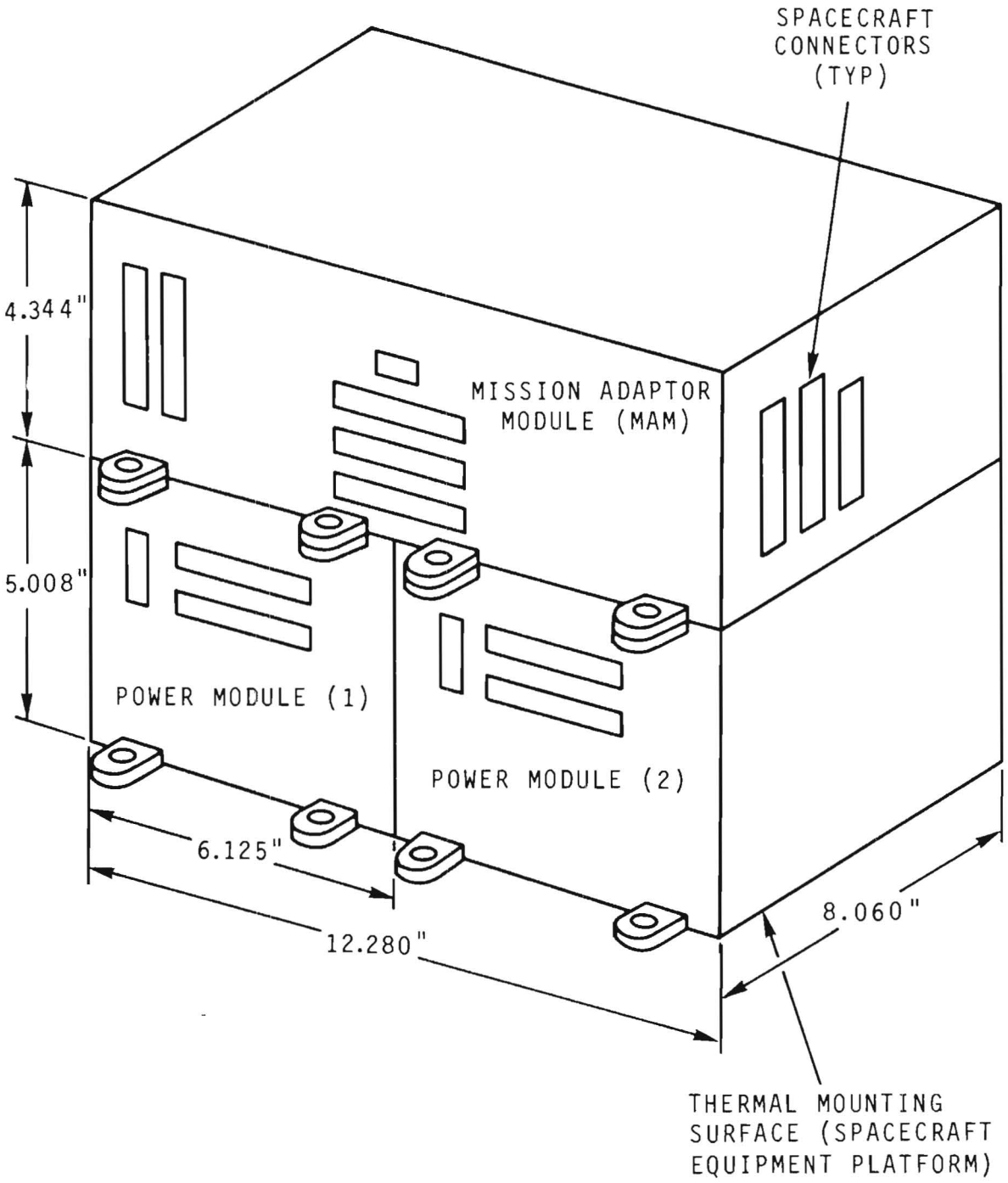

Figure 7-12. PSE Mechanical Configuration

an amount equal to approximately 5.2 percent of the spacecraft load. Maximum total PSE power dissipation could be as high as 24 watts under some modes of operation. Standby power losses for the PSE (i.e., no loads on the power subsystem) are estimated to be as follows:

a. Control unit: 560 mW.

b. Shunt driver: 1000 mW.

c. Shunt elements: 2400 mW.

d. Battery charger: 1000 mW.

e. Boost regulator: 600 mW.

f. Relay drivers: 0

g. Total: 5.56 watts.

7.6 DIODE FILTER BOXES

The IUE power subsystem uses two diode filter boxes to interface the solar array with the Power Supply Electronics (PSE). The two boxes (one per solar array paddle) are located external to the PSE near the solar array hinges on the main equipment platform. The diode filter boxes contain the solar array blocking diodes and filter pin connectors. The purpose of the filter pin connectors is to shield the solar array input to the PSE from EMI. Each box weighs approximately .6 lb. Total power dissipation from the array blocking diodes is approximately 3.2 percent of the solar array power. With a maximum array output of approximately 432 watts (BOL at winter solstice), the dissipation in the blocking diodes is approximately 13.8 watts.

FROM: IUE SYSTEM DESIGN REPORT
VOL.II - SPACECRAFT DESIGN - JUNE 1976

SECTION 8. STABILIZATION AND CONTROLS SUBSYSTEM

8.1 DESIGN PHILOSOPHY

8.1.1 OBJECTIVES

The principal objective of this phase of the study has been the design of an attitude control system that is simple and reliable on one hand and has the best chance of meeting the IUE mission requirements on the other. The need to conform to IUE project ground rules and spacecraft physical constraints, which are relatively stringent, and at the same time satisfy the pointing and slew accuracy specifications, which are quite precise, has necessitated the study of many alternatives before one viable design approach was finally selected and pursued in detail. A deliberate attempt has been made to use proven design concepts, utilize flight qualified or readily available hardware, draw from the experience of previous and ongoing Goddard programs of a comparable nature and achieve component commonality with the SATS program as much as practicable. In terms of the more important control requirements, the IUE mission is quite similar to the Orbiting Astronomical Observatory (OAO) missions. The IUE and the OAO control systems are fundamentally alike. They, however, differ significantly in several respects because of important differences in mission characteristics and operational requirement.

8.1.2 CRITICAL REQUIREMENTS

Section 8.2.2 describes in detail the IUE mission profile, the various spacecraft operating modes and the functional requirements during these modes, as well as the various ACS modes, and the performance specifications of these modes. In this section, an attempt is made to describe the more critical ACS requirements that would satisfy the IUE scientific objectives and to explain the rationale behind the four important choices that must be made during the ACS design of any spacecraft: the selections of the basic design concept, the torquing devices, the attitude sensors, and the logic circuitry and electronics to mechanize the control laws and provide information flow from the attitude sensors to the torquing devices. Figure 8-1 shows the spacecraft control system axis definition and figure 8-2 presents an overall block diagram of the control system including interface with other subsystems.

The block diagram shows the intimate interrelationship of the other IUE systems with the Attitude Control System (ACS). This is particularly true for the interface with the Data Multiplex Subsystem (DMS). Since all control modes of the IUE ACS have either a software backup or are implemented solely with a software algorithm, the DMS interface with the ACS is the

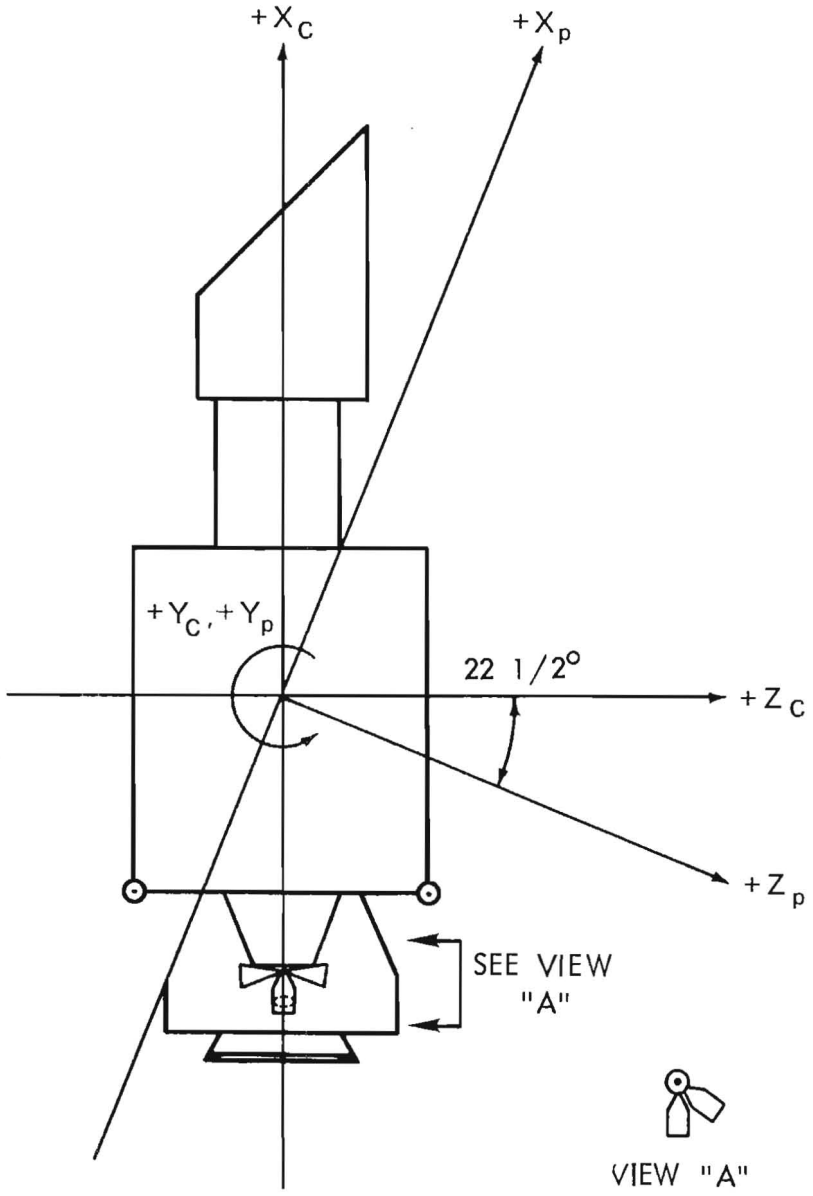

Figure 8-1. Axis Definition for IUE Controls System

source of all information inputs to the OBC regarding ACS sensors. The source of all control decisions from the OBC to the ACS must proceed through the Command Subsystem. In this respect, the IUE ACS conforms to the conventional control system loop using input sensors, processors and actuators/drivers with vehicle dynamics closing the loop.

Also evident from the block diagram is the complete redundancy used throughout the ACS loop. All input sensors except the Spin Mode Sun Sensor and Coarse Analog Sun Sensor set are duplicated with identical, isolated sensors. All inputs to and through the DMS are hardware redundant as are the OBCs and the Command Subsystem. All the actuators and their drivers are redundant in some fashion. This redundancy is also obvious in the portion of figure 8-2 showing the RF Subsystem and Power Subsystem.

The principal IUE requirements that have largely influenced the ACS design philosophy are:

a. Three-axis stabilization in inertial space with ± 1 arc-second pointing accuracy requirement in pitch and yaw, for periods typically ½ hour and more. There is no rate stability or jitter requirement. There is also no precision pointing requirement in the roll axis. However, for reasons described later (section 8.3.1.4) the hold-mode roll accuracy has been specified to be ± 60 arc-second.

b. Following a slew or a sequence of slew maneuvers, the new target must be acquired within the 8 arc-minute half-cone angle field of the telescope as seen by the Fine Error Sensor (FES). The FES in Field Mode can scan a square of up to 18 x 18 arc-minute. To ensure target acquisition implies an accuracy requirement of ± 2 arc-minute per axis slew for any angle of slew.

c. The pointing accuracy requirement must be satisfied for extended periods of time even when stellar attitude measurements of sufficient accuracy and frequency are not available. This is the case when the Fine Error Sensor is used for stellar updates and there may be many tens of seconds or several minutes of time between consecutive samples.

d. The expected useful operating life should be 3 to 5 years.

e. The spacecraft will be maintained in an elliptical synchronous orbit and a nearly continuous communication and command link will be available.

8.1.3 CONTROL CONCEPT

The control concept considered most suitable for the IUE is a momentum exchange control system, designed on a single-axis basis using reaction wheels, as in the OAO. All-axis stabilization in inertial space implies that the three control axes are essentially decoupled. There is of course, some gyroscopic coupling when the spacecraft is slewing on one axis, but the holding accuracy requirement in the other two axes can be relaxed easily in such circumstances.

The secular momentum buildup caused by the integrated effects of environmental disturbances and orbital-control-thruster misalignments must be relieved to prevent saturation of the reaction wheels. The low level of disturbances at synchronous altitude implies that the task of momentum removal would be a small incremental load on the hydrazine propulsion system already present for orbit control and adjustment. It has therefore been decided to combine the two functions and drive the ACS jets by the hydrazine system. The unpredictability of the earth's magnetic field at synchronous altitude rules it out as a practical choice for IUE.

The 3 to 5 year design life raises the question of reaction wheel reliability. On many Goddard programs, reaction wheels have demonstrated reliable performance over long periods of time. One redundant reaction wheel skewed symmetrically with respect to the orthogonal control axis is being used to provide degraded control in the event of a failure of a prime wheel.

8.1.4 ATTITUDE SENSORS

The choice of attitude sensors is somewhat involved. Other things being equal, a cooperative target is always the easiest to track for any pointing control system primarily because of the self-calibrating nature of the system. The optical design of the IUE has, however, precluded the possibility of using either the spectrometer or a star sensor in close proximity to produce error signals off the target star. An offset pointing model has therefore been selected where one or more guide stars from the star field surrounding the target star generate the error information. Two alternative modes can be used for experimentation with an offset guide star. In the first mode, used with a bright guide star, the Fine Error Sensor is operated in its Track Mode and produces pitch and yaw error voltages of up to one hertz information content from the guide star. The second mode, used for dim guide stars also involves operating the FES in its Track Mode. To operate with such a limited information rate requires that the gyros supply pitch and yaw error signals with corrections to the gyros and pointing made at each software update. Implementation involves Kalman filtering of the gyro signals, processing FES signals through a Butterworth filter and combining both via an OBC algorithm to supply the

error voltages. Decision on which mode to be used is based on guide star magnitude with a goal of using +11 m stars or brighter as direct guidance sources.

A high-accuracy position control loop can be designed using a position sensor as a measurement device if it has sufficiently low noise and sufficiently large bandwidth. With increasing noise and decreasing bandwidth, a high-gain system tends toward instability and an independent rate sensor, such as a gyro, becomes necessary for rate damping. With further reduction in the position sensor bandwidth, as in the case of the IUE with stellar updates on dimmer guide stars, more reliance must be placed on the gyroscopic inertial reference for maintaining attitude in addition to providing rate damping. In a sense, the basic nature of the control system changes. The initial case is a position control system using a star sensor for attitude information and a gyro for rate measurement. The modified system, for the IUE case, is a position control system using a gyroscopic reference for both position and rate information and a star sensor for occasional updates and low frequency drift calibration of the gyro. The feasibility of this concept has been very critically examined and demonstrated. The basic results of this study are documented in Section 8.3.1.5 and Reference 20

The outcome of the above analysis is the requirement of a very precise, well calibrated, gyroscopic inertial measurement system capable of maintaining the reference to sub-arc second accuracy for several minutes of time in pitch and yaw. Independently of this analysis, a study of the slew mode requirements also leads to a similar conclusion about the need of a precise inertial reference system, albeit with somewhat relaxed accuracy specifications. In the absence of a gyroscopic system, well separated guide stars must be sensed by two star trackers to maintain inertial attitude information during slew. This implies use of several gimbaled star trackers as in one mode of the OAO. However, experience on OAO has shown that it is preferable to use an inertial reference unit (MIT-IRU) for slew. The same conclusion is considered valid for the IUE. The required slew accuracy is approximately the same on the IUE and the OAO.

Single-degree-of-freedom, hydrodynamic gas bearing, rate-integrating gyroscopes with pulse-rebalance electronics have been chosen as the instruments to meet the IUE requirements. The gas bearing effectively eliminates the bearing failure mechanism under normal operation and also cuts down significantly on the output noise. Pulse rebalancing provides much better readout accuracy compared to analog rebalancing. These gyros are to be used in a strapdown mode, as are the OAO gyros.

While such long lived spacecraft as the OAO demonstrate that good, high quality gyros can operate for at least 30,000 hours (to date) in orbit without failures or degradation, prudence dictates the use of redundancy

in hardware to ensure meeting the IUE 3 to 5 year operating goal. The usual method of employing redundancy would involve the use of two, three-axis gyro packages with their inputs aligned to the spacecraft control axes. This type of redundancy is often improved by providing that any combination of gyros in either package can be used permitting operation even in the event of gyro failures in both systems. Unfortunately, if both gyros sensing about the same axis should fail, control about that axis is lost.

The mechanization of gyro redundancy on IUE involves the use of six individual gyroscopes mounted in a single package. The input axes of the gyros are skewed in relation to each other and the spacecraft control axes. As a result, each gyro senses some component of input rate about any spacecraft axis. If the outputs of any three gyros are combined in proper fashion, this input can be identified with the axis about which it is occurring and a corrective signal to the actuator(s) for that axis can be developed. With this scheme as many as three, any three, gyros can fail without seriously impacting system performance and accuracy. Section 8.3.2 documents the inertial reference study that was the basis for this design.

8.1.5 CONTROL LOGIC MECHANIZATION

Section 8.3.1 documents the computation requirements required to process the gyro output including performance monitoring. The continuous communication and command link can be utilized to advantage for infrequent operations such as the initial calibration and monitoring of input axis alignments, scale factor instability, failure detection and isolation, and similar nonroutine tasks. Computations needed on a routine operational basis are best done onboard. There are 42 different ways in which three-axis information can be extracted from six gyros, each involving between 9 and 18 multiplications with weighting factors depending on postlaunch calibrations of input-axis alignments. Hardwired, special purpose circuitry for this purpose would tend to become quite complex and inefficient. A small general purpose computer will be used to handle the job, providing more accuracy, flexibility and versatility than hardwired circuitry, and also carrying out the attitude control and some data processing computations. Specifications on the computer are given in Section 6.4.

Use of the ground link will be limited mainly to infrequent and one-shot operations, such as calibration, health check, wheel unload commands and slew commands, more or less in an off-line fashion. All on-line routine computations will be done by the flight computer. Real-time control of the spacecraft via ground command as a regular operational procedure is considered undesirable for many reasons, including cost effectiveness, loss of precision, and the possible drastic effects of loss of data link even for a short time. However, provision has been

made so that the wheels and jets can be commanded from the ground, thus allowing backup ground control modes. There are two special cases where parallel ground computations may be utilized in spacecraft operation. The first is the possibility of tracking a fast-moving stellar object such as a comet. In this case, a ground computer could carry out the navigational computations and generate the three-axis slew commands. The second is to allow modeling the inertial reference system accurately on the ground. Apart from producing more accurate calibrations and bias estimates than is possible via the flight computer calculations, this will be an invaluable aid for a better understanding of precision inertial reference systems, leading to more efficient operation of the IUE mission, in a bootstrap fashion, and also of future space missions utilizing similar inertial components.

8.2 GENERAL SYSTEM DESCRIPTION

8.2.1 CONFIGURATION

The IUE control system has evolved into a much simplified concept centered around an on-board digital computer. A block diagram of the controls concept is presented in figure 8-2, section 8.1.2. The sensors are aligned along the lower left side of the figure with the actuators shown on the lower right hand side. Much attention has been devoted to simplicity and redundancy in this final concept.

8.2.1.1 Sensors. The sensors and their functions during the mission life are summarized below.

a. Six Analog Sun Sensors. These sensors provide sun altitude information (two axes) during initial sun acquisition and settling. Six sensors are utilized and are arranged to provide 4π steradian coverage. The units are identical to those used on OAO and ATS.

b. Panoramic Attitude Sensor (PAS). This system originally developed for RAE-B, provides a redundant 4π steradian coverage during the transfer orbit for earth/moon "look" angle. This system consists of two, redundant sensor heads each having a dedicated electronics package. This system is a major improvement over the fixed earth sensor system formerly used on other spacecraft for attitude determination in the transfer orbit. The sensor system also provides a sun-centered pulse so that "spin-sectoring" can be accomplished during this transfer ellipse. In addition, the PAS will be used to help establish (or reestablish) spacecraft attitude prior to stellar acquisition.

c. Redundant Accelerometer Unit. This unit will be similar to that developed for the SMS program. The package consists of redundant, linear force-rebalanced accelerometers. The redundant acclerometers are algined such that their input axes are parallel to the vehicle thrust (or spin) axes. Information from those units will be used to implement active nutation control during the spin portion of the total mission.

d. Fine Digital Sun Sensors (FSS). This system is comprised of two redundant subsystems - each subsystem consisting of two sensor heads and a dedicated electronics assembly. Each subsystem provides two axis digital attitude information with respect to the sunline. The redundant sensor systems are aligned to provide sun angle information during all experiment modes of operations. The information is required to monitor spacecraft slews and update the precision gyro set. A similar digital sensor head was flown on OAO-C.

e. Inertial Reference Assembly (IRA). This precision gyro set consists of six, gas-bearing gyros with their input axes skewed mutually and relative to the spacecraft control axes. By definition this inertial package is the prime sensor of the stabilization and control system. The incremental position information provided by the IRA will be used in conjunction with the on-board computer to drive the reaction wheels during all fine hold and slew modes. Although the unit is a new development, much effort has been expended to date to ensure adequate performance of this sensor (see section 8.3.1.5).

f. Fine Error Sensor (FES). The redundant fine error sensors are located in front of the experiment aperture. The units utilize the telescope light gathering optics and in addition are mechanized with offset capability out to a half cone of 8 arc minutes. Information from these sensors will be used to trim the precision gyro set for the experiment mode. In addition, they can be used as prime sensors to hold the pitch and yaw axes when a bright star and the experiment star both fall within the FES' field-of-view.

g. Spin Mode Sun Sensor (SMSS). This system consists of a single sensor head and its associated electronics package. The SMSS is used primarily in the transfer ellipse to measure sun angle with respect to the spacecraft x-axis. The sensor field-of-view is 180° x 0.5°. Spacecraft alignment is such that its field-of-view is centered on the $-Z_C$ axis along the spacecraft x-axis. This sensor also provides a sun-centered pulse as the field-of-view sweeps through the sun.

8.2.1.2 Actuators. As shown in figure 8-3 the control system further consists of four reaction wheels and twelve hydrazine engines. These actuators are used together and/or separately to provide the reaction torque in the spacecraft control laws. The actuators and their function during the mission life are summarized below.

a. Hydrazine Engines. The twelve hydrazine engines carried on-board the IUE, are subdivided into four pods. Two pods contain two low thrust (0.3 pound) engines and two high thrust (5.0 pound) engines. The other two pods contain only two low thrust engines each. The low thrust engines provide a redundant set of torques for despin, sun acquisition, and momentum unloading. They can be fired by the ground command systems, the on-board computer and by a hardwired despin and sun acquisition algorithm. The high thrust engines provide a redundant set for nutation control and precession during the transfer orbit, and Delta V corrections to orbital drift after final orbital parameters and longitude have been achieved. Note that the thrust of the small engines will decline from 3.0 to 0.1 pound and the large engines from 5.0 to 3.5 pounds as blow down pressure drops due to hydrazine depletion.

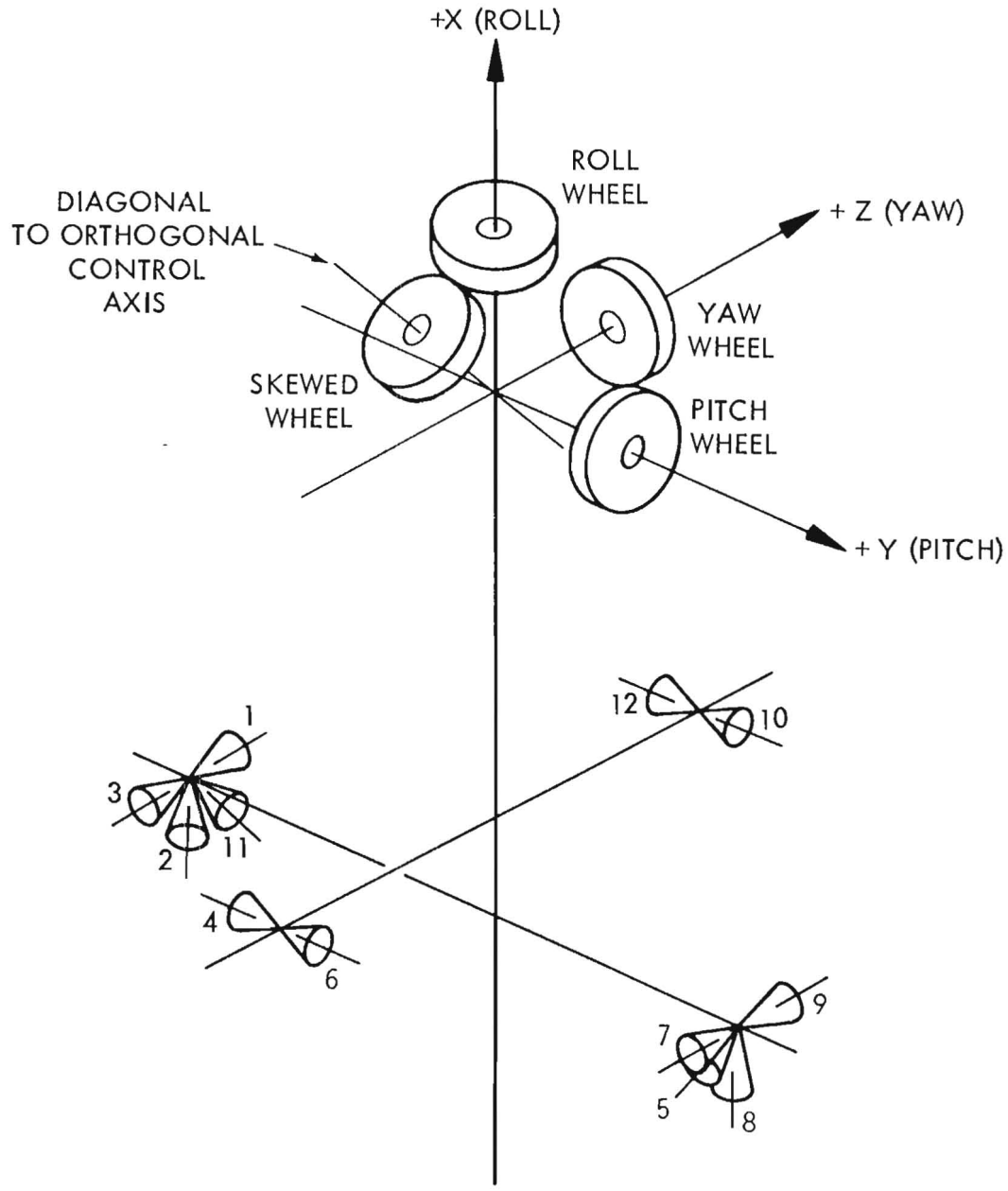

Figure 8-3. IUE Actuator Configuration

b. Reaction Wheels. The four reaction wheels in the control system concept are identical to the Nimbus-D yaw reaction wheel. Three reaction wheels are aligned to the spacecraft pitch, yaw and roll control axes. The fourth wheel is skewed symmetrically with respect to the orthogonal control axes. This unique configuration will provide redundancy in the event the pitch, yaw or roll wheel inadvertently fails during the mission life.

8.2.1.3 Control Electronics Assembly (CEA). This assembly which provides the interface between the sensors and actuators is depicted in figure 8-4, the expanded ACS logic diagram. The unit consists of eight cards with functions as defined below.

a. DAC and Command Decoder. Reaction wheel commands are serially gated into this card from either Command Decoder. The card is totally redundant with command cross-strapping at its input. This module outputs redundant analog wheel commands to the four wheel driver cards in the wheel driver assembly.

b. Engine/Valve Command Logic. Hydrazine System Engine and valve serial commands are gated into this card from either command decoder. The card is totally redundant with command cross-strapping at its input. This module outputs to each of the engine/valve driver cards in the control electronics assembly.

c. Precession/Nutation Card. This card provides the digital logic for spin sectoring, precession commands, active nutation control and engine mode selection. The spin sectoring portion receives a sun-centered pulse from the Panoramic Attitude Sensor and an input from the spacecraft clock. With this information available, the spin period is divided into 128 parts. The current sector status (position) is maintained and updated throughout each spin cycle. This logic information on the spin status is interfaced with both the precession command logic and active nutation control logic. In the precession logic the current sector status is compared with a ground command consisting of three parts: sector ID to start firing a precession thruster, sector ID to stop firing a precession thruster, and the number of consecutive spin cycles during which the precession jet will be fired.

d. Compensation and Mixing Card. This card receives analog sun sensor information and rate information and combines them to form logic levels to drive the low level thrusters during despin and sun acquisition and also to drive the reaction wheels during the sun hold mode of operation. The rate information from the IRA also provides a three-axis, rate limit mode of operation on the reaction wheels.

e. Engine/Valve Driver Cards 1 and 2. These redundant cards serve as the power stage to drive the hydrazine system's engine solenoids and transfer valve solenoids. The outputs from each of the redundant cards are OR'd together via isolation diodes to drive the common solenoids.

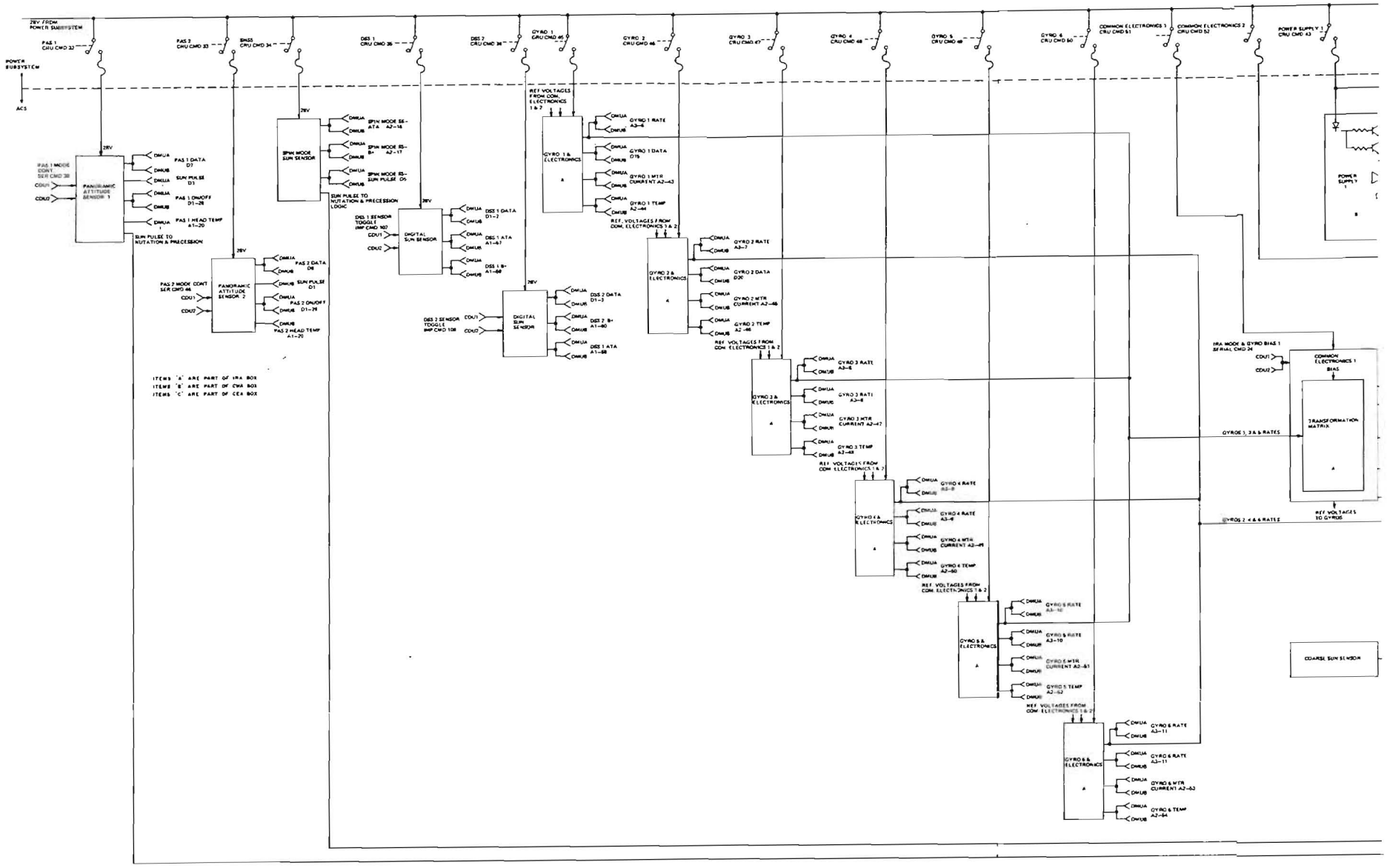
28V FROM POWER SUBSYSTEM
PAS 1 CMD 32
PAS 2 CMD 33
BMSS CMD 34
DSS 1 CMD 36
DSS 2 CMD 36
GYRO 1 CMD 45
GYRO 2 CMD 46
GYRO 3 CMD 47
GYRO 4 CMD 48
GYRO 5 CMD 49
GYRO 6 CMD 50
COMMON ELECTRONICS 1 CMD 51
COMMON ELECTRONICS 2 CMD 52
POWER SUPPLY 1 CMD A3
POWER SUBSYSTEM
ACS
PANORAMIC ATTITUDE SENSOR 1
PAS 1 DATA D7
SUN PULSE D1
PAS 1 ON/OFF D1-28
PAS 1 HEAD TEMP A1-20
SUN PULSE TO NUTATION & PRECESSION
SPIN MODE SUN SENSOR
SUN PULSE TO NUTATION & PRECESSION LOGIC
PANORAMIC ATTITUDE SENSOR 2
PAS 2 DATA D8
PAS 2 ON/OFF D1-28
PAS 2 HEAD TEMP A1-20
DIGITAL SUN SENSOR
DSS 1 DATA D1-2
DSS 1 ATA A1-67
DIGITAL SUN SENSOR
DSS 2 DATA D1-3
DSS 2 ATA A1-68
GYRO 1 & ELECTRONICS
GYRO 1 RATE A3-6
GYRO 1 DATA D19
GYRO 1 MTR CURRENT A2-43
GYRO 1 TEMP A2-44
GYRO 2 & ELECTRONICS
GYRO 2 RATE A3-7
GYRO 2 DATA D20
GYRO 2 MTR CURRENT A2-46
GYRO 2 TEMP A2-46
GYRO 3 & ELECTRONICS
GYRO 3 RATE A3-8
GYRO 3 MTR CURRENT A2-47
GYRO 3 TEMP A2-48
GYRO 4 & ELECTRONICS
GYRO 4 RATE A3-9
GYRO 4 MTR CURRENT A2-49
GYRO 4 TEMP A2-50
GYRO 5 & ELECTRONICS
GYRO 5 RATE A3-10
GYRO 5 MTR CURRENT A2-51
GYRO 5 TEMP A2-52
GYRO 6 & ELECTRONICS
GYRO 6 RATE A3-11
GYRO 6 MTR CURRENT A2-53
GYRO 6 TEMP A2-54
REF VOLTAGES FROM COM. ELECTRONICS 1 & 2
IRA MODE & GYRO BIAS 1 SERIAL CMD 24
COMMON ELECTRONICS 1 BIAS
TRANSFORMATION MATRIX
GYROS 1, 2 & 3 RATES
GYROS 2 + 4 & 6 RATES
REF VOLTAGES TO GYROS
COARSE SUN SENSOR
ITEMS 'A' ARE PART OF IRA BOX
ITEMS 'B' ARE PART OF CWA BOX
ITEMS 'C' ARE PART OF CEA BOX

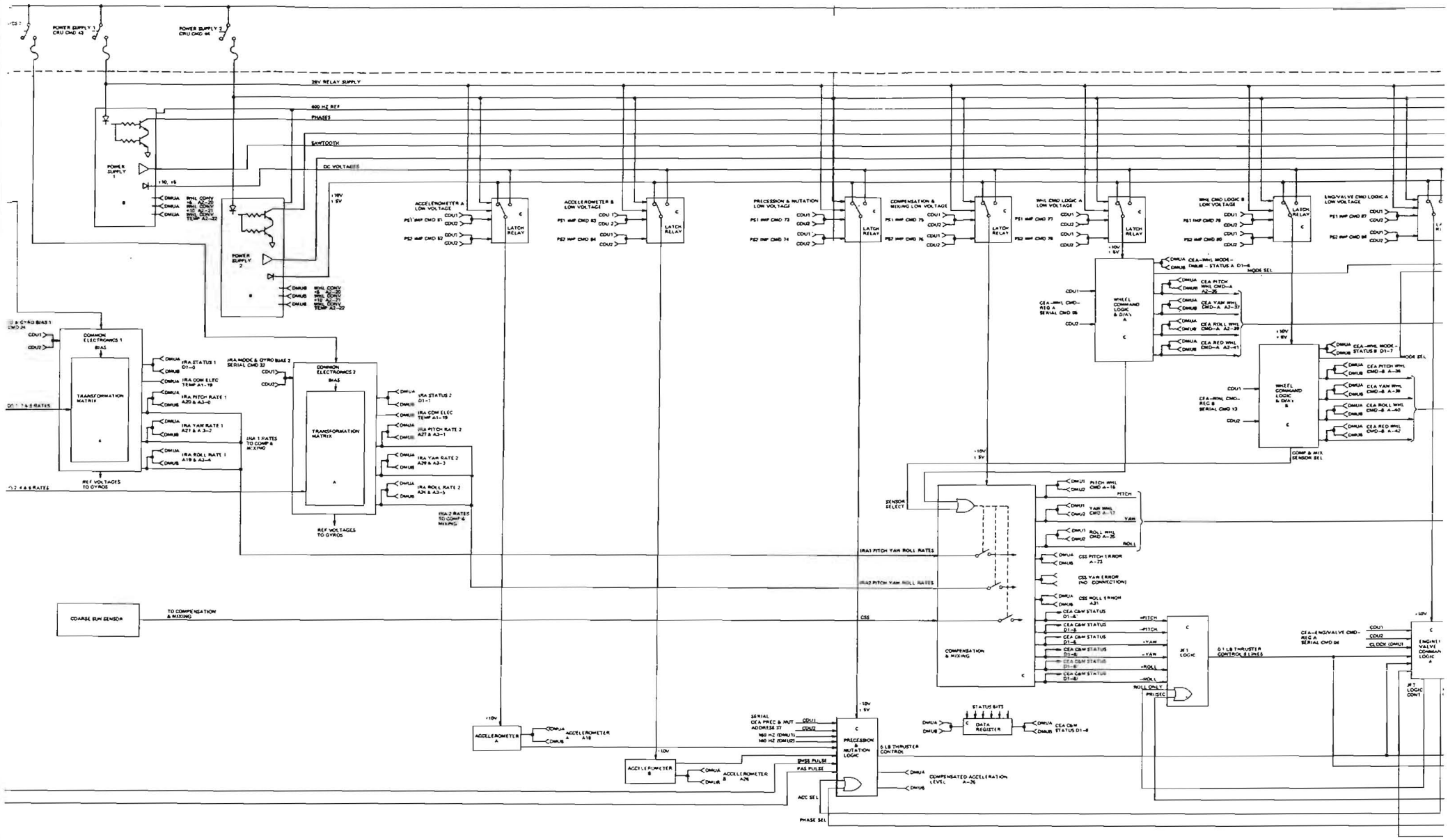
POWER SUPPLY 1 CRU CMD 43
POWER SUPPLY 2 CRU CMD 44
28V RELAY SUPPLY
400 HZ REF
PHASES
SAWTOOTH
DC VOLTAGES
POWER SUPPLY 1
POWER SUPPLY 2
ACCELEROMETER A LOW VOLTAGE
ACCELEROMETER B LOW VOLTAGE
PRECESSION & NUTATION LOW VOLTAGE
COMPENSATION & MIXING LOW VOLTAGE
WHL CMD LOGIC A LOW VOLTAGE
WHL CMD LOGIC B LOW VOLTAGE
ENG VALVE CMD LOGIC A LOW VOLTAGE
LATCH RELAY
COMMON ELECTRONICS 1
TRANSFORMATION MATRIX
COMMON ELECTRONICS 2
IRA STATUS 1 D1-0
IRA COM ELEC TEMP A1-19
IRA PITCH RATE 1 A20 & A3-0
IRA YAW RATE 1 A21 & A3-2
IRA ROLL RATE 1 A19 & A3-4
IRA 1 RATES TO COMP & MIXING
IRA STATUS 2 D1-1
IRA PITCH RATE 2 A27 & A3-1
IRA YAW RATE 2 A28 & A3-3
IRA ROLL RATE 2 A24 & A3-5
IRA 2 RATES TO COMP & MIXING
REF VOLTAGES TO GYROS
COARSE SUN SENSOR
TO COMPENSATION & MIXING
WHEEL COMMAND LOGIC & DRIVE A
WHEEL COMMAND LOGIC & DRIVE B
CEA WHL MODE - STATUS A D1-6
CEA WHL MODE - STATUS B D1-7
MODE SEL
COMP & MIX SENSOR SEL
SENSOR SELECT
IRA1 PITCH YAW ROLL RATES
IRA2 PITCH YAW ROLL RATES
CSS
COMPENSATION & MIXING
PITCH WHL CMD A-16
YAW WHL CMD A-17
ROLL WHL CMD A-26
CSS PITCH ERROR A-23
CSS YAW ERROR (NO CONNECTION)
CSS ROLL ERROR A21
JET LOGIC
JET LOGIC CONT
0.1 LB THRUSTER CONTROL & LINES
ROLL ONLY
PRISEC
ENGINE VALVE COMMAN LOGIC A
ACCELEROMETER A
ACCELEROMETER B
PRECESSION & NUTATION LOGIC
0.1 LB THRUSTER CONTROL
COMPENSATED ACCELERATION LEVEL A-26
STATUS BITS
DATA REGISTER
CEA CAW STATUS D1-8
ACC SEL
PHASE SEL

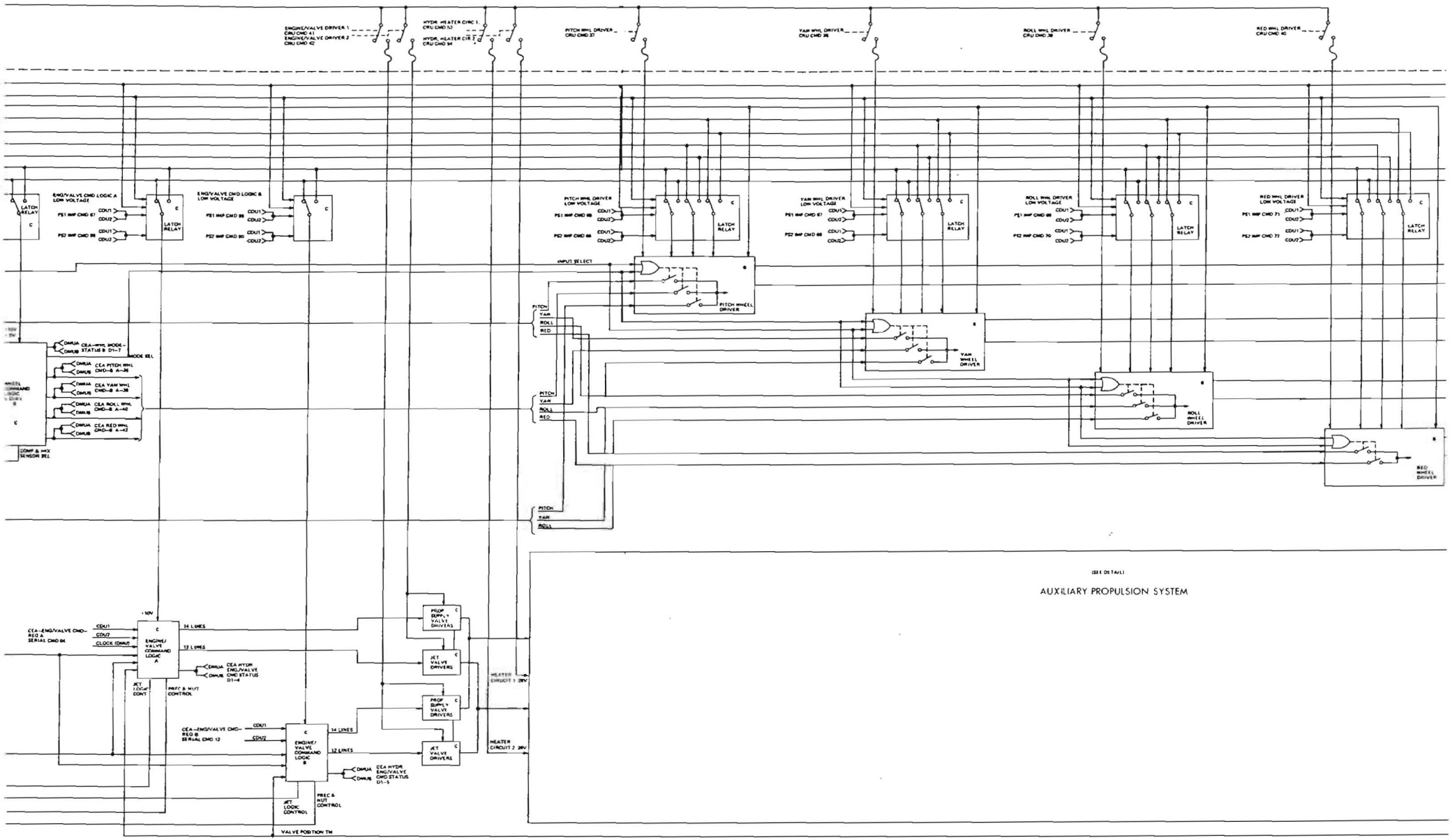
ENGINE/VALVE DRIVER 1 CRU CMD 41
ENGINE/VALVE DRIVER 2 CRU CMD 42
HYDR. HEATER CIRC 1 CRU CMD 53
HYDR. HEATER CIR 2 CRU CMD 54
PITCH WHL DRIVER CRU CMD 37
YAW WHL DRIVER CRU CMD 38
ROLL WHL DRIVER CRU CMD 39
RED WHL DRIVER CRU CMD 40
ENG/VALVE CMD LOGIC A LOW VOLTAGE
ENG/VALVE CMD LOGIC B LOW VOLTAGE
PITCH WHL DRIVER LOW VOLTAGE
YAW WHL DRIVER LOW VOLTAGE
ROLL WHL DRIVER LOW VOLTAGE
RED WHL DRIVER LOW VOLTAGE
LATCH RELAY
INPUT SELECT
PITCH WHEEL DRIVER
YAW WHEEL DRIVER
ROLL WHEEL DRIVER
RED WHEEL DRIVER
PITCH
YAW
ROLL
RED
CEA—WHL MODE—STATUS B D1—7
CEA PITCH WHL CMD—B A—36
CEA YAW WHL CMD—B A—38
CEA ROLL WHL CMD—B A—40
CEA RED WHL CMD—B A—42
MODE SEL
COMP & MUX SENSOR SEL
+10V
CEA—ENG/VALVE CMD—REQ A SERIAL CMD 84
CDU1
CDU2
CLOCK (DMUX)
ENGINE/ VALVE COMMAND LOGIC A
34 LINES
12 LINES
CEA HYDR ENG/VALVE CMD STATUS D1—4
JET LOGIC CONT
PREC & NUT CONTROL
PROP SUPPLY VALVE DRIVERS
JET VALVE DRIVERS
HEATER CIRCUIT 1 28V
CEA—ENG/VALVE CMD—REQ B SERIAL CMD 12
ENGINE/ VALVE COMMAND LOGIC B
CEA HYDR ENG/VALVE CMD STATUS D1—5
JET LOGIC CONTROL
PREC & NUT CONTROL
HEATER CIRCUIT 2 28V
VALVE POSITION TM
(SEE DETAIL)
AUXILIARY PROPULSION SYSTEM

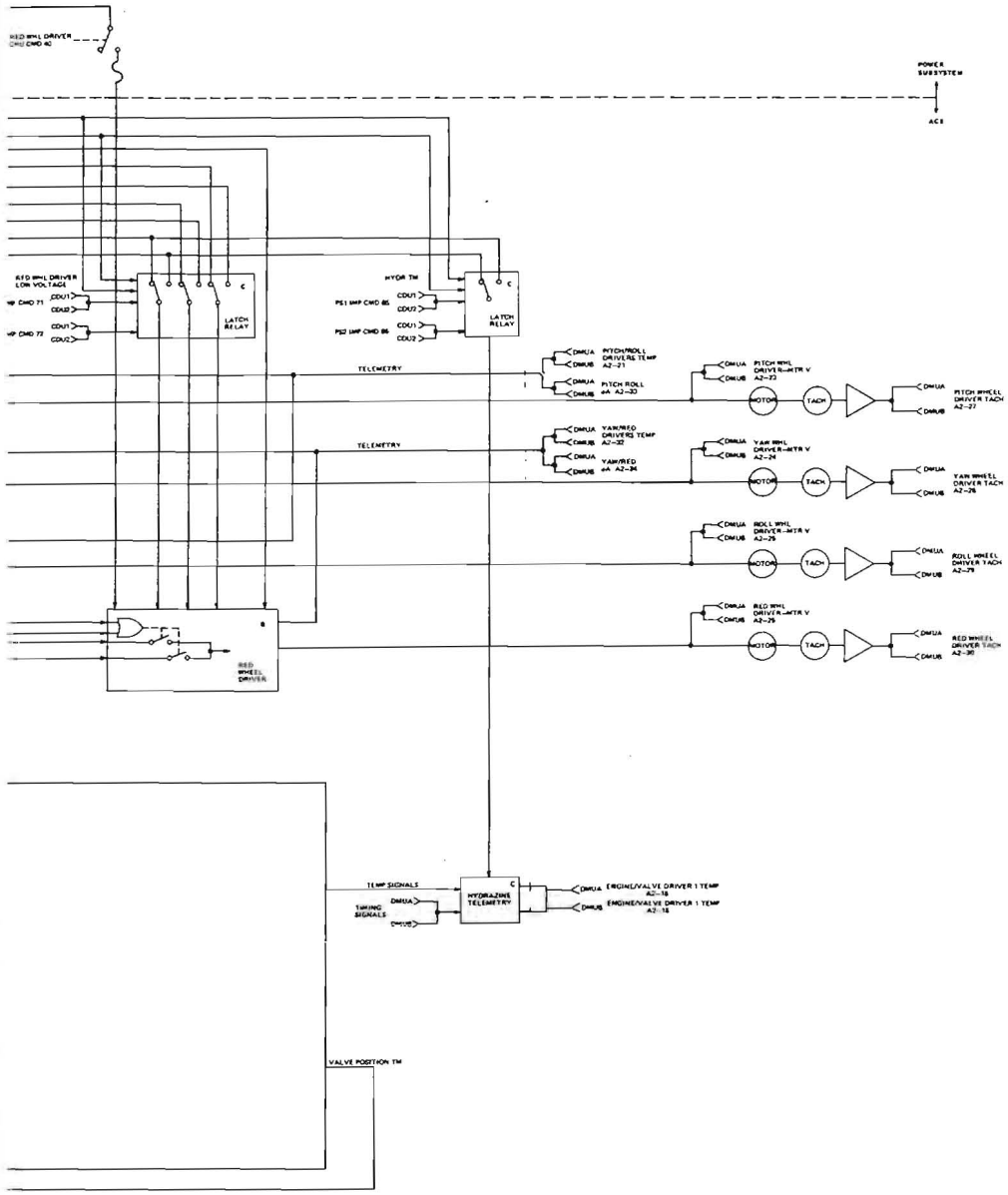

DETAIL OF AUXILIARY PROPI

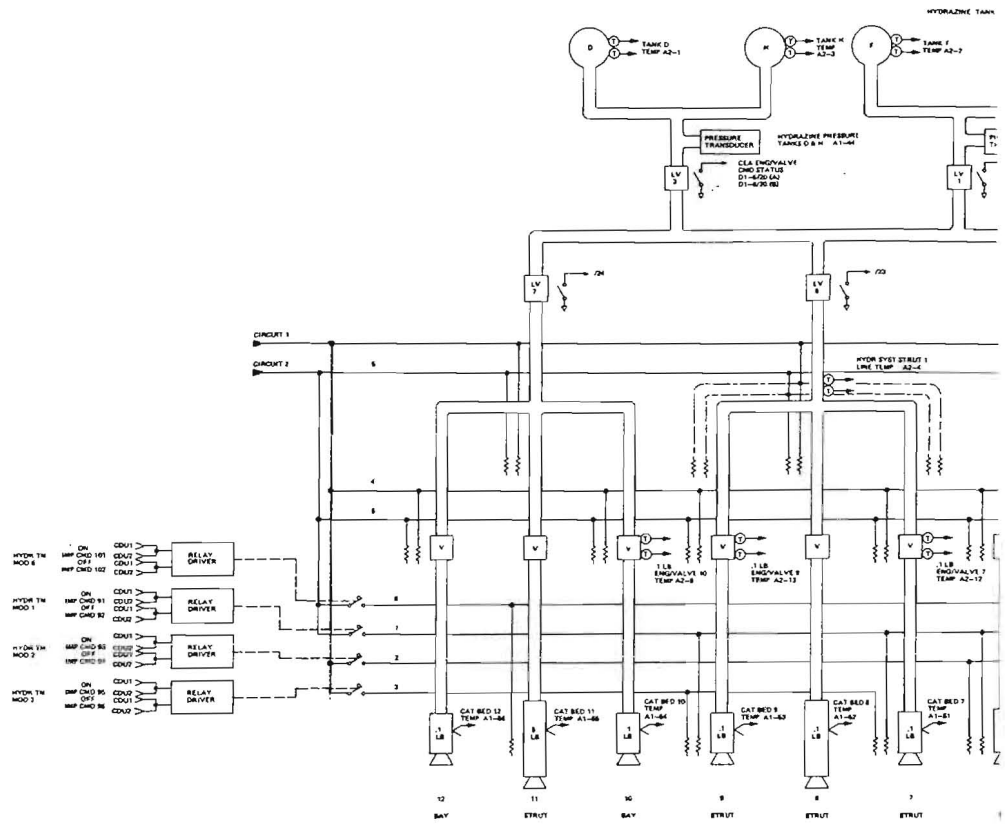

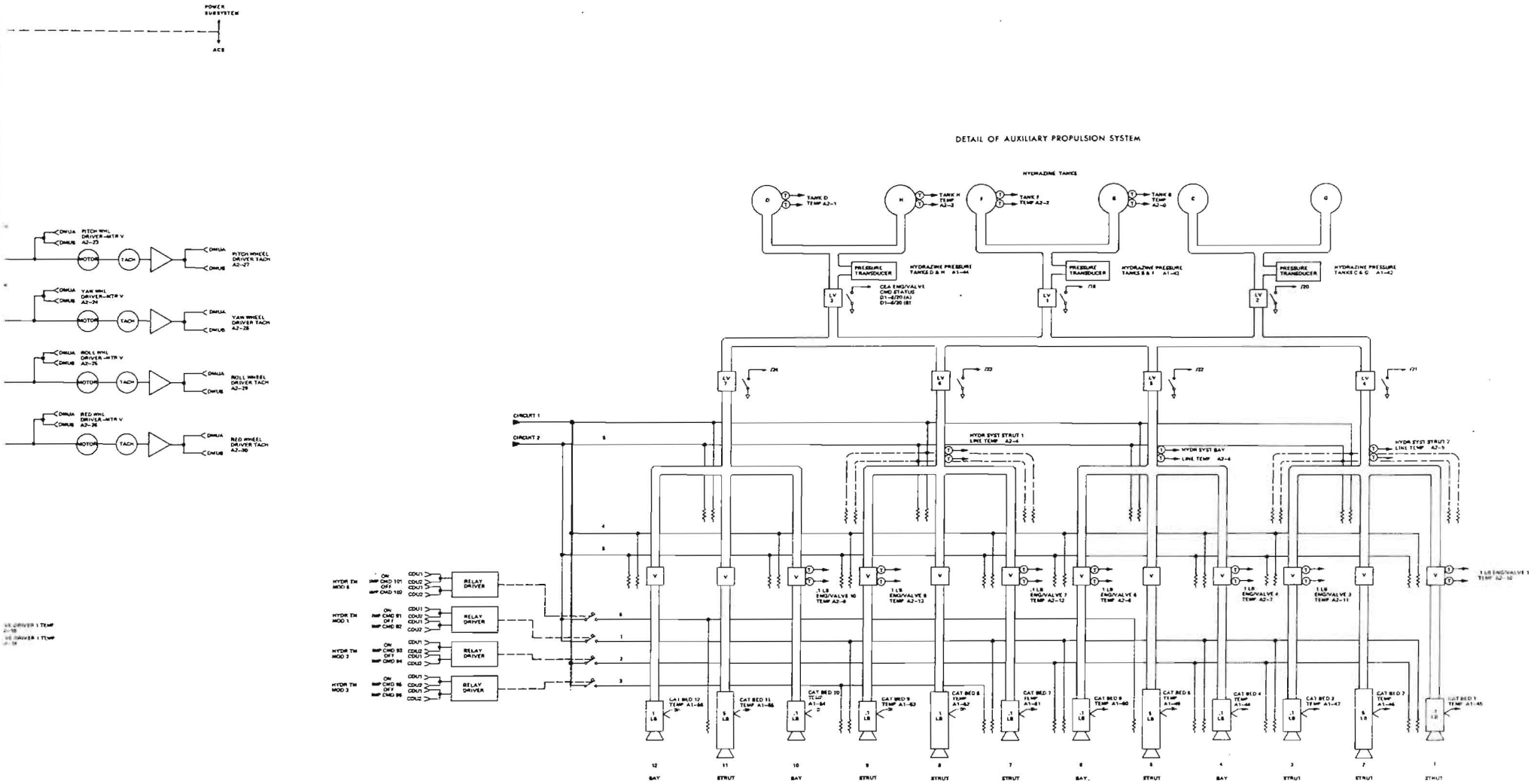

Figure 8.2-2
ATTITUDE CONTROL SUBSYSTEM BLOCK DIAGRAM

Figure 8-4. Attitude Control Subsystem Block Diagram

f. Hydrazine Telemetry Card. This module is provided to condition temperature and pressure functions which must be monitored within the hydrazine system. The card is powered by the redundant power supplies in the wheel driver assembly.

g. Relay Card. This module contains sufficient latch relays and relay drivers to enable power switching (on/off) to all cards within the control electronics assembly and wheel driver assembly. The relays are toggled by impulse command generation by the on-board command decoders.

8.2.1.4 Wheel Drive Assembly (WDA). This assembly provides a redundant power converter and four-wheel driver modules. Each wheel driver module is dedicated to a specific reaction wheel.

a. Wheel Driver Modules. This four module set provides the amplitude controlled, two-phase square wave drive signals to the reaction wheels. Each card separately receives wheel command information from either half of the redundant DAC and command decoder module. In addition, the pitch, yaw and roll wheel driver modules receive wheel commands from the compensation and mixing module in the CEA.

b. Power Supply Modules 1 and 2. These redundant modules in the WDA are powered by the regulated +28 Vdc bus switched by the CRU. Both modules output AC and DC levels to other modules within the CEA and WDA via the relay card.

8.2.1.5 Computer. The on-board computer function in the IUE controls mechanization is two-fold:

a. Primary Function. The unit will serve to execute the control laws during the hold and slew modes of spacecraft operation. During these modes of control, FES and IRA information will be input to the computer and will be processed to logically drive the digital-to-analog converters which address the reaction wheels.

b. Secondary Function. All control modes which are hardwired to the spacecraft actuators will be redundant via computer software programs. These modes are those used during the early mission phase and necessarily include active nutation control, precession, spin sectoring, and initial sun acquisition. Since all sensors input information to the computer under variable format control and since the computer outputs through redundant command decoders to the actuator power stages on-board the IUE, the redundant modes via the computer are simplified.

8.2.2 REQUIREMENTS AND CONTROL CONCEPTS

The controls subsystem is required to perform a wide variety of functions throughout the mission life - each function characterized by specific requirements. The major functions are listed below with each specific requirement associated with that function explicitly defined.

8.2.2.1 Transfer Orbit. During this all critical phase of the mission, the control system is responsible for on-board active nutation control, sensor information to provide ground controllers with data for attitude determination, and finally, the correct execution of precession maneuvers as commanded by ground controllers. The specific requirement for each of these functions is defined below.

a. Active Nutation Control. Since the IUE spacecraft is spinning about an unfavorable moment of inertia axis, the vehicle, if uncontrolled, will enter a flat spin about the transverse axis of maximum moment of inertia. This coning effect about the spin axis which grows to a flat spin is caused by energy dissipation on-board the spacecraft. To prevent this from occurring the coning angle growth must be monitored continuously and removed periodically throughout the spin phase of the mission. A complete analysis of this coning effect and the control mechanization is described in section 8.2.6 of this report. The requirements for control and monitoring are stated here:

(1) Actively monitor the nutation angle growth with an on-board redundant sensor (accelerometer).

(2) Determine when the spacecraft spin axis is coning at a 1.0 degree half-cone angle.

(3) Fire a 5.0 pound thruster through use of an on-board algorithm to effectively remove the cone angle.

(4) Monitor the total operation and its frequency in real-time on the ground.

(5) Ensure that the algorithm is self-adaptive to the spin period.

(6) Compensate for asymmetrical impulse definitions due to cold engine starts and sensor lags.

b. Attitude Determination. Throughout the transfer orbit phase of the mission, ground controllers must continually calculate the spacecraft's spin axis vector with respect to inertial space. This must be accomplished to: ensure that the spacecraft is in a power safe attitude with respect to the sunline; determine a start attitude for

the precession maneuver; and precisely determine the spacecraft attitude for the apogee burn. The last determination must be made to within ±5.0 degrees; the function is the same for all determinations.

To accomplish this attitude definition, ground controllers must receive real-time sensor information from the spacecraft in several forms. The requirements for this information are described below:

(1) Spin axis angle to the sunline must be known within ±½ degree.

(2) Consecutive sun crossings must be defined within ½ degree.

(3) Current state of nutation cone angle must be ensured within 1.0 degree.

(4) The angle between the spacecraft spin axis and the earth scanner look angle must be known to ±0.10 degree at each earth horizon crossing.

The on-board telemetry system with its variable format control must devote a large portion of its time to processing this information to ground controllers in near real-time fashion.

c. Precession Maneuver. Because the spacecraft is launched with apogee engine facing backward, the spacecraft spin axis must be precessed 180 degrees during the transfer orbit in preparation for the apogee burn. This maneuver is accomplished in discrete steps and phased such that a good sun angle is maintained. During each precession step, the active nutation control is turned off. After the precession step is completed, the nutation control is reactivated to remove the induced nutation angle. The total precession is accomplished by firing a precession thruster over a preselected portion of the sectored spin period. Thus, with a given attitude determined before the maneuver, a direction can be selected by ground controllers and the precession command issued. An explanation of the on-board mechanization is given in section 8.2.7.

8.2.2.2 Sun Acquisition Mode. After the apogee engine is burned, the control system must despin the spacecraft and with the arrays deployed, rotate the spacecraft until the sunline is near normal to the major array surface. The maneuver is accomplished with gyros and sun sensor driving the three-axis hydrazine thruster set.

a. Despin After apogee burn the spacecraft is spinning at nominal 60 rpm. The control system is required to reduce the roll spin rate to less than 2-5°/sec so that the array can be deployed. After deployment the rates must be further reduced to 0.25°/sec about each axis.

b. Sun Acquisition With body rates less than 0.25°/sec, the spacecraft is rotated at this maximum rate to the sunline. In this acquisition and hold mode, the array normal is held within ±5 degrees of the sunline and the body rates are less than 0.07°/sec and control is on wheels and gyros.

c. Initial Stellar Acquisition With the spacecraft sun angle known, the PAS is used to find the earth/spacecraft line and this angle in conjunction with position in orbit and ephemeris data allows determination of spacecraft attitude in inertial space with an uncertainty of several minutes in pitch and roll and several degrees in yaw. The spacecraft can now be slewed to the North Ecliptic Pole (NEP) and, using the Fine Error Sensor in the Field Mode, a suitable guide star can be found, locked-on to and used for initial gyro drift calibration. The star field rastered by the FES can be manually matched on the ground to obtain inertial pointing within ±0.5 arc-minute.

8.2.2.3 Slew Mode. With the spacecraft attitude known to within 1.0 arc-minute, the slew angles required to place the spacecraft pointing direction near the experiment star can be determined. The slew to experiment mode is accomplished in two parts. First a major slew is made to place the experiment star within the FES in (Field Mode) field-of-view; then a minor slew is accomplished to place the experiment star in the telescope aperture.

a. Major Slew. Given the initial spacecraft attitude within one arc-minute (three-axis), a slew no greater than 60 degrees in magnitude must be accomplished about two or three axes. The slew rates will be limited to 4.5°/min and have a terminal position accuracy of one part in 2000. The slews will be accomplished about one axis at a time in consecutive fashion. Care must be taken during the slew maneuver to ensure that the optical axis is not moved within a 45° half-cone of the sunline.

b. Minor Slew. Once within the FES (Field Mode) field-of-view, the target star must be recognized and its position identified to an accuracy of 0.5 arc-second with respect to the aperture. The minor slew must then be accomplished to an accuracy of 1 part in 2000 from anywhere within the field-of-view. This will ensure that the target star is within 0.75 arc-second of the aperture center.

8.2.2.4 Hold Mode. Once the experiment star is within the 3 arc-second experiment aperture, the control system (pitch and yaw) must hold this position either on gyros with periodic updates from the FES or on the FES for periods typically of ½ hour. Holding accuracy during this period is defined as follows: 75 percent of the focused star image must be within the 3 arc-second aperture during the observation period. Additionally, the control system must be capable of holding the vehicle within the above defined operating limits on gyros alone for periods of up to 150 seconds. If the star falls outside the experiment aperture in this mode the FES "Field Mode" must be entered and a minor slew accomplished to again center the star.

Because the experiment spectrograph is designed such that the total spectrum is observed through two different apertures (1 arc-minute apart) a minor slew must be accomplished during a single observation to cover the full spectrum. The total time to accomplish this slew operation should not exceed 4 minutes. This slew operation period includes the definition of the new coordinates required, the actual slew, the acquisition of the experiment star in the aperture and the final settling.

8.2.3 CONTROL SYSTEM OPERATING MODES

This section defines the IUE control modes from Delta separation through a final hold mode on the experimenter's star. The mechanization of the specific control laws and limitations of these operating modes are defined in other sections. The planned sequence and sensor actuator combinations used in each mode will be outlined here.

8.2.3.1 Delta Separation. Prior to separation from the Delta second stage the IUE spacecraft will be spun-up to a nominal spin rate of one revolution per second (1 rps). After the third stage Delta burn, the spinning spacecraft/Delta combination will separate. The separation signal will immediately actuate the nutation accelerometers and after a small delay, actuate the active nutation control system. Coning induced at separation will be removed by the primary 5.0 pound thruster in accordance with the nutation control algorithm (section 8.2.6). It should be noted that the nutation control system will remain active through most of the spin phase of the mission and will automatically remove the cone angle when a predetermined threshold is exceeded. Other equipments actuated at Delta separation include the PAS and SMSS systems. Once the spacecraft enters orbit day, sectoring (section 2.3) is initiated and a continual on-board computation will indicate the current sector of a given spin cycle.

8.2.3.2 Attitude Determination. With the spacecraft in orbit and with the sunlit earth visible to the spacecraft, total information is now available to ground controllers for attitude determination. Referring

to figure 8-5 the PAS heads and the SMSS head are located with their field-of-view as pictorially defined. The scanner head is designed such that the 0.71 x 0.71 degree field-of-view is swept through a plane parallel to the vehicle X, Y plane. At each sun crossing the sensor head is incremented 0.71 degree, with an on-board encoder tracking the current position. During each spin cycle the following information is available for attitude determination. The technique is described in section 8.2.5 of this report.

At each PAS sun crossing the sun sensor (blipper) yields a sun-centered pulse. The sun crossing starts the spin sectoring in the Control Electronics Assembly and increments the PAS earth scanner head by 0.71 degrees. The process continues with each sun crossing until the PAS head is incremented at the correct angle to intersect the earth edge. At each edge crossing, the PAS yields information on in-out angle with respect to the sun zenith. The entire earth is quickly mapped as the PAS scanner head is incremented with each sun crossing. The process described above, including total mapping of the earth, will occur once every 4 minutes throughout the transfer orbit. Sufficient information will be available for ground controllers to smooth the attitude determination both before and after spin vector precession.

8.2.3.3 Spin Axis Precession. Since the spacecraft is spin stabilized at Delta release with the apogee engine facing aft, the spacecraft must be precessed 180 degrees at some point in the transfer orbit in preparation for apogee burn. With the spacecraft attitude known, ground controllers will determine over which spin sectors the precession jet must be fired to rotate the spacecraft spin vector 180 degrees and still maintain good sun angle on the folded array (see figure 8-6). The process will be one of commanding the precession jet for (n) spin cycles then actuating the nutation control system to remove induced angle buildup.

8.2.3.4 Despin/Deploy. After apogee burn, the spacecraft is still spinning at the nominal 60 rpm imparted by the Delta spin-up table. This spin must be removed before Sun Acquisition and Three-Axis Hold can proceed. The first step of the despin mode is to reduce the nominal 60 rpm to a nominal 50 rpm by removing approximately 10 rpm (as determined by the PAS). A measurement of hydrazine thruster burn time and knowledge of the spacecraft's moments of inertia will then allow an accurate calibration of thruster torque and thrust. The second step of the despin mode is to reduce the spin rate to a level within the safe operating range of the gyros. Since the nutation induced coning rate and angle will become more severe about the uncontrolled pitch and yaw axes as roll spin rate drops a compromise terminal spin rate yielding acceptable rates in all axes was determined as 5 rpm. When the spin has been reduced to this level, the gyros are enabled into a rate damping mode where,

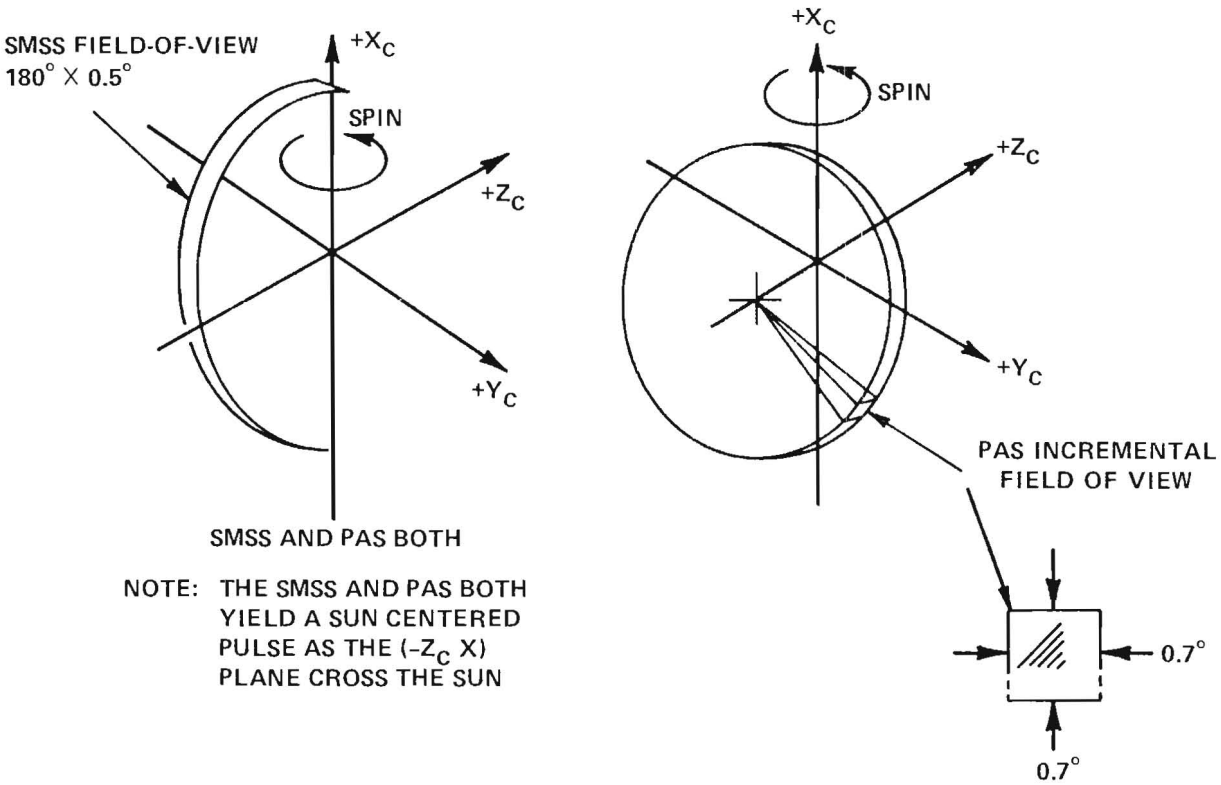

Figure 8-5. SMSS and PAS Field-of-View Location for Attitude Determination

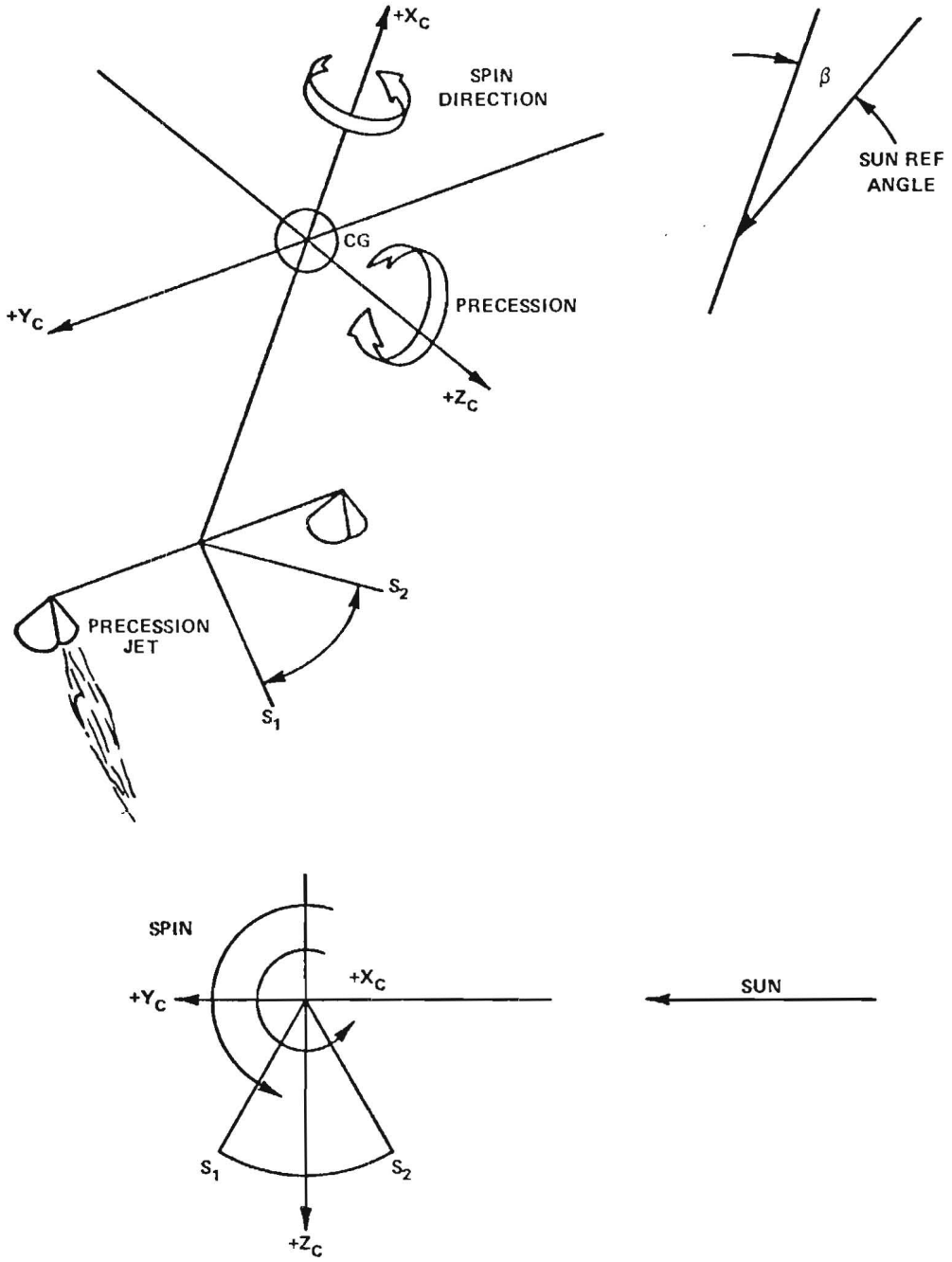

Figure 8-6. Precession Jet Firing

by controlling thruster firing, spacecraft body rates will decline rapidly to less than 0.25°/second. With the spacecraft now under gyro/thruster control, a roll bias is added causing roll thrusters to fire and brings the roll axis spin up to 2 to 5 degree/second rate. After ensuring thermal equilibrium on the solar array hinges the array deployment squibs will be fired unlatching the paddles and allowing them to unfold, extend and lock-up. Rate damping under gyro control will then bring the three-axis body rates down to a level of less than 0.25°/second.

8.2.3.5 Sun Acquisition. By ground command, the sun acquisition mode will be entered and body rates will be mixed with the analog sun sensor signals to drive the acquisition and hold algorithms hardwired in the Control Electronic Assembly.

The sensors are arranged about the spacecraft as shown in figure 8-7. Nominal sensor outputs are shown and their transfer functions defined for the acquisition mode as shown in figure 8-8. The anti-sun side of the fixed array is covered primarily by the pitch set and maneuvers which start from the anti-null side will be primarily about the pitch axis with rate limiting in yaw and roll. Once on the sun side of the fixed array, position errors with respect to the center array Normal will be reduced to 5 degree with three-axis body rates held below 0.075°/second. The initial sun acquisition and settling will occur using gyros and analog sun sensors as inputs and 0.3 pound thrusters for actuators. When body rates and position errors are reduced to the levels defined above, the pitch, yaw, and roll reaction wheels will be energized and perform a vernier control of the spacecraft about the sunline. The thruster set will remain enabled so that control is maintained in the event the switching lines are crossed in this mode of operation.

8.2.3.6 Three-Axis Stabilization. With the sunline held, other equipments on-board the IUE can now be turned on and functionally checked. This verification would necessarily include the digital computer in preparation for the next control mode of spacecraft operations.

Once the control loop that includes the precision gyro set and digital computer is functionally verified, a 3-axes hold on gyro model will be ground initiated. Operation in this mode would be monitored, utilizing the fine sun sensor system.

The redundant sensor heads are collocated and have the same field-of-view about the $+Z_C$ axis. Each system has two heads mounted at an angle of 60° to each other providing an overall field of 64 x 124 degrees with a 1/256 degree resolution. The orientation of the sensors is such that the sunline angle to the spacecraft (β) can be measured over the range of 13 to 137 degrees. The sensor view angles are shown on figure 8-9.

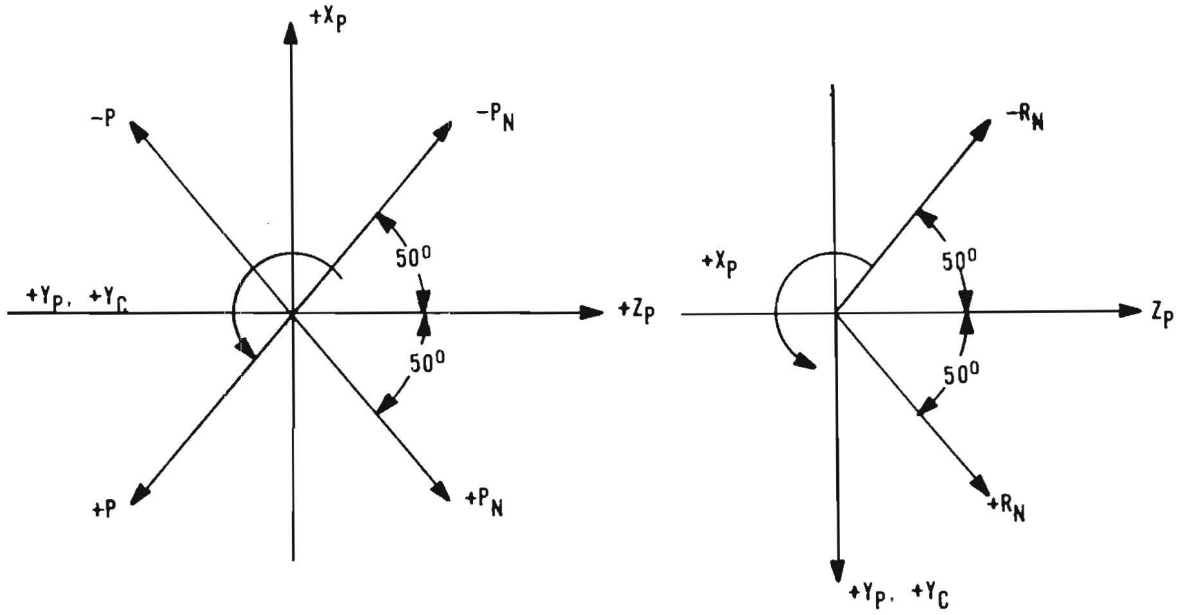

Figure 8-7. Analog Sun Sensor Alignment Definition

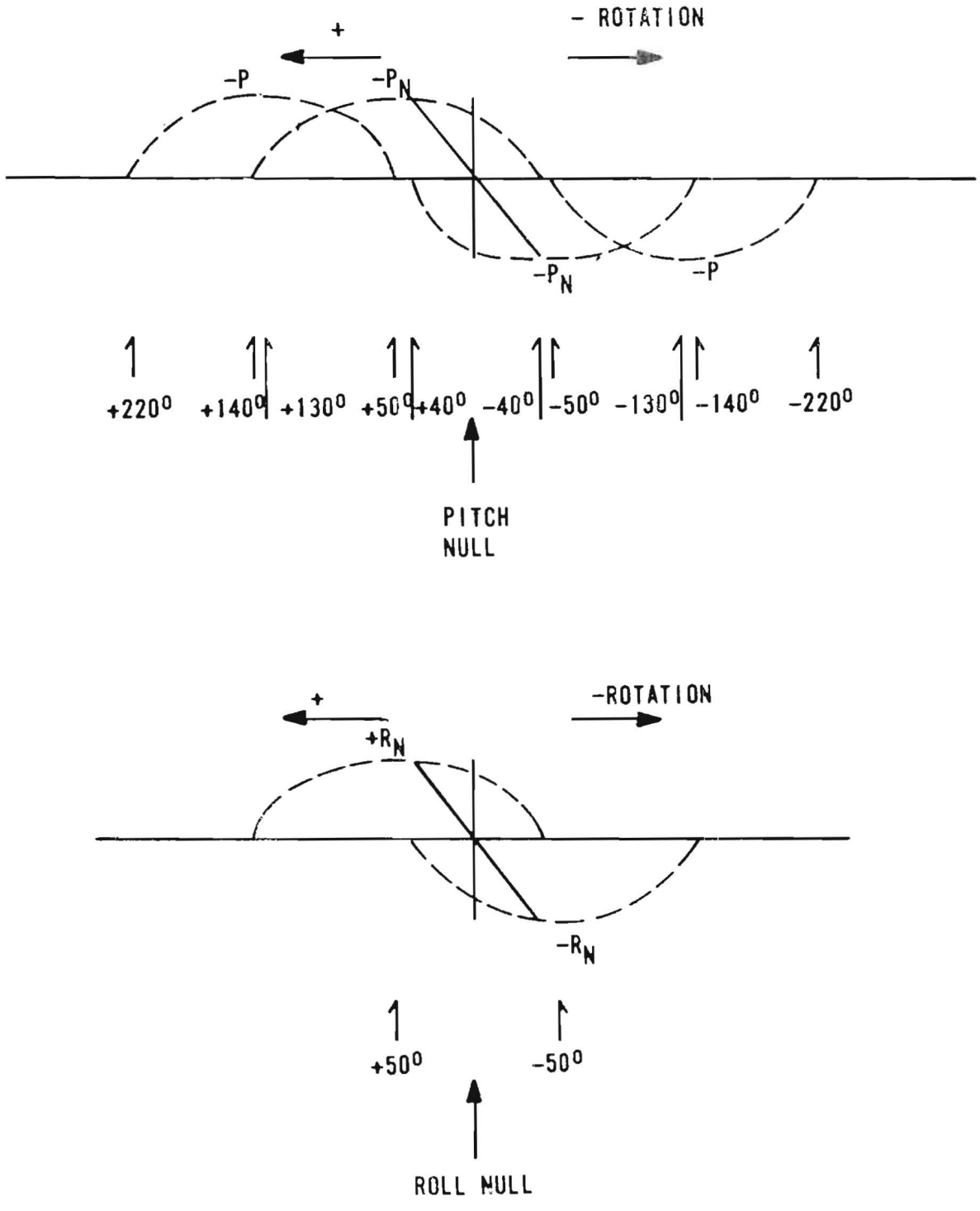

Figure 8-8. Analog Sun Sensor Transfer Function

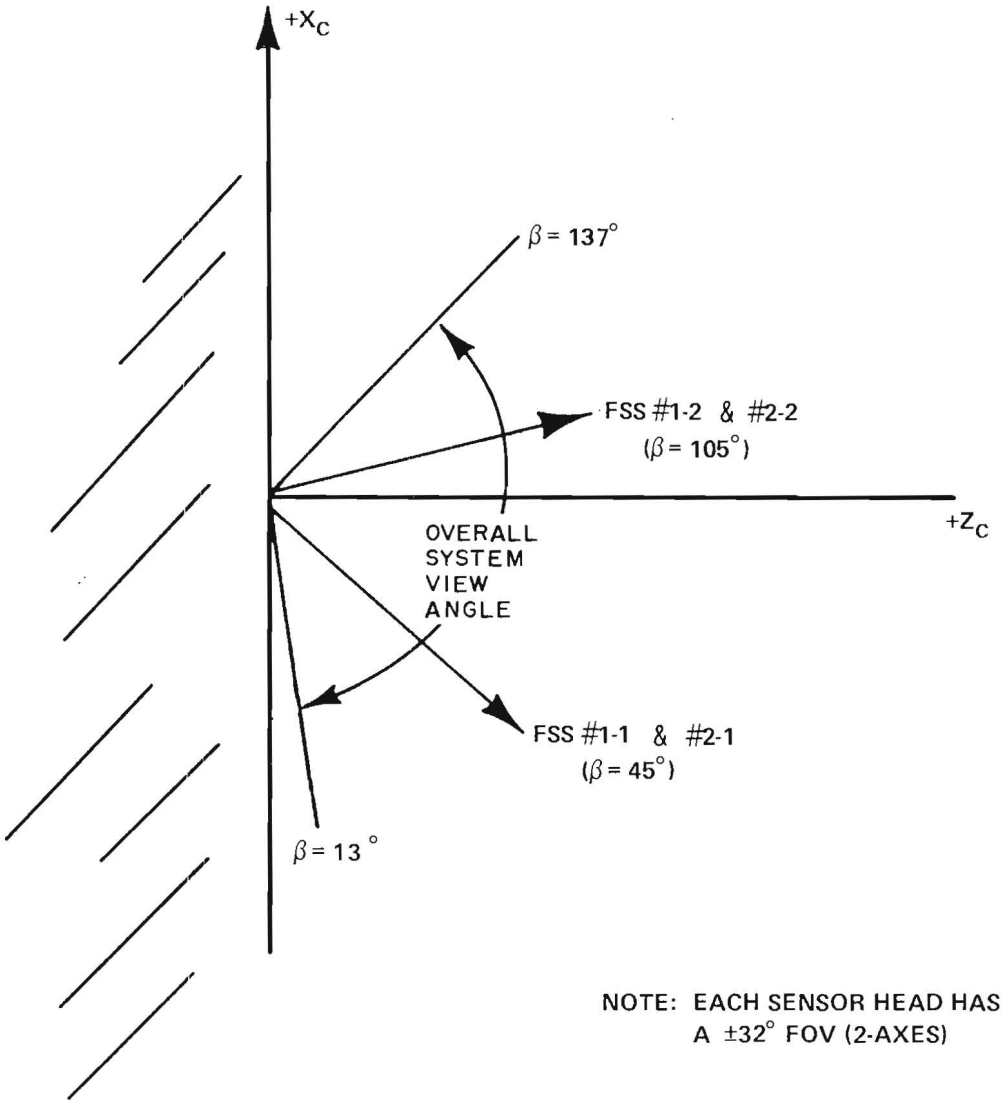

Figure 8-9. Fine Sun Sensor Head Location and Normal Alignment

The completion of sun acquisition with hold on wheels will leave the IUE with the sunline normal to the solar array for maximum power input and at some indeterminate rotation about the sunline. This optimum sun angle corresponds to a β of 67.5 degrees. The first step in stellar acquisition is to change the angle of solar incidence such that the spacecraft experiment pointing indeterminancy, sweeps a great circle about the sunline, including both the North and South Ecliptic Poles. This is accomplished by performing pitch slews while using the FSS to monitor β-angle until a $\beta=90^{o}$ condition is met.

With the spacecraft held inertially in all three axes, the Panoramic Attitude Sensor (PAS), mounted on the anti-sun side of the IUE is operated in its "planar" mode and stepped until it acquires the sunlit earth. From readout of the earth/IUE line obtained by the PAS and knowledge on the ground of the IUE's location in orbit it is possible to perform an attitude determination that will provide the celestial pointing direction with an accuracy of several minutes in pitch and several degrees in yaw.

To avoid generating large numbers of star maps for several degrees about a great circle perpendicular to the sunline and to avoid sensitivity to time of year, the knowledge of celestial pointing is used to generate a series of slews that are used to point the IUE at the North Ecliptic Pole (NEP). The Fine Error Sensor is now used in its Field Mode to scan the pointing zone and generate a star map on the ground. A bright star is chosen in the field and its coordinates relative to the center of the field are determined. The FES is placed in the Track Mode and offset to these coordinates such that pitch and yaw attitude change signals are generated.

The astronomers, using detailed 0.5 x 0.5 degree maps of the NEP will make comparisons with the initial FES star image until a fit is established. From the star map coordinates the IUE pointing can now be accurately determined and entered into the ground computer. The ground computer can now generate slews from this determined pointing attitude to the experimenter's target star.

While the astronomers are determining actual pointing, the IRA drift relative to the fixed stellar pointing is determined for each gyro and a compensating term for the on-board algorithm is developed and commanded into the OBC.

8.2.3.7 Control During ΔV-Burn. Once the spacecraft has moved to the desired longitude, its eastward drift must be stopped. To accomplish this the spacecraft must be maneuvered such that the thrust axis is aligned in the proper direction with respect to the velocity vector. At the correct time, a set of 5.0 pound thrusters aligned parallel to the X_c axis will be fired to end the eastward drift. The alignment maneuver will be accomplished on the precision gyro set using reaction wheels as actuators. During the 5.0 pound thruster burn, the pitch and yaw control axes rates will be limited using the primary 0.3 pound thruster set as actuators. The implementation of this maneuver will be via OBC algorithm.

8.2.3.8 Slew to Experiment Star. Once the spacecraft transients have settled from the ΔV-Burn, three axes control will again be maintained on the trimmed precision gyro set. Position changes that occurred during the burn will be tracked in the computer and removed when the hold-on gyro mode is reentered. Large angle slews will then be commanded about two or three axes (one axis at a time) to place the experiment and guide stars within the field-of-view of the Fine Error Sensor. When the spacecraft settles at the new attitude, the FES will be operated in the Field Mode and the guide star and experiment star identified by the experimenter on the ground. Figure 8-10 (a), (b), and (c), demonstrate the appearance of a typical field as scanned by the FES in Field Mode. The astronomer selects one of these stars (labelled ES) and another, brighter one for guidance (labelled GS). The ground computer determines the pitch error from ES to the aperture (θ) and the yaw error from ES to the aperture (ψ) and generates a small slew command. In addition, the ground computer determines what pitch and yaw offsets must be inserted in the FES to bias out the pitch and yaw errors from GS to the aperture. With the FES in the Track Mode, any tendency of the spacecraft to move from the offset position will be detected as a shift in GS relative to the offset scan of the FES. The FES will then generate corrective error signals.

8.2.3.9 Hold-During-Experiment Modes. This mode of operation is detailed in section 8.3.1 of this report. A brief summary is included here for continuity.

Because the spacecraft must be held on a variety of targets, the operation in the fine-hold mode becomes a function of star availability within the vicinity of the experiment star or target. Three modes of control are defined as follows:

a. Control on Gyros Alone. Because instances will occur where no bright stars exist within the offset capability of the FES, the spacecraft must be held on gyros alone. As the spacecraft drifts and the target falls outside the aperture, the FES in Field Mode must be scanned and a small slew accomplished to place the star within the aperture.

b. Control on Gyros and FES. When the FES can be offset on a very dim star but the position information from the FES is degraded, the spacecraft will be held under gyro control with periodic updates of drift terms as dictated by FES changes.

NOT IMPLEMENTED IN FLIGHT S/W AT LAUNCH.

c. Control on FES. When the FES is locked on a bright star that yields good position information about the pitch and yaw control axes, total position control can be accomplished with the FES. The occurrence of a bright star within the immediate vicinity of the experiment star, however, will not be frequent.

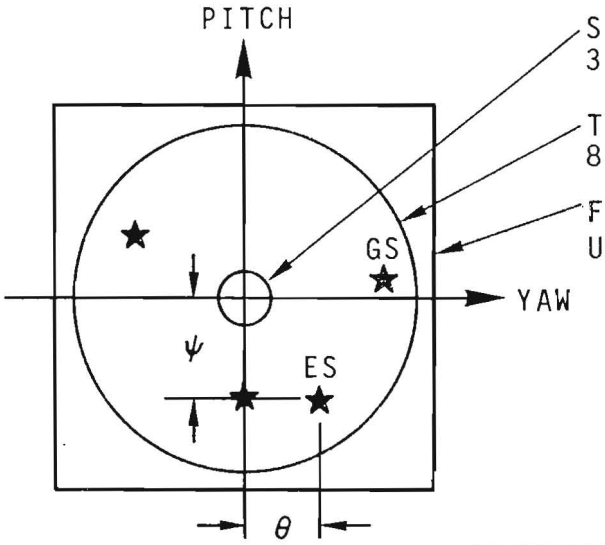

Figure 8.2-8 (a)

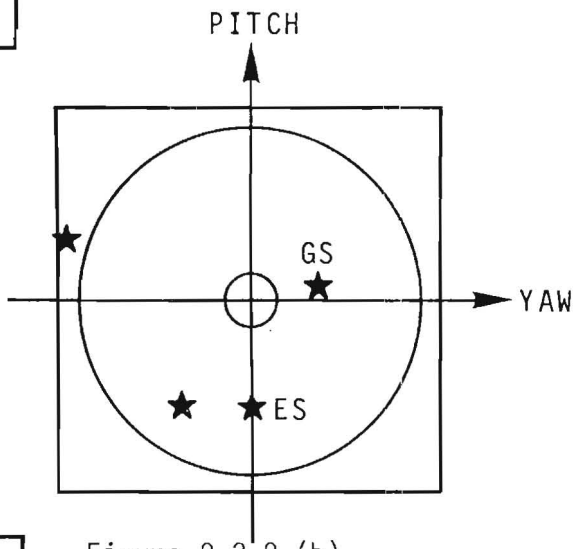

Figure 8.2-8 (b)
SLEW ABOUT PITCH
AXIS COMPLETE

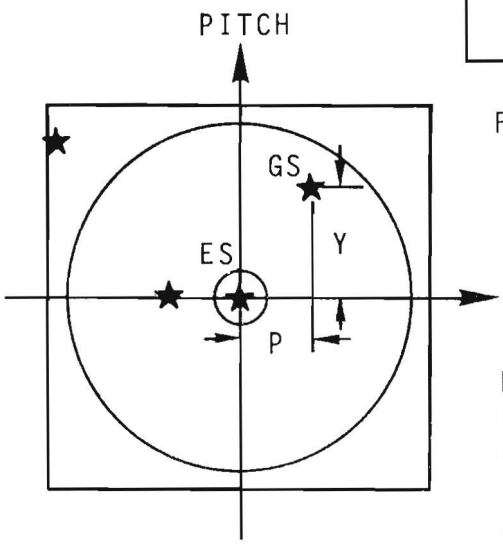

Figure 8.2-8 (c)
SLEW ABOUT YAW
AXIS COMPLETE
'P' & 'Y' OFFSETS
REQUIRED FROM GS TO
HOLD ES IN APERATURE

Figure 8-10. FES Star Field

8.2.4 SPIN SECTORING DURING TRANSFER ORBIT

8.2.4.1 Requirements. As previously mentioned, the Delta third stage and the IUE spacecraft are spun up to 60 rpm prior to third stage injection into the transfer orbit. This spinup of 1.0 rps is a nominal figure and could vary as much as ±10 percent (0.9 to 1.1 rps). Because the spin frequency directly affects on-board and ground computations during the transfer orbit, a good measurement of its period must be maintained until apogee is reached and the spacecraft is despun. To accomplish this spin sectoring on-board, an adaptation of a design used on the satellites IMP and SSS (Reference 21) has been mechanized within the Control Electronics Assembly to yield both a current indication of the spin period and the current sector that the spacecraft has entered in a given spin. All computations including sectoring are indexed from the sun crossing.

a. Spin Sector. Because the IUE spacecraft spin axis must be precessed 180 degrees during the transfer orbit and because the precession direction is completely arbitrary until the initial attitude reference is defined, ground controllers must have the capability to choose the spin sector (or sectors) over which the precession jet will fire. Additionally, knowledge of the spin sector during which earth horizons are crossed will assist in the ground computation of the spacecraft attitude.

b. Spin Period. Because the IUE active nutation control algorithm is dependent on spin period, an onboard estimate of this variable must be maintained so that the nutation control system can be self-adaptive to the current spin period. Since the nutation control utilizes a linear accelerometer aligned parallel to, but offset a radial distance from the X axis, spin period directly affects the angular threshold level at which the nutation control jet will be activated. The nutation control algorithm requires the control jet to be fired for one-half of a nutation cycle.

8.2.4.2 Implementation. Spin sectoring is accomplished via a hardwire algorithm on one of the eight cards of the Control Electronics Assembly (CEA). The basic concept is to develop a "clock" which is synchronous with the spacecraft spin rate, divide this Spin-Synchronous Clock (SSC) into 128 equal segments or sectors and determine in which sector the sunline appears. Figure 8-11 shows an elementary block diagram of this portion of CEA logic.

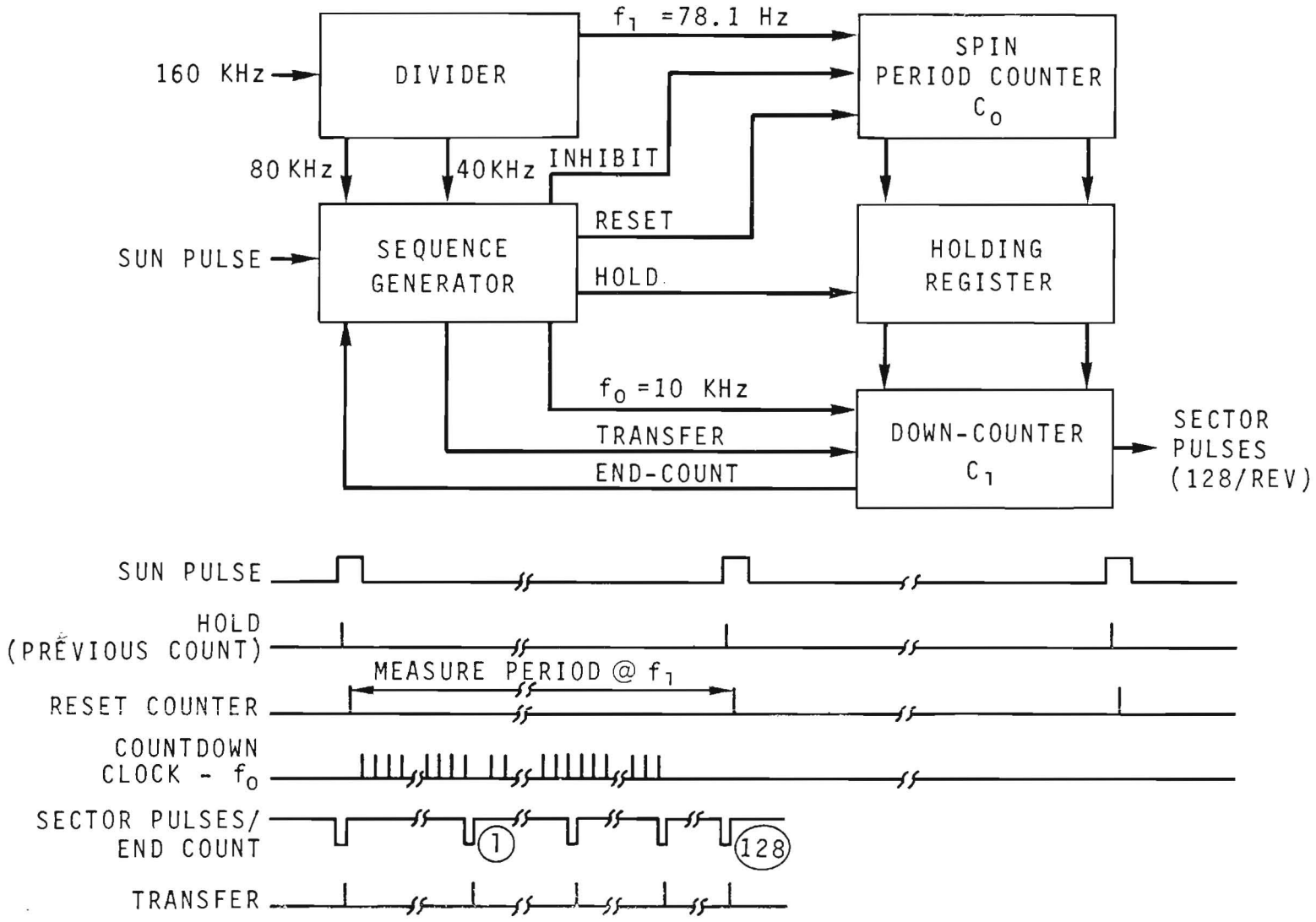

Figure 8-11. Spin Sectoring Logic and Timing Diagram

The inputs to the Spin Sectoring Logic (SSL) are the IUE system clock of 160 kHz and a sun-centered pulse from the Spin Mode Sun Sensor (SMSS) or the Panoramic Attitude Sensor (PAS). These devices, described in detail in sections C.5.2 and C.5.4, respectively generate a pulse each time their field-of-view cuts the sun's zenith. The receipt of a sun pulse in the sequence generator inhibits the 78.1 Hz signal (derived by counting down the 160 kHz clock) to the spin period counter (C_0) and the 10 kHz signal to the down counter (C_1). The sequence generator (driven by 80 kHz and 40 kHz signals) then transfers the count stored in C_0 into the holding register, resets C_0 to zero and transfers the information from the holding register (which was the previous count in C_0) and then reenables the 78.1 Hz signal to C_0 and the 10 kHz signal to C_1. C_1 counts down against its stored count at a 10 kHz rate until the counter reaches zero at which time it produces a sector pulse that is used to reload C_1 from the holding register. This cycle reoccurs 128 times between sun pulses thus dividing the spin period into 128 segments. This resolves the sunline into one of the 128 sectors with an accuracy of $(1/n)(360/128)$ degrees where n is the number of sectors from start. Thus, the worse cast determination is 2.8^0 which is adequate with the spin period computation to perform the precession and nutation functions onboard.

8.2.5 ATTITUDE DETERMINATION DURING TRANSFER ORBIT

8.2.5.1 Requirements of Mission. During the transfer orbit, the attitude of the spacecraft momentum vector must be determined and precessed nominally 180 degrees in preparation for apogee engine burn at altitude. At apogee the spacecraft X axis attitude must be known within 5.0° (two axes). Additionally, the attitude of the spinning spacecraft must be monitored throughout the transfer orbit to ensure a power-safe angle with respect to the sunline (solar arrays are folded around the spacecraft at this time).

8.2.5.2 Requirements of Sensors. Sensors on-board the IUE spacecraft must supply three pieces of information to ground controllers so that the attitude determination of the spin vector can be calculated. A brief explanation of the geometry involved is included here so that alignment and resolution of the sensor readouts can be appreciated (reference 22).

Consider the celestial sphere shown in figure 8-12 with the center of mass of the spacecraft at the center of the sphere. The zenith vector is the line connecting the earth disk center and the vehicle mass center. The spacecraft momentum vector is shown as L with the incident angles to the earth and sun defined as δ and β, respectively. Other terms shown in the figure are defined as follows:

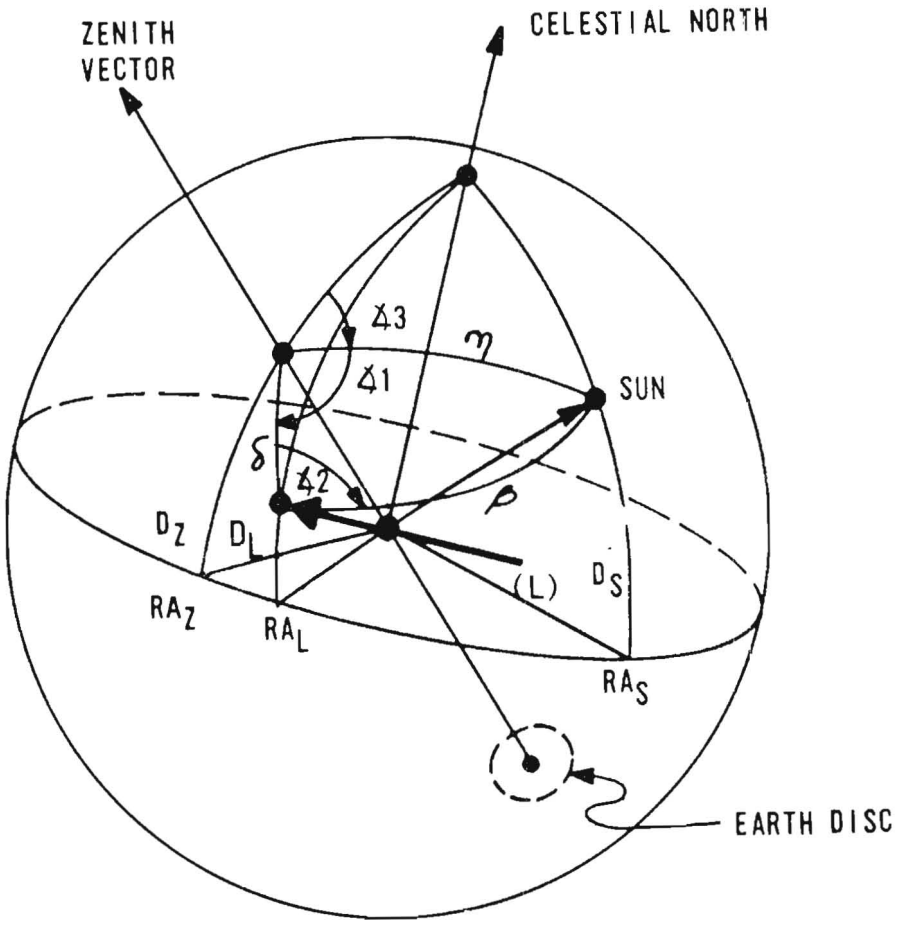

Figure 8-12. Attitude Determination Geometry

RA_Z = right ascension of zenith vector

D_Z = declination of zenith vector

RA_L = right ascension of momentum vector

D_L = declination of momentum vector

RA_S = right ascension of sun

D_S = declination of the sun

η = great circle arc from sun to the zenith vector

Right ascension and declination of the zenith vector and sun are determined on the ground from time of year, orbit inclination, and ranging data. Information relayed from the spacecraft must define β, δ, and $\frac{1}{2}$.

a. β-Measurement. As the spacecraft rotates about its spin axis, the SMSS head sweeps out the total celestial sphere. Since the sensor yields information that defines sun angle with respect to the X axis, the incident sun angle (β) is defined. The SMSS resolution is ½ degree in a digital format.

b. δ-Measurement. Throughout the transfer orbit, the PAS head is incremented across the earth disk in 0.71 degree steps as the vehicle makes successive revolutions about its spin axis. Because the earth is essentially mapped once every 4 minutes during the transfer orbit, good estimates of the angle between the spin vector and the zenith vector can be made, as the look angle between the PAS scanning head and the vehicle X axis can be read to within $\pm$0.1 degree (see Appendix C, Section C.5.4).

c. $\frac{1}{2}$-Measurement. Sequential sun crossings as indicated by the PAS or SMSS sensors yield precise indication of vehicle spin rate ω_X. Since sun crossing to earth crossing time can be measured, $\frac{1}{2}$ can be accurately computed.

8.2.6 ACTIVE NUTATION CONTROL DURING SPIN PHASE

8.2.6.1 Design Description. A spacecraft spinning about an X axis where the ratio of the spin axis inertia I_X to the transfer axis inertia I_t is less than one, represents a system which is divergent in the presence of energy dissipation. The divergence manifests itself as coning of the spin axis about a space vector. If left unchecked, the coning will grow until the vehicle enters a flat spin about the transverse axis at a rate reduced by I_X/I_t. The causes of dissipation on-board a spinning spacecraft are varied and not a subject of this section. If suffices to say that the greater the magnitude of dissipation the more quickly the unstable divergence occurs. There are currently many studies underway which hopefully will enable a

good estimation of the magnitude of dissipation for a given spacecraft configuration. This will lead to an estimate of the dissipation time constant τ, where the half-cone angle θ at time t is defined as:

$$\theta(t) = \theta_0 \, e^{t/\tau}$$

For the purpose of fuel consumption estimates within this report, τ was given a very conservative value of 500 seconds.

For the IUE during transfer orbit, the following are present nominal values:

I_X = 79 slug ft^2
I_Y = 292 slug ft^2
I_Z = 288 slug ft^2
I_X/I_t = 0.27
T = 19 ft/lb
ω_X = 2π rad/s ($\pm$10 percent)
r $\simeq$ 2.0 feet

The primary equations which describe the effects of nutation are listed below with associated terms defined for the IUE.

$$\omega_N = \omega_X \, (1-\delta) \tag{1}$$

$$\frac{2T}{\omega_X^{\,2} I_X (1-\delta)} \tag{2}$$

$$S = r\omega_X^{\,2}(2-\delta) \tag{3}$$

where

ω_N = nutation frequency (rad/s)
ω = spin frequency (rad/s)

δ = I/I_t
θ = amount of nutation removed if torque T is applied for one-half nutation period

I = spin axis inertia

S = g-force/degree of half-cone angle, sensed a distance r from the X axis, along the X-axis when the nutation rate is W_X.

The following parameters are computed from the preceeding equations to be:

ω_N = 4.58 rad/s

θ = 0.0167 rad = 0.96 degree

S = 0.019g force/degree

It should be noted that all parameters defined by the three equations depend heavily on the spin rate, which can vary by ±10 percent at Delta separation. The nutation control mechanization must be self-adaptive to ω_X. Figure 8-13 defines the implications of spin rate variations. For a spacecraft spinning about an axis X with no nutation, the footprint on the ω_Y, ω_Z plot for a nutation thruster firing for one nutation cycle is shown as the nominal ω_X circle. For the unstable spacecraft with energy dissipation present, the vector ω_T in the ω_Y, ω_Z plane is shown as the coning grows in magnitude. If the solid circle represents the half-cone threshold for nutation control and if, when a threshold is exceeded, a properly phased thruster is turned on at the intercept of the solid circle and ω_X circle, the ω_T vector will transfer the nominal ω_X circle back to the origin. The time from intercept to origin on the footprint is exactly one-half nutation period.

From the equation for the half-cone ϕ at time t it is obvious that the half-cone magnitude is a function of ϕ at t_0. Therefore, the closer the nutation control drives ϕ to zero, the smaller ϕ will be at time t. This, of course, will result in a much longer time between required nutation angle reductions, assuming the reductions are initiated by half-cone divergence to a fixed threshold angle. Additionally, if the threshold were chosen such that the total angle were reduced by firing a properly phased nutation thruster for one-half nutation period, optimum fuel utilization would be realized. This mechanization was the design goal for the IUE nutation control system.

If ω_X varies by +10 percent, then from equation (2), θ is reduced by a factor of 1.21. This footprint is shown on figure 8-13 as the smaller ω_X circle. Since the same thruster removes less cone angle for one-half nutation period, the angular threshold for thruster turnon will be smaller. From equation (3), the accelerometer scale factor (g/degree) at +10 percent spin rate will increase by 1.21. Therefore, the present voltage threshold in the mechanization remains the same and only the thruster on-time must be adjusted for the current spin period. The same argument can be made for a spin period 10% lower than nominal.

With the mechanization adaptive to the current spin period, the efficiency of the system will be a function of how well the intercept can be sensed and the total impulse definition (phase and amplitude) of the nutation thruster.

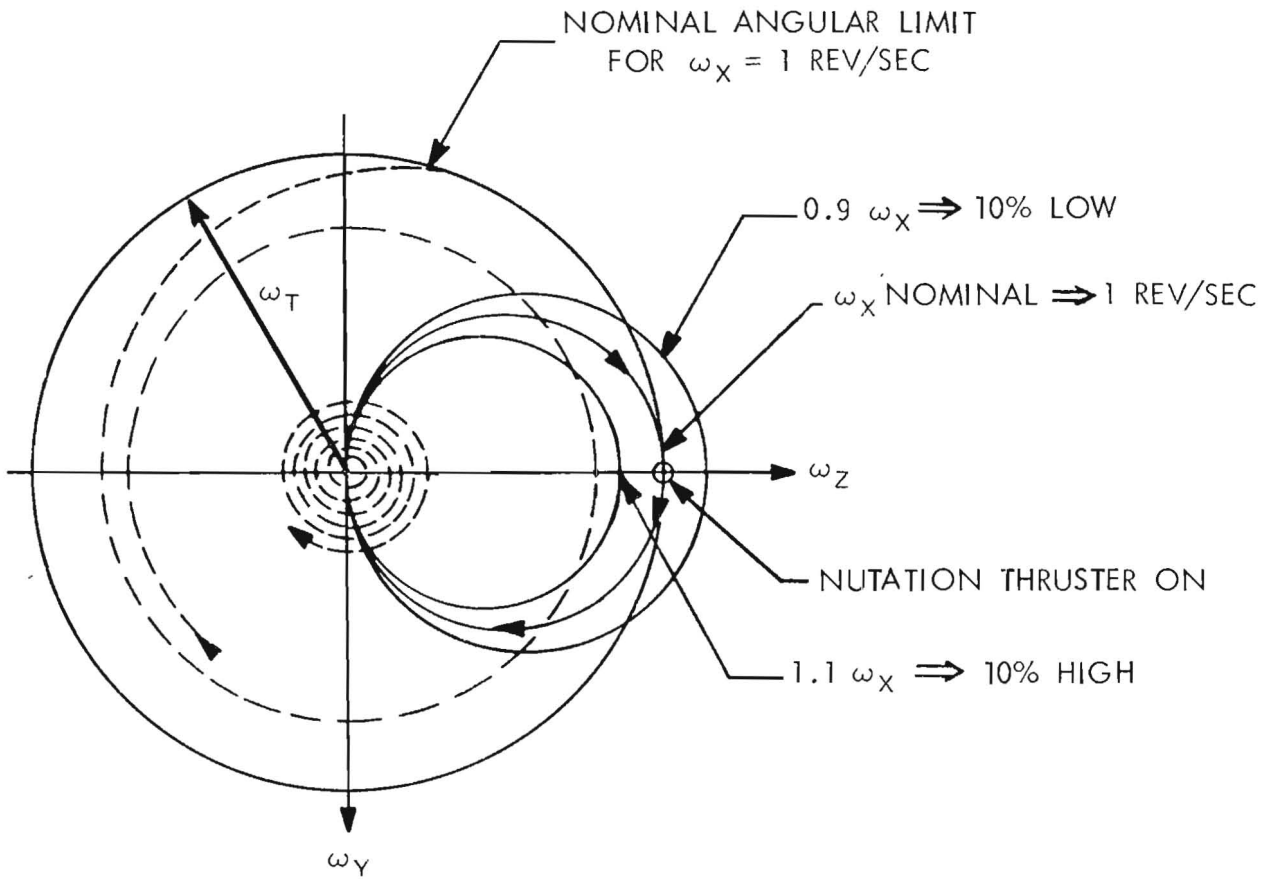

Figure 8-13. Nutation Control Switching Lines

8.2.6.2 Implementation. Like spin sectoring, the implementation of nutation damping is accomplished by hardwire logic on one of the eight CEA cards. Figure 8-14 shows the logic in elementary form.

The input sensors for the nutation logic are the redundant accelerometers. The signal from either is selected by ground command, shaped through a filter network to remove any DC bias caused by misalignment and, depending on whether nutation thruster 5 or 11 is used, phase inverted. The processed accelerometer signal is entered into an adjustable threshold detector which develops an output signal when a preset level of acceleration is exceeded and a zero-crossing detector which senses when the null point of the nutation cycle is present. When the nutation reaches a preset value, the threshold detector enables a counter. At the next zero crossing signal, the counter starts counting clock pulses until the next zero crossing transition with the same polarity. This provides a measurement of the nutation period and generates a measurement completed pulse which causes the nutation period information to be stored in a holding register. At the next accelerometer zero crossing with the same polarity, an up-down counter is preset with the nutation period information in the holding register. The clock now counts down against this register. A nutation signal is also generated and enters the hydrazine thruster drive board where it energizes either thruster 5 or 11. When the clock counts down to a point representing one-half of the stored nutation period, the thruster signal is terminated. Besides the nutation signal to the thruster, an inhibit signal to the timing logic is also generated. This signal is maintained for a period of one and one-half nutation cycles and is used to prevent thruster-induced noise in the accelerometer from falsely initiating another cycle.

Figure 8-15 is a timing diagram showing the gradual buildup of a nutation event, the zero crossing detector square wave, threshold pulses, period measurement, thruster and inhibit signals. Figure 8-16 shows graphically the effect of an increasing nutation coning as it builds to the point where the threshold is exceeded, its period is timed and a thruster fires to remove the nutation. The action is grossly exagerated for clarity.

8.2.7 PRECESSION DURING TRANSFER ORBIT

8.2.7.1 Requirements. As discussed in section 8.2.3.3, the vehicle spin axis must be precessed 180 degrees during the transfer orbit in preparation for the apogee-engine burn. The direction of precession is dictated by two requirements:

a. The precession engines should not be fired in a direction that would lower perigee.

b. A favorable β angle should be maintained for thermal and power considerations.

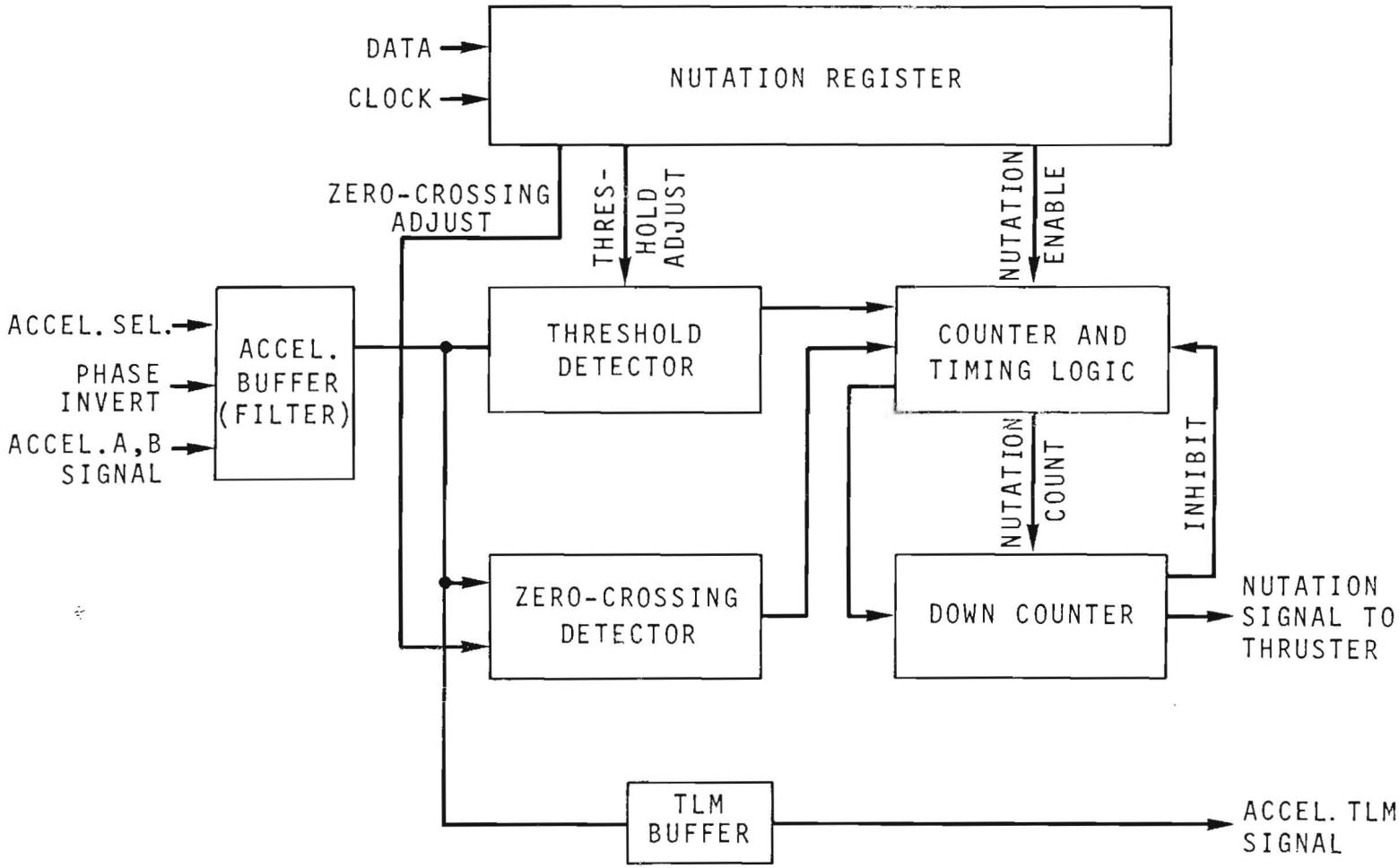

Figure 8-14. Nutation Block Diagram

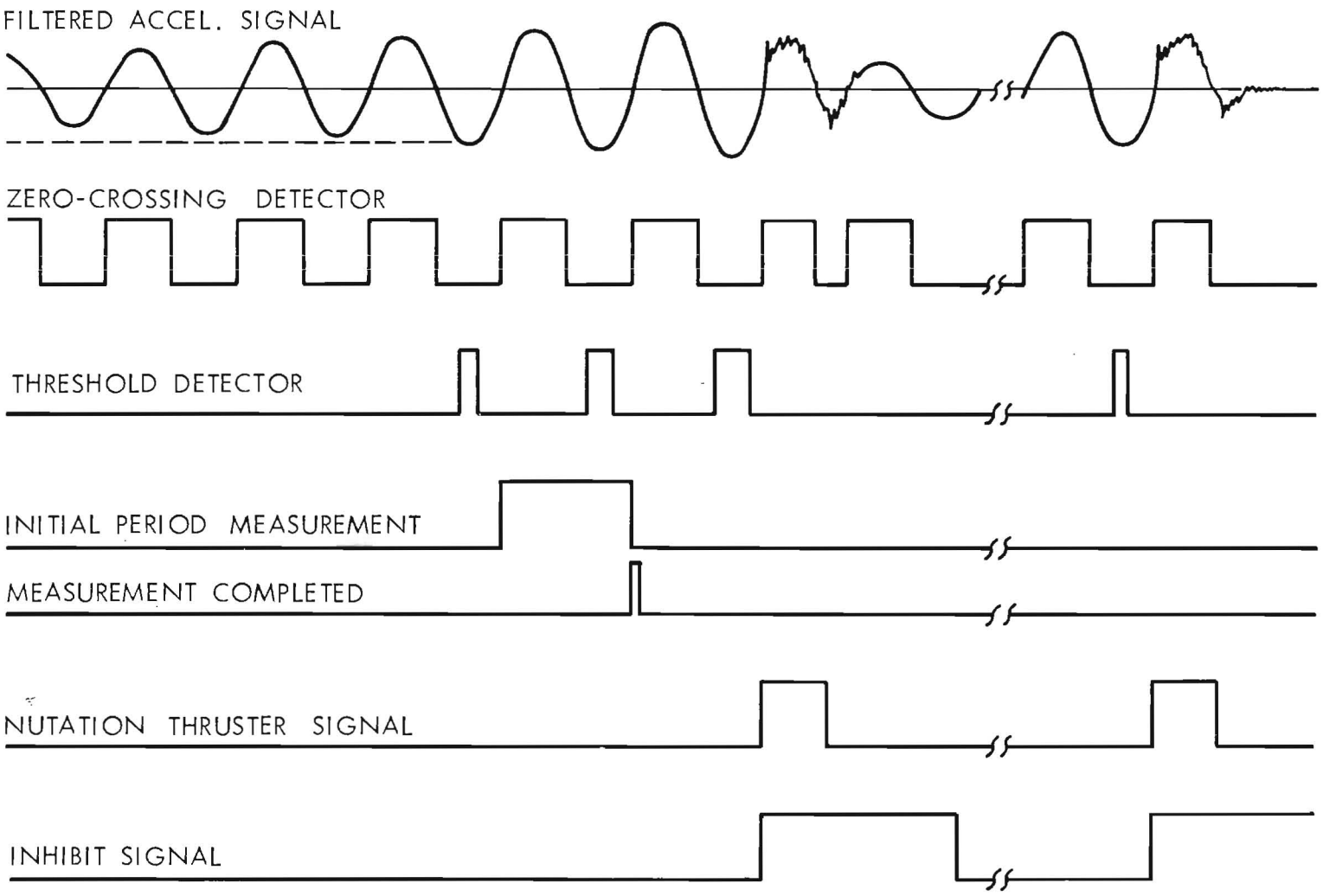

Figure 8-15. Nutation Timing Diagram

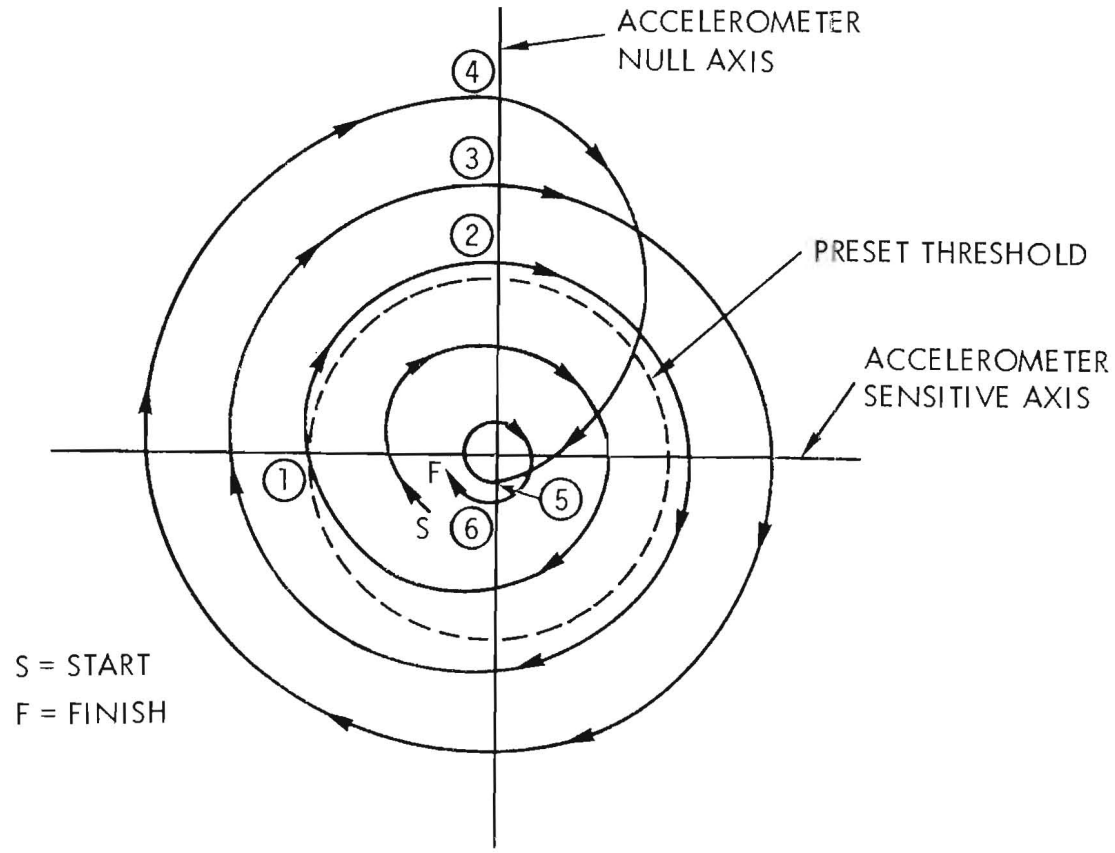

Legend

1. Accelerometer signal exceeds present threshold (at or near sensitive axis).
2. First accelerometer null crossing minus to plus, start determination of nutation period.
3. Second null crossing minus to plus, end nutation period, transfer count to holding counter.
4. Third null crossing minus to plus, transfer count to up-down register, enable hydrazine thruster, start count against register, generate accelerometer inhibit pulse.
5. Reach nutation half period, terminate thruster.
6. Complete one nutation period settle after thrusting, terminate accelerometer inhibit pulse, reset logic.

Figure 8-16. Nutation Trajectory About Accelerometer Input Axis

8.2.7.2 Implementation. A block diagram of the precession mechanization is shown in figure 8-17. With the current spin vector attitude determined on the ground, a three-part command will be issued to the precession logic which will indicate at which spin section S_1, the precession jet is to fire (1-127), at which sector S_2, the jet is to turn off (1-15), (see figure 8-16) and the consecutive number of spin cycles, N, during which the jet is to be operated (1-255). With $N \neq 0$ the precession jet will be gated for comparison with the current spin sector. When a compare is generated, the flip-flop will trigger and fire the jet. In addition, S_2 will now be gated for comparison with the start of the S_2 sector. When S_2 occurs, the trigger flip-flop will again toggle and the jet will be turned off. This process will continue with each spin cycle until N is counted to zero. At this time the precession jet will be inhibited.

8.2.8 DISTURBANCE TORQUES AT SYNCHRONOUS ATTITUDE

The Phase A report listed the worst case disturbance torques that were anticipated for the IUE in a circular synchronous orbit. Since that time the orbit has been revised to an elliptical synchronous orbit defined as follows:

a. Semi-Major Axis: $\approx$ 42,000 km.

b. Radius of Perigee (Rp): $\approx$ 30,000 km.

c. Radius of Apogee (Ra): $\approx$ 50,000 km.

d. Eccentricity: 0.27

8.2.8.1 Gravity-Gradient Torque. The expressions that describe the gravity gradient torque are as follows:

$$T_{ggx} = \frac{3G(I_z - I_y) \sin 2\theta_x}{2r^3}$$

$$T_{ggy} = \frac{3G(I_z - I_x) \sin \theta_y}{2r^3}$$

$$T_{ggz} = \frac{3G(I_x - I_y) \sin \quad z}{2r^3}$$

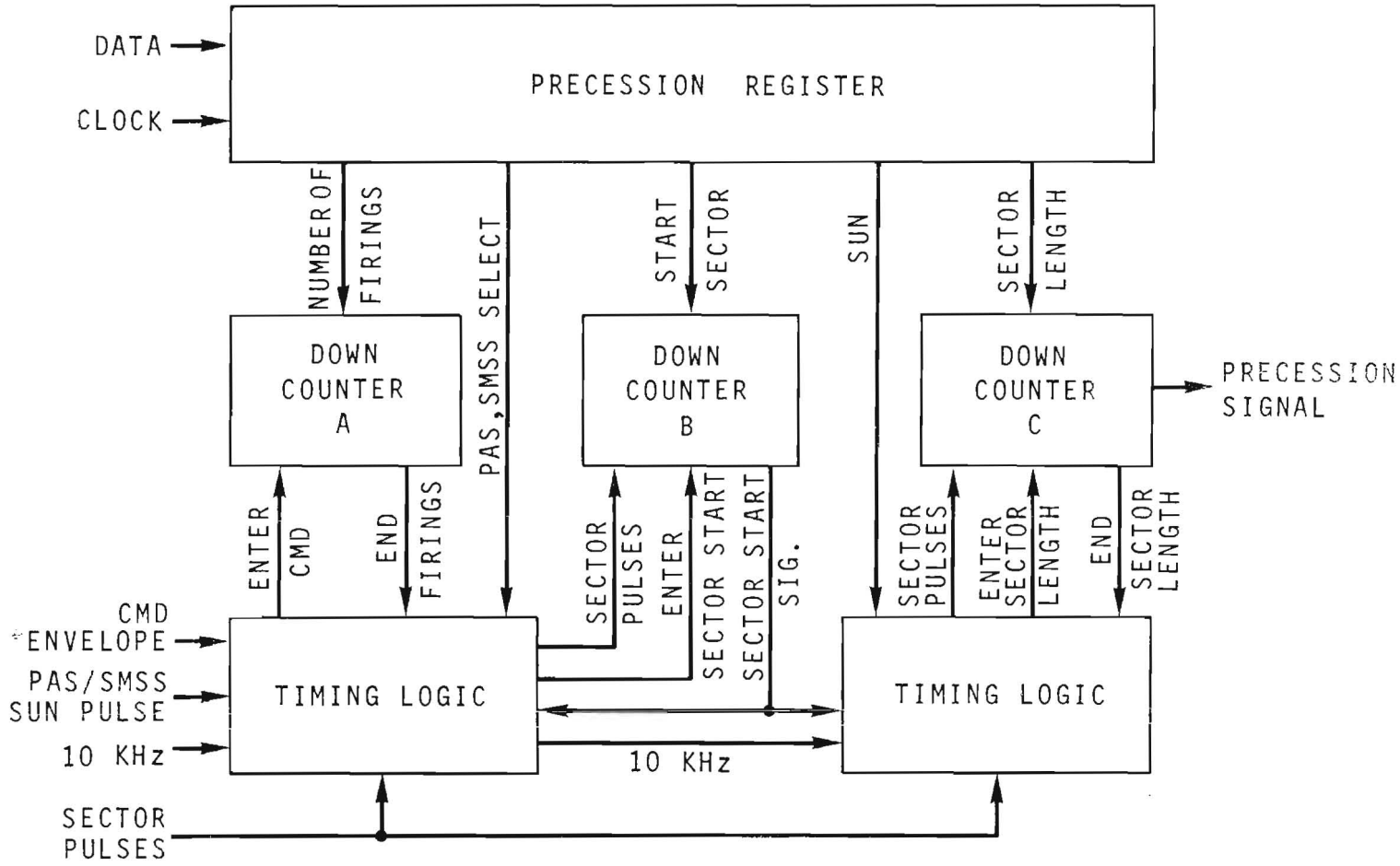

Figure 8-17. Precession Block Diagram

where:

G = the gravitational constant = $1.4 \times 10^{16} ft^3/sec^2$

r = R_p or R_A above = 1×10^8ft and 1.65×10^8ft respectively

θ = angle between the spacecraft radius vector and the body axis (worst case, 45 degrees)

I_x = X-axis moment of inertia = 85 slug ft^2

I_y = Y-axis moment of inertia = 185 slug ft^2

I_z = Z-axis moment of inertia = 203 slug ft^2

Using the above constants, the calculated gravity gradient disturbance torques at perigee and apogee are:

Torque	@ Perigee	@ Apogee
T_{ggx}	0.38×10^{-6}ft-lb	0.085×10^{-6}ft-lb
T_{ggy}	2.48×10^{-6}ft-lb	0.556×10^{-6}ft-lb
T_{ggz}	2.10×10^{-6}ft-lb	0.470×10^{-6}ft-lb

8.2.8.2 Magnetic Torques and Solar Radiation Pressure Torque. External torques resulting from interaction with the earth's magnetic field (m) and from solar radiation pressure (sr) were calculated in the Phase A report. Since that time no basic spacecraft revisions have been made which would modify the anticipated solar pressure torques. A computer study, however, was accomplished to reevaluate the effects of magnetic torques based on the elliptical synchronous orbit. The new estimates assumed an untrimmed dipole of 4000 pole-cms strength parallel to the X-axis for the IUE spacecraft. The study showed a peak momentum buildup of 0.025 ft-lb-sec for a 24 hour period. This would result from an equivalent constant torque of 0.28×10^{-6} ft-lb.

$T_{mx} = 0$

$T_{my} = 0.28 \times 10^{-6}$ ft-lb

$T_{mz} = 0.28 \times 10^{-6}$ ft-lb

$T_{sry} = 10.3 \times 10^{-6}$ ft-lb

8.2.8.3 Summary of Disturbance Torques. The net torques for each axis are summarized as follows:

*Worst case at perigee

Integrating the summed torques over a 5 year period yields the entire momentum which must be removed:

$$M = (5)\ (365)\ (24)\ (3600)\ (0.38 + 13.06 + 2.38)\ (10^{-6})\ \text{ft-lb-sec}$$

$$= 2494\ \text{ft-lb-sec}$$

Assuming an average moment arm of 3 feet for the thruster jet, the impulse is calculated to be 831 lb-sec.

Hydrazine has a specific impulse of 200 lb sec/lb. Consequently, a total of 4.16 pounds of fuel is required to counteract the disturbance torques for 5 years.

8.2.9 FUEL ESTIMATES

8.2.9.1 Nutation Control. Based on the control laws discussed in section 8.2.6, the following estimates are made for fuel consumption during a maximum 50 hour transfer orbit. Assuming that the nutation angle unloading is 80 percent efficient, then $\theta_0 = 0.20$ degree. The time required for θ to build to a 1.00 degree threshold is calculated from:

$$\theta_t = \theta_0\, e^{t/\tau}$$

$$t = 805\ \text{seconds}$$

Considering a 50 hour orbit period, unloading would be required approximately 224 times. If the thruster on-time is taken as 0.68 second, a total impulse of 5 pounds x 152 seconds, or 762 lb-sec, would result. For a specific impulse of 200 lbs/lbm, 3.81 pounds of fuel would be required.

In addition to the above requirement during the transfer orbit, the 3Σ Delta tip-off rates can be as large as 10^0/sec. This would yield a nutation half-cone of approximately 5 degrees that must be immediately removed (Reference 22). Considering nutation angle buildup during this removal, it is estimated that 6 consecutive operations of the nutation algorithm must occur to remove the 5 degree half-cone. This translates to 0.10 lb (5 pounds x 4.08 seconds per 200 lb-sec/lbm) of additional fuel. The total fuel requirements for nutation angle removal is then estimated as 3.91 pounds.

8.2.9.2 Precession. The nominal 180 degree precession scheduled during the transfer orbit will occur as a programmed sequence of torque commands phased with respect to an inertial reference such that the precession trajectory approximates a great circle path. Nutation buildup during the precession of a spin-stabilized spacecraft is discussed in references 24 and 25 where the authors define the bound on the nutation angle as the precession progresses through a number of spin periods. Reference 25 extrapolates the nutation bound analysis to the IUE configuration where the bound on induced nutation is between 1.25 and 1.75 times the induced nutation caused by a single precession pulse. If we assume that the precession torque is applied over one-tenth of the nominal spin period (100 ms) then the precession angle resulting from a single precession pulse is approximated by:

$$\theta_{rad} = \frac{\Delta H}{H_x} \frac{T\ t}{I_x W_x} \frac{19\ (\text{ft lb})\ 0.1\ (\text{sec})}{2\pi \frac{(\text{rad})}{\text{sec}}\ 79.2\ (\text{ft lb-sec}^2)} = 0.0039\ \text{rad}$$

or 0.225 degrees. To precess 180 degrees, approximately 800 precession pulses must be issued. The maneuver would then require approximately 2.0 pounds of hydrazine assuming no losses in maneuver efficiency. A computer simulation has not been accomplished which adequately demonstrates the 180 degree precession maneuver and the deviations from a great circle path.

Because attitude adjustment requirements are uncertain at this time and because a 180^0 precession maneuver may be necessary after apogee, 6.0 lbs of hydrazine should be carried as a worst case fuel estimate for the precession maneuvers and associated losses.

8.2.9.3 Despin. After apogee burn, the spacecraft is spinning at a nominal 6.28 rad/sec rate about the roll axis. Roll torque available to remove this rate is nominally 1.125 ft-lb. Time to despin is calculated at t - $I_x\omega_x$/Torque = 374 seconds. The total impulse required to remove the 6.28 rad/sec spin rate is calculated as 0.51 lb x 374 sec = 187 lb-sec. This requires approximately 0.94 pounds of fuel.

8.2.9.4 Sun Acquisition. The sun acquisition maneuver described in section 8.2.3.5 will be accomplished initially on the 0.3 pound thruster set. Analog simulations indicate that the maneuver requires approximately 0.10 pound of fuel. Assuming that a reacquisition 1.00 pound of fuel should be allotted in the total fuel budget for the function.

8.2.9.5 Momentum Unloading. The total momentum that must be removed as a result of external torques acting on the spacecraft during the 5-year mission was calculated in section 8.2.8.3 as 831 lb-sec. This would require 4.16 pounds of fuel.

8.2.9.6 Fuel Estimate Summary. Table 8-1 shows the fuel requirement budget on a yearly basis as reflected in the previous paragraphs. It should be noted that momentum buildup due to orbit-control-thruster misalignment is charged to the propulsion system and therefore not included in this estimate.

8.2.10 POWER, WEIGHT, AND DIMENSION SUMMARY

Table 8-2 summarizes the weight, power and dimension of those units charged to the control system. In most instances the units have been developed for other spacecraft and demonstrated characteristics are available. The right hand column indicates the development status for each unit.

Table 8-1. Fuel Requirements for Attitude Control

Function	Fuel Requirement Summary (LbM)		
	First Year	Second Through Fifth Years	Total
Nutation control	3.81*	-	3.81*
Precession	6.00	-	6.00
Despin	0.94	-	0.94
Sun acquisition	0.20	0.80	1.00
Momentum unloading	0.83	3.32	4.16**
25% Contingency	-	-	3.98
Total			19.89

*Assumes despin immediately following Apogee Burn
**Based upon most efficient usage of reaction mass by scheduling unloading at optimal times. Experimenter exigencies may require non-optimal unloading with consequent increase in reaction mass required.

Table 8-2. Stabilitzation and Control Weight and Power Summary

Component	Units	Power (Watts)		Weight (Pounds)		Development Status
		Each	Total	Each	Total	
Analog Sun Sensors	6	-	-	-	-	OAO
Spin Mode Sun Sensor Head	1	-	-	0.31	0.31	Univ. of Iowa (Hawkeye)
Spin Mode Sun Sensor Elect	1	-	0.42	1.09	.1.08	Univ. of Iowa (Hawkeye)
Fine Sun Sensor Head	4	-	-	.79	3.16	OAO-C
Fine Sun Sensor Elect	2	1.35	1.35*	1.73	3.46	OAO-C
Panoramic Attitude Sensor Head	2	3.0	3.0*	1.10	2.20	RAE-B
Panoramic Attitude Sensor Elect	2	2.0	2.0*	2.18	4.35	New
Redundant Accelerometer Unit	2	1.0	1.0*	0.50	1.00	SMS
Inertial Reference Assembly	1	-	67.0	-	41.43	New
Reaction Wheels	4	2.0	6.0**	5.10	20.40	Nimbus-D
Wheel Driver Assembly	1	-	8.0	-	7.43	New
Control Electronics Assembly	1	-	1.0	-	12.76	New
				Total Weight	97.58	

* Only one component power at a time
** Power estimate is for hold mode - in slew mode add 4 watts for slewing wheel

8.3 DESIGN ANALYSIS

8.3.1 DIGITAL CONTROL MODES

8.3.1.1 Control Concept. The precision control modes are digitally implemented. To reduce on-board computation requirements, three-axis attitude computations are not carried out on-board. This is allowable because there are no navigational requirements on the spacecraft, and pointing commands can be generated by ground computers. An absolute inertial reference is therefore not maintained by the flight computer, resulting in the elimination of the largest computational load of the usual strapdown gyro mechanizations (reference 3). In effect, there is one high accuracy position control system in each axis. In the normal inertially stable hold mode, the input command is zero and the control system in each axis behaves as an infinite time regulator. To acquire a new target star, the ground computer uses the knowledge of the present orientation, the orbit ephemeris and the coordinates of the desired target to generate sequential, single-axis slew commands which are fed up to the spacecraft to bias the attitude reference. As these angles are nulled, the spacecraft executes the desired slew.

Since the IUE uses only one wheel per axis, slewing must be mechanized in a closed-loop fashion. A rate limited slew mode has also been incorporated which is primarily meant for use when small slew commands are needed. It will also be needed for scale factor and axis alignment calibrations of the gyros.

8.3.1.2 Attitude Sensors. The prime attitude sensor during these modes of operation is the gyroscopic inertial reference. This is described in detail in Appendix A. The other sensors that are used to bound the attitude drift errors of the gyros are the digital solar aspect sensors and the fine error sensor. Because of its coarse resolution (compared to the gyros and other sensors), the sun sensor serves only a monitoring function, particularly in the roll axis, and is not used on-line in closed loop control. When a bright neighbor of the target star can be used as a guide star, the fine error sensor produces pitch and yaw error signals which are directly usable for updating and bias calibrating of the gyros. Since the gyro reference is used for attitude information, it may be replaced by the fine error sensor without changing the control law and filtering computations, except for changes in noise and bandwidth specifications. The present plan is to use the gyro attitude reference as long as the accuracy remains acceptable. The fine error sensor can be switched on (replacing the gyros) in a backup hold-control mode. This backup capability may be useful near the end of the spacecraft life in case of degradation of inertial reference, when it may still meet the accuracy specification for large slew but not for hold-mode of operation. Backup for the FES is provided via a redundant FES.

8.3.1.3 Pitch and Yaw Measurement Accuracy. The requirements on stellar attitude measurement and gyro hold-mode pointing accuracy may now be considered. These relate to the pitch and yaw axes only, and not to the roll axis. Because of the ±1 arc-second pointing requirement, the pointing accuracy (which depends on the attitude measurement accuracy) must be better than 0.33 arc-second rms (or 1σ). This, however, would not allow a very precise gyro trim and update. To investigate this point, let the pointing error with respect to the gyro null and the star sensor measurement error both be taken to be 0.2 arc-second of arc, 1σ. If two star fixes are taken 200 seconds of time apart and the gyro bias trim computed simply as attitude change per unit time, the worst case bias error would be 0.012 arc-second per second, which is unacceptable. However, the rms bias estimation error, using appropriate processing, could probably be brought down to less than 0.005 arc-second per second, with 0.002 arc-second per second as the lower bound. This error originates in the bias estimation and not in the gyro itself, but the effect on pointing stability is the same. The time between updates can be increased in an attempt to decrease this error, but a limit is set by the basic gyro bias instability. At 200-second sampling time, the frequency is 0.0025 hertz and available data (Reference 15) indicate that the gyro noise power is quite high (compared to the base value at 1.0 hertz) at this frequency. A desirable error distribution would be to have equal star-measurement and servo-pointing errors of such magnitude that, for the chosen update interval, the bias estimation error equals the bias instability. This would imply roughly equal error contributions from the major error sources. An investigation of gyro noise characteristics and an ACS simulation test is in progress and extrapolation of the results to space environment will be attempted. Preliminary results as well as available data (Reference 15) indicate that the inherent gyro bias stability is excellent. During the Phase A study, an error analysis was carried out based on an assumed error model (Reference 1, Section 5.5.7). The gyro random drift (1σ) and bias trim error (constant) were taken to be 0.001 to 0.003 arc-second per second, servo pointing error 0.1 to 0.2 arc-second (1σ) and the update measurement error 0.224 to 0.316 arc-second (1σ). It seems quite reasonable to expect that the inertial reference described in Appendix A will meet the 0.001 arc-second per second requirement in space. The preliminary indication from the ACS simulation test is that the requirement of 0.2 arc-second servo pointing error to the gyro null can definitely be met, with possibility of meeting the 0.1 arc-second goal. The gyro bias trim accuracy would therefore be limited mainly by the accuracy of available stellar measurements. From the numbers used at the beginning of this discussion, it seems reasonable to specify that the total stellar update measurement error, including the effects of all error sources,

should be in the neighborhood of 0.1 arc-second (1σ) and be no greater than 0.2 arc-second (1σ). This translates to a requirement of 0.6 arc-second (1σ) for the FES if nine guide stars are utilized. This requirement is compatible with the FES design, because the scan technique yields position resolution to 0.25 arc-second with proper calibration and filtering. The 0.25 arc-second or better requirement on the fine error sensor also permits the hold mode on fine error sensor to maintain ±1 arc second pointing accuracy. As compared to the gyro, the lower bandwidth of the fine error sensor implies a higher ratio of servo pointing error to sensor noise.

8.3.1.4 Roll Control. The hold-mode control on the roll axis would normally orient the spacecraft to an optimum solar aspect angle for the paddles. An accuracy of a few degrees is adequate for this purpose. Roll accuracy is also not critical for the spectrograph. The accuracy requirement arises mainly from the need to limit dynamic cross coupling between axes and to improve star sensor measurement accuracy. One minute of arc roll motion would imply a 0.133 arc-second motion of any corner of the FES/telescope field-of-view. This is below the measurement resolution and is also a satisfactory limit to prevent axis cross-coupling from becoming significant. The inertial reference would provide roll attitude information with less than 5 arc-seconds rms noise and at most 30 arc-seconds attitude shift because of gyro bias. This is more than adequate to maintain ±1 arc-minute using the roll reaction wheel. The digital solar aspect sensor has a resolution of 14 arc-seconds and accuracy of about 30 arc-seconds near null and 1 arc-minute near the edge of the field-of-view. This would therefore serve well as a monitor and could be used in a backup mode in closed loop.

8.3.1.5 Control System Simulation. A high-accuracy position system has been designed for digital implementation. Based on this design, a test program has been written in FORTRAN, including a large amount of housekeeping not needed in the flight version, and verified on an IBM 1800 computer in conjunction with hardware simulation of the single-axis control system. The design details and simulation results will be published later. A block diagram and some preliminary results are shown in figures 8-18, 8-19 and 8-20.

The block diagram is the same for any standard position control system. The major difference is in the compensator, which is digitally implemented in this case. It includes a small model of the remaining portion of the system and specifications of the system noise so that the control voltage can be calculated to a fairly high degree of precision.

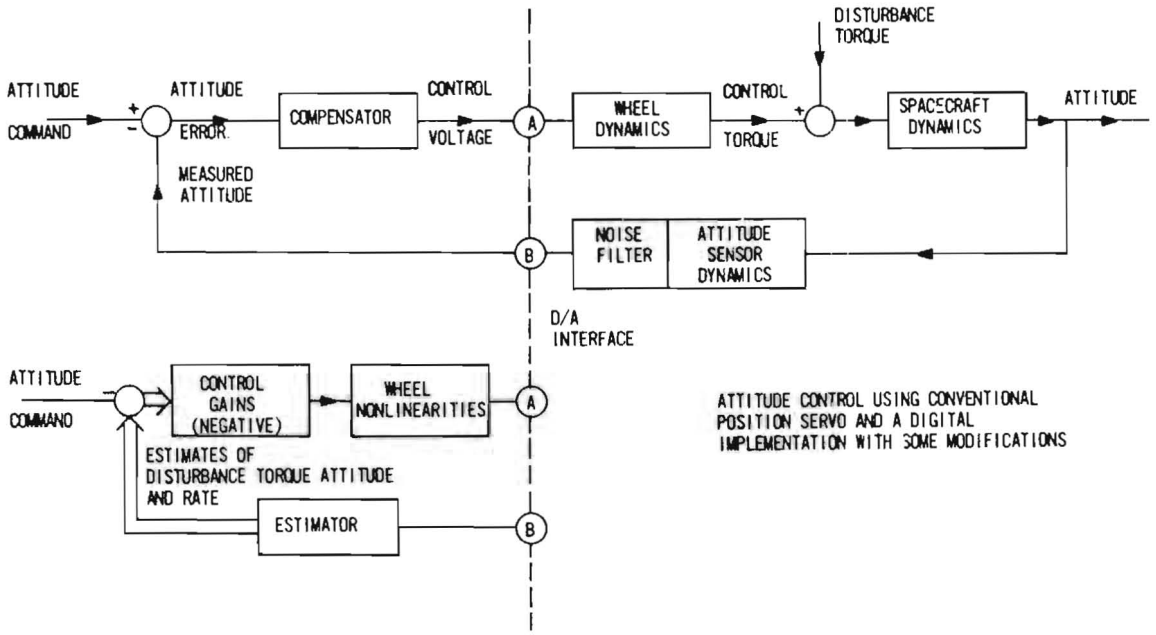

Figure 8-18. Attitude Control Function Diagram

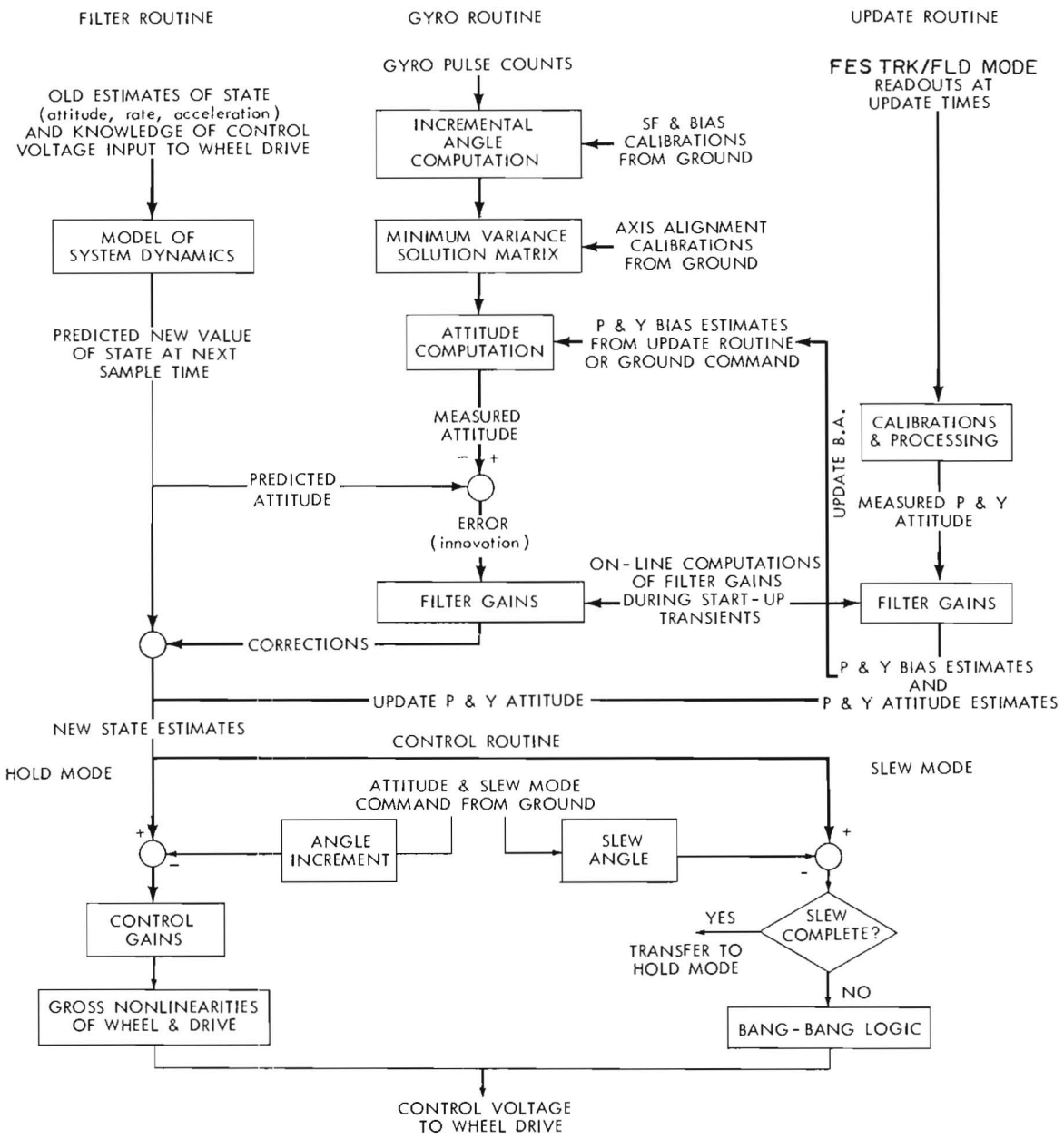

Figure 8-19. ACS Digital Computation Scheme

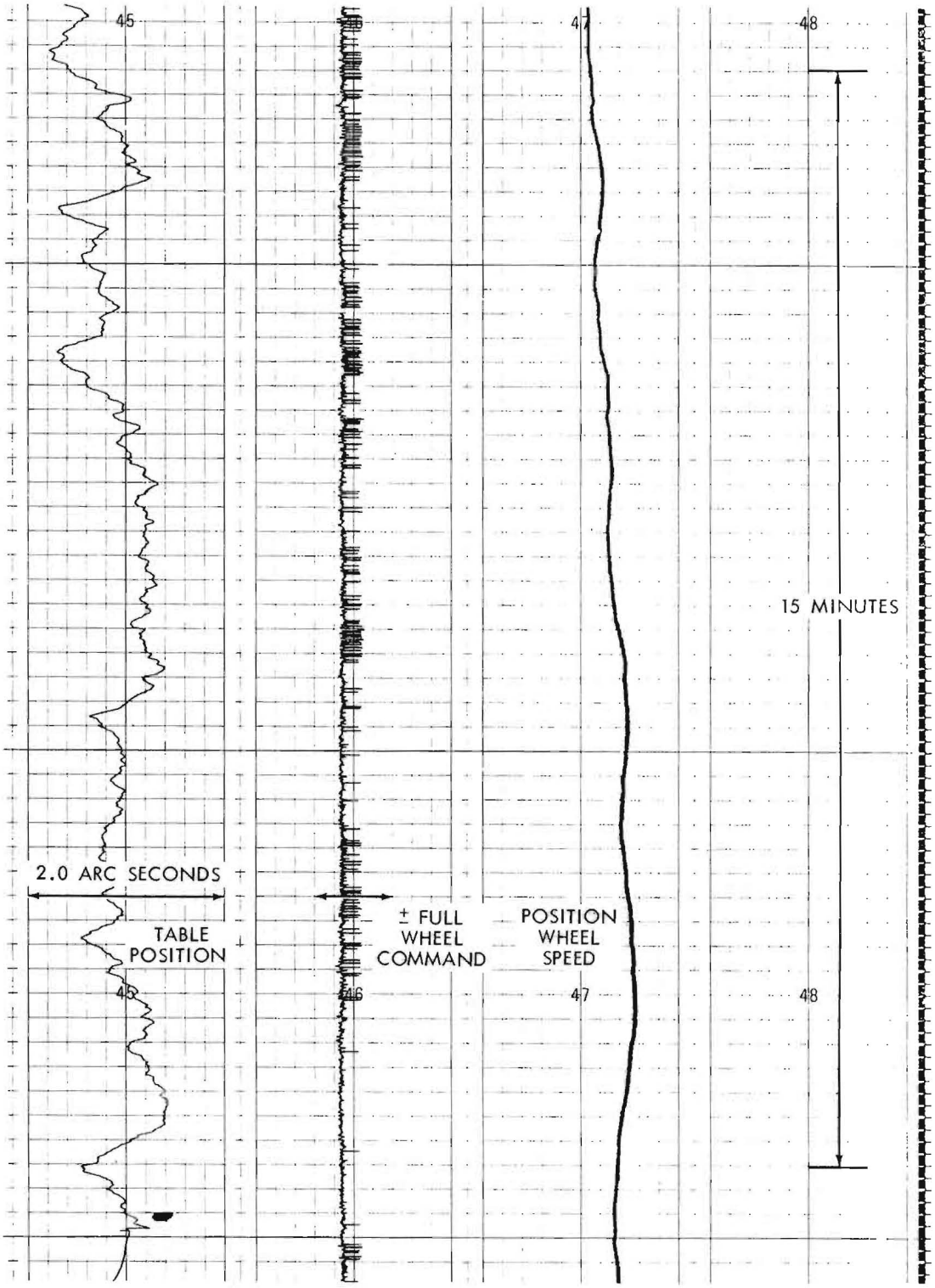

Figure 8-20. Airbearing Test Results

8.3.2 ANALOG MODE SIMULATIONS

The three-axis simulation for attitude control of the spacecraft during sun acquisition and sun hold was programmed on two EAI 231R computers. The primary objectives of the study were to determine control feasibility, to determine the amount of fuel consumed in the sun acquisition maneuver using a three-axis hydrazine thruster set and, to ensure satisfactory hold-mode characteristics using the three-axis reaction wheels. The program was divided into eight major parts which are shown in figure 8-21. A brief description of the function of each block is given, along with a discussion of the simulation results.

8.3.2.1 Parameters. The following spacecraft constants were assumed for the simulation:

Spacecraft inertia about the roll, pitch, and yaw axes, respectively

$$I_x = 90 \text{ Slug ft}^2*$$

$$I_y = 200 \text{ Slug ft}^2*$$

$$I_z = 220 \text{ Slug ft}^2*$$

Wheel inertia

$$I_x = I_y = I_z = 0.0025 \text{ slug ft}^2$$

Wheel momentum

$$H_x = H_y = H_z = 0.327 \text{ ft lbs}$$

Wheel friction constants

Viscous-friction time constant = 292 seconds

Coulomb friction = 0.4 oz in.

Stall torque = 4.0 oz in.

Jet levels

roll = pitch = yaw = 0.6 ft lb

---

*These values have changed but their impact on the analyses was minimal and it was deemed unnecessary to repeat these analyses with the new values.

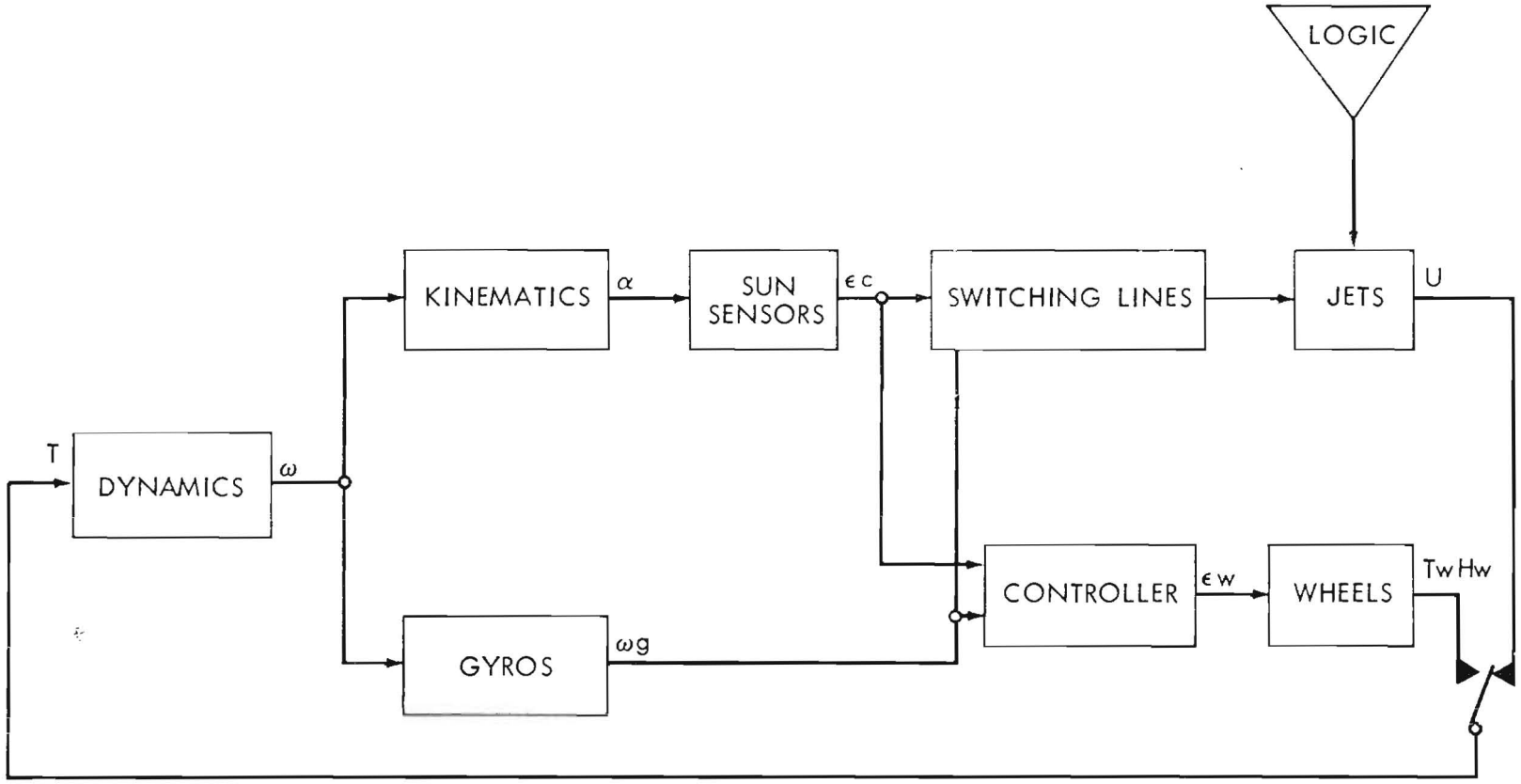

Figure 8-21. Functional Block Diagram Simulation

8.3.2.2 Dynamics. The accelerations of the spacecraft about the roll, pitch, and yaw axes with respect to inertial cooridnates are:

$$\omega_x = \left(\frac{I_y - I_z}{I_x}\right) \omega_y\omega_z - \frac{H_{xw}}{I_x} + \frac{\omega_z H_{yw}}{I_x} - \frac{\omega_y H_{zw}}{I_x} + \frac{T_x}{I_x}$$

$$\omega_y = \left(\frac{I_z - I_x}{I_y}\right) \omega_x\omega_z - \frac{H_{yw}}{I_y} + \frac{\omega_x H_{zw}}{I_y} - \frac{\omega_y H_{xw}}{I_y} + \frac{T_y}{I_y}$$

$$\omega_z = \left(\frac{I_x - I_y}{I_z}\right) \omega_x\omega_y - \frac{H_{zw}}{I_z} + \frac{\omega_y H_{xw}}{I_z} - \frac{\omega_x H_{yw}}{I_z} + \frac{T_z}{I_z}$$

where T_i = jet torques, H_i = wheel torques and H_{ij} = wheel cross-coupling torques. Integration of the accelerations provides the rates about the three axes. Included in the simulation are switches which are used to select either jet or wheel attitude control torques.

8.3.2.3 Kinematics. The time rate of change of the spacecraft position vector components with respect to inertial reference axes are:

$$a_{13} = a_{23}\omega_z - a_{33}\omega_y + K_\varepsilon \left[\sin a_{13}\right]$$

$$a_{23} = a_{33}\omega_x - a_{13}\omega_z + K_\varepsilon \left[\sin a_{23}\right]$$

$$a_{33} = a_{13}\omega_y - a_{23}\omega_x + K_\varepsilon \left[\sin a_{33}\right]$$

Integration of these derivatives provides a_{13}, a_{23}, and a_{33} which are the x, y, and z position components, respectively. The constraint that the sum of the squares of the components equals unity is imposed by defining

$$\varepsilon = 1 - a_{13}^2 + a_{23}^2 + a_{33}^2$$

A value of K = 1 proved sufficient to maintain the constraint.

8.3.2.4 Sun Sensors. The outputs of the four pitch-axis sensors in inertial coordiantes are:

$$-P_n = a_{13} \sin 27\tfrac{1}{2}^0 + a_{33} \cos 27\tfrac{1}{2}^0$$

$$+P_n = -a_{13} \cos 27\tfrac{1}{2}^0 + a_{33} \sin 17\tfrac{1}{2}^0$$

$$+P = -a_{13} \sin 27\tfrac{1}{2}^0 - a_{33} \cos 27\tfrac{1}{2}^0$$

$$-P = a_{13} \cos 17\tfrac{1}{2}^0 - a_{33} \sin 17\tfrac{1}{2}^0$$

(positive values only)

and the error about the paddle pitch axis is

$$-\varepsilon_{yp} = (+P_n) + (+P) - (-P_n) - (-P)$$

However, for simulation purposes the pitch error reduces to

$$-\varepsilon_{yp} = - (\sin 27\tfrac{1}{2}^0 + \cos 17\tfrac{1}{2}^0)\, a_{13} + (\sin 17\tfrac{1}{2}^0 - \cos 27\tfrac{1}{2}^0)\, a_{33}$$

and since the paddle and control pitch axes are coincident, the control pitch error is equal to the paddle pitch error ($\varepsilon_{yc} = \varepsilon_{yp}$).

The outputs of the roll axis sensors are

$$-R_n = -a_{13} \sin 22\tfrac{1}{2}^0 \cos 50 - a_{23} \sin 50 + a_{33} \cos 22\tfrac{1}{2}^0 \cos 50$$

$$R_n = -a_{13} \sin 22\tfrac{1}{2}^0 \cos 50 + a_{23} \sin 50 + a_{33} \cos 22\tfrac{1}{2}^0 \cos 50$$

(positive values only)

The paddle roll axis error is

$$\varepsilon_{xp} = (-R_n) - (-R_n)$$

and the control axis signals required to produce a pure rotation about the paddle roll axis are

$$\varepsilon_{xc} = \varepsilon_{xp} \cos 22\tfrac{1}{2}^0$$

$$\varepsilon_{zc} = \varepsilon_{xp} \sin 22\tfrac{1}{2}^0$$

The outputs of the three control-axis error signals have a magnitude of 2.62V/° and are limited at ±20 degrees.

8.3.2.5 Rate Gyros. Each gyro is implemented with an associated lag circuit with a time constant of 0.1 second.

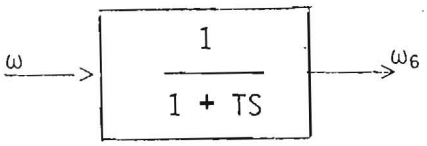

8.3.2.6 Switching Lines. For each axis, the jet switching lines have the characteristics shown in figure 8-22.

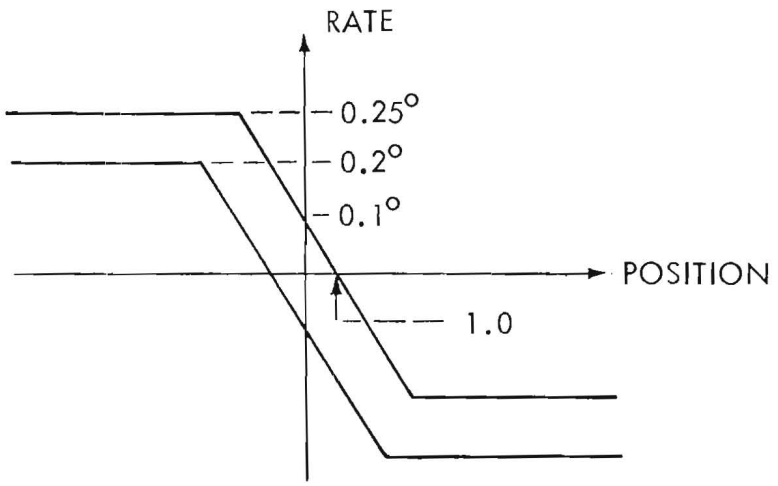

Figure 8-22. Jet Switching Lines

The gyro output (ω_g) is compared to the upper (ω_u) and to the lower (ω_L) switching lines:

If $\omega_g > \omega_u$ a negative jet is on.

If $\omega_g < \omega_u$ a positive jet is on.

If $\omega_L < \omega < \omega_u$ no jets are on.

The addition of hysteresis modifies the above three statements in the following way: If a positive jet is on, it will turn off when

$\omega_g = \omega_U$ - hys; if a negative jet is on, it will turn off when $\omega_g = \omega_L$ + hys. The value of hysteresis used is 5 percent at 0.25°/s, or 0.0125°/s.

8.3.2.7 Jets. Although the primary control of the jets is from the outputs of the switching lines, inhibit logic is included to provide the blanking discussed in Appendix . When opposing yaw-roll jets are commanded to fire simultaneously, the torque on both the X and the Z axes is reduced from 0.6 ft/lb to 0.3 ft/lb.

In order to accumulate the amount of fuel being consumed, the absolute value of the torques is summed and then integrated at a rate of 1 lbm/ 2300 second.

8.3.2.8 Controller. For each axis, the position error (ε_c) and the gyro rate (ω_g) signals are combined to produce an error signal (ε_w) which controls the wheel torque.

$$(\varepsilon_w = \varepsilon_c + 10\omega_g)$$

8.3.2.9 Wheels. The wheel torque is proportional to the controller output (ε_w), having a value of 4 oz./in. when $\varepsilon_w = 1$. The nonlinear speed-torque relationship is approximated by the two-segment characteristic shown in figure 8-23.

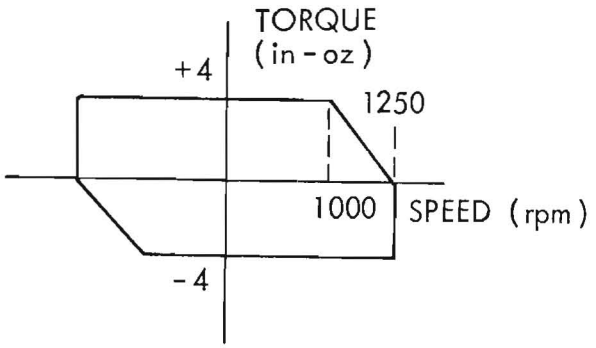

Figure 8-23. Speed-Torque Relationship, IUE Inertia Wheels

Integration of the torques provides the wheel moments, which are then multiplied by the spacecraft rates to provide cross-coupling torques.

8.3.3 SIMULATION RESULTS

The simulation results were recorded on eight-channel stripchart recorders. These have been tabulated and are shown as table 8-3 for Jet Control tests and table 8-4 for Wheel Control tests. As was stated previously, there have been changes in moments of inertia and in limit values as the actual hardware has been realized and evolved. These changes, while significant, were not deemed to be of such magnitude as to require that the analyses be repeated. The differences in actual operation are anticipated to be miniscule.

Table 8-3. Jet Control

a_{13}	a_{23}	a_{33}	Fuel (lbm)	Settling Time (seconds)
0.3826	0	-0.9238	0.0030	800
0	0	-1.0	0.0018	690
0.2930	-0.6420	-0.7071	0.0036	470
0.2930	0.6420	-0.7071	0.0032	730
0	-1.0	0	0.0032	320
0	1.0	0	0.0032	310
0.8850	0	-0.4610	0.0012	630
-0.2990	0	-0.9530	0.0014	620
0.9238	0	0.3826	0.0012	410
-0.9238	0	-0.3826	0.0011	410

Note: The settling time is defined as the time from when a jet first fires to the time when the number of firings is less than one every 10 seconds.

Tabulated below are the results of three runs which were made with the sunline pointing along the +Z paddle axis, and with all wheel rates initially equal to zero.

Table 8-4. Wheel Control

Spacecraft Initial Rates (^{o}/s)			Wheel Final Rates (rpm)			Settling Time (seconds)
ω_x	ω_y	ω_z	ω_x	ω_y	ω_z	
0.075	0	0	400	0	0	600
0	0.075	0	0	1100	0	1200
0	0	0.075	0	0	1150	800

The settling time is defined as the period from time equal zero to the time when all rates are at steady state as observed from the strip chart recordings.

8.4 REFERENCES

(1) Phase A Report for Small UV Astronomy Satellite SAS-D, Technical Plan, March 1971, NASA/GSFC.

(2) Gilmore, J. P. and R. A. McKern, "A Redundant Strapdown Inertial System Mechanization - SIRU," MIT/CSDL Report E-2427, August 1970.

(3) Final Technical Report, Precision Pointing Control System, TRW Systems Group, NASA/GSFC Contract NAS5-2111, July 1971.

(4) Pejsa, A. J., "Optimum Orientation and Accuracy of Redundant Sensor Arrays," AIAA Paper No. 71-59, 9th Aerospace Sciences Meeting, January 1971.

(5) Inertial Package Small Astronomy Satellite-D, Vol. 1, Technical Proposal, Honeywell Government and Aeronautical Products Division, Response to NASA/GSFC RFP No. 37320-164, April 1971.

(6) General GG 2200 IRA Description, Honeywell Aerospace Division, Prepared for NASA/GSFC.

(7) GG 334 Information Package, Honeywell Aerospace Division, Prepared for NASA/GSFC, May 1970.

(8) Final Report for the SAS/D Inertial Package Engineering Model, Honeywell Aerospace Division, July 1972, NASA/GSFC Contract No. NAS5-23033.

(9) GG 334A Gas Bearing Strapdown Gyroscope - Random Drift Performance, Honeywell Aeronautical Division, C.E.L. No. LMSC-70-01, March 6, 1970.

(10) Lory, C.B., J. Feldman, and J. S. Sinkiewicz, "Dynamic Testing of a Single-Degree-of-Freedom Strapdown Gyroscope," (GG334A), MIT/CSDL Report E-2618, October 1971.

(11) Proposed for Inertial Package Engineering Model for the Small Astronomy Satellite D (SAS/D), Vol 1: Technical and Business, Proposal 20364-6001-PO-00, TRW Systems Group and Northrop Precision Products Department, Response to NASA/GSFC RFP No. 37320-164.

(12) GIK7G Information Package, Northrop PPD, January 1969.

(13) Evaluation Testing of a Northrop K7G-3D, Single-Degree-of-Freedom inertial Grade Gyroscope, LEC Document No. 643D.12R.878, August 1970.

(14) Reliability Growth of C5A Gyro, Northrop Memo. No. QA:140:MJP:blh from M. J. Prendergast, dated 17 May 1971.

(15) Gyro Noise Measurements, Report No. PPD-69-E-10288, Northrop Final Report on NASA-ERC Contract NAS 12-580, October 1969.

(16) Truncale, A., W. Koenigsburg, and R. Harris, "spectral Density Measurement of Gyro Noise," MIT/CSDL Report E-2641, NASA/GSFC Contract NAS5-11002, February 1972.

(17) Ogletree, G., J. Coccoli, R. McKern, M. Smith, R. White, "Interim Technical Report No. 1, Candidate Configuration Trade Study, Stellar-Inertial Measurement System (SIMS) for an Earth Observation Satellite (EOS)," MIT/CSDL Report E-2616, November 1971.

(18) Andary, J. F., NASA/GSFC Code 732, Branch Memo Nos. 732:196:JFA: om dated 1 July 1971 and 732:234:AKG:bb dated 6 August 1971.

(19) Guha, A. K., NASA/GSFC Code 732 Memo Nos. 732:194:AKG:pap dated 6 July 1971 and 732:234:AKG:bb dated 6 August 1971.

(20) NASA/GSFC Code 732 Report on Gyro Noise Measurements and ACS Single Axis Air Bearing Test, to be published.

(21) Pyle, J. E., "Imp I Optical Aspect System," NASA Technical Note TN D-7008, Goddard Space Flight Center, Greenbelt, Maryland - March 1971.

(22) Albus, J. S., G. A. Muckel, E. J. Pyle, "Attitude Determination of a Spin Stabilized Spacecraft," NASA Technical Document X-711-68-336, Goddard Space Flight Center, Greenbelt, Maryland, August 1968.

(23) Taylor, J. M., "The SAS-D Nutation Control System, "NASA Technical Document X-732-72-196, Goddard Space Flight Center, Greenbelt, Maryland, June 1972.

(24) Slachmuylders, E., "The Behavior of the Spin Axis of a Spinning Satellite Under the Influence of Various Transverse Torques," NASA Branch Report No. 79 - Goddard Space Flight Center, Code 732, Greenbelt, Maryland, December 1963.

(25) Taylor, J. M., "Nutation During Procession of a Spin-Stabilized Spacecraft," NASA Technical Document X-732-72-278, Goddard Space Flight Center, Greenbelt, Maryland, August 1972.

SECTION 9. SPACECRAFT STRUCTURAL SUBSYSTEM

9.1 STRUCTURAL DESIGN OBJECTIVES

One of the goals of the IUE spacecraft design is to achieve a minimum weight structure while satisfying the many other requirements imposed by the various subsystems. In addition to meeting the obvious strength requirements it must be configured so that all orbital functions and launch sequence operations can be performed, and so that assembly, checkout, and integration can be conveniently done. It is also desirable that removal of a malfunctioning item of equipment be possible without a major disassembly of the spacecraft. The launch itself imposes a combination of unique requirements because it entails two stages of three axis controlled flight and one stage of spin-stabilized flight, followed at some hours later by a spin-stabilized apogee motor burn.

This spacecraft contains a number of major subsystems which, because of their role in these operations, play a significant part in the determination and evolution of the overall configuration. A partial listing of such items include the telescope, the apogee insertion rocket motor, the auxiliary propulsion system, the solar array, the attitude control system, the platform-mounted equipment, and the thermal control system. In the broadest sense the structural design objective is to create a controllable telescope platform in space that can serve to the maximum the scientific goals of the mission.

9.1.1 OPERATIONAL REQUIREMENTS

At launch the spacecraft is protected from aerodynamic loads and aerodynamic heating by the Delta vehicle fairing, which imposes certain limitations on its size. In order to conform to these limitations the solar array is stowed in a folded position, and the telescope length is limited to that which can be accommodated by the fairing. The array, however, must provide electric power during a substantial portion of the launch trajectory and injection sequence after the fairing has been ejected. Therefore, the array has been designed with the solar cells facing outward in the folded configuration. The array will remain folded during the spinning phase of the launch and injection sequence. It will be deployed after the apogee motor insertion burn. For the rest of the mission it must remain in proper orientation to the spacecraft. Attitude determination is required both during the spinning phase and after despin and deployment of the solar array. Therefore placement of the attitude sensors must be such that they are not blocked by the array either in the folded or in the deployed

configuration. Attitude control is effected by the proper use of the auxiliary thrusters after despin and stabilization. Placement of the thrusters must be such as to accomplish three-axis stabilized maneuvers, spinning maneuvers, and trajectory correction maneuvers. This placement must not cause conflicts with other systems and their functions such as shadows on the solar array or contamination on the telescope optics. Likewise, antenna placement must be arranged to satisfy pattern requirements without resulting in conflicts with the solar array, telescope, or thrusters.

The moments of inertia and dynamic balance of the spacecraft are important during the spinning phase of the mission. Since the telescope and apogee motor both lie along the spin axis of the spacecraft, and since the sum of these two items constitutes more than half the weight of the spacecraft, it is not possible to achieve a favorable moment of inertia ratio without a large weight increase. Therefore nutation of the spin axis will occur and it must be controlled. All components in the spacecraft must be located to achieve good dynamic balance and a moment of inertia ratio that is far from 1.0, where the greatest dynamic instability would occur.

In-orbit operation involves three axis stablized pointing of the spacecraft, and thereby the telescope, to any desired point on the celestial sphere, limited only by sun angle to the telescope aperture. This will be accomplished by the inertia wheels, which thus must be properly oriented to the spacecraft axes and rigidly supported solar array position must be such that sufficient power is obtained at all sun angles within the operating range. All components that dissipate heat must be mounted in the structure in a manner which provides for heat loss to space. Those items which must operate at temperatures substantially different from the temperature of adjacent items must be suitably isolated and insulated from undesirable heat exchange.

9.1.2 ASSEMBLY AND HANDLING REQUIREMENTS

For purposes of assembly, integration, and checkout, it is preferable to have the spacecraft designed as separable major subassemblies. For example, the telescope should be removable without disassembly of other unrelated components. Installation and removal of other major subsystems should also be possible with a minimum of impact on other assembled and checked out items. These can be built up separately, partially checked out and then assembled into the spacecraft at the proper time. This concept is of special importance when considering the apogee motor and the auxiliary propulsion system. A rocket motor always constitutes a potential safety hazard and must be stored separately from the rest of the spacecraft prior to final assembly at the launch site. The auxiliary propulsion system becomes a potential hazard when fueled. During those portions of its testing and checkout when it is fueled it is highly desirable that the unit be removable from the spacecraft. It is, therefore, important that flexibility

in assembly sequence be provided in the design. The apogee motor must be installed just prior to mating of the spacecraft to the Delta vehicle third stage, and this operation should not require demating of any electrical connectors or mechanical interfaces except those associated with the propulsion systems and those items located at the bottom of the lower cone structure. The auxiliary propulsion system should, ideally, be manufactured with no disconnects in the fluid lines to achieve high reliability with regard to leakage.

Handling requirements impose a need for strong points at locations where lifting rigs will be attached. These must provide for lifting of the telescope from the spacecraft, lifting of the spacecraft in both the vertical and horizontal positions and mounting it in these positions for moment of inertia measurements and for integration and test operations. These strong points must not be in conflict with other features that must function without interference from handling equipment.

9.1.3 CONFIGURATION REQUIREMENTS

The configuration is generally limited by the needs of the telescope, its size and weight and by the other major items. Size, weight, function, and the spinning mode of operation essentially make it mandatory that both the telescope and apogee rocket motor be located on the centerline of the spacecraft. Functional requirements make it necessary that the auxiliary propulsion system be located near the lower end of the spacecraft and that it be symmetrical about the spin axis. The solar array could have many combinations of dimensions but it must be arranged to fit inside the fairing when folded and must have sufficient area and satisfactory attitude when deployed. Platform-mounted equipment must be arranged to produce a dynamically balanced spacecraft with a minimum of balance weights while also satisfying thermal dissipation requirements. Geometrical arrangements that would optimize one subsystem would frequently conflict entirely with others and thus these must be compromised.

9.2 STRUCTURAL DESIGN REQUIREMENTS

The structural design requirements for the IUE spacecraft are determined primarily by the environment produced by the Delta launch vehicle. With the exception of the apogee motor thrust, and possibly the solar array deployment shock, all of the loads imposed on the spacecraft after separation from the third stage are small. Apogee motor acceleration load will not exceed 6.5 g, which is less than the third stage acceleration of approximately 10.5 g. All of the forces and moments produced by the hydrazine thrusters are small and thus do not govern structural design. Table 9-1 lists the various structural design criteria. This data is derived from the Delta Spacecraft Design Restraints manual DAC-61687 issued by the McDonnell Douglas Astronautics

Table 9-1. Design Criteria

Criteria	Parameter	Units	Requirement	
			Design Qualification	Protoflight Acceptance
Static Balance	Center of gravity offset	inches	0.100	0.05
Dynamic Balance	Angular Deviation of Principal Axis	radians	0.04	0.02
Sinusoidal Vibration				
Thrust Axis	Frequency Range	Hz	5-6.3 / 6.3-15 / 15-21 / 21-200	5-6.3 / 6.3-15 / 15-21 / 21-200
	Level (0 to Peak)	g	0.75 in da. / 1.5 / 5.25 / 1.95	0.75 in da. / 1.5 / 5.25 / 1.95
	Sweep Rate	Oct./Min.	2.0 / 2.0 / 2.0 / 2.0	4.0 / 4.0 / 4.0 / 4.0
Lateral Axes	Frequency Range	Hz	5-40 / 40-80 / 80-200	5-40 / 40-80 / 80-200
	Level (0 to Peak)	g	0.75 in da. / 1.16 ips / 1.5	0.75 in da. / 1.16 ips / 1.5
	Sweep Rate	Oct./Min.	4.0 / 4.0 / 4.0	4.0 / 4.0 / 4.0
Random Vibration				
All Axes	Frequency Range	Hz	20 / 20-300 / 300-2000	20 / 20-300 / 300-2000
	PSD Level	g^2/Hz	0.0044 / 3dB/Oct. / 0.068	0.0044 / 3dB/Oct. / 0.068
	Acceleration	g-rms	11.3	11.3
	Duration	min./axis	2	1
	Rate of Increase	db/octave	3	3
Acceleration	First Stage	g	17.4 Thrust and 1.5 Lateral Simultaneously (1 minute duration)	N/A
	Third Stage	g	17.0 Thrust (Covered by first stage test)	
	First Stage (Pogo oscillation)	g	(Covered by 15-21 Hz band, Thrust Sinusoidal Vibration and the first stage 17.4 combined acceleration)	
Spin Rate	Initial	rpm	75	60
	Final	rpm	0.001	0.001
Max. Ang. Accel.	Spin-up	rad/sec^2	9.0	6.5
	Despin, Prescession, Pitch, Yaw	rad/sec^2	0.2	0.13

Company, and from a proposed revision to the General Environmental Test Specification for Spacecraft and Components, S-320-G-1 issued by the Goddard Space Flight Center.

In specifying design criteria for subsystems and components, the area of greatest uncertainty are the vibration inputs. These inputs are largely influenced by the stiffness characteristics of the spacecraft structure and the clampband-adapter assembly. Empirical data on the spacecraft and adapter have been obtained in vibration tests on the engineering test unit and are documented in Environmental Test Specification for IUE Subsystems, IUE-320-74-008, Revision 1, December 1975.

9.3 CONFIGURATION AND GENERAL ARRANGEMENT

9.3.1 GENERAL DESCRIPTION

To fulfill the objectives and requirements described above the spacecraft general arrangement and design has evolved from the Phase A design into the configuration shown in this report. An overall view of the IUE spacecraft in the deployed configuration is given in figure 3-1. It is shown with the array folded in figure 3-2. It is an octagon-shaped body with a solar array on each of two opposing sides and with the telescope protruding from the top. The auxiliary propulsion system with its thrusters is at the lower end of the body, and a conical structure at the bottom provides for attachment to the launch vehicle and also supports the apogee rocket motor inside.

9.3.2 PRIMARY SUBASSEMBLIES

The structure has been designed in several major sections to facilitate assembly and disassembly, and to provide the operational and handling characteristics described in Section 9.1 above. These structural sections, when fitted with their various components become primary subassemblies. The primary subassemblies that can be removed from the spacecraft as a unit are as follows:

a. The telescope assembly with or without the Inertial Reference Assembly (IRA).

b. The upper body and telescope support structure.

c. The equipment platform and components.

d. The solar arrays.

e. The upper cone structure.

f. The hydrazine auxiliary propulsion module.

g. The apogee rocket motor.

h. Lower cone structure and rocket motor adapter rings.

Figure 9-1 is an exploded view showing these primary subassemblies. A cut-away view of the assembled spacecraft is shown in figure 9-2.

9.3.3 STRUCTURAL INTERFACES

The subassemblies are joined together as described below:

a. The telescope experiment interfaces mechanically with the spacecraft structure at three points on the telescope strong ring. These points fasten to fiberglass thermal insulation blocks that are bolted to the top of each of the three telescope support columns. This provides a strong thermally isolated connection, and because of three-point suspension it reduces distortions imposed on the ring by spacecraft structural distortions. At two of the three mounting pads an additional mounting feature is provided for the IRA gyro assembly. The IRA electronics package is mounted to the upper equipment platform. The IRA gyro assembly is attached to the strong ring by 2 thin-walled titanium mounting frames. These low thermal conductivity mounting frames provide additional thermal isolation for the gyro assembly. The rigid mounting frames allow the IRA gyro assembly and telescope combination to be removed from the spacecraft structure for integration, alignment, and checkout without disturbing the relationship between the two; and thermal distortions, however large or small in the spacecraft, have no effect on the relationship between the telescope and the IRA gyro assembly.

b. The upper body structure fastens to the top of the upper cone structure and surrounds the main equipment platform, which also fastens to the top of the upper cone structure. The main equipment platform is thermally isolated while the other connections are direct.

c. In the launch configuration the solar arrays will be folded along the X axis of the spacecraft as shown in figure 3-2. The array hinge mechanisms will be mounted with thermal insulators on the main platform at facets C and G which are identified in figure 9-3. In addition, there will be two explosively actuated locking devices for each array. These will be located on the top platform upper body structure at the corners of facets A-B, D-E, E-F, and H-A. These

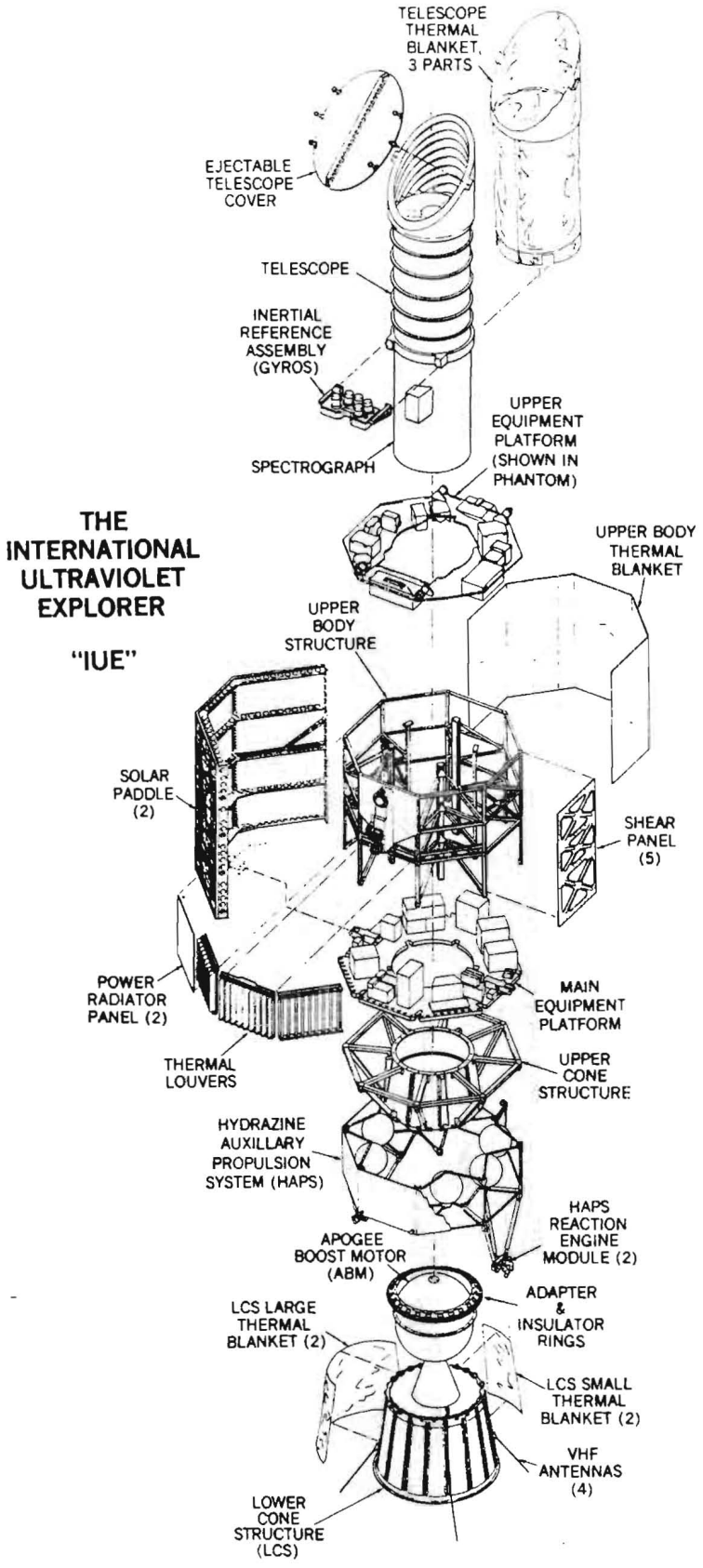

Figure 9-1. IUE Exploded View

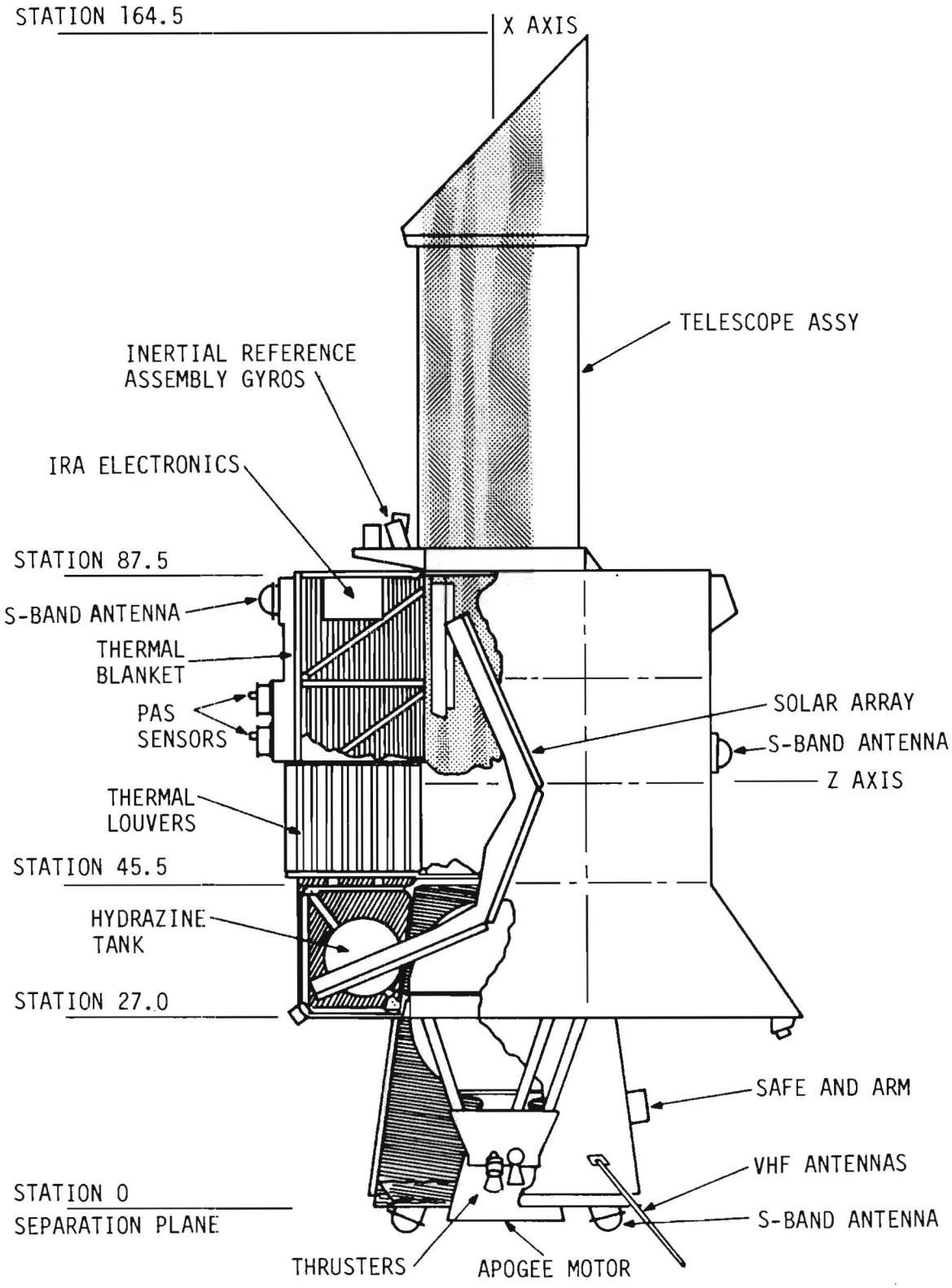

Figure 9-2. IUE Interior and Exterior Features

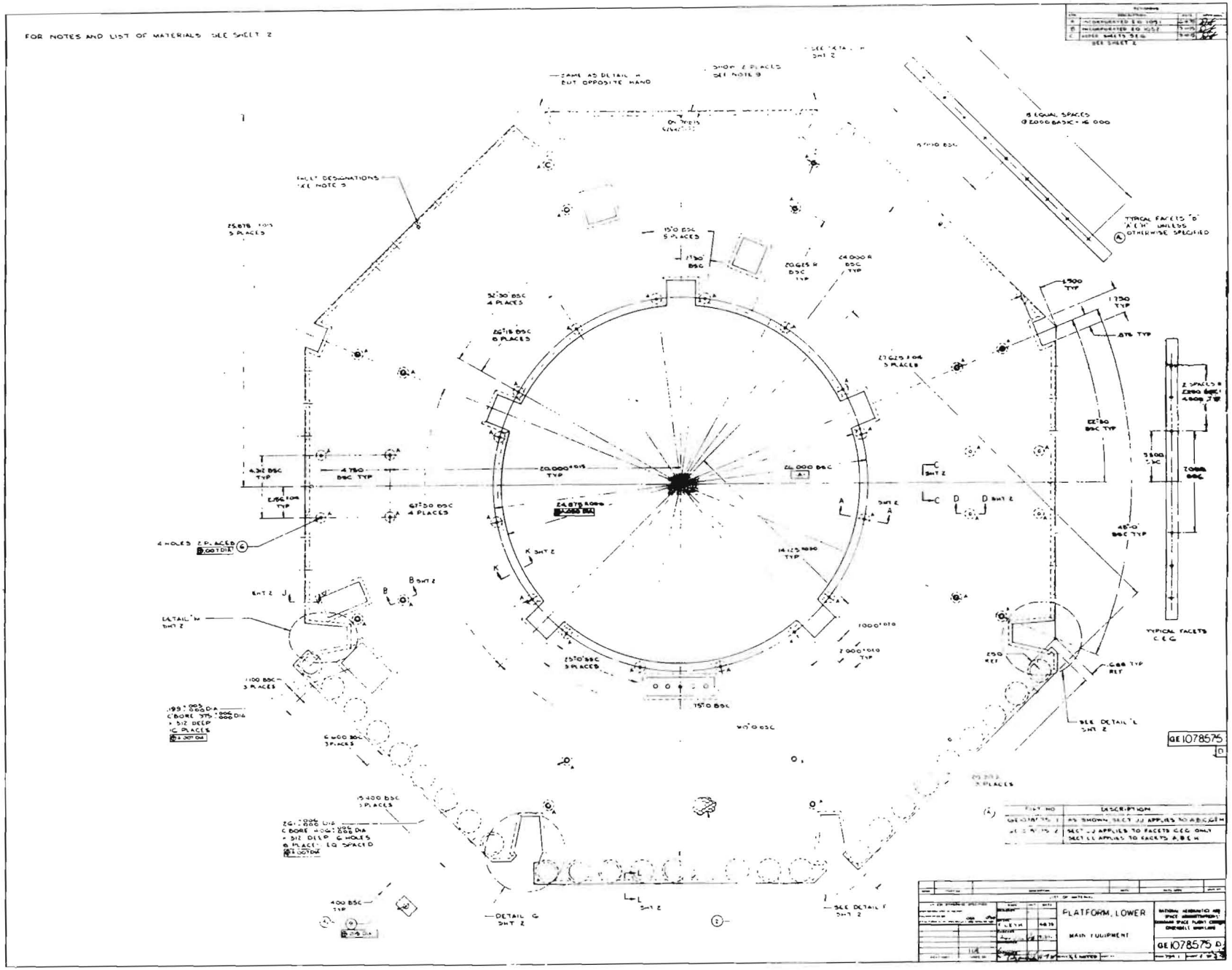

Figure 9-3. Main Platform Assembly

locking devices capture both vertical side frames of each array and provide both vertical and lateral support to the arrays. Each array hinge mechanism provides only lateral support. To optimize the vibration characteristics, swivel pins are used to hold the two lower corners of each array.

d. The hydrazine propulsion bay, an octagonally shaped structure that contains the entire hydrazine system, fastens to the upper cone structure at 16 points. The eight upper corners of the bay structure are bolted to machined corner fittings at the corresponding points on the upper cone structure. At the bottom of the bay structure, there are eight bolt holes which mate with corresponding holes in the lower ring of the upper cone structure. The only other connections into the spacecraft are the electrical connectors that provide power, telemetry data, and control signals for operation of the hydrazine system.

e. The upper cone structure is fastened to the top of the lower cone structure where a 24 bolt flange is provided. Another inner flange at this level provides for the apogee motor adapter ring and insulator ring.

f. The apogee rocket motor is fastened to the top of the adapter and insulator rings. This arrangement allows installation of the rocket motor without disassembly of any portion of the spacecraft except this joint, the access panels on the propulsion bay, the 2 lower S-band antennas and the S-band and VHF antenna cabling.

9.4 STRUCTURAL DESIGN DETAIL

9.4.1 IRA FRAME

The telescope strong ring includes mounting provisions for the attitude control IRA gyro assembly. This arrangement ensures rigid alignment between the telescope and the gyros regardless of any effects occurring in the spacecraft structure. The frame that supports the gyro assembly is a two-piece unit machined from titanium. With this arrangement the IRA gyro assembly is rigidly held in place and yet thermally isolated from the telescope, a condition which is required by the large difference between the operating temperatures of the two.

9.4.2 UPPER BODY STRUCTURE

The telescope strong ring is supported by three columns which are a part of the upper body structure. The upper body structure consists of eight corner columns and a number of horizontal and diagonal members in

addition to the three telescope support columns. It extends vertically from station 45.5 to station 86.875 and is 52 inches wide across the flats. The horizontal and diagonal members provide lateral support to the vertical columns and make the overall structure more rigid. All of these parts are of aluminum alloy and are riveted together using machined corner fittings where necessary. The telescope columns are 6061-T6 alloy with welded end caps. All of the structural members are 2024-T81 or T851 alloy. To mount the rear body mounted S-band antennas and the panoramic attitude sensors, a panel and bracket structure is riveted to the upper E facet of the upper body structure. The lower portion of the D, E, and F facets are used to mount the three thermal louvers. The upper portions of facets D and F are covered with an excess power radiator panel. The remaining five sides of the upper body structure are stiffened with lightweight shear panels.

At the top of the eight vertical corner column is mounted the upper equipment platform. This aluminum honeycomb platform supports the camera electronics box, the experiment electronics assembly, the reaction wheels used for controlling spacecraft attitude when in the three-axis stabilized mode and other miscellaneous components. The IRA electronics is mounted on a removable portion of the upper honeycomb equipment deck. This facilitates the installation and removal of the electronics necessary for calibrating the gyro assembly.

9.4.3 LOWER EQUIPMENT PLATFORM

The lower equipment platform is an aluminum honeycomb sandwich structure. It is octagonal with a dimension of 51.75 inches across the flats and a 24.875-inch diameter hole in the center. Notches at the corners and in the edge of the hole provide clearance for the columns of the upper body structure. This platform is 0.8-inch thick with 0.016-inch face sheets of 2024-T81 aluminum alloy. The honeycomb core is 0.768-inch thick 5056 alloy with 1/4-inch cells and 0.002-inch foil thickness. The platform is mounted to fiberglass blocks on the structural ribs of the upper cone at station 45.5 and to a fiberglass ring in the center, also at this station. Inserts are installed in the platform where required for attachment of components. Much of the electrical equipment is mounted on top of this platform. This platform is also the support structure to the solar array hinge mechanisms. Fiberglass pads will thermally isolate the arrays from the platform. To equalize the temperature of the entire platform and its equipment, the under surface is equipped with two circular heat pipes that fasten to inserts in the platform. In order to control heat loss to space, the three dark sides of the platform (anti-sun sides) are equipped with thermal louvers. Figure 9-3 shows the main platform assembly; figure 9-4 shows the equipment mounted on the platform.

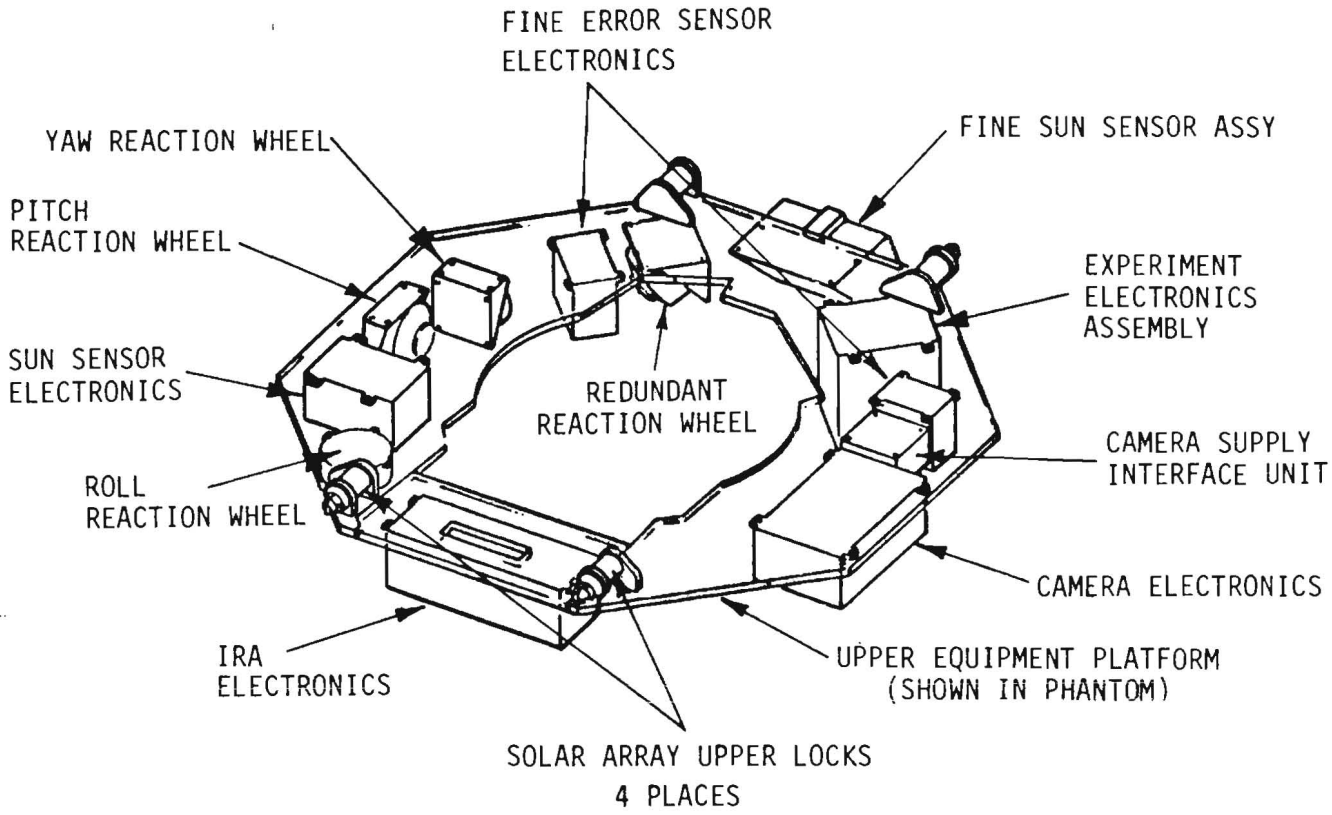

Figure 9-4. Equipment Mounted on Platform

9.4.4 THE SOLAR ARRAY

The solar array of the IUE spacecraft is supplied by the European Space Agency (ESA) with the design and development under the cognizance of the European Space and Technology Centre (ESTEC), Noordwijk, Holland.

The solar array consists of two deployable paddles, one on each side of the spacecraft. Each paddle has a 21.574-inch-wide center panel and two 26.692-inch-wide side panels, all 55.63 inches long. The side panels are permanently fixed at 45 degrees to the center panel to conform to spacecraft geometry when the array is folded, and to provide more power output at high and low sun angles when deployed. In the folded configuration the solar cells are on the outside to provide power while the spacecraft is in the spinning phase of the launch sequence. Each of the flat panels is a honeycomb sandwich structure with aluminum core and fiberglass face sheets. Details of the solar array weight are listed in table 9-2.

In the stowed configuration, each paddle is attached to the spacecraft at five points: the hinge, the two upper locks, and the two swivel pins. Upon command, redundant pyrotechnics release the two upper locks. The swivel pins automatically release as the paddle starts to deploy. During deployment, the hinge rotates the paddle first about the spacecraft Z axis, then the spacecraft Y axis until the final paddle position is reached. In the final position with the arrays rotated 22.5 degrees about the Y axis, the hinge becomes rigidly locked. This, along with the stiffness of the array, gives a natural frequency of 7.03 Hz in the bending mode and 5.47 Hz in the torsional mode.

During deployment, the array motion is damped by a centrifugal brake. This brake gives a virtually constant drag over its operating temperature.

9.4.5 UPPER CONE STRUCTURE

The upper cone structure has a sheet aluminum cone that extends from station 27.0 to station 45.5 and has aluminum alloy rings riveted to it at the top and bottom. Eight horizontal ribs extend outward from the upper ring to the eight corners that form the octagonal body structure. At each of these corners a machined fitting joins the horizontal rib to a diagonal member which rises from the lower ring, and to the angle members which form the outer octagonal shape. Three formed sheet metal "hat" sections riveted to the cone provide support to the three telescope columns of the upper body structure. Five small sheet metal "hat" structures are used to stiffen the cone structure. The cone, horizontal ribs, diagonal members, and hat sections are 2024-T3 alloy. The upper and lower machined rings are of 2024-T351 alloy, and the remainder of the members are of 2024-T4 alloy. Twenty-four bolt holes are provided in the lower ring for attachment to the lower cone

Table 9-2. Solar Array Weight Details

Item	Weight (Pounds)
Solar Cell Modules	8.44
Module Adhesive	1.06
Panel Wiring and Adhesive	0.53
Honeycomb Ground	0.22
Harness	0.91
Main Connector	0.08
Temperature Sensors	0.03
Potting	0.06
Thermal Boards	0.44
Solder and Shrinkable Sleeves	0.14
Frame	17.48
Panels and Screws	13.66
Hinge Assemblies	3.49
Release Mechanism Assemblies	3.96
Swivel Pin Assemblies	0.62
Centrifugal Brakes	0.60
Sun Sensor Shades	.12
Total Solar Array Weight	51.84

structure, and eight bolt holes are provided for the propulsion bay structure in this ring. A bolt hole is provided in each of the eight upper corner fittings for the propulsion bay, and one also for each upper body corner column.

9.4.6 PROPULSION BAY STRUCTURE

The propulsion bay is an octagonally shaped structure similar in width to the upper body structure. It has eight vertical corner columns, with corner fittings at the top and bottom. Each of the lower corners is connected by a horizontal edge member. These form the octagon. All structural frame members are made of aluminum alloy. The propulsion bay frame members consist of both tubular and sheet metal structures joined with machined fittings.

Hydrazine tanks are permanently installed in this structure. The plumbing lines and fittings, which are permanently welded, are secured with nylon clamps to the structure. All valves, filters, and miscellaneous components associated with the auxiliary propulsion system are contained in this bay. The thrusters and their valves are attached to the outside. Thermal blankets are fastened to the sides and bottom of the bay to provide for thermal control. The propulsion bay is shown in figure 9-5.

9.4.7 LOWER CONE STRUCTURE

The lower cone is the main load-bearing section of the spacecraft structure. It is fastened to the vehicle attach fitting by a standard Delta clamp band, which will be tightened to a tension load of 2800 pounds. The lower cone consists primarily of an upper and a lower ring with a sheet cone connecting them. The rings are machined from 2024-T351 aluminum alloy and the sheet is formed using lockalloy, a beryllium-aluminum alloy. Four spring seats for the separation springs are machined from 2024-T4 alloy. All parts are riveted together. The upper ring has 24 threaded holes on an outer bolt circle, and an alignment groove for fastening to the upper cone structure. A similar set of holes and an alignment surface for fastening the apogee motor adapter ring is provided on the inner bolt circle. Accurate alignment of the motor and the upper structure with the lower cone are necessary to achieve coincidence of the thrust vector with the spacecraft spin axis within acceptable tolerances. Additional brackets and doublers are used to accommodate items such as the two S-band antennas and VHF antennas. Figure 9-6 shows the lower cone panel. This supports the thermal blanket, which protects the apogee motor from solar heating.

9.4.8 APOGEE MOTOR ADAPTER RINGS

The apogee motor is fastened to an adapter ring with a fiberglass insulation ring between the motor flange and the adapter. The adapter ring is

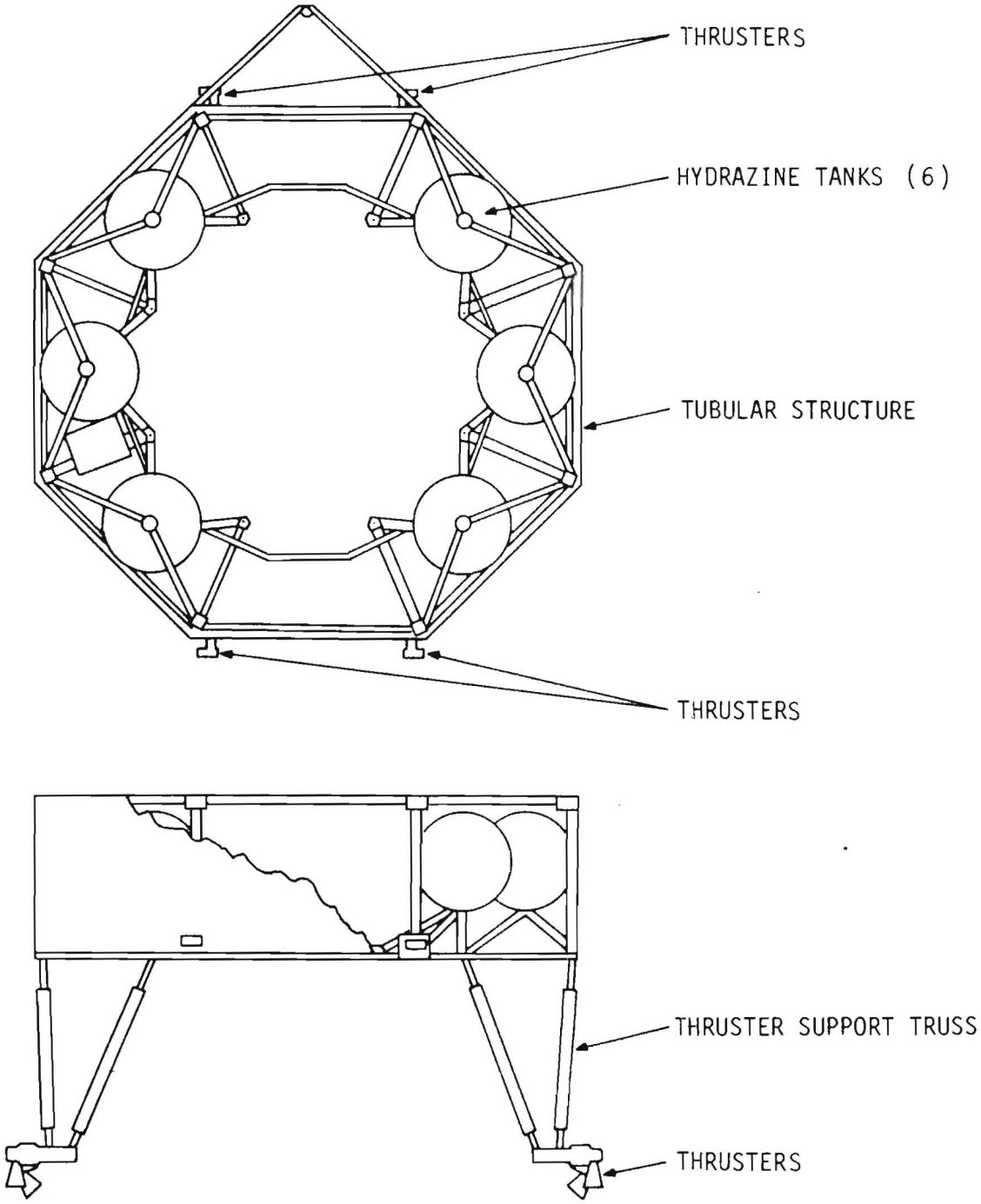

Figure 9-5. Auxiliary Propulsion Bay

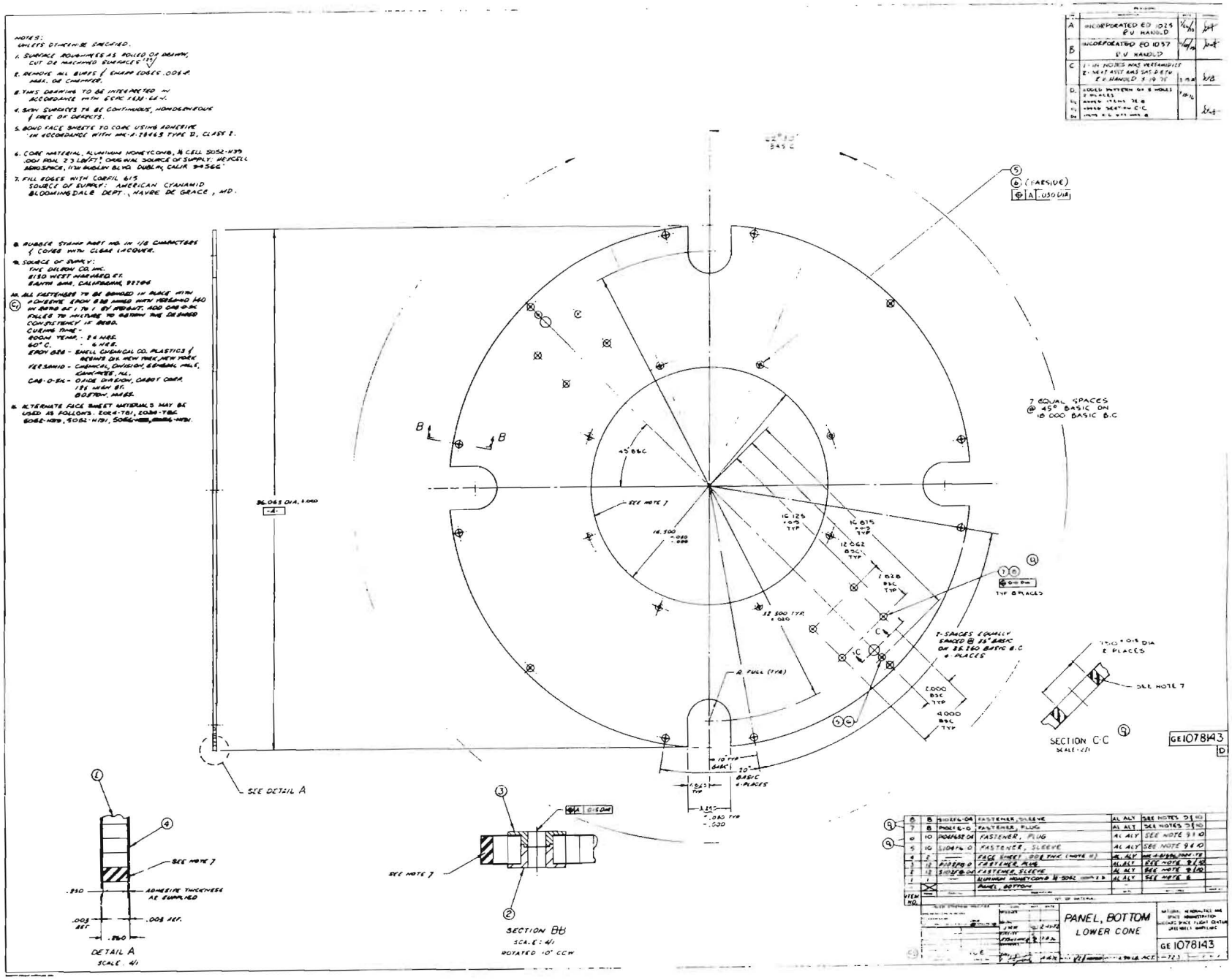

Figure 9-6. Lower Cone Panel

bolted to the lower cone structure at station 27.0. An insulation ring is needed to limit thermal soakback into the spacecraft during and after apogee motor burn. The adapter ring is machined from 2024-T351 aluminum alloy, the insulator from epoxy-fiberglass.

9.5 LAUNCH VEHICLE COMPATIBILITY

The spacecraft has been designed to be launched on the Delta 2914 launch vehicle, which has the new 96-inch diameter fairing. Figure 3-2 shows the spacecraft in this fairing. The folded solar arrays are designed to fit within the 86-inch diameter payload envelope. The exit plane of the nozzle of the apogee motor is located 3.137 inches below the separation plane to minimize effects of the exhaust plume on the structure. This dimension could be as much as 4 inches without interfering with the upper portion of the Delta third stage motor. The spacecraft has been designed to interface with the Delta 3731 A attach fitting, which is intended for spacecraft over 1200 pounds. The lower ring of the lower cone structure meets the spacecraft interface dimensional restraints specified in the Delta Spacecraft Design Restraints Manual (DAC-61687A). The restraints include:

a. Correctly designed clamp band lip.

b. Lower ring cross sectional area of 0.3863 $in.^2$ within 2 inches of the separation plane.

c. Lower ring cross section moment of inertia of 0.010 $in.^4$ within 2 inches of the separation plane.

d. Brackets to accommodate four separation springs.

The IUE spacecraft has been designed within the weight limit for the 2914 Delta vehicle when placing a spacecraft into the inclined high apogee transfer trajectory required for this mission.

9.6 STRUCTURAL ANALYSIS

The primary structure and major mass components are illustrated in the exploded view of figure 9-1. The telescope with the IRA gyro assembly is supported at three points by columns each stabilized by two intersecting trusses. Since loads in all direction, applied at the intersection can be supported by the trusses alone, the outside skin on the upper body structure was considered a redundant load path and thus a target for weight saving. This was inspite of less efficient load paths and a number of clearance problems caused by a much less rigid upper body structure. The upper body attaches to the upper cone structure which redistributes the loads along with approximately 250 pounds of equipment and the 100-pound hydrazine system to a circumferential loading on the lower cone. The lower cone then acts as a compression member and a cantilevered beam for the total spacecraft weight.

The most severe structural loads occur at lift-off in the lateral direction and at MECO in the thrust direction. These thrust levels, combined with vibration expected during flight are multiplied by 1-1/2 to obtain the qualification level used in the centrifuge test. This test was performed on the spacecraft Engineering Test Unit (ETU). The qualification loads were 17.4 g's in the thrust direction with 1.5 g's in the lateral.

The lift-off load is one of many flight transients which affects the design of the spacecraft structure and subsystem components. All such loads were applied during testing by a single sinusoidal vibration sweep. One of the important functions of structural analysis is to assure that the test levels are adequate and to prevent the levels from over testing the spacecraft. The desired test levels are 1-1/2 times the expected flight levels. These are predicted by a transient analysis of the spacecraft coupled to the launch vehicle. The spacecraft model shown in figure 9-7 was used to predict the flight loads. It represents the spacecraft structure with 164 degrees of freedom and incorporates the solar arrays and telescope as a single mass point. The McDonnell Douglas Corporation performed an independent structural analysis to predict the launch vehicle flight loads and the motion at the base of the adapter during lift-off. These motions were used as excitations for transient analysis of the spacecraft model which included the scientific instrument and solar arrays substructures. These substructures are shown in figures 9-8 and 9-9. The results of these analyses were used to develop the qualification test levels.

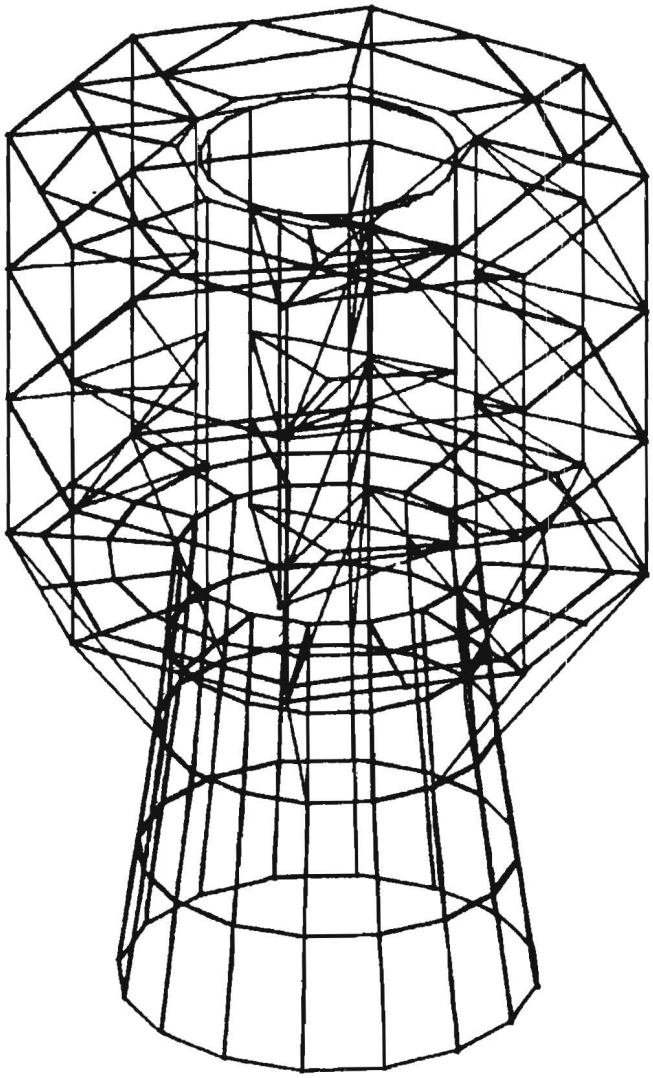

Figure 9-7. Spacecraft Structural Model

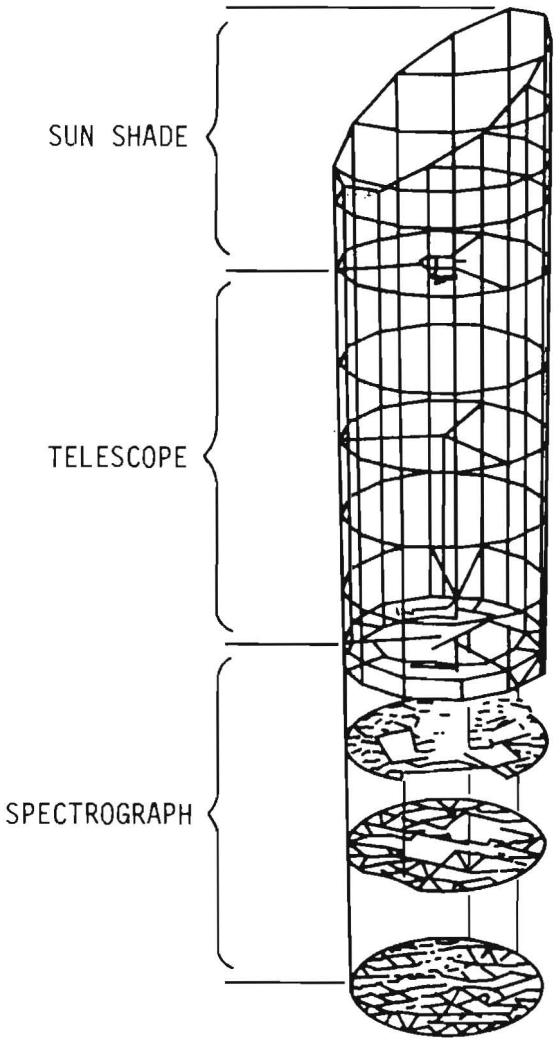

Figure 9-8. Scientific Instrument Structural Model

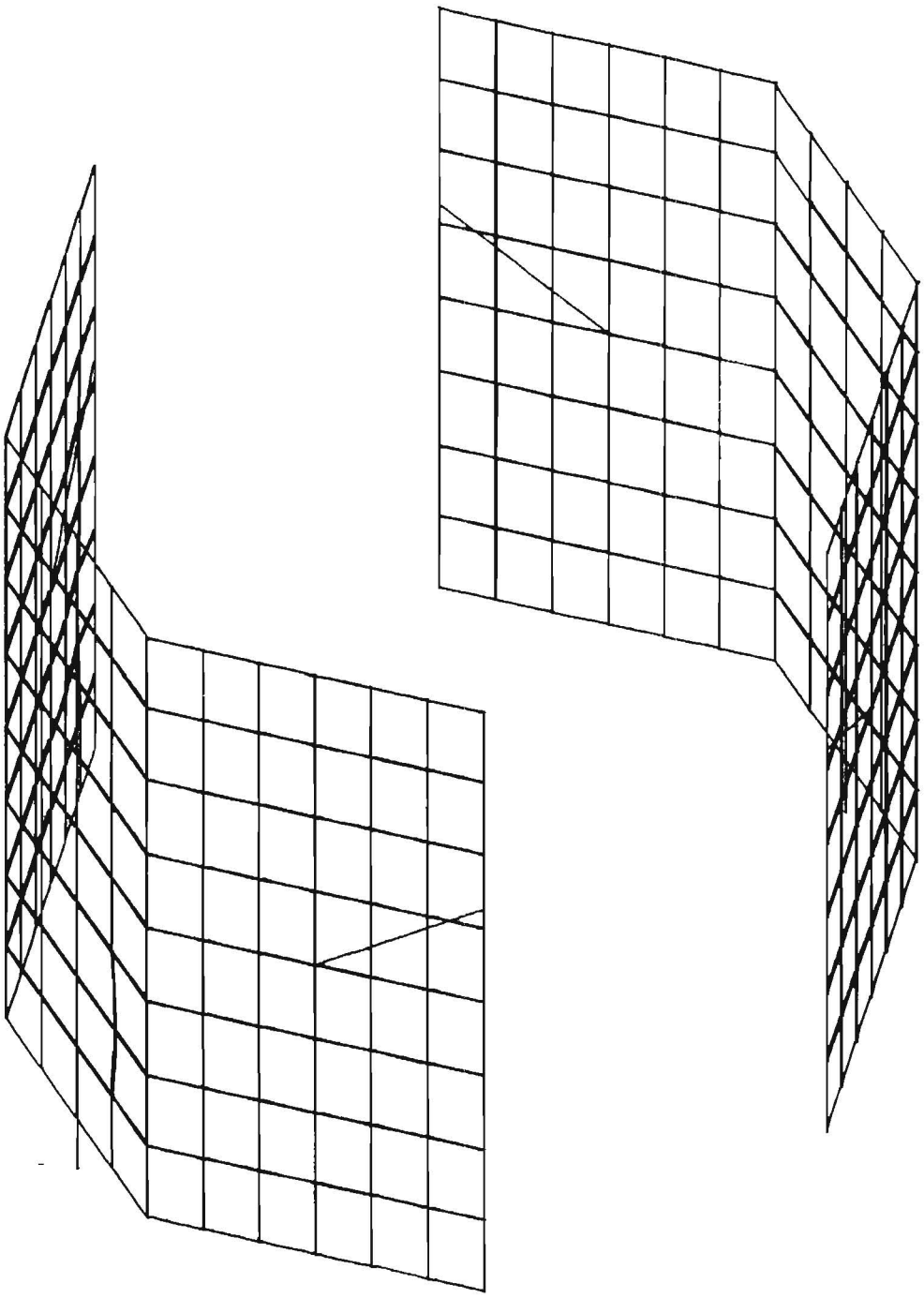

Figure 9-9. Solar Array Structural Model

SECTION 10. SPACECRAFT THERMAL DESIGN

10.1 THERMAL DESIGN REQUIREMENTS

From the thermal design viewpoint, the IUE spacecraft may be conveniently divided into five separate and distinguishable sections, each with its unique thermal problems. Referring to figure 9-2, these areas are: the Hydrazine Auxiliary Propulsion System (HAPS) bay from station 0 to station 45.5, the main equipment bay from station 45.5 to station 87.5, the spectrograph which is mounted in its canister within the main equipment bay, the telescope from station 87.5 to station 164.5, and the solar array. The thermal design of the spectrograph and telescope were discussed in Volume I of the IUE System Design Report.

The HAPS bay consists of the apogee boost motor, the HAPS, and the surrounding spacecraft structure. The only thermal requirement on the ABM is to maintain its temperature between $-15^{o}C$ and $+38^{o}C$ prior to ABM ignition, which may occur up to 50 hours after launch. The HAPS must be kept between $+5^{o}C$ and $+65^{o}C$ throughout the mission.

The main equipment bay is to be maintained between $0^{o}C$ and $+40^{o}C$. The batteries are an exception as are the gyros in the Inertial Reference Assembly (IRA). The batteries are not to exceed $+20^{o}C$ while the gyros contain their own thermal controller to maintain temperature at $+57.3 \pm 1^{o}C$. Most of the electronic equipment is mounted as shown in figure 9-4. The main equipment platform is located at station 45.5 (see figure 9-2). The remainder of the electronic packages are mounted on the upper equipment platform located at station 87.5.

Referring to figure 7-5, the IUE spacecraft is oriented such that the sun is always in the X-Z plane. The solar aspect angle (β) can be anywhere between $0^{o}C$ (sun on aft end of vehicle) to 135^{o}. The total power dissipation is on the order of 186 watts of which approximately 130 watts is dissipated in the main equipment bay. In addition, the spacecraft is required to survive a 72 minute, zero power eclipse.

10.2 THERMAL DESIGN OF THE MAIN EQUIPMENT BAY

Once synchronous orbit is achieved, the sun moves in the X-Z plane from a β angle of 0^{o} to a β angle of 135^{o}, thereby exposing only one side of the spacecraft to sunlight at all times except for the eclipse phase of the orbit. Since the scientific instrument is susceptible to thermal gradients and also changes in gradients, the main equipment bay which

surrounds the spectrograph is covered with multilayer insulation to reduce the effect of solar input. The spectrograph is further decoupled from the main equipment bay by utilizing low emittance surfaces. As a further reduction of the solar effect, the outer layer of the insulation is silverized teflon.

To achieve the required temperatures at the anticipated power dissipation of about 130 watts, approximately .55 m^2 of radiating area is required. Since this power dissipation is not constant and the spacecraft must operate over a wide range of solar aspects, this radiating area is provided by thermal louvers. Three sets of louvers consisting of nine blades each are located on the anti-sun side of the spacecraft. Each louver blade is individually controlled by its own bimetallic spring located within the honeycomb of the main equipment platform (see figure 9-3). The louvers provide approximately .6 m^2 of radiating area in the fully open position and are calibrated to move from fully closed at 0^oC to fully open at 10^oC. They are similar to the louvers flown on the SAS-C satellite. To further reduce thermal gradients, two circular heat pipes are mounted to the underside of the main equipment platform. These pipes are ammonia-filled grooved heat pipes of the type flown on the ATS-6 spacecraft. Each heat pipe is capable of transporting 75 watt-meters, far in excess of expected IUE heat loads. It is calculated that the heat pipes will reduce the gradients on the platform to less than 5^oC.

10.3 THERMAL DESIGN OF THE HAPS BAY

Since the hydrazine system can withstand rather wide temperature limits (5^oC to 65^oC), it was decided to make use of solar energy to reduce the dependence on heaters. The canted side ("sun catcher") of the HAPS bay is a single layer of kapton with a VDA-SiO-SiO_x coating having an absorptance (α) of 0.25 and an emittance (ε) of 0.23. This surface provides a solar input of approximately 20 watts at the $\beta = 135^o$ solar aspect and aids in maintaining a more uniform energy balance over all solar aspects. The sides of the HAPS bay are covered with multilayer insulation with an external surface of Vapor Deposited Aluminum (VDA). The remainder of the propulsion area is covered with multilayer insulation with a black exterior layer. The propulsion area is radiatively isolated from the main equipment platform by a multilayer blanket. Details of the catalyst bed heaters, line heaters, and valve heaters can be found in section 11.3.

The apogee motor is covered with multilayer insulation to prevent heat leaks to the main equipment bay during firing and to prevent heat leaks to space during orbital flight. In addition, a heat shield will cover the nozzle exit plane during the transitional phase of the flight to keep the ABM warm before firing.

10.4 PREDICTED SOLAR ARRAY THERMAL PERFORMANCE

A thermal analysis of the IUE solar array has shown that the array must be deployed within five minutes of completion of the despin maneuver. In addition, it will be necessary to keep the β angle between 45° and 135° before despin in order to control temperatures and maintain a favorable power output from the array.

When the satellite is spinning and the arrays are in the stowed configuration with a β angle of 90°, the highest cell junction temperature is $20.5^{\circ}C$. Under the same circumstances as above but with the satellite not spinning and one paddle directly facing the sun, the hot paddle would reach temperatures as high as $93^{\circ}C$ in spots. The cold paddle could see temperatures as low as $-183^{\circ}C$. This condition could be very serious for two reasons. First, the power from the array would be small because the hot paddle's cells would have a greatly reduced voltage output. Secondly, the cold paddle's deployment mechanism may not function at such cold temperatures. Thus, it is necessary to deploy the array within five minutes of despin.

The average subpanel temperatures at the end of life at summer solstice are shown in figure 10-1 as a function of β angle.

In its elliptical geosynchronous orbit, the IUE will experience eclipses with durations up to 84 minutes. During the longest eclipse periods, parts of the array will occassionally experience temperatures as cold as $-185^{\circ}C$. Because of these severe temperatures, the array design and the array itself will be thoroughly thermal cycled.

Test samples or "Q boards" of the substrate and solar cell stack, which are completely representative of the flight array except for size, have undergone in excess of 2,000 cycles from $-180^{\circ}C$ to $+80^{\circ}C$ with no failures. Although the lowest temperature the array will see was not realized, this thermal cycling still represents a considerable overtest. This is so because the satellite will experience only about 460 eclipses during its lifetime and because the array will nominally experience low temperatures of $-165^{\circ}C$.

In addition to the "Q boards" tests, which are run to verify the design, the mechanical prototype array will be cycled 100 times and the flight array 40 times. The primary reason for cycling these units is to assure good workmanship and, in the case of the mechanical prototype, to verify those parts of the design not tested by the "Q boards".

10.5 THERMAL ANALYSIS

Because of the relatively small thermal interaction between the spacecraft and the Scientific Instrument (SI) - which includes both the

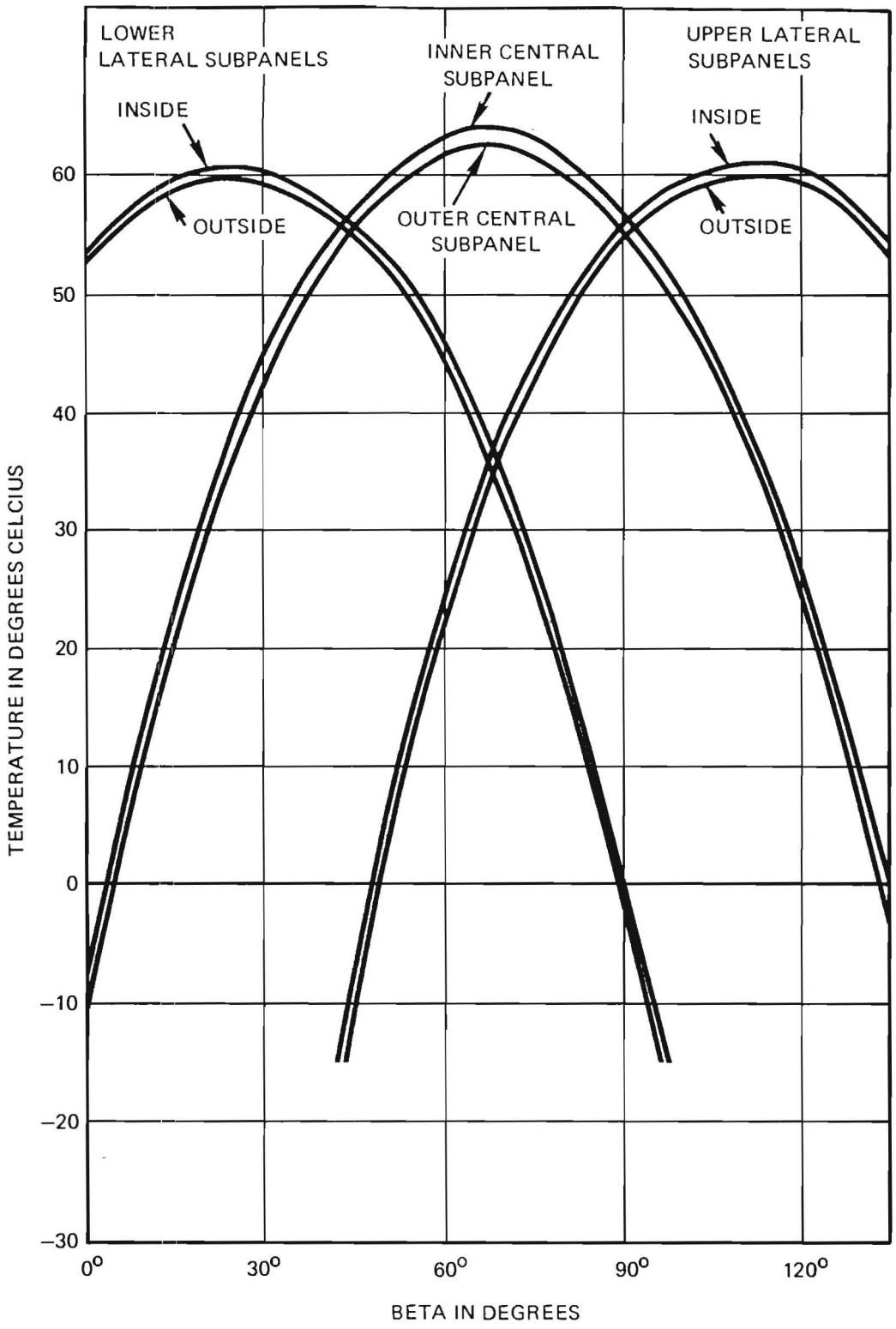

Figure 10-1. Average Subpanel Temperatures At EDL and Summer Solstice

telescope and spectrograph, two separate analytical models were constructed. The analytical model of the SI contains 195 nodes while the spacecraft model, consisting of all components except the spectrograph and telescope, contains 186 nodes. In addition, a 250 node model has been constructed to investigate the thermal conditions of the propulsion area in minute detail. A comprehensive analytical model has yet to be generated.

Table 10-1 is a listing of the major components and the expected nominal temperatures as a function of β angle. It is to be noted that this data is the result of a preliminary analysis performed in May of 1976 using the analytical model. These values will be updated as the components become better defined. A thermal vacuum test will also be run on the flight vehicle to verify the thermal design.

Table 10-1. Predicted Thermal Performance of Major IUE Components (Data Obtained from IUE Analytical Model - May 1976 Run)

NODE	BAY	DESCRIPTION	POWER (W)	$\beta=0^{o}$ (TEMP ^{o}C)	$\beta=67.5^{o}$ (TEMP ^{o}C)	$\beta=90^{o}$ (TEMP ^{o}C)	$\beta=135^{o}$ (TEMP ^{o}C)
17	A-1	Command Subsystem	1.30	20.64	24.82	23.80	20.37
18	E-1	Multiplexer	2.50	9.57	12.90	11.79	8.59
19	B-1	Computer Memories	0.0	22.15	26.19	25.19	21.85
176	B-1	Computer Processors	16.40	35.03	38.70	37.77	34.69
20	C-1	Array Hinge #1	3.00	25.09	28.90	27.90	24.60
21	C-1	Diode Filter #1	3.70	41.92	45.26	44.35	41.43
22	CO-1	VHF Transponder #1	2.50	25.07	28.69	27.67	24.44
160	C-1	S-Band Transmitter	0.0	14.52	18.34	17.19	13.72
23	D-1	S-Band Power Amp. 1	21.00	28.48	32.05	31.02	27.81
24	D-1	VHF Transponder #2	0.0	21.18	24.69	23.63	20.42
25	E-1	Battery #1	4.50	18.18	21.66	20.63	17.45
26	E-1	Battery #2	4.50	18.46	21.96	20.92	17.73
27	F-1	Control Electronics	3.00	14.86	18.38	17.22	13.86
28	G-1	Wheel Drive Assembly	5.00	24.67	28.32	27.17	23.78
29	G-1	Diode Filter #2	3.70	39.63	42.72	41.61	38.48
30	G-1	Array Hinge #2	3.00	23.79	27.56	26.50	23.14
31	H-1	Power Supply Elect.	9.00	22.83	26.76	25.73	22.35
32	C-2	Camera Electronics	7.50	20.31	24.07	23.10	20.54
33	E-2	Inertial Reference	24.60	31.34	34.25	33.30	30.73
34	G-2	Sun Sensor Electronics	1.80	15.75	19.55	18.44	15.54
35	B-2	Experiment Electronics	10.00	24.86	29.02	28.09	25.23
36	H-2	Redund. React. Wheel	0.0	15.98	20.45	19.41	16.30
37	GH-2	Yaw React. Wheel	1.50	16.85	20.93	19.86	16.92
38	F-2	Roll React. Wheel	1.50	16.11	19.63	18.50	15.80
39	G-2	Pitch React. Wheel	1.50	17.97	21.84	20.76	17.97
187	B-2	Fine Error Sensor #1	2.18	22.77	26.84	25.90	23.17
188	H-2	Fine Error Sensor #2	0.0	15.12	19.40	18.34	15.56
189	C-2	Camera Supply Inter.	0.0	20.38	24.33	23.38	20.81
		Total Power Is	133.68				
136	B	Hydrazine Tank	0.0	28.09	44.46	46.10	38.70
137	C	Hydrazine Tank	0.0	29.39	41.58	42.05	34.22
138	D	Hydrazine Tank	0.0	30.01	39.54	39.43	31.38
139	F	Hydrazine Tank	0.0	29.98	39.51	39.40	31.35
140	G	Hydrazine Tank	0.0	29.35	41.54	42.00	34.17
141	H	Hydrazine Tank	0.0	28.07	44.42	46.05	38.65

SECTION 11. PROPULSION SUBSYSTEMS

11.1 INTRODUCTION

The IUE spacecraft uses two different propulsion systems. The first one discussed in this section is the Apogee Boost Motor (ABM). The ABM is a solid propellant motor used for injection into the planned elliptical synchronous orbit. The second system, the Hydrazine Auxiliary Propulsion Subsystem (HAPS), is used for attitude control and stationkeeping maneuvers.

11.2 APOGEE BOOST MOTOR

The Apogee Boost Motor (ABM) is required to increase the spacecraft velocity from that which is attained at apogee of the transfer orbit, to the velocity that is needed to place it into an elliptical near-synchronous drifting orbit. The drift is required in order to place the spacecraft finally over the desired earth longitude. As explained in section 14, Mission Analysis, the expected drift rate is approximately 6^{o}/day eastward. As the target longitude is approached, the HAPS will be used to brake the drift and bring the vehicle on station.

The decision to use an elliptical synchronous orbit was governed primarily by the launch vehicle capability, total IUE weight, and tracking requirements. Compared with the usual synchronous launch, IUE was able to reduce apogee boost motor velocity requirements and, therefore, ABM weight by:

a. Not performing a plane change to equatorial orbit.

b. Targeting the launch vehicle above synchronous altitude.

c. Not requiring a perfect circular orbit.

The rocket motor and data shown in figure 11-1 is for the maximum weight spacecraft. For a lighter weight spacecraft, the motor case dimensions remain the same, but the propellant load is less. With the present Delta 2914 launch vehicle capability, the maximum weight spacecraft that can be placed into the desired transfer trajectory is normally 1470 pounds. If no third stage telemetry is carried, the capacity is 1489 pounds. Using the apogee insertion strategy described above, and allowing for the hydrazine propellant consumed in nutation

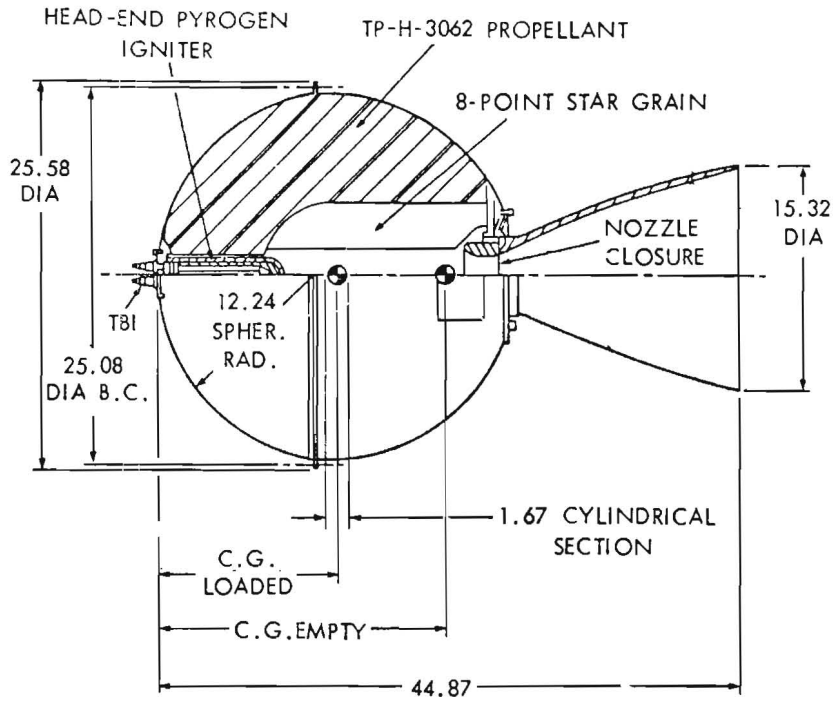

Model	TE-M-604-4
Case Diameter	24.47 inches
Cylindrical Length	1.67 inches
Nozzle Exit Diameter	15.32 inches O.D.
Case Material	Titanium 6AL-4V
Case Weight	38.2 pounds
Expendable Inert Weight + Igniter Prop.	5.8 pounds
Propellant Weight	483.5 pounds
Total Weight (includes RETA, FETA, S&A)	527.5 pounds
Propellant	TP-H-3062
Specific Impulse	285.5 $\frac{\text{LBF-SEC}}{\text{LBM}}$
Effective Specific Impulse	282.4 $\frac{\text{LBF-SEC}}{\text{LBM}}$
Average Thrust	4482 pounds
Maximum Thrust	4967 pounds
Action Time (thrust >10%)	31 secs. @ 55°F

1-Rigid Explosive Transfer Assembly and Flexible Explosive Transfer Assembly

Figure 11-1. Apogee Boost Motor

control and precession prior to apogee motor fire, the apogee motor size and propellant load were determined for this spacecraft weight. The actual propellant load will be selected for the actual total spacecraft weight as determined during assembly. The actual propellant weight will be obtained by an off-loading procedure which involves trimming away propellant at the aft end of the motor case. The maximum amount of fuel which can be trimmed using the off-loading procedure is approximately 40 pounds, which yields a minimum ABM propellant weight of 443.5 pounds.

The motor used as the ABM on IUE is a Thiokol Star 24, model number TE-M-604-4. This motor is the twin (having been cast at the same time) of the 604-3 motor which was used successfully on the LAGEOS satellite. Because of the extensive flight history with this family of rocket motors and the similarity of manufacturing techniques and materials, it was decided that a quantity of three motors would be adequate for this program. One motor is to be used for an altitude chamber firing test after vibration and thermal cycling. The other two motors are designated as flight units - one as prime, the other for backup. However, the IUE motors (dash-4) have been lengthened 1½" thus, providing additional propellant to accommodate S/C weight growth.

Because of the potentially hazardous nature of the solid rocket motor, it must be kept in a hazardous-storage area until ready for assembly at the launch site. To facilitate this assembly, the spacecraft structure has been designed so that the upper part of the propulsion bay, including the upper cone structure, separates from the lower cone and ABM adapter ring at station 27.0. The apogee motor can then be lowered onto the insulated adapter ring on the lower cone structure. The upper part of the spacecraft is then lowered over the motor and adapter structure and bolted in place without disturbing any other subsystem. This also results in a minimum of electrical connections. The spacecraft does not have to be turned upside down or held in a horizontal attitude to install the motor, thereby reducing risks to the telescope and improving handling operations.

The apogee motor has been insulated to prevent heat transfer to the spacecraft structure during the ABM burn and cool down periods. A fiber-glass insulation ring is located between the motor flange and the adapter ring to cut conductive heat flow. In addition, the ABM is covered with thermal blankets to minimize radiative transmission of heat to the surrounding structure. There is some concern that the heat emitted by the ABM exhaust plume may cause damage to the S-band antenna located on the lower cone structure. It is expected that the altitude chamber firing test will confirm the adequacy of thermal protection described above.

Safing and arming of the ABM is discussed in section 5.3 - Command Relay Unit Design.

11.3 HYDRAZINE AUXILIARY PROPULSION SYSTEM

11.3.1 INTRODUCTION

The Hydrazine Auxiliary Propulsion System (HAPS) provides the spacecraft with the attitude control torquing capability needed to perform the maneuvers described in Section 8 and with the velocity correction capability needed to perform the trajectory maneuvers described in Section 14. These functions, which were discussed in the Phase A Report, have been analyzed further and are as follows:

a. Nutation control.

b. Precession of the spin axis.

c. Despin of the spacecraft.

d. Spacecraft torquing to acquire the proper sun angle.

e. Spacecraft torquing to unload the reaction wheels when they become saturated.

f. Velocity correction to trim the orbit initially.

g. Velocity correction as required to maintain east-west stationkeeping.

Contract NAS5-20658 was awarded to Hamilton Standard Division of United Aircraft Corporation on July 18, 1974, for a protoflight HAPS, a Design Test Unit DTU/HAPS, Spare Parts, and GSE.

The HSD design reduces heater power by extended surfaces (sun catcher) on the HAPS bay and by placing two Reaction Engine Modules (REM's) on the Y-axis where they will be warmed by the sun. Each REM contains two 5 LB_F thrusters and two 0.1 LB_F*thrusters. The remaining four 0.1 LB_F thrusters are located on the HAPS bay. The REM mounted 5 LB_F thrusters are used for active nutation control and precession are canted 30^o and therefore have a longer moment arm than if they were mounted on the Bay. This saves propellant weight.

Propellant requirements have been re-examined and changed as required to reflect the needs of the mission with its present sequence of operations and the new design parameters of the spacecraft. Some fuel economies have been achieved but total tank capacity has been maintained at a level which will permit the loading of excess hydrazine in the event that total spacecraft weight after final assembly is less than vehicle capability.

*The Low Thrust Engines (LTE) are referred to herein as 0.1 LB_F thrusters for purposes of documentation continuity; actual thrust is described on page 11-5.

The precession and nutation thrusters are redundant, but in the case of velocity correction the thrusters must operate in pairs. The loss of one thruster would mean that the pair of canted precession and nutation thrusters would take over for the normal velocity correction engines. The velocity correction thrust would be reduced by the cosine of the canted angle (30^{o}) or 0.866. An additional 3.8 pounds of hydrazine would be required in this backup mode.

All thrust values given pertain to steady-state operation of the thrusters. For pulse type operation, thrust becomes a function of on-time. In addition, thrust is also a function of propellant tank pressure. The five LB_F thrusters have a nominal beginning-of-life thrust of 4.8 at a tank pressure of 350 PSIA. Nominal end-of-life thrust is 2.8 @ 161 PSIA. The 0.1 LB_F thrusters have a nominal BOL thrust of .29 @ 350 PSIA. Nominal thrust is .095 @ 105 PSIA.

11.3.2 MISSION REQUIREMENTS

Propellant quantities needed to perform the functions listed above for the full five-year mission lifetime were calculated as described in Sections 8 and 14. These fuel quantities are shown in table 11-1. for a nominal case starting from an initial tank pressure of 350 PSIA.

Table 11-1. Hydrazine Requirements

Maneuver	First Year		2-5 Years		Total	
	Kg	Lb	Kg	Lb	Kg	Lb
Nutation Control	1.73	3.81			1.73	3.81
Precession	2.38	5.25			2.38	5.25
Despin	.43	.94			.43	.94
Sun Acquisition	.09	.20	.36	.80	.45	1.00
Momentum Unloading	.38	.83	1.51	3.32	1.89	4.15
Station Acquisition	7.4	16.4			7.4	16.4
East-West Stationkeeping	.18	.4	.73	1.60	.91	2.00
Totals	12.63	27.83	2.60	5.72	15.19	33.55
25% Contingency	3.16	6.96	.65	1.43	3.80	8.39
Totals	15.8	34.8	3.3	7.2	19.0	42.0

The following assumptions were used in calculating the hydrazine requirements:

a. Useful load of 694.6 Kg (1531 lbs.)
b. Nutation control for 50 hours maximum.
c. New proposed transfer and mission orbits (i.e. e=.25, i=28.7°)
d. 99 percent transfer orbit apogee errors of 1480 Km (800 N.M.)
e. Excludes nitrogen.
f. No misalignments of jets.
g. No extra unloading considered.
h. Precession allows for three 180 degrees reorientation.

The hydrazine capacity of the six propellant tanks is 61.5 pounds.

If 50 pounds of usable hydrazine are loaded initially, the tank pressure will blow-down from 350 to 185 PSIA.

11.3.3 SYSTEM CONFIGURATION

The system uses monopropellant hydrazine fed in a blowdown mode from six tanks pressurized with nitrogen. The plumbing lines and fittings are brazed or welded to eliminate leak sources. There are four rocket thrusters of nominally five pounds thrust and eight thrusters of nominally 0.1 pounds thrust. For nutation control and precession where a large torque is required, a long moment arm has been obtained by canting these two five-pound thrusters at approximately 30^{o}. A schematic of the HAPS is shown in figure 11-2 with the thruster arrangement, functions, and moment arms. A general view of the system is shown in figure 11-3.

The six tanks are 9.5 inches in diameter and have an elastomeric diaphram to separate the liquid propellant from the pressurizing gas. This feature is required for the non-spinning phase of the mission. Tanks are connected together in pairs, diametrically opposed so that fuel usage from any pair will not adversely affect the balance of the spacecraft. Each pair is equipped with a fill and drain valve for hydrazine and each tank has a fill and vent valve for nitrogen. These values will be accessible for filling and draining by removal of a part of the insulation blanket from the propulsion bay. Thus, filling and draining can be done with the propulsion system mounted to the spacecraft. A crossover latching valve network is required to control the flow from each tank pair to the proper thrusters for proper fuel management and redundancy. A valve for each thruster is also required to feed the fuel to the thruster at the desired time.

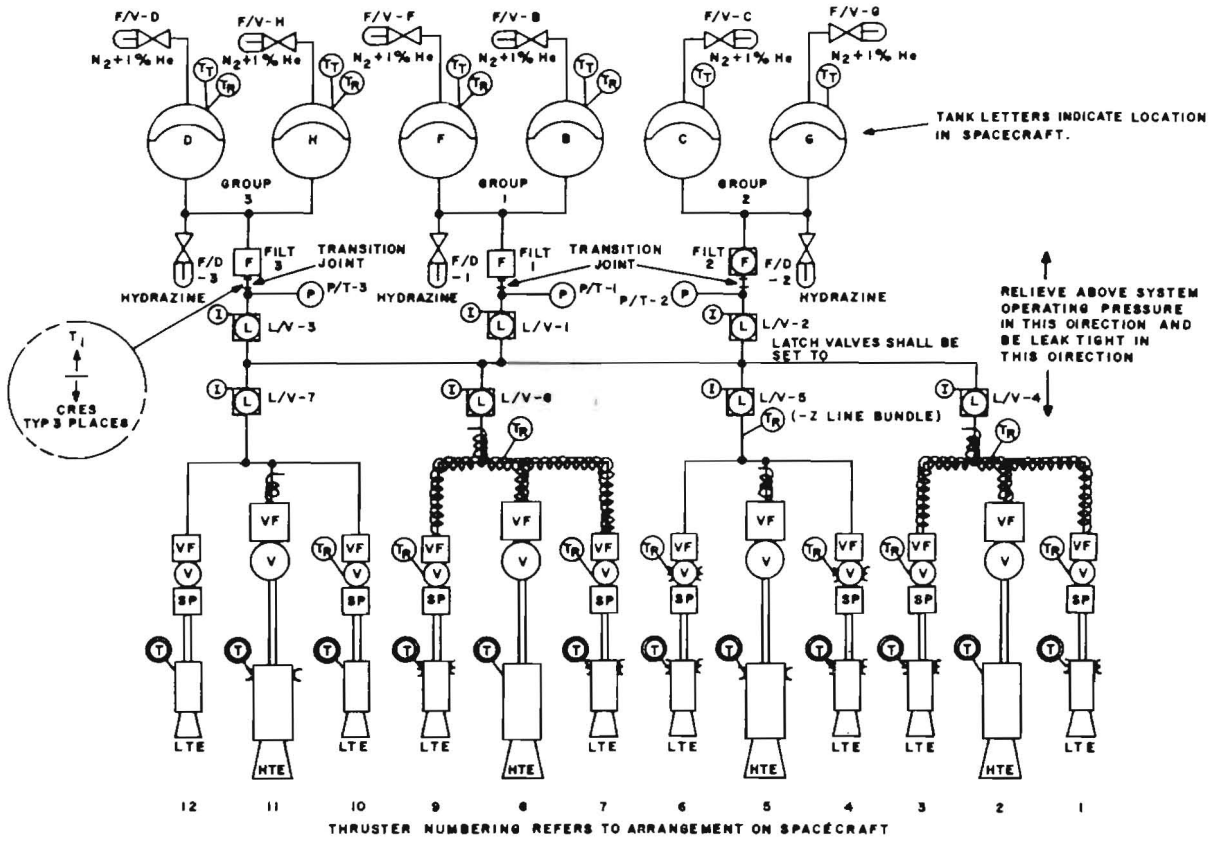

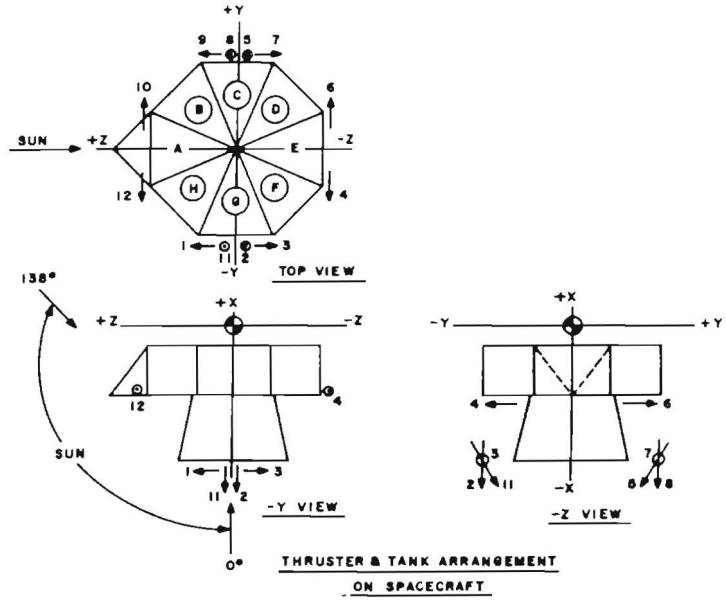

THRUSTER FUNCTIONS

FUNCTION	PRIMARY (+)	PRIMARY (-)	SECONDARY (+)	SECONDARY (-)
ROLL XX	10 & 4	12 & 6	7 & 1	9 & 3
PITCH YY	7 & 3	9 & 1	7 OR 3	9 OR 1
YAW ZZ	10 & 6	12 & 4	10 OR 6	12 OR 4
PRECESSION & NUTATION	5		11	
VELOCITY CORRECTION	8 & 2		11 & 5	
SPIN	10 & 4	12 & 6	7 & 1	9 & 3

KEY

- TT — TEMPERATURE INDICATOR-GROUND TEST THERMISTOR-SINGLE
- TR — TEMPERATURE INDICATOR-THERMISTOR-REDUNDANT
- T — TEMPERATURE INDICATOR-THERMOCOUPLE-SINGLE
- FILL AND DRAIN VALVE-CAPPED
- V — THRUSTER SOLENOID VALVE
- THERMAL STANDOFF TUBE
- P — PRESSURE INDICATOR
- I L — LATCH VALVE WITH POSITION INDICATOR
- SP — SCREEN PLATE
- ELECTRIC COMPONET HEATER-REDUNDANT
- ELECTRIC COMPONENT HEATER-SINGLE
- ELECTRIC LINE HEATER-REDUNDANT
- TRANSITION JOINT

(C) THRUSTER MOMENT ARMS

FUNCTION	PRE-APOGEE BURN	POST-APOGEE BURN
ROLL XX & SPIN	2.26 FT	2.26 FT
PITCH YY	-	4.64
YAW ZZ	-	2.82
PRECESSION & NUTATION	3.79	4.32

Figure 11.3-1. Hydrazine Auxiliary Propulsion System, Schematic

Figure 11-2. Hydrazine Auxiliary Propulsion System, Schematic

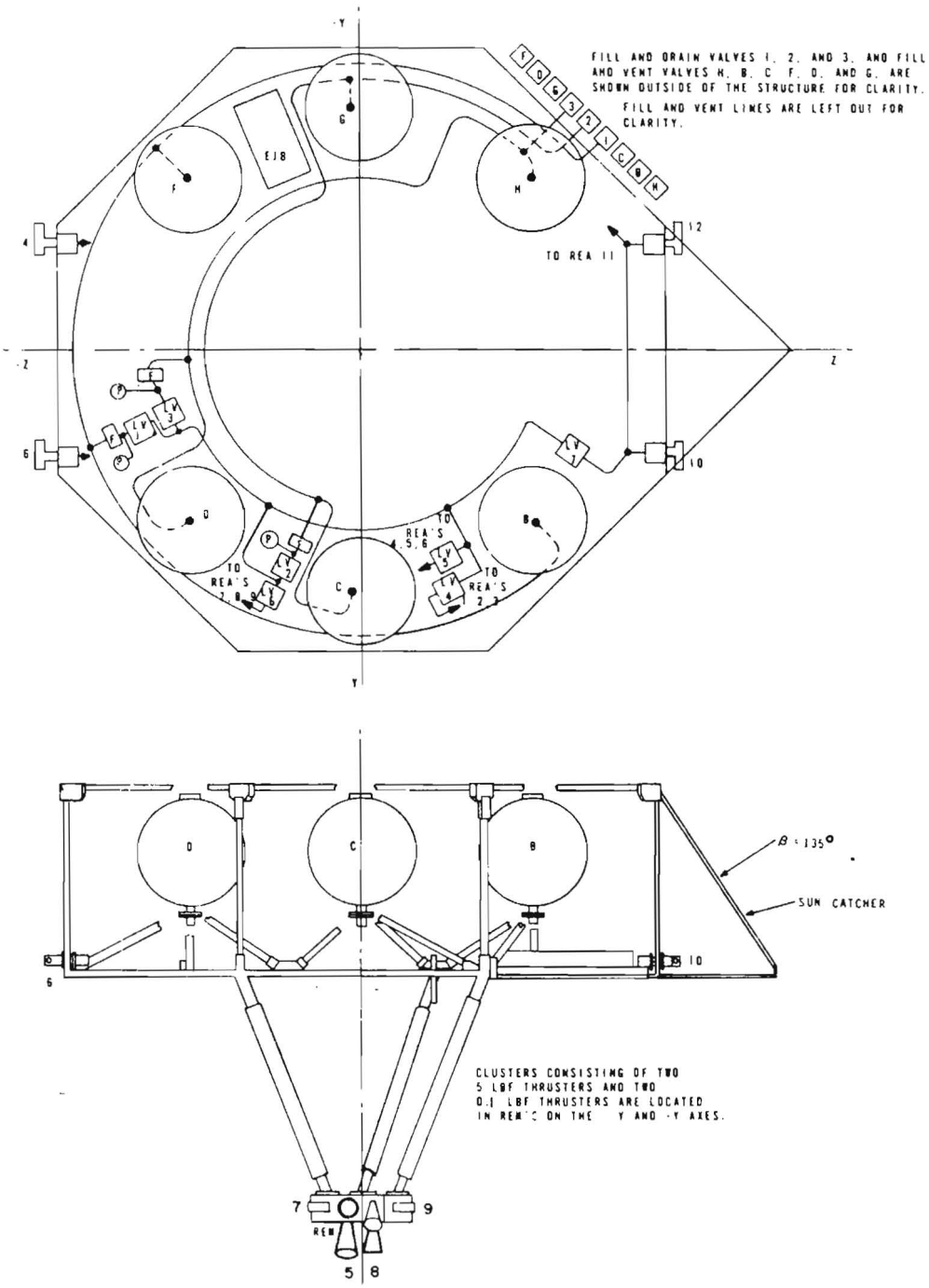

Figure 11-3. Reaction Engine Assemblies (REA) - IUE-HAPS Fuel System

Filters are placed in the hydrazine supply lines to prevent particle contamination over a specified size from reaching the valves, where it could prevent complete closure of the valves and result in leakage through the seat. System filters are located at the tank outlets and before the latch valves. Each thruster valve has an integral upstream filter. Downstream from each low-thrust engine at the entrance to the capillary tube is a screen plate with holes smaller than the inside diameter of the tube to prevent plugging from any debris generated by the valve.

The thruster assemblies are equipped with catalyst beds containing Shell catalyst 405, which has been used successfully on a number of space flights with monopropellant hydrazine systems. Electrical heaters are installed to maintain adequate temperature of the catalyst beds and the thruster valves as needed. No freezing in the valves or lines will be allowed to occur.

Pressure and temperature transducers, appropriately placed will be used to monitor the operation of the system. Potentiometer type pressure transducers will be placed in the hydrazine feed line. For proper operation, the hydrazine subsystem must be maintained between $5^{o}C$ and $65^{o}C$.

Transition joints are located at the outlet from each of the three systems filters and provide a means of changing from titanium to stainless steel. The tanks, fill and drain valves, fill and vent valves, system filter, and associated piping is titanium and the other side of the transition joint is stainless. This arrangement is a compromise between weight savings, cost, and availability.

A listing of the HAPS components with additional specifications is given in table 11-2.

An Electrical Junction Box (EJB) is located in the HAPS bay and is shown schematically in figure 11-4. The EJB provides for the test connector and contains suppression and monitoring circuitry for the thruster valves and the latching valves.

Table 11-2. IUE Hydrazine Auxiliary Propulsion System Components

ITEM	NUMBER REQUIRED	REMARKS
Tanks	6	9 1/2-inches diameter titanium. EPT-10 diaphram.
Latch Valves	7	Closed for launch-normally open for operations. Position indicators. Seals in one direction and relieves in opposite direction, above system pressure.
Fill and Drain	9	Adapt to RAE-B loading cart fittings. 3/16-inch fill and drain; 1/8-inch fill and vent.
System Filters	3	10 Microns nominal, 25 Microns absolute, etched disc type.
Temperature Sensor-Thermistor	34	28 flight (14 redundant pairs) plus 6 ground test GFE, YSI-44006.
Temperature Sensor-Thermocouple	12	Mounted on each catalyst chamber surface. Range -20 to 2000^{o}F chromel-alumel
Pressure Sensor	3	Range 0 - 400 PSIA
Thrusters (5 LBF) 22.2N (HTE)	4	Nominal 22N (5 LBF) assembly with heat shield, Shell 405 catalyst.
Valves (5 LBF)	4	Shall incorporate 25 Micron absolute upstream filter. Dropout 4 VDC minimum; pull-in 18 VDC maximum
Thrusters (0.1 LBF) 0.445N (LTE)	8	Nominal .44N (0.1 LBF) assembly with shield. Entrance to capillary tube shall incorporate a screen plate having 14 or more parallel holes no larger than 75% of the capillary diameter. Shell 405 catalyst.
Valves (0.1 LBF) 0.445N	8	Shall incorporate 25 Micron absolute upstream filter dropout 4 VDC minimum; pull-in 18 VDC maximum.

Table 11-2. IUE Hydrazine Auxiliary Propulsion System Components (cont)

ITEM	NUMBER REQUIRED	REMARKS
Heater for 22.2N (5 LBF) Thruster Catalyst Bed	2	One heater shall keep catalyst bed above 90°C when on and facing sunless space, redundant bolt-on design.
Heater for 0.44N (.1 LBF) Thruster Catalyst Bed	12	One heater shall keep catylst bed above 90°C when on and facing sunless space, redundant bolt-on design.
Heater for 0.44N (.1 LBF) Thruster Valve	4	One heater shall keep valve temperature above 10°C when thruster is facing sunless space with its heater off, redundant design.
Transition Joint	3	Provides means to change system material from titanium to stainless steel.

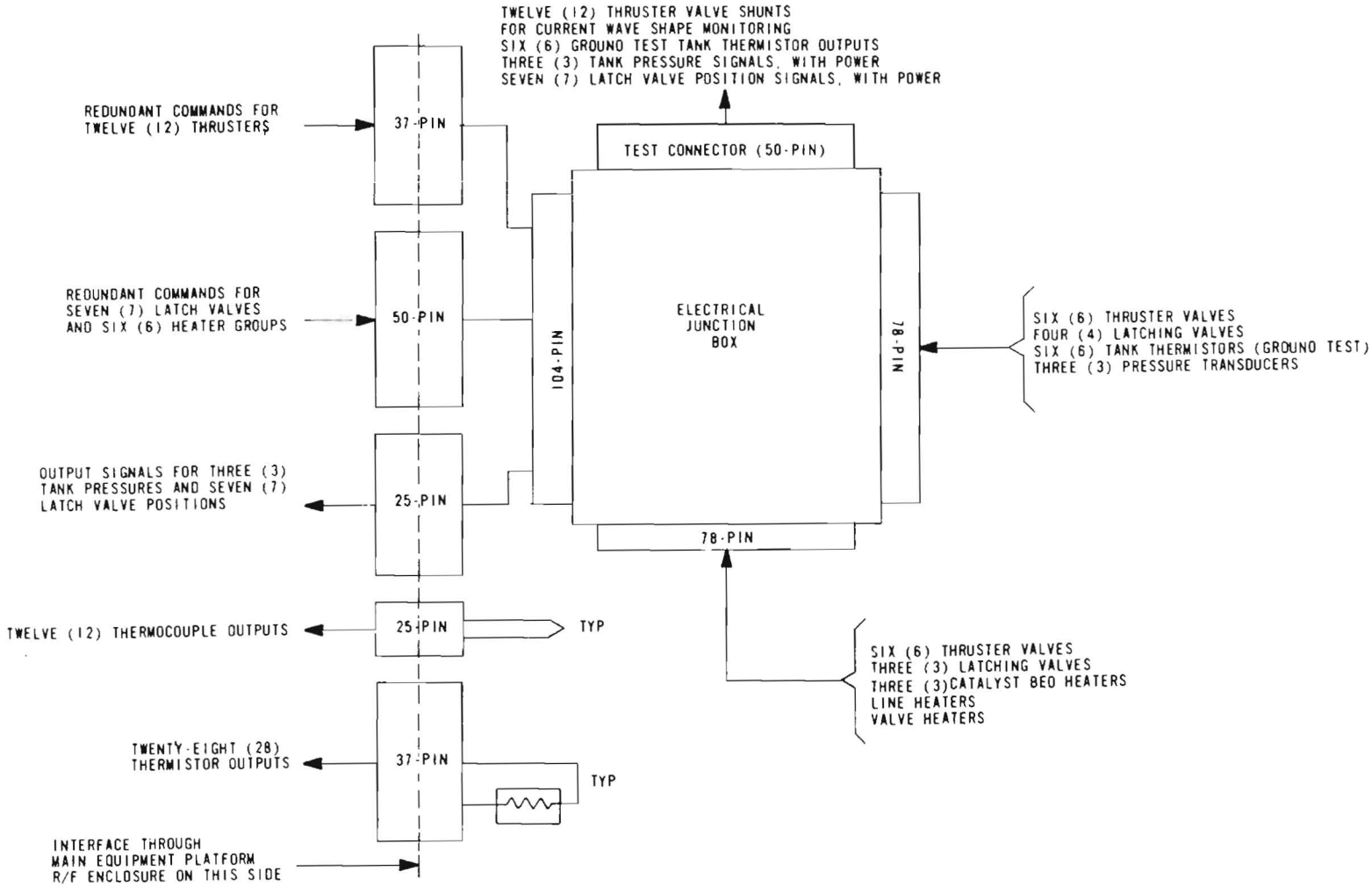

Figure 11-4. IUE/HAPS Electrical Schematic

SECTION 12. SPACECRAFT WEIGHT AND MASS PROPERTIES

12.1 WEIGHT

The IUE spacecraft weight is limited by the capacity of the Delta launch vehicle, which has been assigned for this mission. In the Phase A report redundancy in the spacecraft design was limited to the most critical functions in order to keep spacecraft weight within the capability of the Delta 904 vehicle, which was the largest version at that time. Since publication of that report a more advanced version of the vehicle has been added to the Delta series. In order to optimize the spacecraft and increase reliability, additional redundant features and design improvements have been added, taking advantage of the increased weight capacity of the new Delta 2914. Many of the components described in Phase A have been improved, combined with other units to improve efficiency, or eliminated. Some new components have been added and some existing components were increased to provide redundancy that was not available in the Phase A design. Total spacecraft weight is therefore greater than in the Phase A report and from the System Design Report of September 1973.

Table 12-1 presents the weight tabulation for the IUE spacecraft as now configured and is based on the weights used in Revision J of the Weight Control Program (WECOP). The total launch weight is estimated to be 1439 pounds which includes 437.7 pounds of propellant for the ABM. This weight is derived from the actual weights of units fabricated for the IUE spacecraft and from estimates of the weights of units which are still in the design stages. As these later units are fabricated, the Weight Control Program will be updated to improve the accuracy of the spacecraft weight estimate.

The current weight estimate provides a weight contingency of 1.6% assuming a maximum payload weight of 1463 pounds for the Delta. This payload capability implies that the Delta will not use the third stage telemetry kit. A portion of the 24.3 pound contingency can be used to increase the IUE spacecraft weight, the remainder of the contingency must be used to increase the propellant in the ABM. This gives a useful payload contingency of 16.4 pounds or 1.1 percent.

12.2 BALANCE WEIGHTS

The spacecraft will be balanced by adding weights, if necessary, at stations 47.0 and 86.8. Additionally, stations 2.0 and 27.0 are available for balancing weights. The weights will be attached to the honeycomb platform at stations 47 and 86.8 or to the outside frame members at the other required

Table 12-1. Spacecraft Weight (pounds)
(As of Feb. 1976; for latest data see current WECOP printout)

Subsystem	Item Weight	Subsystem Weight
Experiment		258.1
Telescope	91.7	
Spectrograph Structure	44.8	
Spectrograph Cameras, Optics, and Electronics	121.6	
Attitude Control		99.2
SMSS Electronics	1.1	
FSS Electronics (2)	3.5	
PAS Electronics (2)	4.4	
Electronic Assy. Top, Bottom, Bolts	1.5	
CSS Head (6)	0.1	
SMSS Head	0.3	
FSS Head (4)	3.1	
PAS Head (2)	2.2	
NSA (2)	1.0	
RWA (4)	20.4	
WDA	7.4	
CEA	12.8	
IRA Sensor	23.2	
IRA Electronics	18.2	
Communications		28.5
S-Band Transmitter A	2.0	
S-Band Transmitter B	2.0	
S-Band Antennas (4)	2.0	

Table 12-1. Spacecraft Weight (cont)

Subsystem	Item Weight	Subsystem Weight
S-Band Cables	1.0	
Dividers (2)	0.0	
S-Band Power Amp Module	5.3	
VHF Transponder (A) (Incl. Conv.)	5.9	
VHF Transponder (B) (Incl. Conv)	5.9	
VHF Antennas (4) and Cables	2.2	
VHF Antenna Distribution Unit	1.5	
S-Band Transmitter Spider	0.5	
S-Band Antenna Blanket	0.2	
Command and Data Handling		72.0
OBC		
Processor Module A	2.5	
Processor Module B	2.5	
Memory Module A	5.6	
Memory Module B	5.6	
Memory Module C	5.6	
Power Conv. A	3.7	
Power Conv. B	3.7	
OBC Peculiar Harness	1.2	
DMS		
Dataplexer A	4.4	
Dataplexer B	4.4	

Table 12-1. Spacecraft Weight (cont)

Subsystem	Item Weight	Subsystem Weight
Subplexer (Analog) A	2.5	
Subplexer (Analog) B	2.5	
Subplexer (Digital) A	2.1	
Subplexer (Digital) B	2.1	
Power Conv. A	2.0	
Power Conv. B & Mounting Hardware	2.6	
Command		
Command Relay Unit	8.9	
Command Decoder A (Incl. Conv.)	4.7	
Command Decoder B (Incl. Conv.)	5.4	
Power		107.8
Mission Adapter Module	10.5	
Power Module A	8.3	
Power Module B	8.3	
Battery A (6 AH)	13.6	
Battery B (6 AH)	13.6	
Solar Paddle A	25.9	
Solar Paddle B	25.9	
Diode Box A	0.6	
Diode Box B	0.6	
Dump Resistors (24)	0.5	

Table 12-1. Spacecraft Weight (cont)

Subsystem	Item Weight	Subsystem Weight
Thermal		24.3
Upper Structure (ABCGH) Blankets	3.5	
Louvers	2.1	
Louver Base Plate	0.9	
Heat Pipes	4.2	
Thermal Paint	0.0	
Lower Cone Heat Shield Blanket	0.6	
Tape, Blanket Fasteners	1.6	
Lower Cone Blanket (2)	3.2	
Upper Cone Blanket (Inside)	0.2	
Apogee Motor Blanket	3.0	
Lower Platform Blanket	1.0	
Upper Structure Blanket	1.2	
Upper Platform Blanket (3)	1.8	
Solar Array Locks Blanket (4)	0.4	
Upper Cone Blanket (Outside)	0.6	
Spacecraft Structure		135.9
Lower Cone Structure	26.0	
Apogee Motor Rings	3.7	
Upper Cone Structure	22.3	
Bottom Panel	2.0	
Shear Panels	7.7	
Lower Platform	15.8	
Upper Platform	8.9	

Table 12-1. Spacecraft Weight (cont)

Subsystem	Item Weight	Subsystem Weight
Upper Body Str., E-Panel and Bracket	27.8	
Brackets	4.3	
IRA Electronics Platform	3.0	
Misc. Hardware	5.2	
Support Blocks and Rings	2.0	
Lower S-Band Brackets and Heat Sheilds	2.0	
Power Radiator Panels	1.5	
Brackets	0.9	
Misc Hardware	2.8	
Hydazine Aux. Propulsion System		64.9
Dry Weight	54.1	
Blankets and Attachment Hardware	8.8	
Heaters and Miscellaneous	2.0	
Miscellaneous		73.5
Balance Weights	16.8	
Lower Elec. Harness and Clamps	33.0	
Upper Elec. Harness and Clamps	16.0	
Special RF Shields	2.1	
Safe & Arm Mech. & Lines	4.3	
RF Shield	1.3	

Table 12-1. Spacecraft Weight (cont)

Subsystem	Item Weight	Subsystem Weight
Basic Spacecraft Dry Weight	864.2	
HAPS Propellant (N_2H_4 and N_2)	36.6	
Basic Spacecraft Weight (fueled)	900.8	
Apogee Motor		
1. Case	34.7	
2. Inerts	4.5	
3. Propellant	437.7	
Total Spacecraft Launch Weight	1377.7	
Delta Attach Fitting	61.0	
Total Launch Weight	1438.7	
Contingency	24.3	
Delta 2914 Payload Capability	1463.0	

stations. Preliminary weights and positions will be calculated using a mass properties computer program. The final weights and positions will be determined by measurements made on a balancing machine. Precut weights of various thicknesses will be stacked at each required position to facilitate the balancing operation, as was done on the Explorer 32. Analysis shows a total balance weight of approximately 16.8 pounds is required at this time. Components have been arranged to keep this number to a minimum. The components on the main platform have been arranged so they are nearly balanced. The equipment on the upper platform has been located to achieve an optimum balance commensurate with the equipment cabling requirements.

12.3 MASS PROPERTIES

The mass properties presented in table 12-2 are based on the weights as tabulated in Revision J of the Weight Control Program with the exception that the balance weights have been reduced from 16.8 pounds to 6.8 pounds. This weight reduction, although not presently implemented, is expected in the near future.

As each event in the mission sequence takes place, the weight of the spacecraft decreases. These weight reductions, shown in table 12-2 are those which result from a normal launch and operation sequence. This occurs if the Delta vehicle and the apogee rocket motor performance are nominal, and the apogee motor is fired on the second apogee as planned. In this case the hydrazine consumed prior to arriving on station at 48° W longitude is minimized. The spacecraft will be spin stabilized prior to and during apogee motor burn and will utilize active nutation control to prevent a large cone angle from developing. After apogee motor burn and determination of a positive eastward drift, the spacecraft will be despun and the solar array deployed. Thereafter the spacecraft will be three axis stabilized. During the spinning phase of the mission the moment of inertia ratio is approximately 0.26 which provides a satisfactory condition for nutation control.

Table 12-2. IUE Spacecraft Mass Properties History

CASE NO.	CASE DESCRIPTION	SOLAR ARRAYS	S.I. COVER	ABM	HAPS FUEL (lbs)	TOTAL S/C WEIGHT (lbs)	CM HEIGHT (in)	MOMENTS OF INERTIA (Slug-ft^2) I_x	I_y	I_z	INERTIA RATIOS I_x/I_y	I_x/I_z
1.	AT LAUNCH	Folded	On(1)	Full(2)	36.6(3)	1,367.7	50.53	78.3	297.2	295.9	.263	2.65
2.	AT APOGEE, PRIOR TO ABM BURN	Folded	On	Full	32.6	1,363.7	50.57	77.9	297.0	295.5	.262	.264
3.	AT APOGEE, AFTER ABM BURN OUT	Folded	On	Empty	32.6	921.4	62.55	72.2	202.3	201.0	.357	.359
4.	AFTER DESPIN AND DEPLOYMENT	Depl'd	On	Empty	30.4	919.2	61.29	97.5	199.6	227.5	.448	.429
5.	AFTER ALL TRAJECTORY CORRECTIONS (BOL)	Depl'd	Off	Empty	7.4	892.2	61.53	95.3	189.0	216.1	.504	.441
6.	AFTER FIVE YEARS IN ORBIT (EOL)	Depl'd	Off	Empty	0	884.8	61.74	94.6	187.8	214.7	.504	.440

Note

(1) 4.0 lbs
(2) 442.2 lbs, including 4.5 lbs inerts
(3) Includes 1.3 lbs nitrogen

SECTION 13. LAUNCH VEHICLE

13.1 GENERAL

The IUE spacecraft will be launched by the Delta launch vehicle. For this mission, the three stage Delta 2914 launch vehicle (figure 13-1) will be used. This launch vehicle has an overall length of approximately 116 feet and a maximum body diameter of 8 feet. A staging and separation schematic is shown in figure 13-2. A brief description of the vehicle's major characteristics follows.

13.1.1 FIRST STAGE

The first stage is a McDonnell Douglas Astronautics Company (MDAC) modified Thor booster incorporating nine strap-on Thiokol solid fuel rocket motors. The booster is powered by a Rocketdyne engine using liquid oxygen and liquid hydrocarbon propellants. The main engine is gimbal mounted to provide pitch and yaw control from lift-off to Main Engine Cutoff (MECO). Two liquid propellant vernier engines provide roll control throughout first stage operation and pitch and yaw control from MECO to first stage separation.

13.1.2 SECOND STAGE

The second stage is powered by a TRW liquid-fuel, pressure fed engine employing nitrogen tetroxide and aerozine 50 propellants. The second stage main engine is also gimbal mounted to provide pitch and yaw control through second stage burn. A nitrogen gas system using 8 fixed nozzles provides roll control during powered and coast flight, as well as yaw and pitch control after Second Stage Cutoff (SECO). Two fixed nozzles fed by the propellant tank helium pressurization system, provide retro-thrust after third stage separation.

13.1.3 THIRD STAGE

The third stage is the TE-364-4 spin-stabilized solid propellant motor manufactured by the Thiokol Chemical Corporation (TCC). The third stage motor is secured in a spin table mounted to the second stage. The firing of two to eight solid propellant rockets fixed to the spin table accomplishes spin-up of the third stage assembly.

13.1.4 ATTACH FITTING

The IUE spacecraft is attached to the third stage motor by means of the standard 3731A attach fitting that incorporates the third stage sequencing and separation system.

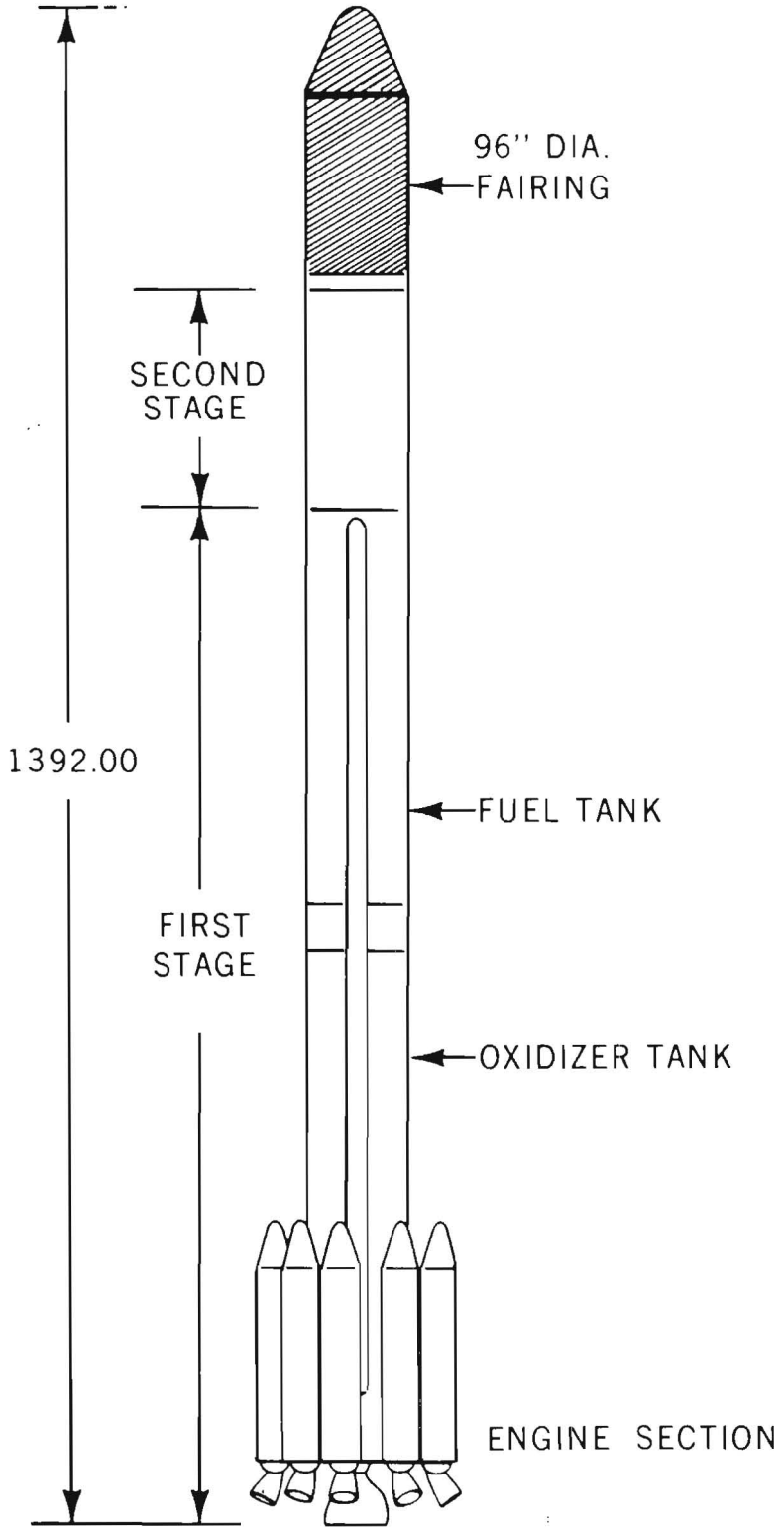

Figure 13-1. Delta 2914 Vehicle

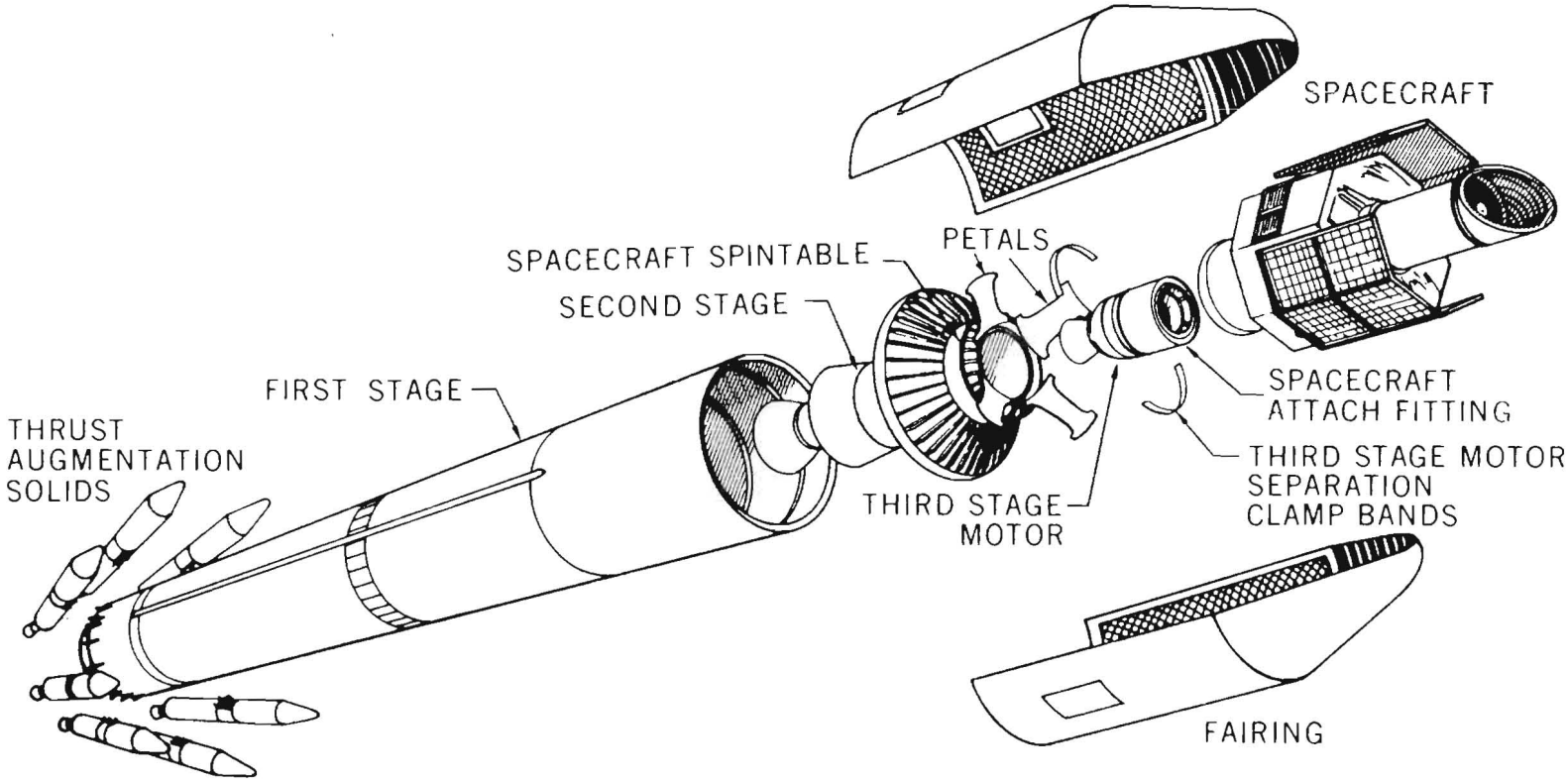

Figure 13-2. Delta Staging and Separation Schematic

13.1.5 FAIRING

The standard 96-inch-diameter fairing will be utilized for the IUE mission. This fairing, which protects the spacecraft from aerodynamic heating during the boost flight, is jettisoned as soon as the vehicle leaves the sensible atmosphere shortly after second stage ignition. Figure 13-3 shows the Delta 3rd Stage and the fairing dimensions.

13.1.6 GUIDANCE AND CONTROL

The Delta Inertial Guidance System (DIGS), consisting of an inertial sensor package and digital guidance computer, controls the vehicle and sequence of operations from lift-off to spacecraft separation. The sensor package provides vehicle attitude and acceleration information to the guidance computer. The guidance computer generates vehicle steering commands to each stage to correct trajectory deviations by comparing computed position and velocity against prestored values.

In addition, the guidance computations perform the functions of timing and staging as well as issuing preprogrammed command attitude rates during the open loop and coast guidance phases.

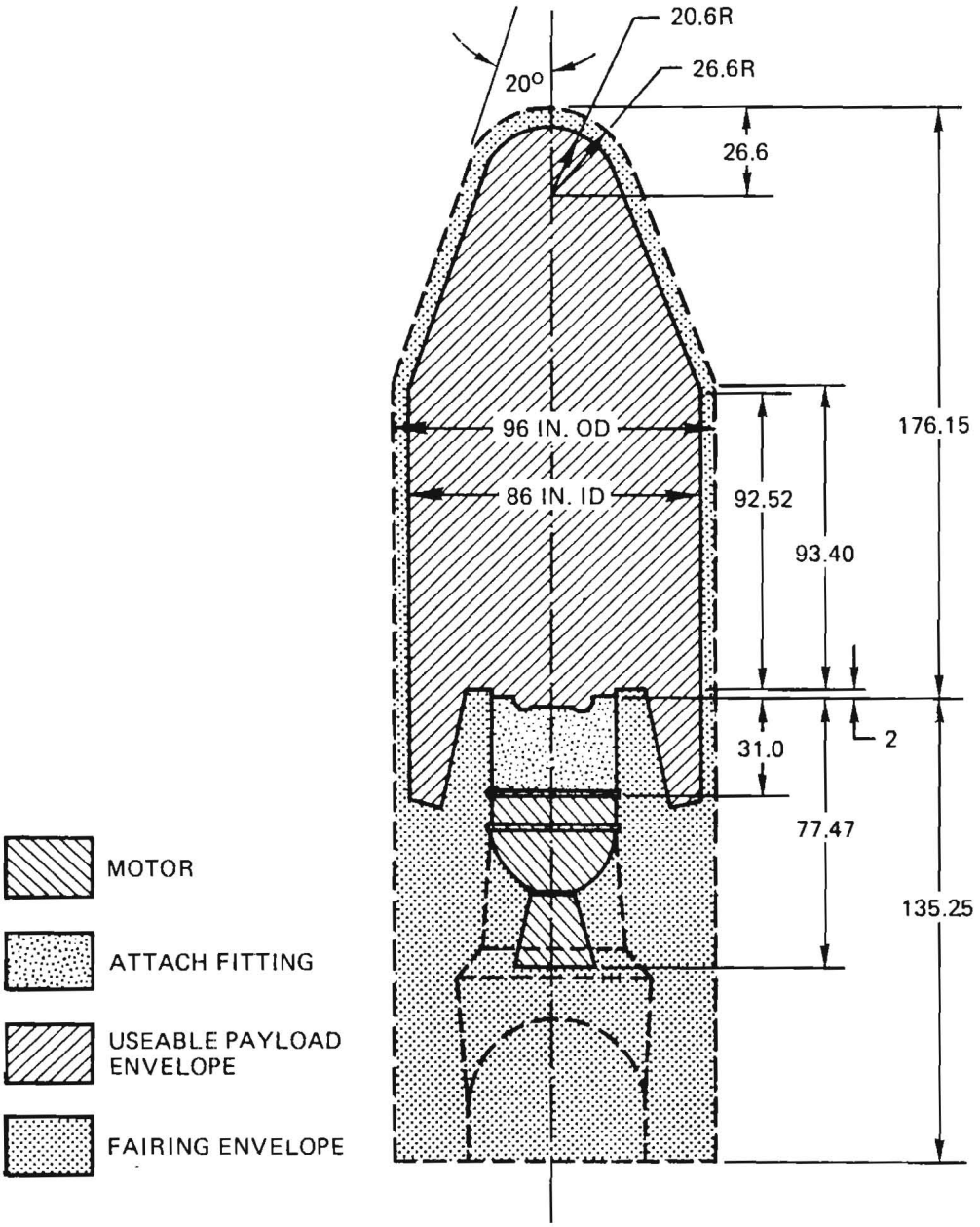

Figure 13-3. Payload Envelope, TE-364-4, 3731A Attach Fitting

SECTION 14. IUE MISSION ANALYSIS

14.1 INTRODUCTION

The purpose of the mission analysis for IUE is to select a flight profile beginning with insertion into the park orbit and then into the transfer orbit, and finally into the elliptical synchronous orbit. The overall strategy will involve numerous trade-offs in an attempt to maximize launch window availability and coverage from the tracking stations and to minimize fuel requirements to conserve weight.

The scope of the analysis consists of a detailed study of matching the final elliptical synchronous orbit with the necessary transfer orbit parameters and suitable injection location of the third stage from the park orbit. The transfer orbital elements are selected from (1) park orbital elements, (2) desired elliptical synchronous orbital elements, and (3) optimum apogee height based on minimizing fuel requirements. The fuel requirements for the IUE concern the amount of solid fuel propellant for the apogee boost motor and the amount of liquid hydrazine needed for orbit trim and east-west station-keeping. Tracking coverage for the transfer and elliptical synchronous orbits is investigated as well as tracking error analysis. A maneuver sequence is discussed involving the primary maneuvers of reorientation of spin axis for apogee motor fire, the apogee motor fire strategy and a plan for target acquisition. The selection of specific target longitude and desired shadow conditions for the final elliptical synchronous orbit are presented. Also included is a launch window analysis showing the yearly launch window conditions as well as desirable daily launch times.

Specific updates to this section of the IUE system design report include the following:

a. The launch window analysis was updated to reflect a nominal launch date of July 20, 1977. The FORTRAN Launch Analysis Program (FLAP) was used to determine the launch opportunities as a function of launch data and right ascension of the ascending node. The launch window is presented for a one-year period beginning July 29, 1977.

b. The spacecraft weight was increased to accommodate higher payload requirements. The Two-Body Error Analysis (TBERR) Program was used to resize the Apogee Boost Motor (ABM), assuming an apogee yaw maneuver in order to satisfy tracking requirements in the synchronous orbit. The resulting ABM fuel weight (including inert expendables) is 455 pounds (206

kilograms) which corresponds to a velocity change of 3540 feet per second (1078.9 meters per second). The hydrazine fuel requirements were computed for a nominal drift rate of 6 degrees per day east. The study assumed that drift rate errors would be corrected. The 99th percentile hydrazine required for station acquisition is 23 pounds (10 kilograms).

c. The shadow time history of the elliptical synchronous orbit was reevaluated in light of recent changes in the constraints. To achieve maximum sunlight over a 5-year mission, a node and argument of perigee were selected to assure a high ecliptic inclination and apogee position well above the shadow cone of the earth. The nominal node angle is 220 degrees and argument of perigee is 234 degrees.

d. The synchronous orbit inclination was chosen to satisfy tracking requirements at Goddard Space Flight Center (GSFC) and Villafranca del Castillo, Spain (VILFRA). The tracking time prediction program (SANDTRACKS) was used to determine tracking coverage as a function of inclination and station longitude.* If the nominal inclination is chosen to be 26.5 degrees, then the tracking constraints are satisfied. Furthermore, there is no significant loss of tracking time for points inside the .90 probability error ellipse centered at the nominal inclination.

e. The nominal trajectory parameters were computed for a July 20, 1977 launch. The transfer orbit node and argument of perigee were compensated for the Apogee Motor Firing (AMF) maneuver. Second apogee was selected as nominal position for the AMF because of extensive tracking coverage from the U.S. sites. The drift orbit was divided into three phases to achieve station acquisition in approximately 10 days. The nominal elliptical synchronous orbit has an eccentricity of 0.272, inclination of 26.5 degrees, and initial station longitude of about 42 degrees west.

Section 14.2 presents the launch window extending from July 20, 1977 to July 20, 1978. Section 14.3 updates the spacecraft weight breakdown, including the resized ABM and hydrazine fuel required for station acquisition. Section 14.4 outlines the nominal IUE mission profile, presents the trajectory constraints, and tabulates the nominal orbital elements designed to satisfy these constraints.

---

*Station longitude is defined as geographic longitude of the ascending node when the spacecraft is at the ascending node.

14.2 LAUNCH WINDOW ANALYSIS

14.2.1 LAUNCH WINDOW CONSTRAINTS

The launch window analysis for IUE was updated to extend from July 20, 1977 for a one-year period.* The launch window constraints assumed for this study are as follows:

a. Maximum continuous shadow duration prior to AMF must be less than 60 minutes.

b. Third-stage solar aspect angle must lie between 45 and 135 degrees.

c. Fourth-stage solar aspect angle must lie between 45 and 135 degrees.

d. Earth-spacecraft-sun separation angle must be between 30 and 150 degrees for the 3-hour period prior to apogee.

e. Minimum daily launch window duration must be at least 20 minutes.

f. Synchronous orbit shadow duration must be less than 72 minutes per revolution for the entire mission.

The pre-AMF shadow constraint must be satisfied from fairing ejection up to AMF. The solar aspect angle is measured between the spacecraft spin axis and the spacecraft-sun vector (figure 14-1). The separation angle is measured between the spacecraft-sun vector and the spacecraft-earth vector (figure 14-2). The third stage injects the satellite into the transfer orbit from the parking orbit (figure 14-3). The fourth stage is the ABM and is used to inject the satellite into the desired drift orbit.

14.2.2 LAUNCH WINDOW DEFINITION

The launch window is defined in terms of launch data and node of the parking orbit. The composite launch window plot is presented in figure 14-4. The individual constraints can be found plotted in Appendix D of Reference 2, section 14.5.

The acceptable launch periods are approximately as follows:

a. July 20, 1977 to August 24, 1977

*See Reference 3, section 14.5.

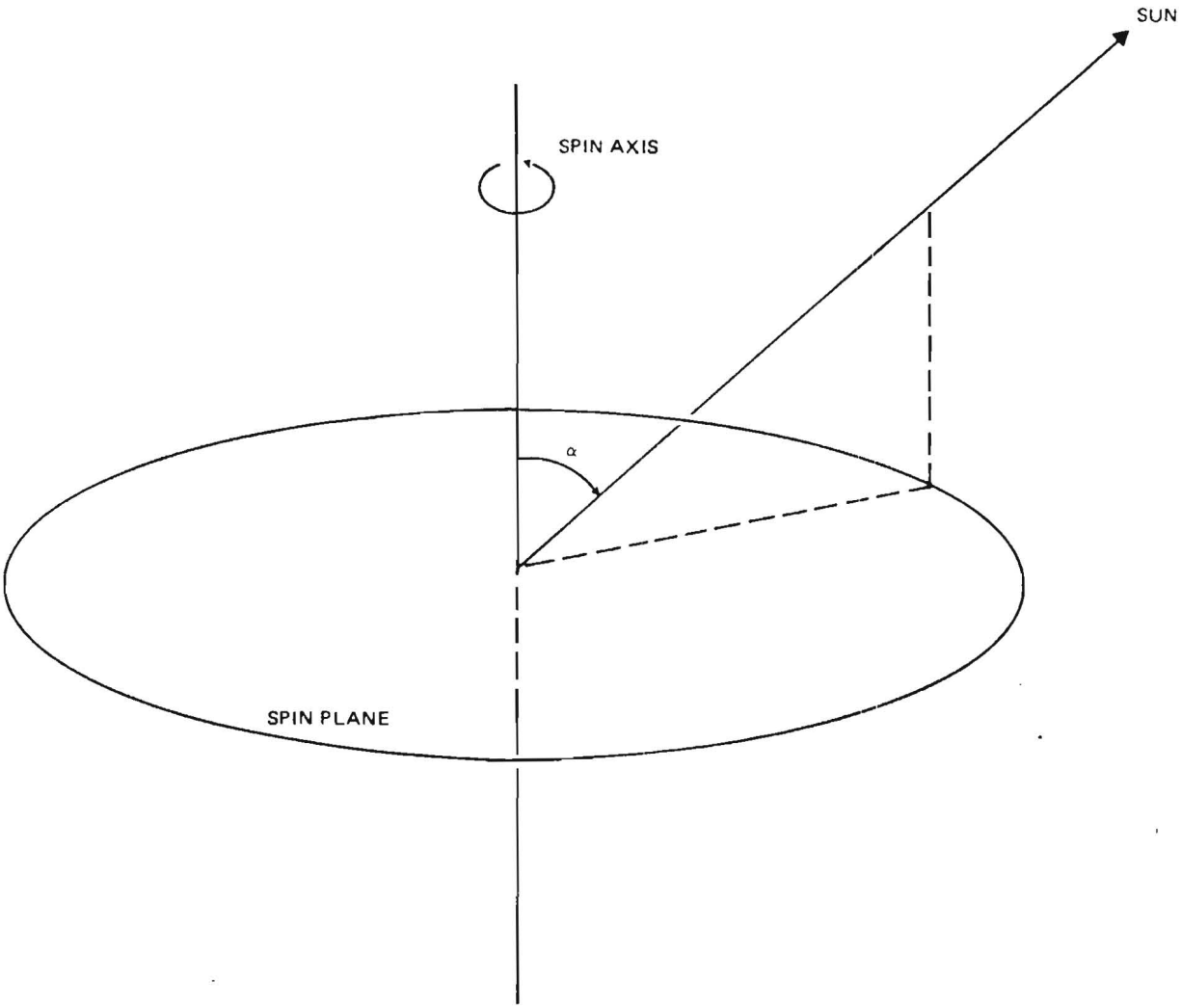

Figure 14-1. Definition of Solar Aspect Angle (α)

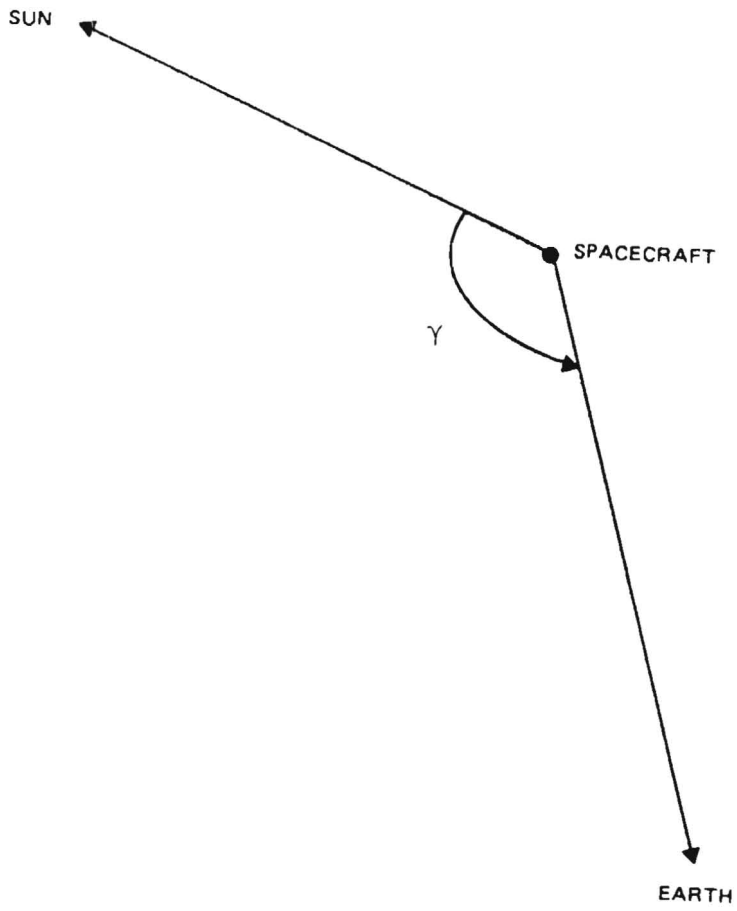

Figure 14-2. Definition of Separation Angle (γ)

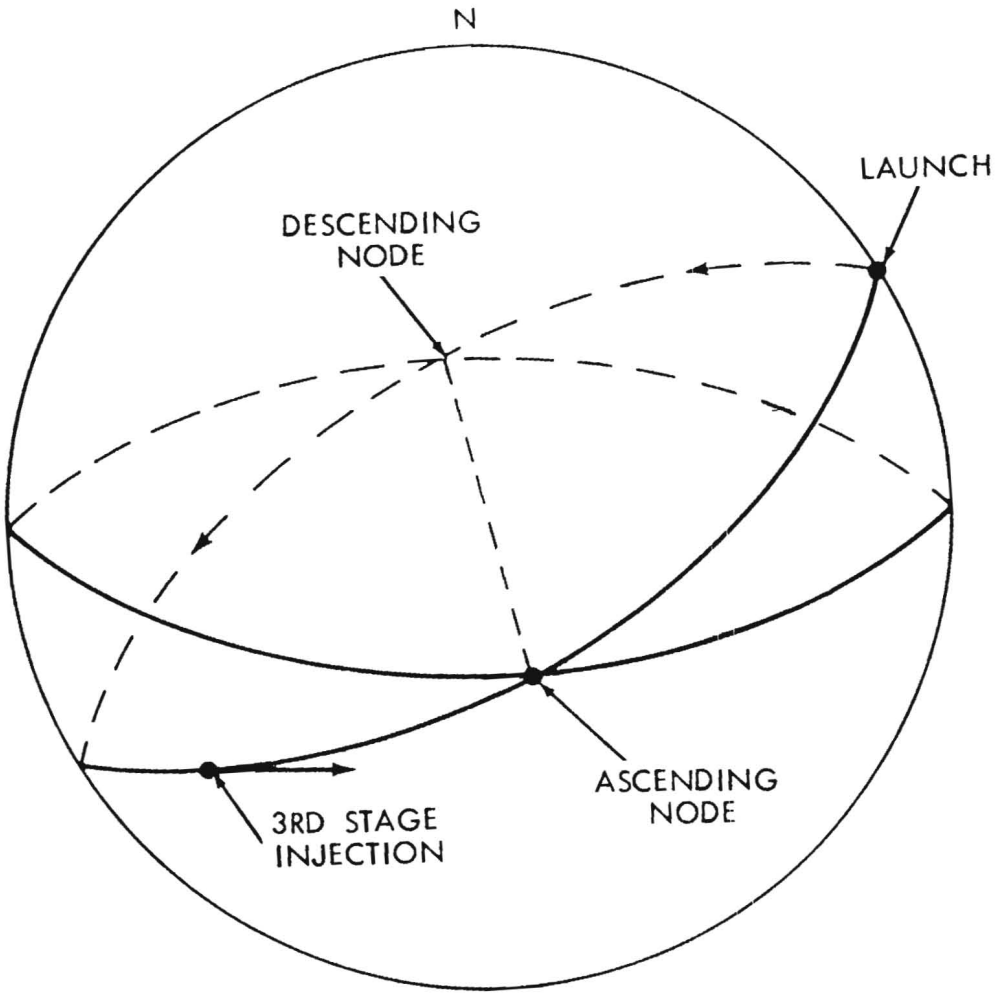

Figure 14-3. Injection into Transfer Orbit

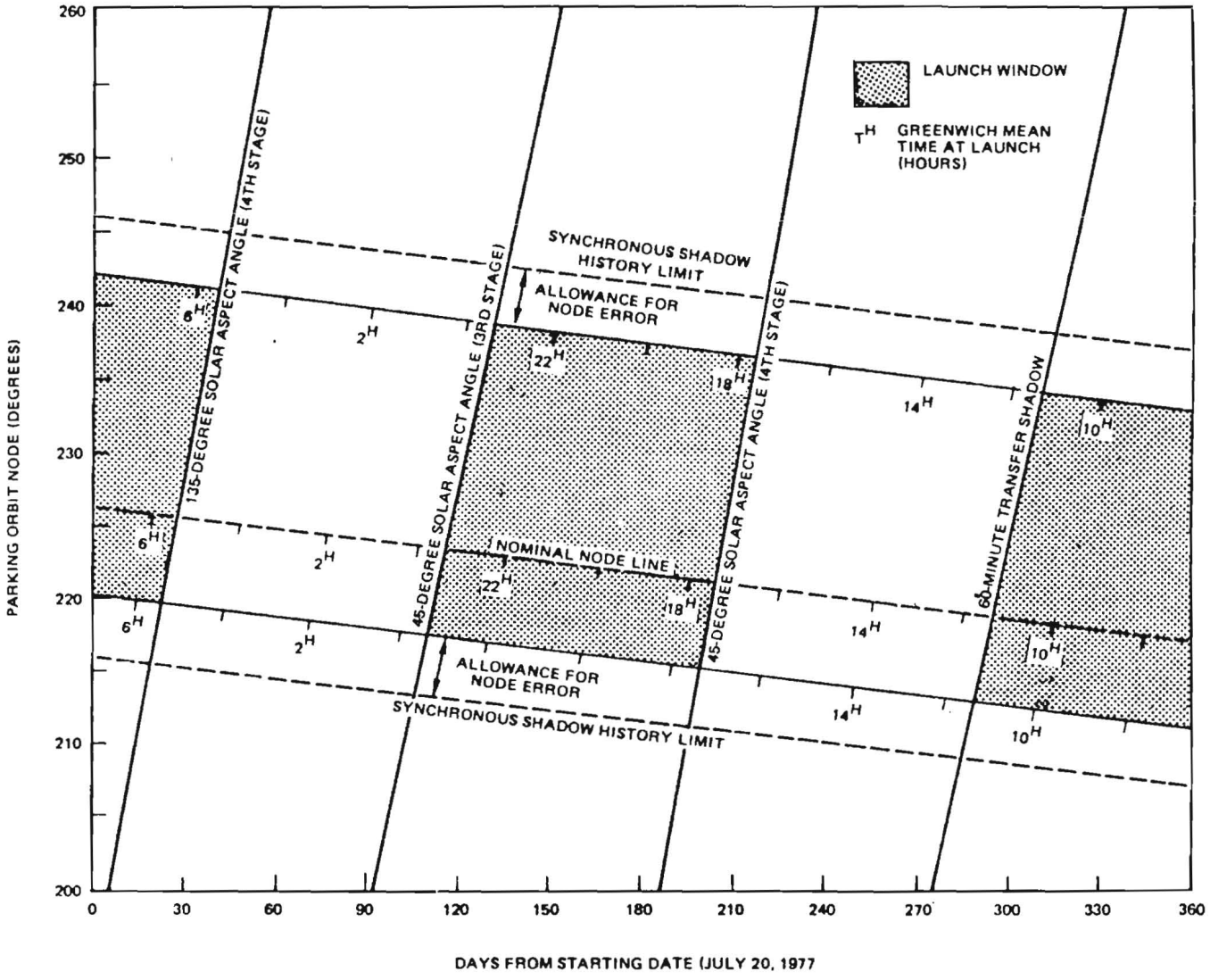

Figure 14-4. IUE Launch Window

b. November 10, 1977 to February 14, 1978

c. May 9, 1978 to July 20, 1978

These dates are determined primarily by the third- and fourth-stage solar aspect angle constraints, which rule out a total of about 5 months of the year. The acceptable node values are limited by the synchronous shadow history constraints, which are discussed in detail in Section 14.4. These limits slope downward in order to account for node regression in the synchronous orbit. For example, on the launch date of July 20, 1977 the shadow history can be computed with a given initial node value. To achieve the same shadow history for a launch date 5 months later, for example, the initial node must be compensated by an amount equal to a 5-month node regression.

It should be noted that the synchronous orbit node values will be about 6 degrees less than the parking orbit nodes because of the plane change at AMF. This is true for any launch date. In figure 14-4, this constant node shift has been accounted for in plotting the node limits associated with the synchronous orbit shadow history constraints. Also, in figure 14-4, note that there are no violations of the earth-sun separation angle constraint for the node range under consideration. This is due to the relatively high inclination of the orbit with respect to the ecliptic plane.

14.3 FUEL REQUIREMENTS

14.3.1 APOGEE BOOST MOTOR SIZING

Using the TBERR Program, the ABM was resized to account for increased spacecraft weight. The transfer orbit inclination used was 28.7 degrees (defined by launch azimuth) and the apogee bias was 5,700* nautical miles (10,556 kilometers). The target inclination was varied from 24.0 to 28.7 degrees, and the ABM fuel was computed assuming a nominal target drift rate of 6 degrees per day east. The ABM fuel penalty versus inclination is shown in figure 14-5, where zero penalty represents no plane change between the transfer and and synchronous orbits. The selection of the nominal inclination (26.5 degrees) is discussed in Section 14.4.2. For an inclination of 26.5 degrees, the impulsive velocity change (ΔV) is 3,540 feet per second (1,078.9 meters per second). The corresponding ABM fuel required is 455 pounds (206 kilograms), assuming an effective specific impulse of 280.6 seconds.

14.3.2 HYDRAZINE AND ON-STATION WEIGHT

To determine the station acquisition hydrazine required, a Monte Carlo simulation was performed using the TBERR Program. The covariance matrix for position and velocity at transfer orbit injection is presented in table 14-1. This study assumed launch vehicle errors of $\pm$1,100 kilometers (3σ) for apogee height and 0.3 degree (3σ) for transfer orbit inclination error. Additional errors are introduced during the AMF. The ABM 3-sigma pointing error was assumed to be 5 degrees in both yaw and pitch. The 3-sigma error in ABM ΔV was assumed to be 0.75 percent.

Two hydrazine maneuvers were simulated in the drift orbit. If the sample drift rate deviated by more than 0.1 degree per day from the nominal value of 6 degrees per day, a hydrazine burn was performed to correct the drift rate back to the nominal value. A second hydrazine burn reduces the drift rate to zero to achieve a synchronous orbit. (The purpose of the drift orbit is to allow the spacecraft to acquire a specified station longitude.) If the sample eccentricity was greater than nominal, two hydrazine burns were performed to achieve the synchronous orbit. The eccentricity was lowered to the nominal value, while the drift rate was reduced to zero. In either case, the 99th percentile* hydrazine fuel is 23 pounds (10 kilograms), assuming a specific impulse of 220 seconds. This does not include any fuel required for spin rate control or attitude trim maneuvers. Table 14-2 presents an approximate IUE weight breakdown. The pre-AMF and post-AMF reorientation hydrazine values are estimated to be 4 and 2 pounds, respectively.

*For hydrazine used to acquire station, N percent of the sample values are less than the Nth percentile value.

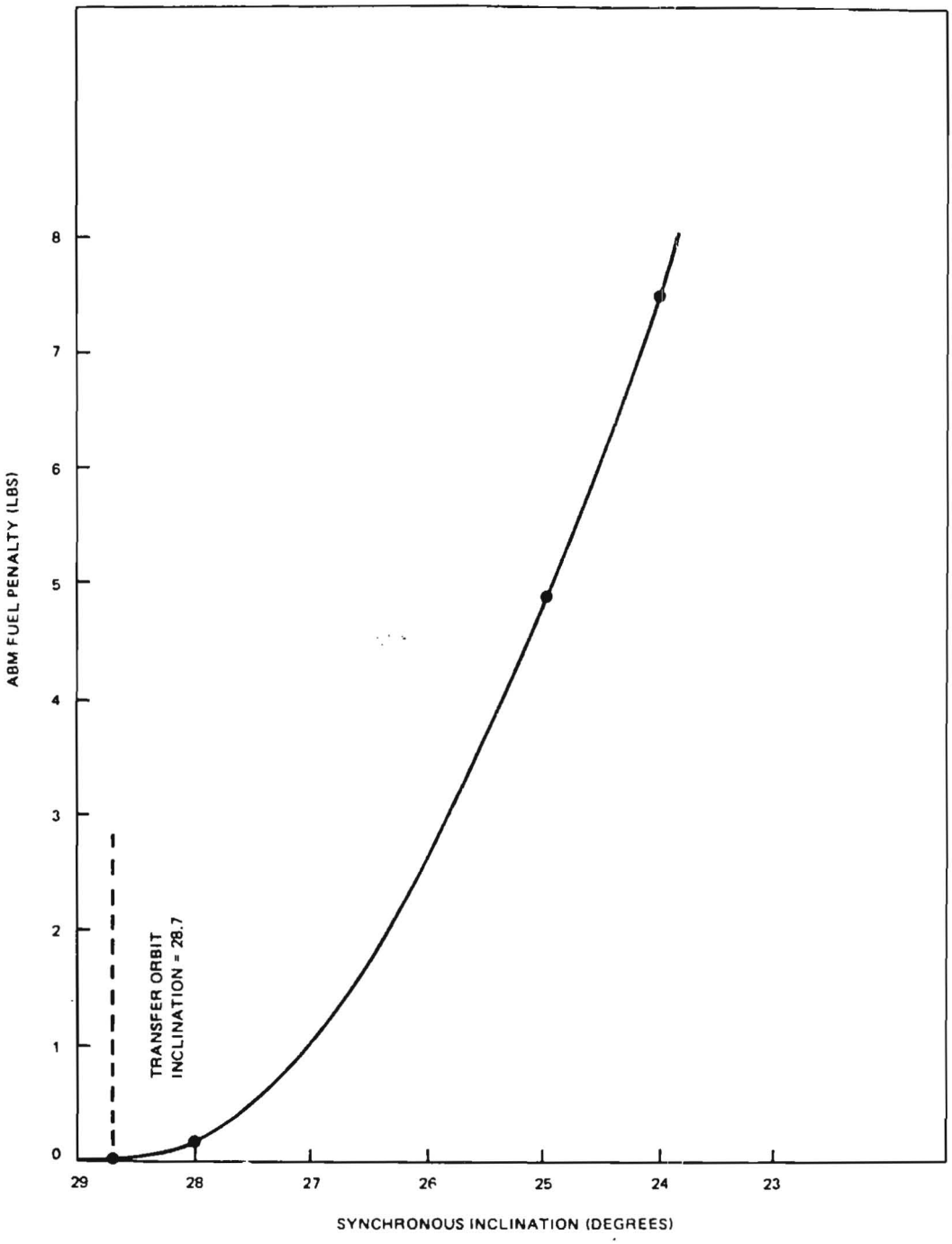

Figure 14-5. ABM Fuel Penalty Versus Inclination (for Fixed Apogee Bias and Fixed Drift Rate)

Table 14-1. Covariance Matrix at Transfer Injection

	x	y	z	$\dot{x}$	$\dot{y}$	$\dot{z}$
x	116322450.0	−1528932.4	−30565341.0	59126.868	83.506098	−142975.58
y	−1528932.4	63602375.0	706100.71	−1191.2372	5900.6438	1863.5505
z	−30565341.0	706109.71	25449260.0	−22264.382	16.078010	64165.883
$\dot{x}$	59126.868	−1191.2372	−22264.382	255.0	117.07503	−200.2417
$\dot{y}$	83.506098	5900.6438	16.078010	117.07503	8836.1771	−0.11295046
$\dot{z}$	−142075.58	1863.5595	64165.883	−200.2417	−0.11295046	9050.9395

Legend

1. POSITION IN FEET; VELOCITY IN FEET/SECOND.

2. COORDINATE SYSTEM:
   $Z = \underline{R}$
   $Y = \underline{R} \times \underline{V}$
   $X = (\underline{R} \times \underline{V}) \times \underline{R}$
   WHERE $\underline{R}$ AND $\underline{V}$ ARE THE INERTIAL POSITION AND VELOCITY VECTORS.

Table 14-2. Approximate Weight Breakdown for IUE

Item	English Units	Metric Units
WEIGHT AT THIRD STAGE BURN-OUT	1415 LBS	642 KG
PRE-AMF REORIENTATION HYDRAZINE (ESTIMATE)	−4	−2
WEIGHT AT AMF	1411	640
ABM PROPELLANT AND INERT CONSUMMABLES	−455	−206
POST-AMF WEIGHT	956	434
POST-AMF REORIENTATION HYDRAZINE (ESTIMATE)	−2	−1
STATION ACQUISITION HYDRAZINE (99TH PERCENTILE)	−23	−10
ON-STATION WEIGHT (99TH PERCENTILE)	931	422

14.4 NOMINAL TRAJECTORY

14.4.1 SHADOW TIME CONSTRAINT

The nominal node and argument of perigee of the elliptical synchronous orbit were chosen to satisfy the shadow time constraint. Synchronous shadow duration must be less than 72 minutes per revolution over a 5-year mission. Due to the orbital eccentricity, the actual shadow durations could be as high as 95 minutes. To avoid these situations, the orientation geometry of the orbit plane must be controlled. The shadow constraint is satisfied when the orbit plane achieves a relatively high ecliptic inclination (figure 14-6) and when the apogee position is well above the shadow cone of the earth (figure 14-7; ecliptic argument of perigee near 270 degrees). These conditions are met using an initial node of 220 degrees and argument of perigee of 234 degrees. For node angles from -10 to +20 degrees about the nominal value, the umbra shadow curves are acceptable and provide launch window durations of about 88 minutes per day (after compensating for possible node errors). For higher or lower node angles, the shadow curves are marginal or unacceptable.

14.4.2 TRACKING REQUIREMENTS AND ERROR ANALYSIS

The synchronous orbit inclination was chosen to satisfy tracking requirements at GSFC and VILFRA. GSFC tracking time must be 24 hours per day and VILFRA tracking time must be at least 10 hours per day. The physical mask plus 10 degrees was used in computing all tracking time for VILFRA. SANDTRACKS was used to compute tracking time as a function of inclination, argument of perigee, and longitude at the ascending node. A representative sample of this data is presented in table 14-3. The western-most limit of longitude at the ascending node is determined by the VILFRA tracking constraint, and the eastern-most limit is determined by the GSFC tracking constraint.

As the orbit evolves, the inclination tends to decrease and the argument of perigee increases, resulting in better tracking coverage. For nominal initial conditions, the orbit was allowed to evolve over a 5-year mission, and the longitude limits were determined as shown in figure 14-8. To keep the orbit within these limits, it is necessary to perform stationkeeping maneuvers throughout the mission.

A tracking error analysis has been done for the transfer orbit involving Rosman, Alaska, and Santiago. Figures 14-9 and 14-10 are plots of the root-mean-square position and velocity errors as a function of time after start of the transfer orbit. These values of position and velocity error are quite acceptable for the performance of maneuvers including apogee motor fire. Figures 14-9 and 14-10 show that the position error is maximum at apogee of the transfer orbit (approximately 7 hours after injection and every 14 hours afterwards), conversely, at perigee

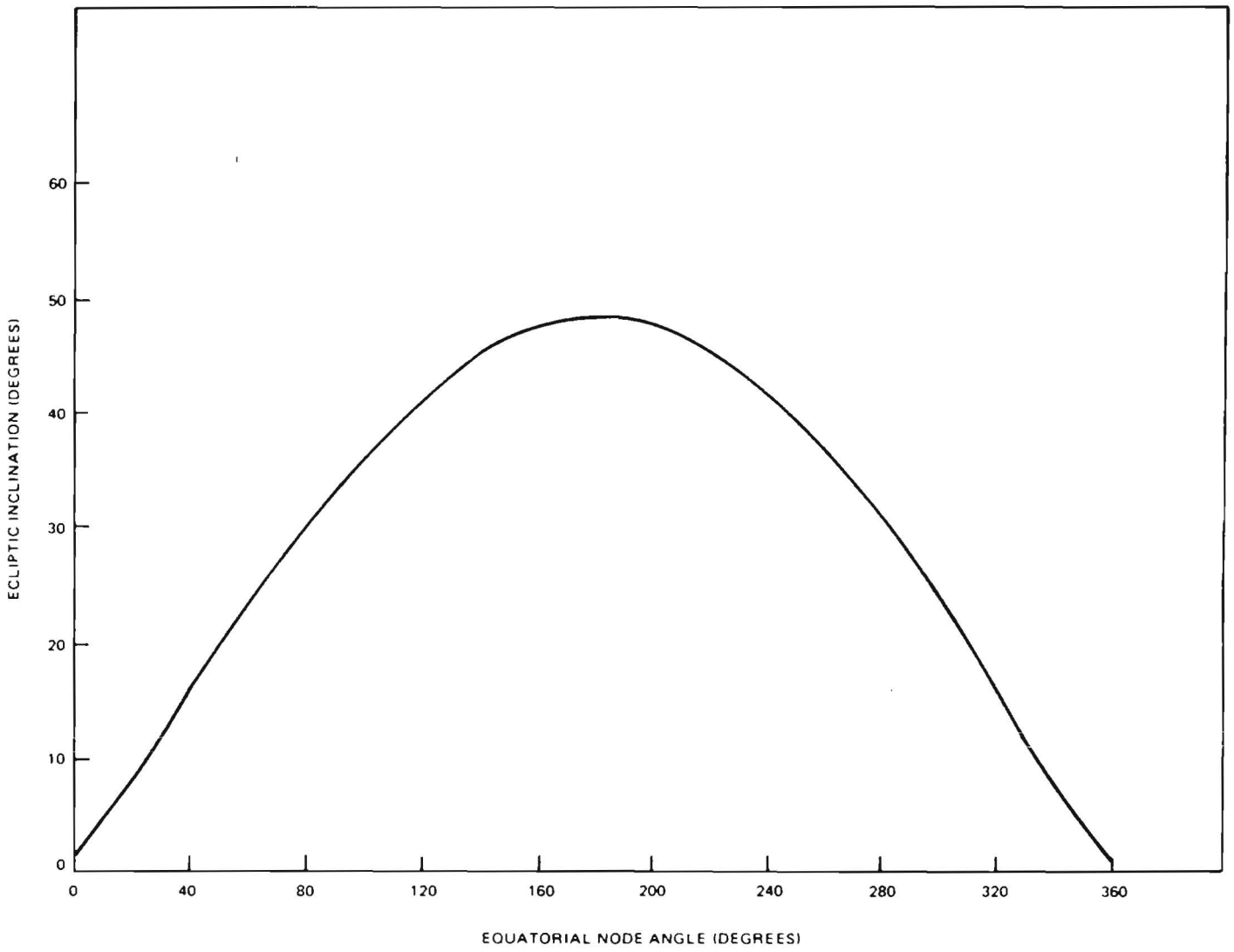

Figure 14-6. Ecliptic Inclination

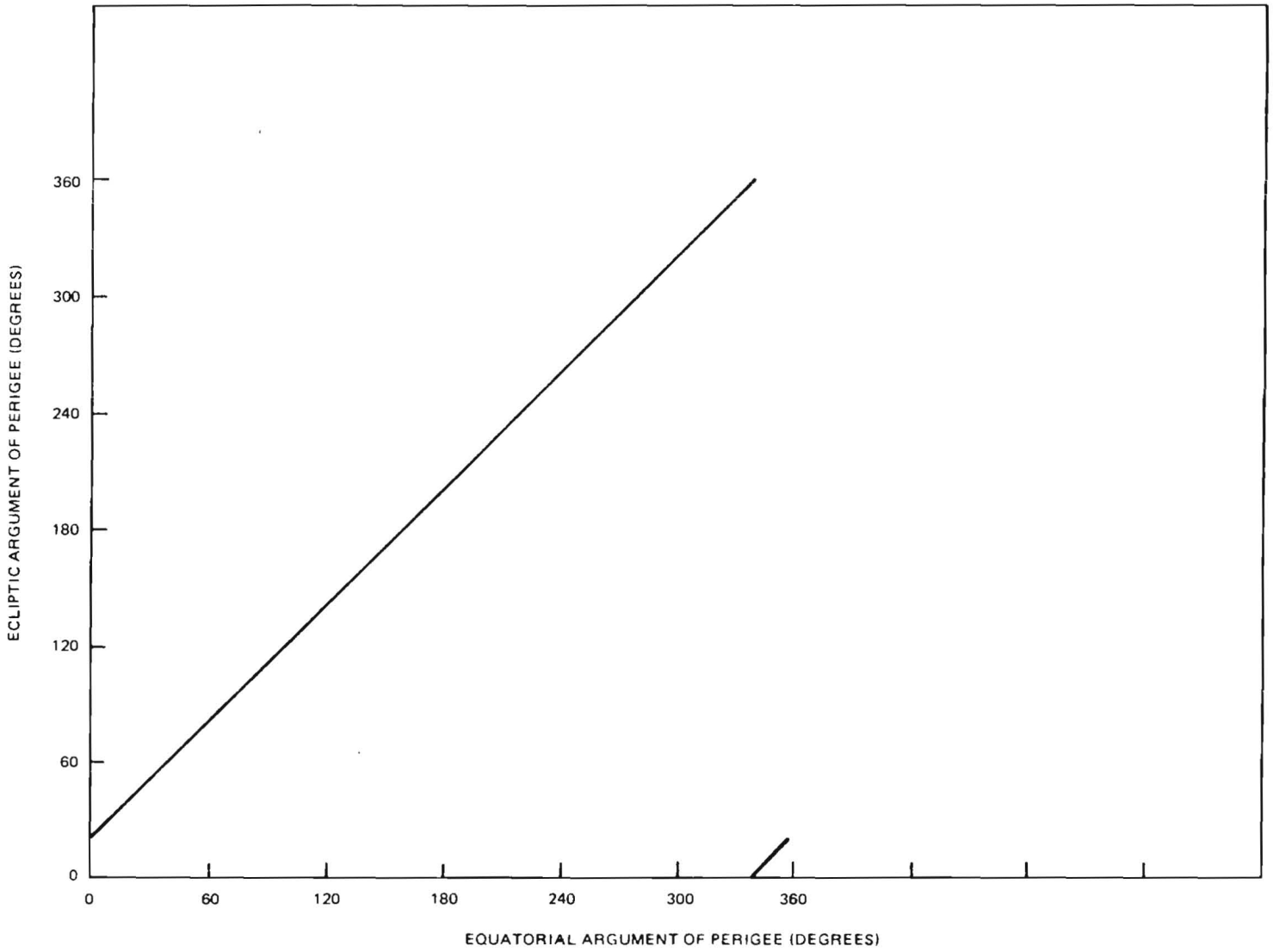

Figure 14-7. Ecliptic Argument of Perigee

Table 14-3. Longitude Intervals for Good Tracking

ARGUMENT OF PERIGEE (DEGREES)	VILFRA MINUS GSFC STATIONKEEPING LONGITUDES (DEGREES WEST)		
	INCLINATION = 25 DEG	INCLINATION = 26 DEG	INCLINATION = 26.5 DEG
226	44 – 36 = 8	44 – 38 = 6	44 – 38 = 6
230	44 – 34 = 10	44 – 36 = 8	44 – 36 = 8
234	44 – 32 = 12	44 – 34 = 10	44 – 40 = 4

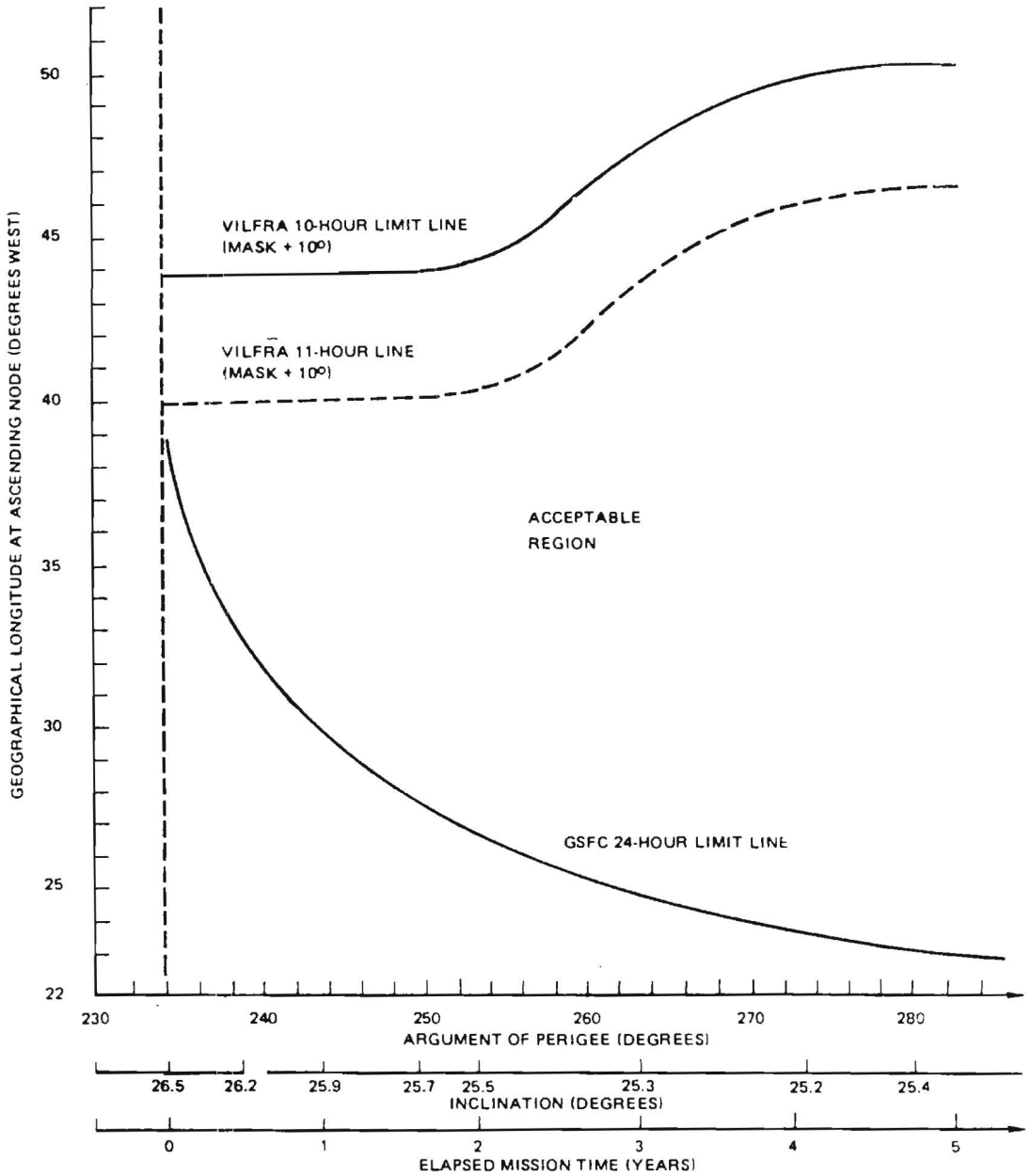

Figure 14-8. Stationkeeping Limits for Nominal Orbit

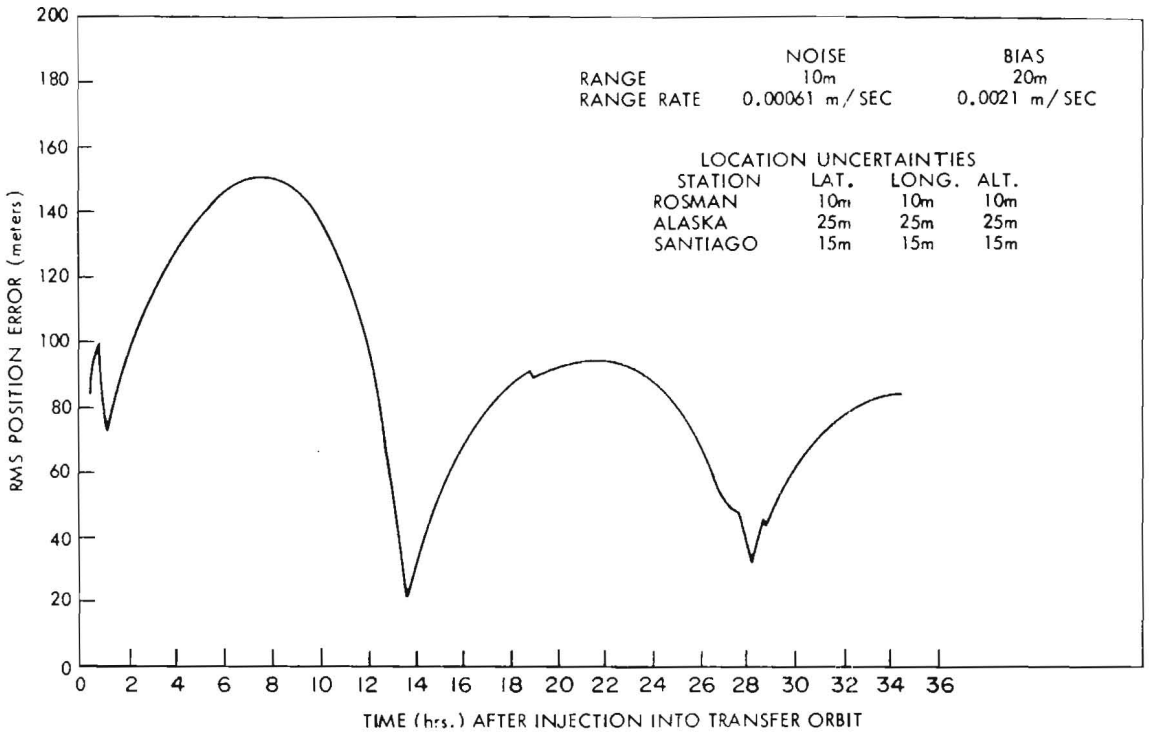

Figure 14-9. Position Accuracy of Tracking

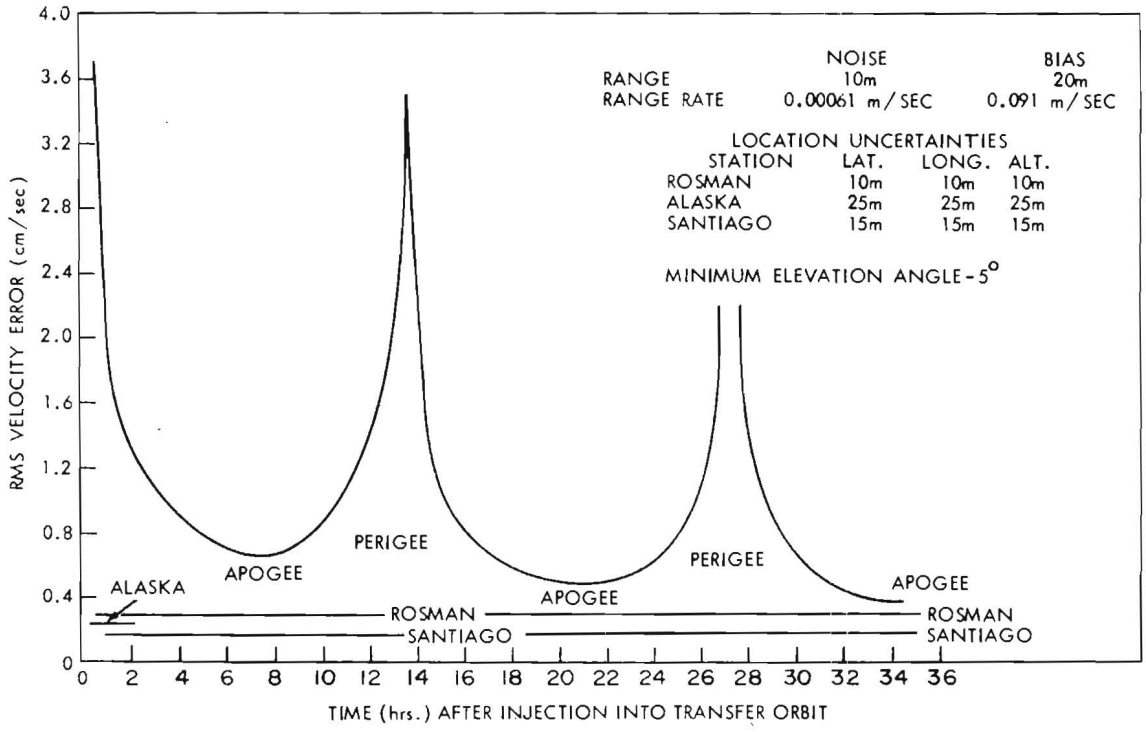

Figure 14-10. Velocity Accuracy of Tracking

(every 14 hours) the position error is at a minimum. Similarly, the velocity error is minimum at apogee and maximum at perigee of the transfer orbit. These conditions occur because at perigee of the transfer orbit the velocity of the spacecraft is at its largest value and a fixed percentage of this velocity (due to tracking error) will yield a larger value of error than at apogee where the velocity has its smallest value and therefore its smallest error. Also, at apogee of the transfer orbit the altitude of the spacecraft is at a maximum and a fixed percentage of this value will yield a larger error than at perigee, where the altitude is very low. For multiple orbits (every 14 hours), the errors of both position and velocity are reduced as the orbit becomes better defined due to the accumulated tracking data.

14.4.3 NOMINAL ORBITAL ELEMENTS

The parking orbit is defined by the parameters listed in table 14-4. The transfer, drift, and synchronous orbits are defined in table 14-5. At AMF, the spin axis right ascension is 5.27 degrees, and the declination is 11.26 degrees, for the nominal orbit. Errors in the orbital elements are listed in table 14-6.

14.4.4 NOMINAL MISSION PROFILE

The current nominal launch date for IUE is July 20, 1977. On this date, the launch window is open from approximately 6.9 to 8.4 hours GMT. This corresponds to a transfer node range of 220 to 242 degrees, or a synchronous node of 214 to 236 degrees.

IUE will be launched by a three-stage Delta 2914 vehicle from Kennedy Space Center at a launch azimuth of 95 degrees. At an altitude of 100 nautical miles, it will be injected into a circular parking orbit with an inclination of 28.7 degrees. After coasting for about 26 minutes, the booster injects the spacecraft into a transfer orbit with an argument of perigee of 228.7 degrees. At the end of this third-stage burn, the thrust axis remains in the same attitude position since there are no forces acting to change it. In order for the apogee motor to be fired, there must be a reorientation of the thrust axis of 180 degrees using the HAPS. After approximately 1 to 2 hours into the transfer orbit, there should be enough tracking data to adequately determine the trajectory. Also, there should be enough attitude data to determine the pointing direction of the spin axis. Almost all of the 180 degrees reorientation will be performed at one time (requiring about 20 minutes); the rest of this maneuver will be done later in the transfer orbit when more tracking and attitude data are available. Figure 14-11 presents the tracking coverage up through second apogee. The attitude of the thrust axis is then firmly determined for apogee motor firing.

Table 14-4. Nominal Parking Orbit Parameters

Parameter	Description
Altitude	100 nautical miles (185 kilometers)
Eccentricity	0
Inclination	28.7 degrees
Injection latitude	24.77 degrees
Injection longitude	59.49 degrees west
Injection azimuth	105.28 degrees
Time from launch to injection	539.37 seconds
Coast time	1599.35 seconds
Epoch date	July 20, 1977
Epoch time	$7^{H}\ 13^{M}\ 42^{S}$

Table 14-5. IUE Nominal Orbits

PARAMETER	TRANSFER ORBIT	DRIFT PHASE 1	DRIFT PHASE 2	DRIFT PHASE 3	SYNCHRONOUS ORBIT
SEMIMAJOR AXIS (KM)	29642	41703	42010	42119	42164
ECCENTRICITY	0.77858	0.26417	0.26955	0.27144	0.27221
INCLINATION (DEG)	28.7	26.5	26.5	26.5	26.5
ASCENDING NODE (DEG)	225.9	220	220	220	220
ARGUMENT OF PERIGEE (DEG)	228.7	234	234	234	234
MEAN ANOMALY (DEG)	0.0	180	0.0	0.0	0.0
EPOCH DATE	7/20/77	7/21/77	7/24/77	7/27/77	7/29/77
EPOCH TIME	$7^{H}49^{M}21^{S}$	$4^{H}53^{M}21^{S}$	$15^{H}17^{M}27^{S}$	$14^{H}41^{M}53^{S}$	$14^{H}29^{M}30^{S}$
DRIFT RATE (DEG/DAY EAST)		6.0	2.0	0.577	0.0
PERIOD (HR)	14.110	23.543	23.803	23.896	23.934
PERIGEE RADIUS (KM)	6563	30686	30686	30686	30686
APOGEE RADIUS (KM)	52720	52720	53334	53552	53642

INITIAL STATION $\approx 42^{o}$ W

Table 14-6. 99th Percentile Errors in Orbital Parameters

PARAMETER	TRANSFER ORBIT ERRORS		DRIFT ORBIT ERRORS		SYNCHRONOUS ORBIT ERRORS	
ECCENTRICITY	−0.003	+0.004	−.004	+0.007	−.014	+0.0
INCLINATION (DEG)	−0.2	+0.2	−1.0	+1.1	−1.0	+1.1
NODE (DEG)	−0.6	+0.6	−3.4	+3.1	−3.4	+3.1
ARGUMENT OF PERIGEE (DEG)	−1.0	+1.1	−5.6	+5.6	−5.6	+5.6
RADIUS OF PERIGEE (KM)	−3.6	+3.3	−696	+504	0.0	+590
RADIUS OF APOGEE (KM)	−972	+1004	−993	+1017	−590	0.0
DRIFT RATE (DEG/DAY)			−11.0	+9.9	0.0	0.0

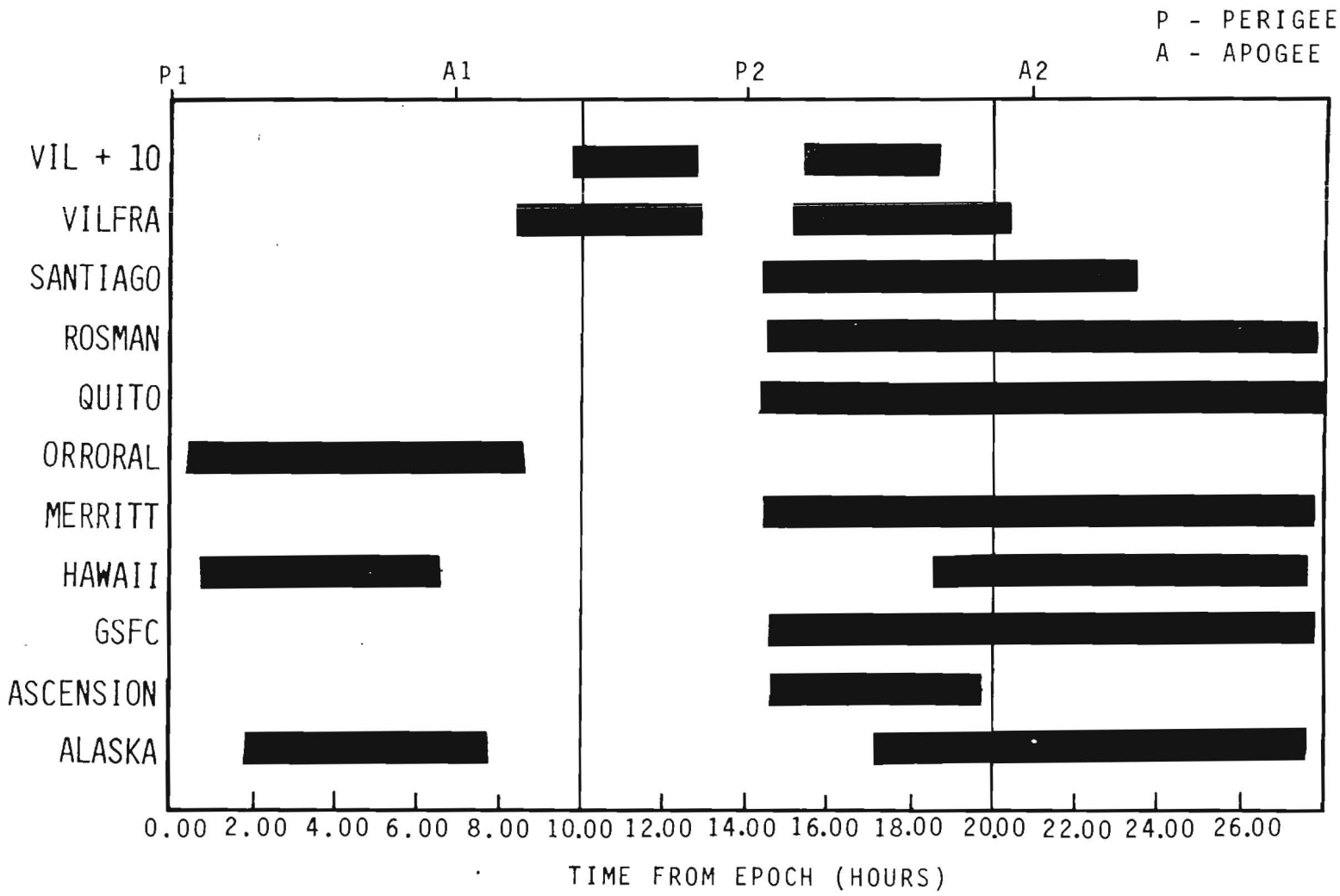

Figure 14-11. Tracking Coverage for First Apogee and Second Apogee in Transfer Orbit

The current strategy for IUE calls for apogee motor burn at the second apogee passage of the transfer orbit which will inject the satellite into a near-synchronous drifting orbit. The ABM will perform a plane change resulting in an inclination of 26.5 degrees, node of 220 degrees, and argument of perigee of 234 degrees . However, if for some reason it is not possible to fire on second apogee, then fourth or sixth apogee must be considered. At the end of every other apogee pass the spacecraft will move longitudinally by about 45 degrees. Fourth apogee firing would then be at a longitude of 80 degrees and sixth apogee would be at 17 degrees east. Both of these cases would place the spacecraft farther from the target longitude of 42 degrees west. In addition, there would be slightly more fuel used for nutation control.

14.4.5 NOMINAL STATION ACQUISITION SEQUENCE

As discussed above, the strategy selected for IUE is to fire the apogee motor at the second apogee pass which would place the spacecraft at 69 degrees west longitude. The nominal orbit would then drift to the target longitude of 42 degrees west at the rate of 6 degrees per day. As presented in table 14-5, the drift orbit is divided into three phases with drift rates of 6 and 2 degrees per day east. The major portion of the drift rate is removed by two Hohmann type burns of the hydrazine thrusters. The rest of the drift rate will be removed by eventual fine tuning. This represents only one of many possible station acquisition sequences to achieve a synchronous orbit. Table 14-7 indicates time to acquire station for easterly and westerly drift rates of 6 degrees per day, assuming AMF occurs on one of the first five transfer apogee passes (second apogee is nominal).

It should be noted that although the nominal drift rate is 6 degrees per day east, the three-sigma value can be as high as 18 degrees per day which would be a fast drifting orbit and would require a revision of the acquisition schedule. Furthermore, the orbit could also be drifting westward and in this case would have to be changed to eastward as soon as tracking data has verified the orbit. More specifically, the range of three-sigma drift rates is from 18 degrees per day east to 6 degrees per day west. It would be acceptable to have a drift rate of at least 3 degrees east although it would take several days longer to reach the target longitude. However, a drift rate of less than 3 degrees east or a westward drift rate is not acceptable and the spacecraft would then require a reorientation maneuver and then a maneuver to decrease the semi-major axis of the orbit to cause an eastward drift. It would take between two to four hours of tracking to determine a fairly precise orbit that would determine the existing drift rate. If it has been established that the drift rate is unacceptable, then reorientation of the spin axis is necessary so that the spacecraft is thrusting in the proper direction. In order to perform this initial ΔV, the spacecraft will remain spinning in order to use the panoramic scanner for attitude determination. Once the reorientation has been completed, a hydrazine

Table 14-7. Time to Acquire Station for Easterly and Westerly Drift Rates

TRANSFER APOGEE PASS	DEGREES TO STATION		DAYS TO STATION	
	EAST	WEST	DRIFT 6 DEG/DAY	DRIFT 6 DEG/DAY
1	176	184	29	31
2	27	333	5	55
3	238	122	40	20
4	90	270	15	45
5	301	59	50	10

burn will be initiated to decrease the semi-major axis for the desired drift. The final drift removal maneuvers, once on target, will be performed with the spacecraft in a three-axis stabilized mode using experiment and sun sensors for attitude determination. The fuel requirements for a three-sigma drift error have been included in the fuel budget.

14.4.6 EAST-WEST STATIONKEEPING

Effects of the equatorial bulge and the sun and moon will combine to alter the orbital radius of the IUE satellite by a small amount. The major in-plane perturbation is caused by the ellipticity of the earth's equatorial section, which causes large in-plane angle oscillations of the satellite around the nearest minor axis of the equatorial section. The earth's minor axis(which contains a stable point at either end) is located at approximately 105 degrees west longitude and 75 degrees east longitude. As the IUE satellite will be located at 42 degrees west longitude, the nearest stable point will be at 63 degrees west of this station. The satellite will then oscillate through 126 degrees and return to its original position to complete the cycle. The period of oscillation will be about 3 years. The drift rate will reach a maximum of 0.38 deg/day at the stable point and reduce to zero at half of the period length. At this point, the sign of the drift rate will change and the satellite will return in a reverse pattern.

The total drift off-station is 126 degrees which will, of course, cause tracking station view problems. The velocity requirements needed to keep the satellite from this oscillatory drift are approximately 1 meter/second per year. It is estimated that 6 to 8 stationkeeping maneuvers are needed over the mission lifetime of 5 years to keep the spacecraft within the required longitudinal band for satisfying tracking coverage and shadow constraints (see Sections 14.4.1 and 14.4.2; also figure 14-8).

14.5 REFERENCES

1. International Ultraviolet Explorer (IUE) Satellite Mission Analysis. CSC/TM-75/6137, Ronald Cook, November 5, 1975.

2. Error Studies for Synchronous Satellites, J. L. Cooley, January 1972.

3. Launch Window Analysis for the International Ultraviolet Explorer (IUE) Satellite, CSC, 3000-2700-07TN, J. H. Griffin, March 1975.

APPENDIX A. FUNCTIONAL DESCRIPTION OF NEW DEVELOPMENT ACS COMPONENTS

A.1 HARDWARE PHILOSOPHY

A.1.1 INTRODUCTION

The ACS for the IUE is a combination of proven, presently flown (or flying) hardware with a minimum of mission unique items. This approach was taken to minimize the risk associated with new components and to minimize the costs of necessary qualification testing required on new hardware. Those items chosen as new hardware are intimately related to the extensive redundancy required to achieve the IUE design goal of 3 to 5 years orbital life. In these cases it was felt to be more expendient to go for a new design incorporating this redundancy than attempt to redesign existing devices. However, in keeping with the low risk development nature of the program, even these new devices generally consist of preexisting and preflown components, circuits and/or assemblages with their uniqueness restricted to packaging, interconnection or conceptual usage. This section will describe the new components while Appendix B will describe those that have previously been used.

A.1.2 FUNCTION

The prime functions of the IUE unique components are to process data from various proven sensors, perform hard programmed algorithms on these sensory inputs and develop the driving signals for the various torque or reaction devices. Some of these logic functions have been explained in section 8.2 and the interconnection of the various sensors, processors and actuators is shown graphically in figure 8-2 and figure 8-4. Figure 8-4 shows the relay functions in the Control Electronics Assembly (CEA), which accepts power from redundant regulated buses and switches it to the various external sensors, logic circuits, and actuators. Also shown is the Wheel Drive Assembly (WDA), which generates the redundant regulated voltages and selects and amplifies the wheel drive signals from the CEA to the level required for the four reaction wheels. The CEA is a NASA/GSFC designed and fabricated unit using proven techniques while the WDA is procured from Ithaca and contains various individual card designs that have flown on other spacecraft. Also shown on figure 8-4 are the six gyro units. These are relatively standard devices fabricated by the Bendix Corporation.

A.2 INERTIAL REFERENCE ASSEMBLY

A.2.1 DESIGN REQUIREMENTS

As the prime attitude sensor of the IUE, the IRA must provide attitude sensing of sufficient accuracy to meet the IUE mission requirements. Its accuracy requirements are most stringent in the hold mode of operation when spectrograph data are being collected and can be relaxed somewhat

at other times. It must also have a design life expectancy to match that of the IUE and must satisfy the physical constraints of the IUE spacecraft. Consideration of these factors has led to the following design requirements for the IRA.

a. Accuracy and stability of ±1 arc-second in pitch and yaw for at least 150 seconds, with a design goal of ±0.7 arc-seconds for 30 minutes; ±1 arc-minute in roll; and ±2 arc-minute slew accuracy for any slew angle.

b. Reliability for 3 to 5 year life expectancy.

c. Physical constraints of low weight, power and volume requirements. Present budgeted values are 42 pounds and 11 watts/channel. The size is not a very critical limitation.

To meet the most critical accuracy requirements when the spacecraft is inertially stabilized in a benign environment, the decision was made to use a strapdown, single degree-of-freedom, gas bearing, rate integrating gyro. To provide the readout accuracy required for strapdown operation with a digital computer, a pulse-rebalance capture loop is required. A study of the performance of the selected gyro shows that the following characteristics are quite realistic and reasonable to expect expect from this instrument.

a. Accuracy and Stability. The readout resolution is 0.01 arc-second nominal. A study was completed to determine the ACS pointing stability using such gyros. Available data indicates that a stability of ±2 arc-seconds or better for 30 minutes in laboratory environment, after a precise gyro bias calibration, is achievable. Some gyro test data has shown a drift rate of only 1.0 arc-second per hour for a 60 minute period, thus there is every likelihood that the design accuracy requirements of ±1 arc-second for 150 seconds will be exceeded.

b. Slew Accuracy. Differences in the actual and assumed orientations of the input axes, and the actual and assumed values of the overall scale factor, produce errors in slew. Roughly speaking, for an orthogonal triad of gyros, a 1 arc-second input axis misalignment and a 5.3 ppm scale factor error produce equivalent slew errors. For the gyros and rebalance electronics being used, the input axis orientations are defined to better than four minutes of arc and the alignments are stable to better than ±15 arc-second for fairly long periods of time (depending on environment). The overall scale factor linearity and stability, including the effects of torquer, signal pickoff, and rebalance electronics are such that after proper calibration, the scale factor variation will be no greater than 500 ppm over the whole range of input rates

and about 10 ppm at each calibrated input rate point. The 15 arc-second alignment stability and 500 ppm scale factor stability are adequate for the ±2 arc-minute IUE slew accuracy requirement. The 10 ppm scale factor stability at very low input rates is desirable because fairly rapid fluctuations of the scale factor are indistinguishable from bias variations and therefore affect pointing stability.

c. Reliability. The gyro loop MTBF is greater than 30,000 hours as discussed in the following paragraphs.

d. Physical Characteristics. Approximately 7.0 pounds and 11 watts per gyro loop are good estimates, assuming proper structural and thermal design, good thermal environment, and well regulated power supply.

A final design IRA is undergoing fabrication and test by the Bendix Corporation at this time.

A.2.2 RELIABILITY

The MTBF of one gyro and its associated electronics has been determined as 30,000 hours minimum. Available data on gyros currently operational in NASA spacecraft (OAO, ATS-6) show this to be a realistic lower bound for IUE application. While most previous applications of these gyros have been in short duration aircraft and missile applications (under far more severe environment) the various gyro manufacturers have been able to perform studies and analyses of their gyros under field conditions and project their longevity under the more benign space environment. Thus, an aircraft gyro exhibiting a tested 34,000 hour MTBF is projected to have at least equal space life while two other manufacturers whose gyros demonstrated 30,000 hour MTBF in "field" use project orbital lives of 125,000 and 275,000 hours.

In summary, it is probably fair to state that it is impossible to specify a particular MTBF figure with any great confidence. During design and manufacture, great emphasis will be put on good engineering and careful quality control rather than on an attempt to meet a specific MTBF figure. However, it appears that extensive redundancy must be used to satisfy the 3- to 5-year design life requirement. Table A-1 should be examined with this background in mind. It is assumed that 3 or more gyros are used in a skewed configuration so that any 3 can provide three-axis information. The entries should be considered in the relative sense rather than an absolute one— entries in any column going down show the effect of increased redundancy (increased number of gyros) and entries in any row going right show the effect of better engineering (larger MTBF). The MTBF values used bracket the expected MTBF range. Entries in parentheses refer to a 5-year mission and others to a 3-year mission.

Consideration of above factors, as well as the physical constraints, has led to the decision to use six gyros. Making the assumption that a 60,000 hour MTBF is realizable in IUE application, this yields an 88 percent probability of success for a 3-year mission, and 62 percent for a 5-year mission. The IUE weight, power and volume budgets allow use of up to six gyros. The present plan is to run all healthy gyros continuously, except during emergencies.

Table A-1. Probability (Life) Chart for Redundant Gyros

Number of Gyros	MTBF (Hours)				
	20,000	40,000	60,000	80,000	100,000
3	2 (0)	14 (4)	27 (11)	37 (19)	45 (27)
4	6 (1)	34 (11)	55 (29)	69 (44)	77 (55)
5	12 (1)	53 (21)	76 (47)	86 (64)	92 (76)
6	20 (2)	69 (32)	88 (62)	94 (79)	97 (88)

A.2.3 COMPUTATIONAL REQUIREMENTS

Each of the six rebalanced gyro modules emits two pulse trains on two channels, the positive and negative pulse repetition frequencies being proportional to that component of spacecraft body rates sensed by that gyro.

For a given maximum pulse repetition frequency, the design required a pulse weight of 0.01 arc-second. Stability (and linearity) of this scale factor depends primarily on the quality of the torquer, the signal pick-off, and the rebalance electronics (primarily the current generator). A short term (several hours) scale factor stability for low input rates of 0.01 percent (100 ppm) is achievable.

These requirements lead to the specification of the digital interface. The gyro bias drift— the measured output rate for zero input rate— is about 1 arc-second per second. It has to be estimated as accurately as possible with a measurement resolution of about 0.001 arc-second per second. Any high-frequency variations in the scale factor— either in individual pulse weights or differences in positive and negative pulse weights— appear as an apparent bias instability. A gyro with a 10 arc-second per second fixed bias drift and a 100 ppm short term scale factor instability

would have an acceptable bias estimate resolution. The two pulse trains may therefore be summed in one up-down counter. The extra accuracy to be gained by calibrating and counting the positive and negative pulses independently is not required in this application.

The counter is sampled between two and five times per second. The corrected output of one gyro is therefore an angle increment during one sample interval $\Delta\theta = WN - \bar{B}$ where W is the calibrated weight of one pulse in arc second, N is the net number of pulses during the sample interval, and $\bar{B}$ is a bias correction term in arc second. Occasional recalibration of W and $\bar{B}$ would be required and can be done via ground command every few hours. During experimentation, additional bias corrections will be carried out every few minutes using onboard computations from the fine error sensor.

Let the output of k gyros, $3 \leq k \leq 6$, be denoted by the column vector $g = \text{col}\ (g_1, g_2, \ldots, g_k)$ and let $\omega = \text{col}\ (\omega_1, \omega_2, \omega_3)$ be the incremental angular rotations about the orthogonal reference axes fixed in the spacecraft. For the i-th gyro, $g_i = l_i\omega_1 + m_i\omega_2 + n_i\omega_3 + B_i$, where B_i is the residual bias drift and l_i, m_i; and n_i, are the direction cosines of the input axes of the gyro. Since the uncertainty in the definition of the input axes—several minutes of arc—would introduce unacceptable errors, a post-launch calibration will be carried out to determine the orientations of these axes. The stability of these calibrations will be 15 arc second (1σ) or better and will hold for very long periods of time in a benign environment.

For all k gyros, in matrix notation $g = L\omega + B$ where L is the matrix of direction cosines and $B = \text{col}\ (B_1, B_2, \ldots, B_k)$ is the residual bias drift. Since the best estimates of the fixed bias have already been taken out of the gyro output, B must behave like a weakly correlated (high frequency), zero-mean (vector-valued) random variable which includes the basic instabilities of the gyro and the rebalance electronics as well as the bias estimation errors. If the gyros are assumed to be independent, the covariance matrix of B is diagonal and from all possible solutions for ω (for $k > 3$), the best, or minimum variance, solution is (Reference 4-8) $\hat{\omega} = Hg$ where $H = (L^T L)^{-1} L^T$ and is assumed to exist. L^T is the transpose of L. The solution of ω, including the effect of bias variability, may therefore be assumed to be $\omega = Hg + b$ where $b = HB = \text{col}\ (b_1, b_2, b_3)$ is the resultant bias drift along the spacecraft axes.

Only two of these, about pitch and yaw, can be measured with sufficient accuracy using the fine error sensor. The fine solar aspect sensor may be used to monitor the roll bias, but the best estimate for the roll bias, from available measurements, would be zero most of the time. These bias estimates can be used to update the individual gyro bias calibrations through the relation $\Delta B = Lb$ and then setting $b = 0$. This is not a complete bias correction because B has up to six elements and b contains

only two independent entries. A minimum of three updates at three different inertial orientations are needed, the optimum orientations being three orthogonal directions. Initial postlaunch calibration, and recalibrations, will require three stellar measurements as close to 90 degrees apart as practicable. During normal operation, the observation sequence may be arranged to avoid nearly unchanging inertial orientation of the spacecraft for extended periods of time.

The determination of the direction cosines (elements of L) and subsequent computation of H (for all the 42 different ways 3-axis information may be derived from 3 to 6 gyros) requires double precision arithmetic which is a significant computer load. For IUE, the H matrix is determined on the ground as a function of which gyros are active (normally all good gyros will be used.) This matrix is uplinked to the OBC and the direction cosines are developed onboard the IUE. Monitoring of performances of individual gyros, diagnosis and isolation of failures and necessary configurations, infrequent calibrations, and similar service functions will all be done using the ground link and ground computer. A computation flow diagram for the complete ACS, including that of IRA, is shown in figure 8-19 in section 8-3.

A.2.4 LAYOUT

The number of gyros has been chosen to be six for reliability considerations. The only restriction on their relative orientation was that three of them must be capable of providing complete three-axis information. This implies that no more than two input axes could lie on any given plane. Mathematically, the requirement is that the H matrix must exist, which, in turn, requires that the direction cosine matrix L has rank 3.

The usual method of implementing an assemblage of six, skewed axes gyros is a duodecahedron configuration. This has a covariance matrix that describes a sphere and, if gyro failures are independent, the equivariance surface stays close to a sphere. However, IUE does not require the same degree of pointing and holding about all axes. While the pitch and yaw axes require 1 arc-second holding and can be resolved to about 0.1 arc second, the roll axis only requires 1 arc-minute holding and can be resolved only to about 14 arc-second with a 30 arc second accuracy.

This ratio of 20 to 1 roll error to pitch-yaw error in the IRA attitude information argued for a skew configuration favoring the pitch and yaw axes. The requirement called for the equivariance surface to be an ellipsoid of revolution with the major axis 20 times the magnitude of the minor axis along the spacecraft roll axis. This was achieved by distributing the gyro input axes symmetrically about pitch and yaw and at 85 degree half-cone angle around roll. This configuration is shown schematically in figure A-1, although the actual gyro package contains all gyros in six-pack fashion within a rectangular outline. Figure A-2

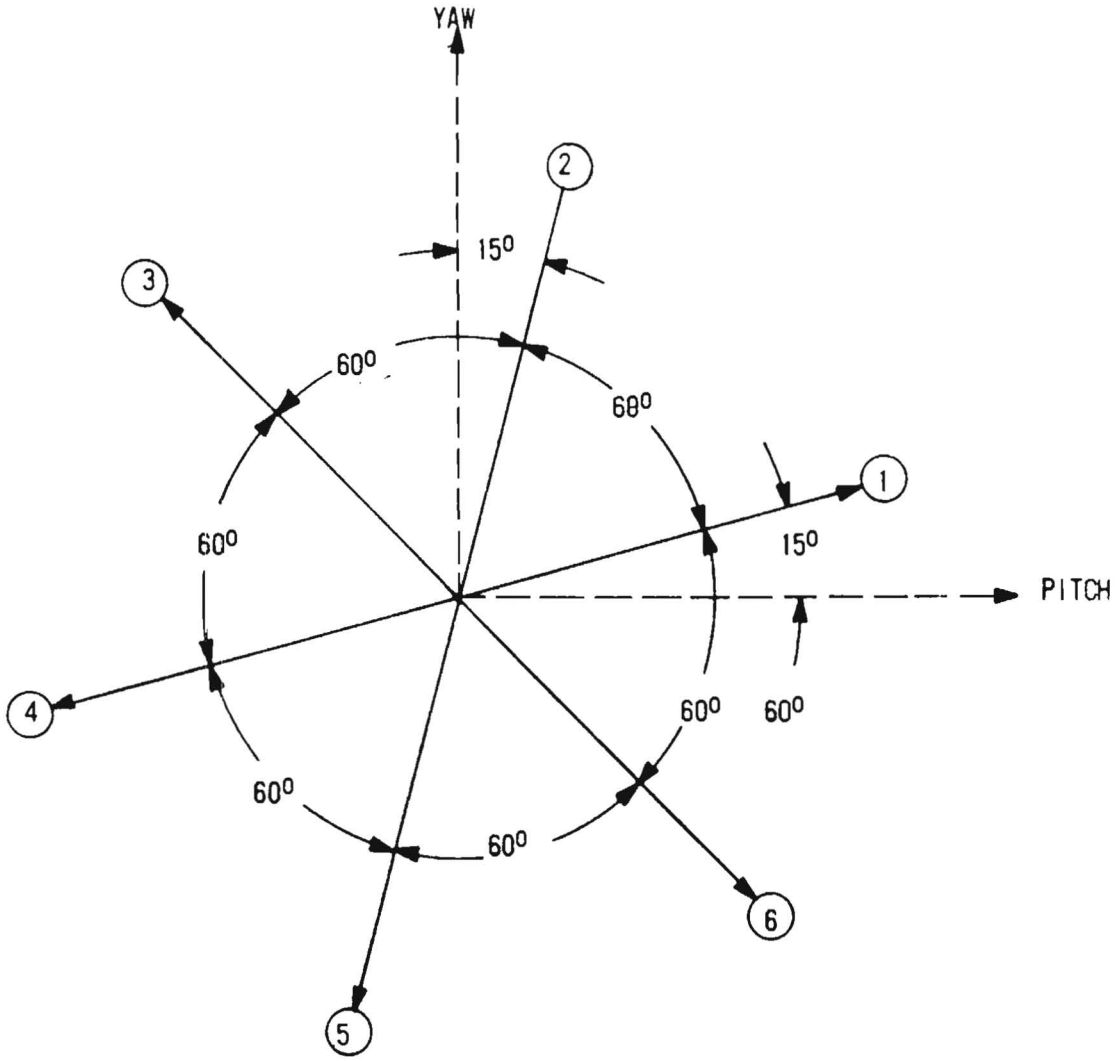

PROJECTIONS OF THE INPUT AXES OF THE SIX GYROS ON SPACECRAFT PITCH-YAW PLANE

INPUT AXES LIE ON A CONE ABOUT ROLL AXIS WITH 85° HALF CONE ANGLE

Figure A-1. Projections of the Input Axes of Six Gyros

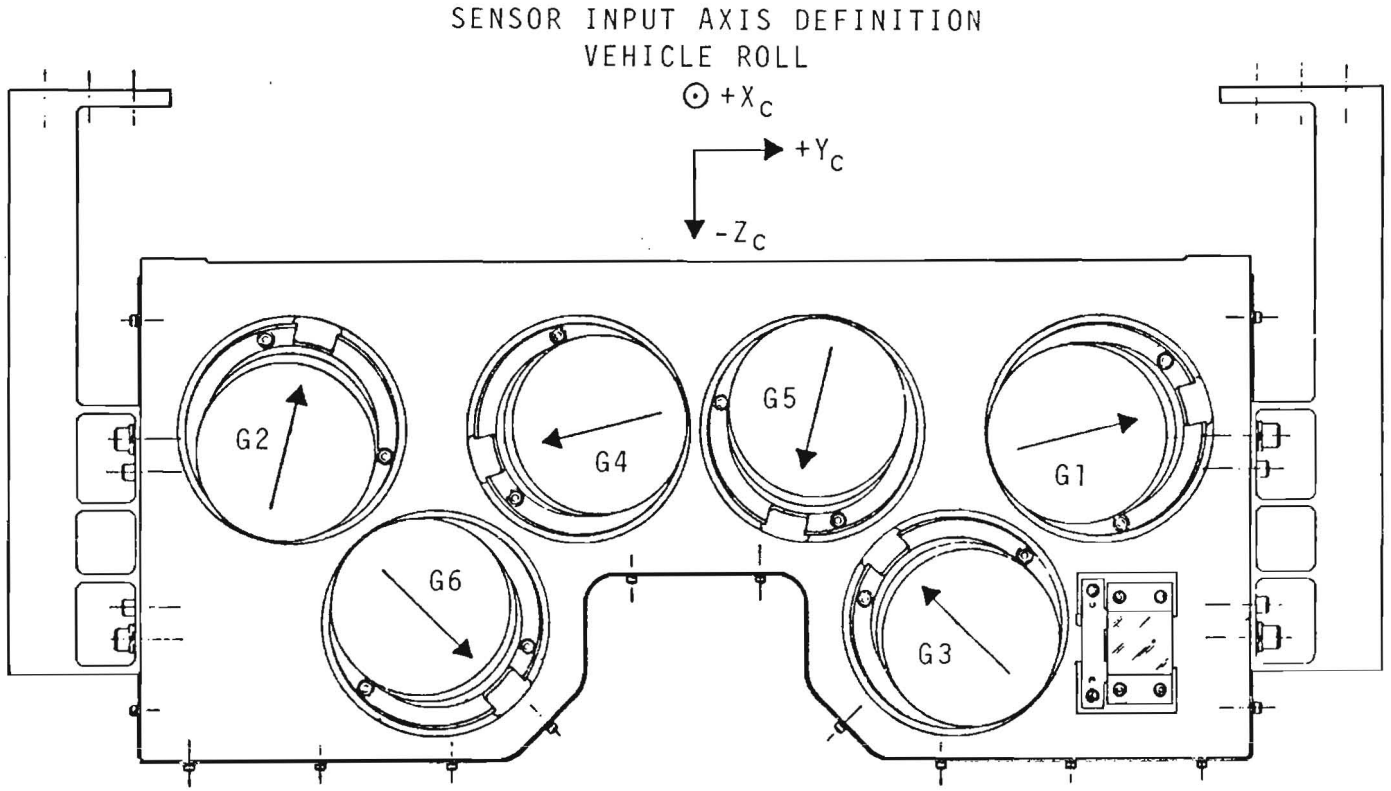

Figure A-2. IRA Gyro Input Axes Orientation

gives a top view of the gyro six-pack showing the orientation of the six-pack to the spacecraft control axes and the sensitive or input axes of the six gyros. In order to facilitate test of the gyros and to permit easy replacement of failed units, the gyro package is split into two parts. The upper part contains the six, identical gyros with a small amount of electronics physically part of each gyro and trimmed to match the mechanical characteristics of that gyro. The lower part contains all the other electronics required to develop motor drive power, sensor pick-off energization, regulated voltages, buffering of input and output, pulse rebalancing torque words, etc. With this arrangement, shown in figure A-3 a single gyro can readily be unplugged, removed and replaced with a spare without any need to retrim any other part of the system.

Table A-2 shows the overall IRA altitude errors in seconds of arc (1δ) assuming that all six gyros have independent, random attitude errors of 1 arc-second (1δ). From the entries in table A-2 note that symmetry about the roll axis is important for maintaining accuracy. If gyros fail (or are turned off to conserve power), the desirable triads would be gyros 1, 3 and 5 running or gyros 2, 4 and 6 running.

A.2.5 IRA HARDWARE DESCRIPTION

The mechanization of the IRA function is performed using six, identical, single degree-of-freedom, gyros each with a certain amount of unique circuitry and a separate package with common circuitry. Figure A-4 is a top level diagram of the IRA. To the right can be seen the six separate sensors. Each contains a heater to elevate the gyro to 135^{0}F, a thermistor to sense the gyro temperature and control the heater via a thermal controller in the common box and an internal loop to generate a rate sensing signal. The internal loop consists of a Torque Generator (TG) that positions the gyro rotating mass (H), a Signal Generator (SG) that senses position changes of H as a result of input rates, a pulse width modulator to digitize the SG rate signal, a quantizer to develop a scaled rate signal and a current bridge or amplifier to energize the TG to reposition the gyro mass. The quantizer signal is also used in the IRA as a rate and direction signal for that component of input rate sensed by the gyro. Not shown in the sensor but part of it are the motor and the suspension/suspension drive functions. The motor is a three phase device energized with a 960 Hz signal that causes it to spin the gyro mass at 28,800 rpm. At this speed, the gyro sensitivity of 'H' is 432,000 gm-cm^{2}/sec. The suspension drive is electromagnetic and is driven at 9.6 KHz to avoid varying disturbance torques caused by beats between sub-harmonics of the suspension signal and the motor drive signal.

In the common electronics package are six identical circuit areas supporting each gyro. These accomplish the following:

a. Individual power supplies for generating wheel drive and suspension drive voltages.

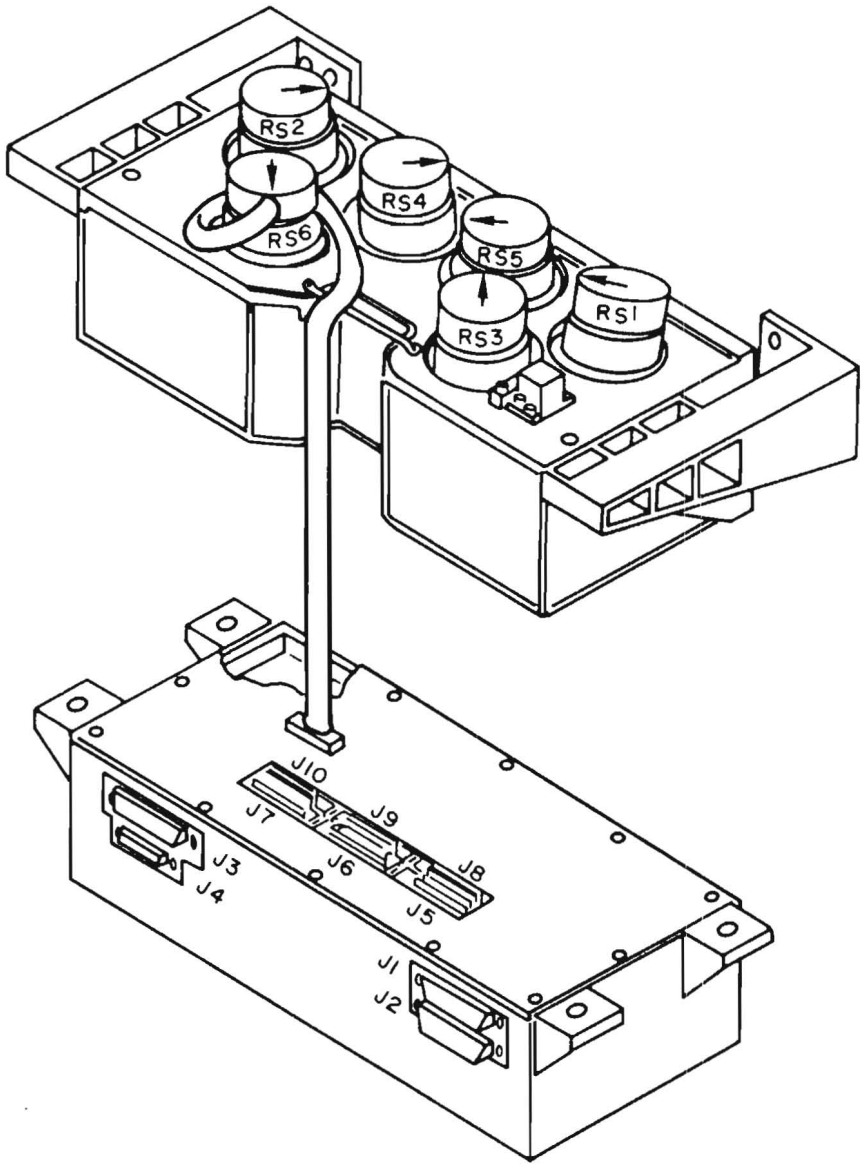

Figure A-3. Inertial Reference Assembly Mechanical Outline Drawing

Table A-2. Error Distribution of 6-Gyro IRA

Half-cone angle around roll: 85.0 degrees

Angles on pitch-yaw plane: 1 (15), 2 (75), 3 (135), 4 (195), 5 (255), 6 (315) Gyro (degrees)

Gyro Numbers Eliminated	Roll	One-Sigma Errors (Normalized to Triad)			
		Pitch	Yaw	Ratio R/P	Radial (In FOV) 1.414 for Triad
0	4.684	0.580	0.580	8.082	0.820
1	5.409	0.738	0.592	7.328	0.946
2	5.409	0.592	0.738	9.131	0.946
3	5.409	0.669	0.669	8.082	0.946
4	5.409	0.738	0.592	7.328	0.946
5	5.409	0.592	0.738	9.131	0.946
6	5.409	0.669	0.669	8.082	0.946
12	8.113	0.935	0.935	8.682	1.322
13	6.047	0.818	0.680	7.462	1.058
14	5.737	0.981	0.617	5.847	1.159
15	6.047	0.748	0.748	8.082	1.058
16	6.113	1.132	0.683	7.170	1.322
23	8.113	0.683	1.132	11.884	1.322
24	6.047	0.748	0.748	8.082	1.058
25	5.737	0.617	0.981	9.296	1.159
26	6.047	0.650	0.810	8.889	1.058
34	8.113	1.132	0.683	7.170	1.322
35	6.047	0.680	0.810	8.889	1.058
36	5.737	0.820	0.820	6.099	1.159
45	8.113	0.935	0.935	8.682	1.322
46	6.047	0.810	0.680	7.462	1.058
56	8.113	0.683	1.132	11.884	1.322
123	19.873	1.016	2.385	19.565	2.592
124	8.113	1.278	1.026	6.346	1.639
125	8.113	1.026	1.278	7.908	1.639
126	19.873	2.385	1.016	8.334	2.592
134	8.113	1.489	0.686	5.450	1.639
135	6.624	0.820	0.820	8.082	1.159
136	8.113	1.388	0.873	5.847	1.639
145	8.113	1.278	1.026	6.346	1.639
146	8.113	1.489	0.686	5.450	1.639
156	19.873	1.833	1.833	10.843	2.592
234	19.873	1.833	1.833	10.843	2.592
235	8.113	0.686	1.489	11.823	1.639
236	8.113	0.873	1.388	9.296	1.639
245	8.113	1.026	1.278	7.908	1.639
246	6.624	0.820	0.820	8.082	1.159
256	8.113	0.686	1.489	11.823	1.639
345	19.873	2.385	1.016	8.334	2.592
346	8.113	1.388	0.873	5.847	1.639
356	8.113	0.873	1.388	9.296	1.639
456	19.873	1.016	2.385	19.565	2.592

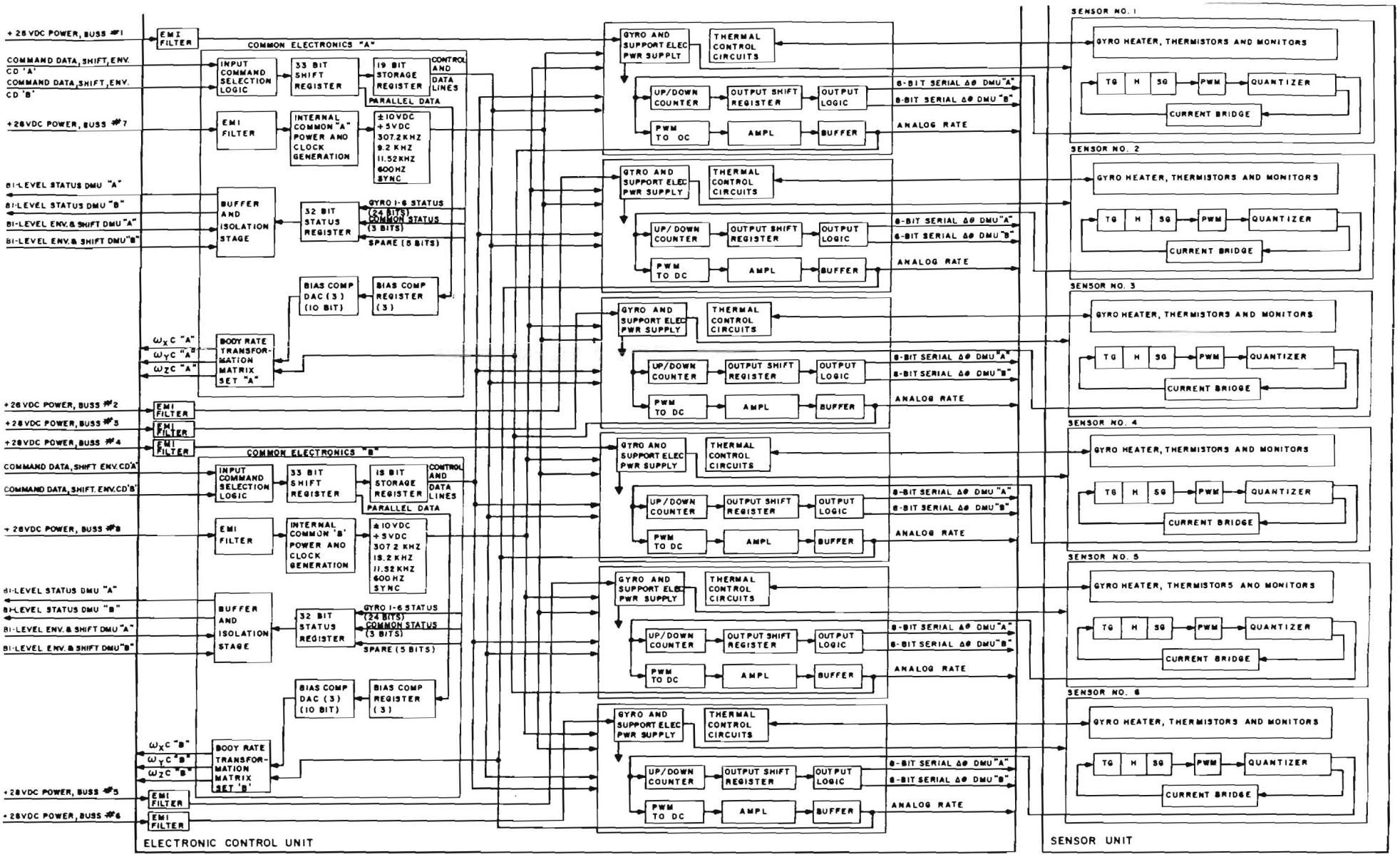

Figure A-4. IUE/IRA Top Level Block Diagram

b. Thermal control circuitry for maintaining proper gyro temperature.

c. Up/down counter, output shift register, and logic unit to present gyro rate as redundant, 8 serial-bit words to the DMU, and thus the OBC.

d. Demodulator, amplifier, and buffer that present the rate as a bipolar analog error signal.

This analog rate along with the analog rates from the other five channels are combined in three matrices wherein pitch, yaw and roll analog rate signals are derived. These signals are used to implement the hardwire sun acquisition/sun hold modes without need of OBC algorithm.

The body rate transformation along with other functions common to all six sensors is part of two, redundant electronic control units. Besides matrix transformation these units select between the redundant command decoder inputs, convert serial command words to parallel data that is used to develop bias compensation to be added to the analog rate transformation, develop control signals for the various sensor functions, generate three regulated dc voltages (+ -10v, +5v) for all internal circuitry and four different frequencies for synchronizing internal events. In addition they receive and combine the sensor digital error bit streams and combine them with other information to generate a 32 serial bit status word that is buffered, isolated and presented to the redundant DMU's. External +28v power to the IRA is supplied by eight, individually switched lines, one for each of the six sensors (gyros) and one for each of the two electronic control units. The actual power switching is shown as part of the Master ACS Logic Diagram, figure 8-4.

The flow of a rate signal from its detection through matrixing for a single axis is shown in much greater detail in figure A-5 which is a block diagram of a single channel in the IRA. Rate sensing commences in the upper left corner where the rotating mass, H, driven by the 960 Hz supply is influenced by an input to its sensitive axis. The resulting motion is sensed by the microsyn pickoff, preamplified, bandpass filtered and demodulated and passed through a lead/lag network. This output is presented as a buffered analog rate output signal. It is also digitized in a pulse width modulator where it can be summed with a simulated rate input. The output is quantized through either a normal or test channel quantizer and the selected output is current amplified and used to drive the gyro mass torquer. The normal quantized output is logic gated and fed to a 16-bit up/down counter and a 16-bit shift register. External envelope and transfer signals from the DMU control the register and present it via isolating buffers to the redundant DMU's.

The normal quantizer output is converted to a bipolar dc signal and matrixed with similar signals from two other sensors to generate pitch, yaw and roll analog error signals.

Also shown as part of the sensor are the suspension device and the suspension drive generator, the heater, thermal sensor and the thermal controller.

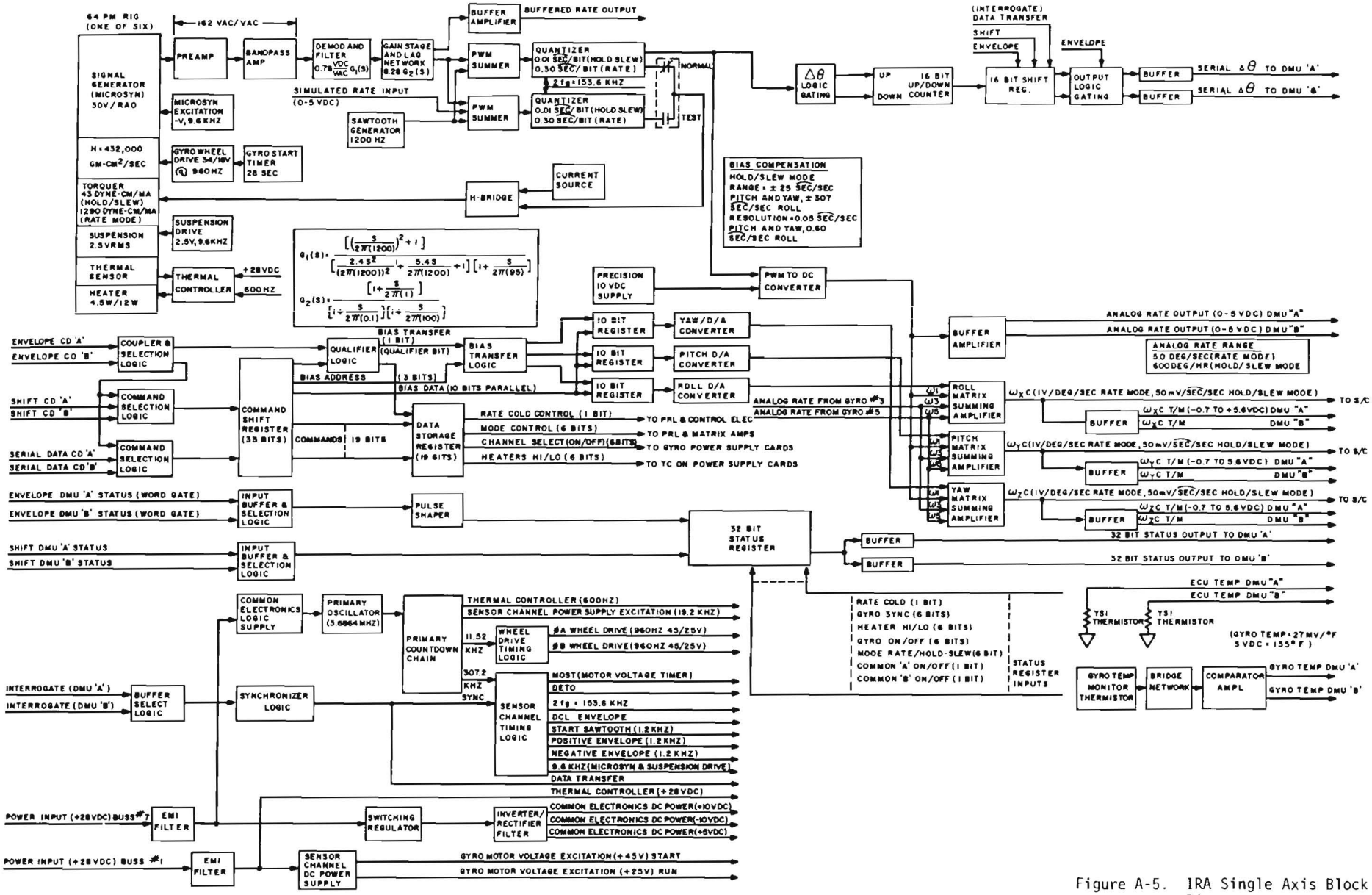

Figure A-5. IRA Single Axis Block Diagram

The digital control word from the redundant CD's is shown being processed and decoded to develop the 19 control bits, the 10-bit bias data with the 3-bit bias address and the bias transfer logic. This latter drives three 10-bit registers followed by D/A convertors resulting in three analog bias voltages that are matrixed with the analog rate signals and are used to bias out any offsets from the gyros. The lower part of the block diagram is concerned with the low voltage electronics power generation; primary oscillator, countdown chain and sync generator; and the circuitry for converting gyro housekeeping telemetry into a 32-bit serial word for presentation to the DMU. Implementation of most gyro logic is via standard CMOS circuits while the sensor unique electronics is packaged on the end of the gyro as developmental, thick-film hybrid chips.

A.3 CONTROL ELECTRONICS ASSEMBLY

A.3.1 FUNCTION

The function of the CEA is to provide certain hardwire logic functions, primarily through the launch phase commencing at Delta Separation and ending after Sun Acquisition in elliptical synchronous orbit, to provide power switching internal and external to the unit, to decode digital command words from the OBC and generate analog signals for inertia wheel driving, to provide high level signals for energizing hydrazine thrusters, and to provide telemetry conditioning for the various telemetry sensors in the Hydrazine Auxiliary Propulsion System (HAPS). An overall block diagram of the CEA is shown as figure A-6 and its interrelationship in the overall ACS can be seen in the Master ACS Logic Diagram figure 8-4.

A.3.2 CONFIGURATION

The basic configuration of the CEA is an assemblage of eight cards of similar length and breadth but with varying thickness. The cards are of six types with the remaining two cards being redundant versions of the unique six. The mechanical configuration of the eight-pack showing the functions of the cards is illustrated in figure A-7. The various cards and their functions are described in the following paragraphs.

A.3.3 PRECESSION/NUTATION CARD

This consists of the spin synchronous clock (Para. 8.2.4.2, figure 8-11), circuitry to perform precession maneuvers (Para. 8.2.7.2, figure 8-17), and circuitry to perform active nutation damping including redundant accelerometer switching and filtering (Para. 8.2.6.2, figures 8-14, 8-15, and 8-16 showing logic, timing and a typical event). In addition, this card contains inhibit circuitry to prevent opposing jets from firing with zero net torque and fuel wastage. The various logic functions on this card are implemented with standard CMOS logic chips of the RCA CP XXXX family type. CMOS logic was chosen because of its low power consumption (most CMOS devices consume power only while transitioning

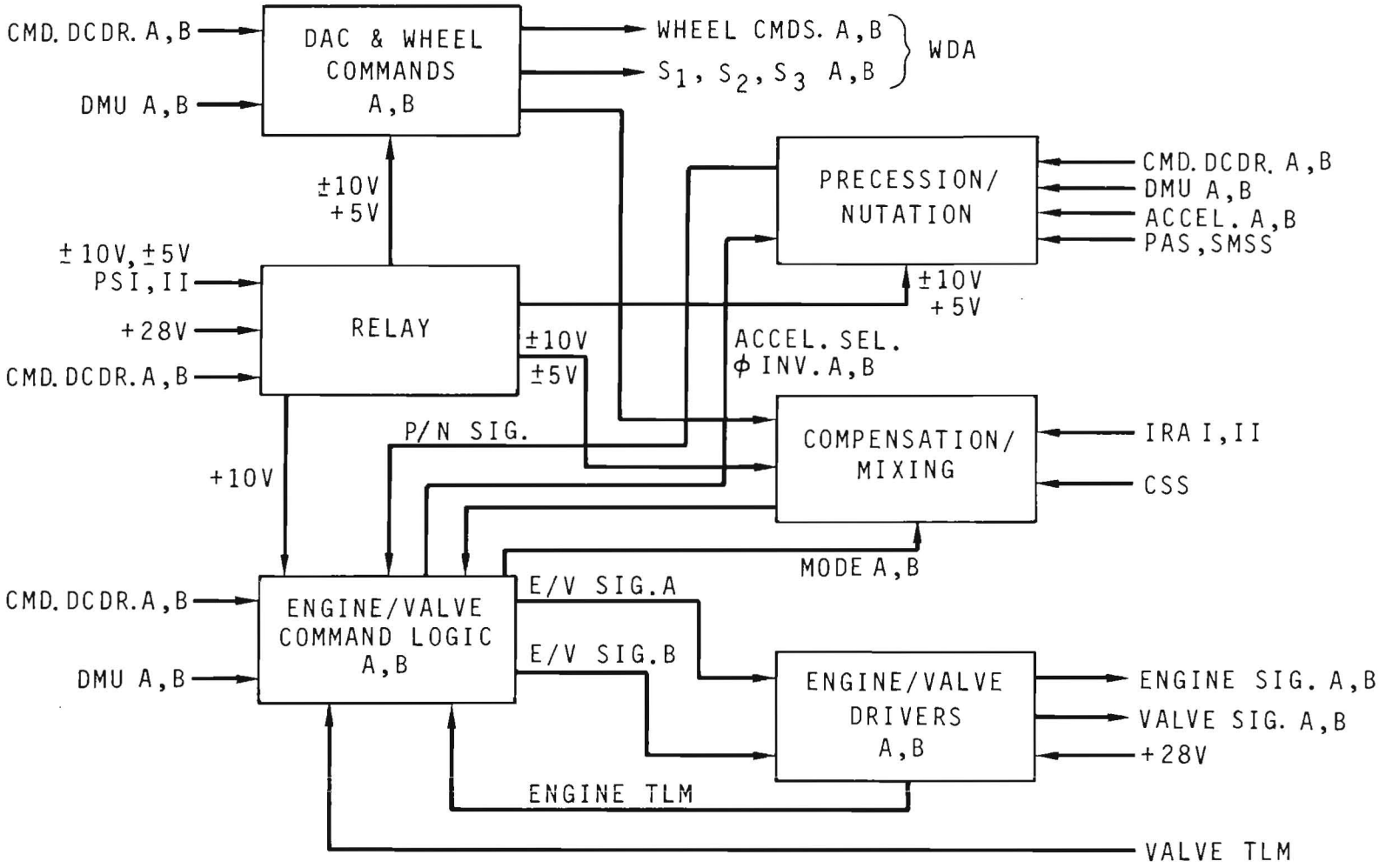

Figure A-6. CEA Block Diagram

CONTROL ELECTRONICS ASSEMBLY

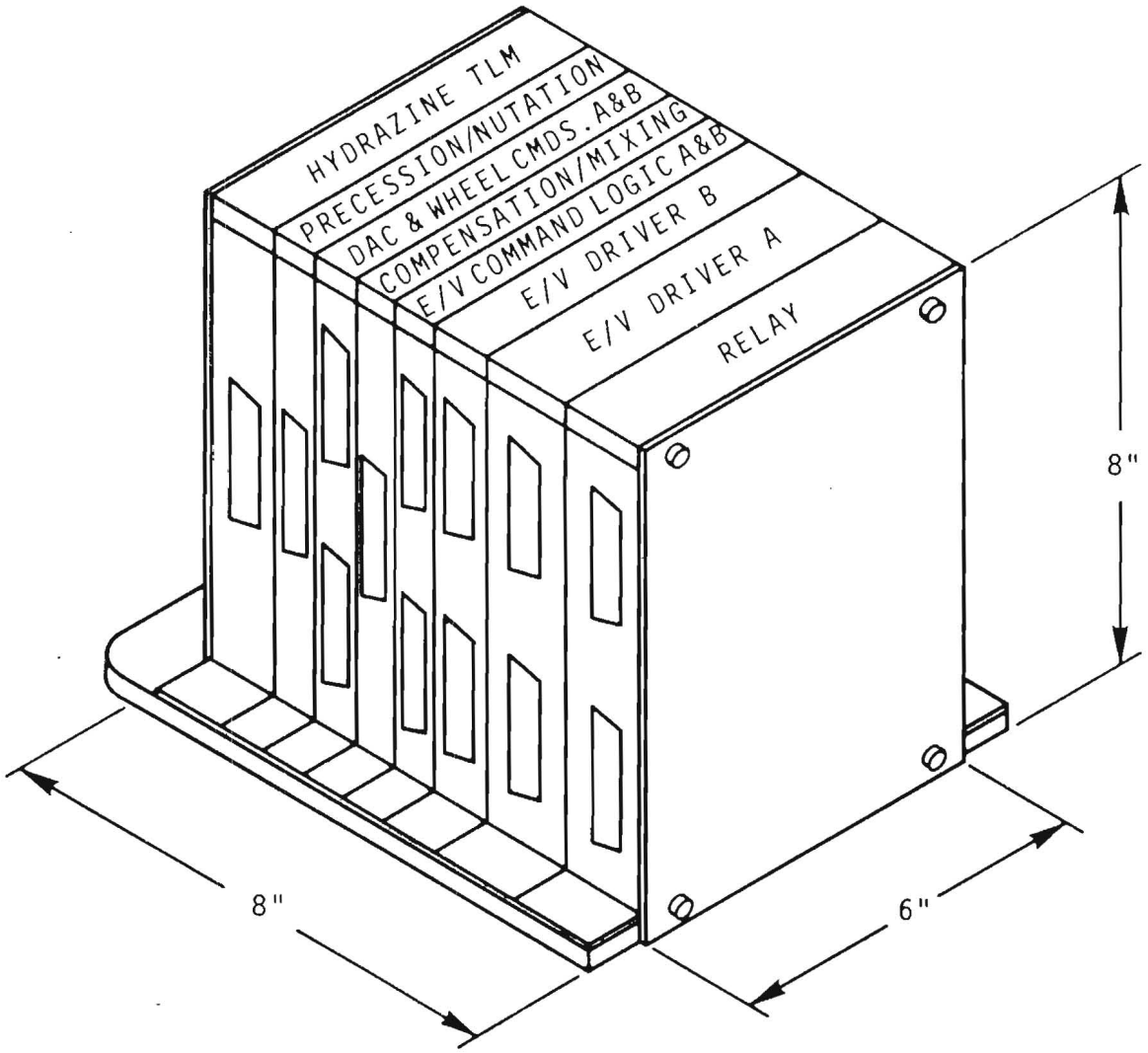

Figure A-7. Control Electronics Assembly

logic state), great immunity to line noise and relative immunity to high energy particulate bombardment.

The initiation of events in the Precession/Nutation Card is via a 37-bit serial command word from the Command Decoder. This controls the number of engine firings, start fire sector, sector width, sun enable, selection between the PAS and SMSS as sources of sunline information, and allows adjustment of nutation threshold and zero crossing adjustment. Following is the bit assignment for the P/N control word.

Bit	Function
1-8	Number of engine firings Bit 1=LSB, Bit 8=MSB
9-15	Sector start fire Bit 9=LSB, Bit 15=MSB
16	Sun enable "0"=disable, "1"=enable
17-20	Sector width Bit 17=LSB, Bit 20=MSB
21	PAS/SMSS select "0"=SMSS, "1"=PAS
22	Enable bits 23-37 "0"=disable, "1"=enable
23	Nutation Inhibit "0"=enable nutation "1"=inhibit nutation
24	Threshold gain adjust "0"=Threshold adjust (.4v $\pm$ .04 v) "1"= .64v $\pm$ .04v
25-28	Threshold adjust Bit 25=LSB, Bit 28=MSB
29-32	Zero-crossing adjust Bit 29=LSB, Bit 32=MSB

Threshold Adjust

Bit					Voltage (Typical)
24	25	26	27	28	
0	0	0	0	0	0.43v
0	0	0	0	1	0.39v
0	1	1	1	1	0.36v
1	0	0	0	1	0.63v
1	0	0	0	0	0.67v
1	1	1	1	1	0.60v

Zero-crossing Adjust

Bit				Voltage (Typical)
29	30	31	32	
0	0	0	0	0.034v
0	0	0	1	-0.006v
1	1	1	1	-0.042v

A.3.4 RELAY CARD

This card contains a bank of latching relays and their driver circuits used to switch power from an external source to circuitry both within and without the CEA. These external regulated voltages of + and -10v + and -5 v are generated in the Wheel Drive Assembly (WDA) from two power supplies, only one of which is energized at any time. Thus, the effect of switching between the buses is not only to ensure power by being able to select between redundant buses but to remove power from unneeded functions by switching them to the standby (off) bus. The full complement of relays showing the ACS circuits they control can be seen on the Master ACS Logic Diagram, figure 8-4.

Figure A-8 shows a typical relay driver in schematic form. The relays used are of the latching type and are driven independently by separate pulsing circuits. The energy to toggle a relay is supplied by the 22 μf capacitor, C_1 shown between the relay coil high side and ground.

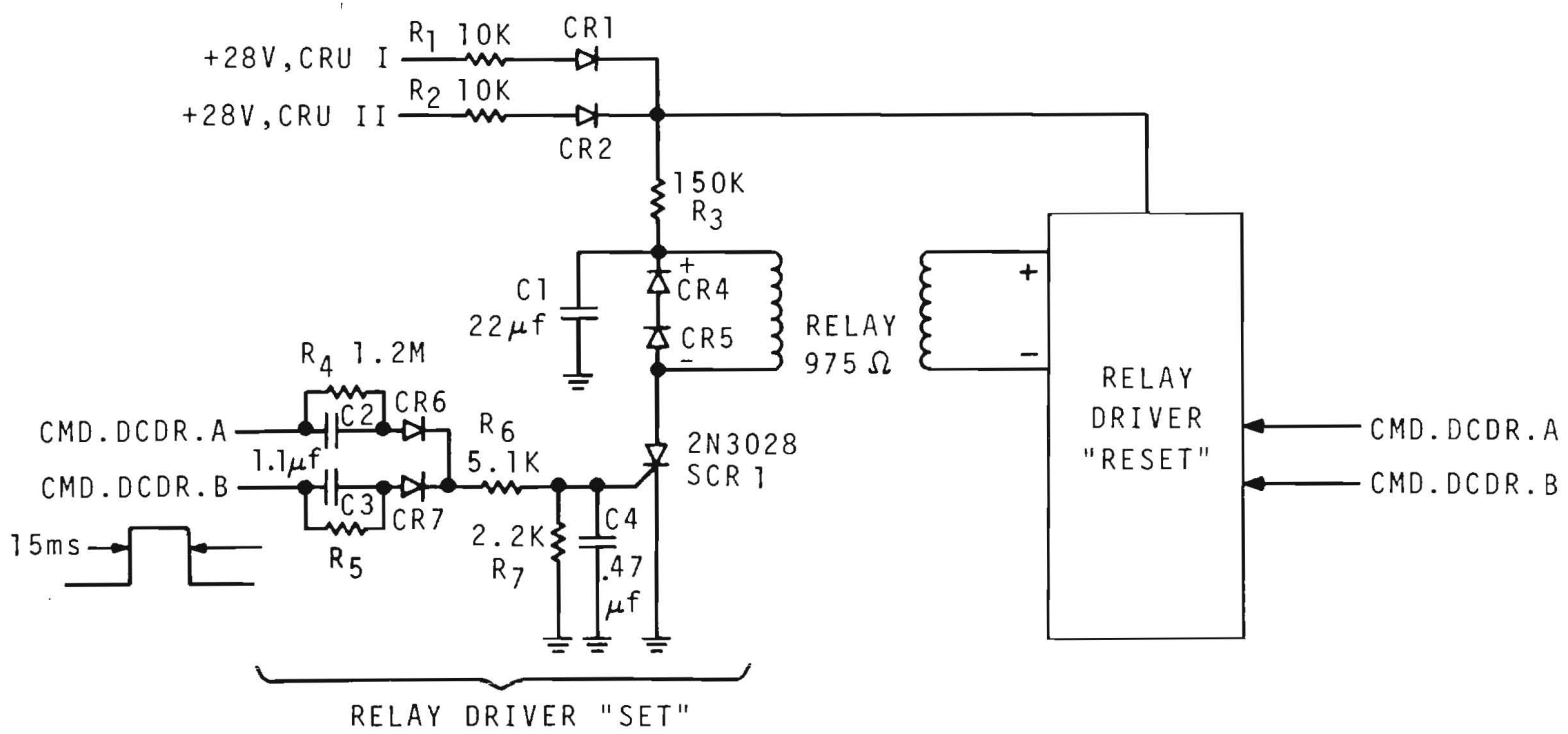

Figure A-8. Relay Driver

This capacitor is charged to +28v from either bus CRU 1 or CRU II (whichever is active) via isolation resistors R_1 and R_2 and isolation diodes CR_1 and CR_2 and current limiter, R_3. When SCR 1 is triggered by the 15 ms pulse from Command Decoder A or B, it goes into conduction and latches up. This causes C_1 to discharge to ground through the relay coil. The holding current from the +28v pulse is limited by R_3 to a value insufficient to permit SCR 1 to remain latched and it goes out of conduction as e_{C1} drops to zero and the trigger pulse disappears. This allows C_1 to recharge through R_1/R_2 and R_3. CR_4 and CR_5 are conventional flyback diodes to suppress transient voltage from the collapsing magnetic field in the relay coil from damaging SCR 1. They are placed in series to provide redundancy against a short failure mode that would prevent energizing that side of the relay. DC isolation between the two Command Decoders is provided by R_4, R_5 and CR_6 and CR_7. Capacitors C_2 and C_3 are "speed-up" capacitors to couple the command pulse rapidly into SCR 1 with input current limited by R_6 and noise immunity provided by C_4 and R_7. The circuit shows clearly the thought involved in providing capability to trigger with faults in either power source or command source and to provide isolation between these sources. Repeat actuation time would appear to be limited to about one time constant of the energy storage source, C_1, charged through R_1 (R_2) and R_3 or 3.5 milliseconds. (A one time constant charge would bring C_1 to about 19v which should be adequate to toggle type SLDB relays.)

A.3.5 DAC AND WHEEL COMMANDS CARD(S)

These are redundant cards that develop the analog signals used by the wheel drivers. Figure A-9 shows a block diagram of the card. These cards can be addressed from either ground command or from the on-board computer. A 37-bit serial word from the command decoder is transferred to a holding register. The first 32 bits are decoded as four 8-bit wheel commands and converted to analog voltages for the pitch, yaw, roll and redundant wheel drivers. Figure A-10 shows a typical D/A converter and its associated outputs. The wheel command signal ranges from -2.48v to +2.50v and the wheel command telemetry signal from 0v to +5.0v.

Bit 33 of the serial command is used to enable the transfer of bits 34-37 into the holding register. Bits 34-37 are used by a 4-bit decoder to generate enable states for the wheel driver cards (S_1, S_2, S_3) and the Compensation/Mixing card (R_1, R_2, Css). The status of the 4-bit (Mode) decoder is telemetered through the data system.

The following describes the breakdown of the 37-bit DAC and Wheel Command serial word.

Last bit out of Command Decoder

First bit out of Command Decoder

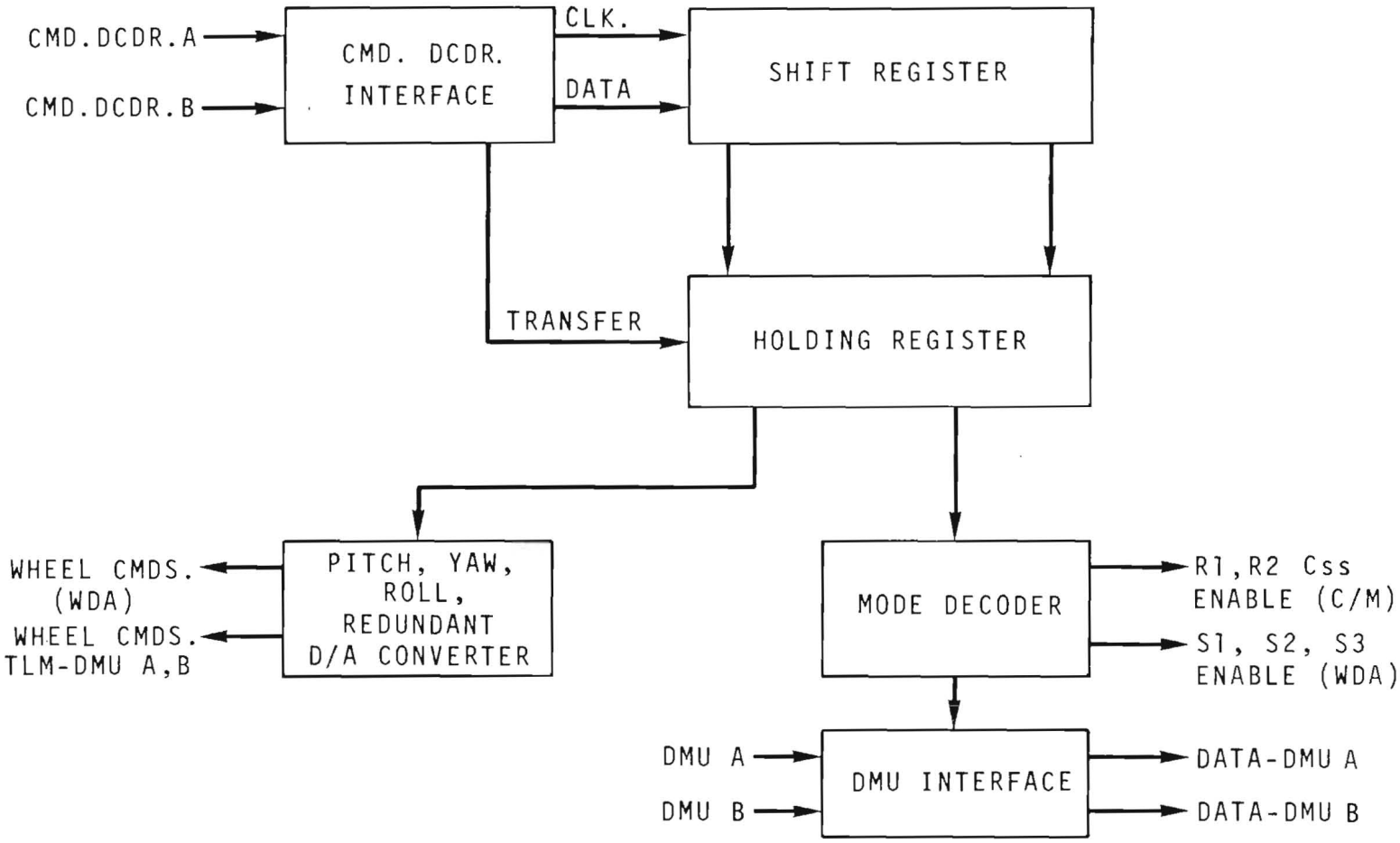

Figure A-9. DAC and Wheel Command Card

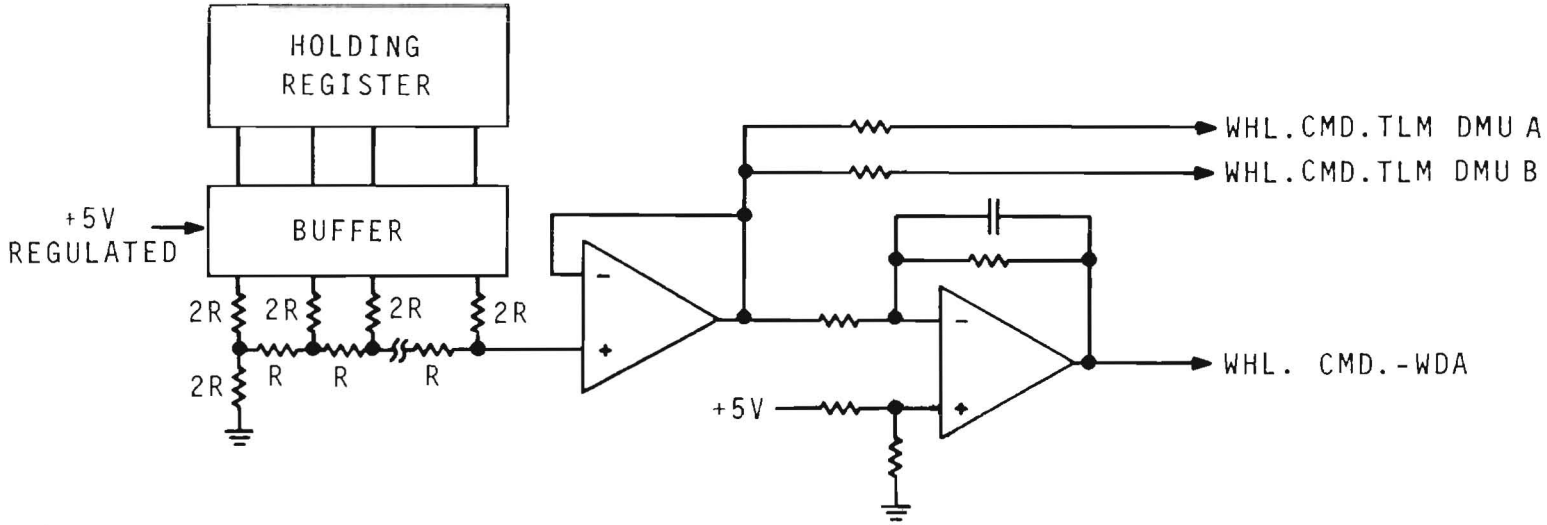

Figure A-10. D/A Converter

Command Decoder Bit Assignments

Bit	Function
1-8	Pitch Wheel Command Bit 1=LSB, Bit 8=MSB
9-16	Yaw Wheel Command Bit 9=LSB, Bit 16-MSB
17-24	Roll Wheel Command Bit 17=LSB, Bit 24=MSB
25-32	Redundant Wheel Command Bit 25=LSB, Bit 32=MSB
33	Transfer enable for bits 34-37
34-37	Mode decoder - enable bits for wheel drivers and Compensation/Mixing card.

A.3.6 ENGINE/VALVE COMMAND LOGIC CARD(S)

These are redundant cards that provide low level signals used by the Engine/Valve Drivers to activate the hydrazine system. Inputs to the card are through the spacecraft command system, DMU, Compensation/Mixing card (TR=torque request) and the Precession/Nutation card.

A 37-bit serial command contains information to enable/disable the engines and open/close the hydrazine transfer valves. The engines can be activated using the Torque Command (TC) portion of the serial word (Bits 1-12), from the Torque Request (TR) signals generated in the Compensation/Mixing card and from signals produced in the Precession/Nutation card. Also available is a mode that allows the engines to be pulsed. If selected, the JETPULSE mode allows the 0.3 lb engines to be activated for approximately 100 milliseconds after each command update, and the THR.PULSE mode allows the 5 lb engines to be activated in the same manner. The resulting engine signals can be written as:

$$0.3 \text{ lb engine sig.} = (TR + TC) \cdot EN \cdot JPULSE$$

$$5.0 \text{ lb engine sig. (2\&8)} = TC \cdot EN \cdot TPULSE$$

$$5.0 \text{ lb engine sig. (5\&11)} = (P + N + TC) \cdot EN \cdot TPULSE$$

TR = Torque request signal from Compensation/Mixing card.

TC = Torque command signal from command decoder.

EN = Engine enable from command decoder.

JPULSE, TPULSE = "1" when JETPULSE = "0", THR.PULSE = "0"

= ~100 milliseconds pulse when JETPULSE = "1",

THR.PULSE = "1"

P = Precession signal

N = Nutation signal

The card also provides the Primary/Secondary mode enable bits for the Compensation/Mixing card and the Accelerometer Select and Invert Phase bits used by the Precession/Nutation card.

Figure A-11 shows a block diagram of the Engine/Valve Command Logic Card while figure A-12 shows an actual circuit for both a high or low engine thruster and for a latch valve driver. Following is a listing of the number and function of the 37-bit serial command word that controls the HAPS.

Command Decoder Bit Allocation

Bit	Function
1-12	Torque command. Engines 1-12 "0" = OFF, "1" = ON
13	Transfer enable for bits 14-37
14-25	Enable/Disable engines 1-12 "0" = Disabled, "1" = Enabled
26-32	Open/Close valves 1-7 "0" = Close, "1" = Open
33	THR.PULSE "0" = OFF, "1" = ON (52 msec)
34	Primary/Secondary Mode Control "0" = Secondary, "1" = Primary
35	Accelerometer A/B select "0" - Accel 1, "1" = Accel 2
36	Invert Accelerometer Phase "0" = Non-invert, "1" = Invert
37	JET.PULSE "0" = OFF, "1" = ON (52 msec)

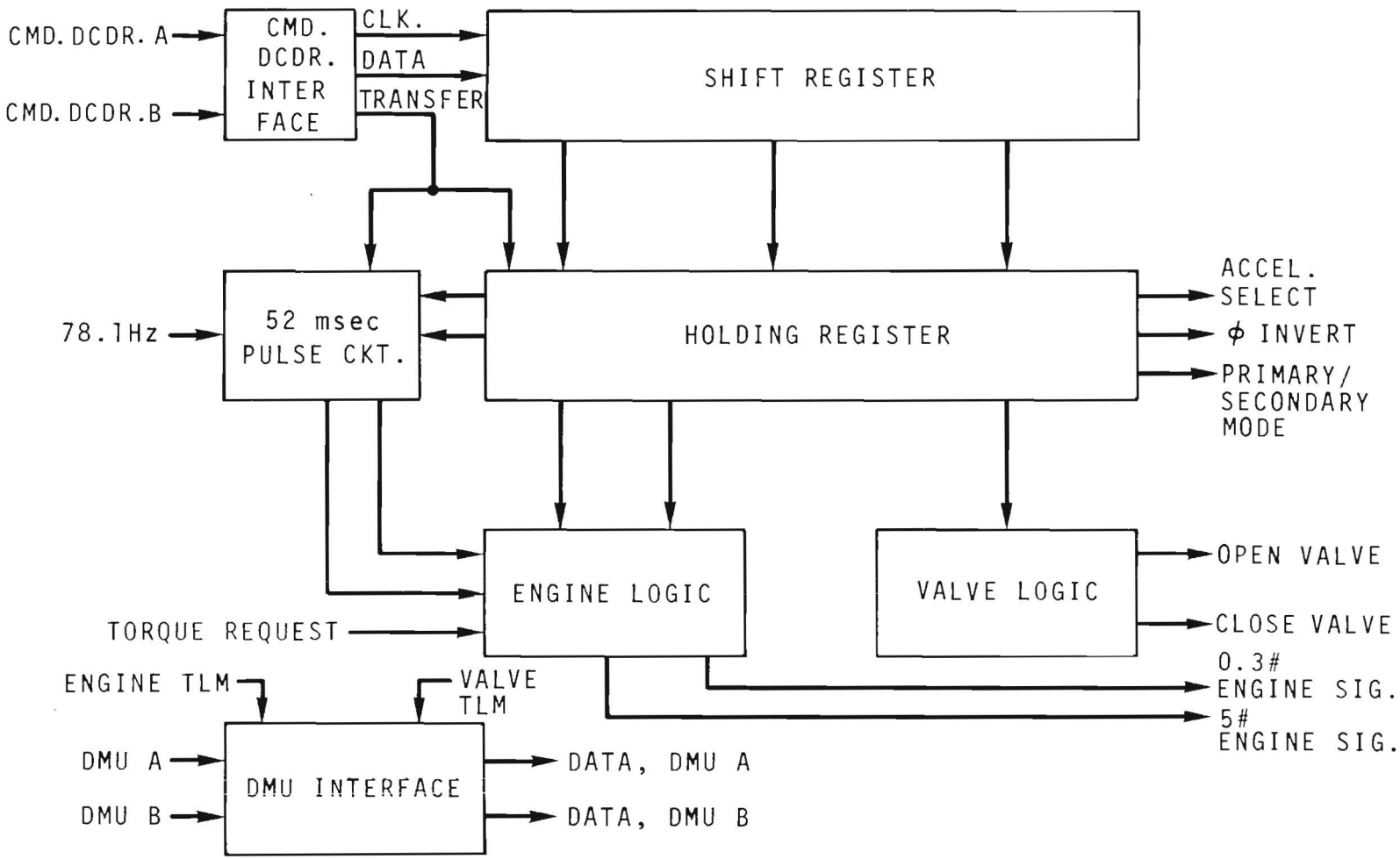

Figure A-11. Engine/Valve Command Logic

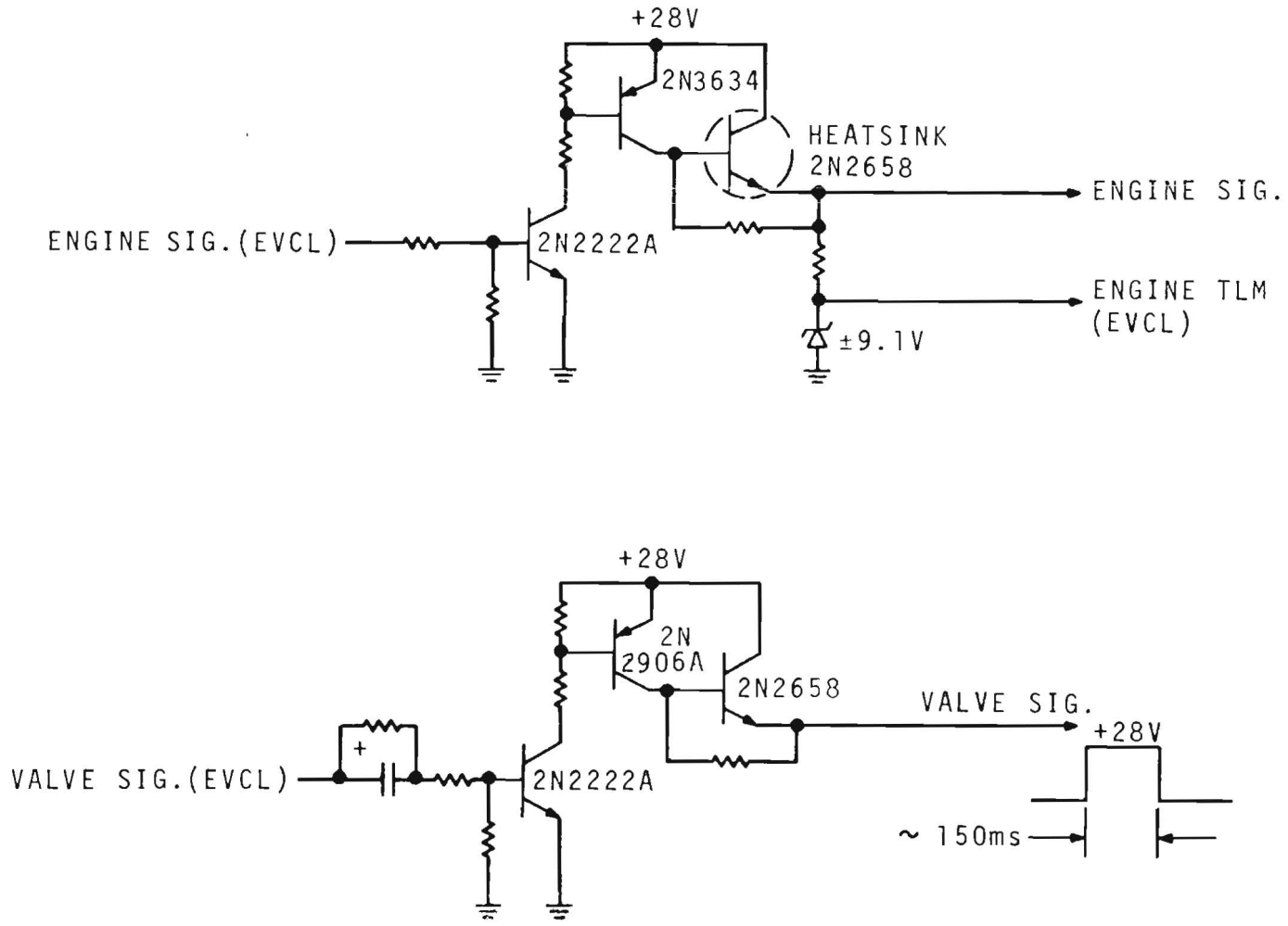

Figure A-12. Engine/Valve Driver

A.3.7 COMPENSATION/MIXING CARD

Like the Precession/Nutation card, the prime function of this card is to provide a hardwire logic algorithm to control some phase of IUE ACS operation. However, while the need for precession and nutation control is of a one shot basis (during the transfer orbit) the hardwire function of the Compensation/Mixing card will be used not only for initial sun acquisition but at any future time when, for some reason or other, inertial reference via stellar sources is lost and reinitialization is required. In addition, since the logic is hardwire and analog, this serves as a backup in the event of an OBC hangup preventing the normal digital control algorithm from being processed. The card receives position from the set of six coarse sun sensors distributed about the IUE spacecraft and rate information from the IRU. These signals are combined and the analog error signals are used to drive the inertia or reaction wheels and, when certain thresholds are exceeded, to energize the HAPS for bang-bang control primarily during despin and sun acquisition. The overall block diagram of the C/M card is shown as figure A-13, while figure A-14 expands in detail the Pitch axis including transfer functions and error gradients.

Rate and position information is switched to the card with the R_1, R_2, C_{SS} enable bits developed in the redundant DAC and Wheel Command cards. The sun sensor signal is amplified by a current-to-voltage convertor and clipped to ± 2.5 v by a precision limiter. This signal is summed with the rate information to produce a wheel command. For the Pitch axis this can be written as:

$$E_p = (27.5\text{v/deg/sec} + 2.5\text{v/deg}) \begin{matrix} +5.6\text{v} \\ -5.6\text{v} \end{matrix}$$

Slightly different gains are used for the Roll-Pitch and Yaw cases. The resulting transfer curves or wheel drive signals for position control on the sunline (i.e. in the absence of significant rates) are shown on figure A-15a. A single gain equation for rate inputs with the spacecraft at the proper sun position is used and this transfer function is shown as figure A-15b.

Because of different moment arms and thruster angles, different switching lines are used for jet control about the three axes. From figure A-16a it can be seen that for the Pitch axis the zero position switching occurs at + or - .090 deg/sec with zero rate switching at + or - 1.00 degrees. The Roll axis is shown on figure A-16b and the zero position switching occurs at + or - .095 deg/sec with zero rate switching at + of - 1.10

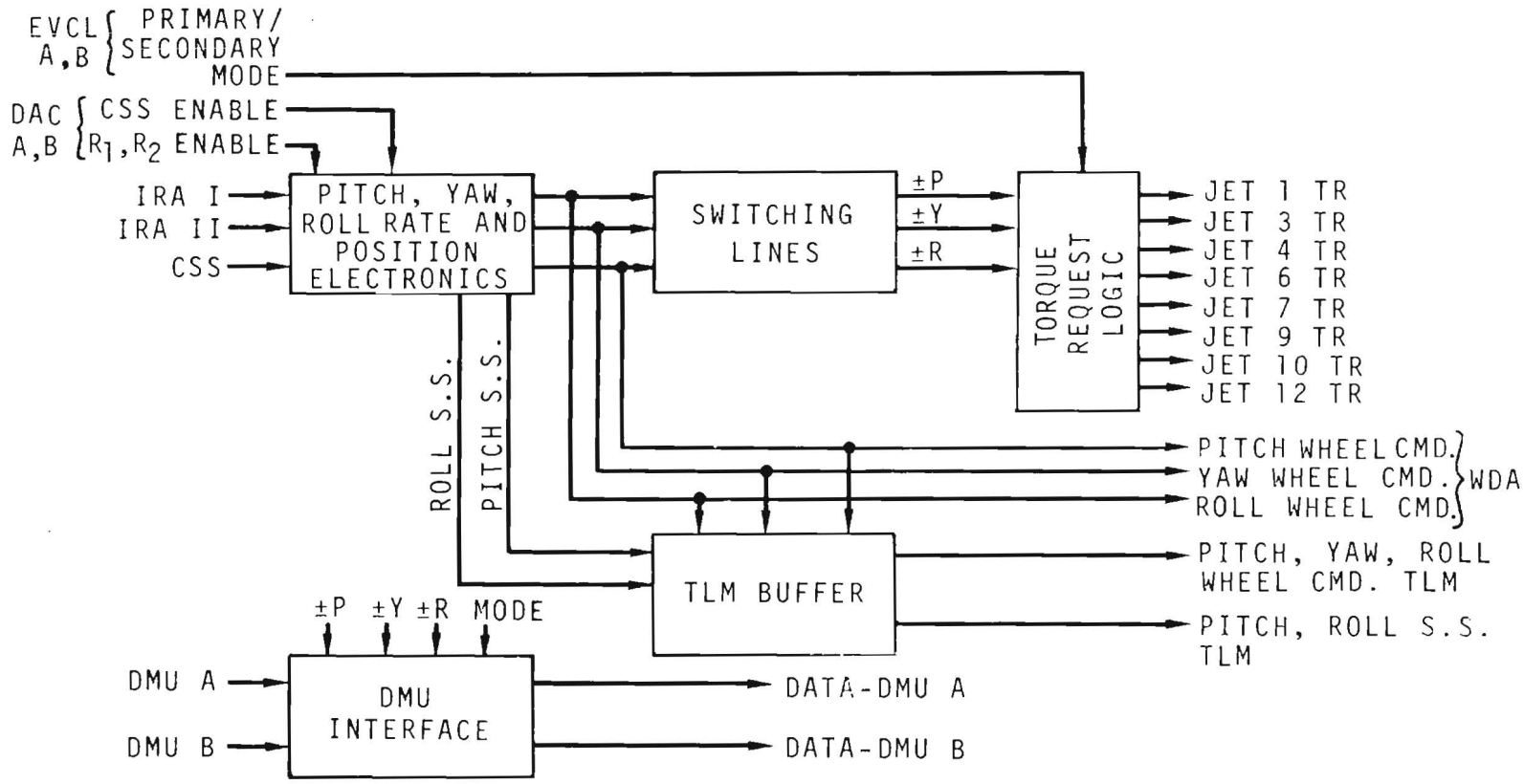

Figure A-13. Compensation/Mixing

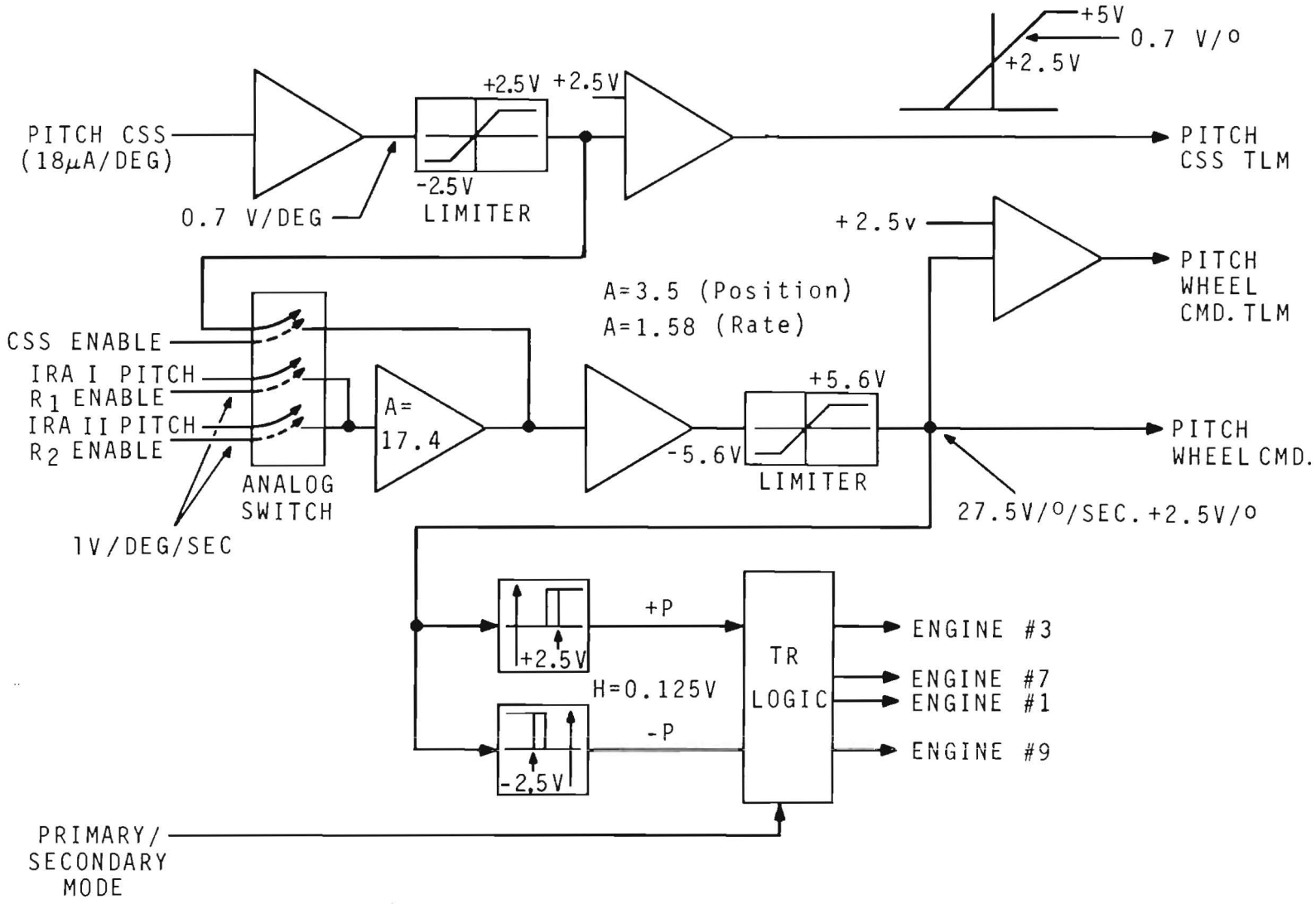

Figure A-14. Pitch Axis Block Diagram

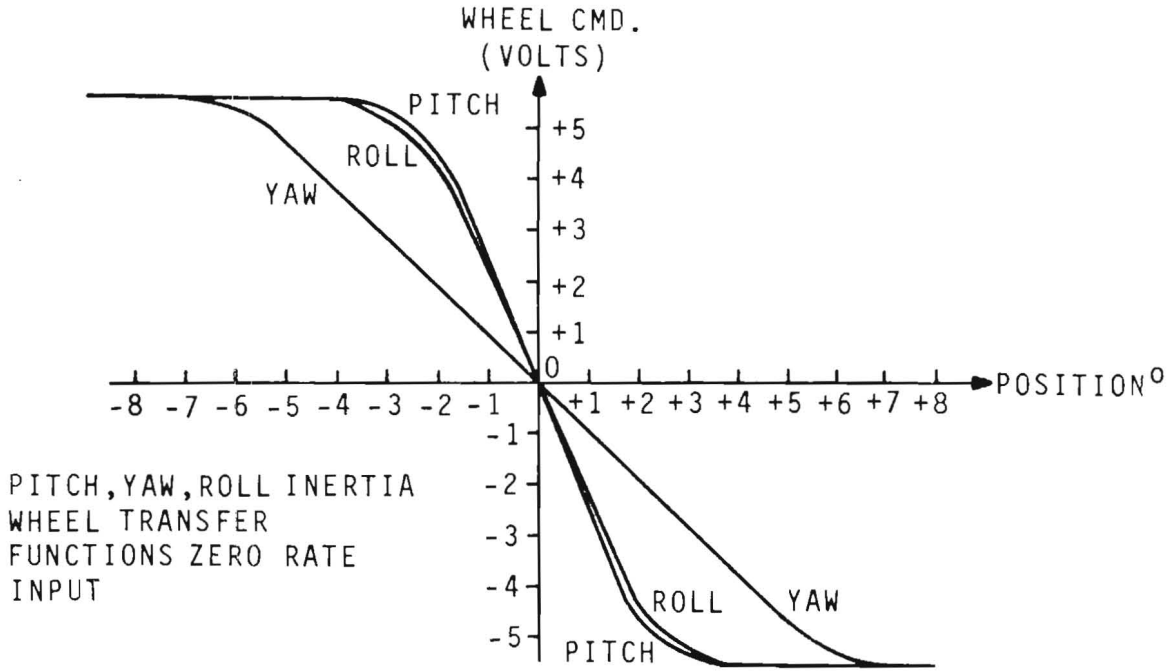

Figure A-15a. Pitch, Yaw, Roll Inertia Wheel Transfer Functions Zero Rate Input

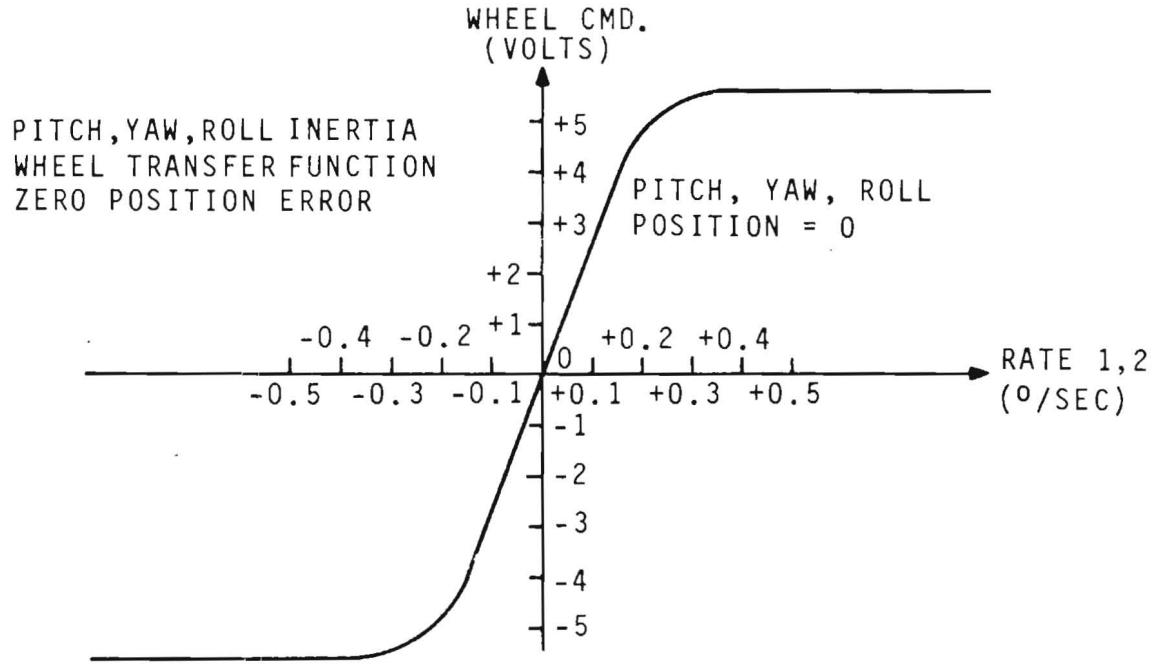

Figure A-15b. Pitch, Yaw, Roll Inertia Wheel Transfer Function Zero Position Error

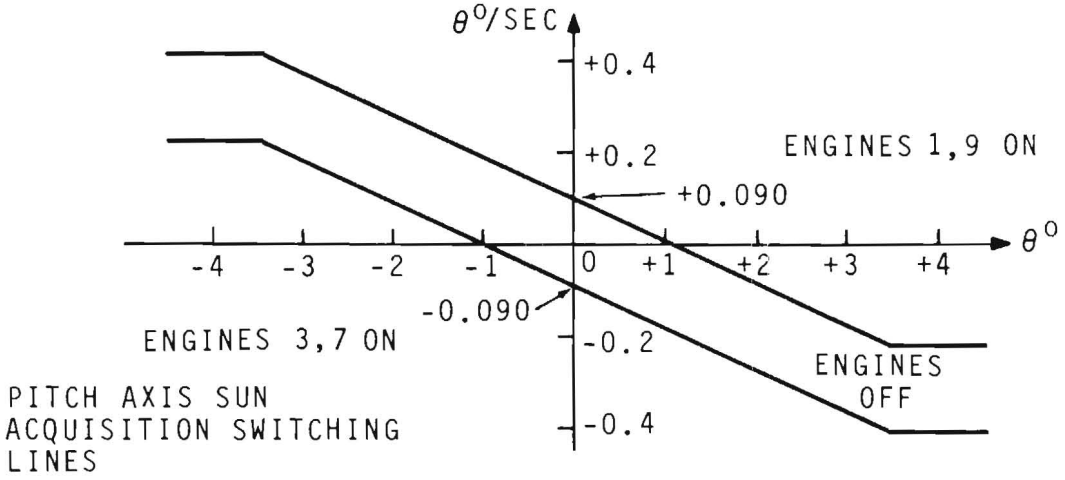

Figure A-16a. Pitch Axis Sun Acquisition Switching Lines

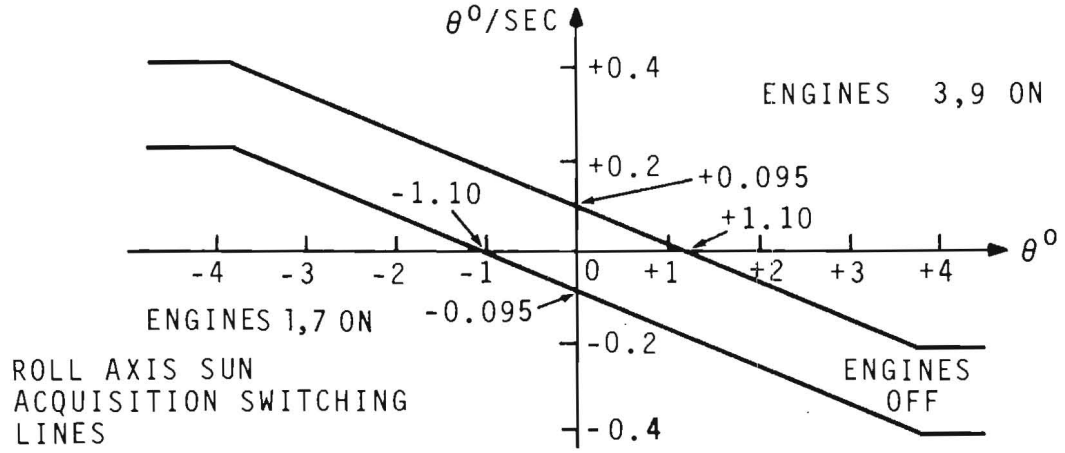

Figure A-16b. Roll Axis Sun Acquisition Switching Lines

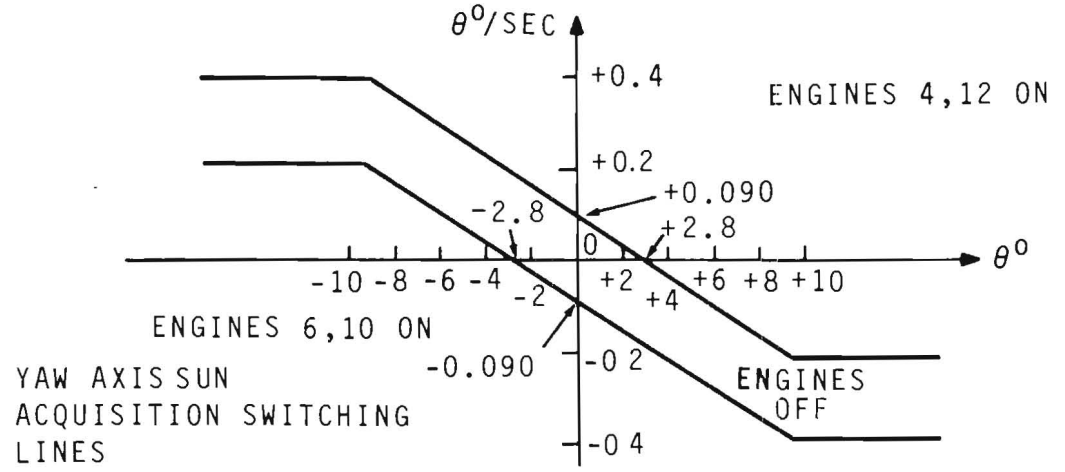

Figure A-16c. Yaw Axis Sun Acquisition Switching Lines

degrees. For the Yaw axis zero position switching is similar to the Pitch and Roll at + or -.090 deg/sec, but the zero rate switching occurs at + or -2.8 degrees in keeping with the small sun position error component that can be sensed in the Yaw axis. This is shown as figure A-16c.

As was mentioned in the discussion of the Precession/Nutation card, situations can arise where opposing engines could fire with zero net torque. This occurs because the Roll engines are shared with the Pitch and/or Yaw engines, (e.g. +Pitch and +Roll Torque Request fires engines 1, 7 and 3, 7 with 1 and 3 firing in opposition). To avoid this, the Torque Request Logic performs a blanking operation for the opposing engines.

Firing of the engines in pairs as either Primary or Secondary torques is governed by the Primary/Secondary Mode bit developed in the Engine/Valve Command Logic Card. Following is a listing of axis torque and the engines that produce it in Primary or Secondary mode.

0.3-Pound Thrusters

(Momentum Unloading, Sun Acquisition and Despin)

Axis	Primary		Secondary	
	Pos	Neg	Pos	Neg
Pitch	3 & 7	1 & 9	3 or 7	1 or 9
Yaw	6 & 10	4 & 12	6 or 10	4 or 12
Roll	4 & 10	6 & 12	1 & 7	3 & 9

5.0-Pound Thrusters

(Nutation, Precession and ΔV Burn)

Function	Primary	Secondary
Nutation and Precession	5	11
ΔV Burn	2-8	5-11

A.3.8 HYDRAZINE AUXILIARY PROPULSION SYSTEM (HAPS) TELEMETRY CONDITIONING CARD

The functions of this card are to condition the signals to and/or from the various temperature and pressure sensors in the HAPS and to monitor

and indicate the positions of various latch valves between tanks and manifolds as well as jet firings. Telemetry leaving the CEA is in a serial bit word form and the following tables A-3, A-4, A-5 and A-6 show the TLM bits and their meanings for the various CEA functions such as DAC and Wheel Drive, Compensation/Mixing Precession/Nutation Cards and Engine Firings.

Table A-3. DMU Bit Assignments

Bit	Function
1	R_1 Enable
2	R_2 Enable
3	C_{SS} Enable
4	S_3 Enable
5	S_1 Enable
6	S_2 Enable
7	Transfer enable. Bit 33 of command word.
8	+10v

Table A-4. Mode Decoder

Bit				Output
34	35	36	37	
1	0	0	0	R_1, C_{SS}
0	1	0	0	R_1, C_{SS}, S_3
1	1	0	0	R_2, C_{SS}
0	0	1	0	R_2, C_{SS}, S_3
1	0	1	0	R_1
0	1	1	0	R_1, S_3
1	1	1	0	R_2
1	0	0	1	R_2, S_3

Table A-4. Mode Decoder (cont)

Bit				Output
34	35	36	37	
0	1	0	1	C_{SS}, S_3
1	1	0	1	S_1
0	0	1	1	S_2

R_1 = enable Rate 1 to Compensation/Mixing card.

R_2 = enable Rate 2 to Compensation/Mixing card.

C_{SS} = enable Coarse Sun Sensor to Mixing card.

S_1 = enable D/A 1 to Wheel Drivers.

S_2 = enable D/A 2 to Wheel Drivers.

S_3 = enable Compensation/Mixing card wheel commands to Wheel Drivers.

Table A-5. DMU Bit Allocation

Bit	Function
1-12	Engine 1-12 ON/OFF "0" = OFF, "1" = ON
13	THR.PULSE Status (Cmd. Bit 33)
14	+10v
15	Accelerometer Select Status (Cmd. bit 35)
16	Phase Invert Status (Cmd. bit 36)
17	JET.PULSE Status (Cmd. bit 37)
18-24	Valve 1-7 Open/Closed "0" = Closed, "1" = Open

Table A-6. DMU Bit Allocation

Bit	Function
1	- Roll Error
2	+ Roll Error
3	- Yaw Error
4	+ Yaw Error
5	- Pitch Error
6	+ Pitch Error
7	Mode Control
8	+10v

A.3.9 COMMAND DECODER INTERFACE

Commands to the CEA come from the Onboard Processor or directly via RF link from the ground in either of three formats:

(1) 37 bit serial data line shifted at 4.27 Kbps and consisting of data, clock and gate envelope. This configuration is shown as figure A-17.

(2) Impulse lines of 15 millisecond duration at +10 v which are used to latch and unlatch relays in the CEA.

(3) Steady levels, generally of 28 v unregulated power, obtained by toggling latch relays.

Examples of all three types can be seen on the Master ACS Logic Diagram, figure 8-4.

Figure A-18 is a schematic of the command interface circuit used in the CEA. The circuit provides the OR function for the signals from each decoder, the gating of the clock and data with the envelopes and also AC coupling for the envelopes. The gating with the envelopes is used so that both lines (envelope and data or envelope and clock) must fail "high" before the incoming data can be disrupted. The envelopes are AC coupled in case that line should fail "high." Since the decoder shifts the data on the leading edge of the clock pulse, the clock signal from the command decoder interface is inverted to give sufficient delay before the data is entered into the CEA serial shift register. The trailing edge of the

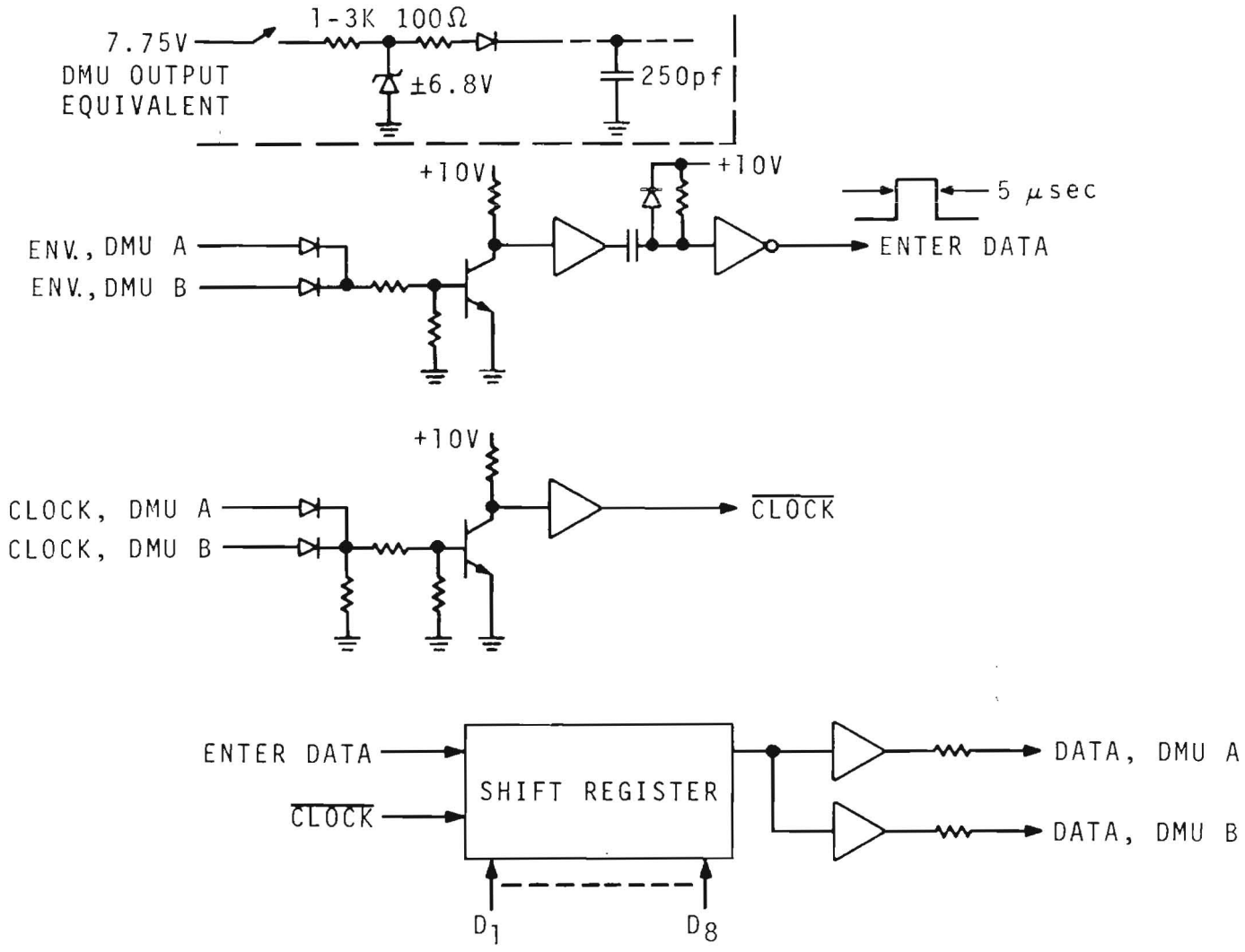

Figure A-17. 37 Serial Bit Decoder

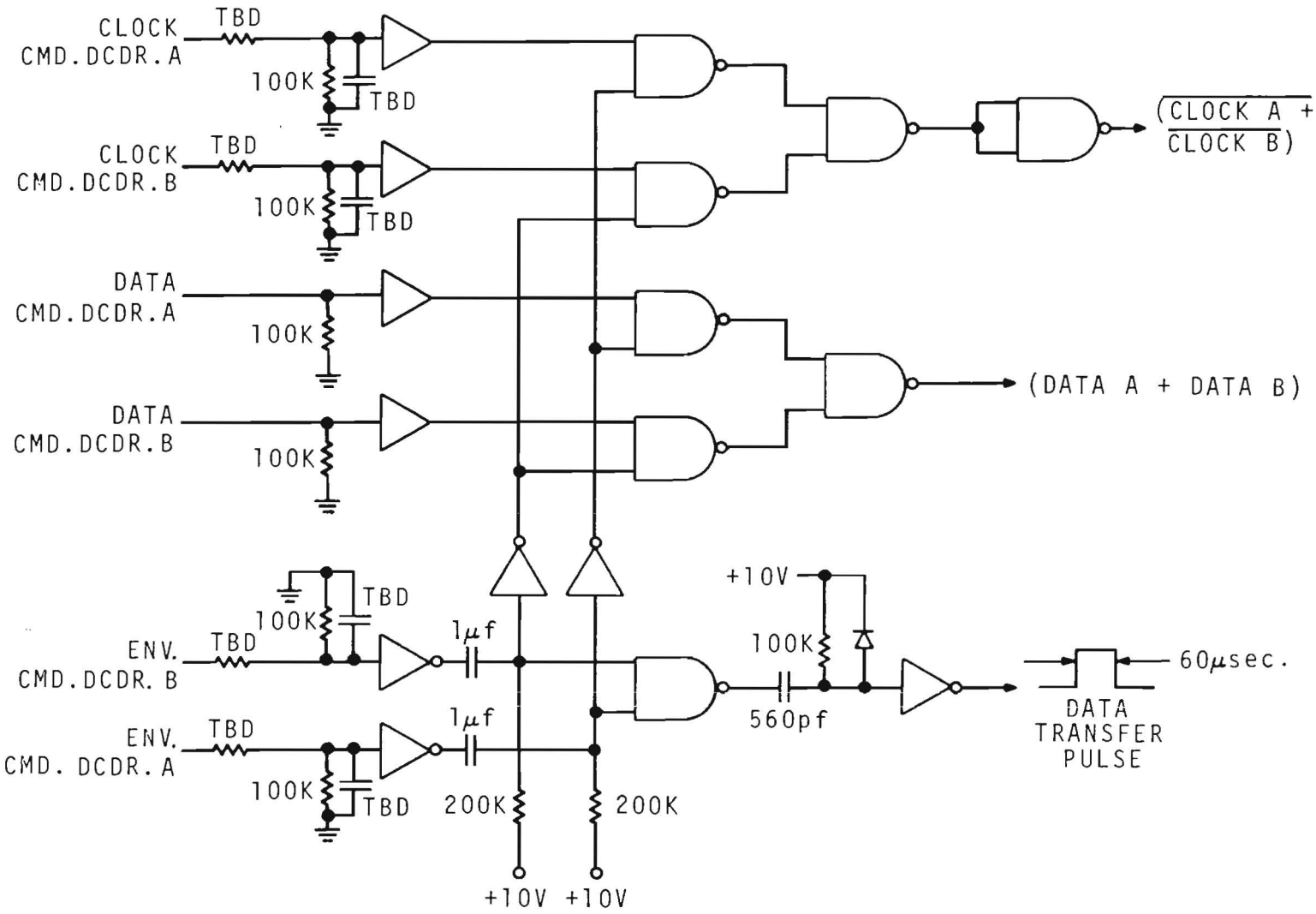

Figure A-18. CMU Interface Circuit

envelope is used to develop a pulse which enters the data into the CEA storage register.

The input buffers of the decoder interface circuit, CD 4049 and CD 4050, are used for these reasons:

(1) Since CMOS contains protective diodes from the input pin to the supply pin, a voltage at the input, greater than the supply voltage, could damage the CMOS chip. CD 4049 and CD 4050 do not have these diodes and can handle up to +15 v at the input.

(2) When power is removed from a CMOS circuit, an input voltage could energize it through the protective diodes.

The 100 Kohm resistors at the inputs are used for open-circuit protection since a floating input on a high current type, such as the CD 4049 and CD 4050, can cause maximum power dissipation to be exceeded and may result in damage to the device.

A.4 WHEEL DRIVE ASSEMBLY

A.4.1 DESIGN REQUIREMENTS

The basic design requirements of this third and final component designed specifically for the IUE ACS is to develop redundant sources of regulated voltages for use in the CEA and the WDA and to accept the wheel torque signals from the CEA, convert them to two phase 400 Hz signals and power amplify them to drive the inertia wheels. As is the case of the CEA, the WDA is an assemblage of cards having identical lengths and breadths stacked to form a complete unit. The cards or at least some of their circuitry have been flown previously on other spacecraft. A total of six cards of two different types are used. These consist of two identical Power Supply Cards and four interchangeable Motor Driver Cards. Figure A-19 is a block diagram of the overall WDA showing both Power Supply Cards, external switching relays (CEA Relay Card) and a block diagram of one of the four Motor Driver Cards. The overall interrelationship of the WDA Power Supply Cards and the various WDA and CEA loads and CEA relay switching can be best seen by referring back to figure 8-4, the Master ACS Logic Diagram.

A.4.2 POWER SUPPLY CARDS

The Power Supply Cards generate +/-10v @ +5% power ground isolated voltages to power the CEA cards and the four WDA Motor Drive Cards. In addition, two 5 volt supplies (+ and -) with 1% regulation are derived from the +/-10 volt supplies . Externally switched +28 volt bus power is the input to the PSC's and this input, suitably filtered and diode isolated is also provided as an output. The power supplies are current

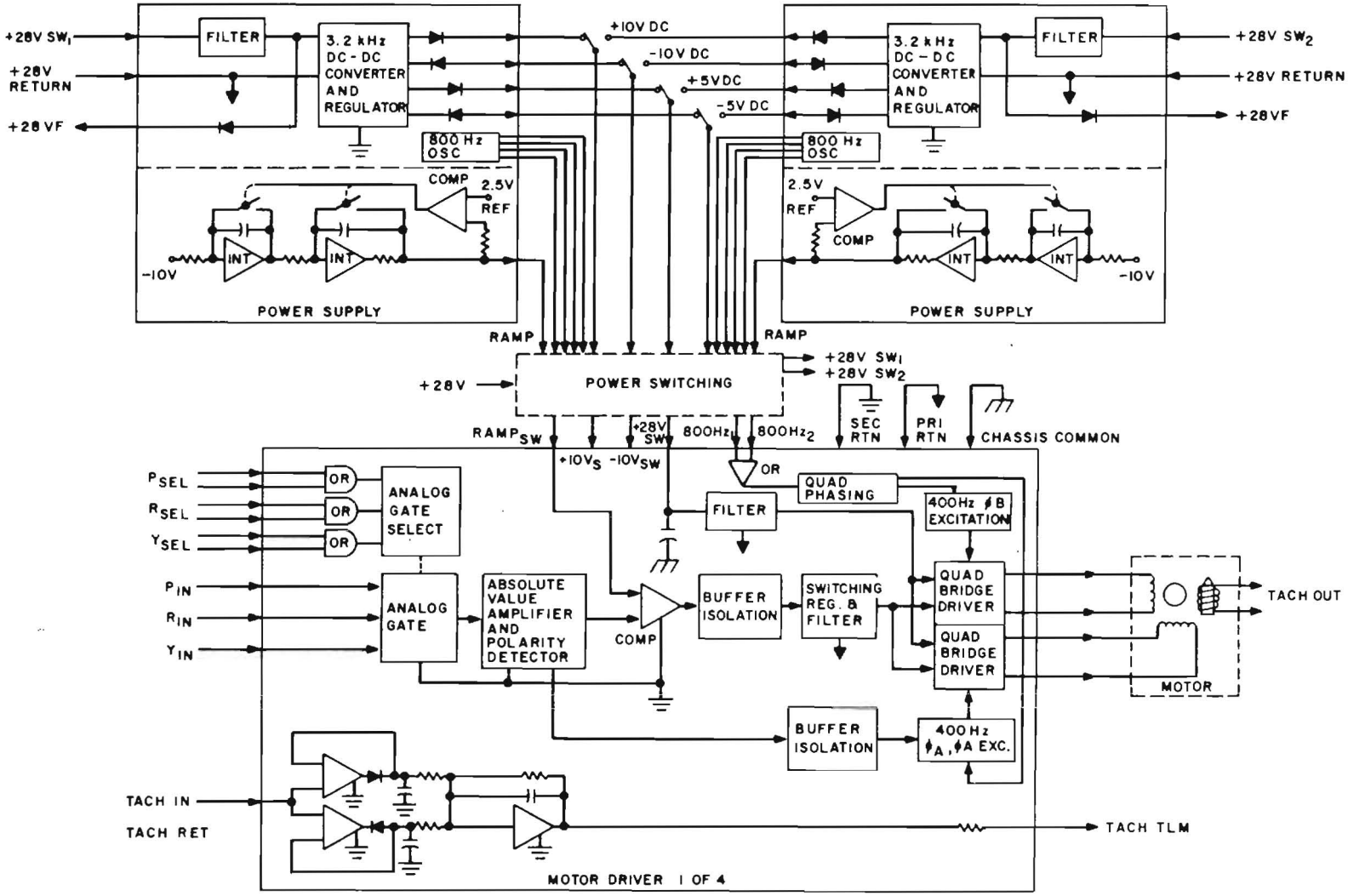

Figure A-19. IUE WDA Block Diagram

limited and interrelated such that an excessive load on the +/-10 v line causing that voltage to be limited will result in identical limiting of the -10 v line. The converse is likewise true.

Figure A-20 is the block diagram of a PSC. A DC to DC conversion is made by chopping the 28 v input at a 3.2 KHz rate, stepping down the voltage and rectifying and filtering the transformer output. Regulation is accomplished in an energy efficient manner by sensing the output voltage and using it to regulate the base drive current of the chopper oscillator transistors. As can be seen from the block diagram, the more tightly regulated 5 volt supply is obtained by using a unity gain op amp and emitter follower following a temperature compensated zener diode driven by the -10 volt bus and then inverting and buffering this +5 v with another unity gain op amp/emitter follower to derive a -5 v source with the same ultimate reference and regulation.

Besides generating regulated or isolated power, the PSC's also have two additional functions. The first of these is to generate an 800 Hz signal which is divided and phase shifted in the MDC's to create two 400 Hz signals in phase quadrature. The remaining function is a square law generator that develops a 2.5 v peak signal with a 10 KHz fundamental frequency that is used in the MDC's to modulate the motor voltage such that the developed motor torque will be proportional to the commanded torque signal from the CEA.

A.4.3 MOTOR DRIVE CARD

Each of these four identical cards contain two, four transistor, power bridge circuits which drive two windings of an induction motor with 400 Hz signals in quadrature (90^0) phase relationship. The amplitude of the 400 Hz voltage is determined by the level of the input from the CEA while the phase relationship (i.e. ØA leading or lagging ØB) and thus the torque direction are controlled by the polarity of the input signal. Any of three inputs can be selected by digitally energizing an analog gate. Once selected, the analog signal is scaled and applied to a unity gain absolute value circuit. At this point the input signal polarity is detected and used to control the drive phase relationship. The signal amplitude is compared with the 10 KHz square law waveform of zero to 2.5 v peak and the output of the comparator controls the duty ratio of a switching regulator. Since both windings of the motor are being driven by the modulated signal, the motor torque varies as the square of the duty ratio of the switching regulator. It is for this reason that the input signal is square law modulated. Otherwise a 50% signal would generate a 70% torque level. Duty ratio modulation of both motor windings, although more complex, results in substantial power savings over the more conventional technique of energizing one winding at some continuous nominal or discretely switchable level while modulating and phasing shifting the other winding. Figure A-21 shows a block diagram of a MDC. Note that besides developing drive voltages the MDC also provides amplification, direction sensing and telemetry

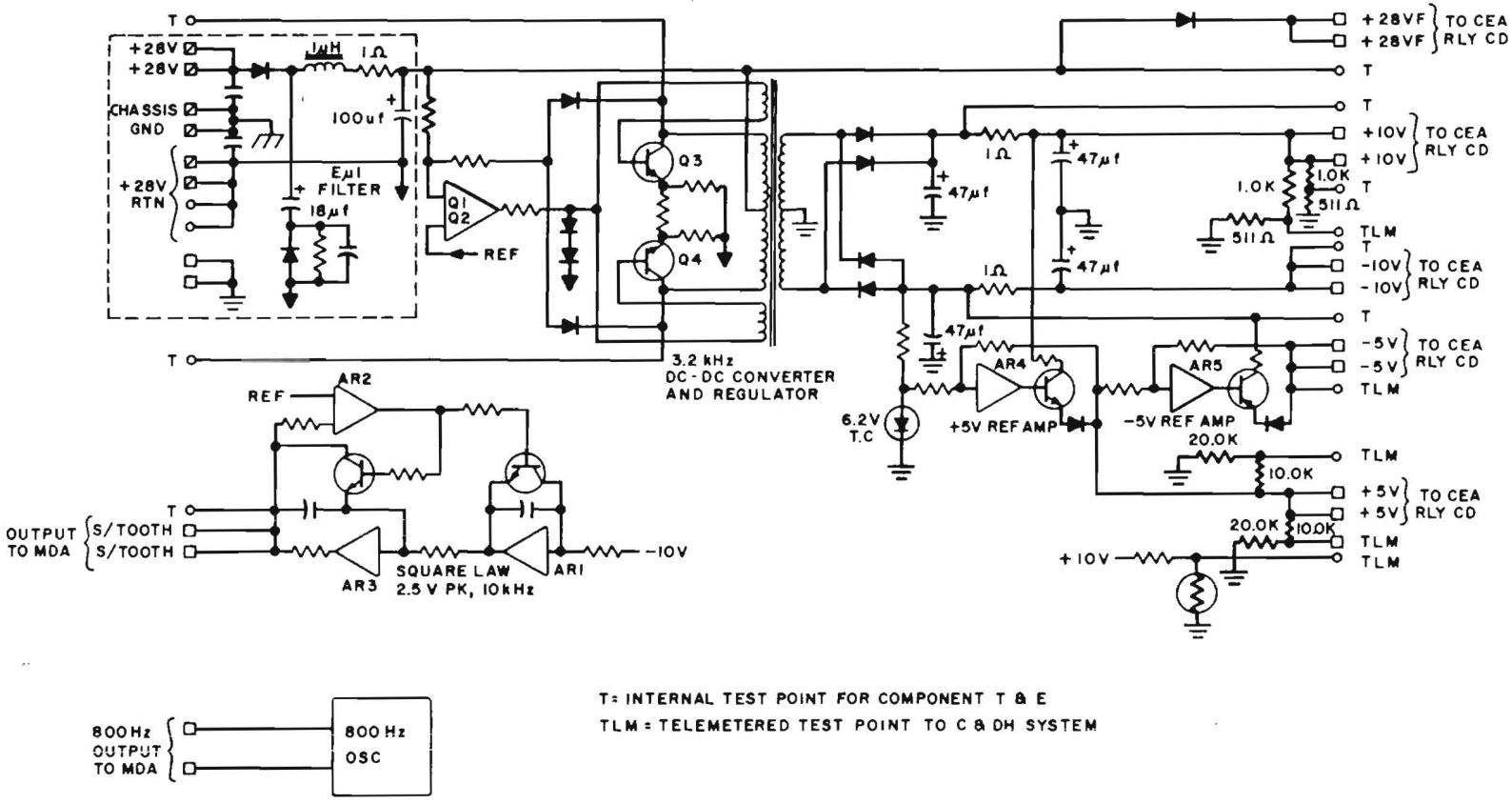

T= INTERNAL TEST POINT FOR COMPONENT T & E

TLM = TELEMETERED TEST POINT TO C & DH SYSTEM

Figure A-20. WDA Power Supply Block Diagram

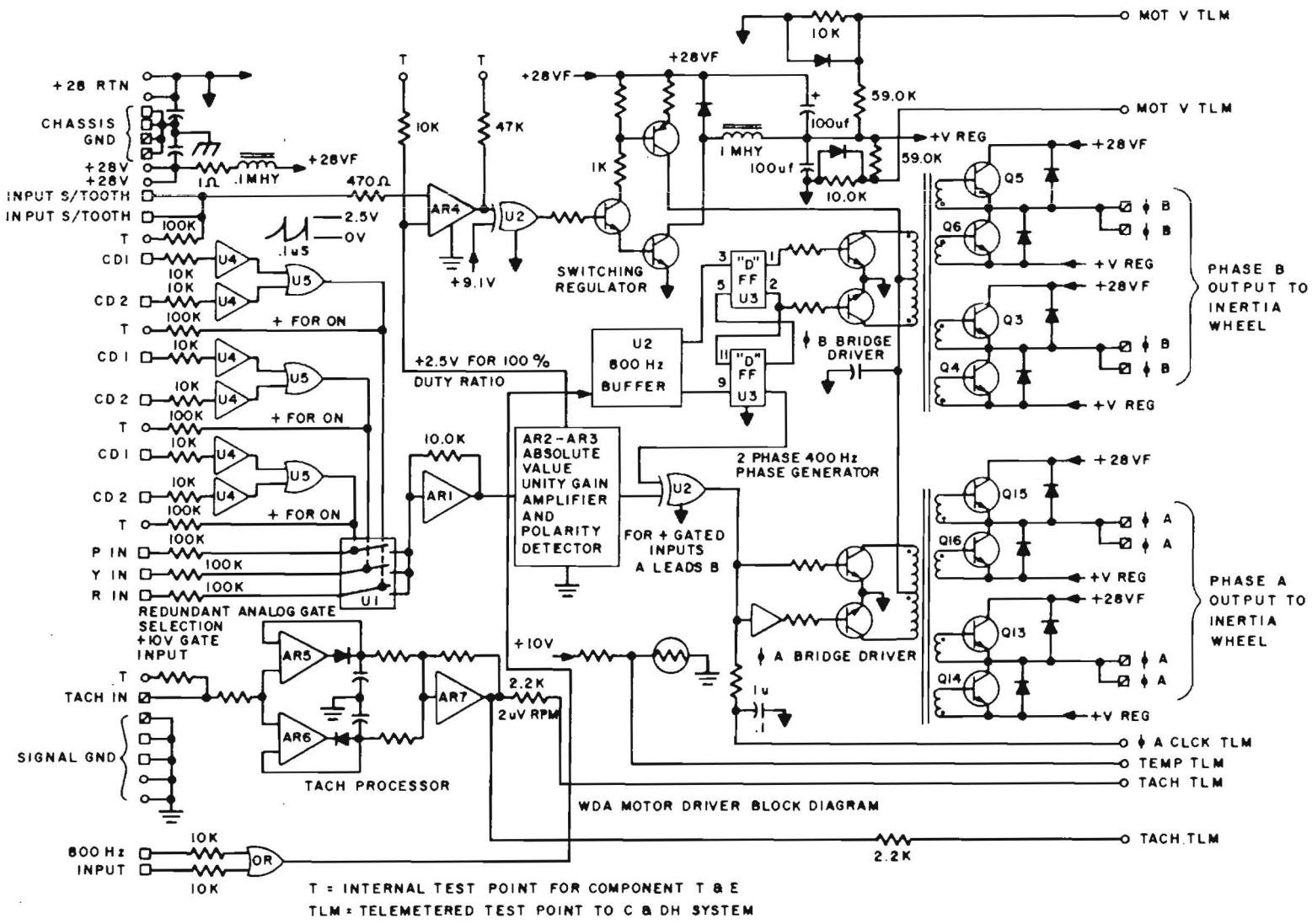

Figure A-21. IUE Motor Driver Block Diagram

conditioning of the inertia wheel tachometer signal. This information is used in the OBC as a basis for momentum unloading and slewing.

APPENDIX B. ACS FLIGHT PROVEN COMPONENTS

B.1 INTRODUCTION

A previous section, 8.3, dealt in detail with those components of the IUE ACS system that were developed essentially as new devices and specifically for use on the IUE. The components described in this section are devices that have previously flown on other NASA programs. Some, such as the Coarse Sun Sensors (CSS), are completely unchanged from their usage on OAO. Others, such as the Spin Mode Sun Sensor (SMSS) and the Fine Sun Sensor(s) (FSS) are essentially the same as they were on Hawkeye and OAO but with relatively minor modifications to make their command and telemetry formats compatible with the IUE C&DH/OBC subsystems. A third type of sensor, the Panoramic Attitude Sensor(s) (PAS), while previously flown on RAE-B, has had to be modified drastically both to correct flight observed deficiencies and to achieve compatibility with the IUE C&DH interface. It is, however, considered basically flight proven and included herein.

B.2 COARSE ANALOG SUN SENSOR

B.2.1 PURPOSE

This sensor set is used to provide two-axis attitude information with respect to the spacecraft pitch and roll paddle axes. The attitude information will be combined with body rate information to allow sun acquisition and hold via the 0.30 pound hydrazine engines and/or the reaction wheels.

B.2.2 DEVELOPMENT

No development is required for this sensor set. Identical sensors have been flown on the three latter OAO flights.

B.2.3 EQUIPMENT LOCATION

This sensor set is body mounted on the IUE at locations which minimize sun shading by spacecraft appendages. Each sensor normal is directed such that the relative angles between individual sensors and the spacecraft axes are preserved as shown in figure B-1. This figure includes the electrical polarity convention for the two sets.

B.2.4 PERFORMANCE

The following characteristics and definitions shall be associated with the CSS.

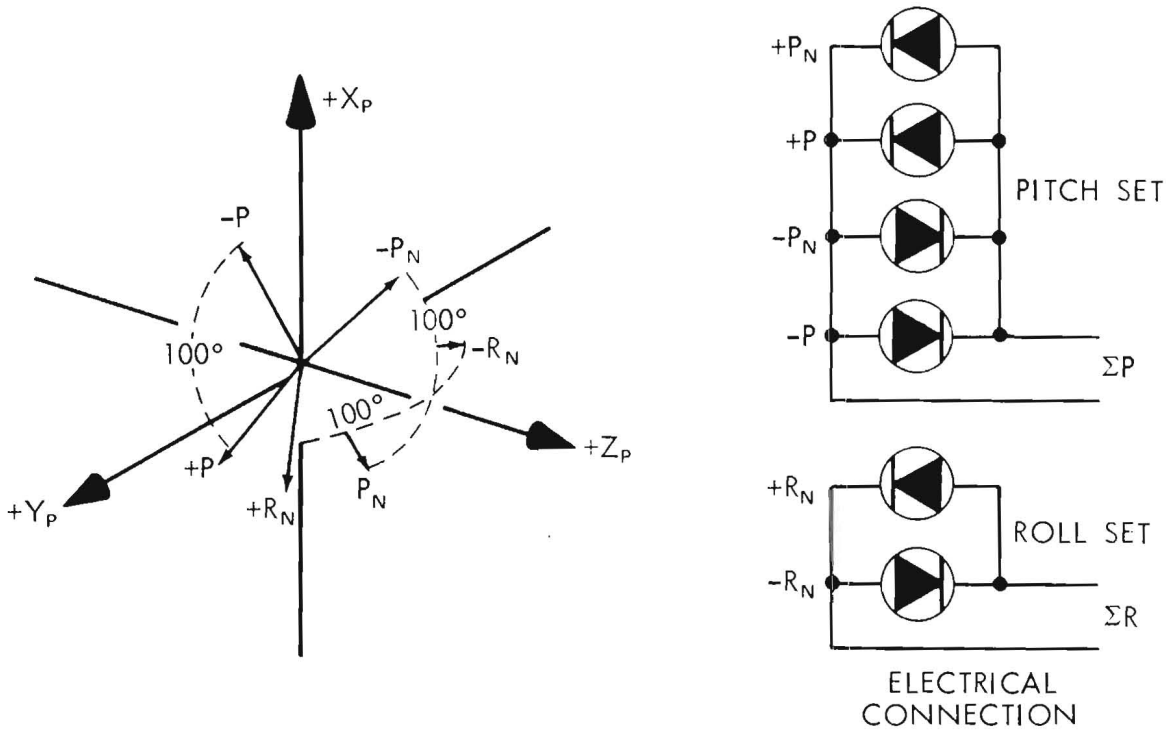

Figure B-1. Coarse Sun Sensor View Angles Relative to IUE Control Axes

(1) Control Planes. The two planes defined by the X_p, Z_p and Y_p, Z_p axes sets are further defined as the pitch and roll control planes respectively.

(2) Field-of-View. The field-of-view of each sensor head is described by a hemisphere whose axis is coincident with the sensor normal. The field-of-view of the total sensor set is spherical with a two axis null directed coincident with the $+Z_p$ axis (array normal).

(3) Transfer Function. The approximate transfer functions of the pitch and roll sensor sets relative to the sun in the pitch and roll control planes respectively are shown in figure 8-8 The individual sensors are parallel connected as shown in figure B-1.

(4) Null Accuracy. The pitch and yaw sets shall both yield a sensor null when the sun is at some point within 1.0 degree half-cone of the $+Z_p$ axis over the entire life of the sensor set.

(5) Transfer Function. The sensitivity of the pitch or yaw sensor sets shall be 18.0 $\pm$3.6 micro amperes per degree for $\pm 10^o$ from the sensor set null when the summed set is terminated in a 100 ohm load.

(6) Linearity. The transfer function shall be linear within $\pm$5% of the output at $\pm 10^o$ over the range of $\pm 10^o$ from null.

(7) Cross-Coupling. When the sun is in the roll control plane the output from the pitch sensor set shall not exceed 5% of the maximum output of a single sensor.

(8) Power. The CSS requires no power.

(9) Weight. Each sensor head including pigtails shall not exceed 0.04 pounds. This does not include the weight of the sensor mount which is charged to the spacecraft structural weight.

(10) Dimensions. The individual sensor size shall not exceed 1.0" diameter by 1.0" depth.

(11) Electrical Connections. Each sensor shall be provided with two pigtail leads at least 12 inches in length.

(12) Telemetry Requirements. The individual sensors require no telemetry. The pitch and roll sensor set signals shall be amplified in the Control Electronics Assembly and conditioned in that unit for telemetry sampling.

B.3 SPIN MODE SUN SENSOR (SMSS)

B.3.1 PURPOSE

The prime SMSS function is to provide a sun presence or blip as the sunline impinges on the rotating IUE during the transfer orbit phase of control. This sun blip, achieved by the SMSS's narrow field-of-view of 0.5° transverse to the x-axis, is used in the CEA to accurately time the period of rotation of the spinning IUE. The sensor has a 180° field-of-view parallel to the x-axis in order to provide this signal regardless of Beta angle.

B.3.2 DEVELOPMENT

The SMSS was developed for the University of Iowa for use on the Hawkeye vehicle. It has been modified in its electronics to make it compatible with the IUE C&DH subsystem.

B.3.3 DESCRIPTION

The SMSS consists of a sensor head with photocells that detect the sunlight as it falls upon them and an electronics unit that amplifies, combines and performs logic functions on the photocell signals. Figure B-2 is a general block diagram showing the interface between the two units while figure B-3 is a logic diagram of the overall system. As was stated previously, the SMSS has a field-of-view of 180° x 0.5 degrees and this swath has a resolution of 0.5 degrees with an accuracy of ±0.25 degrees over the entire field. The sun pulse produced by the IUE rotation shall occur within

$$\theta = \pm \tan^{-1} \frac{0.25}{\cos \beta} \times \frac{\pi}{180}$$

of the command plane where β is the angle of the sunline relative to the normal of the sensor (i.e. spacecraft β angle).

B.3.3.1 Sensor Head. The sensor head consists of two fused silica blocks with silicon solar cell arrays mounted beneath them. The two blocks are tilted 90° with respect to each other in order to provide the 180° coverage about the command plane. This plane is defined by two slits, one above the other. When both slits are aligned to the sunline (as the IUE rotates), sunlight passes through and impinges on a photocell beneath them. This causes a sun pulse to be produced. The sun pulse causes the SMSS electronics to read out the sun angle as a function of which photocells behind a Gray code mask are illuminated. In addition to the data bit patterns there is an Automatic Threshold Adjust (ATA) pattern and photocell. The ATA output is used to set the thresholds of the data bit amplifiers to prevent spurious response from inputs other than the full sun. As can be seen in figure B-3, the

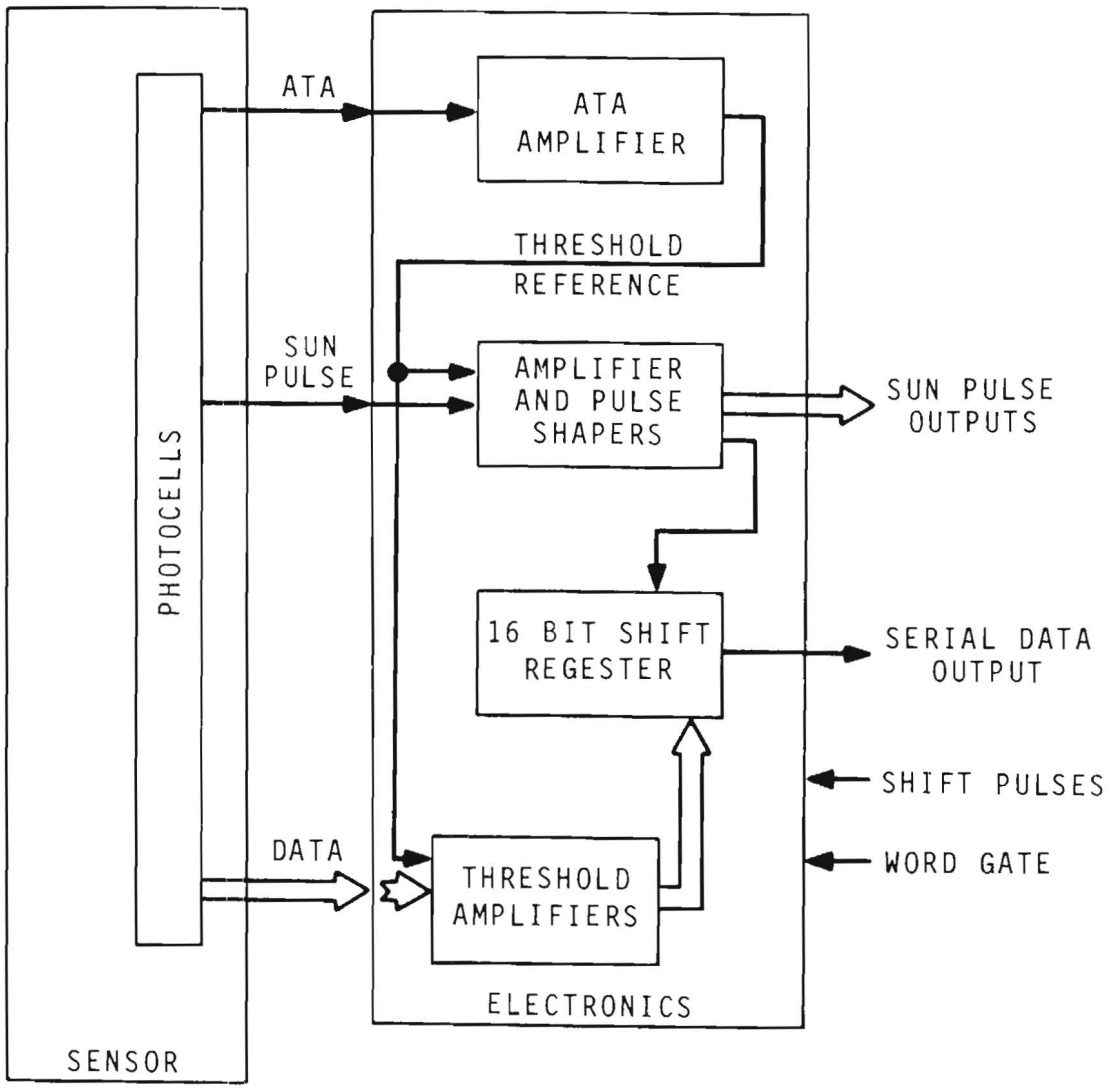

Figure B-2. SMSS General Block Diagram

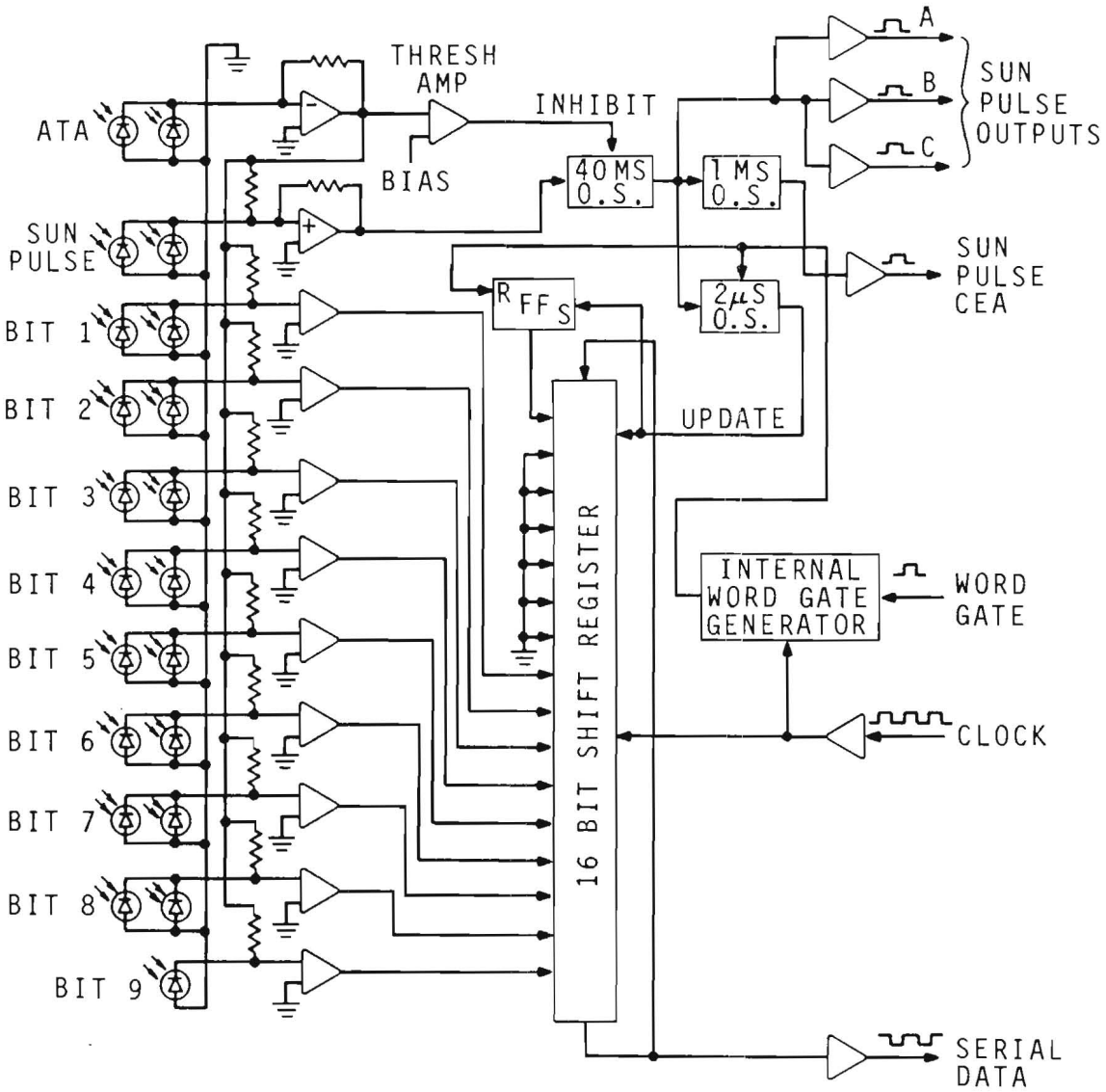

Figure B-3. SMSS Logic Diagram

photocells of both arrays except the MSB or sign bit (Bit 9) are in parallel. This ninth bit indicates which of the two reticles (quadrants) is being illuminated.

B.3.3.2 Sensor Electronics. Referring to the logic diagram, note that the photocell outputs are amplified and then fed to nine inputs of a 16-bit shift register. This register is updated each time a sun pulse occurs unless it occurs during a register readout. Two 8-bit data words are used with the word gate present during the first data word. An internal word gate generator produces a signal which extends from the beginning of the word gate to the end of the last clock pulse of the second data word. This signal is used to inhibit register update during the readout interval. The shift register recirculates so that if two data readouts occur without the occurrance of a command pulse between them the readouts will have the same data content. The 16th bit is a data status bit that indicates a '1' if a command pulse (sun pulse) occurs between two readouts. The timing sequence is shown as figure B-4. The output word is a 9-bit Gray coded serial word which encodes the 180° aspect angle into 360 parts of 0.5° each. The MSB is the sign bit with '0' indicating a minus angle and '1' a positive angle. The remaining eight bits are converted into a decimal number (N) using a standard Gray-to-binary-to-decimal conversion. The aspect angle is:

$$\beta = \text{SIGN (plus or minus)} \ (0.25 + 0.5N)$$

B.3.4 REDUNDANCY

The SMSS is not, in itself, a redundant device nor are a pair of them flown for redundancy since it is required only during transfer orbit and since its function can be duplicated with either of the PAS's. However, to maintain integrity of the IUE overall redundancy scheme, both the input circuits (Redundant Word Gate and Shift Pulse) and output circuits (T/M Sun Pulse and Serial Data Word) are redundant and isolated to prevent shorts on one input or output from loading the others out of specification.

B.3.5 POWER

Also in keeping with IUE philosophy, the SMSS is designed to accept the roughly regulated +28v supply bus and use this, via a DC-DC converter, to develop regulated, power/signal ground isolated, voltages for use within the SMSS.

B.4 FINE DIGITAL SUN SENSOR (FSS)

B.4.1 PURPOSE

This redundant sense system provides the means of either holding the spacecraft roll attitude during the experiment mode or of updating

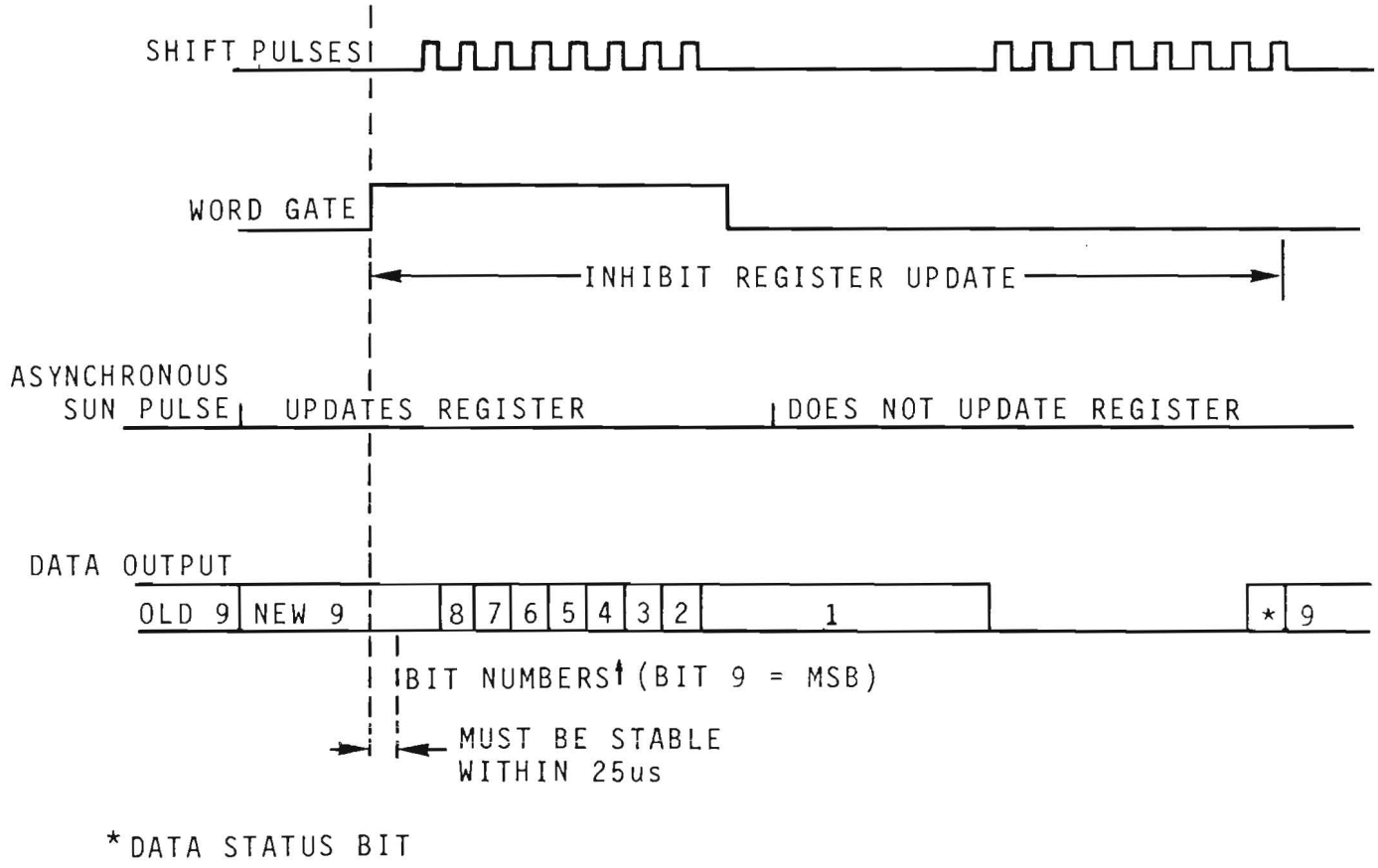

Figure B-4. SMSS Timing Diagram

the roll component of IRA gyro drift while the spacecraft is being held on the IRA.

B.4.2 DEVELOPMENT

This sensor head plus electronics has been flown on OAO-C with excellent performance demonstrated. The OAO system, however, was designed to process data from only one sensor head. The IUE FSS system must accept inputs from multiple heads and therefore some gating modifications must be accomplished in the processing electronics. In addition, the electronics had to be made compatible with the C&DH interface.

B.4.3 EQUIPMENT LOCATION

The four FSS heads shall be mounted on a body mounted bracket such that relative angles between sensor heads and the spacecraft control axes are as depicted in figure 8-9.

B.4.4 PERFORMANCE

B.4.4.1 Field-of-View. The field-of-view of each sensor shall be $+32^{o}$ in two orthogonal axes. Total coverage shall be from $\beta = +13^{o}$ to $\beta = +137^{o}$.

B.4.4.2 Resolution. The average resolution of the data output shall be 1/256 degrees or 15 arc-seconds.

B.4.4.3 Accuracy. The transition accuracy shall be one minute of arc or better.

B.4.4.4 Output Data Word

(a) Format. The output data word shall consist of a 32-bit serial output with the bits designated as follows (all outputs MSB first).

Bits 1-6 :	A-axis coarse Gray coded output	
Bits 7-15 :	A-axis fine binary coded output	
Bit 16 :	Sensor Selected:	Sensor #1 - "0" Sensor #2 = "1"
Bits 17-22 :	B-axis coarse Gray coded output	
Bits 23-31 :	B-axis fine binary coded output	
Bit 32 :	Sun Presence:	not present "0" present "1"

(b) Amplitude

"1" level: 3-6 volts

"0" level: 0-1 volts

(c) Output Impedance: shall be less than 30 K for the "1" state and less than 2 K for the "0" state.

(d) Timing. See figure B-5 for the timing requirements.

(e) Register Update. The register shall be updated at a rate greater than 1500 Hz except that it shall not be updated during the period extending from the leading edge of the first word gate pulse to the trailing edge of the last shift pulse.

B.4.4.5 Transfer Function. The output of the system consists of a nine bit fine angle number (N_F) and a six-bit coarse bit number (N_C) for each axis. The coarse angle data first has to be logically converted as follows:

(a) Convert the six bit Gray coded coarse data to six-bit binary data.

(b) Compare the resulting least significant bit with the most significant bit of the fine angle data:

1. If these bits are the same, leave the coarse data as is.

2. If these bits differ, and if the next to MSB fine bit is a one, subtract one from the binary coarse data; however, if the next to MSB fine bit is a zero, add one to the binary coarse data.

(c) Define N_C as the five most significant bits of the result (ignore the LSB).

N_F is a number from 0 to 511. N_C is a number from 0 to 31. The effective number to be used in the transfer function is as follows:

$$N = N_F + 512\ N_C$$

The coordinate system for the high resolution sensor is shown in figure B-6. Angle α is defined as the angle between the projection of the sunline on the XZ plane and the Z-axis. Angle β is defined as the angle between the projection of the sunline on the YZ plane and the Z-axis. N_A and N_B are the processed data for the two axes respectively where:

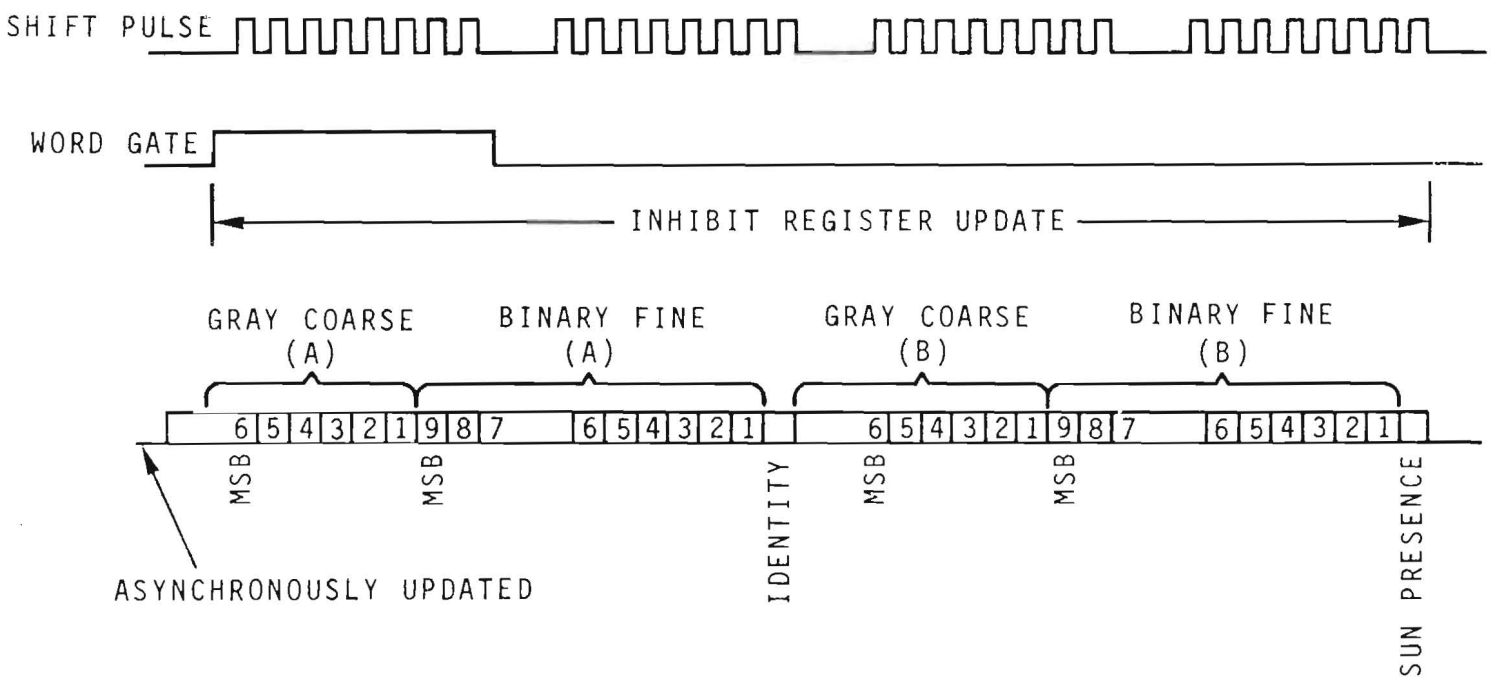

Figure B-5. Fine Sun Sensor Timing Diagram

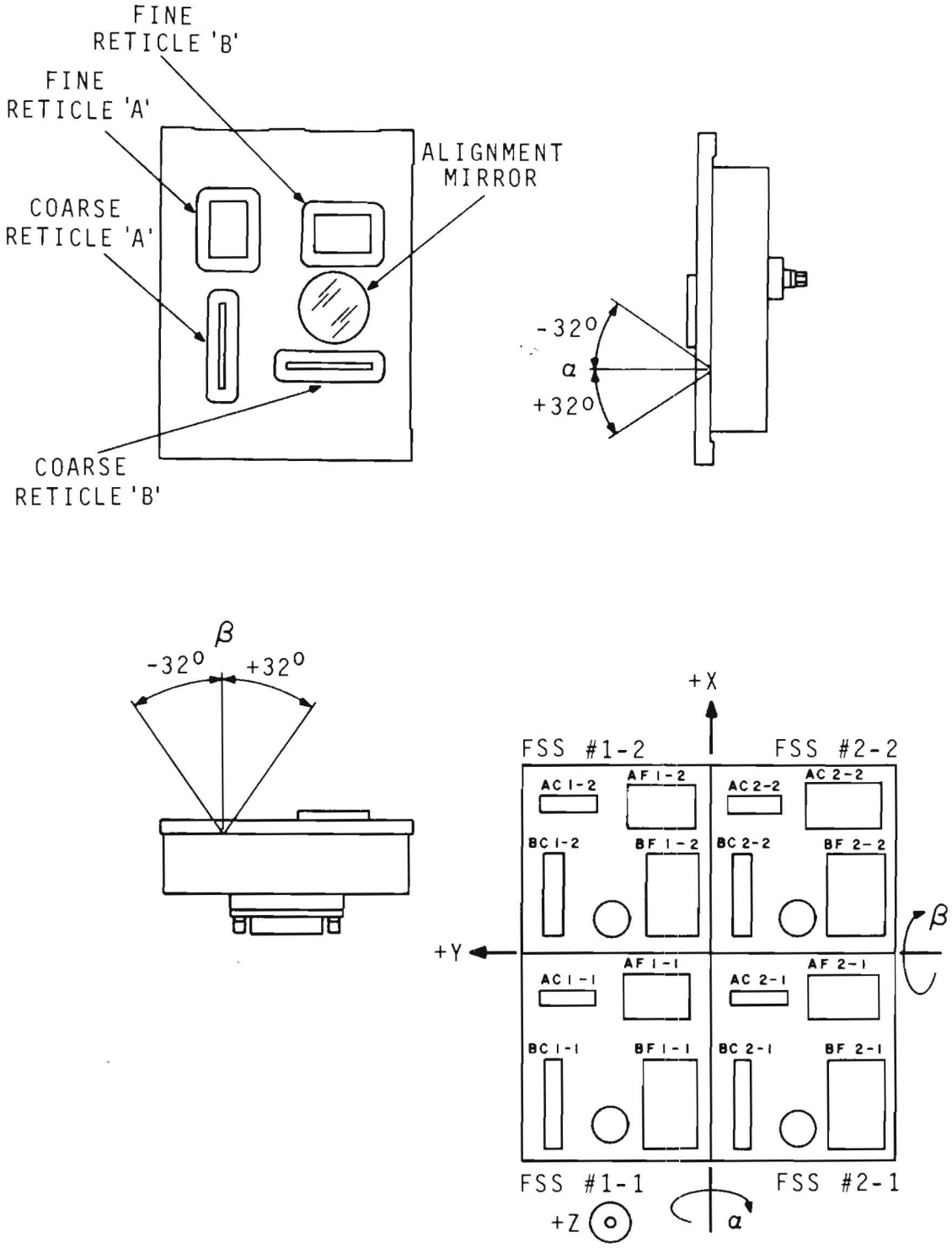

Figure B-6. Fine Sun Sensor Coordinate System

$$N_{A \text{ or } B} = N_F + 521\ N_C \text{ for each axis}$$

$$\alpha = \tan^{-1}\ A_{1(M)}\ (N_A + 0.5) + A_{2(M)} + A_{3(M)}$$

$$\beta = \tan^{-1}\ B_{1(M)}\ (N_B + 0.5) + B_{3(M)} + B_{3(M)}$$

Where M is the serial number of the sensor, A_1 and B_1 are nominally 7.62780×10^{-5}, A_2 and B_2 are nominally -0.624869, and A_3 and B_3 are offset angles that will not exceed 0.1 degree.

B.4.4.6 Input Control Signals

a. Word Gate and Shift Pulse. Amplitude and input impedance. The amplitude will be five volts minimum when loaded with 2.5 K ohms. The effective input impedance is at least 2.4 K ohms with a five volt input. The timing is as shown in figure 8-5.

b. Sensor Select Command. The sensor select command is 10 volt 15 millisecond pulse with a diode and 1 K ohm (max) resistor in series. The input impedance is greater than 20 K ohms.

After initial power turn on, Sensor #1 shall be selected. Subsequent sensor select commands shall cause the selection to alternate between Sensor #1 and Sensor #2.

B.4.4.7 Redundancy. The serial data output is redundant. A short circuit on one output shall not cause an out of specification condition on the other output. Redundant Word Gate and Shift Pulse inputs shall be accepted. The redundant inputs are diode OR'd together in the electronics unit. Redundant Sensor Select Command inputs are accepted. The input ORing circuit is such that if either input fails in the "0" or "1" state, the other input will function correctly.

B.4.4.8 Auxiliary Outputs. A thermistor is located within the electronics unit and both leads brought out to the vehicle interface connector to provide capability of monitoring electronics temperature. A B+ output monitors the internal plus 5 volt supply. Proper operation will result in a signal of 3.5 v ±2% when internal supply is at 5.0 v. The ATA output monitors the internal ATA signal. Sun

presence is generated when the ATA voltage equals or exceeds 0.5 v. $V_{ATA} \sim 3.0 \cos \theta$ volts where θ is the angle between the sunline and sensor normal.

B.4.4.9 Power Input. The power input shall be +28 V ±2%. Power consumption shall be less than 1.7 watts.

B.4.5 SENSOR SYSTEM DESCRIPTION

Figure B-7 is a general block diagram of the overall FSS showing the two sensor heads, each with an A-axis and B-axis output, the FET switches used to select the active sensor pair, the two-axis processors and the shift registers that combine the outputs into a 32-bit serial data word for presentation to the C&DH interface. A more detailed depiction of a single channel is shown as figure B-8, FSS Logic Diagram. The ability to resolve the sun position to an accuracy considerably greater than the 32 arc minutes the sun subtends at 1 A.U. is accomplished by using coarse and fine reticle patterns with Gray coded patterns to prevent bit ambiguity at transistions and quadrature gating of individual cell outputs to obtain sun angle as a function of phase shift between a reference sine wave and the sine wave resulting from the quadrature gating. The ATA signal provides threshold for gating on the coarse pattern sensor amplifiers. As can be seen from the Logic Diagram, there are four "fine" photocells, six "coarse" photocells and one ATA or sun presence detector.

The outputs of the four "fine" photocells are amplified and then chopped by four quadrature square waves derived from a chain of flip-flops counting down from a 1.5552 MHz frequency reference source. The chopped outputs are summed and passed through a 3.037 KHz bandpass filter to obtain the fundamental sine wave which has a relative phase that is an indication of sun angle. The phase angle is measured by counting the number of reference frequency pulses that occur between the zero crossing of the phase reference signal (one of the chopping signals) and the zero crossing of the sine wave. The compute cycle operates at a rate of one half the chopping frequency with the phase count being accumulated during one cycle, and the count transferred to the shift register and the counter reset during the next cycle. The shift register thus will be updated every 658 microseconds. Referring to the logic diagram, two signals are decoded within the second cycle. The first signal is gated with the Inhibit Generator output and triggers a one shot multivibrator. The output of the multivibrator is used to update the shift register. The second decoded signal is used to reset the accumulator and set the Count Control Flip-Flop. This flip-flop which is reset when the phase encoded signal passes through zero, gates the 1.5552 MHz pulses into the accumulator.

Coarse Angle determination is the function of the remaining photocells. The Automatic Threshold Adjust (ATA) cell and associated amplifier serve

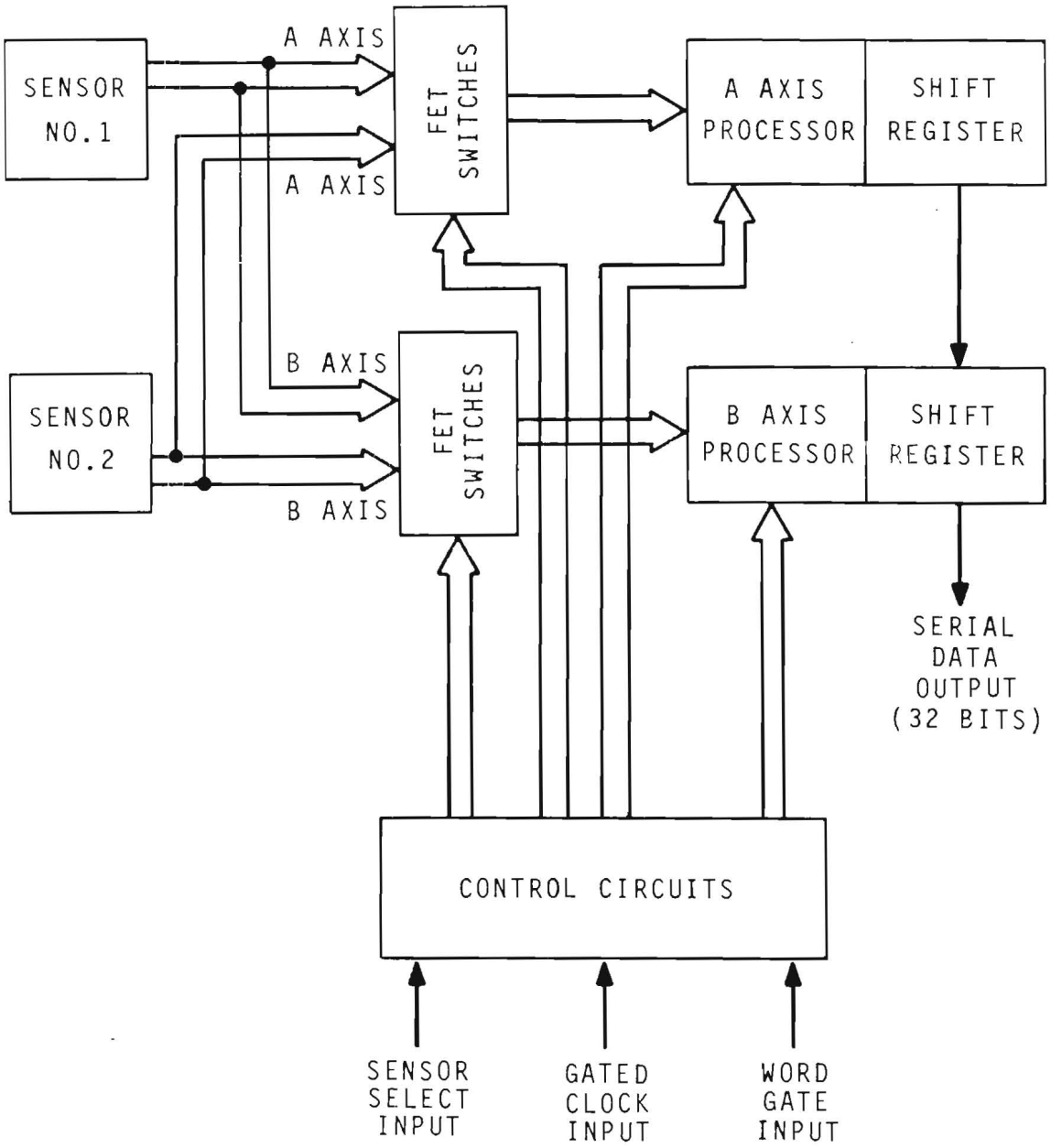

Figure B-7. FSS General Block Diagram

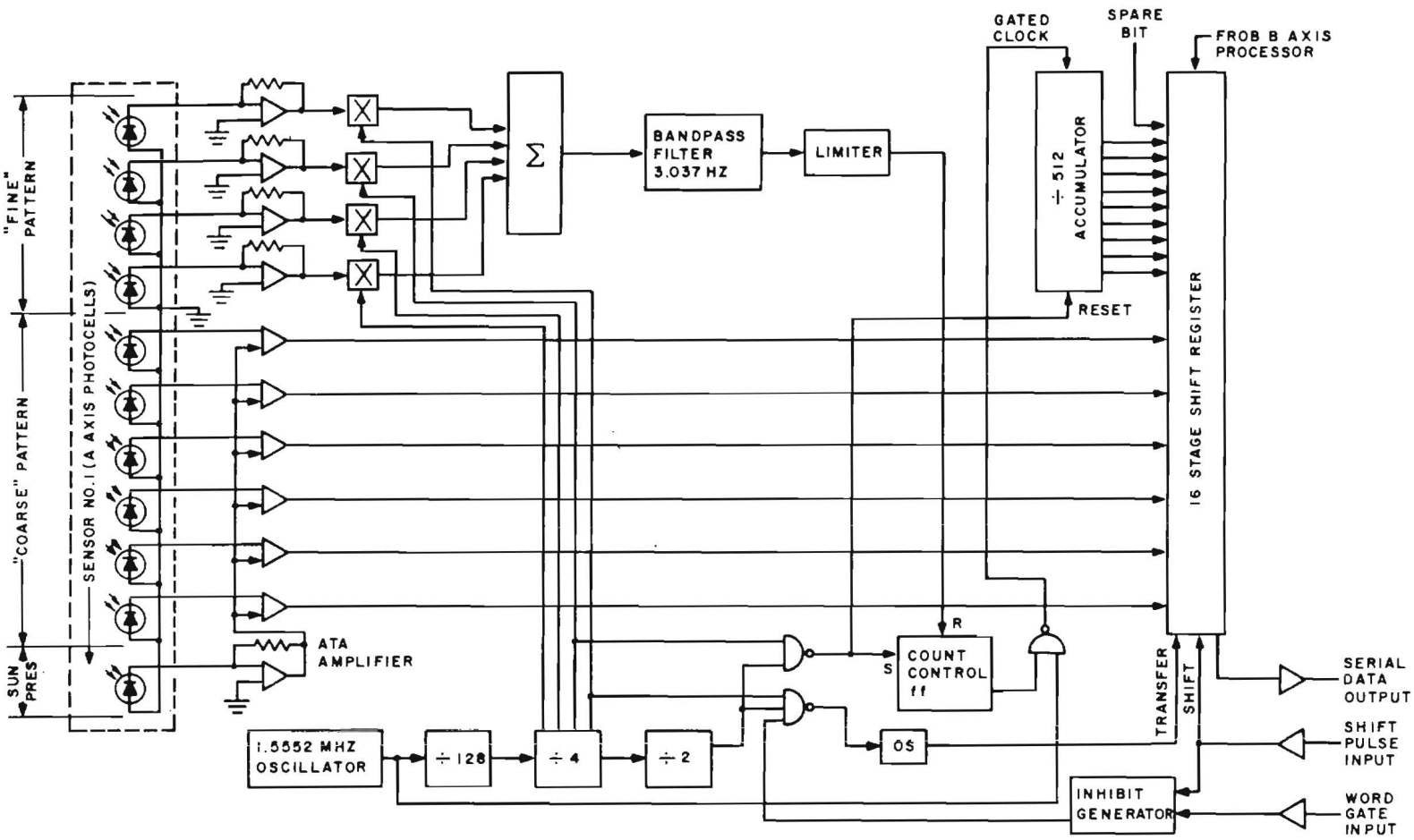

Figure B-8. FSS Logic Diagram

to set the threshold current for the six coarse bit, open loop operational amplifiers. If the output from a photocell exceeds the output of the ATA cell, the output of the bit amplifier is a one; if not, the output is a zero. The coarse data is transferred into the shift register at the same time as the fine data.

The data is shifted out under control of the Gated Clock input pulses which consist of four eight-bit word blocks of pulses. The B-axis processor output is shifted out after the A-axis processor output. The Word Gate input is present during the first three of the four word blocks. An inhibit generator produces a signal that extends from the leading edge of the Word Gate to the trailing edge of the eighth shift pulse of the fourth word block. This signal is used to prevent updating of the register while reading out. The output from each axis consists of 9 bits of binary coded fine data and 6 bits of Gray coded coarse data. Two additional bits of information in the data word are (1) an indication of the selected sensor and (2) a sun presence indicator.

The electronics also includes a preregulator and DC/DC converter which isolates the signal return line from the power return line and produces conditioned voltages for the system operation. The converter operates in a non-saturated mode at 19 KHz.

B.5 PANORAMIC ATTITUDE SENSOR

B.5.1 PURPOSE

The purpose of the Panoramic Attitude Sensor (PAS) is severalfold. It is used during the transfer orbit period as a backup to the SMSS for obtaining spin period and Beta angle of the sunline, it is also used to find the satellite-earth line during transfer orbit which is necessary for the ground operators to perform the precession maneuver, and it is used after insertion into elliptical synchronous orbit in conjunction with the FSS to obtain adequate inertial attitude location to permit slewing the telescope to sight the NEP region and allow initial stellar acquisition (or reacquisition). This latter function is considered of sufficient importance to require flying two, redundant PAS systems in order to ensure this capability over the 3 to 5 year IUE operational life.

B.5.2 DEVELOPMENT

The PAS was developed for and qualified on the RAE-B mission. Some unforeseen difficulties with the sensor optics caused severe limitations in instrument usage and therefore the electronics has been redesigned. To provide utility beyond the IUE mission, the electronics has been given expanded capabilities beyond those required solely for the IUE flight. These are primarily in the areas of scan step rate and clock frequency options.

B.5.3 LOCATION

The redundant PAS sensor heads are mounted on the spacecraft E-side and scan the plane defined pictorially in figure 8-5. The mounting is such that the scan plane will not intercept any spacecraft appendages.

B.5.4 GENERAL DESCRIPTION

The sensor is a two mode operational aspect sensing system. The two modes are spherical and planar. Each of the two modes has two submodes which are the continuous and sector scan. The objective is to detect a crossing of the sensor field-of-view by either the Sun, Earth limb or Moon and encode data sufficient to determine the spacecraft attitude. This is accomplished by either measuring the crossing times relative to the Sun crossing (Spherical) or the angle relative to a set of body fixed coordinates (Planar mode). The worst case resolution of this sensor is 0.7 degrees in all modes.

The sensor operation is controlled by a serial digital command word. The output is also serial digital data which can be read out at variable rates depending on the frequency of the DMU word gate and read out clock.

The sensor consists of a solid state silicon, 0.5° by 180° sun slit sensor and a 0.7° by 360° scanner angle sensor. The sun sensor has a fixed field-of-view and is activated at each sun crossing of the 180° by $.5^{\circ}$ fan shaped field-of-view. The scanner is a 0.7° field-of-view sensor which can be positioned by a stepper motor to 512 positions of about $.7^{\circ}$ each. Figure B-9 is a cutaway view of the PAS mechanical head showing the sun slit, telescope, prism, baffle tube, stepper and scanning mechanisms.

B.5.5 OPERATIONAL MODES

There are two operational modes, spherical mode and planar mode.

B.5.5.1 Spherical Mode. The spherical mode is used when the spacecraft is spinning. As the spacecraft spins, the sun slit crossing is used to start a counter. The sun sync can be provided either by the PAS or by the SMSS (selected by the PAS CMD). When the Sun, Earth or Moon crosses the scanner field-of-view, two times are stored. The Acquisition of Signal (AOS) and Loss of Signal (LOS) times are stored in separate holding registers. The registers are in reality counters that start counting on a sun crossing and stop on an AOS and LOS. The steering logic then will accept the next AOS and LOS into two more counter/registers. The unit is designed to hold up to three sets of AOS and LOS pairs. If more than three targets are detected, a target overflow flag is set in the TM data. Data is transferred to the storage buffer A (or B) after one sun crossing to sun crossing and held there until Digital Word Gate (DWG)

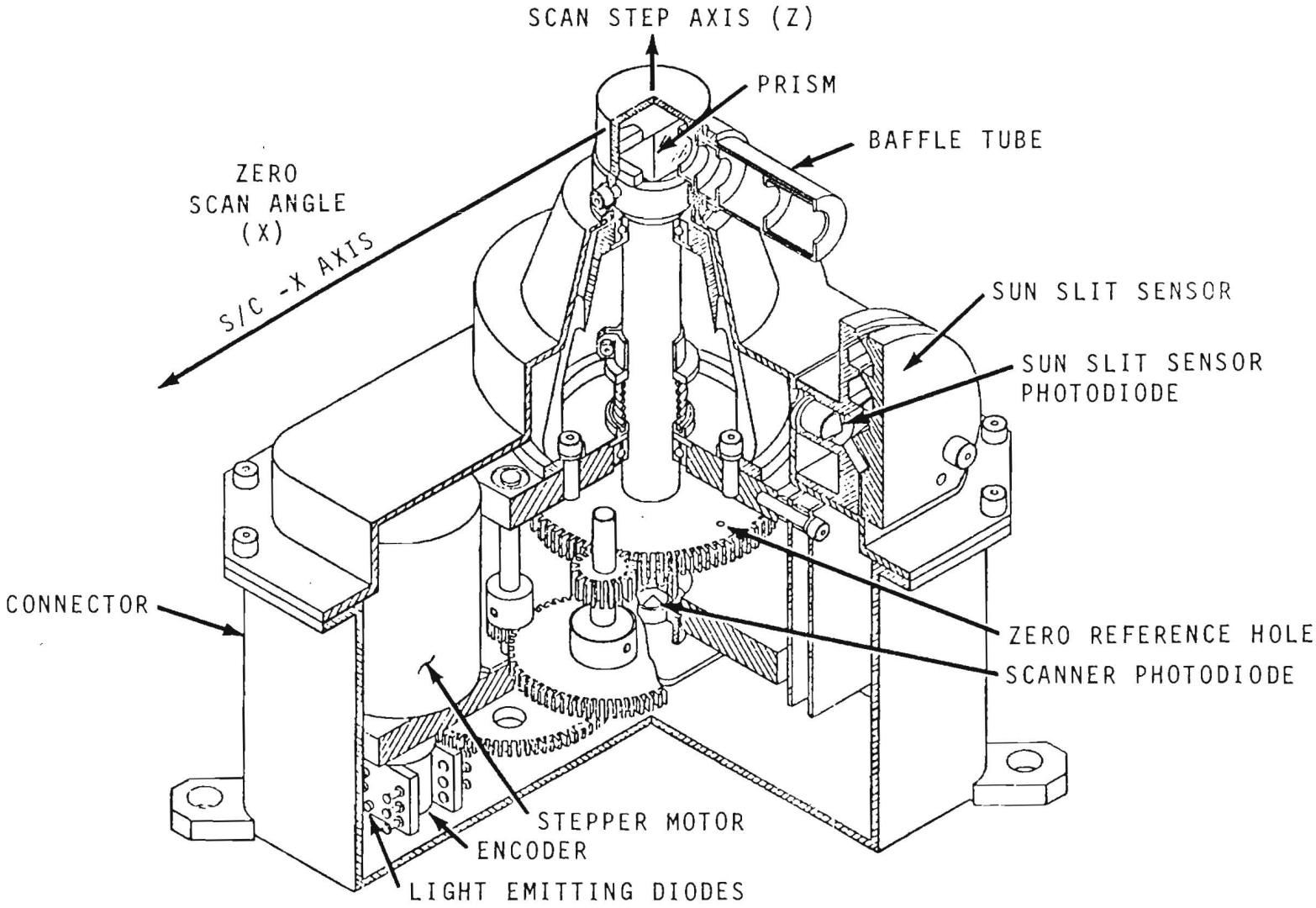

Figure B-9. PAS Head Design

occurs. At this time, storage buffer A (or B) is read out and the next sun crossing dumps data into storage buffer B (or A). (Figure B-10 allows data to be read out and updated simultaneously.)

If only one of the three pairs of AOS/LOS signals are encountered in any one sun-to-sun crossing time, the second and third AOS/LOS positions will contain the spin period. There are two submodes in the spherical mode; continuous and sector.

a. Continuous Submode. The scanner is advanced one step in the commanded direction on the first sun crossing after a DWG. This then permits the complete map of the sky in 256 spin periods or DWG's whichever is the longer time, (i.e., provided the field-of-view of the spin periods are non-overlapping). For example, the scanner advances from 0° to 180°. This is shown in figure B-11, the PAS field-of-view.

The intent here is to permit operation with many DWG's per spin period as well as many spin periods per DWG with no circuit modification.

b. Sector Submode. In the sector submode, the scanner steps one step on each first sun crossing after DWG as before except now only between θ max and θ min (θ max and θ min are commanded through the command words). The scanner steps until θ max is encountered and then reverses direction. The scanner then steps to θ min and again reverses direction. If θ min comes before θ max on the first pass, the scanner will go through θ min to θ max. If θ max is encountered first, the scanner reverses at θ max and goes to θ min. The commanded slew direction of scan determines if the scan is between an inside or outside angle, (see figure B-12). The scanner will continue to scan between θ max and θ min until switched to another mode or submode. There is one condition which is unique to the sector mode and that is where θ max equals θ min. When this condition is commanded, the scanner will step as before until θ min at which time the scanner is stopped. The data will be read out before but the position of the scanner head will remain fixed at θ max. Data is valid in this mode.

B.5.5.2 Planar Mode. The planar mode is used when the spacecraft is in a non-spinning state. In this mode, the sun sensor is not used. The only data will be the angular position of the scanner relative to the scanner zero angle, (figure B-9). Up to three AOS/LOS pairs can be recorded per rotation of the scanner. The scanner head can be stepped at different rates upon command. The rates are 78, 39, 19.5, and 9.8 steps per second. On occurrences of AOS/LOS, the angular positions of the scanner are recorded in separate holding registers. Data is then

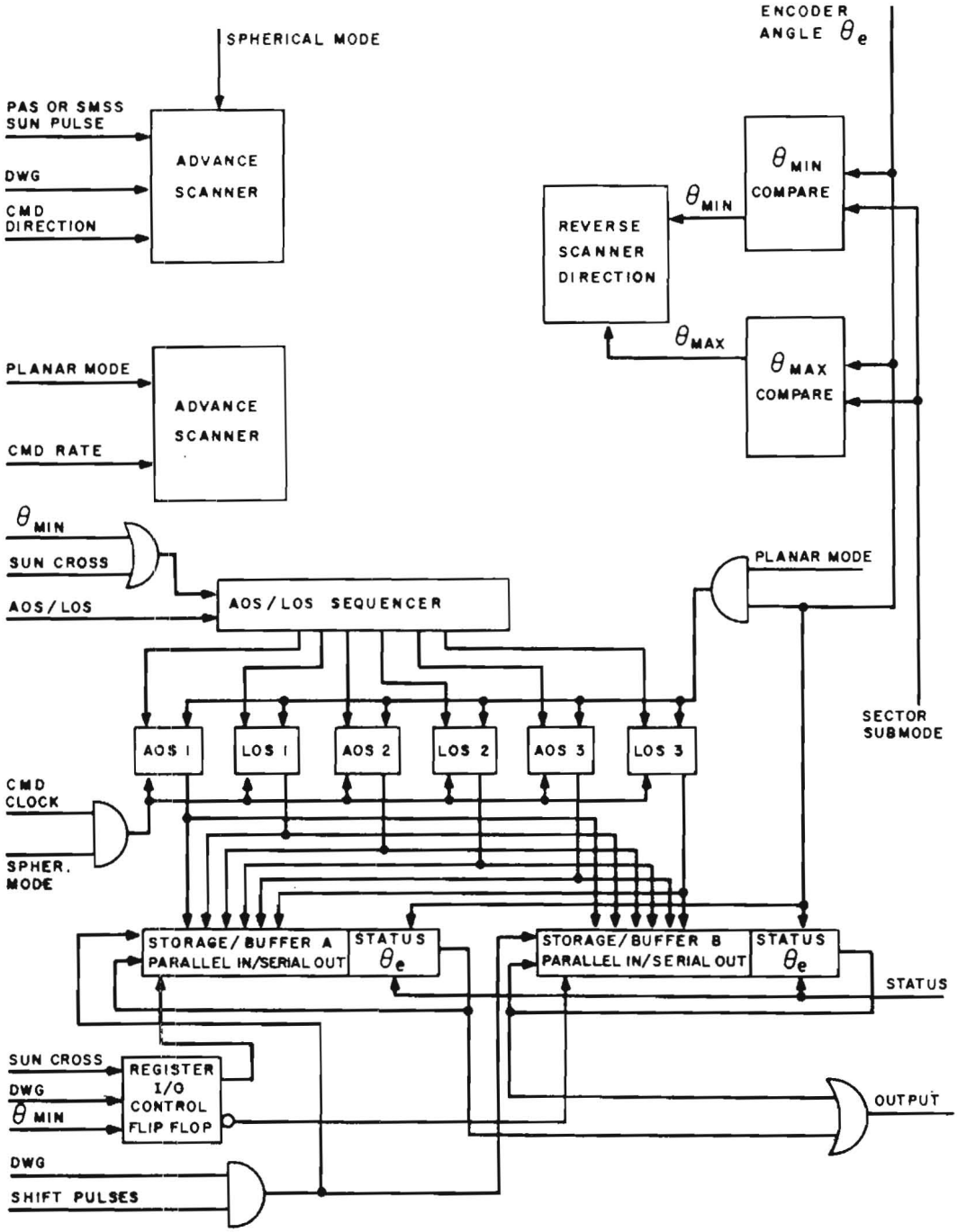

Figure B-10. PAS Logic Block Diagram

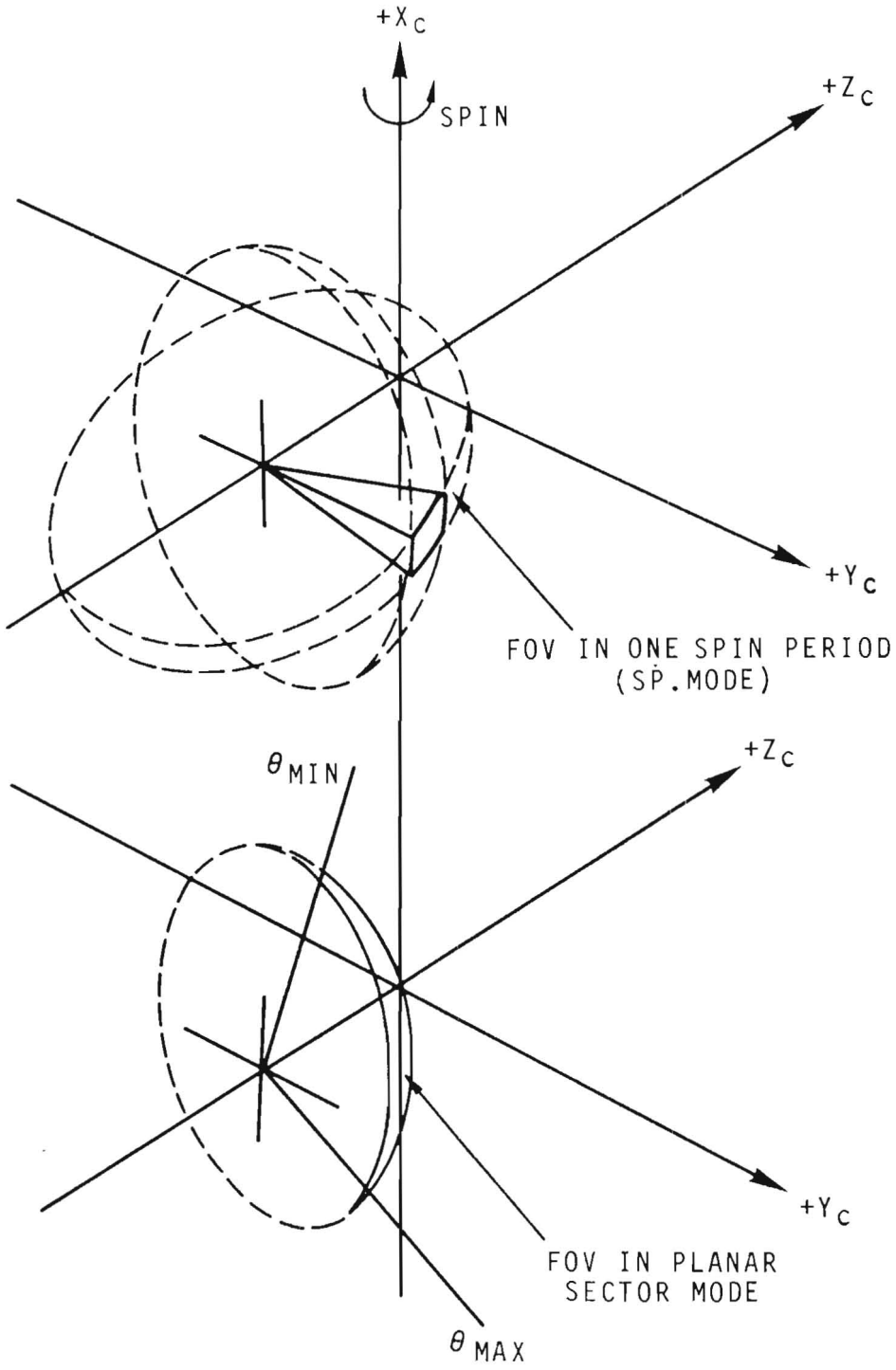

Figure B-11. PAS Field-of-View

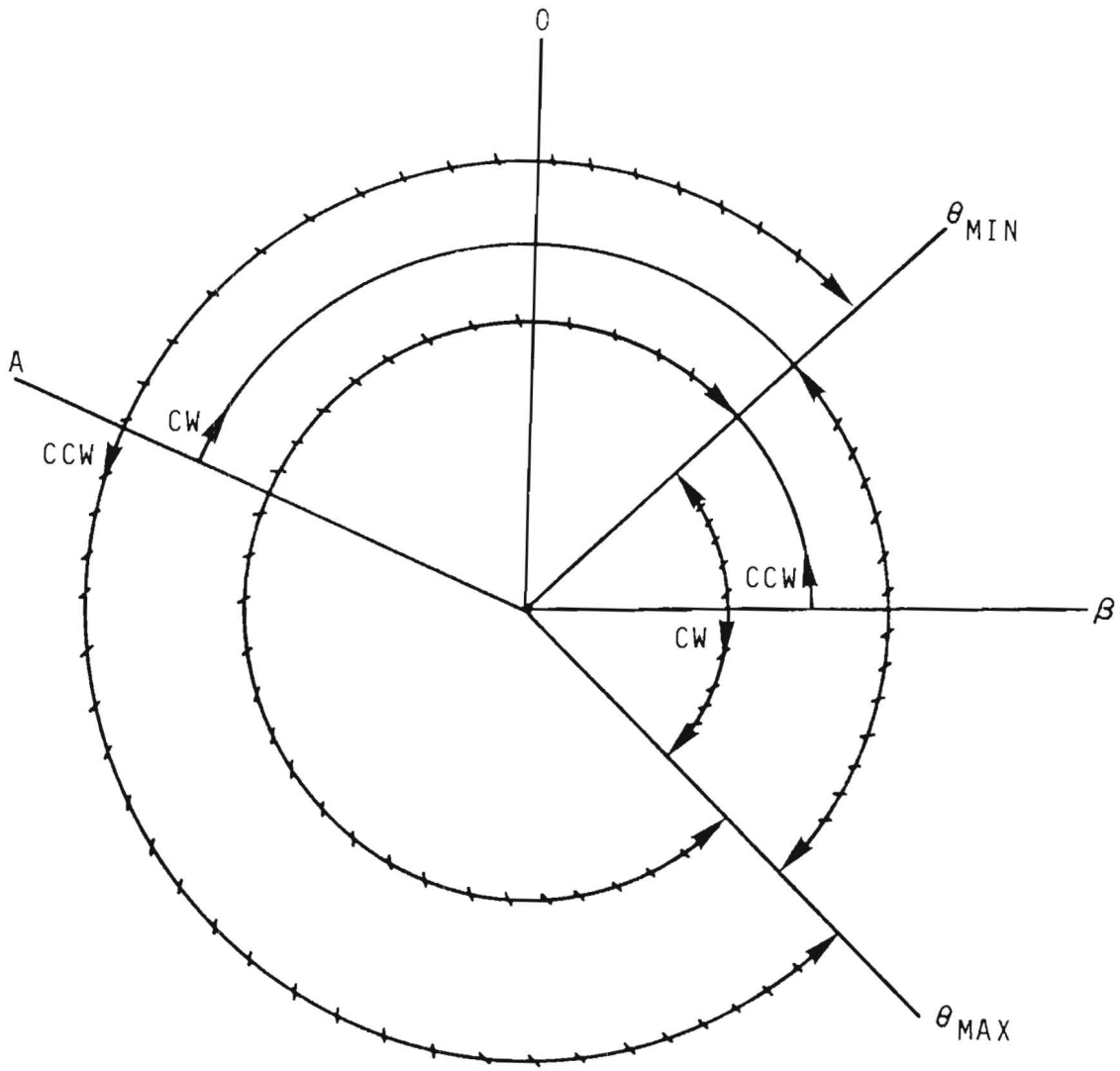

Figure B-12. Inside or Outside Angle Scan in Sector Submode

transferred to storage buffer A or B on the first θ min crossing after a DWG. A New Data status bit is used in the planar mode (but not used in spherical mode) to indicate the acquisition of new data at the buffer storage register. This bit is set high at each θ min crossing and is reset to low after a DWG.

a. Continuous Submode. In the continuous submode, the scanner steps at the commanded rate and direction. θ max is not used in this submode.

b. Sector Submode. In the sector submode, the scanner steps at the commanded rate between θ max and θ min. The scanner steps until θ max is encountered and reverses direction. If θ min comes before θ max on the first pass, the scanner will go through θ min to θ max. The commanded slew direction of scan determines if the scan is between an inside or outside angle, (figure B-12). If θ max is set equal to θ min, the scanner will step to θ max/θ min and stop. Data is not meaningful in this mode.

B.5.6 ACCURACY AND LIMITATIONS

The scanner resolution will depend on the commanded clock frequencies and the actual spacecraft spin rate. This relationship is expressed as:

$$\text{Spin Rate (RPM)} = \frac{\text{Clock Rate (Hz)}}{\text{No. of Counts}} \times 60$$

There are limitations on what minimum spin rate can be on the spacecraft for a given clock rate without causing an overflow of the 10-bit counter. This is shown in tabular form as follows:

Clock Rate	Min RPM w/o Overflow
1250 Hz	73.17 RPM
625 Hz	36.62 RPM
312 Hz	18.31 RPM
156 Hz	9.16 RPM

A high clock rate can be used with a low spin rate to obtain greater resolution by observing the data telemetry and noting when the 10-bit counter transitions from all one's to all zeros. Each of these transitions add 1024 counts. This feature will be of considerable value as the spacecraft roll is braked.

High resolution of spin period is of value in obtaining high resolution of angle-to-target measurement. For a given spin rate, an LOS or AOS angular position is:

$$\text{AOS} = \frac{\text{AOS Counts} \times 360 \times 60 \times \text{RPM}}{\text{Clock Rate Hz}}$$

or

$$\frac{\text{AOS Counts}}{\text{Counts per Spin}} = 360 = \text{degrees}$$

$$\text{Resolution} = \frac{360}{\text{Counts per Spin}} = \text{degrees}$$

B.5.7 SERIAL DIGITAL COMMAND

Control of the PAS is via a serial, digital command from the C&DH interface. The serial digital command is composed of 10 command words. The names of these command words, listed in the order they are received by the PAS are shown in table B-1. The first bit received by the PAS, in each command word, is the Most Significant Bit (MSB). The θ min and θ max angles are represented by a hybrid Gray/binary code. The coding and decoding scheme is shown in table B-2.

B.5.7.1 Serial Digital Output Data. The PAS provides 80 bits of serial digital output data. The loading of this data into the output register and the shifting out is under the control of the DMU.

The data is valid provided that a DWG is received followed by 80 shift pulses prior to the next DWG.

In addition, during initiation or change of command, a TM status bit is used to indicate validity of the received data. The Invalid Data bit is set high whenever a command envelope occurs and is reset to low on the first sun slit crossing (of the PAS or SMSS in the spherical mode) or on the first θ min crossing (in planar mode) after the command envelope. The 80 bits of output data are composed of data words of 10 bits each. The names of these words, listed in the order that they are shifted out are shown in table B-3. The encoder angle and the LOS/AOS's (in the planar mode only) are represented by a hybrid Gray/binary code. The coding and decoding scheme is shown in table B-2. The Most Significant Bit (MSB) is the direction of scan.

Table B-1. PAS Command

(12)	(1)	(2)	(1)	(9)	(1)	(1)	(1)	(9)
N/A	PASMOD	PASCLK	PASDIR	PASMAX	PASLEW	PASCAN	PASSUN	PASMIN

Mnemonic	Bit #	Function
N/A	1-12	Not Used
PASMOD	13	0=Spherical Mode 1=Planar Mode
PASCLK	14-15	0=1250 Hz Clock, 78.0 Hz Step. 1= 625 Hz Clock, 39.0 Hz Step. 2= 312 Hz Clock, 19.5 Hz Step. 3= 156 Hz Clock, 9.8 Hz Step.
PASDIR	16	0=CCW Scan Direction 1=CW Scan Direction
PASMAX	17-25	Theta Maximum Angle
PASLEW	26	0=Slew Disable 1=Slew Enable
PASCAN	27	0=Select Continuous Submode Scan 1=Select Sector Scan
PASSUN	28	0=Select PAS Sun Sensor 1=Select SMSS Sun Sensor
PASMIN	29-37	Theta Minimum Angle

Bit 1 is MSB

Bit 1 is the first bit out of the command decoder

PAS - 1 Serial Command #38 Hex Address B2

PAS - 2 Serial Command #46 Hex Address BA

Table B-2. Hybrid Grey/Binary Code

Position	Bit 1 MSB 1=CW 0=CCW	Bit 2-7 Binary Code	Bits 8-10 Gray Code	Encoder Angle in Degrees
0	1	000000	000	0
1	1	000000	001	.703°
2	1	000000	011	1.406°
3	1	000000	010	2.109°
4	1	000000	110	2.312°
5	1	000000	111	3.515°
6	1	000000	101	4.218°
7	1	000000	100	4.921°
8	1	000001	000	5.624°
9	1	000001	001	6.327°
10	1	000001	011	7.030°
11	1	000001	010	7.331°
12	1	000001	110	8.437°
13	1	000001	111	9.140°
14	1	000001	101	9.843°
15	1	000001	100	10.547°
16	1	000010	000	11.250°
17	1	000010	001	11.953°
.	.	.	.	.
.	.	.	.	.
.	.	.	.	.
32	1	000100	000	22.500°
.	.	.	.	.
.	.	.	.	.
.	.	.	.	.
64	1	001000	000	45.000°
.	.	.	.	.
.	.	.	.	.
.	.	.	.	.
128	1	010000	000	90.000°
.	.	.	.	.
.	.	.	.	.
.	.	.	.	.
256	1	100000	000	180.000°
.	.	.	.	.
.	.	.	.	.
.	.	.	.	.
504	1	111111	000	354.375°
505	1	111111	001	355.078°
.	.	.	.	.
.	.	.	.	.
.	.	.	.	.
511	1	111111	100	359.297°
512	1	000000	000	360.00 or 0°

To decode angle data, use the following:

$$\theta = \frac{\text{Position}}{512} \times 360^{\circ}$$

Table B-3. PAS Telemetry

PAS - 1 Digital Maincom Channel #7

PAS - 2 Digital Maincom Channel #9

80 Bit Register

(10)	(10)	(10)	(10)	(10)	(10)	(10)	(10)
PASANG	PASTAT	LOS 3	AOS 3	LOS 2	AOS 2	LOS1	AOS1

80

Mnemonic	Bit #	Function	
PASANG	1	0 = CCW, 1 = CW	
	2-10	Encoder Angle (Bit 2 = MSB)	
PASTAT	11	1 = Invalid Data	
	12	1 = New Data (Planar Mode Only)	
	13	1 = Target Overflow (Over 3)	
	14	1 = Slew Enable	
	15	1 = Sector Scan Mode	
	16	1 = Select SMSS	
	17-18	0 = 1250 Hz Clock, 78.0 Hz Step 1 = 625 Hz Clock, 39.0 Hz Step 2 = 312 Hz Clock, 19.5 Hz Step 3 = 156 Hz Clock, 9.8 Hz Step	
	19	1 = CW Scan Direction	
	20	1 = Planar Mode	
Mnemonic	Bit #	Planar Mode	. Spherical Mode
	21		
LOS 3	22-30	Bits 22/32/42/52/62/72	
	31	Are MSB's	
AOS 3	32-40		
	41		
LOS 2	42-50	Six 9 Bit Hybrid Grey	Six 10 Bit Ctrs.
	51	Codes Representing	
AOS 2	52-60	Encoder Position	Bits 21/31/41/51/
	61		61/71 are MSB's
LOS 1	62-70	Bits 21/31/41/51/61/71	
	71	Represent Direction	Bits 30/40/50/-
AOS 1	72-80	of Scan, 1 = CW	60/70/80 are LSB's

B.6 REACTION WHEELS

B.6.1 PURPOSE

The IUE reaction wheels will provide the vernier control torques which will enable the control system to hold and slew the spacecraft in accordance with onboard control laws and ground commands. Four wheels will be hard mounted to the spacecraft structure - one each on the three control axes and one symmetrically skewed with respect to the orthogonal control axes. This unique configuration provides functional redundancy in pitch, yaw, and roll.

B.6.2 MODIFICATIONS

This reaction wheel will be identical to the Nimbus yaw reaction wheel. No modifications in operating characteristics and/or physical characteristics are anticipated.

B.6.3 LOCATION

The four wheels will not be located on the equipment shelf. Provisions shall be made to mount the wheels just under the primary mirror strong ring and attached to the spacecraft structure.

B.6.4 PERFORMANCE

The following definition and characteristics shall apply to the reaction wheel design:

a. Configuration. The wheel motor is an inside out design two-phase induction motor. The stator, containing the field windings, is internal to the rotor and is secured to the housing assembly (spacecraft). The motor armature and tachometer sawtooth cam are integral parts of the flywheel subassembly forming the rotor. The rotor spin axis is perpendicular to the mounting base of the housing. The housing is sealed to maintain internal, positive pressure in a vacuum environment. The magnetic pickoff for the tachometer is attached to the housing.

b. Flywheel Inertia. The inertia of the flywheel is 0.0025 slug ft^2 $\pm$5% about its spin axis.

3. Motor. The following characteristics apply to the wheel motor:

Type	Induction
No. of Poles	32
No. of Phases	2
Stator Windings/Phase	2
DC Winding Resistance	15.2 Ω ±20%
Excitation	Square Wave
Rotation	Bi-directional

d. Tachometer. The tachometer cam is an integral part of the flywheel and consists of eight magnetic sawtooth cams equally spaced about the flywheel axis of spin. The tach signal generator consists of a single magnetic pick-up coil mounted to the stator. The tachometer produces eight pulses per revolution.

e. General Characteristics. The following characteristics apply to the overall wheel design:

No-load Speed: > 1350 RPM.

Torque (stall): > 5 oz-in.

Angular Momentum: 0.327 ft-lb-sec ±5% @1250 RPM.

Coast Down Time (t): 5 min < t < 11 min.

Momentum Vector: within 15 arc-minutes of mounting base normal.

B.7 NUTATION SENSOR ASSEMBLY (NSA)

B.7.1 PURPOSE

The NSA will be configured to support the IUE transfer orbit control function. The unit will contain two force rebalanced accelerometers. The accelerometers will be co-aligned and redundant. During the transfer orbit their outputs will be utilized to indicate the nutation cone angle build-up and to control the decay in accordance with the nutation control algorithm.

B.7.2 LOCATION

The NSA will be mounted on the equipment shelf at a maximum radial distance from the vehicle spin axis. The redundant accelerometers shall have their input axes parallel to the vehicle spin axis. An optical reference shall be provided to define the sensitive axis.

B.7.3 POWER

The NSA shall operate directly from the WDA ±10v bus. The unit shall draw no more than 1.0 watt of power under steady state operating conditions (assuming only one accelerometer powered). Provisions shall be made to operate each accelerometer independently from the other. This switching is accomplished in the CEA.

The following performance characteristics shall apply to the force rebalanced accelerometers.

Range: ±1.0 g.

Null Bias: < 0.001 g.

Linearity: 200 µg max.

Threshold: 100 µg.

Scale Factor Stability: 0.05%
(over environment)

APPENDIX C. ACS SOFTWARE ALGORITHMS

C.1 INTRODUCTION

As was stated in previous sections, there are both hardwire logic and software logic algorithms controlling various phases of ACS operation. The hardwired functions are used during the transfer orbit stage, orbit insertions, appendage deployment and sun acquisition. The logic is contained in the CEA and was described in sections 8.2 and Appendix A. These hardwire algorithms are backed up by ground initiated software algorithms, some of which will be described herein. The prime software algorithm, however, is the one whereby the rate inputs to the six gyros are measured, combined, separated into control axes and used to generate wheel drive signals to close the loop for attitude hold. Subsets to this algorithm permit decision making as to what errors should be used for control during experimentation and to permit both small multi-axis slews and large single axis slews. This section will describe these logic flows in simplified fashion.

C.2 PRECESSION ALGORITHM

Section 8.2.3.3 discussed the requirement to perform a 180^0 rotation of vehicle spin axis during the interval between Delta separation and arrival at apogee in order to align the thrust vector of the Apogee Boost Motor (ABM) along the spacecraft velocity vector. Section 8.2.7 described in detail the hardware implementation of the precession maneuver. This section will describe the algorithm and show the logic flow to accomplish the precession maneuver via OBC.

C.2.1 PRECESSION ALGORITHM REQUIREMENT

The basic requirement for the algorithm is to provide the capability of firing a precession engine over a portion (ARC) of the spacecraft spin cycle and phasing this ARC so a predetermined precession direction relative to the Sun can be achieved. The magnitude of the precession motion obtained for each spacecraft revolution can be controlled by varying the ARC over which the precession engine is fired. Thus a summation of the incremental precession angle per revolution will yield the total precession angle required. This capability can be implemented in an algorithm whereby a single, 37 bit serial command word can enable the algorithm, specify the time delay with respect to sun crossing to start firing the engine, specify the number of consecutive OBC command windows to repeat the "ON" command (which normally shuts off approximately 100 milliseconds after an "ON" command as a fail safe measure) thus determining the amount of precession per revolution, and specify the number of consecutive spins to repeat the operation before automatically terminating the Precession Maneuver.

C.2.2 MEASUREMENT TIMING

Any of three different sensors (PAS 1, PAS 2, or SMSS) can be used to generate a Sun Presence signal to index the algorithm. The appropriate sensor will be ground command selected. All will develop a Sun Presence signal of $\frac{1}{2}^0$ width which, at a nominal 360^0/sec rotation rate will yield a signal about 20 milliseconds in duration. The OBC operates at a 40 kbit rate and will sample this Sun Presence signal at least 3 times. Since sampling occurs once every 6.4 milliseconds, there can be a maximum error of only 6.4 milliseconds. Because the OBC and the command system run asynchronously and because the command system is time shared between OBC and ground commands, use of a simple algorithm generating an engine fire command a fixed time after Sun Presence could be in error as much as 53.67 milliseconds. (Fixed delay of 23.67 milliseconds plus variable delay of 0 to 30 milliseconds as a function of OBC command relative to CDU command windows.) With the added Sun Presence error of up to 6.4 milliseconds, engine fire could be delayed as much as 60.07 milliseconds beyond nominal. This could be half of the nominal firing period of 1/8 revolution (125 milliseconds) and is intolerable. To minimize this effect, a more complex algorithim has been implemented that corrects the commanded time by subtracting the fixed delay (23.67 milliseconds) and one-half the random, variable delay (8.2 milliseconds) or a total of 41.87 milliseconds from the desired time. The Time Delay (TD) can be up to 1200 milliseconds and should be resolvable to one millisecond. Up to 10 consecutive engine commands are required (R) and up to 256 spin revolutions (C) for a complete maneuver may be required. In addition, two bits are required to select one of the three sun sensors and two bits are required to enable the maneuver. The command word structure is as follows:

Bits 1 through 11: TD (Delay to start engine).

Bits 12 through 15: R (Number of engine starts).

Bits 16 through 23: C (Number of revolutions).

Bits 24 and 25: SS (Sensor Select).

Bits 26 and 27: PME (Precession Maneuver Enable).

Bits 28 through 37: Spare.

The logic flow for the Precession Algorithm is shown as figure C-1.

C.3 NUTATION ALGORITHM

Section 8.2.2.1.a discussed the reasons that the IUE would require an active nutation control during the spin-stabilized transfer orbit while Section 8.2.6 described in detail the analysis, hardware implementation and graphical time sequencing of nutation buildup and cancellation. This

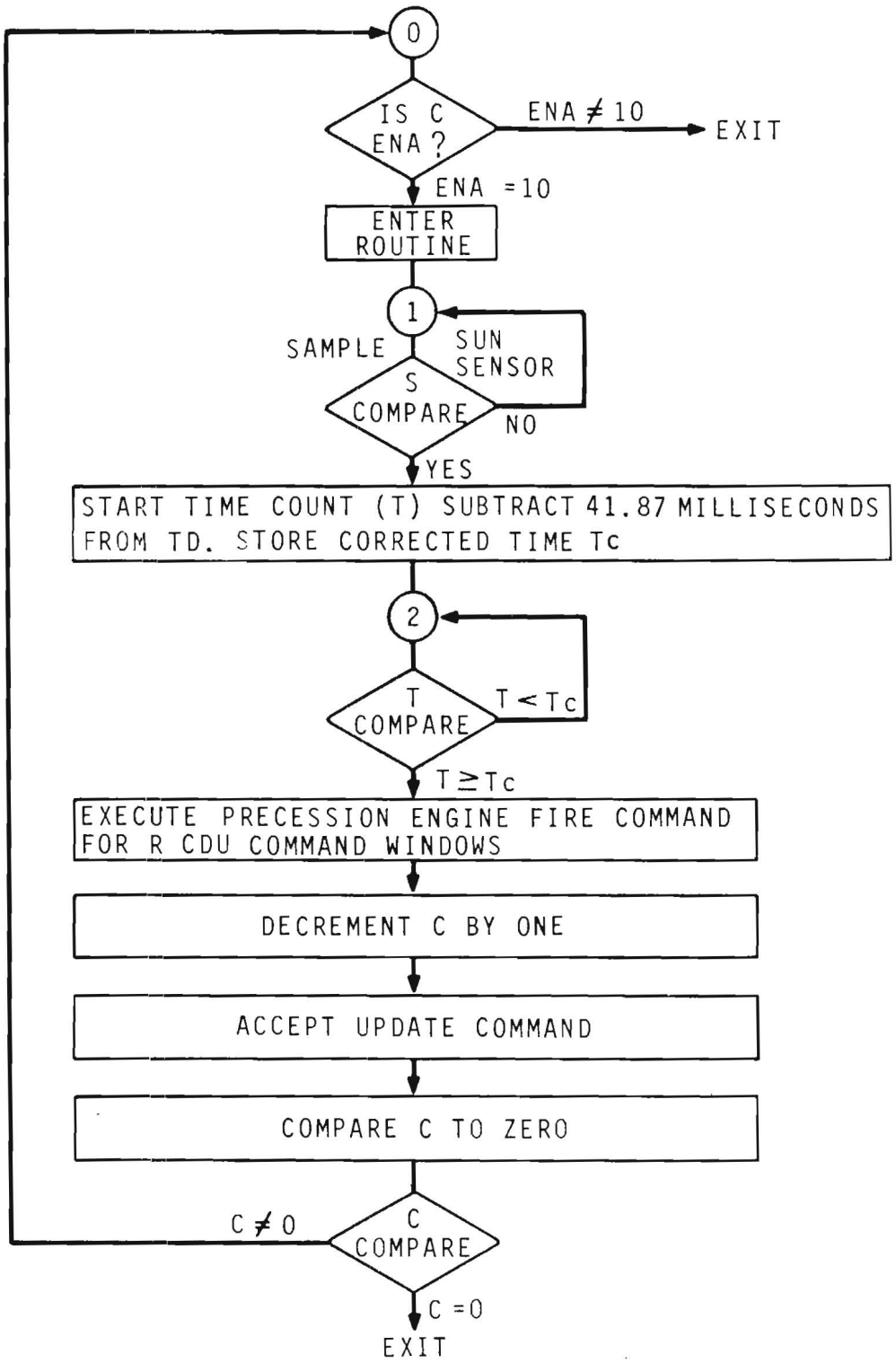

Figure C-1. Precession Logic Flow Diagram

section will describe the algorithm and show the logic flow to accomplish nutation damping.

C.3.1 NUTATION ALGORITHM REQUIREMENT

The basic requirement of the nutation algorithm is to work with active sensors to determine a coning angle buildup, to eliminate any offset or bias in these sensors and to then fire a hydrazine jet at the proper time and for the proper duration to cancel out the coning angle when a threshold is exceeded.

C.3.2 IMPLEMENTATION

The algorithm first selects one of the two, redundant accelerometers in the logic flow diagram (figure C-2). This is unit A and the accelerometer is designated as NSA = A. The output of this accelerometer is sampled by the OBC once every 6.4 milliseconds for several cycles. This allows a DC Bias (B_T) to be calculated and arithmetically removed from subsequent samples. Since the sampling period is quite frequent relative to the nominal spin period, the algorithm also obtains an accurate figure for the nutation cycle. With B_T removed, each sample of NSA, A is compared against a commanded threshold. Once the threshold is exceeded, the next null transition is detected and a nutation control engine fire signal is generated over a period correctly phased with respect to the null transition. To minimize the effects of command decoder/OBC asynchronous operation on firing interval, the algorithm performs a time averaging operation similar to that used in the precession algorithm. Also as with the precession algorithm, the nutation control command word will be generated and executed via ground command. Figure C-3 shows a nutation cycle with a typical period of 1.4 sec before and after determination and removal of DC Bias, a Time Delay (TD) after threshold is exceeded, and a firing period, R, over which the jet is enabled. Also shown is a delay, TS, that allows the system to settle after a firing before accepting as valid accelerometer signals exceeding the threshold. Table C-1 shows the 37 bit nutation command word functions and their definitions.

C.3.3 LOGIC FLOW

Referring to figure C-2, the OBC enters the routine and checks to see if a ground command has enabled operation. If this is affirmative, the bias measured bits, TR 1 and TR 2 are set to zero and the selected accelerometer, NSA = A is sampled for 10 seconds. B_T is determined as shown and TR 1 is set to a '1' and the routine is rechecked. With a valid B_T term in A, a new value A_C which is the sum of A and B_T is entered. A check is made for the state of TR 2. If it is zero, the routine compares A_C to the threshold value of A_T. If A_C is less than the threshold, the routine loops. When A_C is finally equal or exceeds A_T, TR 2 is set as a '1' and the next loop allows A_C to be compared with a threshold of 2.5. If A_C exceeds this, the routine loops until A_C is below the 2.5 limit.

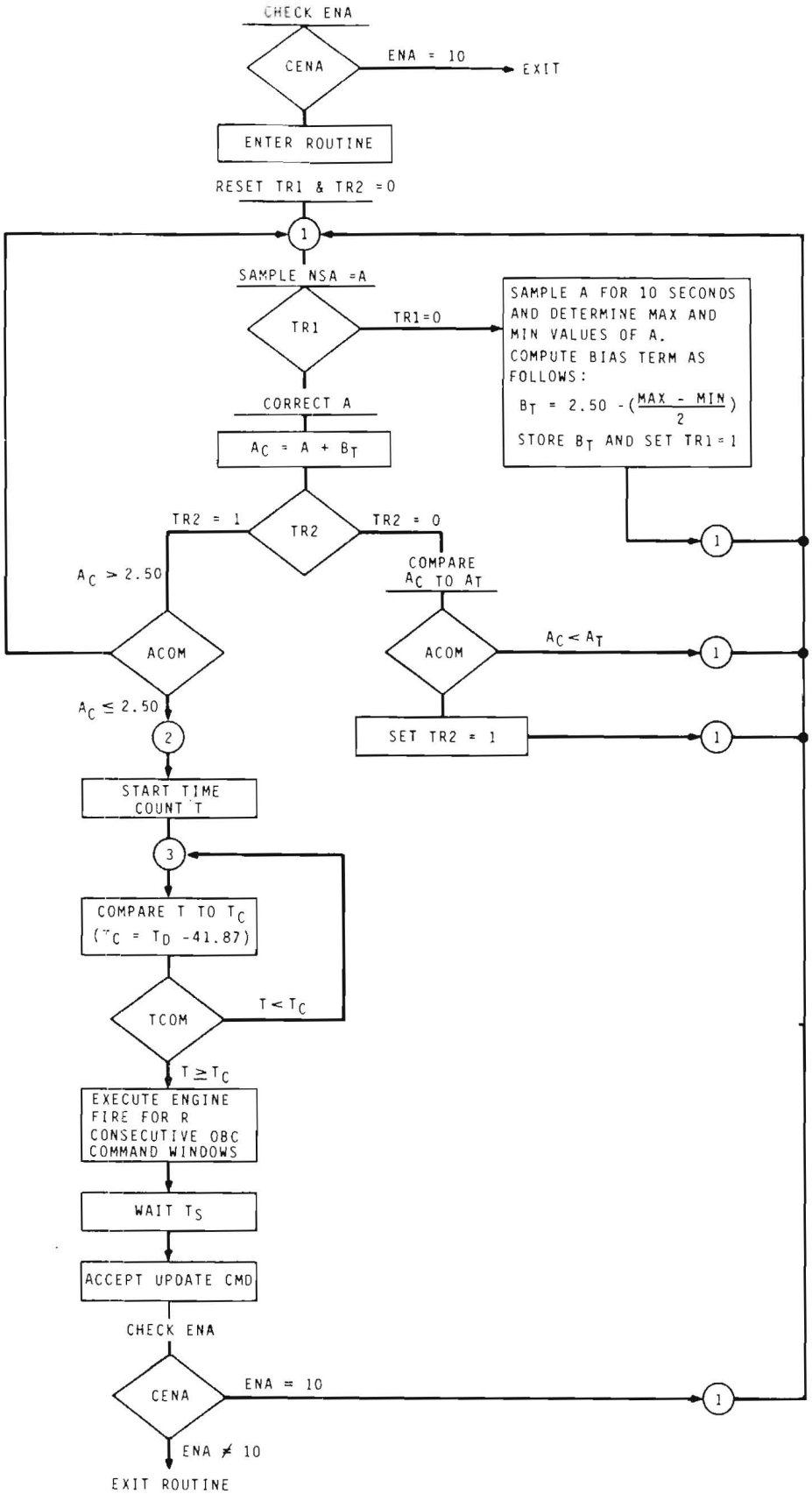

Figure C-2. Nutation Logic Flow Diagram

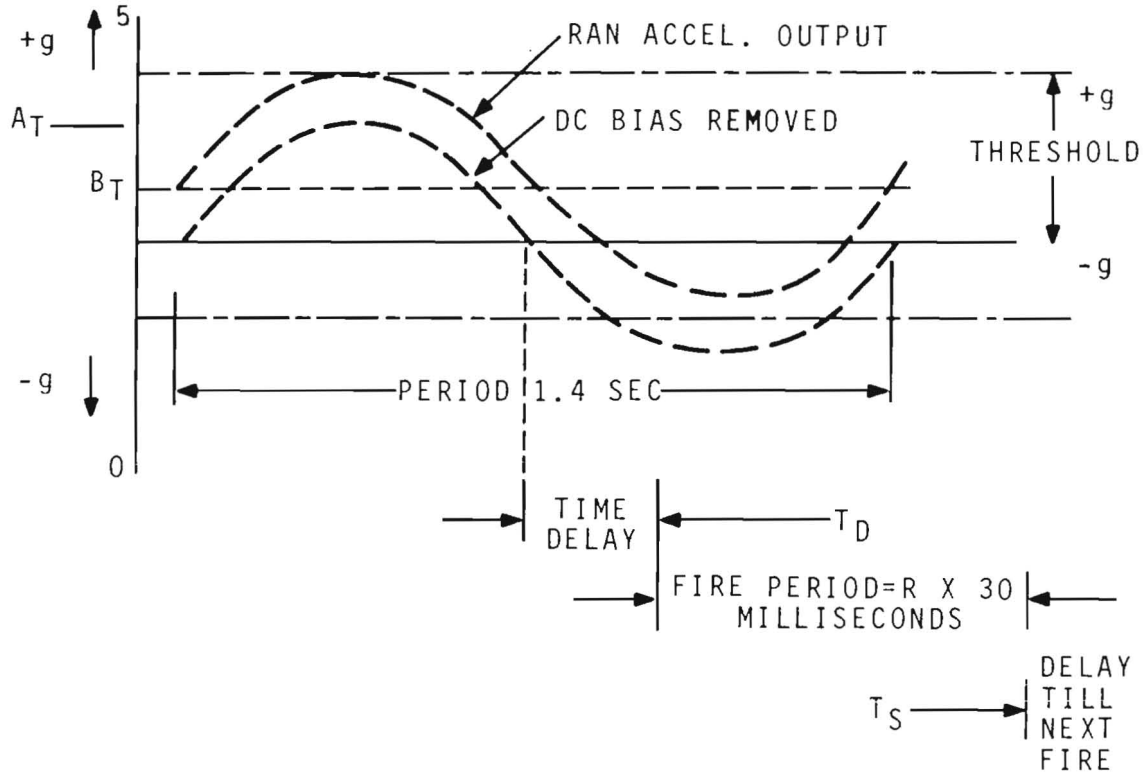

Figure C-3. Adjusted Nutation Cycle

Table C-1. 37 Bit Nutation Command Definition

A_T = 8 Bits	T_D = 11 Bits	R = 5 Bits	T_S = 10 Bits
	NSA = 1	ENA = 2	

1. A_T represents a commandable threshold over the 0 to 5.0 VDC Telemetry range. Maximum sense range is $\pm$ 0.5 g's.

2. T_D represents a commandable time delay from an algorithm event (A_C crossover from $A_C > 2.50$ to $A_C \leq 2.50$). Bit resolution should be approximately one millisecond or 2.048 seconds maximum.

3. R represents a commandable firing time by specifying the consecutive number of OBC command windows over which the nutation control engine should be fired. Maximum firing time is 32 x 30 milliseconds or 960 milliseconds.

4. T_S represents a commandable time delay before re-entering the nutation control algorithm at (1). Bit resolution should be equivalent to 10 milliseconds or 10.24 seconds maximum.

5. ENA represents two bits which must be in the 10 state before the algorithm is entered.

At this point a timer is started and a comparison is made with the value T_C. T_C is the T_D required for phasing less 41.87 milliseconds as an average correction for OBC sampling, command decoder command windows, and asynchronous operation between the devices, when the time, point and the compensated accelerometer output, A_C, is compared with zero level or +2.5 v. If A_C is less than +2.5 v indicating the accelerometer is sensing -g's, the routine returns to nexus 1 and loops until such time as A_C exceeds +2.5 v indicating a zero crossing in the positive sense. At this point the routine continues and starts a time delay prepatory to jet firing. This delay, T, is compared to a value T_C which equals T_D, the time required for proper jet firing phasing, less 41.87 msec, the statistical average correction required to compensate for OBC sampling, command decoder windows and asynchronous operation between these two devices. When the compensated time, T_C, is greater than T, the routine recompares until T equals or exceeds T_C. At this point the OBC generates an engine fire command for R consecutive OBC command windows, this value R having been part of the ground command word. After completion of jet firing, the routine waits an interval, T_S, for the system to settle out from the firing transient and then accepts an update ground command. If the routine is still enabled, the OBC loops back to nexus 1 and repeats. If the routine has been disabled as a result of a new ground command, the routine is exited.

C.4 HOLD (EXPERIMENT)/SLEW

By far the most complex algorithm and the one that not only is the greatest load on the OBC but is the rationale for flying an OBC, is the routine or program that generates inertia wheel commands (eventually control voltages) to either maintain a current attitude and permit experimentation (Hold Mode) or to slew to a different attitude (Slew Mode). To understand the flow of the logic frequent (or continuous) reference to the Hold/Slew Logic Flow Diagram (figure C-4) should be made. The Hold/Slew program is called by the OBC Executive every 204 milliseconds. The following logic operations transpire:

C.4.1 IRA RATE ASSESSMENT

Each of the 6 gyros in the IRA has its digitized output word interrogated to obtain new gyro counts (NNEW) proportional to the rate about that gyro's sensitive (input) axis. The difference in counts, (NDEL) between this update and the previous reading is computed for Ith gyros (I = 1 through 6) by subtracting the previous reading from the current one [NDEL(I) = NNEW(I) - NOLD(I)]. The absolute value, |NDEL(I)|, is checked against a counter limit (NDMAX) and corrected by $\pm 2^{16}$ if it exceeds (NDMAX). Either NDEL(I) or the corrected NDEL(I) - ISIGN (65536 NDEL) now has a gyro scale factor, (WG), of 0.01 arc-second/count (nominal), applied to the delta counts and bias estimate, (BGDT) subtracted to yield a gyro delta angle value, (AGD). The AGD of each operative gyro (normally all six) is now resolved onto the spacecraft control axes via the gyro-to-body direction cosine matrix (LI) yielding

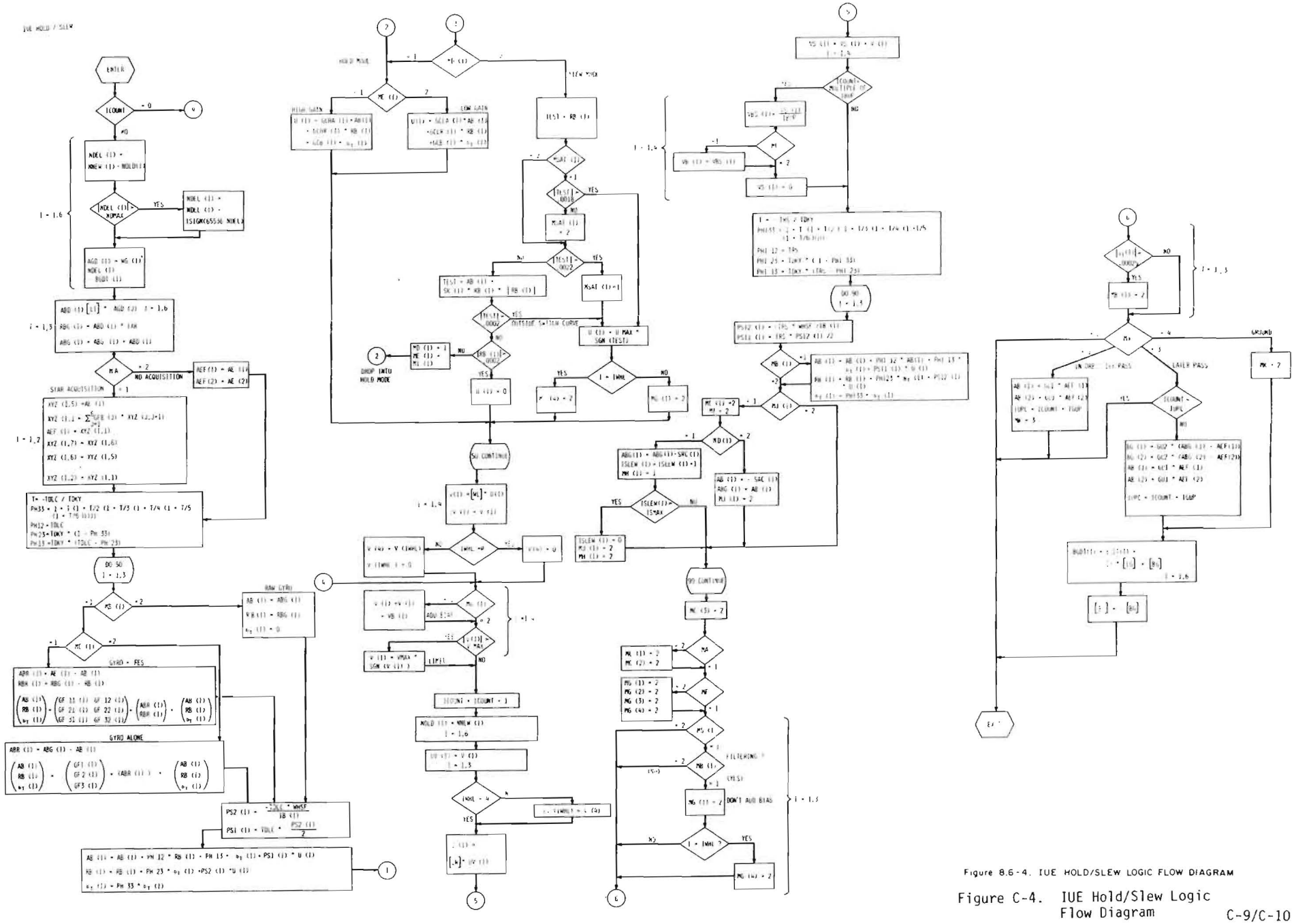

Figure 8.6-4. IUE HOLD/SLEW LOGIC FLOW DIAGRAM

Figure C-4. IUE Hold/Slew Logic Flow Diagram

body delta angles which are then divided by the OBC cycle time of 204 milliseconds to obtain an average rate about each of the control axes over the control interval, (RBG). In addition the body delta angles are also used to update the gyro-estimated body angles, (ABG).

C.4.2 HOLD MODE SELECTION

At this point the program performs a test to determine which of several Hold Modes will be selected. A mode switch, MA, is tested. If a suitably bright guide star is being tracked by the FES, MA will be '1'. In this case, the FES pitch and yaw delta position data is passed through a Butterworth low pass filter to remove high frequency star-image noise/jitter on this data. A matrix (PH) describing the state's transition from time = 0 (cycle start) to time = TDLC is set up. The state is a three-term vector consisting of estimated position error, rate error, and what are termed "bias accelerations" or noise. The Executive-provided TDLC is an estimated time lag between the start of the cycle and the issuance of a wheel voltage command. If there were no star presence from the FES, switch MA would have been set to a '2'. In this case, only the IRA gyro data would be available for control.

C.4.3 AXIS HOLD MODE SELECTION

Before the data of C.4.2 is processed any further, a per-axis mode switch, (MB(I) where I is 1, 2 or 3) is tested. If MB = 2, the FES data is ignored and the gyro data bypasses the Kalman Filter. The gyro-estimated position and rate errors are utilized as the state vector elements. If, on a given axis, MB = 1, the state estimates are corrected by amounts outputted by a Kalman Filter. The selection of input data to the Kalman Filter is determined by a switch, (MC(I) where I is 1 or 2). If MC is a '1', the filter will accept gyro-provided rate information and FES-provided attitude information. If MC is a '2', only gyro attitude information will enter the Kalman Filter. In either case, the Kalman Filter partially removes the noise corrupting the measurement accuracies and permits near optimal estimates of the position and rate errors to be made. At this point an input-coupling matrix, (PS), is established to tie the control voltage to the state vector. This matrix is supplied either raw gyro data (MB(I) = 2), Kalman Filtered gyro data (MB(I) = 1, MC(I) = 2), or Kalman Filtered gyro rate plus FES attitude data (MB(I) = 1, MC(I) - 1) and ties the control-axes-resolved wheel voltage, (U) for the Ith wheel computed on the last cycle to the current state estimate. The state of the system at time TDLC is now determined. This state vector is now ready to be voltage transformed by the wheel control laws.

C.4.4 WHEEL MODE SELECTION

Prior to using these estimates of rate and attitude errors, a per-axis mode switch, (MD), is tested. If MD equals '2', this axis is in SLEW mode. A bang, bang control voltage, (U MAX), of $\pm$2.5 volts is applied

to drive the system to a near zero state: (rate less than $\pm$.0002 radian per second and attitude error less than ~ $\pm$.0002 radian) at which time the system will return to the Hold mode for this axis by setting switch, (MD(I)) to the '1' state, (2). In the Hold mode the wheel volts are set as a function of the current state in a continuing attempt to null out attitude and rate errors.

C.4.5 WHEEL HOLD MODE GAIN SELECTION

The program having determined that the Ith axis is in the Hold mode as a function of switch, (MD(I)), set to a '1', now tests switch, (ME(I)), for the proper gain. If ME(I) is in the '2' state, a Low Gain or slow decay to zero in a second-order step response fashion is applied to the attitude error, (AB). If (ME(I)) is set to the '1' state, a High Gain or fast decay is used to drive (AB) to zero. The step response is characterized by an angular control frequency, (ω_C) and damping ratio, (ξ). The control axis voltages are resolved onto the three operational wheels and a per-wheel mode switch, (MG(I)), where I is 1, 2, 3 or 4, is checked. If (MG(I)) is set to a '1', a computable wheel bias is added to the signal for that wheel. If (MG(I)) is set to a '2', the bias is omitted. The wheel voltage, (V(I)), with or without bias (V_B(I)) is limited or clipped to $\pm$ (V_{MAX}) or $\pm$2.5 volts and issued as a command to the appropriate channel of the CEA.

C.4.6 CYCLE PREPARATION

Having generated a new wheel voltage command for each wheel, the OBC algorithm now performs the necessary computations to prepare the system for the next cycle. I_{COUNT}, the number of times the update algorithm has been run, is updated by adding a one. The present gyro counts, (NNEW(I)), become NOLD(I) for use in the next cycle comparison. The present wheel voltages, (V(I)), are projected back onto the control axes to become a control-axis voltage, (U(I)), which will be available for the state correction at the Kalman Filter (5). If switch, (MB(I)) was set to the '1' state, a prediction as to what the system state will be at the start of the next computation cycle must now be made. A transition matrix, (PHI), for the time period, T = TDLC to T = Cycle End, is established and the prediction is made. If (MB(I)) was set to the '2' state, a "predicted state" as an input to the Kalman Filter will not be required since raw gyro data will be the basis of the next cycle's wheel voltage computation.

C.4.7 SLEW INITIATION

With the "predicted state" developed, if necessary, the routine proceeds to sample the SLEW command switch, (MJ(I)), to determine whether to accept slew commands for execution during the next cycle. If (MJ(I)) is in the '1' state on this axis, slewing commands will be accepted. Switch, (MC(J)), the FES filter switch, will be set to a '2' state to prohibit the acceptance of FES error data while slewing and switch (MF(I)), the refine bias

switch, will also be set in the '2' state to prevent the refinement of wheel bias while slewing. The slew can be a "Slew in Hold Mode" wherein a fixed (low) rate, fixed-angle-increment per cycle slew is performed by leaving the program logic in Hold mode while repeatedly nulling out a small angle, (SRC). This results in a fixed rate of (SRC) radians/sec on the spacecraft and is useful for tracking a slowly moving object. This type of slew will continue for a commandable number of computation cycles, (ISMAX), and the routine will set the slew complete mode switch, (MH) to a '2' state. A normal or "any angle" slew (mode switch, (MD(I)) set to a '2' state) is executed by accepting the slew command angle, (SAC), generating an equivalent angle of opposite polarity, (-SAC), and inserting this as a sudden "position" error in the state vector. The program will respond in the normal error null mode and will drive the wheels until the error is null thereby performing the desired slew. Switch, (MJ(I)) is set to the '2' state on the slewed axis and this prohibits acceptance of any further commands by the program until the slew is complete at which time a new slew can be commanded.

C.4.8 MODE INTERLOCKING

As part of the cycle preparation, the program now proceeds to set various logic switches to limit mode configurations. The roll axis Kalman Filter input switch, (MC(3)), is forced to the '2' state whereby gyro data only is Kalman Filtered in that axis. This prevents a program failure caused by an attempt to process non-existent FES roll axis data. If FES pitch/yaw data is unsuitable (i.e. no FES Star Presence), switch, (MA(I)), will be set to a '2' state and this will force switches (MC(I)) pitch and (MC(2)) yaw to the '2' state to prevent Kalman Filtering of non-existent FES data. Next the "refine bias" switch, (MF), is checked. If (MF) is set to a '2', then the per-wheel bias addition switches, (MG(I)), where I is 1, 2, 3 and 4, are set to the '2' state to prevent addition of bias to the wheel voltage and the routine exits. If (MF) is set to the '1' state, ("refine bias"), and if (MG(I)) switch is set to the '1' state (add bias), then the per-axis switch, (MB(I)), is checked for state. If set to a '2', filtered data will not be used. If (MB(I)) is in the '1' state, then filtered data is available and the per-wheel switches, (MG(I)) where I is 1, 2, 3 and 4, are set to the '2' state to prevent the addition of bias to the wheel voltage. The next check is to determine whether the processed wheel is a failed wheel. If it is not, the routine exits. If it is, then the redundant wheel is in use and the bias addition switch for the redundant wheel (MG(4)), is set to a '2' to prevent bias addition and the routine exits, (6).

C.4.9 GYRO UPDATE CALIBRATION

The final step in the processor is gyro update calibration. A switch, (MK), has four states. If (MK) is set to a '2', no update calibration

is performed and the routine exits. If MK is set to a '4', then ground-computed estimates of the expected gyro drift, (BG), are projected onto the six gyro sensitive axes via (LG), the body-to-gyro direction cosine matrix and are then multiplied by the 204 millisecond program cycle time to get an estimate of drift during one control cycle. This drift per cycle, (BGDT), is added into NDEL(I) on the next cycle. If switch MK is in either the '1' or '3' state, the pitch and yaw attitude error estimates, (AB(1), AB(2)), are updated by passing the filtered FES data through a Kalman Filter, GU1 for these angles. The MK = '1' state is applicable only for the first pass through the processor. For succeeding passes, MK = '3' and the gyro drifts are computed as the output of a Kalman Filter, (GU2), which operates upon the difference between the gyro measured body angle errors and the FES measured error angles. These drifts are then projected in the same fashion as (BG) to develop a value for (BGDT) to be used on the next computation cycle. With completion of this operation, the program exits until recalled by the OBC Executive. Note that on the first pass, $I_{COUNT} = 0$ and the program jumps to (4). On succeeding passes, $I_{COUNT} \neq 0$ and the program runs as described.

C.5 ADDITIONAL OBC ALGORITHMS

At this time, not all of the algorithms required to provide a software backup for the CEA hardwire logic have been developed. The two that have, Precession and Nutation, were described in C-2 and C-3. At such time that the remaining three or so algorithms are developed, they will be added to this section of the SDR.